Exploiting DNA Repair Vulnerabilities to Modulate Anti-Cancer Immunity : a Study of the Immunological Potential of PARP inhibitors

Roman Chabanon

université PARIS-SACLAY

Thèse de doctorat

NNT : 2019SACLS007

Exploiting DNA repair vulnerabilities to modulate anti-cancer immunity: a study of the immunological potential of PARP inhibitors.

Thèse de doctorat de l'Université Paris-Saclay
préparée à l'Université Paris-Sud

Unité Inserm U981, Gustave Roussy (Villejuif)
Gene Function Laboratory, The Institute of Cancer Research (Londres)

École Doctorale N°582 :
Cancérologie – Biologie – Médecine – Santé

Disciplines :
Sciences de la vie et de la santé
Aspects moléculaires et cellulaires de la biologie

Soutenue publiquement le 31 janvier 2019 à Gustave Roussy par

Roman Chabanon

Composition du jury

Pr. Chris Lord Directeur de Recherche, Institute of Cancer Research, Londres	**Président**
Dr. Philippe Pasero Directeur de Recherche, Institut de Génétique Humaine, Montpellier	**Rapporteur**
Pr. Fabrice Barlesi Professeur des Universités-Praticien Hospitalier, Hôpital Nord, Marseille	**Rapporteur**
Dr. Olivier Delattre Praticien Hospitalier et Directeur de Recherche, Institut Curie, Paris	**Examinateur**
Dr. Jean-Luc Perfettini Directeur de Recherche, Gustave Roussy, Villejuif	**Examinateur**
Dr. Sophie Postel-Vinay Praticien Hospitalier et Directrice d'Equipe, Gustave Roussy, Villejuif	**Directeur de thèse**
Pr. Jean-Charles Soria Professeur des Universités-Praticien Hospitalier, Gustave Roussy, Villejuif	**Co-directeur de thèse**
Dr. Aurélien Marabelle Praticien Hospitalier et Directeur d'Equipe, Gustave Roussy, Villejuif	**Co-directeur de thèse**

Acknowledgements

Avec sincérité et humilité, je souhaiterais dédier ce travail au Dr. Sophie Postel-Vinay, qui a admirablement dirigé mes recherches et sans conteste contribué à leur aboutissement. La confiance qu'elle m'a rapidement accordée et le soutien inconditionnel qu'elle m'a apporté tout au long de mon doctorat ont façonné un cadre de travail extrêmement enrichissant, tant sur le plan scientifique qu'humain. Dans cette atmosphère bienveillante et positive, Sophie m'a à chaque instant poussé à l'excellence ; avec douceur et professionnalisme, elle m'a permis de grandir scientifiquement et humainement et a souvent créé des opportunités pour me mettre en avant à travers mon travail. Grâce à elle, j'ai appris à me lancer, oser faire des hypothèses, expérimenter, et plus que tout, avoir confiance dans mon travail et mes résultats. Sophie m'a également transmis sa passion pour la recherche translationnelle en cancérologie, et m'a aidé à garder à l'esprit que tout ce que nous faisons, nous le faisons pour le bénéfice des patients. Enfin, Sophie a concrétisé mon envie de découvrir un autre environnement de travail, une autre approche de la recherche, en me permettant d'effectuer une partie de mon doctorat à l'ICR à Londres. Pour tout cela, je souhaite la remercier chaleureusement, et lui dire que je ne suis pas peu fier d'avoir été son premier étudiant en thèse !

Je souhaiterais ensuite exprimer ma plus grande gratitude au Pr. Jean-Charles Soria, qui m'a initialement accepté comme étudiant en thèse dans son équipe, et qui, avec une clairvoyance déconcertante, a tout de suite su que je pourrais m'épanouir sous la supervision de Sophie. En tant que directeur puis co-directeur de thèse, Jean-Charles m'a soutenu tout au long de mon doctorat et je suis aujourd'hui très heureux qu'il puisse faire le déplacement depuis les Etats-Unis pour assister à ma soutenance de thèse.

Un grand merci également au Dr. Aurélien Marabelle, qui m'a accompagné avec beaucoup de bienveillance et de gentillesse durant ces trois années, et m'a donné un autre regard sur la recherche et sur les parcours possibles au-delà de la thèse.

Sophie, Jean-Charles et Aurélien ont tous les trois contribué au succès de mes recherches, mais plus que cela, ils ont chacun à leur manière enrichit ma personnalité, et sont pour moi des modèles inspirants pour mon futur parcours professionnel.

I would like to warmly thank Prof. Chris Lord, for having welcomed me in his lab at the ICR in London. I am very grateful for his high-quality scientific input on my project, and for the confidence he has placed in me since our very first meetings. A big thank you also goes to his team members, Steve, Drago, Ilirjana, Rachel, Feifei, Ger, Marta and all the others that made my time at the ICR a really enriching experience.

Merci aussi à toutes les personnes à Gustave Roussy qui m'ont, de près ou de loin, aidé à mener mon projet de recherche durant mes deux premières années de thèse : je pense tout d'abord à Marlène et Nicolas, mais aussi Isabelle, Kariman, Daphné, Chloé et Mei-Shue.

Je voudrais aussi remercier mes parents, Chantal et Christian, et mes grands-parents, Raymonde et René, qui ont toujours cru en moi et m'ont soutenu sans relâche, depuis toujours.

Last but not least, je voudrais remercier de tout mon cœur ma petite chérie, Laetitia, pour le soutien sans faille qu'elle m'a apporté depuis le début de cette aventure, pour sa compréhension face à mes craintes, mes inquiétudes et mes moments de doutes, pour son aide précieuse dans la mise en forme de ce manuscrit de thèse, et pour tout le bonheur qu'elle m'a donné, adoucissant un quotidien parfois rude. Sans elle, je n'en serais pas là aujourd'hui.

Abstract

Poly(ADP-ribose) polymerase inhibitors (PARPi) selectively target cancer cells with DNA repair deficiencies such as *BRCA1/2* mutations or ERCC1 defects. Clinically, several PARPi are currently approved for the treatment of *BRCA*-mutant or platinum-sensitive advanced ovarian and breast cancers, and ongoing clinical trials are investigating the efficacy of PARPi in platinum-sensitive Non-Small Cell Lung Cancer (NSCLC). While PARPi constitute potent targeted therapies for the treatment of DNA repair-deficient malignancies, an increasing number of clinical trials are also evaluating their efficacy in combination with immune checkpoint inhibitor (ICI) in various populations. In this context, it is of critical importance to better understand how PARPi might modulate immune responses against cancer, and to investigate the inherent immunological potential of these agents.

In this study, we show that ERCC1-defective NSCLC cells exhibit an enhanced type I interferon (IFN) transcriptomic signature and that low ERCC1 expression correlates with increased lymphocytic infiltration in human NSCLC tumours. Using isogenic cell lines and patient-derived xenografts, we further demonstrate that several clinical PARPi, including olaparib and rucaparib, display cell-autonomous immunomodulatory properties in ERCC1-defective NSCLC and *BRCA1*-mutant triple-negative breast cancer (TNBC) models. Mechanistically, PARPi generate cytoplasmic chromatin fragments with micronuclei characteristics; this activates the cGAS/STING pathway and elicits downstream type I IFN signalling and CCL5 secretion. Importantly, these effects are suppressed in BRCA1-reverted TNBC cells and ERCC1-rescued NSCLC cells, suggesting that DNA repair defects exacerbate the innate immunity-related phenotypes triggered by PARPi. Similarly, these effects are totally abrogated in PARP1-null TNBC cells, supporting the on-target effect of PARPi in mediating such phenotypes.

Besides this potential to activate tumour cell-autonomous immunity through cGAS/STING and type I IFN signalling, we also observed that PARPi synergize with type II IFN to induce PD-L1 expression in NSCLC cell lines and fresh patient tumour cells, especially in the ERCC1-deficient setting. Moreover, we show that lethal concentrations of some PARPi independently activate the key damage-associated molecular patterns dictating the immunogenicity of cancer cell death, including calreticulin exposure at the tumour cell surface, ATP secretion and HMGB1 release in the extracellular compartment.

Together, these preclinical data suggest that PARPi have intrinsic immunomodulatory properties that activate anti-cancer immune responses; this could be exploited clinically in combination with ICI in appropriately molecularly-selected populations.

Publications and Presentations

Publications included in this thesis

Roman M. Chabanon, Gareth Muirhead, Dragomir B. Krastev, Julien Adam, Daphné Morel, Marlène Garrido, Clémence Hénon, Nicolas Dorvault, Rebecca Marlow, Ilirjana Bajrami, Marta Llorca Cardeñosa, Asha Konde, Benjamin Besse, Alan Ashworth, Stephen J. Pettitt, Syed Haider, Aurélien Marabelle, Andrew N.J. Tutt, Jean-Charles Soria, Christopher J. Lord and Sophie Postel-Vinay. ERCC1-deficiency exacerbates tumor cell-intrinsic immunity in response to PARP inhibitors in non-small cell lung cancer. **The Journal of Clinical Investigation**, 2018.

Roman M. Chabanon, Marion Pedrero, Céline Lefebvre, Aurélien Marabelle, Jean-Charles Soria, and Sophie Postel-Vinay. Mutational landscape and sensitivity to immune checkpoint blockers. **Clinical Cancer Research**, 2016.

Contribution to other publications

Mehdi Touat, Tony Sourisseau, Nicolas Dorvault, **Roman M. Chabanon**, Marlène Garrido, Daphné Morel, Dragomir B. Krastev, Ludovic Bigot, Julien Adam, Jessica R. Frankum, Sylvère Durand, Clement Pontoizeau, Sylvie Souquère, Mei-Shiue Kuo, Sylvie Sauvaigo, Faraz Mardakheh, Alain Sarasin, Ken A. Olaussen, Luc Friboulet, Frédéric Bouillaud, Gérard Pierron, Alan Ashworth, Anne Lombès, Christopher J. Lord, Jean-Charles Soria, et Sophie Postel-Vinay. DNA repair deficiency sensitizes lung cancer cells to NAD+ biosynthesis blockade. **The Journal of Clinical Investigation**, 2018.

Ruth Pidsley, Mitchell G. Lawrence, Elena Zotenko, Birunthi Niranjan, Aaron Statham, Jenny Song, **Roman M. Chabanon**, Wenjia Qu, Hong Wang, Michelle Richards, Shalima S. Nair, Nicola J. Armstrong, Hieu T. Nim, Melissa Papargiris, Preetika Balanathan, Hugh French, Timothy Peters, Sam Norden, Andrew Ryan, John Pedersen, James Kench, Roger J. Daly, Lisa G. Horvath, Phillip Stricker, Mark Frydenberg, Renea A. Taylor, Clare Stirzaker, Gail P.

Risbridger and Susan J. Clark. Enduring epigenetic landmarks define the cancer microenvironment. **Genome Research**, 2018.

Presentations

November 2018: 30th EORTC/AACR/NCI conference, Dublin, Ireland. **Poster presentation.** PARP inhibitors activate cancer cell-intrinsic immunity via cGAS/STING in ERCC1- and BRCA1-defective contexts. **Roman M. Chabanon**, Gareth Muirhead, Dragomir B. Krastev, Julien Adam, Marlène Garrido, Daphné Morel, Nicolas Dorvault, Thomas Eychenne, Clémence Hénon, Rebecca Marlow, Christophe Massard, Alan Ashworth, Stephen J. Pettitt, Syed Haider, Aurélien Marabelle, Andrew N.J. Tutt, Jean-Charles Soria, Christopher J. Lord and Sophie Postel-Vinay.

September 2018: Institute of Cancer Research Science Bites, London, United Kingdom. **Oral presentation.** Potential of PARP inhibitors to modulate tumour-intrinsic immunity. **Roman M. Chabanon**.

May 2017: Journées Scientifiques de l'Ecole Doctorale de Cancérologie, Roscoff, France. **Poster presentation.** Beyond DNA repair: Bringing the immunological potential of PARP inhibition to light. **Roman M. Chabanon**, Aurélien Marabelle, Jean-Charles Soria, and Sophie Postel-Vinay.

April 2017: Gustave Roussy Research Days, Tours, France. **Oral presentation.** Beyond DNA repair: Bringing the immunological potential of PARP inhibition to light. **Roman M. Chabanon**.

Contribution to other presentations

January 2019: Keynote Symposium "DNA Replication and Genome Instability: From Mechanism to Disease", Snowbird, United States of America. **Oral presentation.** Combining DNA damage response (DDR) inhibitors with immunotherapy: The next step change in cancer therapy? Sophie Postel-Vinay.

Table of Contents

List of Figures

List of Tables

List of Abbreviations

5-FU	5-Fluorouracil
7-AAD	7-aminoactinomycin D
ADCC	Antibody-Dependent Cellular Cytotoxicity
ALL	Acute Lymphoid Leukaemia
APC	Antigen-Presenting Cells
ATCC	American Type Culture Collection
BCG	Bacillus Calmette-Guérin
CAR T cells	Chimeric Antigen Receptor T cells
CCF	Cytoplasmic Chromatin Fragments
CDC	Complement-Dependent Cytotoxicity
CDK1i	CDK1 inhibitor
cGAMP	Cyclic GMP-AMP
CI	Confidence Interval
CLL	Chronic Lymphoid Leukaemia
CRC	Colorectal Carcinoma
DAMPs	Damage-Associated Molecular Patterns
DAPI	4',6-diamidino-2-phenylindole
DC	Dendritic Cells
DEGs	Differentially Expressed Genes
DSB	Double-Strand Break
dsDNA	Double-Stranded DNA
ELISA	Enzyme-Linked Immunosorbent Assay
EMT	Epithelial–Mesenchymal Transition
EpCAM	Epithelial Cell Adhesion Molecule
ER	Endoplasmic Reticulum
FACS	Fluorscence-Activated Cell Sorting
FDR	False Discovery Rate
FSC	Forward Scatter
GSEA	Gene Set Enrichment Analysis
HCC	Hepatocellular Carcinoma
HGSOC	High-Grade Serous Ovarian Cancer
HLA	Human Leucocyte Antigen
HNSCC	Head and Neck Squamous Cell Carcinoma
HR	Homologous Recombination
HRP	Horseradish Peroxidase
HU	Hydroxyurea
ICC	Immunocytochemistry
ICD	Immunogenic Cell Death

IF	Immunofluorescence
IHC	Immunohistochemistry
IO	Immunotherapy
IR	Ionizing Radiation
IRF	Interferon Regulatory Factor
LAK	Lymphokine-Activated Killer
LFC	$\log_2$ Fold-Change
Mb	Megabase
mCRPC	Metastatic Castration-Resistant Prostate Cancer
MDSC	Myeloid-derived Suppressor Cells
MFI	Mean Fluorescence Intensity
MHC	Major Histocompatibility Complex
miRNA	Micro-RNA
MMR	Mismatch-Repair
mRNA	Messenger Ribonucleic Acid
MSI	Microsatellite-Instability
MTX	Mitoxantrone
NCI	National cancer Institute
NCZ	Nocodazole
NER	Nucleotide Excision Repair
NES	Normalized Enrichment Score
NGS	Next-Generation Sequencing
NHEJ	Non-Homologous End Joining
Nira	Niraparib
NK	Natural Killer
NKT	Natural Killer T
NSCLC	Non-Small Cell Lung Cancer
nsSNV	Non-Synonymous Single-Nucleotide Variants
Ola	Olaparib
ORR	Overall Response Rate
OS	Overall Survival
PAMP	Pathogen-Associated Molecular Pattern
PBMC	Peripheral Blood Mononuclear Cells
PDX	Patient-Derived Xenograft
PE	Phycoerythrin
PFS	Progression-Free Survival
PMSF	Phenylmethylsulfonyl Fluoride
PRR	Pattern Recognition Receptors
PS	Phosphatidyl-Serine
RCC	Renal Cell Carcinoma
RNA-seq	RNA sequencing
RT-qPCR	Quantitative Reverse Transcription Polymerase Chain Reaction
Ruca	Rucaparib
SASP	Senescence-Associated Secretory Phenotype

SCLC	Small Cell Lung Cancer
siRNA	Small-Interfering RNA
ssDNA	Single-Stranded DNA
Talazo	Talazoparib
TAM	Tumour-Associated Macrophages
TAN	Tumour-Associated Neutrophils
TCGA	The Cancer Genome Atlas
TCR	T Cell Receptor
TILs	Tumour-Infiltrating Lymphocytes
TLR	Toll-Like Receptors
TLS	Tertiary Lymphoid Structures
TMB	Tumour Mutational Burden
TME	Tumour Microenvironment
TNB	Tumour Neo-antigen Burden
TNBC	Triple-Negative Breast Cancer
Treg	Regulatory T cells
UBC	Urothelial Bladder Carcinoma
UPR	Unfolded Protein Response
WB	Western Blot
WES	Whole-Exome Sequencing

List of Genes and Proteins

ANXA1	Annexin A1
ATF6	Activating Transcription Factor 6
ATM	Ataxia Telangiectasia Mutated
ATR	Ataxia Telangiectasia and Rad3 related
B2M	Beta-2 Microglobulin
BARD1	BRCA1 Associated RING Domain 1
BLM	Bloom Syndrome RecQ Like Helicase
BRCA1/2	Breast Cancer Susceptibility Gene ½
BRIP1	BRCA1 Interacting Protein C-Terminal Helicase 1
CALR	Calreticulin
CCL5	C-C Motif Chemokine Ligand 5
CD4	T-Cell Surface Glycoprotein CD4
CD47	Antigenic Surface Determinant Protein OA3
CD8	T-Cell Surface Glycoprotein CD8
CD91/LRP1	LDL Receptor Related Protein 1
CDK12	Cyclin Dependent Kinase 12
cGAS	Cyclic GMP-AMP Synthase
CHK1/2	Checkpoint Kinase 1/2
CTLA-4	Cytotoxic T-Lymphocyte Associated Protein 4
CXCL5/9/10/12	C-X-C Motif Chemokine Ligand 5/9/10/12
CXCR4	C-X-C Motif Chemokine Receptor 4
DNASE2	Deoxyribonuclease 2, Lysosomal
ERCC1	Excision Repair Cross-Complementation Group 1
EXO1	Exonuclease 1
FANCA	Fanconi Anemia Complementation Group A
FANCD2	Fanconi Anemia Complementation Group D2
FANCF	Fanconi Anemia Complementation Group F
FAS-L	FAS Ligand
FRP1	Formyl Peptide Receptor 1
Gal9	Galectin-9
GM-CSF	Granulocyte/Macrophage Colony-Stimulating Factor
HER2	Human Epidermal growth factor Receptor-2
HMGB1	High-Mobility Group Box 1
HSP70/90	Heat Shock Protein 70 kDa/90 kDa
IDO	Indoleamine 2,3-Dioxygenase
IFN-γ	Interferon Gamma
IFNAR1	Interferon Alpha and beta Receptor subunit 1

IFNα	Interferon Alpha
IKK	Inhibitor of Nuclear Factor Kappa B Kinase Subunit Beta
IL	Interleukin
IRE1α	Inositol-Requiring Enzyme 1 Alpha
KLRK1/NKG2D	Killer Cell Lectin Like Receptor K1
LKB1/STK11	Serine/Threonine Kinase 11
MLH1/3	MutL Homolog 1/3
MRE11	MRE11 Homolog, Double Strand Break Repair Nuclease
MSH2/3/6	MutS Homolog 2/3/6
mTOR	Mammalian Target Of Rapamycin
MUS81	MUS81 Structure-Specific Endonuclease Subunit
MYC	MYC Proto-Oncogene, BHLH Transcription Factor
NF-κB	Nuclear Factor-kappa B
NFKB1/2	Nuclear Factor Kappa B Subunit 1/2
NSB1/NBN	Nibrin
PALB2	Partner And Localizer of BRCA2
PANX1	Pannexin 1
PARP1/2	Poly(ADP-Ribose) Polymerase 1/2
PD-1	Programmed Cell Death 1
PD-L1/CD274	Programmed Cell Death 1 Ligand 1
PDIA3/ERp57	Protein Disulfide Isomerase family A member 3
PERK	Protein Kinase R-like ER Kinase
PGE2	Prostaglandin E2
PMS2	PMS1 Homolog 2, Mismatch Repair System Component
POLD1	DNA Polymerase Delta 1, Catalytic Subunit
POLD3	DNA Polymerase Delta 3, Accessory Subunit
POLE/Pol-ε	DNA Polymerase Epsilon
pTBK1	Phosphorylated TBK1
PTEN	Phosphatase And Tensin Homolog
RAD17	RAD17 Checkpoint Clamp Loader Component
RAD50	RAD50 Double Strand Break Repair Protein
RAD51C	RAD51 Paralog C
RAD54L	RAD54 Like
RAGE	Advanced Glycosylation End product-specific Receptor
RELB	RELB Proto-Oncogene, NF-KB Subunit
RNASEH2	Ribonuclease H2
SAMHD1	SAM And HD Domain Containing Deoxynucleoside Triphosphate
STING	Stimulator of Interferon Genes
TAP	Transporter associated with Antigen Processing
TBK1	TANK Binding Kinase 1
TGF-β	Transforming Growth Factor beta
TLR3	Toll-like receptor 3

TLR4	Toll-Like Receptor 4
TNF-α	Tumour Necrosis Factor alpha
TRAIL	Tumour necrosis factor–Related Apoptosis-Inducing Ligand
TREX1	Three Prime Repair Exonuclease 1
VEGF	Vascular Endothelial Growth factor
XPF	Xeroderma Pigmentosum Group F-Complementing Protein
XRCC1	X-Ray Repair Cross Complementing 1

Chapter I. Introduction

A. Cancer and immunity: the emergence of a paradigm

Cancer is a genetic disease. It arises from alterations in genes controlling key biological processes, collectively responsible for the maintenance of cellular homeostasis. Both gain-of-function mutations in proto-oncogenes and loss-of-function mutations in tumour suppressor genes can lead to the transformation of normal cells into malignant cells, thereby initiating tumour development. This genetic-based description of carcinogenesis has enabled the identification of many oncogenic drivers involved in tumour development, among which some of them are currently exploited as actionable targets for the treatment of cancer. Beyond the cancer cell itself, the contribution of the tumour microenvironment (TME) – and notably the immune system – to carcinogenesis has been recognized for more than a century, but has only very recently led to significant therapeutic advances.

1. From cancer immunosurveillance to cancer immunoediting

The involvement of immunity in tumour recognition and control was first hypothesized by the German physician and scientist Paul Ehrlich in 1909. He postulated that cancer occurred spontaneously in human, but that in the majority of people, the host immune system was able to prevent neoplastic cells from developing into tumours (1). In the late 1950s, the idea of a host immune protection against cancer was revisited through the concept of cancer immunosurveillance by two prominent immunologists: Frank Macfarlane Burnet and Lewis Thomas. Burnet's pioneering theory stated that tumour cells-specific neo-antigens could challenge host immune tolerance and trigger an effective anti-tumour immunological reaction capable of eliminating nascent neoplasms (2,3). Thomas's theory was shaped by an evolutionary point of view and suggested that long-lived organisms must possess protecting mechanisms against cancer, similar to those mediating allograft rejection. Both

theories were supported by the functional demonstration of mouse tumour-specific antigens (4) and converged towards the concept of cancer immunosurveillance, which defined the critical role of sentinel thymus-dependent immune cells in constantly monitoring the appearance of early neoplasms in host tissues. This concept gained recognition, but was rapidly challenged by studies showing no differences in primary tumour development between athymic nude mice and syngeneic wild-type mice (5,6). Later discoveries demonstrated that lymphocytes and interferon-gamma (IFN-γ) play a beneficial role in the protection of hosts against the development of carcinogen-induced sarcomas and spontaneous epithelial carcinomas, but that they also promote selection of tumour cells with reduced immunogenicity, capable of escaping immune recognition and destruction (7). This process of immunoselection of tumour cells could explain the apparent paradox of tumour formation in immunologically competent individuals, by raising the possibility of escape from immunosurveillance. These findings were the basis for the development of the immunoediting theory in 2002 (8), which described for the first time how both innate and adaptive immunity contribute to tumour development through a dynamic process of Darwinian immunoselection of tumour cell variants. This process classically consists of three distinct steps (**Figure I.1**):

(1) Elimination: the innate and adaptive compartments of the immune system coordinately drive immune rejection;

(2) Equilibrium: through a clonal selection process, the dynamic balance between tumour and immune cells results in the emergence of specific tumour cell variants with increased resistance, which take advantage of acquired mutations;

(3) Escape: the immune-resistant clones freely expand, circumventing both innate and adaptive immune responses.

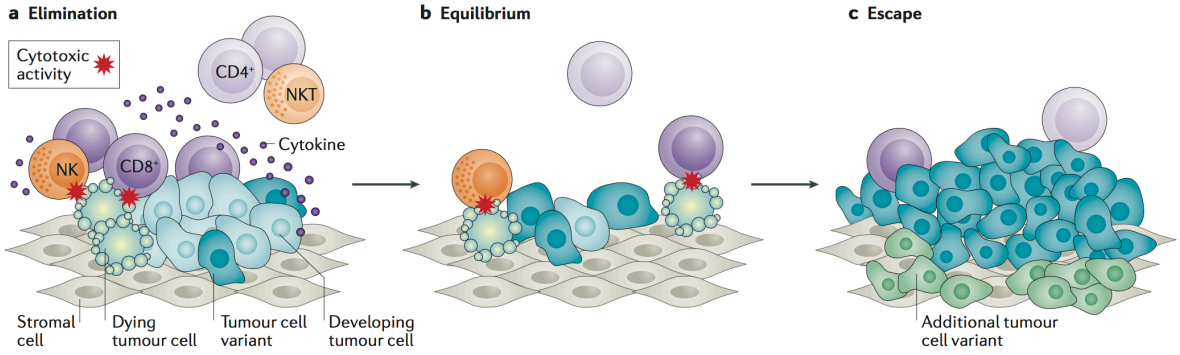

Figure I.1. The three phases of cancer immunoediting.

Cancer immunoediting describes the intricate relationship between a tumour and its infiltrating immune system, during which genetic instability and tumour heterogeneity increase and immune selection of tumour cell variants occurs. (**A**) The first phase encompasses the classical concept of cancer immunosurveillance. Tumour invasion generates inflammatory signals and recruitment of innate immune cells to the tumour site such as NK cells, γδ T cells, macrophages, and dendritic cells (DCs). Tumour antigens expressed by malignant cells are recognized by infiltrating NK or γδ T cells, which are in turn stimulated for the production of IFN-γ. This key soluble cytokine primarily induces the production of other mediators by the tumour cells themselves – such as the lympho-attractant CXC-chemokine ligand CXCL9, CXCL10, and CXCL11 –, and also directly triggers tumour cell death through the activation of angiostatic, anti-proliferative or apoptotic mechanisms (9). While chemokines produced during this escalating inflammatory process recruit more NK cells and macrophages to the tumour, apoptotic tumour cells and debris are engulfed by local DCs; these migrate to lymph nodes and activate tumour-specific CD4+ T helper cells expressing IFN-γ, that in turn stimulate the proliferation of tumour-specific cytotoxic CD8+ T cells. Tumour-infiltrating NK cells and macrophages destroy more tumour cells through the production of tumour necrosis factor-related apoptosis-inducing ligand (TRAIL) and perforin. In parallel, newly activated CD4+ and CD8+ T cells migrate to the tumour site, and cytotoxic CD8+ T cells eradicate the remaining antigen-bearing tumour cells whose immunogenicity has been enhanced by IFN-γ. Hence, in the elimination phase, both innate and adaptive immunity cooperatively participate to cancer rejection. (**B**) During the intermediate phase, the host immune system and surviving tumour cell variants enter into a dynamic equilibrium. Indeed, T infiltrating lymphocytes (TILs) and IFN-γ cooperate to exert a potent selection pressure that is sufficient to contain, but not fully eliminate, a bulk of genetically unstable and highly mutating tumour cells. Occurring over a long period of time, this Darwinian selection eventually leads to the extinguishment of originally escaping variants, and concomitant emergence of new variants bearing different mutations that confer them both a proliferative advantage and an increased resistance to immune aggression. (**C**) The ultimate phase corresponds to the expansion of surviving tumour variants that have acquired resistance to immunological detection or rejection through mutations or epigenetic changes. This leads to aggressive tumour development and clinically observable malignant disease.

Figure and legend adapted from Van der Burg et al., Nature Reviews, 2016.

The immune system therefore plays a dual role of (i) orchestrating tumour rejection, and (ii) sculpting the molecular profile and immunogenicity of developing tumours, by favouring tumour cell variants with low immunogenicity through a T cell-dependent immunoselection – which eliminates clones with strong rejection antigens (10) – and a T cell-independent immunoselection mediated by innate immune cells (11). Type I and type II IFN further play a key role in the coordination of tumour-immune interactions during immunoediting (12), and in particular, IFN-γ was recently described as an essential mediator of cytotoxic T cell-dependent tumour genome immunoediting (13).

Besides immunoselection, other immune-independent mechanisms, such as neutral evolution (14) – that is, the accumulation of passenger mutations without selective sweeps –, have been described to contribute to tumour heterogeneity in some cancers. A recent study showed using an *in vivo* model of microsatellite-instable (MSI) colorectal carcinoma (CRC), that immunoediting effects were weak and dominated by neutral accumulation of mutations (15) during CRC tumour development. Interestingly, the use of immune checkpoint inhibitors (ICI) in this model effectively potentiated immunoediting through increased immunoselective pressure, thereby inducing changes in the clonal and subclonal composition of the tumour, and changing the evolutionary dynamics from neutral to selective evolution. This underlines the plasticity of cancer immunoediting processes, and further suggests that modulation of the tumour-immune interactions via anti-cancer therapies having immunomodulatory properties can favour immunoediting, and potentially facilitate immune evasion through acquired resistance to therapy.

2. When oncology meets immunology: the cancer-immunity cycle

The cancer immunoediting approach describes a continuous evolution of the interactions between cancer and immunity which eventually favours tumour development despite the initiated immune rejection. How the immune system actually eliminates tumour cells during the elimination phase of cancer immunoediting is a well-known process, which has been recapitulated and nicely illustrated with the concept of cancer-immunity cycle (16).

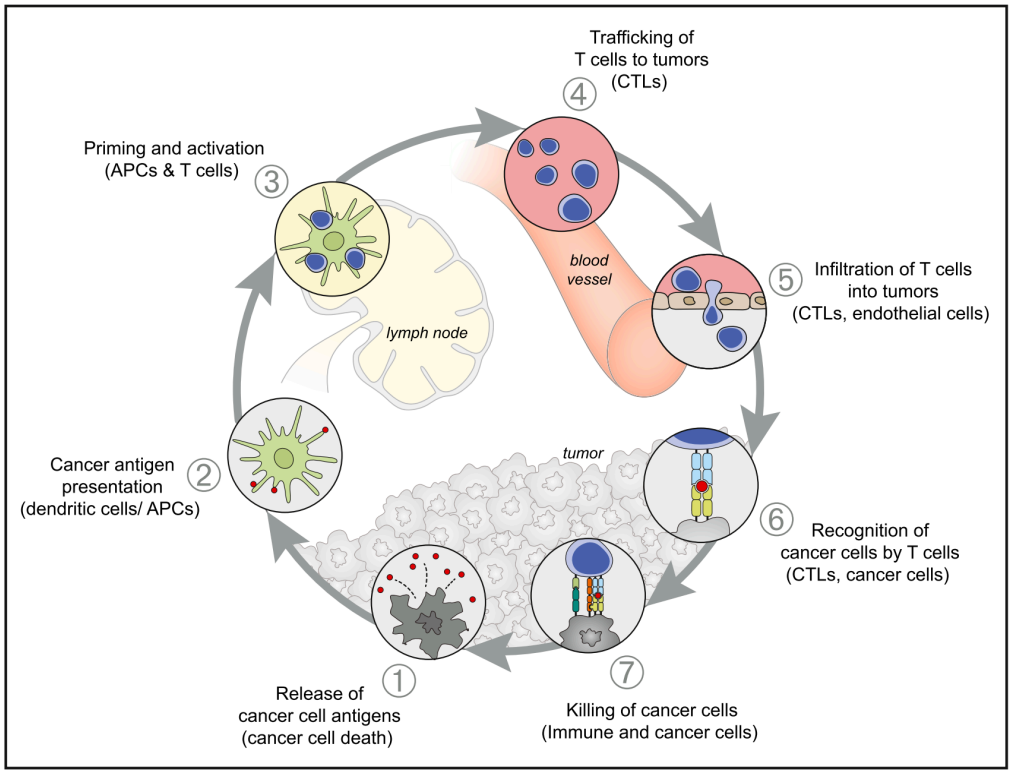

Figure I.2. The cancer-immunity cycle.

(**1**) Rapidly growing tumours display high levels of tumour cell death and apoptosis because of their elevated growth rate. This generates neo-antigens that are captured by DCs upon release in the TME. In addition, dying tumour cells produce immunogenic signals, such as pro-inflammatory cytokines, that stimulate DCs and further activate other innate immunity effectors such as macrophages. (**2**) Stimulated DCs migrate to the lymph nodes and efficiently process tumour neo-antigens to present them on major histocompatibility complex (MHC) Class II to T cells through cross-presentation. (**3**) These neo-antigens are detected as "non-self" because of their specificity to cancer cells or because the central tolerance has been incomplete towards them. This results in the priming and activation of CD4+ helper T cells and CD8+ effector T cells, and eventually leads to the expansion of tumour cell-specific T cell clones, that constitute the adaptive arm of anti-tumour immunity. At this stage, the nature of the immune response is already determined, especially since the critical balance between effector T cells and regulatory T cells (Treg) is defined. (**4**) CD8+ effector T cells traffic through blood circulation to the tumour site. (**5**) T cells infiltrate the tumour bed, and become the so-called tumour-infiltrating lymphocytes (TILs). (**6**) TILs specifically recognize and bind tumour cells through the interaction between their T cell receptor (TCR) and the cognate neo-antigen presented on MHC class I by tumour cells. (**7**) This results in killing of the cancer cells, a process which releases additional neo-antigens and eventually increases the breadth and depth of the immune response in subsequent revolutions of the cycle. Abbreviations: APCs, antigen presenting cells; CTLs, cytotoxic T lymphocytes.

Figure and legend adapted from Chen and Mellman, Immunity, 2013.

This concept describes a series of seven sequential events required for the establishment of an effective anti-tumour immunity (detailed in **Figure I.2**). Importantly, the cycle involves various immune cell types circulating from and towards distinct anatomic locations, and constitutes a self-propagating process. However, failure in any step of the cycle leads to evasion of the tumour from immunological control, and eventually cancer progression.

3. Mechanisms of immune escape in cancer

Immune evasion is a hallmark of cancer (17), which arises from genetic or epigenetic alterations of cancer cells (**Figure I.3**), and involves various mechanisms: (i) mechanisms that affect tumour immunogenicity; (ii) mechanisms that restrain anti-tumour activity of immune effectors; (iii) mechanisms that corrupt suppressive immune effectors; (iv) mechanisms that involve modulation of immune checkpoints.

a. Immune escape through reduction of tumour immunogenicity

Tumour immunogenicity is primarily determined by the antigenicity of tumour cells, which derives from their ability to generate and present tumour-associated antigens, recognized as "non-self" by the cells of the immune system, and responsible for the activation of anti-tumour immunity. Tumour-associated antigens originate from various sources, and are classically comprised by two distinct types of antigens (18,19) (**Figure I.4**):

- **Mutated tumour-specific antigens**, also known as neo-antigens, are exclusively expressed by tumour cells and directly originate from the large number of somatic mutations that are found in human tumours; most of the time, point mutations are responsible for the expression of mutant peptides that are not tolerated by the immune system, and eventually trigger anti-tumour immune responses. Such neo-antigens may be newly displayed at the surface of tumour cells because a mutation increases the binding affinity of a peptide to major histocompatibility complex (MHC) molecules. Alternatively, the mutation can alter the T cell receptor (TCR)-exposed area of a peptide that is also presented by MHC in its non-mutated form.

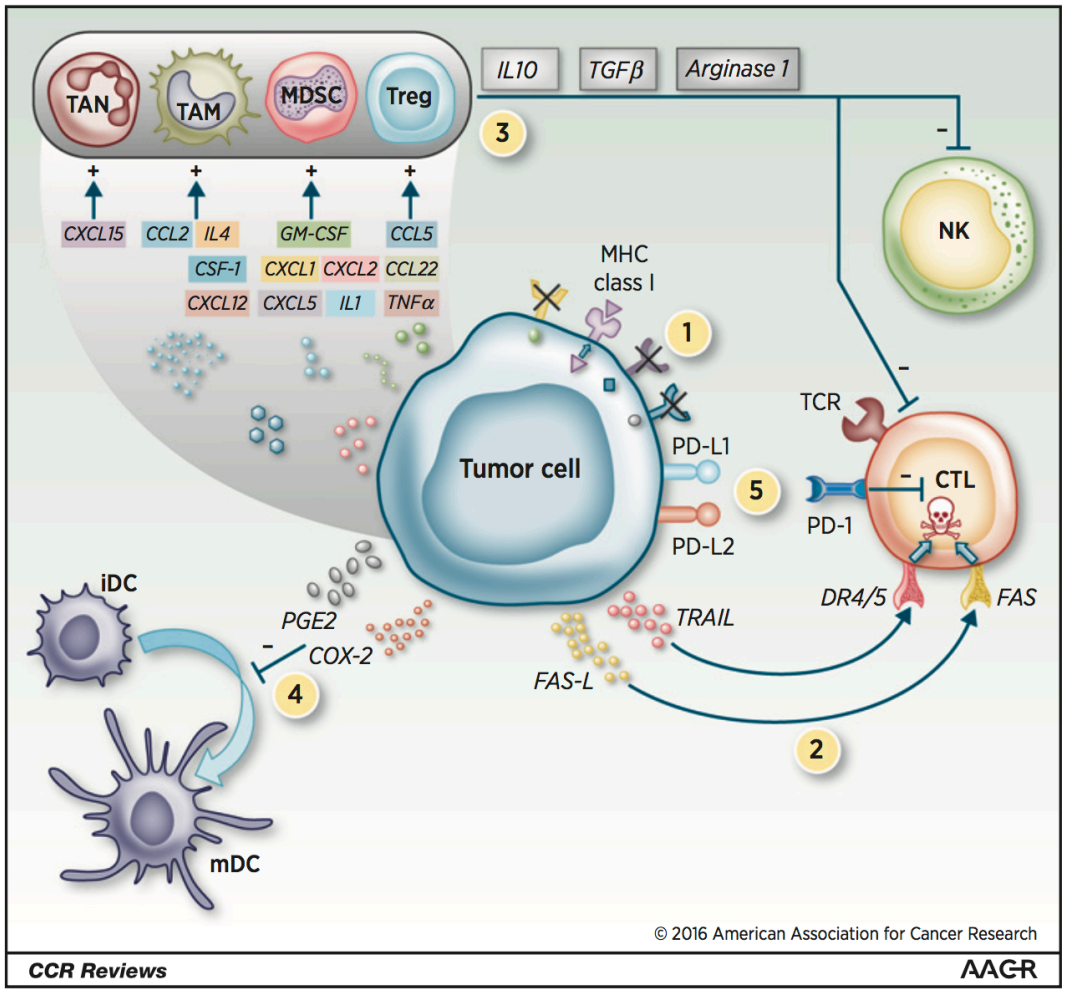

Figure I.3. Mechanisms of immune escape in the tumour microenvironment.
Several mechanisms, involving multiple immune components, contribute to tumour immune escape. (**1**) Immune recognition can be impaired following reduced expression of MHC class I molecules in malignant cells, resulting in decreased antigen presentation and consequently reduced detection by cytotoxic CD8+ T lymphocytes. (**2**) Cancer cells can activate immunosuppressive mechanisms by inducing apoptosis of immune cells through the expression of death signals (including FAS- and TRAIL-ligands). (**3**) Tumour cells release in the microenvironment a variety of immunomodulatory molecules that inhibit the immune system by inducing immunosuppressive cells. (**4**) This cytokine imbalance, combined with the secretion of TGF-β, cyclooxygenase-2 (COX-2), and prostaglandin E2 (PGE2), inhibits DCs differentiation and maturation, thereby affecting antigen presentation and recognition by T cells. (**5**) Disrupted expression of immune checkpoint ligands by cancer cells provides co-inhibitory signals to CD4+ and CD8+ T lymphocytes. Abbreviations: CCL, chemokine ligand; CXCL, chemokine (C-X-C motif) ligand; FAS-L, FAS-ligand; GM-CSF, granulocyte macrophage colony-stimulating factor; iDC, immature dentritic cell; IDO, indoleamine-2,3-deoxygenase; mDC, mature dentritic cell; MDSC, myeloid-derived suppressor cell; PD-1, programmed cell death 1; PD-L, programmed cell death ligand; TAN, tumour-associated neutrophil; TCR, T cell receptor; Treg, regulatory T cells.
Figure and legend adapted from Chabanon et. al, Clinical Cancer Research, 2016.

- **Non-mutated self-antigens**, by contrast, are not exclusively expressed by tumour cells, but also by other cells in a restricted set of cell types. These include (i) "cancer-testis antigens" whose expression is normally restricted to male germline cells in the testis: in tumour cells of many cancer types, these derive from the abnormal expression of cancer-germline genes due to transcriptional regulation defects or demethylation events; (ii) "tissue-differentiation antigens", which emanate from the expression of tissue-specific genes in tumour cells, but whose expression is shared with cells of the tissue they originated from; (iii) "protein-overexpression antigens", that derive from proteins that are overexpressed in tumours, but are also expressed in healthy tissues (e.g. HER2).

While most neo-antigens are very likely to trigger anti-tumour immunity because of their tumour-specificity, non-mutated self-antigens do not always activate immune responses.

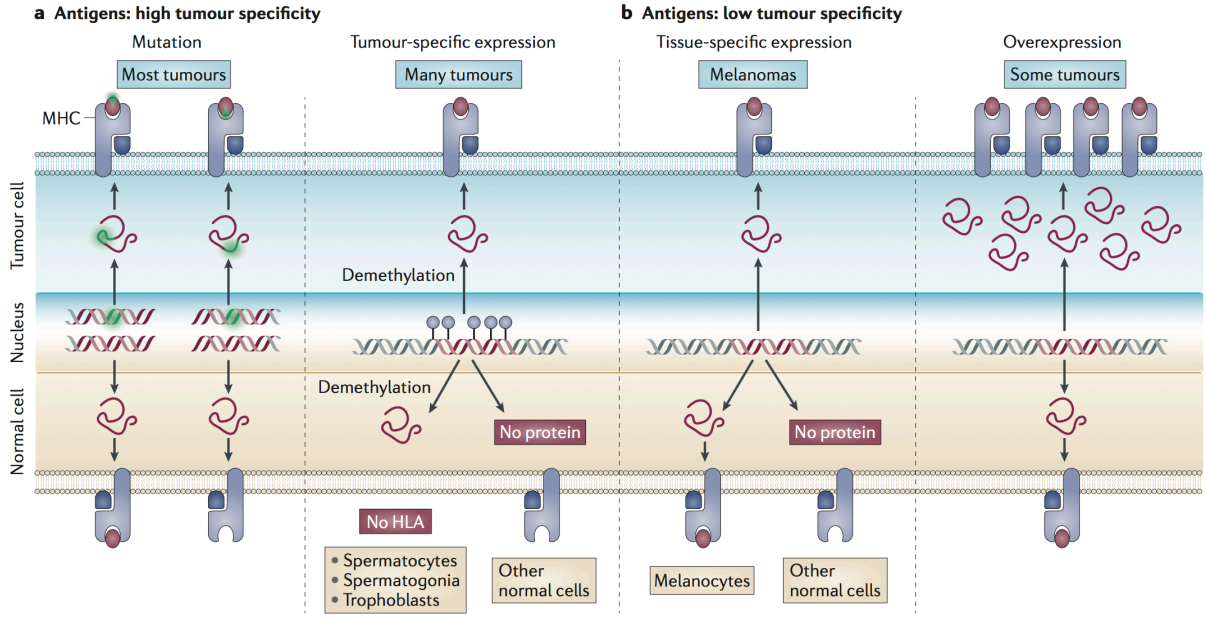

Figure I.4. Classes of human tumour antigens that are recognized by T lymphocytes. **A.** Tumour antigens with high tumour specificity usually originate from point mutations. Cancer-testis antigens can also be considered as tumour-specific because of their selective expression in tumours – germline cells, which lack HLA molecules, do not express them. **B.** Antigens with low tumour specificity arise from tissue-specific gene expression or overexpression of particular proteins. Only HLA class I molecules are represented, but the genetic processes shown can also lead to the presence on tumour cells of antigenic peptides that are presented by MHC class II molecules to CD4+ T cells.
Figure and legend adapted from Coulie et. al, Nature Reviews, 2014.

The process of neo-antigen presentation in tumour cells involves six successive steps, illustrated in **Figure I.5** (19). As this multistep process involves various independent but complementary components, a defect in any of them is sufficient to impede the whole antigen presentation machinery, reduce tumour immunogenicity and eventually favour immune escape. For example, TAP1 protein deficiency in tumour cells has been associated with evasion from immune surveillance and increased tumourigenesis (20). Similarly, immunoproteasome deficiency has been linked to reduced antigen presentation, immune escape and poorer outcome in non-small cell lung cancer (NSCLC) (21).

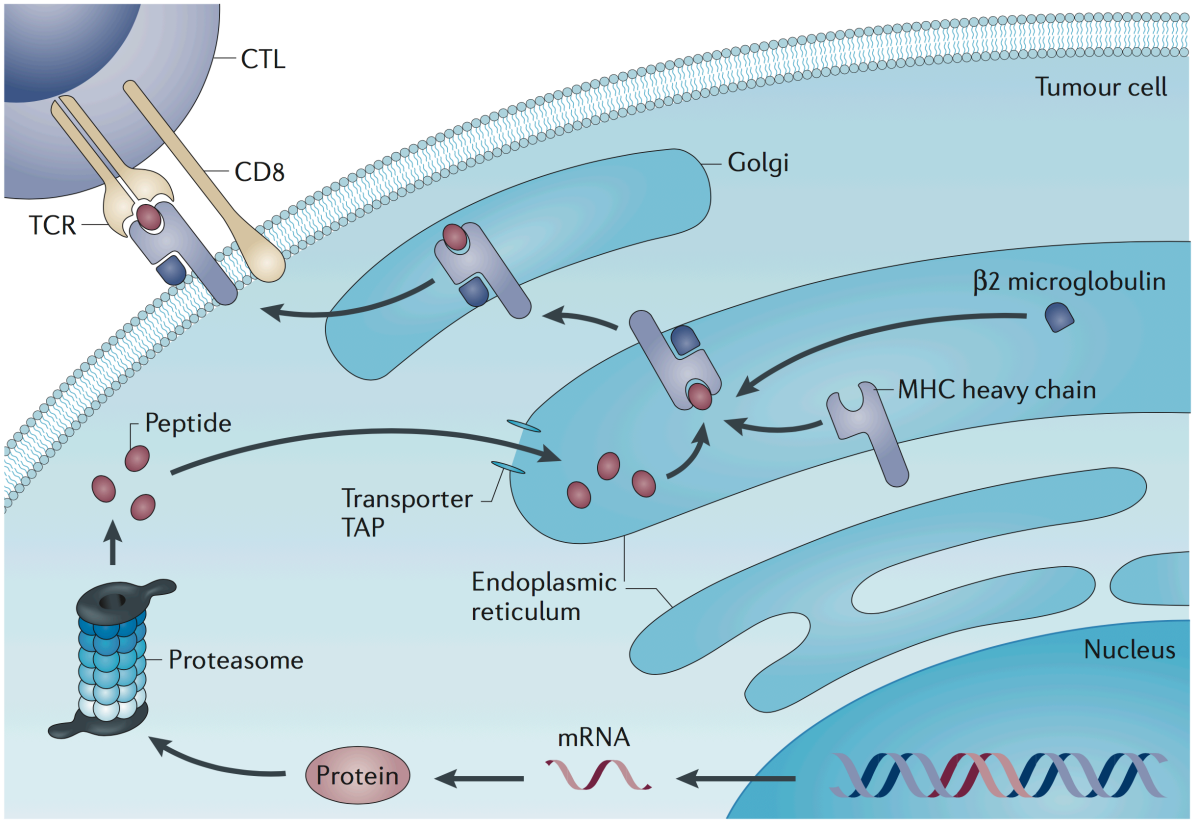

Figure I.5. Processing of tumour antigens that are recognized by CD8+ T cells.
(**1**) A somatic mutation occurs in the genome of the cancer cell; this leads to (**2**) the transcription of a mutated messenger RNA (mRNA) and subsequent translation into a mutated, presumably non-functional protein. (**3**) The mutated protein is processed through the proteasome and degraded into multiple peptides, that are subsequently (**4**) transported into the endoplasmic reticulum (ER) lumen by transporter associated with antigen processing (TAP) proteins, and (**5**) loaded on MHC Class I. MHC-bound peptides are then translocated to the cell-surface and eventually (**6**) presented to a TCR-matching T cell.
Figure and legend adapted from Coulie et. al, Nature Reviews, 2014.

But the most frequent and best documented cause of immune escape through reduced tumour immunogenicity is MHC Class I deficiency. Loss of the MHC Class I components human leukocyte antigens (HLA)-A, -B and -C has been reported in a number of cancers, including approximately 96% of breast carcinomas, 63% of melanomas, 87% of CRC, 70% of head and neck squamous cell carcinomas (HNSCC), 39% of pancreatic carcinomas, and 88% of papillary thyroid cancer (22). This can result from point mutations, gene deletions or loss-of-heterozygosity (LOH) on the locus of HLA genes in chromosome 6, or defects in their transcription (23). Alternatively, loss of beta-2 microglobulin (B2M), a necessary component of MHC Class I, has also been associated with lack of cell-surface expression of MHC Class I (24–27). In either case, reduced or impaired MHC Class I expression was shown to facilitate immune evasion. Recent studies have also found that genetic or epigenetic alterations of the key MHC Class I transactivator NLRC5 [NOD-like receptor family, caspase recruitment (CARD) domain containing 5], promote immune evasion through inhibition of MHC Class I genes transcription (28,29), thus reinforcing this line of evidence.

Interestingly, some genetic characteristics of human cancers also modulate tumour immunogenicity: for example, tumour aneuploidy, also known as tumour somatic copy number alterations, has recently been found to correlate with markers of immune evasion and reduced CD8+ T cells infiltration (30), potentially following weakened antigen presentation.

In totality, reduction of tumour immunogenicity is an important mechanism of immune evasion, that is clearly favoured by cancer immunoediting: as T cells primarily destroy tumour cells with high immunogenicity, they maintain a tumour bed predominantly made of clones with low immunogenicity that are more likely to evade immunosurveillance.

b. Immune escape through restriction of immune effectors activity

Tumour cells are known to develop a myriad of stratagems to prevent immune effectors activity.

First, they express death molecules such as Fas ligand (FAS-L) or TNF-related apoptosis-inducing ligand (TRAIL) that directly mediate apoptosis of tumour-infiltrating lymphocytes

(TILs) (**Figure I.3**, (31)). Recent studies have showed that FAS-L expression was also induced in cells of the TME following increased IFN-γ, leading to the suppression of TILs and associated tumour progression (32,33).

Second, tumour cells release immunosuppressive chemokines and express cell-surface receptors which negatively regulate the function of innate and adaptive immune cells. For example, expression of the "don't eat me signal" receptor CD47 has been shown to prevent macrophages activity through the engagement of the signal-regulatory protein alpha (SIRPα), which serves as an inhibitory receptor on these cells (34,35). Release of transforming growth factor beta (TGF-β) has recently been shown to promote immune evasion via T cell exclusion in CRC (36), but other immunosuppressive chemokines, such as vascular endothelial growth factor (VEGF), interleukin 10 (IL-10) or prostaglandin E2 (PGE2) are also known to inhibit the function, proliferation or differentiation of immune effectors (**Figure I.3**, (31,37)).

Third, tumour cells often exhibit activation of one or few oncogenic pathways, which are known to promote immune evasion via restriction of immune cells activity. A recent article nicely reviewed the various aspects of tumour-immune interactions that can be altered by specific oncogenic pathways, and described how these pathways indirectly mediate T cell exclusion from the TME and block recruitment of other immune cells to the tumour site (**Figure I.6**, (38)).

Finally, tumour cells often have functional defects in key immune pathways due to the deletion of immune genes in their genome. A recent study demonstrated that deletion of a number of genes in tumour necrosis factor (TNF) signalling, or IFN-γ signalling provides protection of tumour cells from CD8+ T cell-mediated killing. In addition, defects in the TNF signalling pathway also provide resistance to killing from primary NK cells (39). This demonstrates that the function of these pathways in tumour cells is key to allow immune-mediated tumour surveillance. Another example of tumour immune dysfunction leading to immune escape is the downregulation of IFN-alpha and -beta receptor subunit 1 (IFNAR1), frequently found in CRC, which is detrimental to TILs activity and survival, and associated with a poor prognosis in CRC patients (40).

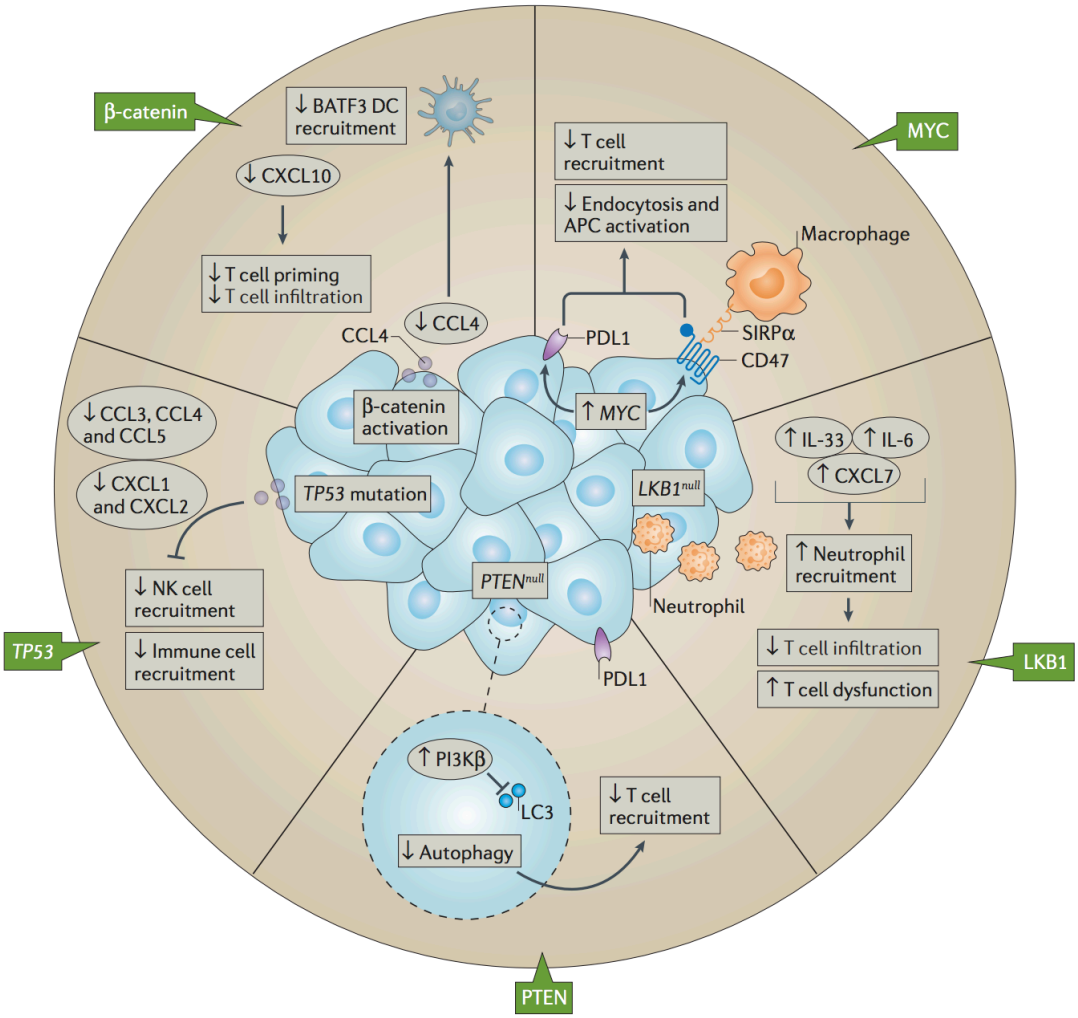

Figure I.6. Impact of oncogenic signalling on immune inhibitory pathways and cell populations.

MYC: Activation of MYC signalling enhances the expression of leukocyte surface antigen CD47 and PD-L1 on tumour cells, which interferes with antigen uptake by APCs via engagement with SIRPα and inhibits T cell function via PD-1 engagement. **LKB1**: Loss of LKB1 signalling results in the expression of interleukin-6 (IL-6), a chemokine that mediates recruitment of immunosuppressive neutrophils responsible for reduction of T cell infiltration and activity. **PTEN**: Loss of PTEN leads to impaired autophagy, which prevents T cell priming and mediates resistance to T cell-mediated apoptosis. ***TP53***: Oncogenic mutations of *TP53* in tumour cells lead to the defective production of key cytokines required for the recruitment of NK cells and T cells. **β-catenin**: Activated WNT/β-catenin signalling impairs CCL4 secretion by tumour cells and prevents recruitment of BATF3 DCs to the tumour site, which in turn blocks T cell priming and recruitment because of low CXCL10 production by BATF3 DCs. Abbreviations: BATF3, basic leucine zipper transcriptional factor ATF-like 3 lineage; PD-1, programmed cell death 1; PD-L1, programmed cell death ligand 1; SIRPα, signal regulator protein-α.

Figure and legend adapted from Spranger and Gajewski, Nature Reviews, 2018.

c. Immune escape through corruption of suppressive immune cells

In addition to inhibiting immune effectors activity, tumour cells also mobilize and recruit various suppressive immune cells through the production of specific cytokines, such as CXCL5 [C-X-C motif chemokine 5], granulocyte/macrophage colony-stimulating factor (GM-CSF), PGE2, or indoleamine 2,3-dioxygenase (IDO) (41). In particular, the following immunosuppressive cells can be stimulated by such signals (**Figure I.3**):

- **Tregs**, which are often hijacked by tumour cells to suppress CD8+ T cells and DCs expansion and function (42).
- **MDSC** (43), which inhibit the anti-tumour activity of T cells, DCs and NK cells, and also directly promote tumour growth, neo-vascularization and metastasis through the production of VEGF (44).
- **TAM/TAN**, which block CD8+ T cell-mediated immune responses and favour Tregs recruitment (41).

d. Immune escape through modulation of immune checkpoints

Immune checkpoint proteins are regulators of immune activation which provide co-stimulatory or -inhibitory signals to the cells of the immune system, thereby modulating the duration and amplitude of physiological immune responses in peripheral tissues. These regulatory functions are key for maintaining self-tolerance and mitigating tissue damage brought by inflammation. A plethora of immune checkpoint pathways are involved in the regulation of immune responses (**Figure I.7**, (45)). These involve the interaction between a receptor expressed on T cells and its ligand located at the surface of antigen-presenting cells (APCs) or tumour cells. Two major immune checkpoint pathways have so far been exploited in anti-cancer therapy: (i) the CD28/cytotoxic T lymphocyte-associated antigen 4 (CTLA4) axis, which activates T cells upon engagement of CD28 with CD80 and CD86, and conversely inhibits T cells when CTLA4 is engaged; and (ii) the programmed cell death 1 (PD-1) axis, which provides a strong inhibitory signal following binding of programmed cell death ligand 1 (PD-L1) or 2 (PD-L2) to the PD-1 receptor (46). Contrary to CTLA4, PD-1 is

thought to act predominantly in the TME, where PD-L1 is overexpressed by multiple cell types, including DCs, M2 macrophages, and cancer-associated fibroblasts (47).

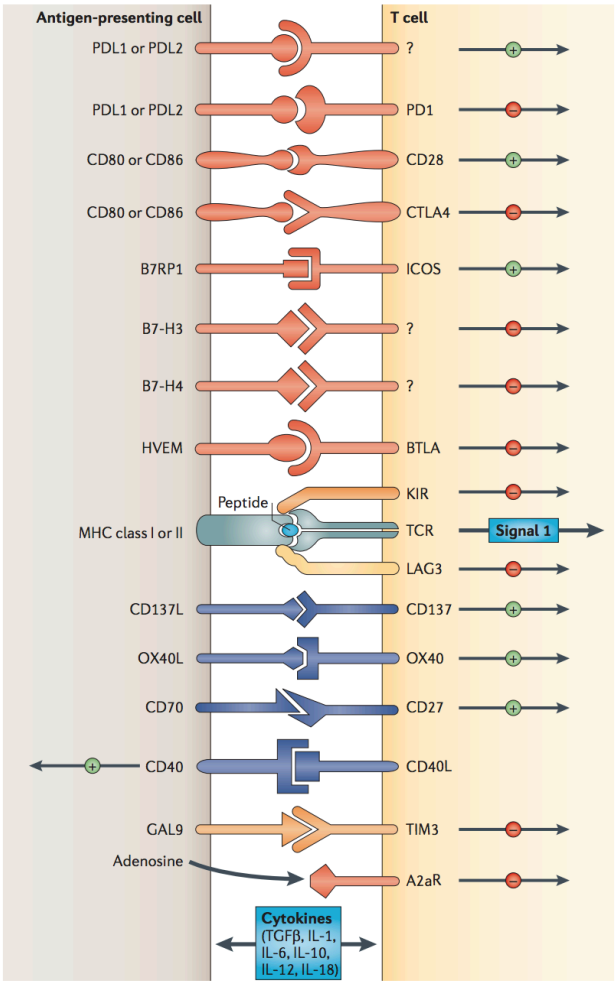

Figure I.7. Multiple co-stimulatory and co-inhibitory interactions regulate T cell responses.

Depicted are various ligand–receptor interactions between T cells and APCs that regulate the T cell response to antigen (mediated by peptide-MHC molecule complexes that are recognized by the TCR). These interactions can occur at the initiation of T cell responses in lymph nodes (where the major APCs are dendritic cells) or in peripheral tissues or tumours (where effector responses are regulated). In general, T cells do not respond to these ligand-receptor interactions unless they first recognize their cognate antigen through the TCR. Many of the ligands bind to multiple receptors, some of which deliver co-stimulatory signals and others deliver inhibitory signals. Abbreviations: A2aR, adenosine A2a receptor; B7RP1, B7-related protein 1; BTLA, B and T lymphocyte attenuator; GAL9, galectin 9; HVEM, herpesvirus entry mediator; ICOS, inducible T cell co-stimulator; IL, interleukin; KIR, killer cell immunoglobulin-like receptor; LAG3, lymphocyte activation gene 3; PD-1, programmed cell death protein 1; PD-L, programmed cell death ligand; TGF-β, transforming growth factor β; TIM-3, T cell membrane protein 3.

Figure and legend adapted from Pardoll, Nature Reviews, 2012.

Corruption of immune checkpoint pathways signalling by tumour cells constitutes a major mechanism of escape from immunosurveillance. In particular, activation of the PD-1/PD-L1 pathway through upregulation of tumour PD-L1 is a common and well-described feature of immune escape in many solid tumours (48), including NSCLC (49), melanoma (50) and CRC (51). Exploration of this phenomenon as a key process by which tumour cells resist elimination by T cells has revealed two central mechanisms for PD-L1 upregulation in cancer, referred to as intrinsic and adaptive immune resistance (see **Figure I.8**, (46)). Both mechanisms are not mutually exclusive and may co-exist in the same TME.

Of note, abnormal expression of other immune checkpoint molecules has also been associated with carcinogenesis and tumour immune evasion in some contexts (52–55), underlining the critical role of these pathways in modulating tumour-immune interactions.

Together, all the above-mentioned studies highlight that evasion from the immune system is a key characteristic of cancer cells. The improved understanding of the mechanisms by which tumours evade immunosurveillance has prompted the development of new therapeutic strategies capable of restoring an immunological control of cancer, collectively known as immunotherapy (IO). Among these strategies, immune checkpoint inhibitors (ICI) have emerged in the late 2000s as a novel generation of IO, and have brought unprecedented therapeutic benefits in many histologies, thereby revolutionizing cancer treatment. It is important to mention that this late revolution has been preceded by more than a century of research, exciting discoveries and remarkable therapeutic attempts in the field of immuno-oncology, that have finally allowed IO to enter the therapeutic arsenal against cancer.

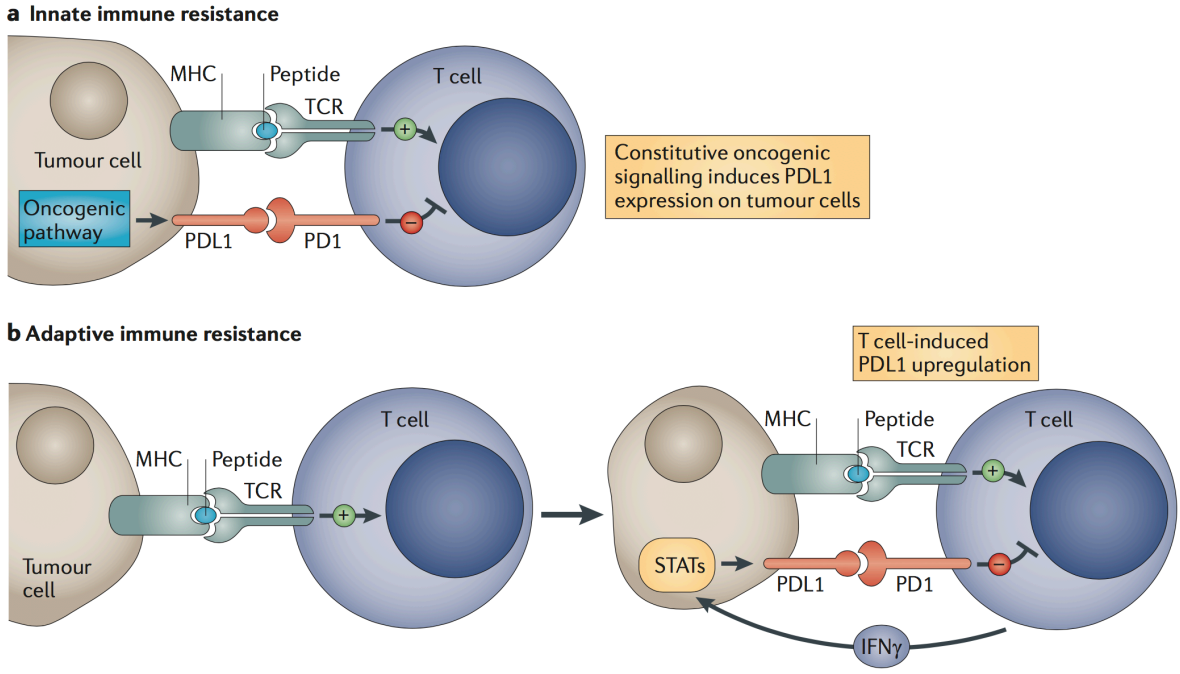

Figure I.8. Two general mechanisms of expression of immune-checkpoint ligands on tumour cells.

Intrinsic immune resistance: This refers to the upregulation of PD-L1 via various tumour cell-intrinsic mechanisms including genetic, epigenetic and transcriptional mechanisms. First, genetic upregulation of PD-L1 caused by frequent structural variations disrupting the 3′ region of the PD-L1 gene has been described as a common mechanism of immune escape in human cancers (56). Second, transcriptional upregulation of PD-L1, which often results from the activation of oncogenic signalling pathways, or specific transcription factors such as those of the JAK/STAT family, also results in resistance to immune attack. For example, activating mutations in *EGFR* have been associated with PD-L1 upregulation and establishment of an immunosuppressive microenvironment in lung cancer (49). Similarly, oncogenic RAS signalling was described to facilitate tumour immune evasion through the stabilization of PD-L1 mRNA (57). Other oncogenic pathways involved in PD-L1 upregulation include MYC (58), AKT-mTOR (59), MEK-ERK (60), and WNT/β-catenin signalling (61). Finally, epigenetic modulation through promoter/gene methylation changes or histone modifications (62) has also recently emerged as a mechanism of PD-L1 overexpression in cancer. Interestingly, the expression of microRNAs probably also contributes to the regulation of PD-L1 expression in tumour cells, as miR-200 and possibly other microRNAs decrease its expression, a mechanism of control that has been found disrupted in cancer, and associated with metastasis (63). **Adaptive immune resistance**: In this context, PD-L1 expression can be induced on tumour cells in response to specific cytokines, in particular IFN-γ. This was evidenced by significant correlations found between PD-L1 expression, levels of TILs and IFN-γ in the TME (64,65). PD-L1 upregulation represents in this case an adaptation mechanism consequent to the sensing of an inflammatory immune microenvironment comprising IFN-γ-producing activated Th1-type helper CD4+ T cells, activated CD8+ T cells and/or NK cells.

Figure and legend adapted from Pardoll, Nature Reviews, 2012.

B. Immunotherapy: a novel generation of cancer therapeutics

Since the early days of cancer treatment, most therapeutic strategies including radiotherapy, chemotherapy, targeted therapies as well as the first immune therapies have focused on a single target: the cancer cell. The advent of ICI brought a paradigm shift in cancer treatment, by demonstrating that targeting the immune system to eliminate cancer is a potent anti-tumour strategy.

1. The many faces of immunotherapy

According to the National Cancer Institute (NCI) Dictionary of Cancer Terms, IO is "a type of therapy that uses substances to stimulate or inhibit the immune system to help the body fight cancer, infection, and other diseases."

Behind this simple definition are hidden a myriad of approaches that have in common to use immune-related effectors to directly block tumour development or indirectly generate and enhance anti-tumour immune responses through modulation of the immune system characteristics. These approaches are classically categorized into two major classes of immune therapies: (i) passive IO which uses effectors of the immune system (antibodies, immunomodulatory molecules, immune cells) as direct anti-tumour agents and (ii) active IO which develops immune system-targeted strategies to activate anti-tumour immunity.

William B. Coley, a renowned surgeon at Memorial Hospital in New York was the first to introduce IO in the treatment of cancer in 1893. His invention was to create a filtered mixture of bacteria and bacterial lysates, composed of *Streptococcus pyogenes* and *Bacillus prodigiosus*, called the Coley's Toxin, in order to treat human tumours. Coley reported impressive results on inoperable tumours with his therapy, and enabled complete remission of some of his patients, especially those having bone and soft-tissue sarcomas (66). Supporting this initial discovery more than 60 years later, in 1959, the tuberculosis vaccine Bacillus Calmette-Guérin (BCG) was shown to have anti-tumour effects in mice (67), and later proved its efficacy in human, allowing the regression of melanoma tumours (68).

The discovery of IFNs in 1957 (69) and the demonstration of their intrinsic non-antiviral cytotoxic effects a few years later (70) initiated a series of studies evaluating the anti-tumour potential of these immunomodulatory molecules. This was first evidenced *in vivo* in 1969 when mice inoculated with tumour cells were cured with the use of various IFN preparations (71), and allowed realisation of the first rigorous adjuvant clinical trial of recombinant IFN for the treatment of cancer in 1984 (72). Later, another immunomodulatory molecule, interleukin-2 (IL-2), also showed interesting anti-tumour properties when used at high doses (73). In the meantime, other IO approaches were developed, including immune cells-based approaches: lymphokine-activated killer (LAK) cells, first described in 1982 (74), were later used as potent anti-tumour agents in combination with IL-2, enabling the regression of renal cell carcinoma (RCC) tumours and melanoma metastases in 1985 (75). In 1987, Steven A. Rosenberg and colleagues treat the first patient with autologous TILs cultured *in vitro* with IL 2, and demonstrate tumour regressions in 9 of 15 melanoma patients (76).

But one of the major discoveries and probably the most important for IO in the past century was the development of the first technology allowing the production of monoclonal antibodies (mAbs) *in vitro* by Georges Kohler and César Milstein: the hybridomas (77). This discovery paved the way to the development of a number of mAbs that brought significant improvement in the treatment of several aggressive diseases, including rituximab in B-cell lymphoma (78), trastuzumab in HER2-amplified breast cancer (79), bevacizumab initially used in metastatic RCC (80), and cetuximab in EGFR-mutated CRC (81) or HNSCC (82).

The second revolution in IO history was brought by the discovery of CTLA4 (83), PD-1 (84) and PD-L1 (85) as major regulators of physiological immune responses, which later enabled the development of mAbs targeting these immune checkpoints that transformed cancer treatment: the ICI.

a. Passive immunotherapy approaches

Passive IO encompasses therapeutic approaches that use effectors of the immune system to substitute an immune response against cancer. These approaches usually do not induce

memory immune responses *in vivo*, and thus rather generate short-term anti-tumour immunity.

(1) Monoclonal antibodies: mAbs exert cytotoxic effects against tumour cells through various mechanisms that include (i) direct trigger of apoptotic signals through binding to their target; (ii) complement-dependent cytotoxicity (CDC), that activates the complement cascade through stimulation of cell-surface Fc receptors and leads to the formation of the membrane attack complex (MAC) responsible for plasma membrane permeabilization of tumour cells; and (iii) antibody-dependent cellular cytotoxicity (ADCC), which mediates tumour cells phagocytosis through the recruitment of immune effectors whose membrane-surface antigens have been bound to the antibody. All mAbs do not have such properties, and the relative importance of each of these mechanisms in determining mAbs clinical response remains partly unclear. The first approved mAb, rituximab, was developed for the treatment of non-Hodgkin lymphoma and chronic lymphoid leukaemia (CLL): it was known to induce direct apoptosis of malignant B cells through binding to CD20, and to trigger both CDC and ADCC (86). Trastuzumab, a mAb targeting the oncogenic protein HER2 (amplified in a subset of breast cancer patients) induces tumour regression by interrupting HER2-mediated oncogenic signals and through CDC, but interestingly, its therapeutic effects were shown to depend on both innate and adaptive immunity (87). More recently, the development of bispecific mAbs has emerged as a novel therapeutic strategy: capable of recognizing two different targets, those mAbs can bind tumour cells concurrently with T cells and thus facilitate their interaction. For example, catumaxomab (bispecific mAb recognizing CD3 and EpCam) has shown efficacy in the treatment of malignant ascites due to epithelial cancers (88), and blinatumomab (bispecific mAb recognizing CD3 and CD19) was recently approved for the treatment of relapsed ALL, after having shown impressive efficacy in the setting of minimal residual disease (89,90).

(2) Non-antigen-specific cell-based approaches: LAK cells and cytokine-induced killer (CIK) cells have been early developed as substitutive IOs. Based on the principle of culturing immune cells *ex vivo* in order to re-inoculate them in patients to elicit non-MHC-dependent cytotoxicity of tumours cells, both approaches have shown safety and

activity *in vivo* (91,92). While the LAK cells approach has led to few successful clinical trials (93,94), CIK cells have been tested in multiple clinical settings including hepatocellular carcinoma (HCC), NSCLC or gastrointestinal tumours, and were shown to be successfully expanded from patients treated with chemotherapy (95).

(3) Antigen-specific cell-based approaches: Adoptive T cell transfer is a new area of transfusion medicine consisting in the inoculation of autologous T lymphocytes to mediate anti-tumour effects. The field has rapidly advanced from a promising form of IO in preclinical models to the recent approvals of chimeric antigen receptor (CAR) T cells to treat leukaemia and lymphoma (96). CAR T cells are T lymphocytes from patients that have been genetically engineered *in vitro* to make them express genes encoding receptors that recognize tumour-specific antigens (**Figure I.9**, (97)). The first demonstration of CAR T cells efficacy was brought in 2013 with a pilot study evaluating autologous T cells expressing a CD19-specific CD28/CD3ζ second-generation dual-signalling CAR in B cell ALL patients (98). The exceptional responses obtained in this study prompted the implementation of larger clinical trials which led to the approval of first-in-class CAR T cell IO for the treatment of relapsed B cell ALL in 2017 (99).

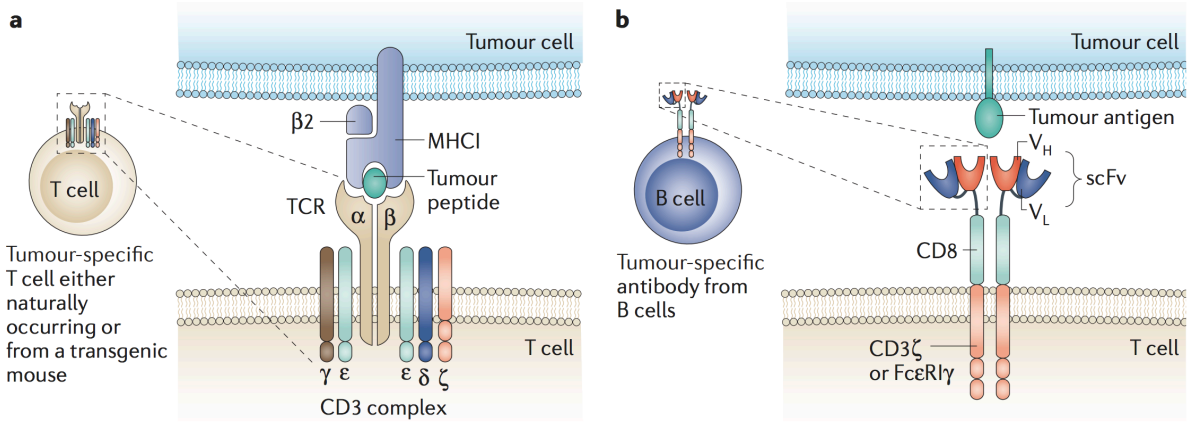

Figure I.9. Derivation of TCRs and CARs for the genetic modification of T cells. **A.** TCR genes, made up of α- and β-chains, can be derived from tumour-specific T cells, which can naturally occur in humans, or from the immunization of HLA-transgenic mice. Alternatively, they can be derived from screening bacteriophage libraries of antibodies. The α- and β-chains associate with the γ-, δ-, ε- and ζ-chains of the CD3 complex. When the TCR encounters a processed tumour antigen peptide fragment displayed on the MHC of the tumour cell, phosphorylation of immuno-receptor tyrosine-base activation motifs (ITAMs) occurs, leading to a cascade of intracellular signalling that results in the release of cytokines and cytotoxic compounds from T cells. **B.** CARs are composed of a scFv extracellular domain linked through hinge and transmembrane domains to a cytoplasmic

signalling region. Genes encoding the scFv are derived from a B cell that produces a tumour-specific antibody. An scFv is shown linked by a CD8 hinge to transmembrane cytoplasmic signalling regions derived from CD3ζ. CARs usually exist as a dimer, and they recognize tumour antigen directly (with no requirement for MHC) on the surface of a tumour cell. Abbreviations: CARs: chimeric antigen receptors; ITAMs: immuno-receptor tyrosine-base activation motifs; MHCI, MHC class I; scFv: single-chain antibody variable fragment.

Figure and legend reproduced from Kershaw et al., Nature Reviews, 2013.

b. Active immunotherapy approaches

Active IO encompasses therapeutic approaches that aim to stimulate the immune system in order to reactivate or enhance an established durable memory anti-tumour immune response.

(1) Vaccines (antigen-specific approaches): Cancer vaccines were developed as cells- or peptides-containing solutions capable of inducing positive, desirable T cell- and B cell-mediated immune responses against cancer. The first cancer vaccine, GVAX, was composed of tumour cells irradiated and genetically modified to express GM-CSF. Its use in preclinical studies showed induction of potent, specific, and long-lasting anti-tumour immune responses in multiple mouse tumour models (100). Peptide vaccines were subsequently developed: for example, the antigen glycoprotein 100 (gp100) vaccine showed efficacy in melanoma patients (101), and the MAGE-A3 cancer-testis antigen vaccine, which showed anti-tumour activity in mice (102), is currently evaluated in human in various metastatic diseases. Other vaccination approaches have focused on the design of cell-based vaccines, especially containing *ex vivo*-maturated DCs, loaded with tumour-specific antigens emanating from autologous tumour extracts. A number of clinical trials have evaluated the safety and efficacy of such approach; the induction of specific anti-tumour immune responses was reported in RCC but no clinical response could be observed in patients, mainly because *in vivo* administration of the vaccine was followed by a massive increase of Tregs (103). The only autologous cell-based vaccine currently licensed is Sipuleucel-T, an agent which demonstrated efficacy in metastatic castration-resistant prostate cancer (mCRPC) (104).

(2) Non-antigen-specific approaches: Several active IO approaches have focused on the activation of innate immunity through non-antigen specific methods. Anti-cancer therapy using BCG instillations is one of them: indicated for prophylaxis of primary recurrence in papillary urothelial bladder carcinoma (UBC) following transurethral resection, this approach showed benefit in approximately 50% of patients following activation of local innate immunity (105). Toll-like receptors (TLR) agonists, which exploit a similar principle by providing danger signals to immune cells, have demonstrated induction of marked local and systemic immune responses in combination with ionizing radiation (IR) in preclinical models of gastrointestinal cancers (106). However, results of clinical trials have so far been disappointing (107). Finally, the direct use of immunomodulatory agents such as cytokines has proved efficacy as active IO in immunogenic tumours such as RCC, although this has generated less enthusiasm because of more modest results compared to BCG therapy (108).

Last but not least, ICI are also a type of active IO which uses mAbs to target negative immune checkpoints in order to reactivate anti-tumour immunity against tumours. The next paragraph will focus on the mechanism of action and clinical impact of these therapies.

2. The advent of ICI: a revolution in cancer treatment

a. Principle and mechanism of action

To date, two major classes of ICI have been developed towards clinical use: anti-CTLA4 and anti-PD(L)1, which correspond respectively to the two central axes of immune checkpoints regulation in human.

While PD-1 predominantly regulates the activity of CD8+ T effector cells in the TME, CTLA4 is thought to primarily regulate CD4+ T helper cells and Tregs in the distant lymphoid tissue (**Figure I.10**, (109)). In order to be activated, T cells initially require priming via recognition of processed tumour antigens presented by APCs, through a unique TCR that binds an MHC molecule and tumour-derived peptide antigens at the surface of APCs. This priming

phase generally occurs in lymphoid tissue and involves CD4+ T cells which provide "help" for CD8+ T cells priming through release of adequate cytokines. Subsequently, both CD4+ and CD8+ T cells require stimulation via co-stimulatory checkpoint pathways such as CD28/CD80 and CD28/CD86 to proliferate, secrete inflammatory cytokines, acquire cytolytic properties and eventually migrate to sites of antigen display, that is, tumour sites. CTLA4 is the primary regulator of CD4+ and CD8+ T cell priming in lymphoid tissue, which makes it an attractive target for immune checkpoint blockade at this level. Anti-CTLA4 mAbs block the interaction between CTLA4 and its cognate receptors CD80/CD86 on APCs, thus allowing preferential binding of their co-activator CD28 and stimulation of T cell priming. Upon migration to the tumour site and within hours to days, activated T cells start expressing the co-inhibitory receptor PD-1. In the TME, activated T cells release a number of inflammatory cytokines, including IFN-γ which stimulates antigen display by tumour cells but also induces PD-L1 expression in macrophages and tumour cells. This results in the functional inhibition of PD-1-expressing CD8+ T cells in the TME and constitutes a central mechanism of tumour immune evasion. Blockade of PD-1 or PD-L1 by mAbs thus represents a potent strategy to restore the ability of T cells to eliminate antigen-expressing cancer cells. Additionally, blockade of CTLA4 in the TME may also be of critical interest to interrupt the immunosuppressive actions of Tregs, which have an enhanced ability to suppress CD8+ T cell cytolytic activity upon expression of CTLA4.

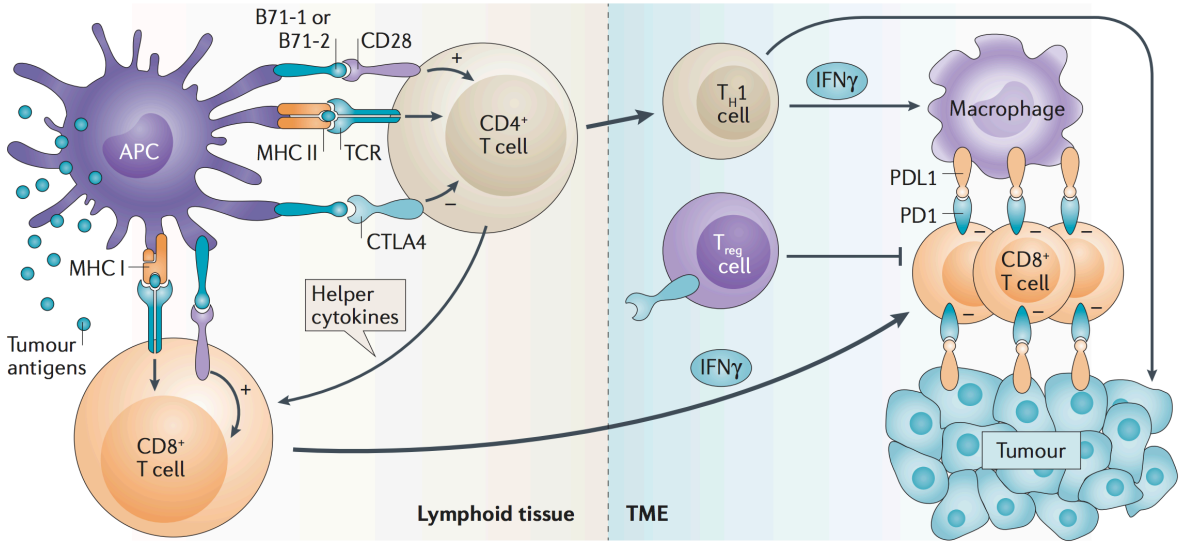

Figure I.10. Mechanistic nodes in immune checkpoint pathways.
The immune checkpoint pathways CTLA4/CD80/CD86 and PD-1/PD-L1 are major down-modulators of immune function that operate at different levels of the cancer-immunity cycle and hamper its progression by providing inhibitory signals to immune cells. Antibodies targeting CTLA-4, PD-1 and PD-L1 interrupt these immunosuppressive interactions and restore the ability of T cells to eliminate antigen-expressing cancer cells.
Figure and legend adapted from Topalian et al., Nature Reviews, 2016.

b. Clinical development and initial successes

The first ICI to enter clinical development was the anti-CTLA4 ipilimumab (Yervoy®, Bristol-Myers Squibb), which rapidly demonstrated efficacy and benefit in patients with metastatic melanoma (110,111), and subsequently obtained approval in this disease in 2011. Other anti-CTLA4 are being developped, such as tremelimumab (112).

In 2012, anti-PD-(L)1 therapies including the anti-PD-1 pembrolizumab (Keytruda®, Merck) and nivolumab (Opdivo®, Bristol-Myers Squibb), and the anti-PD-L1 atezolizumab (Tecentriq®, Genentech/Roche), durvalumab (Imfinzi®, Astra Zeneca/MedImmune), and avelumab (Bavencio®, Pfizer) entered clinical development. Very promising overall response rates (ORR) in relapsing/refractory malignant melanoma, RCC, and NSCLC (113), associated with prolonged progression-free survival (PFS) and overall survival (OS), led to their accelerated approval in 2014-2015, and the outstanding activity observed in several histologies awarded them "drugs of the year" in 2013 (114).

Further reflecting the significance of these advances, the Nobel Prize in Physiology and Medicine 2018 was awarded jointly to James P. Allison and Tasuku Honjo, for their discovery of cancer therapy by inhibition of immune checkpoints.

c. Current clinical impact of ICI

Following these initial successes, an exponential number of monotherapy or combination trials evaluating anti-CTLA4 and anti-PD-(L)1 have been launched in multiple cancer types, leading to a series of approval that have broadened the clinical spectrum of these therapies. In particular, anti-PD-1 have allowed significant therapeutic successes in many

solid tumours and hematologic malignancies, including melanoma (115,116), NSCLC (117,118), HNSCC (119), metastatic RCC (120), MSI-high CRC (121), metastatic UBC (122), gastric cancer (123), cervical cancer (124), Merkel cell carcinoma (125) and classical Hodgkin lymphoma (126). Responses obtained with anti-PD-(L)1 are often durable, lasting years sometimes even after treatment discontinuation, suggesting that some responding patients have a pre-existing T cell-mediated anti-tumour immunity that is mainly restrained by PD-1/PD-L1 activation.

The best example illustrating the impact of anti-PD-(L)1 therapy today is probably NSCLC, a histology in which the outcome has been drastically changed with the introduction of these agents (**Table I.1**). In this very deadly disease classically associated with poor prognosis, remarkable 5-year survival rates of 16% have recently been reported (127) with nivolumab, highlighting the ability of anti-PD-(L)1 to provide long-term tumour control. In addition, very impressive results of large phase III trials in NSCLC have reported unprecedented improvements in OS and PFS when using anti-PD-(L)1 in first-line therapy alone (128), or in combination with chemotherapy (129). In this latter trial (KeyNote189), Gandhi and colleagues observed a significantly higher 1-year OS rate in the pembrolizumab plus chemotherapy group (69.2%; 95% confidence interval (CI), 64.1 to 73.8) than in the placebo plus chemotherapy group (49.4%; 95% CI, 42.1 to 56.2), and also reported a significant prolongation of PFS (8.8 months; 95% CI, 7.6 to 9.2 vs 4.9 months; 95% CI, 4.7 to 5.5, respectively). More importantly, improvement in OS was obtained in all PD-L1 categories that were evaluated. These results led to the approval of pembrolizumab plus chemotherapy as the new standard treatment in first-line for metastatic NSCLC.

Table I.1. Clinical trials of anti-PD-(L)1 and their results in NSCLC.

For phase III trials, the control arm and its associated endpoint are italicized. Abbreviations: Atezo, atezolizumab; Ave, avelumab; Beva, bevacizumab; Carbo, carboplatin; Durva, durvalumab; Nivo, nivolumab; Pacli, paclitaxel; Pembro, pembrolizumab; PFS, progression-free survival; ORR, overall response rate; OS, overall survival.

Study/Agent	Setting	Experimental arms	Primary endpoint	Reference
KeyNote189 Phase III Pembrolizumab	Metastatic NSCLC First-line	Pembro + platinum-doublet *Platinum-doublet*	1-year OS rate 69.2% *1-year OS rate 49.4%*	(129)

Study/Agent	Setting	Experimental arms	Primary endpoint	Reference
KeyNote021 Phase II Pembrolizumab	Advanced NSCLC First-line	Pembro + platinum-doublet *Platinum-doublet*	ORR 55% *ORR 29%*	(130)
KeyNote024 Phase III Pembrolizumab	Metastatic NSCLC PD-L1 positive First-line	Pembro 200 mg /3 weeks *Platinum-doublet*	PFS 10.3 months *PFS 6.0 months*	(128)
KeyNote010 Phase II/III Pembrolizumab	Advanced NSCLC PD-L1 positive Second-line	Pembro 2 mg/kg /3 weeks Pembro 10 mg/kg /2 weeks *Docetaxel*	PFS 10.4 months PFS 12.7 months *PFS 8.5 months*	(131)
KeyNote001 Phase I Pembrolizumab	Advanced NSCLC PD-L1 positive	Pembro 2 mg/kg /3 weeks Pembro 10 mg/kg /2 weeks Pembro 10 mg/kg /3 weeks	ORR 28% ORR 40% ORR 41%	(132)
CheckMate227 Phase III Nivolumab	Advanced NSCLC Previously-treated	Nivo + Ipilimumab *Platinum-doublet*	1-year PFS rate 30.9% *1-year PFS rate 17%*	(133)
CA209-003 Phase I Nivolumab	Advanced NSCLC Previously-treated	Nivo 1 mg/kg /2 weeks Nivo 3 mg/kg /2 weeks Nivo 10 mg/kg /2 weeks	5-year OS rate 13% 5-year OS rate 26% 5-year OS rate 11%	(127)
CheckMate017 Phase III Nivolumab	Metastatic NSCLC Squamous Previously-treated	Nivo 3 mg/kg /2 weeks *Docetaxel*	OS 9.2 months *OS 6.0 months*	(134)
CheckMate057 Phase III Nivolumab	Metastatic NSCLC Non-squamous Previously-treated	Nivo 3 mg/kg /2 weeks *Docetaxel*	OS 12.2 months *OS 9.4 months*	(118)
IMPower150 Phase III Atezolizumab	Metastatic NSCLC Non-squamous First-line	Atezo + Beva + Carbo + Pacli *Beva + Carbo + Pacli*	PFS 8.3 months *PFS 6.8 months*	(135)
POPLAR Phase II Atezolizumab	NSCLC Previously-treated	Atezo 1200 mg /3 weeks *Docetaxel*	OS 12.6 months *OS 9.7 months*	(136)
OAK Phase II Atezolizumab	NSCLC Previously-treated	Atezo 1200 mg /3 weeks *Docetaxel*	OS 13.8 months *OS 9.6 months*	(137)
PACIFIC Phase III Durvalumab	Stage III NSCLC Previously-treated	Durva 10 mg/kg /2 weeks *Placebo*	2-year OS rate 66.3% *2-year OS rate 55.6%*	(138)
JAVELIN 200 Phase III Avelumab	Advanced NSCLC PD-L1 positive Previously-treated	Ave 10 mg/kg /2 weeks *Docetaxel*	OS 11.4 months *OS 10.3 months*	(139)

Combined anti-CTLA4 and anti-PD-(L)1 therapy has also demonstrated efficacy in some contexts, such as metastatic melanoma (140,141) and NSCLC (133), although results obtained in NSCLC were not reproduced in another study (142) (ARTIC trial, NCT02352948).

In a nutshell, the advent of ICI has recently revolutionized the prognosis of a number of diseases in oncology, and these therapies are today considered as key in the therapeutic armamentarium against cancer. However, still only a minority of patients receive benefit from ICI, which reinforces the need for better understanding the elements that determine response to ICI, and for developing novel rationale combinations.

C. Key determinants of response to ICI

Anti-cancer immunity is influenced by a variety of elements involving not only the tumour and its microenvironment, but also the host and its macroenvironment, which govern the amplitude and duration of immune responses against the tumour. In this context, response to ICI is determined by a complex combination of several tumour-related, microenvironment-related and host-related factors. Importantly, these parameters can undergo dynamic variations over time, which greatly complicates the identification of definite predictive biomarkers of response to ICI, needed for appropriate patient selection.

1. Tumour-related factors influencing response to ICI

a. Tumour mutational burden and neo-antigen burden

The anti-tumour immune response is predominantly governed by the recognition of cancer-associated antigens by T cells. The idea that T cells can recognize neo-epitopes generated by mutations or transcriptional aberrations in cancer originated from early studies that for the first time identified mutant neo-antigens in mice responsible for the priming of tumour-specific T cell responses associated with tumour regression (143,144).

Checkpoint blockade with anti-PD-1 or anti-CTLA4 in mice was later shown to reactivate T cell responses against sarcoma tumours through recognition of tumour-specific neo-antigens (145). Yet, the recognition by T cells of neo-antigens originating from point mutations is thought to be relatively inefficient, as only a very small fraction of non-synonymous single-nucleotide variants (nsSNV) eventually give rise to neo-epitopes bound to MHC class I molecules with high affinity (144).

In human, direct evidence of the recognition of tumour neo-antigens by T cells in the context of active anti-tumour immune responses has been provided by studies in which the specificity of TILs towards mutant neo-antigens was determined using complex bioinformatics pipelines, capable of identifying or rather predicting the neo-epitopes expressed in patient tumours based on their mutational profile (146,147).

These lines of evidence supported the concept that the large number of passenger mutations occurring in cancer provides a reservoir of neo-antigens that constitute the most probable targets of protective anti-cancer T cells. This further suggested that tumour mutational burden (TMB) and neo-antigen burden (TNB) are important drivers of anti-cancer immunity, which could thus represent key determinants of response to ICI.

Although we can anticipate that highly mutated tumours are more prone to form neo-antigens, the stochastic nature of neo-antigen generation calls for a functional validation, as all formed neo-antigens may not be immunologically relevant. In particular, if nsSNV obviously represent a mine of immunogenic mutations, frameshift, splice site mutations, and intragenic fusions are also liable to generate neo-epitopes when non-functional proteins are directed to the proteasome (148). The identification of relevant mutations likely to generate active anti-tumour T cell responses through immunogenic neo-antigens has been allowed by recent advances in next-generation sequencing (NGS) technologies, notably whole-exome sequencing (WES) and RNA-sequencing (RNA-seq). In particular, the estimation of TMB and predicted TNB (as defined by the number of neo-antigens potentially presented by MHC class I molecules) has been achieved through modelling the key steps of the antigen presentation machinery *in silico* using dedicated bioinformatics pipelines operated on genomic and transcriptomic data (**Figure I.11**).

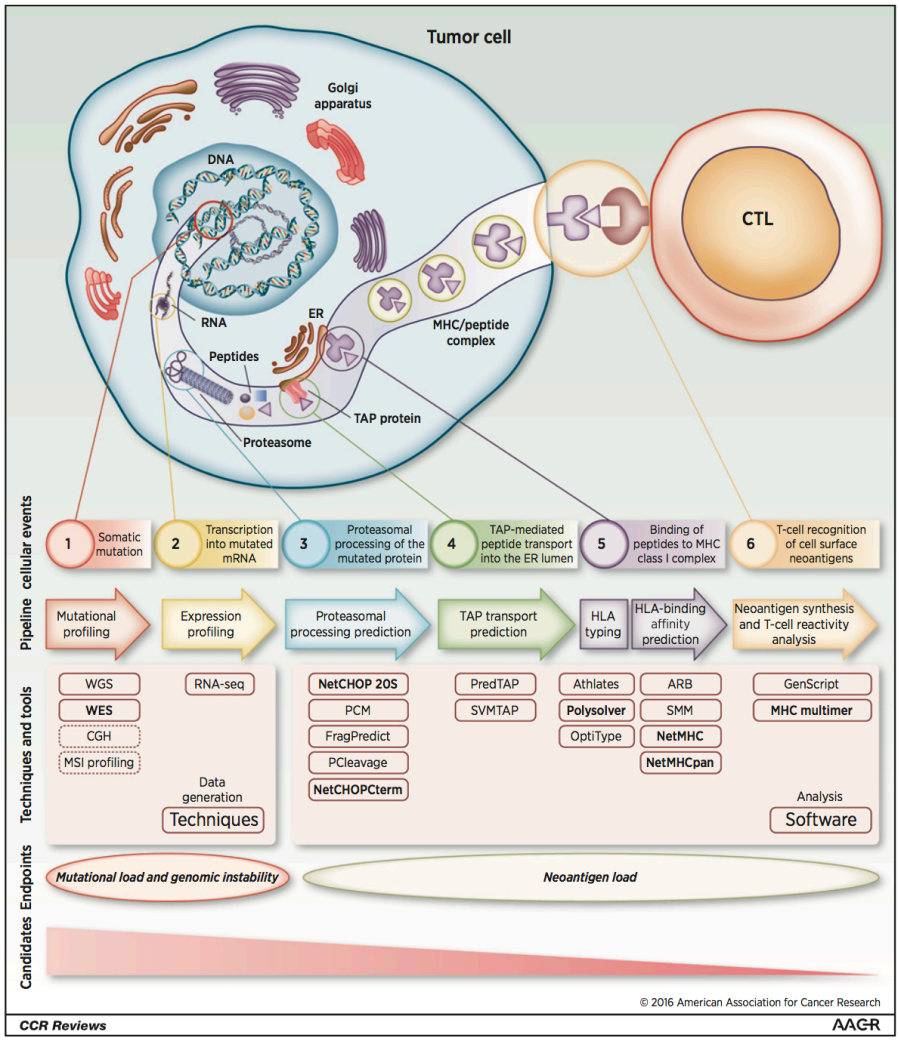

Figure I.11. Pipeline for the identification of immune-relevant neo-antigens.
The typical bioinformatics pipeline consists of six main steps: **(1)** TMB and specific mutations are identified using WES or WGS. Additional techniques such as CGH or MSI-profiling might be of interest to evaluate genomic instability but have not been validated yet in this indication. Moreover, WES is always a required starting point as the DNA sequence information is required for subsequent prediction tools. **(2)** Using RNA-seq, previously generated sequencing data are filtered for gene expression to restrict neo-antigen prediction to the set of translated mutations ("expressed nsSNV"). Subsequently, predictions for **(3)** proteasomal processing and **(4)** TAP-mediated transport of peptides are completed using dedicated algorithms. **(5)** To predict binding of peptides on MHC class I molecules, the previously selected peptides are implemented in a dedicated software that infers binding affinity to HLA molecules according to the HLA type of the patient. **(6)** Eventually, the predicted peptides may be synthesized to test for T-cell reactivity *in vitro* using the MHC multimer technology. Key technologies most often used in the literature are highlighted in bold. Techniques exclusively used to measure genomic instability are presented in dotted rectangles. Abbreviations: ARB, average relative binding; CGH, comparative genomic hybridization; SMM, stabilized matrix method; WGS, whole-genome sequencing.
Figure and legend reproduced from Chabanon et al., Clinical Cancer Research, 2016.

These modelling pipelines have been overall successful in correlating TMB with predicted TNB, and both parameters have therefore been evaluated as potential biomarkers of response to ICI in several studies. High TMB, defined as >100 nsSNV per exome, was first correlated with high predicted TNB and clinical benefit in melanoma patients treated with anti-CTLA4 therapy (149,150). Subsequently, Rizvi and colleagues showed association between high TMB (defined as >178 nsSNV per exome) and durable clinical benefit in two partially independent cohorts of NSCLC patients receiving pembrolizumab (151). Consistent with these studies, it was later suggested that tumours displaying >10 nsSNV/Mb may produce sufficient neo-antigens to generate anti-tumour immunogenicity, whereas tumours with <1 nsSNV/Mb may not (148).

The identification of immunogenic neo-antigens in ICI-responding patients has also been a focus of some clinical studies, which revealed the existence of a very high attrition rate resulting in few neo-epitopes eventually capable of producing anti-tumour immune responses. In the case report of a melanoma patient who experienced complete response after ipilimumab treatment, it was shown that, out of 1,657 nsSNVs, only 448 neo-epitopes were displayed in the whole tumour, and no more than two of them induced potent anti-tumour T cell responses (152). In a similar analysis, Rizvi and colleagues demonstrated that response to pembrolizumab in a NSCLC patient was associated with the T cell response against a single neo-antigen resulting from a nsSNV in *HERC1* (151). Likewise, Snyder and colleagues identified a set of consensus tetrapeptide sequences exclusively shared by melanoma patients exhibiting long-term clinical benefit from anti-CTLA4 (149), and being necessary and sufficient for the activation of an anti-tumour T cell response; these results were unfortunately not confirmed in two later studies (150,153).

If these examples illustrate well the complexity of predicting response to ICI using genomic data alone, it is besides important to note that the established correlation between TMB and response to ICI conceals a significant overlap in mutation range between responders and non-responders (149,150). Indeed, some patients still benefit from ICI despite very low TMB, and conversely, high TMB does not always correlate with response. This is best illustrated by Hodgkin lymphoma, which is highly sensitive to PD-1 blockade (154) despite carrying virtually no mutation. Further, TMB analysis only provides an "instantaneous and

descriptive" picture of the tumour genome as a bulk, but does not take into account the clonal and subclonal evolution of the tumour, which favours the generation of immunogenic neo-antigens, but also allows the emergence of less immunogenic new clones that escape immunosurveillance – thereby favouring primary or acquired resistance. High intra-tumour heterogeneity (ITH) has indeed been correlated with poorer outcome, whereas sensitivity to ICI was associated with low ITH and high clonal neo-antigens (155). This underlines the fact that several parameters remain to be optimized in order to improve the robustness of TMB in predicting response to ICI, including the threshold for defining "high" and "low" TMB, the optimal tumour purity and sequencing depth needed to produce reliable data, and the incorporation of alternative factors such as neo-antigen clonality.

b. Tumour PD-L1 expression is a biomarker of responses to anti-PD(L)1 therapy

Beyond the tumour "antigenome", other biomarkers are being developed to predict response to anti-PD-(L)1 therapies. The historical and best validated one is probably PD-L1 expression assessment by immunohistochemistry (IHC) on tumour and/or immune cells (113,118,132,156,157). Although trial results from initial studies in various cancer types revealed different predictive values for PD-L1 expression on tumour cells (158), the relevance of this biomarker has been validated later in meta-analytic studies. Khunger and colleagues demonstrated that PD-L1 expression was predictive of favourable response across all tumour types in a meta-analysis evaluating 41 distinct clinical trials involving a total of 6,664 patients (159), with the best predictive value being observed in NSCLC – where pembrolizumab is approved in first-line therapy based on PD-L1 positivity (128).

However, this biomarker currently lacks sensitivity, as some PD-L1-negative patients consistently experience clinical benefit (160,161), and specificity, as not all PD-L1-positive tumours benefit from anti-PD-(L)1 therapy (115,116). Furthermore, the parameters of PD-L1 staining and scoring are highly variable, notably the anti-PD-L1 antibody (clone SP142 and clone SP2063, Ventana; and clone 28-8 and clone 22C3, Dako), the platform (PD-L1 IHC pharDx, Dako; OptiView DAB IHC Detection Kit, Ventana), the positivity threshold (1%, 5%, 10%, or 50%), as well as the tumour material used for analysis (fresh versus archived material, and primary versus metastatic tumour (162)). Moreover, PD-L1 expression can be

constitutive or inducible (e.g. IFN-γ-mediated induction (163)). Together, these elements represent significant hurdles for reaching the reproducibility and analytic validity that is required for any companion biomarker development and clinical implementation.

2. Microenvironment-related factors influencing response to ICI

The TME is a critical determinant of cancer development and is also known to modulate response to therapy (164). In particular, T cell infiltration critically influences response to IO, which led to the distinction or "hot, T cell-inflamed" or "cold, non-T cell inflamed" tumours.

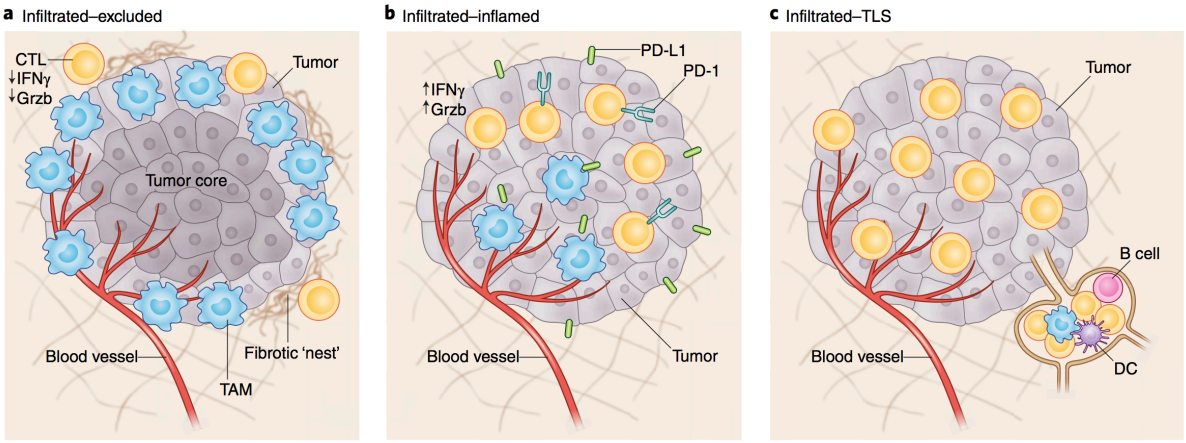

Figure I.12. General classes of TME.
A. Infiltrated-excluded TME are characterized by the exclusion of cytotoxic CD8+ T cells from the tumour bulk. These TME are broadly populated with immune cells but relatively void of CD8+ T cells, which are instead present along the tumour margins where they are usually found in contact with TAM – which prevent their infiltration – or trapped in fibrotic nest. Lack of expression of activation markers and T cell exclusion from the tumour mass are features associated with immunological ignorance, a state in which adaptive immunity is unable to recognize or respond to malignancy. Therefore, infiltrated-excluded TME are thought to be poorly immunogenic or "cold". **B. Infiltrated-inflamed TME**, by contrast, are defined by an abundance of activated CD8+ T cells expressing Granzyme B, IFN-γ and PD-1 in the tumour core, associated with the presence of PD-L1-expressing tumour and myeloid cells. These TME are considered as immunologically "hot". **C. Tertiary lymphoid structures (TLS)-infiltrated TME**, are a subset of infiltrated-inflamed TME, which are characterized by the presence of immune cells aggregates whose cellular composition is similar to that of lymph nodes. These structures, also known as TLS, comprise naïve and activated T cells, B cells, DCs and Tregs. Abbreviations: CTLs: cytotoxic T lymphocytes; TLS: tertiary lymphoid structure.
Figure and legend adapted from Binnewies et al., Nature Medicine, 2018.

Binnewies and colleagues recently described three classes of TME according to the nature of the immune infiltrate (**Figure I.12**, (165)): (i) infiltrated-excluded TME which are characterized by the exclusion of cytotoxic CD8+ T cells from the tumour bulk and are thus considered as poorly immunogenic or "cold"; (ii) infiltrated-inflamed TME, which define tumours that are highly populated with activated CD8+ T cells and considered as immunologically "hot"; and (iii) tertiary lymphoid structures (TLS)-infiltrated TME, which are characterized by the presence of immune cells aggregates whose cellular composition is similar to that of lymph nodes.

Exploration of the immune infiltrate characteristics in patients treated with ICI using low-resolution (e.g. IHC, bulk expression array) or high-resolution (NGS-based) techniques has allowed the identification of important biomarkers of response to these therapies.

a. T cell infiltration determines response to ICI

T cell infiltration, mostly represented by infiltrating CD8+ T cells, has for long been associated with improved survival in retrospective studies of multiple tumour types (166–168). The presence of TILs in tumours has also been linked to clinical benefit from active IO approaches such as the MAGE-A3 vaccine (169) and high-dose IL-2 (170).

More recently, the predictive value of TILs was evaluated in the context of treatment with ICI. A prospective phase II trial of ipilimumab in patients with metastatic melanoma demonstrated that the level of TILs at baseline was not predictive of clinical activity, whereas TILs density at the time of the second injection was clearly associated with response to therapy (171). Several studies assessed the immune infiltrate characteristics of melanoma or NSCLC patients treated with the anti-PD-1 pembrolizumab, and showed that tumour regression following therapeutic PD-1 blockade was dependent on the presence of pre-existing CD8+ T cells in the tumour mass (172); consistently, responders have enriched CD8+ T cell levels at the tumour-invasive margin as compared with non-responders (173). Importantly, Tumeh and colleagues also demonstrated that responders had a narrower T cell repertoire at baseline (i.e. high TCR clonality corresponding to a less diverse population) compared to patients with disease progression (172), suggesting that the pre-

existing TILs in responders originated from tumour-specific T cell clones. Moreover, comparison of the TCR clonality at baseline and in post-treatment biopsies in responders showed a 10-fold increase in clone expansion after anti-PD-1 therapy, supporting the involvement of a tumour-specific response to therapy in these patients. Interestingly, baseline TCR clonality did not highly correlate with TILs density, which supports the idea that some patients exhibiting low T cell infiltration could still benefit from anti-PD-1 therapy if their TIL population has restricted TCR clonality, specific to few tumour neo-antigens (174). Conversely, no correlation between TNB and T cell inflammation could be found in a recent study evaluating this association in melanoma (175). This does not exclude that within T-cell-inflamed tumours, clinical efficacy of ICI may be favoured in the context of tumours with high TNB, displaying a greater range of neo-antigens available for T cell recognition. Related observations support that higher degrees of cytolytic activity correlate with higher TMB/TNB in some solid tumours (176).

Considering the pivotal role of T cell infiltration in triggering response to PD-(L)1 blockade, other groups have investigated strategies to turn "cold" tumours into "hot" tumours. Tang and colleagues have developed an innovative approach to increase T cell infiltration in initially "cold" tumours, by creating an antibody-conjugated fusion protein that enables the delivery and overexpression of tumour necrosis factor superfamily member 14 (TNSFR14) in tumour cells, a factor responsible for the activation of lymphotoxin beta receptor signalling in immune cells (177). The use of this strategy stimulated the production of chemotactic chemokines, resulting in lymphocytic infiltration and improved response to PD-(L)1 blockade in previously T cell-excluded tumours.

b. Role of immune checkpoints expression in TILs

Expression of immune checkpoints in TILs has also been associated with sensitivity or resistance to ICI. For example, low expression of PD-1 in TILs was shown to predict better outcome and enhanced response to nivolumab in NSCLC patients (178). By contrast, upregulation of the checkpoint molecules TIM-3 and LAG3 has been proposed as a mechanism of adaptive resistance to anti-PD-1 treatment (179).

c. Immune gene signatures associated with response to ICI

Recently, a lot of efforts have been made towards the improvement of immune infiltrate estimation in tumour tissue. Techniques such as CIBERSORT (180) and XCell (181) can now easily and accurately assess the abundance of immune infiltrates into the tumour by using gene expression data from bulk tissues. Other approaches, such as "immunomics" (182), use a combination of IHC and bulk tissue gene expression profiling to stratify patients according to immune-related criteria and subsequently predict disease outcome.

Assessment of the nature and activation status of immune cells populations within the TME has also been achieved through gene expression profiling using NGS or Nanostring™ technologies, and consistently, several immune gene signatures have been developed to predict response to ICI in various tumour types (183,184). The best validated signature is probably the eight-gene "T effector/IFN-γ" signature, which was explored in the phase II POPLAR trial, and predicted OS (but not PFS or ORR) benefit in atezolizumab-treated NSCLC patients. If the robustness of predictive signatures associated with IFN-γ expression is supported by the already described link between tumour PD-L1 expression and response to PD-(L)1 blockers, it is also corroborated by data showing that high tumour MHC class II expression is associated with improved clinical response, longer OS and PFS in melanoma patients treated with anti-PD-(L)1 therapies (185).

Other signatures, such as the "innate anti-PD-1 resistance" (IPRES) signature, have been successfully established to predict resistance to ICI (153). Of note, although this signature was not predictive of resistance to anti-CTLA4 therapy, it was found at variable frequencies across most human cancers, suggesting that some mechanisms of ICI resistance might be shared between histologies.

d. Immuno-monitoring approaches and peripheral blood biomarkers

Immuno-monitoring strategies, that involve the repeated assessment of circulating immune biomarkers, have also been proposed to assist the prediction of response to ICI (31). These dynamic biomarkers, which include notably cell surface proteins, cytokines and inflammatory mediators (**Table I.2**), can be monitored at several time points on trial using

a simple blood test. Although associations of some parameters with survival and clinical benefit from checkpoint blockade have been noted (174,186), these circulating biomarkers have not been robust enough so far to solely predict response to ICI (187), and none have been yet validated as predictive biomarkers in prospective studies.

Assessment of TCR gene sequences in peripheral T cell populations has also been suggested as a predictive biomarker for immune checkpoint blockade therapy. Postow and colleagues (188) demonstrated that the baseline TCR repertoire diversity, assessed using the ImmunTraCkeR tool (189), was correlated to patient PFS (but not OS) upon ipilimumab treatment. Other studies have evaluated the TCR repertoire diversity in patients by testing their PBMCs for T cell recognition of specific tumour neo-antigens, previously predicted from tumour WES and synthesized *in vitro* (151). These analyses revealed autologous T cell responses against cancer neo-antigens in the context of a clinical response to anti-PD-1 therapy, confirming the relevance of this kind of approaches.

Table I.2. Immune-related biomarkers for anti-PD-(L)1 therapy.

Biomarker Family	Biomarker	Reference
Cell-surface interaction molecules (evaluated on peripheral immune cells)	**MHC Class I/II** HLA-DR+ on CD8+ T cells	(187,190)
	T-Cell Repertoire Diversity	(188)
	Immune-Checkpoints Expression PD-1, CTLA4, TIM-3, PD-L1, PD-L2	(191)
Cytokines/Chemokines	**IFN-γ**	(187,190)
	IL-6	(187,190)
	IL-18	(187,190)
	CXCL9	(192)
	CXCL10	(192)
	CXCL11 (ITAC)	(187,190)
	CXCL13	(193)
	CCL2	(193)
	CCL5	(193)
Other immunomodulatory molecules	**Soluble CD25**	(194)

Biomarker Family	Biomarker	Reference
Peripheral immune cells	**"Anti-tumour T cells"** CD3+/CD69+, CD3+/Ki67+, CD8+	(187,190)
	Th1-related T cells CD3+/EOMES+, IFN-γ+, PD-L1+, IDO1+	(193)
Tumour burden	**Serum LDH**	(195)

3. Host-related factors influencing response to ICI

Beyond factors associated with the tumour and its microenvironment, the general immunological status of the host is also an important determinant of response to ICI. Defined by extrinsic factors that influence physiological immune responses such as host genetics, the gut microbiota or the presence of infection, this immunological status varies from patient to patient. Recent studies have explored the potential of these factors to influence response to immune checkpoint blockade.

In particular, for the past five years, there has been a growing interest in the gastrointestinal microbiome and its role in the modulation of anti-tumour immune responses. This interest was brought by several preclinical studies showing that the gut microbiota may promote anti-tumour immunity by stimulating innate and adaptive immune effectors (196,197), and that therapeutic responses to chemotherapy may be improved through this stimulation (198,199). Very recently, several studies have analysed the gut microbiome of patients treated with anti-PD-1 (200–202), and reported significant differences between responders and non-responders in terms of the diversity and composition of their microbiome. Indeed, "good" bacterial species such as *Bifidobacterium longum*, *Collinsella aerofaciens*, and *Enterococcus faecium* were found enriched in responding patients, while non-responders had an imbalance in gut flora composition, which correlated with impaired immune cells activity (200,202). In line with these observations, Matson *et al.* and Routy *et al.* described improved tumour control, enhanced T cell responses, and greater efficacy of anti-PD-(L)1 therapy in germ-free or antibiotic-treated mice reconstituted with faecal material from responding (but not non-responding) patients (201,202). These data reveal an unexpected impact of the commensal microbiome on anti-tumour immunity and response to ICI.

4. Cancer-immune phenotypes and the cancer–immune set point

Data from clinical studies have revealed the existence of three cancer-immune phenotypes that reflect the previously described classes of TME, but are also associated with response to anti-PD-(L)1 ((203), **Figure I.13**):

(1) The immune-inflamed phenotype corresponds to tumours that display a substantial immune infiltrate, presumably emanating from a pre-existing anti-tumour immune response that was arrested. This phenotype is mostly associated with patients exhibiting clinical response to anti-PD-(L)1.

(2) The immune-excluded phenotype corresponds to tumours that are not infiltrated by immune cells, because of the retention of these cells in the stroma. Treatment with anti-PD-(L)1 is usually ineffective and clinical responses are rarely observed in patients with this phenotype.

(3) The immune-desert phenotype corresponds to tumours that are totally devoid of T cells either in their core or in the stroma, which reflects the absence of pre-existing anti-tumour immunity. Patients carrying this phenotype are mostly refractory to anti-PD-(L)1 therapy.

Although most patients can be classified into one of the three basic cancer-immune phenotypes, the inherent immunological status of an individual is much more complex, as a multitude of factors contribute to determining anti-tumour immunity – and response to ICI. In the current personalized medicine era, the above-presented data could soon translate into the definition of a unique "immunological profile" per patient, which would recapitulate the contribution of tumour-, microenvironment- and host-related factors at a given time to define its likelihood of response to therapy. This kind of approach has been proposed by Chen and Mellman in the form of a "cancer–immune set point", that would use complex modelling systems to integrate multiple variables and define the threshold that must be overcome to generate effective anti-cancer immunity (203).

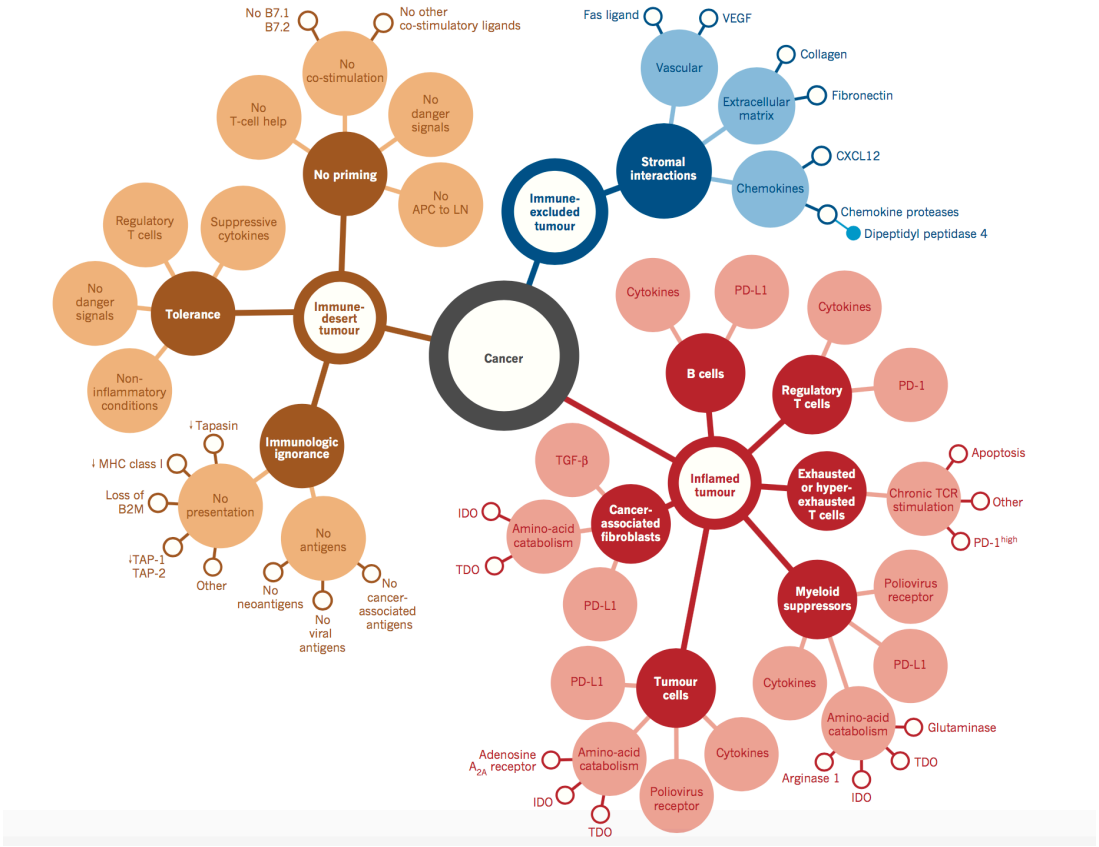

Figure I.13. Cancer-immune phenotypes.
(1) The immune-inflamed phenotype (red) corresponds to tumours that display a substantial immune infiltrate composed of both CD4+ and CD8+ T cells, often accompanied by myeloid cells and monocytes, in close proximity with tumour cells. Immune-inflamed tumours are also characterized by the sustained expression of pro-inflammatory and effector cytokines, as well as immune checkpoints such as PD L1. This supposes the presence of a pre-existing anti-tumour immune response that was arrested – probably through immunosuppressive mechanisms operating in the tumour core. The immune-inflamed phenotype is mostly associated with patients exhibiting clinical response to anti-PD-(L)1. **(2) The immune-excluded phenotype** (blue) is also characterized by an abundance of immune cells, but these do not penetrate the tumour core and are instead retained in the stroma of the tumour. This suggests that a pre-existing anti-tumour immune response might have been present but was rendered ineffective by the retention of immune cells in the stroma, or a block in tumour infiltration. Treatment with anti-PD-(L)1 can lead to the activation and proliferation of stroma-associated T cells, but as these cannot penetrate the tumour core, clinical responses are rarely observed in patients with this phenotype. **(3) The immune-desert phenotype** (brown) defines tumours totally devoid of T cells either in their core or in the stroma. Despite the possible presence of myeloid cells, these tumours have a non-inflamed TME with few or no CD8+ T cells. This reflects the absence of pre-existing anti-tumour immunity, and highlights that the generation of tumour-specific T cells is the rate-limiting step. Consequently, patients carrying this phenotype are mostly refractory to anti-PD-(L)1 therapy. Abbreviations: LN, lymph node; TDO, tryptophan 2,3-dioxygenase.
Figure and legend adapted from Chen and Mellman, Nature, 2017.

D. The DNA damage response determines anti-cancer immunity

We have previously described that the tumour mutational landscape plays a major role in determining anti-tumour immune responses, primarily through its direct impact on tumour antigenicity. The mutational landscape is a "record" of the tumour history which carries the traces of a number of endogenous and exogenous mutational processes that have been operating throughout disease development. Understanding how these "genomic scars" were formed brings important information about the factors that determine tumour genomic instability and might consequently influence response to therapy.

1. Mutational processes control genomic instability in cancer

Genomic instability is known as an important hallmark of cancer (17), that drives the first steps of carcinogenesis and fuels tumour evolution throughout disease development. It is determined by the effects of all mutational processes to which a tumour may be exposed; these include exogenous processes essentially represented by DNA damage (following chronic exposure to carcinogens for example) and endogenous processes which are the results of tumour-specific DNA repair or DNA damage response (DDR) defects.

Although genomic instability is a common denominator of cancer, the prevalence of somatic mutations is highly variable across tumour types ((204), **Figure I.14**); this reflects the diversity and irregular frequency of mutational processes that operate in cancer. Each of these processes – which not only influence the level of somatic mutations but also the type of mutations generated – is distinctively associated with a characteristic imprint, known as mutational signature, that is determined by the type of DNA damage and DNA repair processes involved in the formation of genetic alterations. The analysis of large genomic datasets has enabled the identification of 21 distinct mutational signatures (204), that are characterized by a substantial diversity in terms of mutation type, frequency of apparition, and association with known mutational processes. For example, exogenous DNA damage following exposure to UV light is known to promote the formation of pyrimidine dimers, which eventually create C>T transversions in the genome. The preponderance of these

mutations constitutes a characteristic feature of cutaneous cancers that are associated with UV exposure such as malignant melanoma (205). Similarly, the prevalence of C>A transitions, that result from the mutagenic effects of polycyclic hydrocarbons of tobacco smoke, are characteristically found in lung carcinomas (206). Of note, these two DNA damage-related mutational signatures are usually associated with high TMB, and in lung cancer, the smoking molecular signature correlates with response to anti-PD-1 (151).

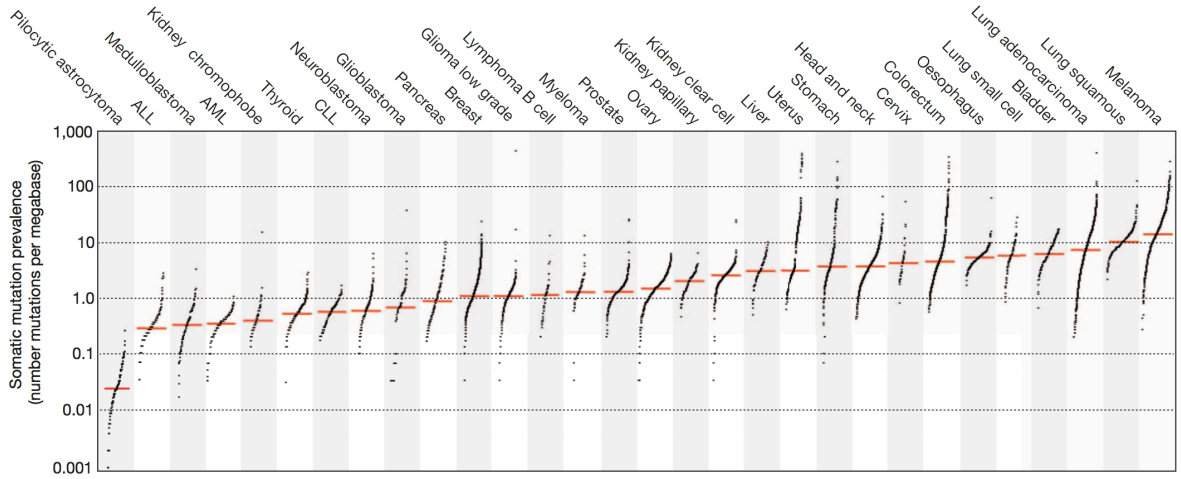

Figure I.14. The prevalence of somatic mutations across human cancer types.

Every dot represents a sample whereas the red horizontal lines are the median numbers of mutations in the respective cancer types. The vertical axis (log-scaled) shows the number of mutations per Mb whereas the different cancer types are ordered on the horizontal axis based on their median numbers of somatic mutations. Abbreviations: ALL, acute lymphoblastic leukaemia; AML, acute myeloid leukaemia; CLL, chronic lymphocytic leukaemia.

Figure and legend reproduced from Alexandrov et al., Nature, 2017.

If some histologies display a higher prevalence of one or two particular mutational signatures, it is very likely that, in patients, the mutational landscape obtained after sequencing is a composite of multiple mutational signatures – although one of them might be prominent among the others. Indeed, an individual tumour comprises subclonal populations that might have been variably exposed to several mutational processes across tumour development, which eventually promotes the complexity of the final landscape of somatic mutations in a cancer genome (207). Importantly, if some of these signatures are

traces of historical mutational processes that are no longer actively promoting cancer development, others indicate exposure to ongoing mutational processes, and may serve as prognostic or predictive biomarkers of therapeutic sensitivity, or even as targets for disease control.

In some tumour types, DDR defects represent the predominant form of operative mutational processes, and are therefore important determinants of the tumour mutational landscape. In these histologies, DDR defects also represent critical biomarkers of response to therapy, including chemotherapy, targeted therapies and IO.

2. The extent of DNA repair alterations in cancer

DDR dysfunction is closely associated with cancer and is thought to participate to neoplastic development at an early stage (208). Markers of Double-Strand Breaks (DSBs), such as nuclear γH2AX foci (a histone phosphorylation event occurring on the DNA surrounding DSB) have been found at elevated levels in some precancerous lesions, as a result of replication stress induced by oncogenes activation (209,210). Subsequent transformation of those precancerous lesions into mature tumours is thought to occur via inactivation of key DDR and cell-cycle checkpoint proteins such as ataxia telangiectasia mutated (ATM), ataxia telangiectasia and Rad3-related (ATR) and the master tumour suppressor protein p53, which promotes cell-cycle progression at the expense of the DDR, thereby increasing mutagenesis (208). DDR deficiency is thus a fundamental characteristic of cancer, which actively promotes tumour development by maintaining a high degree of genomic instability.

Further evidence of the role of DDR dysfunction in cancer development was brought by the association between germline mutations in DDR genes and a number of rare cancer-predisposing syndromes, including Louis–Bar syndrome (also known as ataxia telangiectasia, associated with *ATM* mutations), Fanconi anaemia (associated with mutations in *FANC* genes, including *BRCA1* and *BRCA2*), Lynch syndrome (associated with

mutations in *MSH2*, *MLH1, MSH6*, or *PMS2*) but also Bloom syndrome, Rothmund–Thomson syndrome, Werner syndrome or Nijmegen breakage syndrome (208).

A multitude of DDR alterations can be found in cancer, and their type and frequency vary across tumour types (**Table I.3**). In some histologies, an incontrovertible link exists between a particular DDR defect and a specific mutational signature in the tumour genome. For example, 15% of sporadic CRC exhibit a mutational signature characterized by an abnormal shortening and lengthening of dinucleotide repeat sequences. This signature, known as microsatellite instability (MSI), is caused by a dysfunction in the mismatch-repair (MMR) pathway of the DDR, responsible for the repair of DNA replication errors. Hence, the MMR genes *MSH3/6* and *MLH3* are frequently found mutated in MSI-high CRC. Similarly, a subset of both sporadic and familial cancers harbour substantial numbers of large deletions (up to 50 base pairs) with overlapping micro-homology at breakpoint junctions. This mutational signature is associated with defects in homologous recombination (HR), a DNA repair process involved in the resolution of DSBs. These HR defects, often caused by loss-of-function mutations in genes such as *BRCA1, BRCA2, PALB2,* and *RAD51C*, are present in 50% of high-grade serous ovarian cancers (HGSOC), 15% of triple-negative breast cancers (TNBC) and 2% of pancreatic cancers. Another example is the ultra-mutated phenotype encountered in a subset of endometrial cancers, which has been associated with altered activity of the error-prone polymerase Pol-ε, consequent to mutations in the gene *POLE*.

These data demonstrate that specific DDR defects cause characteristic mutational patterns that shape the tumour mutational landscape. This has important implications for tumour immunogenicity, as each DDR defect is likely to generate specific antigens at a certain frequency, thereby leaving a particular imprint on the tumour "antigenic landscape" and potentially influencing response to ICI.

Table I.3. Type and frequency of DNA repair alterations in solid tumours.

Genes in blue are related to DSB repair, in green to MMR, in red to NER, in orange to nucleotide synthesis, and in grey to DNA replication. Genes marked with an asterisk refer to data reported in cell lines only. Abbreviations: N.R., not reported.

Cancer type	Gene	Alterations		Reference
		Type	Frequency	
Non-Small Cell Lung Cancer	***BRCA1***	Reduced mRNA and protein expression	44%	(211)
	FANCF	Promoter methylation	14%	(212)
	ATM	Somatic mutations	6%	(212)
	MSH2	Reduced protein expression	18-38%	(212)
	ERCC1	Reduced protein expression	22-66%	(212)
	RRM1	Loss of heterozygosity	65%	(212)
Small-Cell Lung Cancer	***POLD4****	Reduced mRNA expression	N.R.	(213)
Clear-Cell Renal Cell Carcinoma	***ATM***	Somatic mutations	3%	(214)
	NSB1	Somatic mutations	0.5%	
	MLH1	Homozygous deletion	3-5%	(215)
	MSH2	Promoter hypermethylation	N.R.	(216)
Urothelial Carcinoma	***BRCA1***	Somatic mutations	14%	(217–219)
	BRCA2	Somatic mutations	14%	
	PALB2	Somatic mutations	14%	
	ATM	Somatic mutations	29%	
	MSH2	Loss of protein expression	3%	(220)
	ERCC2	Somatic mutations	12%	(221)
Head and Neck Cancer	***FANCB****	Promoter methylation	31%	(222)
	FANCF*	Promoter methylation	15%	
	FANCJ	Reduced protein expression (IHC)	N.R.	
	FANCM	Reduced protein expression (IHC)	N.R.	
	BRCA1	Reduced protein expression (IHC)	N.R.	
	BRCA2	Reduced protein expression (IHC)	N.R.	
	FANCD2	Reduced protein expression (IHC)	N.R.	
Ovarian Cancer	***BRCA1/ BRCA2***	Germline mutations	15%	(223,224)
		Somatic mutations	35%	
		Promoter methylation	11-35%	
	FANCF	Promoter methylation	N.R.	
	FANCD2	Reduced protein expression	N.R.	
	BARD1	Germline mutations	6%	(225)
	BRIP1	Germline mutations	6%	
	PALB2	Germline mutations	6%	
	MRE11	Germline mutations	6%	
	RAD50	Germline mutations	6%	
	RAD51C	Germline mutations	6%	
	NSB1	Germline mutations	6%	
	MSH6	Inactivating mutations	6%	(225)

Cancer type	Gene	Alterations		Reference
		Type	Frequency	
Triple-Negative Breast Cancer	***BRCA1***	Germline mutations	5-10%	(223,226)
	BRCA2	Somatic mutations	10%	
Gastric Cancer	***MLH1***	Loss of protein expression (IHC)	18%	(227)
		Promoter hypermethylation	15%	
	MSH2	Loss of protein expression (IHC)	3%	
MMR-deficient Colorectal Cancer	***MRE11***	Somatic mutations	75%	(228–230)
	RAD50	Somatic mutations	21-46%	
	BRCA2	Somatic mutations	2%	
	MSH3	Somatic mutations	22-51%	(228–230)
	MSH6	Somatic mutations	9-38%	
	MLH3	Somatic mutations	9-28%	
	POLD3	Somatic mutations	37%	(228–230)
Hepatocellular carcinoma	***NSB1***	Somatic mutations	10%	(231)
	MSH2	Promoter hypermethylation	25%	(232,233)
		Reduced protein expression	18%	
	PMS2	Promoter hypermethylation	15%	
	MLH1	Promoter hypermethylation	8%	
		Reduced protein expression	38%	
Biliary tract cancer	***MSH2***	Loss of protein expression (IHC)	7%	(234,235)
	MSH6	Loss of protein expression (IHC)	7%	
	MLH1	Loss of protein expression (IHC)	1.5%	
	PMS2	Loss of protein expression (IHC)	1.5%	
Prostate Cancer	***BRCA2***	Homozygous deletion/ Heterozygous deletion/ Frameshift mutation	14%	(236,237)
	ATM	Frameshift mutation	12%	
	PALB2	Frameshift mutation	4%	
	CHK2	Homozygous deletion	4%	
	FANCA	Homozygous deletion	6%	
	BRCA1	Homozygous deletion	2%	
	MRE11	Frameshift mutation	2%	
	NSB1	Frameshift mutation	2%	
	MLH3	Frameshift mutation	4%	(236,237)
Endometrial cancer	***MLH1***	Promoter hypermethylation	30%	(238,239)
	POLE	Somatic mutations	10%	(238,239)
Pancreatic Cancer	***BRCA2***	Germline mutations	1.5%	(211,240)
	MSH2	Loss of protein expression (IHC)	15%	(241)
	MSH6	Loss of protein expression (IHC)	15%	
	MLH1	Loss of protein expression (IHC)	15%	
	PMS2	Loss of protein expression (IHC)	15%	

3. DNA repair pathway alterations are associated with response to ICI

Initial studies that evaluated a correlation between TMB and response to ICI had already identified DDR defects as potential biomarkers of response to these therapies. Indeed, Rizvi and colleagues found that, in NSCLC, pembrolizumab responders showing the highest TMB had specific mutations in DDR genes, including *POLD1, POLE, MSH2, BRCA2, RAD51C,* and *RAD17*. Multiple subsequent studies, presented below, further investigated this link between DDR, TMB and sensitivity to ICI.

a. MMR-deficiency predicts response to ICI

The most robust evidence for the association between DDR defects and response to ICI was initially established in MMR-deficient tumours (242). Early IHC and genomic studies had identified an interaction between the MSI-high phenotype, the increased presence of TILs and an improved prognosis in CRC (243,244), thus suggesting that MMR deficiency may influence the immune microenvironment of these tumours. Later, it was shown that the enhanced immune infiltrate found in MSI-high CRC tumours was counterbalanced by the upregulation of inhibitory immune checkpoints including PD-1, PD-L1, and CTLA-4 (245). This supported the hypothesis that these tumours escape anti-tumour immunosurveillance via upregulation of immune checkpoints, and that checkpoint blockade therapy could represent an effective treatment strategy in this context.

Based on these observations, and on the initial description of exceptional responses in MMR-deficient patients receiving ICI, a phase II clinical trial was initiated to test the activity of pembrolizumab in three cohorts of patients with treatment-refractory disease: (i) MMR-deficient CRC patients, (ii) MMR-proficient CRC patients, and (iii) MMR-deficient non-CRC patients including cholangiocarcinoma, endometrial carcinoma, and gastric carcinoma patients (121). The immune-related ORR was 40% in the MMR-deficient CRC cohort and 71% in the MMR-deficient non-CRC cohort, versus 0% in the MMR-proficient CRC cohort. These results established the first compelling clinical evidence for activity of anti-PD-(L)1 agents in MMR-deficient tumours. In addition, consistent with initial studies, the analysis of genomic data from patients revealed that both TMB and predicted TNB were higher in

MMR-deficient tumours compared with MMR-proficient tumours, and that MMR-deficient tumours had a higher CD8+ T cell infiltrate associated with an increased PD-L1 expression on tumour cells.

This proof-of-concept study was later expanded in a larger cohort of patients with advanced MMR-deficient tumours of 12 different histotypes; impressive ORR of 53% and complete response rate of 21% were achieved (246). The median PFS and OS were still not reached at the time of publication, indicating that most responses were durable. Furthermore, functional analysis in a responding patient established that a rapid expansion of neo-antigen-specific T cell clones was engaged upon treatment with anti-PD-1. This data was the basis for the first FDA approval of an anti-cancer drug in a histotype-agnostic fashion: in May 2017, pembrolizumab was granted accelerated approval for any adult or paediatric advanced tumour presenting MMR deficiency or high MSI.

Considering the important benefit brought by ICI in this population, many institutions have now implemented routine MSI testing (using IHC and/or PCR-based assays) for all patients newly diagnosed of CRC and endometrial carcinoma. The development of targeted sequencing panels, that can be used to measure TMB and infer MSI status, will also enable more efficient patient screening and diagnosis "automatization" to better predict clinical benefit to ICI.

b. POLE/POLD1 proofreading mutations are associated with exceptional responses to ICI

Pol-ε and Pol-δ are two major DNA polymerases in human, responsible for the majority of nuclear DNA replication. Because of their proofreading exonuclease activity, these polymerases also play a preponderant role in the correction of DNA replication errors, and are thus considered as important components of the DNA repair machinery. Somatic point mutations in the exonuclease domain of Pol-ε and Pol-δ occur in certain tumours, and are associated with the highest TMB identified to date (247). Ultra-mutated tumours associated with *POLE* mutations, primarily found in a subset of endometrial carcinomas, exhibit a consistently high predicted TNB and were shown to have high levels of TILs and PD-1/PD-L1

expression (238,248). Moreover, recent case reports described exceptional responses to pembrolizumab in patients with *POLE*-mutant endometrial carcinoma (249) and glioblastoma (250), associated with local immune activation after treatment initiation. These results suggest that *POLE*-mutant tumours are sensitive to ICI due to their elevated genomic instability and increased immunogenicity; clinical trials are currently ongoing to validate this hypothesis (NCT02899793).

c. Defects in HR correlate with markers of immune activation

Tumours with HR dysfunction have also been shown to elicit specific anti-tumour immune responses. Initial evidence for an association between HR defects and immune activation was brought by IHC studies which demonstrated that loss of *BRCA1* or *BRCA2* (following mutation or promoter methylation) in ovarian tumours correlated with increased immune infiltration and higher levels of PD-1 and PD-L1 expression (251,252). In parallel, analysis of the genomic profile of HGSOC tumours with *BRCA1/2* alterations or mutations in other HR genes associated with the "BRCAness" phenotype (such as mutations in *RAD51, ATM*, or *ATR* and *PTEN* deletions) revealed a significantly higher predicted TNB compared with HR-proficient tumours (253). Very recently, loss of *CDK12*, a kinase involved in the transcription of several HR genes including *BRCA1*, was shown to define a distinct class of mCRPC, associated with increased genomic instability due to high levels of focal tandem duplications (FTD) and gene fusions (254). This subset of *CDK12*-mutant cases was shown to harbour elevated TNB driven by fusion-induced chimeric open reading frames, and consistent increased T cell infiltration. Interestingly, *CDK12*-mutant tumours do not exhibit the mutational signature classically linked to HR defects (i.e. nsSNVs or insertions/deletions associated with LOH), suggesting that their high TNB may not directly result from HR dysfunction, and that specific neo-antigens may drive the immunogenicity of these tumours.

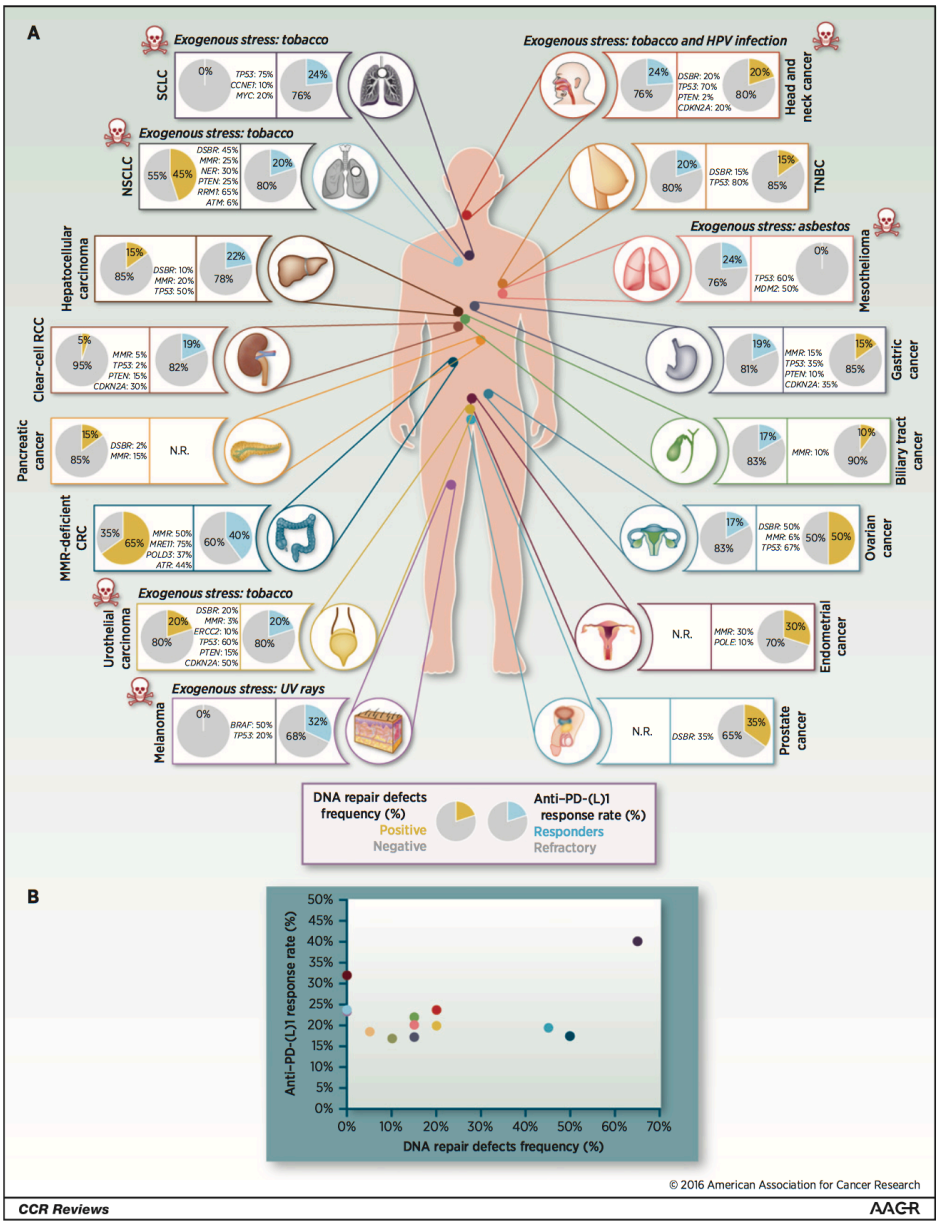

Figure I.15. DNA repair defects and their association with anti-PD-(L)1 efficacy in solid tumours.

A. Representation, per tumour type, of the median frequency of DNA repair deficiency (yellow pie charts) and the median efficacy of anti-PD-(L)1 (blue pie charts). For each histology, the median rate of DNA repair defects was calculated on the basis of literature data. When DNA repair defects in distinct pathways were mutually exclusive, the sum of their frequency was taken; when overlaps were observed between several DNA repair defects, the median of all DNA repair defects was chosen. The frequency of additional defects in other genes relevant for DNA repair (i.e. genes involved in cell cycle regulation or DNA replication) were also evaluated and are depicted on the side of the pie chart graphs. Tumour types resulting from exposure to a mutagenic agent are highlighted by a skull. ORR reported in phase I, II, or III trials performed in the corresponding histologies were taken for estimating the efficacy of anti-PD-(L)1 inhibitors. The data cut-off for collecting anti-PD-(L)1 efficacy was January 2016. **B.** Scatter plot illustrating the lack of statistically significant correlation between DNA repair mutation frequency and response

to anti-PD-(L)1 therapies, highlighting the need to take into account additional parameters for predicting response to these drugs. Abbreviations: DSBR, double-strand break repair; HPV, human papillomavirus; NER, nucleotide-excision repair; N.R., not reported.
Figure and legend reproduced from Chabanon et al., Clinical Cancer Research, 2016.

Additional studies have shown correlations between the HR status and response to ICI. In a small cohort of 38 patients with metastatic melanoma treated with pembrolizumab or nivolumab, Hugo and colleagues observed that 29% of ICI responders harboured a deleterious mutation in *BRCA2* versus only 6% of non-responders (153), and that *BRCA2*-mutated melanomas had a significantly higher TMB compared with *BRCA2*-wildtype melanomas. Similarly, better ORR, PFS and OS have been reported in HR-deficient metastatic prostate cancer patients receiving nivolumab plus ipilimumab, although the difference with HR-proficient patients was not statistically significant – probably due to low patient number (255). Other clinical trials are ongoing to determine the predictive value of HR defects as a biomarker of response to ICI in other histologies (NCT01772004).

Very recently, a retrospective study has evaluated the impact of DDR alterations on the clinical efficacy of atezolizumab or nivolumab in advanced urothelial cancers (256). The presence of any DDR defect, regardless of the pathway affected, was associated with a higher ORR, and patients with known or likely deleterious DDR defects had a higher ORR than patients with DDR defects of unknown significance. Although these data and the above-presented studies suggest that DDR deficiency results in higher TMB and increased immunogenicity in some histologies, a definite correlation between DDR deficiency, TMB and sensitivity to ICI cannot be claimed (**Figure I.15**), which suggests that TMB-independent factors also influence response to ICI.

4. The cGAS/STING pathway: another interface between the DNA damage response and innate immunity

In recent years, an emerging body of data has supported the involvement of neo-antigen-independent mechanisms in the recognition and elimination of tumour cells by the immune

system. In particular, the cyclic GMP-AMP synthase / stimulator of interferon genes (cGAS/STING) pathway has generated significant interest in immuno-oncology, because of its central role of interface between the DDR and innate immunity (257). If this pathway was initially characterized as a cellular system of sensing of foreign DNA – originating from viral or bacterial sources in the setting of cellular infection –, several lines of evidence have later suggested its implication in the detection of endogenous damaged nuclear DNA in the context of auto-inflammatory diseases (258) and cancer (259). In either case, recruitment of this pathway results in innate immune responses through the activation of a signalling cascade connecting the cytoplasmic DNA sensor cGAS, several signal transducers including STING and TBK1, and eventually transcription factors (mainly IRF3 and NF-κB) that are collectively responsible for the induction of a type I IFN response.

a. Function of the cGAS/STING pathway

The cGAS/STING pathway owes its sensing functions to the DNA sensor cGAS, a protein which contains a nucleotidyl-transferase domain and two major DNA-binding domains. cGAS operates in the cytosol and primarily detects double-stranded DNA (dsDNA) molecules, independently of their DNA sequence, through binding to their sugar-phosphate backbone. Single-stranded DNA (ssDNA) can also be detected in the form of internal duplex structures. Biochemical *in vitro* studies have shown that dsDNA molecules as short as ~15 base pairs are sufficient to bind and activate cGAS; in cells cytoplasm, it is likely that cGAS activation relies on the detection of longer DNA molecules because of the presence of nucleases and other cellular regulatory factors (257).

cGAS binding to DNA induces a conformational change in the nucleotidyl-transferase active site of the protein, which allows the synthesis of cyclic GMP-AMP (cGAMP) from ATP and GTP (**Figure I.16**, (257)). The cGAMP synthesized by cGAS is a 2′-3′-cGAMP isomer, containing two phosphodiester bonds, one between the 2′-OH of GMP and 5′-phosphate of AMP, and the other between the 3′-OH of AMP and 5′-phosphate of GMP. This molecule functions as a second messenger that activates the ER-membrane adaptor STING through binding via extensive hydrophobic interactions and hydrogen bonds. Binding of cGAMP to STING induces (i) STING translocation from the ER to the Golgi apparatus, and during this

process (ii) a conformational change in STING that is postulated to release a carboxy-terminal tail which recruits and activates TANK binding kinase 1 (TBK1) and IκB Kinase (IKK). Upon activation, TBK1 in turn phosphorylates STING at several serine and threonine residues, and phosphorylated STING binds to a positively charged region of interferon regulatory factor 3 (IRF3), thereby recruiting it and allowing its phosphorylation by TBK1. Once IRF3 is phosphorylated, it forms a homodimer and enters the nucleus to activate the transcription of interferons. Similarly, STING-mediated activation of IKK results in the phosphorylation of the IκB family of inhibitors of the transcription factor NF-κB. This allows the release of NF-kB and its translocation to the nucleus where it functions together with IRF3 to induce the expression of interferons and inflammatory cytokines.

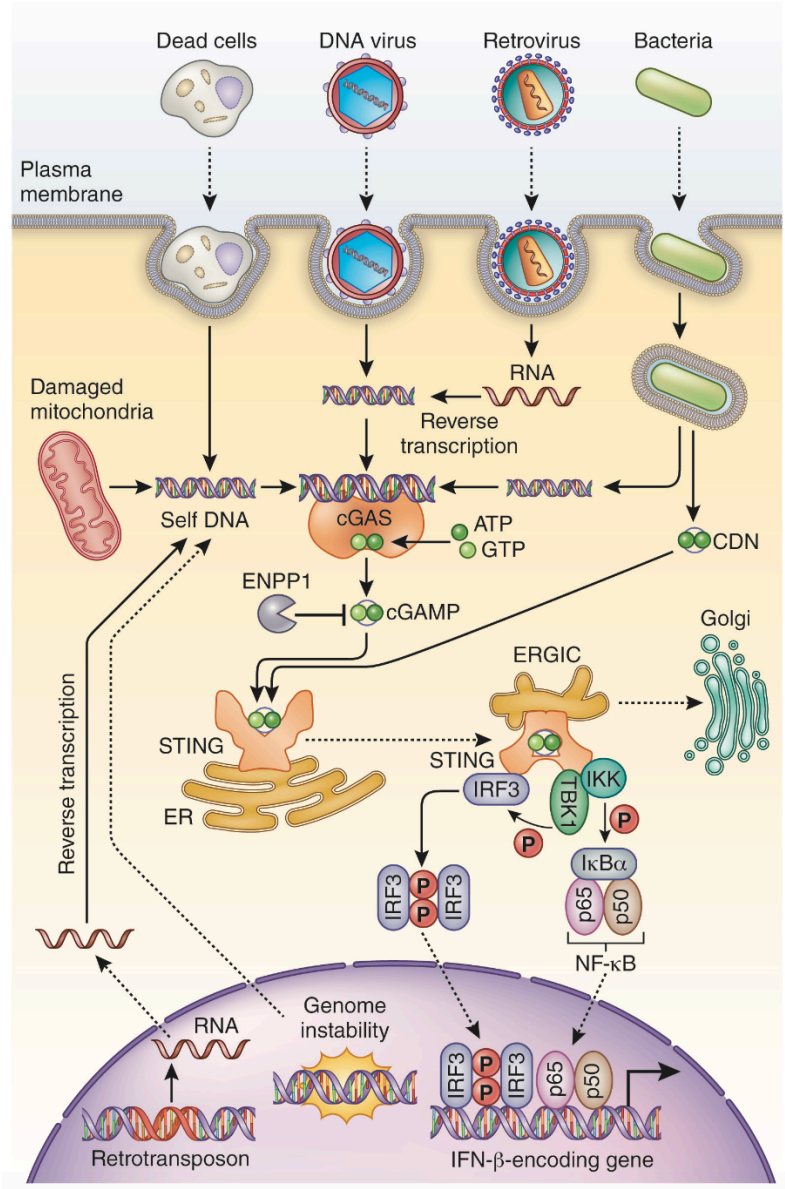

Figure I.16. The cGAS/STING pathway of cytosolic DNA sensing.
DNA is a pathogen-associated molecular pattern (PAMP) when it is delivered to the host cytoplasm by microbial infection, and is a danger-associated molecular pattern (DAMP) when it enters the cytoplasm from the nucleus (e.g., through DNA damage and reverse transcription of retro-elements), mitochondria or dead cells. Cytosolic DNA binds to and activates cGAS, which catalyzes the synthesis of 2′3′-cGAMP from ATP and GTP. 2′3′-cGAMP binds to the ER adaptor STING, which traffics to the ER-Golgi intermediate compartment and the Golgi apparatus. STING then activates IKK and TBK1. TBK1 phosphorylates STING, which in turn recruits IRF3 for phosphorylation by TBK1. Phosphorylated IRF3 dimerizes and then enters the nucleus, where it functions with NF-kB to turn on the expression of type I IFN and other immunomodulatory molecules.
Figure and legend adapted from Chen et al., Nature Immunology, 2016.

b. The cGAS/STING pathway is activated in the context of DDR deficiency

The cGAS/STING pathway appears to be a major innate immune sensing machinery for the detection of tumours (260). Indeed, this pathway was shown to be activated in APCs following engulfment of dying tumour cells, thus resulting in T cell activation and priming against tumour-associated antigens via type I IFN-mediated stimulation (261,262). More importantly, the activation of cGAS/STING has also been evidenced in tumour cells undergoing DNA damage. For example, exposure of tumour cells to IR or S-phase-specific chemotherapies has been associated with a cell cycle-dependent formation of cytoplasmic chromatin fragments (CCF) or micronuclei involved in the induction of a STING-mediated type I IFN response (263–266). Exogenous DNA damage-induced IFN responses have also been observed in the context of treatment with other clinically relevant drugs, such as etoposide, camptothecin, mitomycin C, and adriamycin (267). Furthermore, the presence of specific DDR defects, *per se*, has been associated with cGAS/STING activation: Parkes and colleagues reported that defects in HR genes (*BRCA1/2* or *FANCD2*) promote the accumulation of CCF in cancer cells and trigger STING-mediated phosphorylation of TBK1 and IRF3, thereby resulting in a type I IFN response characterized by the upregulation of the lympho-attractant chemokines CXCL10 and CCL5 (268). They further showed in a cohort of 184 breast cancer samples that DDR-deficient tumours (identified by molecular profiling using a validated DDR-genes signature) displayed higher CD4+/CD8+ T cell infiltration and higher expression of CXCL10 and CCL5 compared to their DDR-proficient

counterparts, thus supporting that HR defects in breast tumours favour the establishment of an immune-activated microenvironment. Other DDR defects such as ATM deficiency have been associated with activation of cGAS/STING and subsequent type I IFN response in cancer cells (269), suggesting that the accumulation of cytosolic DNA is a common feature of DDR-defective cells.

Beyond DDR defects, chromosomal instability – which results from ongoing errors in chromosome segregation during mitosis – has recently been identified as a major mechanism contributing to the activation of the cGAS/STING cascade (270). The proposed model is that chromosomal missegragation creates a preponderance of micronuclei whose rupture spills genomic DNA into the cytosol, thereby activating DNA-sensing pathways. Interestingly, activation of the cGAS/STING pathway in this context has been associated with tumour evasion and metastasis, because chromosomally unstable cancer cells develop multiple mechanisms that largely suppress type I IFN signalling in favour of alternative inflammatory STING-dependent signalling, such as NF-κB, that actively participate to cellular migration and distant metastasis (271). This suggests the ambiguous role of cGAS/STING in modulating cell-autonomous immune responses in cancer and highlights the precarious balance that mediates the expression of immuno-stimulatory and pro-inflammatory signals in response to genomic instability.

Overall, the mechanism by which free DNA arises in the cytoplasm is not yet fully understood, and whether CCF result from "leakage" of nuclear DNA into the cytoplasm, from rupture of micronuclei, or from the putative cytosolic functions of DDR enzymes requires further investigation (272).

Importantly, considering the potential of cGAS/STING signalling to mediate anti-tumour immune responses, direct activation of this pathway using STING agonists represents an attractive therapeutic strategy and an intense research area, with several ongoing phase I trials evaluating such molecules (273), in monotherapy or combination – notably with anti-PD-(L)1 agents, as cGAS recently appeared to be essential for the anti-tumour effects of ICI (274).

5. Other neo-antigen-independent mechanisms connecting the DDR and immunity

Some groups have investigated other tumour cell-intrinsic neo-antigen-independent mechanisms as potential mediators of anti-tumour immunity. For example, an original study from McGrail and colleagues used a multi-omics approach to show the absence of correlation between TNB and T cell infiltration in copy number alterations-driven cancers, such as breast cancer (275). Conversely, they identified *ATM* as a major driver of T cell infiltration in these cancers, which potentially controls the expression of lympho-attractant chemokines through phosphorylation of specific transcription factors. This study opens novel perspectives on the potential of DDR defects to influence anti-tumour immune responses, and supports the existence of transcription-dependent mechanisms modulating tumour immunogenicity.

E. Targeting DDR deficiencies to modulate anti-cancer immunity

We have previously detailed how DDR alterations modulate the characteristics and outcome of anti-tumour immune responses via neo-antigen-dependent and -independent mechanisms. Given the importance of these effects, therapeutically targeting DDR deficiencies represents an attractive approach to stimulate anti-cancer immunity. In the context of IO, the identification of rationale combinations with ICI that would increase the proportion of patients benefiting from these therapies is an intense research area. Several therapeutic modalities have been assessed toward this aim, including chemotherapy, IR and DNA repair-targeted therapies.

1. Immunogenic properties of cytotoxic chemotherapy

Although most conventional chemotherapies, including direct DNA-damaging agents, have been traditionally considered as immunosuppressive because of their deleterious effects on immune cells (lymphopenia), a significant body of evidence has established that

at least some chemotherapies can promote anti-tumour immunity by generating immunogenic cell death (ICD) of tumour cells. This peculiar form of cell death actually comprises various cell death modalities that share the common feature of activating immune effectors through the emission of a variety of danger signals collectively known as damage-associated molecular patterns (DAMPs). At least four individual types of ICD have been identified so far, including ICD driven by pathogens, ICD elicited by chemotherapeutics, ICD elicited by physical interventions, and necroptotic ICD (276). Each type of ICD is characterized by the emission of a specific panel of DAMPs, which activates a more or less wide range of immune effectors.

a. ICD elicited by chemotherapeutics

The demonstration that chemotherapeutic agents trigger ICD has first been achieved *in vivo* using vaccination assays. This kind of assay involves (i) the inoculation of dying tumour cells, pre-treated *in vitro* with a putative ICD inducer, into syngeneic immunocompetent mice (vaccination step) and (ii) the subsequent challenge of vaccinated mice with living cancer cells of the same type. As tumour cells dying through ICD have been proposed to trigger memory immune responses against tumour-specific antigens, vaccination of mice with these cells is thought to provide a protective effect against subsequent tumour challenge. In this scenario, the percentage of tumour-free mice after re-challenge provides a robust estimate of the capacity of a given drug to induce ICD. A number of chemotherapeutic agents have been screened in this system, and some of them, currently used in the clinic such as doxorubicin, mitoxantrone, oxaliplatin or bortezomib, were shown to trigger *bona fide* ICD (277–279), with vaccination rates ranging from 80% to 90%.

These *in vivo* observations called for a mechanistic dissection of the ICD process. Thus, during the past ten years, the molecular mechanisms underlying ICD have been extensively studied, resulting in the identification of several DAMPs as critical molecular events triggered in the context of chemotherapy-induced ICD (**Figure I.17**, (276)). These include: (i) cell-surface exposure of calreticulin (CALR) and other ER chaperones, (ii) secretion of ATP in the extracellular milieu, (iii) activation of a cancer cell-intrinsic type I IFN response

resulting in the secretion of CXCL10 and (iv) release of immunomodulatory molecules including High-Mobility Group Box 1 (HMGB1) and Annexin A1 (ANXA1).

(1) Exposure of CALR: Chemotherapy-driven ICD relies on the exposure of ER chaperones at the plasma membrane of dying tumour cells. These include primarily CALR (280), but also protein disulfide isomerase family A member 3 (PDIA3, also known as ERp57) (281), heat shock protein 70 kDa (HSP70) and 90 kDa (HSP90) (282). The exposure of these proteins is dependent on the phosphorylation of the ER factor eukaryotic initiation factor 2 (eIF2α), which is characteristic of an ER stress triggered by DNA-damaging agents. Once exposed on the plasma membrane of dying tumour cells, the chaperones act as "eat-me" signals for phagocytes, promoting the uptake of cell corpses and debris by APCs (283). For example, CALR-exposing cells are recognized and engulfed by CD91-positive cells (mostly represented by macrophages and DCs), unless they simultaneously express an antagonist signal (such as CD47) on their surface. Conversely, depletion of CALR (or that of any of the proteins that are required for CALR exposure) prevents phagocytosis and abolishes ICD as elicited by multiple ICD inducers. CALR exposure is thus a critical DAMP which dictates the immunogenicity of cancer cell death (280).

(2) Secretion of ATP: Stress-induced ATP secretion is an important feature of ICD. It occurs via various mechanisms including the active exocytosis of ATP-containing vesicles as well as the passive release of cytoplasmic ATP via gap junction hemi-channels, pannexin channels or transporters of the ATP-binding cassette family (284). Autophagy is involved in the active secretion of ATP; being strictly required for cells exposed to immunogenic chemotherapeutics to release ATP in amounts that are compatible with the engagement of adaptive immunity, this process was shown to be essential for ICD (285). Passive release of ATP, by contrast, occurs secondary to caspases-mediated cleavage and activation of pannexin 1 (PANX1), and is not sufficient to induce the high levels of extracellular ATP required for ICD (286). ATP is the most abundant intracellular metabolite but also an important autocrine/paracrine messenger that operates by binding to ionotropic (P2RX) or metabotropic (P2RY) purinergic receptors. Thus, extracellular ATP constitutes a potent "find-me" signal for phagocytes: by interacting

with P2RY2 and P2RX7 receptors, respectively, on APCs and their precursors, ATP mediates robust chemotactic effects, promoting the recruitment of macrophages and DCs to the tumour site (287).

(3) Secretion of type I IFN: Anthracyclines have been shown to stimulate the rapid production of IFN-α and IFN-β by cancer cells through activation of the endosomal pattern recognition receptor Toll-like receptor 3 (TLR3) (288). The secretion and subsequent binding of these factors to IFN receptors on cancer cells was shown to trigger autocrine and paracrine circuitries that result in the release of CXCL10, a chemokine mediating the recruitment and activation of macrophages, DCs and NK cells. Importantly, this type I IFN response is required for the anti-cancer immune responses elicited by anthracyclines *in vivo*, as (i) tumours lacking TLR3 or IFNAR fail to respond to chemotherapy (unless type I IFN or CXCL10, respectively, is artificially supplied) and (ii) IFNAR1-deficient mouse cancer cells killed by doxorubicin cannot vaccinate syngeneic hosts in conditions in which wildtype cells efficiently do so.

(4) Release of HMGB1/ANXA1: Another hallmark of chemotherapy-induced ICD is the release of immunomodulatory molecules in the extracellular milieu. Among them, HMGB1 and ANXA1 represent important mediators of the anti-cancer immune responses elicited by chemotherapy. HMGB1 is a nuclear factor, normally bound to chromatin. Upon exposure to chemotherapy, stressed cells undergo nucleo-cytoplasmic translocation of HMGB1, and eventually, passive release of this molecule through loss of plasma membrane integrity following post-apoptotic necrosis (284). Once released, HMGB1 operates as a potent pro-inflammatory stimulus for immune cells, by interacting with various pattern recognition receptors, including TLR2, TLR4 and receptor for advanced glycosylation end-products (RAGE) (289,290). Binding of HMGB1 to TLR4 on monocytes/macrophages stimulates the secretion of pro-inflammatory cytokines (291), while interaction of nucleosome-bound HMGB1 to TLR2 induces a humoral immune response, resulting in the production of anti-DNA and anti-histone antibodies (292). HMGB1 can also form a complex with CXCL12, thus mediating the recruitment of mononuclear cells to inflammatory lesions through interaction with CXCR4 (293). Importantly, the interaction with TLR4 appears to be the most important for the perception of cell death as immunogenic, primarily because HMGB1 also binds

to TLR4 on DCs to facilitate processing and cross-presentation of antigens from dying tumour cells (294). Consistently, depletion of HMGB1 via small-interfering RNA (siRNA) or neutralizing antibodies totally compromises the efficacy of anti-tumour vaccination and abrogates ICD. Similarly, ANXA1 controls the immunogenicity of cell death by promoting stable interactions between dying cancer cells and DCs, through binding to formyl peptide receptor 1 (FRP1) on these latter (295). Lack of FRP1 has been shown to impair the approach of DCs to dying cancer cells, thus preventing the initiation of anti-tumour T cell responses.

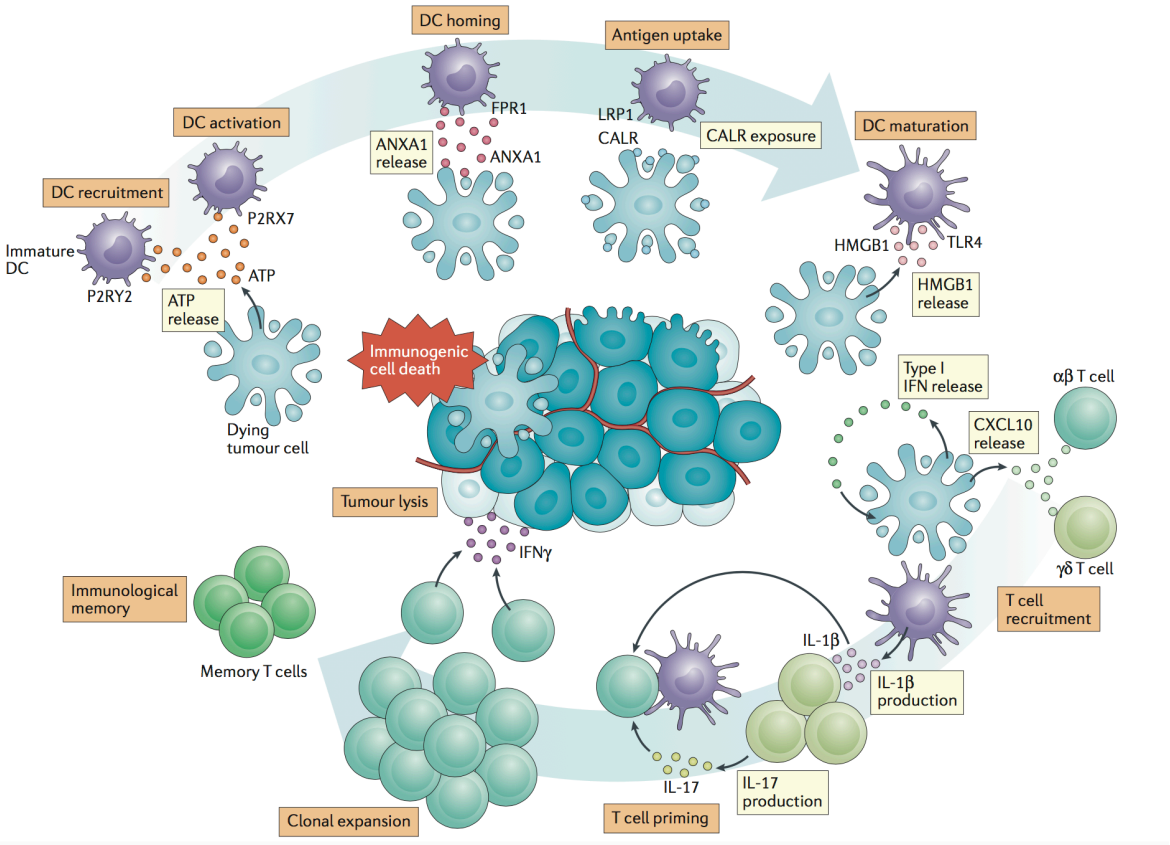

Figure I.17. Mechanisms of chemotherapy-driven ICD.
In response to ICD inducers, malignant cells produce a series of DAMPs that favour the uptake of cell corpses and debris by APCs, including DCs, and eventually lead to the priming of an adaptive immune response involving both αβ and γδ T cells. Such response is associated with the establishment of immunological memory, and has the potential to eradicate malignant cells that survive chemotherapy via an IFN-γ-dependent mechanism. CXCR3, CXC-chemokine receptor 3; FPR1, formyl peptide receptor 1; IFNAR1; interferon α/β-receptor subunit 1; IL, interleukin; LRP1, LDL receptor related protein 1; P2RX7, purinergic receptor P2X7; P2RY2, purinergic receptor P2Y2; TLR4, Toll-like receptor 4.
Figure and legend adapted from Galuzzi et al., Nature Reviews, 2017.

The previously described DAMPs constitute the molecular basis of ICD, and are as such, critical determinants of the immunogenic effects of chemotherapy. Experimental strategies aiming to interfere with the release of any of these DAMPs were shown to abolish the immunogenicity of cell death, as assessed by vaccination assays. This demonstrates the complexity and fragility of ICD, underlining the fact that this process is dependent on the spatiotemporally coordinated emission of immunogenic signals, that are triggered by simultaneous exposure to several stresses (ER stress, autophagy, cell death), and orchestrated by multiple intracellular and extracellular effectors. This may explain why only a subset of chemotherapeutic agents, able to gather these conditions, can effectively trigger ICD.

Although ICD may appear as a largely theoretical concept, the immunogenic properties of conventional chemotherapies have been shown to be essential for their clinical efficacy (288,296), which highlights the significance and clinical relevance of this process.

b. Other immunogenic effects of chemotherapy

Beyond the well-described effects of chemotherapy-driven ICD, other immunogenic properties have been associated with cytotoxic agents. For example, 5-fluorouracil (5-FU) can increase tumour cells immunogenicity by inducing cell-surface expression of MHC Class I molecules and tumour-specific antigens (297); Mitomycin C, hydroxyurea or 5-FU can induce expression of NK cell stimulatory ligands, such as killer cell lectin-like receptor K1 (KLRK1, also known as NKG2D), thereby stimulating NK cells activity (298). Other chemotherapeutic agents were demonstrated to upregulate death receptors present on the tumour cell surface, such as mannose-6-phosphate receptor or TRAIL, thus rendering tumour cells more susceptible to elimination by TILs (299,300). Finally, certain chemotherapy regimens such as TPF (docetaxel plus cisplatin plus 5-FU) have been associated with PD-L1 upregulation in tumour cells (301), which suggests that these agents may have antagonist effects on the modulation of immunity.

In addition to tumour-based effects, DNA-damaging chemotherapies have also been shown to modulate anti-tumour immune responses via direct effects on the TME (302).

Regulation of immune cell populations constitutes an important characteristic of certain chemotherapies: for example, drugs such as gemcitabine, paclitaxel, or 5-FU have been shown to suppress Treg or MDSC function in experimental models (303), thereby enhancing anti-tumour immunity. Similarly, cyclophosphamide has been shown to activate anti-tumour immune responses through increasing the number and activity of DCs. However, the applicability of these discoveries remains limited as, in many cases, the observed immunomodulatory effects appear to occur at non-toxic, non-clinically-relevant concentrations.

c. Combinatorial approaches of chemotherapy with immunotherapy

Several lines of evidence now suggest that cytotoxic chemotherapy can sensitize tumours to immune checkpoint blockade. In a recent preclinical study, Pfirschke and colleagues demonstrated that pre-treatment of ICI-resistant tumours lacking T cell infiltration with an appropriately selected combination of immunogenic chemotherapy (oxaliplatin plus cyclophosphamide) could successfully initiate host immune responses via direct stimulation of cancer cell TLR4 signalling (304). This strategy resulted in a rapid CD8+ T cell infiltration and eventually sensitized tumours to ICI, thus allowing durable control of tumour growth. Similar observations were made in studies evaluating other chemotherapeutic agents (decitabine, gemcitabine) in combination with anti-CTLA4 (305,306).

Clinically, most recent results of the combination of pembrolizumab with pemetrexed and cisplatin brought impressive results in advanced NSCLC, as previously described (129). These results were practice-changing and led to the recommendation of combining anti-PD-(L)1 agents with platinum-based doublet chemotherapy in NSCLC. Interestingly, drug administration schedule and sequence may be key in optimising the effects of such combination as, in lung cancer, initial studies demonstrated a benefit for ipilimumab plus carboplatin and paclitaxel using a phase dosing schedule (but not using a concurrent schedule), compared with chemotherapies alone (307,308).

More than 200 clinical trials are currently evaluating DNA-damaging chemotherapies in combination with ICI, with a variety of cytotoxic agents being tested in different dosing and

timing regimens (309). This will hopefully contribute to the definition of an optimal dosing and scheduling to eventually improve patient outcome.

2. Radiotherapy enhances anti-tumour immune responses

Historically, radiotherapy was considered as an immunosuppressive therapy because of frequent bone marrow irradiation and exquisite sensitivity of lymphocytes to radiation-induced apoptosis (310). Despite these observations, early studies have demonstrated the implication of the immune system in the therapeutic effects of radiotherapy. Stone and colleagues first showed that stimulation of the host immune system with a crude bacterial preparation prior to IR could reduce the dose of radiation needed to control tumour growth, while immunosuppression had the opposite effect (311). It was further described that immune cells, notably CD8+ effector T cells, have a key role in tumour elimination within the radiation field (312–314).

Radiotherapy has been shown to stimulate the immune system through local and systemic effects. The so-called "abscopal effect", which refers to regression or disappearance of lesions outside of the irradiated field, has been increasingly observed and is the best example of the immuno-stimulatory potential of radiotherapy.

a. The multiple immunogenic properties of radiotherapy

By inducing tumour cell death, radiotherapy initiates a variety of immunogenic mechanisms that participate to the activation of anti-tumour immunity (**Figure I.18**, (315)).

(1) Radiotherapy increases tumour cells immunogenicity: One of the best-described mechanisms by which radiotherapy enhances immune responses is the upregulation of MHC Class I in cancer cells (316–318). Dose-dependent increase in MHC Class I cell-surface expression has been observed following IR, and proposed to result from the stimulation of translation and peptide production via mammalian target of rapamycin (mTOR) pathway activation (319,320). These effects were associated with an enhanced degradation of existing proteins and a translation of novel proteins in response to

radiation, both resulting in an expanded intracellular peptide pool that stimulated antigen presentation on MHC Class I. Exposure to IR has also been shown to upregulate other cell-surface stimulatory ligands such as NKG2D (321), thus suggesting that its immunogenic effects may involve both innate and adaptive immunity.

(2) Radiotherapy induces ICD: Several lines of evidence support the idea that radiotherapy triggers an immunogenic form of cell death, that resembles the one triggered by anthracyclines and other ICD inducers (276). Indeed, irradiation was shown to mediate CALR exposure on cancer cells through the induction of an unfolded protein response (UPR) and consequent ER stress (322,323), but also ATP secretion driven by autophagy (324), type I IFN signalling activation (325,326) and HMGB1 release (323,327). Additional processes such as HSP70 secretion, TLR3 signalling stimulation, or IL-1β release were shown to be associated with IR-induced ICD but their involvement in the engagement of adaptive immunity remains to be tested formally (276).

(3) Radiotherapy stimulates cytokines/chemokines secretion: Exposure of cells and tissues to IR has been shown to result in the secretion of multiple cytokines and growth factors, including TNF-α, IL-1α, IL-1β, type I IFN, GM-CSF, IL-4, IL-5, IL-6, IL-10, IL-12 and IL-18, VEGF and TGF-β (328). This cytokine efflux is thought to participate to immune cell infiltration by inducing changes in vascular endothelium and by transmitting chemoattractant signals, that favour immune cells extravasation, migration, and invasion (329). This results in the infiltration of important mediators of anti-tumour immune responses such as DCs, macrophages, and effector T cells but also of suppressive immune cells such as Tregs and MDSC.

(4) Radiotherapy sensitizes tumour cells to T cell-mediated killing: IR exposure has been shown to induce expression of FAS on tumour cells, thereby facilitating their elimination by T cells (330,331). This mechanism is thought to play a major role of stimulation of anti-tumour immunity within the irradiated field.

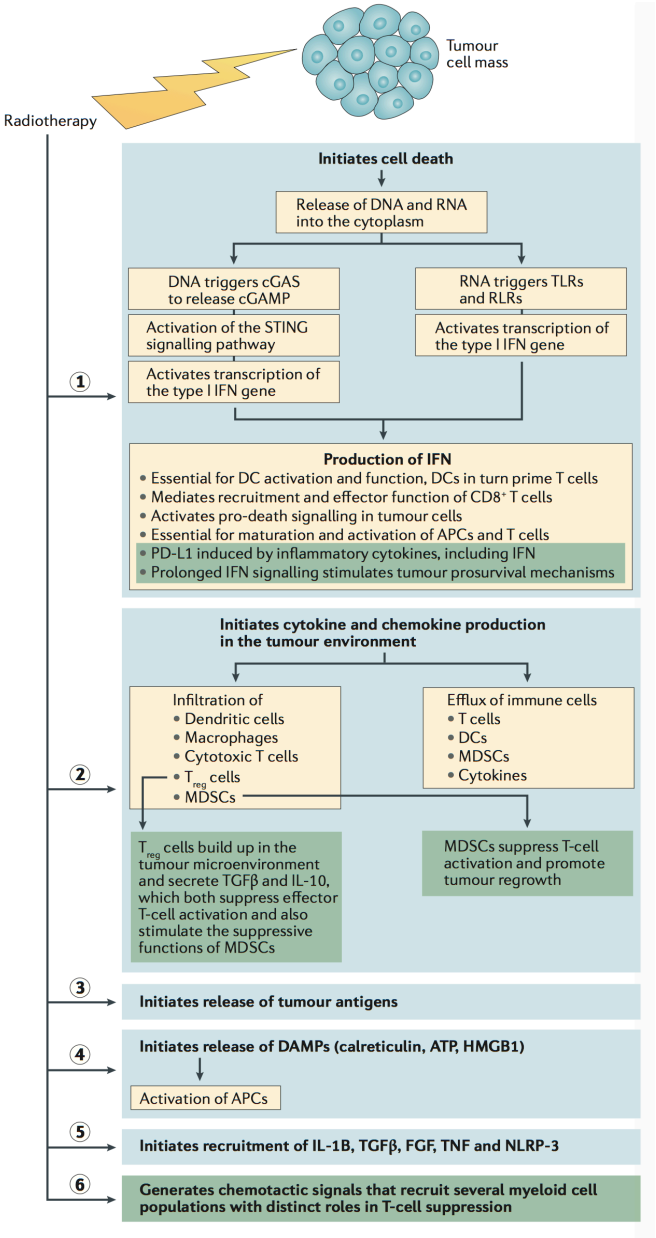

Figure I.18. Radiation-induced effects on tumour cells.

IR initiates: **(1)** cell death, **(2)** cytokine and chemokine production in the TME, **(3)** release of tumour antigens, **(4)** release of DAMPs, **(5)** recruitment of IL-1β, TGFβ, FGF, TNF, and NLRP-3, and **(6)** the generation of chemotactic signals that recruit several myeloid cell populations with distinct roles in T cell suppression. These primary events are the catalysts for an elaborate succession of processes. Cell death **(1)** causes the release of DNA and RNA into the cytoplasm leading to the production of IFN. Cytokine and chemokine production **(2)** triggers the infiltration of DCs, macrophages, cytotoxic T cells, Tregs, and MDSC, as well as the efflux of immune cells. The release of DAMPs **(4)** activates APCs. These complex and sometimes conflicting events are reflective of the struggle between host immune response and tumour pro-survival mechanisms. Abbreviations: FGF, fibroblast growth factor; IL-1β, interleukin 1β; IL-10, interleukin 10; NLRP3, NACHT, LRR and PYD domains-containing protein 3; RLRs, RIG-I-like receptors; TLRs, Toll-like receptors.

Figure and legend adapted from Weichselbaum et al., Nature Reviews, 2017.

b. The abscopal effect

First described in the 1950s (332), the abscopal effect is an important peculiarity of radiotherapy that has only recently been associated with activation of the immune system (333). Experiments carried out in nude mice have demonstrated that T cell effector function within the irradiated TME was a driver of the abscopal effect and that a memory immune response was involved in this phenomenon (333). Cytokine release is another important element of the abscopal effect (334): notably, TNF-α secretion by activated T cells reduces the number of immunosuppressive cells both locally and systemically (335).

If the abscopal effect has rarely been observed in routine clinical practice when radiotherapy was administered alone, this phenomenon has been increasingly reported in combination with IO (315), suggesting that combinatorial strategies of radiotherapy plus ICI may be beneficial in the metastatic setting for patients with advanced cancers.

c. Combinatorial approaches of radiotherapy with IO

Initial pre-clinical studies evaluating the combination of local tumour irradiation plus anti-CTLA4 therapy obtained immune-mediated regression of metastatic lesions in various tumour models including breast and colon cancer, indicative of potent abscopal effects (336,337). Similarly, addition of anti-PD-(L)1 therapy to local IR treatment was shown to enhance the efficacy of radiotherapy through a cytotoxic T cell-dependent mechanism (335), both locally and at distant sites in several mouse models (315,338). Moreover, as IR may participate to immunosuppression in the TME via upregulation of immune checkpoint molecules such as PD-L1 (329), combination with PD-(L)1 blockade has been proposed as a strategy to overcome acquired resistance to fractionated radiotherapy (339,340).

Clinically, the abscopal effect has been successfully achieved in the setting of combination with anti-CTLA4 in isolated cases (341–344), but clinical trials specifically addressing this question have shown little clinical benefit of this combination so far (345), although anti-tumour activity with disease control has been observed (346) and very recently associated with potent systemic T cell responses in some cases (347). Currently, more than 300 clinical trials are evaluating ICI in combination with radiotherapy in various histologies (348).

3. DNA repair-targeted therapies: another class of immunomodulatory agents?

Based on the immunomodulatory potential of conventional cytotoxic agents, an increasing interest has emerged towards the use of DNA repair-targeted therapies, notably poly(ADP-ribose) polymerases inhibitors (PARPi), as immunomodulatory agents.

a. PARPi: the advent of synthetic lethal approaches in the clinic

The DDR relies on the incredibly complex function of a series of interrelated molecular pathways that recognize diverse DNA damage patterns, mediate cell cycle arrest, and orchestrate DNA repair in order to maintain genome integrity. Key to the DDR are the poly(ADP-ribose) polymerases 1 and 2 (PARP1 and PARP2) enzymes, that operate as DNA damage sensors and signal transducers through the synthesis of negatively charged, branched poly(ADP-ribose) (PAR) chains on multiple target proteins as post-translational modifications (349). This poly(ADP)ribosylation (PARylation) process is involved in most of the known functions of PARP1 in DNA repair, including repair of single-strand breaks (SSBs) and DSBs, in the stabilization of DNA replication forks, as well as in chromatin remodelling (350). PARP1 primarily binds damaged DNA at sites of SSBs, although other DNA lesions are known to trigger its recruitment. This binding to DNA stimulates the catalytic activity of PARP1 through the induction of a series of allosteric changes in its structure (**Figure I.19**), which eventually promote PARylation and recruitment of various DNA repair effectors to the damage site, and facilitate remodelling of the chromatin structure around the lesion as part of the DNA repair process. In particular, PARP1 mediates the rapid recruitment of X-ray repair cross-complementing protein 1 (XRCC1) to SSBs, a core factor in SSB repair which acts as a scaffold for a number of SSB repair proteins. At the end of the repair process, PARP1 auto-PARylates itself, which causes its release from repaired DNA. PARP1 also plays a major role in the remodelling of chromatin within the nucleotide excision repair (NER) pathway, which mediates repair of bulky DNA lesions that arise from exposure to mutagenic agents such as platinum salts (350). The involvement of PARP1 in other DNA repair processes such as HR or non-homologous end joining (NHEJ) has also been evidenced, demonstrating the predominant and ubiquitous functions of this protein in the DDR.

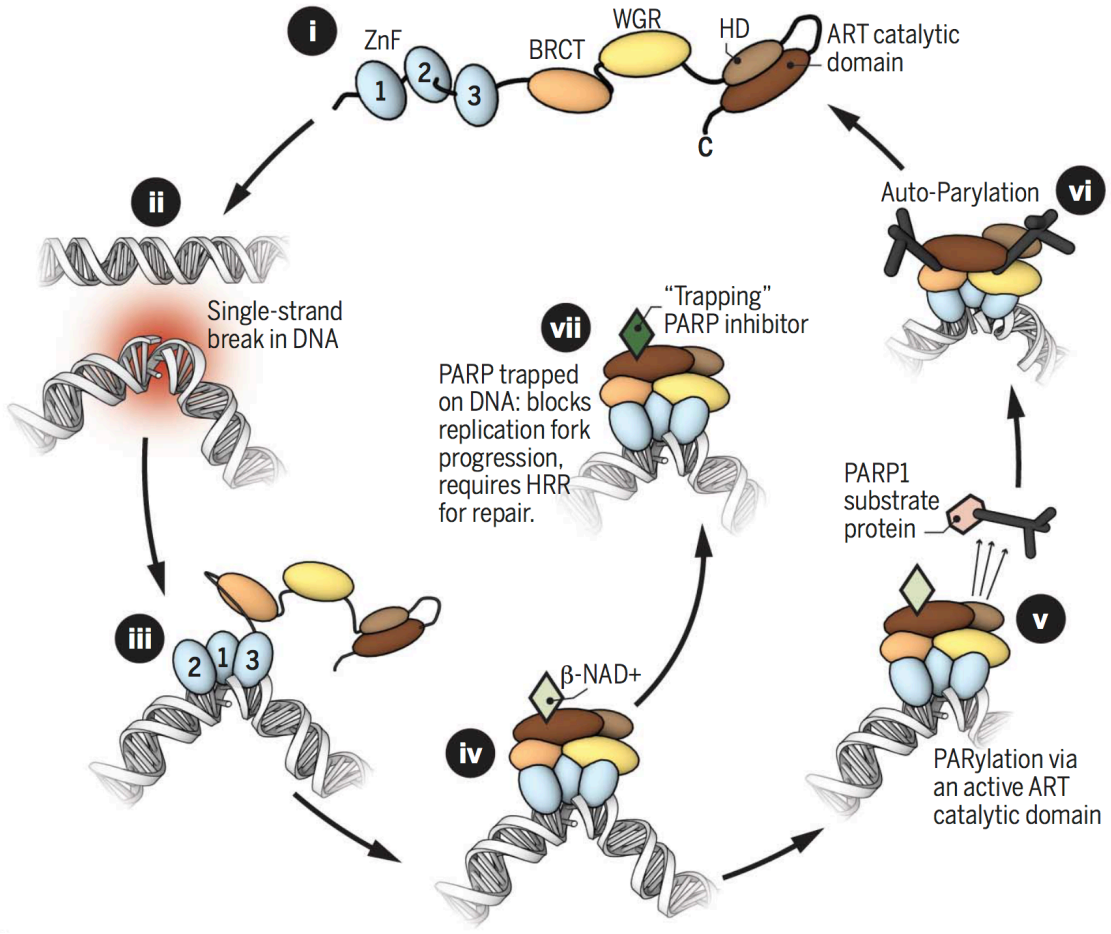

Figure I.19. A model describing PARP1 catalytic cycle.
(i) In its non-DNA bound state, PARP1 exists in a relatively disordered conformation, commonly referred to as "beads on a string". The domain structure of PARP1 includes three zinc finger–related domains (ZnF 1, 2, and 3): the BRCA1 C-terminus domain (BRCT), the tryptophan-, glycine-, arginine-rich domain (WGR), and the catalytic domain, which encompasses two subdomains, a helical domain (HD) and an ADP-ribosyltransferase (ART) catalytic domain. In this non-DNA bound state, HD acts as an auto-inhibitory domain preventing binding of the PARP-superfamily cofactor, β-NAD+, to its ART binding site. **(ii)** DNA damage often causes the formation of SSBs, which induces a change in the normal orientation of the double helix. **(iii)** In turn, this provides a binding site for DNA binding PARP1 ZnF domains. **(iv)** The interaction of ZnF 1, 2, and 3 with DNA initiates a stepwise assembly of the remaining PARP1 protein domains onto the PARP1/DNA nucleoprotein structure, which leads to a change in HD conformation and resultant loss of its auto-inhibitory function, and allosterically activates PARP1 catalytic activity. **(v)** ART catalytic activity drives the PARylation of PARP1 substrate proteins, mediating the recruitment of DNA repair and chromatin remodelling effectors. **(vi)** PARP1 auto-PARylation finally causes its release from DNA and the restoration of a catalytically inactive state. **(vii)** Several clinical PARPi, each of which binds the catalytic site, prevent the release of PARP1 from DNA: this "trapping" of PARP1 at the site of damage removes PARP1 from its normal catalytic cycle.
Figure and legend adapted from Lord et al., Science, 2017.

The understanding that PARP1 functions as a key mediator of DNA repair processes has led to the development of small-molecule inhibitors targeting PARP1 and its paralogs (351). The original rationale was that PARPi could sensitize tumours to conventional DNA-damaging agents, including various chemotherapy and radiotherapy regimens, by inhibiting PARP1-mediated repair of DNA lesions generated by these agents. Following the observation that small-molecule nicotinamide analogs inhibit PARylation and enhance the cytotoxicity of DNA-damaging agents such as dimethyl sulfate (352), several clinical PARPi were developed (**Figure I.20**), including the first generation inhibitors veliparib (ABT-888, Abbvie), rucaparib (Rubraca®, Clovis), olaparib (Lynparza®, AstraZeneca) and niraparib (Zejula®, Tesaro), and the second generation inhibitor talazoparib (Talzenna®, Pfizer), which exerts more potent activity. But the full clinical potential of PARPi was only revealed in 2005, when two research groups demonstrated the synthetic lethal interaction between PARP inhibition and loss of *BRCA1* or *BRCA2* function, suggesting for the first time a novel therapeutic strategy for treating patients that carry deleterious mutations in these tumour suppressor genes (353,354).

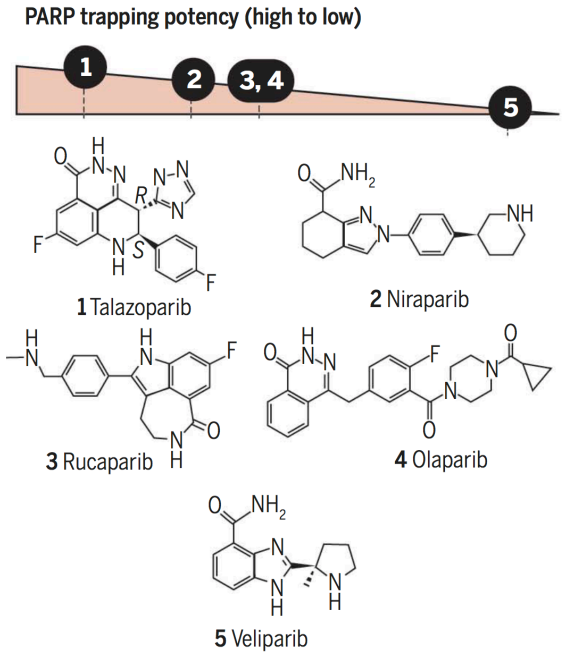

Figure I.20. Clinical PARP inhibitors.
Chemical structures of five clinical PARPi are shown. The ability of each PARPi to trap PARP1 on DNA differs (talazoparib being the most potent PARP1 trapping inhibitor, veliparib being the least potent) and broadly correlates with cytotoxic potency.
Figure and legend adapted from Lord et al., Science, 2017.

Both BRCA1 and BRCA2 are critical mediators of HR, a conservative DDR pathway that uses homologous DNA sequences to guide repair of DSBs. Mutations in either of these proteins impair HR and result in the preferential use of error-prone repair mechanisms – such as NHEJ – to repair DSBs, which promotes mutagenesis and tumour progression. Germline *BRCA1/2* defects are frequent alterations found in 5-10% of TNBC and 15-35% of HGSOC (**Table I.3**), thus forming an important distinct molecular subtype of patients. Synthetic lethality refers to the situation whereby a defect in either one of two genes has little effect on cell fitness, but a combination of defects in both genes results in cell death (349). Initially, the proposed mechanism for explaining PARP/BRCA synthetic lethality was that PARPi promote the persistence of SSBs, which, when encountered by a replication fork, sometimes result in collapse of the fork and subsequent formation of DSBs (353). Left unrepaired in the context of HR dysfunction, these DSBs accumulate in the genome and eventually trigger tumour cell death. Later, this model was completed by the idea that some PARPi promote PARP1 "trapping" on DNA by preventing auto-PARylation and subsequent PARP1 release from the damage sites, thus resulting in the formation of cytotoxic lesions that enhance the accumulation of collapsed replication forks and consequent DSBs (355,356). Clinical PARPi differ in their PARP trapping potential, talazoparib being approximately 100 times more potent than niraparib in trapping PARP1, which in turns is more potent than olaparib and rucaparib in this respect (349) (**Figure I.20**).

Discovery of the PARP/BRCA synthetic lethality and demonstration that *BRCA*-mutant tumour cells are highly sensitive to PARPi provided the biological rationale for testing PARPi as single-agents in *BRCA*-deficient populations. Data from the first phase I clinical trial evaluating olaparib, which was enriched in patients with germline *BRCA1/2* mutations showed impressive ORR and observed clinical benefit for a majority of patients, thus validating the clinical applicability of the concept of synthetic lethality (357). Subsequently, phase II clinical trials involving *BRCA*-mutant patients in breast, ovarian, pancreatic or prostate cancers confirmed the clinical benefit offered by olaparib (358–360), and led to its approval by the U.S. Food and Drug Administration (FDA) for treatment of patients with germline *BRCA*-mutant advanced ovarian cancer in 2014. In 2018, a randomized phase III clinical trial evaluating olaparib in monotherapy for germline *BRCA*-mutant HER2-negative

breast cancer patients demonstrated a significant benefit over standard therapy (361), leading to the FDA approval of Lynparza® for treatment of this disease.

In the meantime, other synthetic lethal interactions involving PARP inhibition have been discovered, starting with the demonstration that deficiencies in a number of tumour suppressor genes involved in HR, such as *ATM, ATR, PALB2*, *RAD51* and the *FANC* gene family confer sensitivity to PARPi (362,363). Importantly, large-scale cancer genome sequencing projects have established that HR defects occur in a wide range of tumour types, suggesting that a number of HR-deficient cancers could benefit from PARPi (349). Sensitivity to PARPi has also been evidenced in the context of other DDR defects such as excision-repair cross-complementation group 1 (ERCC1) deficiency (364), a frequent DDR alteration in NSCLC (**Table I.3**). ERCC1 is an essential component of the NER pathway, which mediates the excision of bulky adducts caused by platinum salts and other mutagenic agents, thus allowing repair of these lesions by other NER proteins (208). Interestingly, ERCC1 is also thought to be involved in the excision of PARP trapping lesions; it has thus been suggested that in the absence of ERCC1, trapped-PARP1 lesions that generate DSBs cannot be adequately excised, which prevents their processing through HR, and eventually causes cell death (364). Given the high frequency of ERCC1 deficiency in NSCLC, this DDR defect represents a potential therapeutic target for PARPi in this histology, and clinical trials evaluating olaparib in patients with platinum-sensitive advanced NSCLC are currently testing this opportunity (NCT02679963). Finally, defects in other components of the DDR, such as the chromatin remodelling complex SWI/SNF have been associated with sensitivity to PARPi: in particular, *ARID1A*, a tumour suppressor gene mutated in a broad spectrum of human cancers has demonstrated synthetic lethality with PARP inhibition (365).

These recently-described synthetic lethal interactions suggest that the tumour-specific cytotoxic effects of PARPi can be exploited in a variety of molecular contexts, and that their clinical use may be extended to a wide range of cancers, non-restricted to HR-deficient cancers. Alternatively, this has also prompted their clinical assessment in combination with ICI in a number of histologies, including primarily *BRCA*-mutant breast and ovarian cancers, but also NSCLC, HNSCC, mCRPC, CRC, gastric carcinomas and other advanced solid tumours (309).

b. PARPi plus ICI: a beneficial combination?

Along with their well-established functions in DNA repair, a wide immunological role has been attributed to PARP enzymes. In particular, PARP1 has been shown to participate to the development of inflammatory responses, and is thought to be involved in adaptive immunity by directly affecting the differentiation and functions of T cells and B cells (366). In line with these data, it has recently been demonstrated that *PARP1*- and *PARP2*-knockout mice have impaired adaptive immune function due to defective thymocyte maturation with reduced numbers of peripheral CD4+ and CD8+ T cells (367).

Despite this involvement of PARP proteins in immune processes, very little is known about the immunological properties of PARPi. So far, few pre-clinical studies have evaluated the impact of PARP inhibition on the immunological rejection of tumours, and available data only refer to a very restricted histological and molecular context, represented by BRCA1-deficient ovarian cancer models. Huang and colleagues have shown that administration of talazoparib led to increased levels of peritoneal CD8+ T cells and NK cells associated with an enhanced production of IFN-γ and TNF-α in syngeneic *BRCA1*-deficient murine ovarian tumours (368), suggesting the immuno-stimulatory potential of PARP inhibition in this context. Combination of veliparib and anti-CTLA4 therapy in a similar BRCA1-deficient ovarian cancer model resulted in immune-mediated tumour clearance and long-term survival in a majority of mice (369). The efficacy of this combination was T cell-mediated and dependent on the increased production of IFN-γ in the peritoneal tumour environment. Interestingly, another study evaluating the combination of rucaparib plus anti-PD-(L)1 therapy in *BRCA1/2*-mutant and -wildtype syngeneic ovarian cancer models revealed that treatment efficacy could only be achieved in the *BRCA1/2*-mutant model, suggesting that the anti-tumour activity of this combination was BRCA-dependent (370).

An increased number of clinical trials have been initiated over the past years to evaluate the safety and efficacy of combined PARPi plus anti-PD-(L)1 therapy in both DNA repair-deficient and -proficient settings (303,309). Preliminary results from the phase II basket study MEDIOLA (NCT02734004), evaluating olaparib plus durvalumab with a PARPi monotherapy priming phase schedule, suggested a strong activity of the combination in

the germline *BRCA*-mutated, platinum-sensitive relapsed ovarian cancer cohort (72% ORR; 95% CI, 53.0 to 86.0) (371). Moreover, the elevated 12-week durable clinical response rate obtained in the *BRCA*-mutated metastatic breast cancer cohort suggested that the administration of durvalumab may enhance the efficacy of olaparib monotherapy in *BRCA*-mutated patients (372). Interestingly, baseline PD-L1 expression and TILs levels did not appear to correlate with clinical outcomes in these two cohorts. Further, preliminary data from the biomarker analysis of a limited number of patients in the small cell lung cancer (SCLC) cohort suggested that olaparib monotherapy resulted in a modest reduction in circulating immune cells, and could conversely increase levels of TILs (373). These results show promising efficacy of PARPi plus anti-PD-(L)1 combination in germline *BRCA*-mutated patients, and further support the hypothesis of an immunomodulatory potential of PARPi.

Further pre-clinical studies are now needed to properly define the molecular processes by which PARPi may enhance anti-tumour immune responses and to understand how these DNA repair-targeted therapies may affect sensitivity to ICI. This will eventually provide a scientific rationale for the combination of PARPi with ICI in upcoming clinical trials.

F. Aims and approaches

PARPi are among the most promising adjuvant therapies that may increase the clinical efficacy of ICI, for the following reasons: (i) as DNA repair-targeted therapies, they constitute an interesting alternative to conventional chemotherapy, carrying a putative potential to stimulate tumour immunogenicity through increased genomic instability while having less immunosuppressive effects; (ii) they can be easily integrated into new clinical protocols as several PARPi are currently licensed or in advanced clinical development (iii) few, but several pre-clinical studies have demonstrated their anti-tumour potential in combination with ICI, and preliminary clinical data show promising efficacy of this strategy.

Notwithstanding the recent growing interest for using PARPi as immunomodulatory agents, there is a very little understanding of the immunological effects of PARPi. In a context where

an increasing number of combination trials with ICI are initiated, it is urgent to properly investigate the immunomodulatory potential of PARPi in relevant pre-clinical models.

In this thesis, we evaluated the potential of PARPi to elicit tumour-intrinsic immunity in various DDR-deficient and -proficient models. Overall, the following aims were pursued:

Aim 1: Characterize the effects of ERCC1 deficiency on the modulation of immunological signalling in NSCLC cells. (Chapter III)

Loss of ERCC1 is a frequent DDR abnormality in NSCLC. It confers sensitivity to platinum-based therapy (374) and PARPi (364), and therefore represents an attractive candidate for harnessing immune activation in this disease – where ICI have shown unprecedented efficacy. Our first aim was to characterize the immunological impact of ERCC1 deficiency in NSCLC cells, through the assessment of transcriptional differences in a unique in-house isogenic cellular model of ERCC1-deficient NSCLC.

Aim 2: Evaluate the cell-autonomous immunomodulatory potential of PARPi in ERCC1-deficient NSCLC cells and *BRCA1*-mutant TNBC cells. (Chapter IV and V)

PARPi selectively target cancer cells with DDR deficiencies such as those caused by *BRCA1* mutations or ERCC1 defect (349). Our second aim was to test whether PARPi can selectively trigger cancer cell-autonomous immune phenotypes in DDR-deficient cells; we notably assessed the activation the cGAS/STING pathway, and the induction of specific cellular responses such as type I IFN response, cytokine secretion and PD-L1 expression.

Aim 3: Assess the ability of PARPi to generate ICD in NSCLC cells. (Chapter VI)

A number of DNA-damaging agents have been tested for their potential to trigger ICD of cancer cells, and to this aim, specific standardized assays have been developed *in vitro* and *in vivo* (375). PARPi, as potent DDR modulators, are promising candidates for the induction of ICD. Our third aim was thus to evaluate the ICD-inducing potential of PARPi in NSCLC cells, through the detection of the canonical cellular markers of ICD *in vitro*, and through the implementation of vaccination assays *in vivo*.

Chapter II. Materials and Methods

A. Reagents

1. General chemicals and solutions

All chemicals were purchased from Sigma Aldrich unless otherwise stated. Common solutions and buffers were prepared as follows:

- **PBS**: Phosphate-buffered saline – 137nM NaCl, 2 mM KCl, 8mM Na_2HPO_4, 1.5 mM KH_2PO_4 in H_2O, pH adjusted to 7.4 with HCl.
- **Trypsin solution**: Trypsin, 0.25% ethylenediaminetetraacetic acid (EDTA), phenol red (Gibco).
- **Pen-Strep solution**: Sterile-filtered solution of penicillin (10,000 units/mL) and streptomycin (10 mg/mL) in water.
- **DMSO**: Dimethyl-sulfoxide solution.
- **RIPA lysis buffer**: RIPA Lysis and Extraction Buffer (ThermoFisher), 0.5% phenylmethylsulfonyl fluoride (PMSF), 1% Halt™ Protease Inhibitor Cocktail (ThermoFisher).
- **MOPS**: Running buffer for WB – 3-(N-morpholino)propanesulfonic acid (Invitrogen).
- **Transfer buffer**: 14.4 g glycine, 3.03 g tris(hydroxymethyl)aminomethane (TRIS), 200 mL methanol made up to 1 L with water.
- **TRIS**: tris(hydroxymethyl)aminomethane (Invitrogen).
- **10X TBS**: 200 mL TRIS (1 M) pH 7.5, 300 mL NaCl (5 M) made up to 1 L with water.
- **TBS-T**: Washing buffer for WB – 100 mL 10X TBS, 1 mL Tween-20 in 1 L with water.

- **Blocking solution**: 5% bovine serum albumin (BSA) in TBS-T or 5% milk in TBS-T.
- **PFA**: Fixation solution – 4% (v/v) paraformaldehyde solution.
- **IFF**: Incubation buffer for IF – PBS, 2% BSA, 2% foetal bovine serum (FBS) (Life Technologies), filtered through a 0.2 µm filter.
- **Triton solution**: Permeabilization buffer for IF – 0.05% Triton-X 100 in PBS.
- **DAPI**: 4',6-Diamidino-2-Phenylindole, Dihydrochloride (ThermoFisher).
- **PicoGreen®**: 2-(n-bis-(3-dimethylaminopropyl)-amino)-4-(2,3-dihydro-3-methyl-(benzo-1,3-thiazol-2-yl)-methylidene)-1-phenyl-quinolinium (ThermoFisher).
- **PI**: 20 µg/mL propidium iodide solution.

2. Drugs and chemotherapeutics

All compounds were dissolved in 100% DMSO to give 50 mM or 100 mM stock solutions, and subsequently aliquoted and stored at -80°C (**Table II.1**).

Table II.1. Summary of the drugs used in this study.

Drug	Supplier	Reference
Olaparib (AZD-2281)	Selleckchem	S1060
Rucaparib (AG-014699)	Selleckchem	S1098
Veliparib (ABT-888)	Selleckchem	S1004
Talazoparib (BMN-673)	Selleckchem	S7048
Niraparib (MK-4827)	MedChem Express	HY-10619
RO-3306	Selleckchem	S7747
Mitoxantrone	Sigma Aldrich	M2305000
Nocodazole	Merck Millipore	#487928
Interferon gamma-1b	Boehringer Ingelheim	#557767-8

3. Antibodies

Primary antibodies are listed in **Table II.2**, **Table II.3**, and **Table II.4**. For western blotting (WB), horseradish peroxidase (HRP)-conjugated secondary antibodies were purchased from Sigma Aldrich and diluted to 1:10000. For immunofluorescence (IF), Alexa Fluor® (AF)-647-conjugated (A21235) and AF-594-conjugated (A11037) secondary antibodies were purchased from ThermoFisher and diluted to 1:1000. For flow cytometry, AF-488-conjugated (A11034) secondary antibody was purchased from ThermoFisher and diluted to 1:300.

Table II.2. Summary of antibodies used for WB and IF in this study.

Target	Species	Dilution	Supplier	Reference
β-tubulin	Mouse	1:20000	Sigma Aldrich	T8328
α-tubulin	Mouse	1:2000	Abcam	ab7291
β-actin	Mouse	1:20000	Sigma Aldrich	A1978
Lamin B1	Rabbit	1:2000	Abcam	ab16048
peIF2α	Rabbit	1:1000	Cell Signalling	#3398
eIF2α	Rabbit	1:1000	Cell Signalling	#5324
LC3B	Rabbit	1:1000	Novus Bio	NB100-2220
cGAS	Rabbit	1:1000	Cell Signalling	#15102
STING	Rabbit	1:1000	Cell Signalling	#13647
pTBK1	Rabbit	1:1000	Cell Signalling	#5483
TBK1	Rabbit	1:1000	Cell Signalling	#3013
pIRF3	Rabbit	1:1000	Abcam	ab76493
IRF3	Rabbit	1:1000	Abcam	ab76409
pIRF7	Rabbit	1:1000	Cell Signalling	#12390
IRF7	Rabbit	1:1000	Cell Signalling	#4920
pNF-κB p65	Rabbit	1:1000	Cell Signalling	#3033
NF-κB p65	Rabbit	1:1000	Cell Signalling	#8242
ERCC1	Mouse	1:200	Santa Cruz	sc-17809
Histone H3	Mouse	1:1000	Abcam	ab1791
H3K9me3	Mouse	1:200	Abcam	ab6002

Target	Species	Dilution	Supplier	Reference
RIG-1	Rabbit	1:1000	Cell Signalling	#3743
MDA5	Rabbit	1:1000	Cell Signalling	#5321
IFI16	Mouse	1:200	Santa Cruz	sc-8023
TLR9	Rabbit	1:1000	Cell Signalling	#13674
TRIF	Rabbit	1:1000	Cell Signalling	#4596
TRAF3	Rabbit	1:1000	Cell Signalling	#4729
TRAF6	Rabbit	1:1000	Cell Signalling	#8028
PD-L1	Rabbit	1:1000	Cell Signalling	#13684
pSTAT1	Rabbit	1:1000	Cell Signalling	#9167
STAT1	Rabbit	1:1000	Cell Signalling	#9172

Table II.3. Summary of antibodies used for IHC and ICC in this study.

Target	Species	Dilution	Supplier	Reference
CALR	Mouse	1:200	Abcam	ab22683
LC3B	Mouse	1:40	Nanotools	#0231-100
HMGB1	Rabbit	1:100	ThermoFisher	PA1-16926
ERCC1	Rabbit	1:1000	Spring Biosciences	M3680
PD-L1	Rabbit	1:200	Cell Signalling	#13684
PAR	Mouse	1:200	Merck Millipore	MABC547
PARP1	Mouse	1:200	BioRad	MCA1522G

Table II.4. Summary of antibodies used for flow cytometry in this study.

Target	Dilution	Supplier	Reference
APC-conjugated PD-L1	5 µL/test	Biolegend	#329708
APC-conjugated PD-L1 isotype	5 µL/test	Biolegend	#400322
FITC-conjugated HLA-ABC	20 µL/test	BD Biosciences	#557348
FITC-conjugated HLA-ABC isotype	20 µL/test	BD Biosciences	#551954
BV421-conjugated TLR4	5 µL/test	BD Biosciences	#564401
BV421-conjugated TLR4 isotype	5 µL/test	BD Biosciences	#562438
CALR	1:100	Abcam	ab2907

4. siRNA oligonucleotides

siRNA oligonucleotides were purchased from Dharmacon or Qiagen and were supplied 2'ACE protected and lyophilized (**Table II.5**). These were reconstituted to 10 µM in RNAase-free water, aliquoted and stored at -20°C. The non-targeting siRNA negative control siCTRL was used in this thesis and is known not to target any human gene.

Table II.5. Summary of the siRNAs used in this study.

siRNA	Type	Supplier	Reference
siCTRL	Non-targeting	Qiagen	#1022076
siPLK1	SMARTpool	Dharmacon	L-003290-00-0005
siSTING	SMARTpool	Dharmacon	L-024333-02-0005
sicGAS	SMARTpool	Dharmacon	L-015607-02-0005
siTBK1	SMARTpool	Dharmacon	L-003788-00-0005
siIRF3	SMARTpool	Dharmacon	L-006875-00-0005

5. RT-qPCR probes

Probes for reverse transcription quantitative PCR (RT-qPCR) were purchased from ThermoFisher (**Table II.6**).

Table II.6. Summary of the RT-qPCR probes used in this study.

Probe	Fluorophore	Supplier	Reference
GAPDH	FAM	ThermoFisher	Hs03929097_g1
CCL5	FAM	ThermoFisher	Hs00982282_m1
IFNB1	FAM	ThermoFisher	Hs01077958_s1
PD-L1	FAM	ThermoFisher	Hs00204257_m1

B. Biological material

1. Tumour cell lines

SUM149, A549, H1975 and CT26 cells were obtained from ATCC. The generation of SUM149-BRCA1$_{rev}$ and SUM149-PARP1$^{-/-}$ secondary mutant cell lines was performed using CRISPR-Cas9 site directed mutagenesis, as previously described (376,377). The secondary mutant cell lines A549-ERCC1$^{-/-}$ and H1975-ERCC1$^{-/-}$ were generated using zinc finger nuclease gene targeting, as described previously (378). SUM149 cells were cultured in Ham's F12 nutrient mixture (Gibco) with 10% foetal bovine serum (FBS, Gibco), 1 µg/mL insulin (Sigma Aldrich), 500 ng/mL hydrocortisone (Sigma Aldrich) and Pen-Strep. A549 cells were cultured in high-glucose Dulbecco's Modified Eagle's Medium (DMEM, Gibco) with 10% FBS and Pen-Strep. H1975 and CT26 cells were cultured in Roswell Park Memorial Institute 1640 (RPMI-1640, Gibco) medium with 10% FBS and Pen-Strep.

2. Fresh pleural effusion samples

Pleural effusion samples from NSCLC patients were collected at Gustave Roussy with informed written consent, in accordance with the Helsinki Declaration 1964 and its later amendments or comparable ethical standards. For each sample, the pleural fluid was centrifuged for 10 min at 400 g and cell pellets were resuspended in 30 mL PBS. In order to isolate mononucleated cells, the cell suspension was subjected to a density gradient centrifugation (20 min at 400g in a swinging-bucket rotor without brake) using Ficoll-Hypaque reagent (GE Healthcare). The mononuclear cell layer was carefully collected from the centrifugation tube and thoroughly washed with PBS. Cells were then washed twice with 100% FBS and subsequently cultured in 6-well plates at a density of 200,000 cells per well with RPMI-1640 medium containing 20% FBS and Pen-Strep.

3. Archival tumour samples

Archival tumour samples from two independent cohorts of resected NSCLC patients were used: (i) a series of 55 human tumour samples derived from resected stage I/II/IIIA lung adenocarcinoma patients; and (ii) a series of 49 human tumour samples derived from resected stage I/II NSCLC (invasive adenocarcinomas and squamous cell carcinomas) patients.

C. Protocols

1. Tissue culture

All cell culture procedures were carried out under sterile conditions in a tissue culture hood. Cells were grown under physiological conditions at 37°C and 5% CO_2 in their respective media. Cells were allowed to reach 80% confluency before passaging as follows: media was aspirated and cells were washed once with sterile PBS; cells detachment took place by incubation at 37°C with a covering volume of trypsin solution. Trypsin was neutralized by resuspending cells in growth media containing FBS and seeded into a new flask. To count cells, resuspended cells were thoroughly mixed by pipetting to generate a single cell suspension, and 10 µL of cells were diluted in 10 µL trypan blue solution (ThermoFisher) for counting using a Countess™ II automated cell counter (Invitrogen). Frozen cell stocks were maintained in liquid nitrogen storage in freezing media (90% FBS, 10% DMSO). All cell lines were short tandem repeat typed (STR typed) using StemElite ID (Promega) to confirm identity prior to the study, and verified for mycoplasma contamination every 2 months using MycoAlert (Lonza).

2. RNAi and transfections

All siRNA silencing experiments were performed using a pre-designed ON-TARGETplus SMARTpool (Dharmacon) of four distinct siRNA species targeting different sequences of

the target transcripts. Forward transfections were performed in 6-well plates; cells were plated at a density of 250,000 cells per well and transfected 24 h after seeding using RNAiMAX transfection reagent (ThermoFisher). Briefly, culture medium was removed and 1.75 mL of fresh medium was added to each well with 250 µL of transfection mix. The transfection mix was prepared by incubating 125 µL serum-free Opti-MEM medium (Gibco) with 7.5 µL of RNAiMAX for 5 min as per manufacturer's instructions. This was then mixed with an additional 125 µL of serum-free Opti-MEM medium containing 2.5 µL of siRNA (concentration 10 µM) and incubated for 20 min at room temperature. The prepared transfection mix was then added to the cells and replaced by fresh culture medium 24 h post transfection.

Transfection efficacy was assessed through concomitant but independent transfection of cells with PLK1 siRNA, which produced more than 95% cell growth inhibition. Validation of siRNA target inhibition was performed via WB from pools of concomitantly transfected cells.

3. Short-term drug survival assays

Short-term survival assays were performed in 96-well plates. Exponentially growing cells were plated at a concentration of 1000 cells/well in 150 µL. 24 h after seeding, culture medium was removed and 120 µL of fresh medium was added to each well. 30 µL of vehicle (DMSO) or drug dilutions in medium were added at a five times concentration to the cells to make a total volume of 150 µL. Cells were then continuously exposed to the drug for 5 days, after which cell viability was estimated using CellTiter-Glo® luminescence (Promega). Medium was removed from each well and 50 µL of CellTiter-Glo® reagent (diluted 1:4 with PBS) was added; the plate was shaken for 10 min at room temperature according to the manufacturer's protocol, and luminescence was subsequently measured on a Victor X5 multilabel plate reader (PerkinElmer). Cell viability was calculated as survival fractions compared to the DMSO-treated control, and survival curves were plotted.

4. Protein manipulation

a. Whole-cell protein extraction

Whole-cell protein extracts were prepared from cells lysed in RIPA lysis and extraction buffer (ThermoFisher) supplemented with 0.5% PMSF and 1% Halt™ Protease and Phosphatase Inhibitor Cocktail (ThermoFisher). All lysates were generated on ice, and centrifuged 10min at 16,900 g prior to supernatant collection. Protein concentrations were estimated using Pierce™ BCA Protein Assay Kit (ThermoFisher).

b. Subcellular protein fractionation

Extraction of subcellular proteins was performed using the Cell Fractionation Kit (Cell Signalling) as per manufacturer's protocol. The whole procedure was performed on ice. This allowed the isolation of three distinct cellular fractions: (i) a cytoplasmic fraction, (ii) a membrane/organelle fraction, and (iii) a nuclear/cytoskeletal fraction. In each fraction, protein concentrations were estimated using the Pierce™ BCA Protein Assay Kit (ThermoFisher).

c. Western blot

For WB, 50-80 µg of proteins from cell lysates were subjected to electrophoresis using NuPAGE™ 4-12% Bis-Tris precast gels (Invitrogen) and MOPS running buffer, with PageRuler™ Prestained Protein Ladder (ThermoFisher) as molecular weight marker. After migration, proteins were transferred to a nitrocellulose membrane (GE Healthcare) and 5% BSA in TBS-T was used to block the membranes, at room temperature for 1 h. Primary antibodies were diluted in 5% BSA in TBS-T, and incubated at 4°C overnight. The next day, membranes were washed three times with TBS-T, each for 10 min, followed by incubation with HRP-conjugated secondary antibodies at room temperature for 1 h, in 5% milk in TBS-T. Membranes were washed again three times with TBS-T, and incubated with Amersham ECL Prime Detection Reagent (GE Healthcare) or SuperSignal™ West Dura Extended Duration Substrate (ThermoFisher) for chemiluminescent visualization of protein

bands. Membranes were developed using X-ray films or digital imaging on a high-resolution charge-coupled device (CCD) Chemidoc™ XRS+ Imaging System (BioRad).

5. RNA manipulation

a. *RNA extraction*

Total RNA from cells was extracted using the RNeasy mini kit (Qiagen) according to manufacturer's instructions. RNA concentration and quality was measured using a NanoDrop™ 2000 spectrophotometer (ThermoFisher).

b. *RT-qPCR and gene expression measurements*

RNA was diluted to equal concentrations across all samples. Reverse transcription was performed using a SuperScript® VILO™ cDNA Synthesis Kit (Invitrogen), as per manufacturer's instructions. Assay-on-demand primer/probe sets were purchased from Applied Biosystems. qPCR were performed using a QuantStudio 6 Flex Real-Time PCR system with TaqMan™ Fast Advanced master mix (ThermoFisher). The following primer/probe sets were used for RT-qPCR: IFNB1 TaqMan® gene expression assay (Hs01077958_s1), CCL5 TaqMan® gene expression assay (Hs00982282_m1), CD274 TaqMan® gene expression assay (Hs00204257_m1) and GAPDH TaqMan® gene expression assay (Hs03929097_g1). Gene expression was calculated relative to expression of *GAPDH* endogenous controls, and normalized to expression in cells exposed to vehicle (DMSO), using the following formulas:

$$\boldsymbol{\Delta Ct = Ct(gene) - Ct(GAPDH)}$$

$$\boldsymbol{\Delta(\Delta Ct) = \Delta Ct(condition) - \Delta Ct(vehicle)}$$

$$\boldsymbol{Expression\ fold\ change = 2^{-\Delta(\Delta Ct)}}$$

where $\boldsymbol{Ct}$ represents the cycle threshold, which indicates the number of PCR cycles required for fluorescence to reach a defined threshold (i.e. above background level).

6. Immunofluorescence and image analysis

IF assays were performed in high-binding black 96-well plates (Greiner Bio-One). Cells were plated at relatively high density (6,000-10,000 cells per well) and exposed to the drugs the following day. After drug exposure, cells were fixed in 4% PFA for 20 min at room temperature, washed twice with PBS, and permeabilized with 0.5% Triton X-100 for 10 min. After two additional washes, cells were blocked with IFF for 1 h at room temperature. Fixed cells were then incubated with primary antibodies in IFF at 4°C overnight. The cells were then washed three times with PBS, each for 10 min, followed by incubation with AF-594-conjugated rabbit and AF-647-conjugated mouse secondary antibodies (ThermoFisher), 1 µg/ml DAPI and 1:400 PicoGreen® (ThermoFisher) in IFF for 1 h at room temperature. After that, cells were washed again three times with PBS, and 100 µL PBS was finally added to each well prior to imaging. Plates were imaged using an Operetta High-Content Imaging System (PerkinElmer). Quantification of the number of CCF, micronuclei, and cGAS foci was performed under identical microscopy settings between samples, using the Columbus image analysis system (PerkinElmer). 25 randomly selected fields containing over 200 cells were analysed within three individual replicates for each sample.

Micronuclei and CCF were distinguished based on staining intensity as per manufacturer's specifications. A micronucleus was defined as a small region of the image having a Picogreen staining intensity > 20% higher than the surrounding cytoplasm; CCF were defined as small regions displaying higher intensity than the surrounding cytoplasm but at an intensity around the sensitivity threshold (i.e. lower than the micronuclei threshold). CCF were identified after the application of (i) a background correction and (ii) a splitting coefficient (to enable the separation of connected foci).

7. Flow cytometry analyses

For flow cytometry applications, cells were plated in 6-well plates at a density of 200,000 to 250,000 cells per well, and exposed to the dugs the following day. After drug exposure, culture supernatants were removed, cells were detached using Versene solution

(ThermoFisher) and cell suspensions were transferred to round-bottom fluorescence-activated cell sorter (FACS) tubes. For detection of CALR exposure and cell death assays, culture supernatants were systematically collected and transferred to the corresponding FACS tubes to allow analysis of dying/dead cells.

- **Direct flow cytometry stainings**: FACS tubes containing the previously collected cell suspensions were centrifuged for 5 min at 500 g. Cell pellets were washed with PBS and incubated at 4°C for 30 min with fluorescently-conjugated antibodies, diluted in 5% BSA in PBS. After centrifugation, the supernatants were removed, and cells were washed twice with PBS. Cells were finally diluted in 250 µL PBS containing 1 µg/ml propidium iodide (PI) prior to analysis. Cell-surface expression of HLA-ABC, PD-L1 or TLR-4 was analysed by flow cytometry on an LSR-II flow cytometer (BD Biosciences) operated by BD FACSDiva™ software. PI was used as a viability marker.

- **Indirect flow cytometry staining of CALR**: All steps of this procedure were performed at 4°C. FACS tubes containing the previously collected cell suspensions were centrifuged for 5 min at 500 g. Cell pellets were washed once with 100% FBS, and a second time with PBS, pH7.4. Cells were then incubated at 4°C for 30 min with anti-CALR primary antibody, diluted in 3% FBS in PBS, pH7.4. After centrifugation, the supernatants were removed, and cell pellets were washed with PBS, pH7.4. Cells were subsequently incubated at 4°C for 30 min with AF-488-conjugated secondary antibody, diluted in 3% FBS in PBS, pH7.4. After centrifugation, the supernatants were removed, and cell pellets were washed again twice with PBS, pH7.4. Cells were finally diluted in 250 µL PBS pH7.4 containing 1 µg/ml PI prior to analysis. Cell-surface exposure of CALR was analysed by flow cytometry on an LSR-II flow cytometer (BD Biosciences) operated by BD FACSDiva™ software. PI was used as a viability marker.

- **Cell death and membrane permeability assays**: Apoptotic cell death was monitored by virtue of phosphatidyl-serine (PS) exposure and the uptake of the vital dye 7-aminoactinomycin D (7-AAD). To detect PS exposure and membrane permeabilization, Annexin-V/7-AAD co-staining was performed on the previously

collected cells using the PE Annexin-V Apoptosis Detection Kit (BD Biosciences), as per manufacturer's instructions. Cytofluorometric analyses were carried out on an LSR-II flow cytometer (BD Biosciences) operated by BD FACSDiva™ software.

For all flow cytometry experiments, data analysis was performed using the FlowJo software package.

8. ELISA detection

Detection of secreted cytokines and immunomodulatory molecules in cell supernatants was performed through ELISA detection. Cells were plated in 6-well plates at a density of 200,000 to 250,000 cells per well, and exposed to the dugs in a reduced volume of culture medium (usually 1 mL) the following day. For CCL5 and IFN-β detection, culture media were collected after 72 h of drug exposure; for HMGB1 detection, culture media were collected after 48 h of drug exposure. Cell numbers were counted for normalization at the time of supernatants collection. The media were dispensed in 96-well V-bottomed plates and centrifuged at 500 g for 5 min to pellet cells and debris. The resulting supernatants were used for ELISA detection with the following kits: Human CCL5 ELISA MAX™ Deluxe kit (Biolegend); Human IFN-β ELISA kit (PBL Assay Science); HMGB1 ELISA kit (IBL International). Assays were performed in four technical replicates following the manufacturers' protocols. Absorbance was evaluated using a Victor multilabel plate reader (PerkinElmer). Protein concentration was calculated using the equation of a standard curve established from the known concentration values and measured absorbance of concomitantly assayed standard samples.

9. ATP secretion assays

Cells were plated in 24-well plates at a density of 60,000 to 80,000 cells per well, and exposed to the dugs the following day.

- **Extracellular ATP detection**: Culture supernatants were collected after 48 h of drug exposure, and cell numbers were counted for normalization. The media were dispensed in 96-well V-bottomed plates and centrifuged at 500 g for 5 min and 4°C to pellet cells and debris. Supernatants were collected and extracellular ATP levels were measured by the luciferin-based ENLITEN ATP Assay kit (Promega), as per manufacturer's protocol. ATP-driven chemoluminescence was recorded on a Victor X5 multilabel plate reader (PerkinElmer).

- **Intracellular ATP detection**: Cells were lysed in Nucleotide Releasing Buffer (Merck Millipore) and plates immediately placed on ice. The lysates were transferred to 1.5 mL tubes and centrifuged at 16,900 g for 5 min and 4°C to pellet cellular debris. Supernatants were collected and intracellular ATP levels were measured by the luciferin-based ATP assay kit (Merck Millipore), as per manufacturer's protocol. ATP-driven chemoluminescence was recorded on a Victor X5 multilabel plate reader (PerkinElmer).

10. Immunohistochemistry and pathological scoring

Archival samples from resected NSCLC (invasive adenocarcinomas and squamous cell carcinomas) were used. For each patient sample, a single representative formalin-fixed paraffin embedded (FFPE) block was selected for the study. FFPE blocks were sectioned (4 µm thick) on a RM2245 microtome (Leica Biosystems) and placed onto histological Polysine™ microscope adhesion slides (ThermoFisher).

- **Manual immunohistochemistry (IHC) stainings**: For PAR, PARP1 and ERCC1 stainings, tissue sections were deparaffinized in xylene rehydrated by incubation in serial ethanol baths (95%, 70%, 50%, 30%, v/v in PBS, 2 min per bath). Epitope retrieval was performed through incubation in 10 mM citrate buffer (pH6.0 or pH7.3) for 30 to 40 min. Endogenous peroxidase activity was inhibited by treatment with peroxidase blocking reagent (Dako). Unspecific binding sites were then blocked for 10 min with protein block reagent (Dako) and the slides were incubated for 1 h at

room temperature with anti-PAR, anti-PARP1 or anti-ERCC1 primary antibodies. After three washes in PBS, the slides were incubated for 30 min at room temperature with Vectastain Universal Elite ABC secondary antibody (Vector Laboratories Inc.), and subsequently revealed by the streptavidin-biotin-peroxidase complex method with 3,3′-diaminobenzidine tetrahydrochloride (DAB) as chromogenic substrate.

- **Automated IHC staining of PD-L1**: Automated IHC was performed using a Ventana Discovery Ultra platform (Ventana Medical Systems). After deparaffinization, and epitope retrieval using CC1 buffer (64 min at 98°C), the slides were incubated with anti-PD-L1 primary antibody during 1 h at room temperature. Detection was performed with the UltraMap DAB detection kit (Ventana Medical Systems).

Following counterstaining with Mayer's haematoxylin (Dako), the slides were mounted with glass coverslips (ThermoFisher) and observed by means of a DM2000 microscope equipped with HC PL Fluotar 20×/0.50 and 40×/0.75 objectives and coupled to a DFC280 CCD camera (Leica Biosystems).

Pathological assessment of ERCC1, PAR, PARP1, and PD-L1 stains as well as evaluation of TILs were performed independently by a senior pathologist. ERCC1 IHC was scored as high or low based on the prominent intensity of staining observed for each case in the nuclei of tumour cells, as previously described (379). Tumours with weak staining (0/1+) were scored as low and tumours with strong staining (2+/3+) were scored as high. PAR and PARP1 expression was evaluated as an H-score (percentage of tumour cells stained multiplied by each intensity from 0 to 3+, value from 0 to 300) as previously described (380). PD-L1 expression was evaluated in tumour cells (membranous staining) and immune cells (cytoplasmic or membranous staining) as performed in PD-L1 complementary and companion assays in NSCLC (381,382). TILs density in stromal areas was evaluated as the percentage of stromal areas covered with mononucleated cells whose morphology correspond to lymphocytes, as previously described in other tumour types (383).

11. Cytoblock preparation and immunocytochemistry

For immunocytochemistry (ICC) applications, cells were seeded in 150 cm^2 flasks at a density of 4,000,000 cells per flask, and exposed to the drugs the following day. After 72 h of drug exposure, cells were detached using Versene solution (ThermoFisher) and cell suspensions were transferred to 15 mL falcon tubes. The tubes were centrifuged for 5 min at 500 g and 4°C, and cell pellets were washed with PBS, pH7.4. After a second round of centrifugation, cell pellets were fixed and stained for 45 min at 4°C in a solution containing 4% PFA and 0.2% eosin. After removal of the fixation solution, cell aggregates were prepared from the pellets using the Shandon™ Cytoblock Cell Block Preparation System (ThemoFisher), as per manusfacturer's instructions, and subsequently transferred into cytoblock cassettes. The cassettes were then placed into a fixative bath (4% PFA solution) until inclusion in paraffin.

Automated ICC was performed using a Ventana Discovery Ultra platform (Ventana Medical Systems). After deparaffinization, and epitope retrieval using CC1 buffer (64 min at 98°C), the slides were incubated with anti-CALR, anti-LC3B or anti-HMGB1 primary antibodies during 1 h at room temperature. Detection was performed with the UltraMap DAB detection kit (Ventana Medical Systems). Following counterstaining with Mayer's haematoxylin (Dako), the slides were mounted with glass coverslips (ThermoFisher) and observed by means of a DM2000 microscope equipped with HC PL Fluotar 20×/0.50 and 40×/0.75 objectives and coupled to a DFC280 CCD camera (Leica Biosystems).

12. Transcriptomic analyses

a. RNA-seq

A549 cells were plated in 6-well plates at a density of 200,000 cells per well, and exposed to the dugs the following day. After 48 h of drug exposure, total RNA from cells was extracted using the RNeasy mini kit (Qiagen). Initial quality control and quantification of the RNA material was performed using Qubit RNA HS Assay kit on a Qubit 2.0 Fluorometer

(Thermo Fisher Scientific). RNA degradation was determined through evaluation of the RIN, using RNA 6000 Pico kit on an Agilent 2100 Bioanalyzer System (Agilent). DNA contamination was then removed using the RNeasy Plus Micro kit (Qiagen). mRNA were isolated using the NEBNext® Poly(A) mRNA magnetic isolation module (New England Biolabs, Ipswich, MA, USA), and library preparation for sequencing was carried out using the NEBNext® Ultra II directional RNA library prep kit for Illumina (New England Biolabs), as per manufacturer's instructions. The completed libraries were then quantified with Tapestation High Sensitivity kit (Agilent) and qPCR using the KAPA Library Quantification kit for Illumina platforms (Kapa Biosystems, Wilmington, MA, USA). The samples were finally clustered using the cBot system (Illumina, San Diego, CA, USA) and sequenced on a HiSeq 2500 platform (Illumina) using a v4 chemistry paired-end flow cell, at 2x100 cycles.

b. RNA-seq data analysis

Bioinformatics analyses of RNA-seq data were performed by Dr. Gareth Muirhead at the Institute of Cancer Research (London).

- **RNA-seq pre-processing**: RNA-seq generated between 22 and 39 million reads per sample (n = 24). FastQC was used to evaluate library quality and were processed using Trim Galore! version 0.4.5 with cutadapt (384) version 1.14 to remove adaptors and trim lower quality reads. Trimmed reads were aligned to the human reference genome (GRCh38) and gene-level counts were quantified using STAR version 2.5.1b (385) in two-pass mode with gene annotations obtained from GENCODE release 22. Post alignment quality control was performed with RseQC (386).

- **RNA-seq differential expression analysis**: Genes with low expression were filtered retaining those with at least 5 counts across 75% of samples. Testing for differential expression was performed using R package edgeR (387) version 3.22.0 with the model ~0 + condition + replicate. Differentially expressed genes were defined as those with a Benjamini-Hocherg adjusted *P*-value of < 0.05 with an absolute $\log_2$ fold-change > 0.58 (approximate to a 1.5 fold change in expression).

- **RNA-seq downstream analysis**: Gene Set Enrichment Analysis (388) was performed with fgsea (389) version 1.4.1 using the c2.cp.reactome.v6.1 gene set obtained from the Broad Institute with the minimum pathway size set to 10. Genes were ranked according to $-\log_{10}$(adjusted p.value) multiplied by the sign of the $\log_2$ fold-change. Significant pathways were defined as those with a Benjamini-Hochberg adjusted *P*-value of < 0.05. The ComBat method implemented in the SVA package (390) version 3.26.0 was used to adjust $\log_2$ transformed counts-per-million (CPM) values for the "replicate" factor in heatmap visualisations. All visualisations were generated in R statistical environment version 3.4.0.

c. Nanostring®

RNA from PDXs tissue sections was extracted using the RNeasy FFPE kit (Qiagen) and quantified with a NanoDrop™ 2000 spectrophotometer (ThermoFisher). The percentage of fragmentation between 50-300 nucleotides length as of the total fragments was evaluated for each sample using Agilent 2100 Bioanalyzer System (Agilent). 80 ng RNA were used per sample for the analysis, and applied to the nCounter® PanCancer Immune Profiling panel (XT-CSO-HIP1-12) on a nCounter® SPRINT Profiler platform (Nanostring).

d. Nanostring® data analysis

Bioinformatics analyses of Nanostring data were performed by Dr. Syed Haider at the Institute of Cancer Research (London).

- **Nanostring pre-processing**: Nanostring profiling of Pancancer immune codeset was pre-processed using R package NanoStringNorm (391) version 1.2.1. Data was assessed for batch effects using R package FactoMineR (392) version 1.39. Raw counts of endogenous genes were normalised using R package edgeR11 version 3.20.9 with TMM method.

- **Nanostring differential expression analysis**: Testing for differential gene expression was performed using R package limma (voom) (393) version 3.34.9 with the model ~0 + condition. Differentially expressed genes were defined as those with

a Benjamini-Hocherg adjusted *P*-value of < 0.1 with an absolute $\log_2$ fold-change > 1. All visualisations were generated in R statistical environment version 3.4.0.

13. TCGA data analyses

Analyses of TCGA data were performed by Dr. Andrew Lamb at Sage Bionetwork (Seattle).

- **Tracking of mutation data from 31 cancer types**: Publically available somatic variant calls in mutation annotation format (MAF) files were retrieved from the TCGA. All MAF files were downloaded from the TCGA data coordinating centre and reprocessed to eliminate known, recurrent false positives and germline single nucleotide polymorphisms (SNP) according to dbSNP database. All variant coordinates were transferred to GRCh38 and re-annotated using the Gencode human transcript annotation imported from Ensembl release 93, following methods described in Shen *et al.* and Kandoth *et al.* (394,395).

- **Pan-cancer analysis**: For ERCC1 mutation rate analysis, we included missense, nonsense, and nonstop mutations, splice site and translation start site mutations, as well as frameshift and in-frame indels. For mutational load analysis, we counted the total number of non-synonymous mutations per tumour.

14. *In vivo* studies

a. *Generation of PDX models*

Breast PDX models were generated at Guy's and St. Thomas's NHS Foundation Trust. Human breast tumour samples were collected with informed written consent, in accordance with the Helsinki Declaration 1964 and its later amendments or comparable ethical standards. Study design was approved by the Guy's Research Ethics Committee, Guy's and St. Thomas's NHS Foundation Trust. Access to pseudo-anonymised samples and

clinical data was obtained in accordance with the principles of the Guy's and St. Thomas' Research Tissue and Data Bank (REC 13/LO/1248).

Female NOD/SCID/Il2rg$^{-/-}$ (NOD.cg-Prkdc SCID Il2rg tm1Wjl/SzJ, NSG) were bred under Material Transfer Agreement (MTA) at King's College London (KCL). Mice were maintained within a barrier facility and handled in accordance with local and international regulations and ethical guidelines and were approved by the KCL Institutional Committees on Animal Welfare and the UK Home Office (The Home Office Animals Scientific Procedures Act 1986).

Briefly, to generate breast PDX models, fresh tumour fragments were surgically implanted orthotopically into the mammary fat pad of female 21-28 day old NSG host mice. If not possible, tumour fragments were cryopreserved before implantation. Once implants were palpable and had grown progressively in size to >10mm diameter, tumour fragments (≈2mm diameter) were cryopreserved between passage and implanted for subsequent passage, again, through orthotropic transplantation of thawed tumour fragments into NSG host mice. This was repeated in further passage to expand tumour material.

b. In vivo *assessment of olaparib immunomodulatory potential*

PDX tumours bearing *BRCA1* germline mutations at passage 3 (BTBC456) and passage 4 (BX102) were implanted through transplantation of viable frozen fragments orthotopically into the mammary fat pad of NSG host mice (female 21-28 day old). Once tumours were palpable and measurable (tumour volume > 50 mm3), hosts were randomized into vehicle and olaparib treatment groups. Technicians were blinded to group status. Vehicle (10% w/v 2-hydroxypropyl-β-cyclodextrin) or olaparib were given daily by oral gavage at 100 mg/kg. Olaparib treatment was suspended if tumours regressed and were no longer palpable (this only occurred in BX102 treatment groups). Mice were weighed once weekly and tumours were measured twice-weekly using calipers. When tumours reached a diameter greater than 12mm in the vehicle group, they were harvested, formalin fixed, and processed for paraffin embedding.

Tumour volume was calculated using the formula:

$$V = \frac{\pi \times L \times W^2}{6}$$

where L is the largest tumour diameter (mm) and W the perpendicular diameter (mm).

c. Evaluation of rucaparib potential to induce ICD in vaccination assays

All vaccination experiments were carried out at Gustave Roussy according to the Federation of European Laboratory Animal Science Association guidelines, and had previously been approved by Gustave Roussy Ethics Committee. All animals were maintained in specific pathogen-free conditions.

A total of $3x10^6$ CT26 cells, pre-treated *in vitro* for 48h with DMSO (vehicle), 2 µM MTX (positive control), or 70 µM/90 µM rucaparib, were inoculated subcutaneously in 200 ml PBS into the lower flank of BALB/c mice (female 6 week old). 7 days later, $5x10^5$ untreated CT26 cells were inoculated into the contralateral flank (277). The appearance of established tumours was monitored every two days by manual palpation at both injection sites. Animals bearing necrotic tumours or tumours exceeding 20–25% body mass were immediately euthanatized.

D. Statistical analyses

1. General statistical analyses

No statistical methods were used to predetermine sample size. The experiments were not randomized, with the exception of PDX experiments. The investigators were not blinded to allocation during experiments and outcome assessment. All bar graphs show mean values with error bars (standard deviation); 95% confidence intervals were used, and significance was considered when * $P < 0.05$, ** $P < 0.01$, *** $P < 0.001$, **** $P < 0.0001$; ns, not significant. Mann-Whitney *U* tests were used to compare two non-parametric datasets; Kruskall-Wallis tests were used to compare multiple (more than two) non-parametric

datasets. Two-way ANOVA was used when comparing more than two datasets defined by two independent variables.

2. Drug dose-response curves

Surviving fractions were calculated for each technical replicate as:

$$\frac{Luminescence\ in\ well\ treated\ with\ drug}{Luminescence\ in\ wells\ treated\ with\ DMSO}$$

Replicate values of surviving fractions were plotted in GraphPad Prism and dose-response curves were drawn using a four-parameter logistic regression. SF50 and SF80 doses were calculated from these curves using GraphPad Prism software. Comparisons of dose-response curves were performed using two-way ANOVA testing. Comparisons of SF50 or SF80 data were performed using Student t tests.

Chapter III. ERCC1 deficiency elicits cancer cell-autonomous immune phenotypes in NSCLC

A. Introduction

NSCLC is the leading cause of cancer-related death worldwide, with 50% of patients presenting with metastatic disease at first diagnosis and less than 20% of patients surviving after 5 years (396). On a molecular level, NSCLC is a diverse disease characterized by genetic alterations – including mutations and translocations – in a number of oncogenes such as *KRAS* (mutated in 5–35% of patients), *EGFR* (5–20%), *ALK* (5–10%), *HER2, BRAF, PIK3CA, MAPK2* and *MET* (all four mutated in <5% of patients) (397), and tumour suppressor genes such as *TP53* (>50%) (398) and *LKB1* (50%) (399). In addition, NSCLC is also characterized by a high genomic instability, associated with elevated TMB, in both smoking-associated and non-smoking-associated tumours (204).

If known oncogenic drivers certainly contribute to the aetiology of NSCLC, DDR defects also represent an important attribute of this cancer, with various DNA repair functions being impaired in a significant proportion of patients due to somatic mutations or reduced expression in DNA repair genes, including *BRCA1*, *ATM*, *MSH2* and *ERCC1* (**Table I.3**). In particular, *ERCC1* deficiency represents the most frequent DDR defect with a prevalence of 22-66% in NSCLC patients (212) and has been defined as an important predictive biomarker of response to platinum-based chemotherapy (374). ERCC1, in complex with Xeroderma Pigmentosum complementation group F (XPF), acts as a structure-specific endonuclease that incises damaged DNA segments, and carries a rate-limiting function in the NER-mediated repair of platinum adducts (212). ERCC1 also plays a predominant role in the repair of DNA inter-strand crosslinks and therefore, low levels of ERCC1 are associated with increased response to cisplatin in NSCLC.

Until recently, platinum-based chemotherapy was the gold standard first-line treatment in NSCLC, and was associated with a median OS of approximately 10–12 months (400). The advent of ICI has brought significant improvements in terms of survival in this aggressive disease, as evidenced by the recent results of large phase III trials evaluating anti-PD-(L)1 agents in first-line therapy. For example, the KeyNote-024 trial comparing pembrolizumab and platinum-based chemotherapy in previously untreated PD-L1-positive NSCLC obtained a median PFS of 10.3 months for pembrolizumab vs 6.0 months for chemotherapy (128). Combination trials further demonstrated the efficacy of anti-PD-1 therapy plus chemotherapy in this disease, as illustrated by the KeyNote-021 study which obtained 55% ORR in the combination group versus 29% in the chemotherapy alone group (130) – a result that has recently been confirmed with the corresponding updated 24-month median follow-up data (401). Likewise, combination of pembrolizumab and chemotherapy in the KeyNote-189 trial allowed to achieve an unprecedented 12-month OS rate of 69.2% in NSCLC patients (129), thus providing the basis for the approval of pembrolizumab plus platinum-based chemotherapy as the new standard treatment in first line for NSCLC.

Tumour PD-L1 expression is currently the most robust biomarker of response to anti-PD-(L)1 therapies in NSCLC, and is routinely used in the clinic to select eligible patients for these therapies. Despite the high prevalence of DDR defects in this tumour type, no correlations have been established between their presence in patients and response to ICI. Furthermore, the impact of these DDR defects on the anti-tumour immune response is mostly unknown, although some of them, such as *BRCA1* deficiency have been shown to modulate the immune microenvironment characteristics and to influence response to ICI in other histologies. Therefore, there is an unmet need to characterize the immunological effects of the DDR defects present in NSCLC; this may allow the identification of novel molecular determinants of anti-tumour immunity in this disease, and more importantly, provide potential new biomarkers of response to ICI.

Here, we hypothesized that the absence of key DNA repair tumour suppressor gene function, such as *ERCC1*, in NSCLC cells, might influence the molecular processes that control anti-tumour immune responses, for example through enhanced genomic instability, increased TMB/TNB and tumour immunogenicity, or through activation of the cGAS/STING

pathway. We thus decided to characterize the effects of ERCC1 deficiency on the immunological signalling of NSCLC cells.

To initiate this work, we took a functional genomics approach that involved: (i) selecting a relevant model of ERCC1 deficiency to work with; (ii) using RNA-seq to explore the effects of ERCC1 deficiency on the expression of immune-related genes in this model; (iii) testing the functional impact of ERCC1 deficiency in patients' tumours, via evaluation of lymphocytic infiltration in a series of NSCLC tumours. The results of these investigations are presented and discussed in this Chapter.

B. Results

1. Isogenic NSCLC model of ERCC1 deficiency

In most cell-based studies, two types of cellular models can be used: isogenic and non-isogenic models. In isogenic systems, all cell lines derive from a unique progenitor, in which a genetic intervention (e.g. gene targeting via Clustered Regularly Interspaced Short Palindromic Repeats (CRISPR)/Cas9 or RNA interference) has been used to disable the gene of interest in the resulting mutant cell lines (402). This type of system is advantageous as any genetic and molecular difference between the parental cell line and the mutant cell lines is minimized and any effect observed is likely due to the perturbed gene of interest. Therefore, isogenic systems provide a simplified model for identifying the consequences of a single genetic modification. By contrast, non-isogenic systems usually comprise a large panel of cell lines that arise from different progenitors, and as such harbour many differences in their genetic background. These cell lines can be categorized according to an alteration of interest (e.g. *KRAS*-mutated vs *KRAS*-wildtype). However, considering the diversity in genetic background of non-isogenic systems, the causality of a single genetic perturbation is usually more difficult to assess in such systems, and large panels of cell lines are required to limit confounding factors.

In order to identify the expression changes in immune genes associated with loss of *ERCC1* in NSCLC, we chose to work with an in-house isogenic model of ERCC1 deficiency developed in the commonly-used A549 NSCLC cell line, which harbours a *KRAS* G12S mutation. A549 cells were used to generate a series of isogenic cell lines displaying various levels of expression of ERCC1. *ERCC1* gene targeting was performed using a Zinc Finger Nuclease technology (ZFN®, Sigma-Aldrich), which offers the advantage of cutting DNA at highly specific sites and with satisfactory efficacy.

The overall procedure for generation of ERCC1-deficient A549 cells was performed at Gustave Roussy by Dr. Luc Friboulet and colleagues, and is described in **Figure III.1**. ERCC1 exists as four distinct isoforms that share exons 4, 5, 6, and 7 in common. A short sequence in exon 7 was consequently chosen as target for ZFN targeting, in order to simultaneously inactivate all four isoforms, with the potential of reintroducing each isoform by cDNA expression as a mean to study isoform-specific effects.

A549 cell lines are aneuploid and *ERCC1* is present as four copies in the parental cell line. The generation of ERCC1-deficient cells therefore required inactivation of each of these four copies. After screening of more than 500 colonies by WB, one *ERCC1*-heterozygous cell line with three altered copies was identified; further targeting with ZFN allowed the generation of three ERCC1-deficient clones, harbouring four altered copies of *ERCC1* and undetectable levels of ERCC1 by WB (**Figure III.1**). An accurate protein dosage analysis by Meso Scale Discovery® (Meso Scale) revealed that the *ERCC1*-heterozygous cell line and the three ERCC1-deficient clones (A549-c216, -c295, -c375) expressed respectively 65%, 6%, 18% and 15% of the original ERCC1 protein amount. Importantly, all three ERCC1-deficient clones were characterized by an exquisite sensitivity to cisplatin (378), highlighting the clinical relevance of this isogenic model.

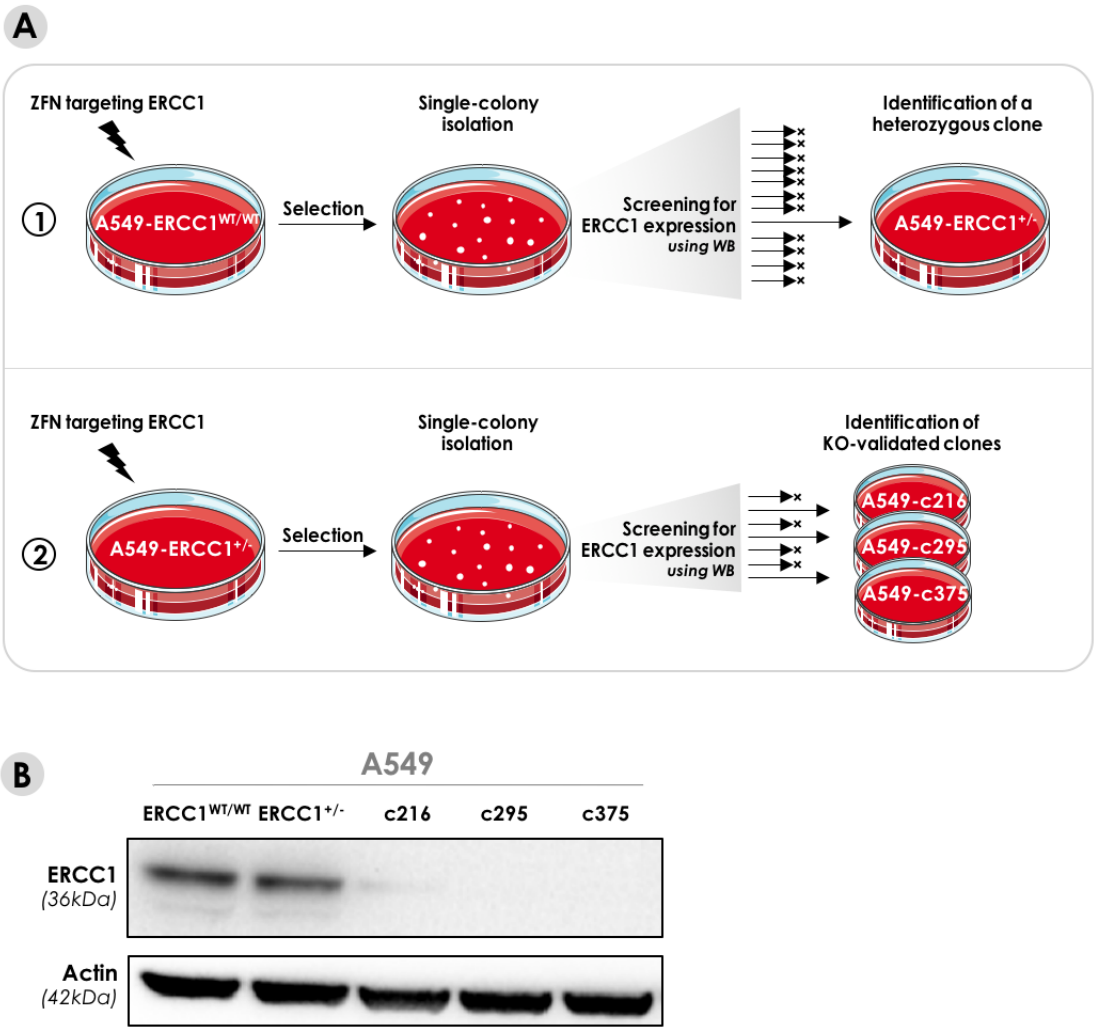

Figure III.1. Generation of an isogenic model of ERCC1-deficiency in the A549 NSCLC cell line.

A. Schematic of the generation of ERCC1-deficient clones from the parental NSCLC cell line A549. Full procedures are detailed in Friboulet et al. **B.** Western blot showing expression of ERCC1 in the parental (ERCC1$^{WT/WT}$), heterozygous (ERCC1$^{+/-}$), and ERCC1$^{-/-}$ knock-out clones (c216, c295 and c375).

2. ERCC1-deficiency in NSCLC drives activation of immune signalling in a cell-autonomous fashion

a. RNA-seq of isogenic ERCC1-deficient A549 cells: general experimental approach

To study transcriptomic differences caused by *ERCC1* loss in a relatively unbiased fashion, we performed RNA-seq on the above-described ERCC1 isogenic model. We specifically used the parental cell line A549-ERCC1$^{WT/WT}$ and one ERCC1-deficient clone (clone c216, referred as to A549-ERCC1$^{-/-}$ below, which harbours the lowest estimated expression of ERCC1) for this analysis. RNA was extracted from these two lines, and sequenced using the Illumina HiSeq 2500 platform. After *in silico* removal of lower quality reads, and subsequent alignment of trimmed reads to the human reference genome (GRCh38), a differential expression analysis was performed to measure gene expression changes between the A549-ERCC1$^{WT/WT}$ and A549-ERCC1$^{-/-}$ cell lines. Differentially expressed genes were defined as those with a Benjamini-Hocherg adjusted P-value of < 0.05 with an absolute $\log_2$ fold change (LFC) > 0.58 (approximate to a 1.5-fold change in expression). Subsequently, a Gene Set Enrichment Analysis (GSEA) was performed using the REACTOME pathway database in order to investigate specific pathway enrichment.

b. RNA-seq results

Comparative transcriptomics of A549-ERCC1$^{WT/WT}$ and A549-ERCC1$^{-/-}$ cell lines identified 1486 significantly differentially expressed genes (DEGs) (**Figure III.2.A**). Subsequent GSEA revealed a significant downregulation of multiple pathways involved in cell cycle regulation, DNA replication, and DNA repair in the A549-ERCC1$^{-/-}$ cell line (**Figure III.2.B**). Among the top 50 downregulated pathways, we found twelve cell cycle-related pathways, seven DNA replication-related pathways, and four DNA repair-related pathways (**Table III.1**) – notably the NER pathway, Normalized Enrichment Score (NES) = -1.728; False Discovery Rate (FDR) = 0.01 –, consistent with the known roles of ERCC1/XPF endonuclease in the DDR.

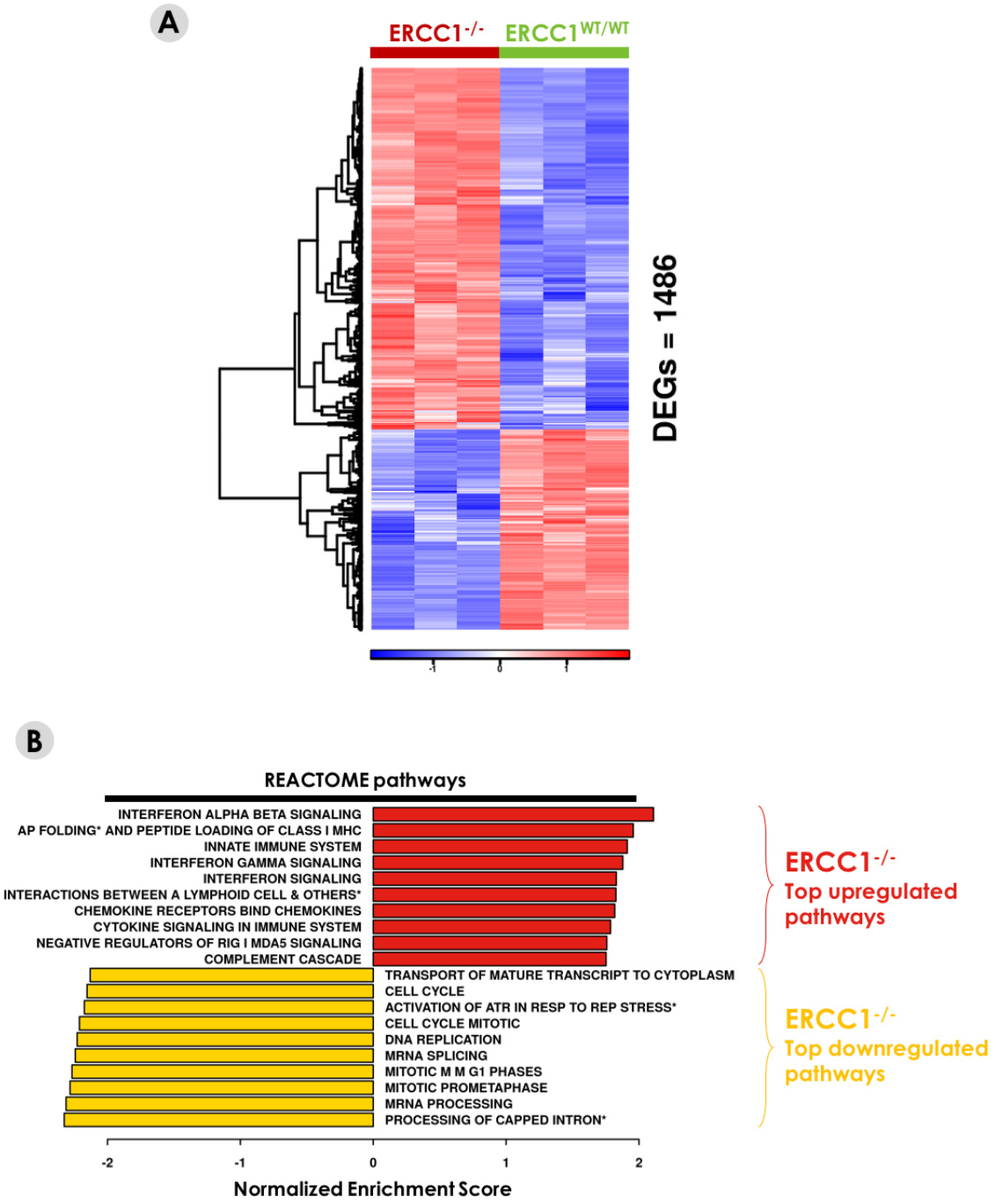

Figure III.2. Differential expression analysis of A549-ERCC1 isogenic cell lines. **A.** Heatmap displaying all significantly DEGs in A549-ERCC1$^{-/-}$ cells compared with A549-ERCC1$^{WT/WT}$, as determined by RNA-seq. N = 3; Heatmap scale is a Z score. Threshold for differential expression was |LFC| > 1 and threshold for significance was FDR < 0.05. **B.** GSEA of REACTOME pathways in A549-ERCC1$^{-/-}$ compared with A549-ERCC1$^{WT/WT}$ cells. Red, top 10 upregulated REACTOME pathways in A549-ERCC1$^{-/-}$ cells; Yellow, top 10 downregulated REACTOME pathways A549-ERCC1$^{-/-}$ cells. All pathways displayed are FDR < 0.05. AP Folding*: Antigen Presentation Folding Assembly; Capped Intron*: Capped Intron Containing Pre-mRNA.

Table III.1. GSEA of REACTOME pathways in A549-ERCC1$^{-/-}$ cells compared with A549-ERCC1$^{WT/WT}$ cells.

Shown are the top 50 downregulated REACTOME pathways in A549-ERCC1$^{-/-}$ cells. Pathways highlighted in forest green relate to cell cycle; pathways highlighted in light green relate to DNA replication; pathways highlighted in dark green relate to DNA repair.

REACTOME pathways	*NES*	*FDR*
REACTOME_PROCESSING_OF_CAPPED_INTRON_CONTAINING_PRE_MRNA	-2.326	0.006
REACTOME_MRNA_PROCESSING	-2.312	0.006
REACTOME_MITOTIC_PROMETAPHASE	**-2.282**	**0.006**
REACTOME_MITOTIC_M_M_G1_PHASES	**-2.267**	**0.006**
REACTOME_MRNA_SPLICING	-2.242	0.006
REACTOME_DNA_REPLICATION	**-2.228**	**0.006**
REACTOME_CELL_CYCLE_MITOTIC	**-2.211**	**0.007**
REACTOME_ACTIVATION_OF_ATR_IN_RESPONSE_TO_REPLICATION_STRESS	**-2.174**	**0.006**
REACTOME_CELL_CYCLE	**-2.154**	**0.007**
REACTOME_TRANSPORT_OF_MATURE_TRANSCRIPT_TO_CYTOPLASM	-2.13	0.006
REACTOME_G2_M_CHECKPOINTS	**-2.088**	**0.006**
REACTOME_ACTIVATION_OF_THE_PRE_REPLICATIVE_COMPLEX	**-2.066**	**0.006**
REACTOME_E2F_MEDIATED_REGULATION_OF_DNA_REPLICATION	**-2.052**	**0.006**
REACTOME_CLEAVAGE_OF_GROWING_TRANSCRIPT_IN_THE_TERMINATION_REGION_	-2.033	0.006
REACTOME_MRNA_3_END_PROCESSING	-2.008	0.006
REACTOME_DNA_STRAND_ELONGATION	**-1.983**	**0.006**
REACTOME_METABOLISM_OF_NON_CODING_RNA	-1.97	0.006
REACTOME_GLYCOLYSIS	-1.946	0.006
REACTOME_TRANSPORT_OF_MATURE_MRNA_DERIVED_FROM_AN_INTRONLESS_TRANSCRIPT	-1.928	0.006
REACTOME_MRNA_SPLICING_MINOR_PATHWAY	-1.906	0.006
REACTOME_MITOTIC_G1_G1_S_PHASES	**-1.905**	**0.006**
REACTOME_CHROMOSOME_MAINTENANCE	**-1.905**	**0.006**
REACTOME_EXTENSION_OF_TELOMERES	-1.884	0.007
REACTOME_RNA_POL_II_TRANSCRIPTION	-1.861	0.006
REACTOME_G1_S_TRANSITION	**-1.828**	**0.006**
REACTOME_TRANSPORT_OF_RIBONUCLEOPROTEINS_INTO_THE_HOST_NUCLEUS	-1.82	0.014
REACTOME_M_G1_TRANSITION	**-1.816**	**0.006**
REACTOME_G1_S_SPECIFIC_TRANSCRIPTION	-1.813	0.021
REACTOME_INTERACTIONS_OF_VPR_WITH_HOST_CELLULAR_PROTEINS	-1.806	0.018
REACTOME_NEP_NS2_INTERACTS_WITH_THE_CELLULAR_EXPORT_MACHINERY	-1.796	0.014
REACTOME_PREFOLDIN_MEDIATED_TRANSFER_OF_SUBSTRATE_TO_CCT_TRIC	-1.795	0.020
REACTOME_CDC6_ASSOCIATION_WITH_THE_ORC_ORIGIN_COMPLEX	-1.781	0.020
REACTOME_ASSOCIATION_OF_LICENSING_FACTORS_WITH_THE_PRE_REPLICATIVE_COMPLEX	-1.777	0.019
REACTOME_REGULATION_OF_GLUCOKINASE_BY_GLUCOKINASE_REGULATORY_PROTEIN	-1.776	0.017
REACTOME_GLUCOSE_METABOLISM	-1.766	0.007
REACTOME_BASIGIN_INTERACTIONS	-1.757	0.037
REACTOME_TRANSCRIPTION_COUPLED_NER_TC_NER	**-1.752**	**0.010**
REACTOME_FORMATION_OF_TUBULIN_FOLDING_INTERMEDIATES_BY_CCT_TRIC	-1.749	0.041
REACTOME_LAGGING_STRAND_SYNTHESIS	**-1.748**	**0.036**
REACTOME_HIV_LIFE_CYCLE	-1.746	0.006
REACTOME_SYNTHESIS_OF_DNA	**-1.746**	**0.008**
REACTOME_ASSEMBLY_OF_THE_PRE_REPLICATIVE_COMPLEX	**-1.738**	**0.010**
REACTOME_NUCLEOTIDE_EXCISION_REPAIR	**-1.728**	**0.010**
REACTOME_S_PHASE	**-1.723**	**0.006**
REACTOME_PROCESSING_OF_CAPPED_INTRONLESS_PRE_MRNA	-1.712	0.041
REACTOME_E2F_ENABLED_INHIBITION_OF_PRE_REPLICATION_COMPLEX_FORMATION	**-1.701**	**0.041**
REACTOME_MITOTIC_G2_G2_M_PHASES	**-1.7**	**0.011**
REACTOME_CYCLIN_A_B1_ASSOCIATED_EVENTS_DURING_G2_M_TRANSITION	**-1.69**	**0.062**
REACTOME_KINESINS	-1.686	0.056

Table III.2. GSEA of REACTOME pathways in A549-ERCC1$^{-/-}$ cells compared with A549-ERCC1$^{WT/WT}$ cells.

Shown are the top 50 upregulated REACTOME pathways in A549-ERCC1$^{-/-}$ cells. Pathways highlighted in orange relate to immune signaling; pathways highlighted in yellow relate to antigen presentation; pathways highlighted in red relate to PRR signaling.

REACTOME pathways	*NES*	*FDR*
REACTOME_INTERFERON_ALPHA_BETA_SIGNALING	**2.109**	**0.006**
REACTOME_ANTIGEN_PRESENTATION_FOLDING_ASSEMBLY_AND_PEPTIDE_LOADING_CLASS_I_MHC	**1.957**	**0.006**
REACTOME_INNATE_IMMUNE_SYSTEM	**1.912**	**0.006**
REACTOME_INTERFERON_GAMMA_SIGNALING	**1.879**	**0.006**
REACTOME_INTERFERON_SIGNALING	**1.830**	**0.006**
REACTOME_IMMUNOREGULATORY_INTERACTIONS_BETWEEN_LYMPHOID_AND_NONLYMPHOID_CELL	**1.827**	**0.007**
REACTOME_CHEMOKINE_RECEPTORS_BIND_CHEMOKINES	**1.817**	**0.006**
REACTOME_CYTOKINE_SIGNALING_IN_IMMUNE_SYSTEM	**1.786**	**0.006**
REACTOME_NEGATIVE_REGULATORS_OF_RIG_I_MDA5_SIGNALING	**1.758**	**0.017**
REACTOME_COMPLEMENT_CASCADE	**1.752**	**0.020**
REACTOME_REGULATION_OF_COMPLEMENT_CASCADE	**1.730**	**0.017**
REACTOME_KERATAN_SULFATE_KERATIN_METABOLISM	1.684	0.041
REACTOME_RIG_I_MDA5_MEDIATED_INDUCTION_OF_IFN_ALPHA_BETA_PATHWAYS	**1.647**	**0.020**
REACTOME_KERATAN_SULFATE_BIOSYNTHESIS	1.629	0.075
REACTOME_TRAF6_MEDIATED_NFKB_ACTIVATION	**1.626**	**0.076**
REACTOME_TOLL_RECEPTOR_CASCADES	**1.597**	**0.020**
REACTOME_TRANSPORT_OF_GLUCOSE_AND_OTHER_SUGARS_BILE_SALTS_ORGANIC_ACIDS_METAL_IONS	1.595	0.049
REACTOME_NOD1_2_SIGNALING_PATHWAY	1.591	0.076
REACTOME_TRAF3_DEPENDENT_IRF_ACTIVATION_PATHWAY	**1.581**	**0.097**
REACTOME_IL_3_5_AND_GM_CSF_SIGNALING	**1.575**	**0.075**
REACTOME_O_LINKED_GLYCOSYLATION_OF_MUCINS	1.575	0.074
REACTOME_TERMINATION_OF_O_GLYCAN_BIOSYNTHESIS	1.553	0.111
REACTOME_NUCLEOTIDE_BINDING_DOMAIN_LEUCINE_RICH_REPEAT_CONTAINING_RECEPTOR_NLR	1.553	0.091
REACTOME_ASPARAGINE_N_LINKED_GLYCOSYLATION	1.550	0.045
REACTOME_N_GLYCAN_TRIMMING_IN_THE_ER_AND_CALNEXIN_CALRETICULIN_CYCLE	1.545	0.123
REACTOME_IL_RECEPTOR_SHC_SIGNALING	**1.531**	**0.146**
REACTOME_PEPTIDE_LIGAND_BINDING_RECEPTORS	1.528	0.091
REACTOME_AMYLOIDS	1.525	0.106
REACTOME_IL_2_SIGNALING	**1.521**	**0.111**
REACTOME_ACTIVATION_OF_CHAPERONE_GENES_BY_XBP1S	1.514	0.091
REACTOME_ANTIGEN_PROCESSING_CROSS_PRESENTATION	**1.505**	**0.086**
REACTOME_INSULIN_SYNTHESIS_AND_PROCESSING	1.500	0.162
REACTOME_METAL_ION_SLC_TRANSPORTERS	1.491	0.183
REACTOME_ACTIVATION_OF_IRF3_IRF7_MEDIATED_BY_TBK1_IKK_EPSILON	**1.484**	**0.183**
REACTOME_RIP_MEDIATED_NFKB_ACTIVATION_VIA_DAI	**1.481**	**0.183**
REACTOME_SIGNALING_BY_ILS	1.481	0.071
REACTOME_CALNEXIN_CALRETICULIN_CYCLE	1.479	0.183
REACTOME_ACTIVATION_OF_CHAPERONES_BY_ATF6_ALPHA	1.478	0.183
REACTOME_ZINC_TRANSPORTERS	1.476	0.186
REACTOME_RAP1_SIGNALLING	1.473	0.192
REACTOME_TRIF_MEDIATED_TLR3_SIGNALING	**1.434**	**0.129**
REACTOME_TRAF6_MEDIATED_IRF7_ACTIVATION	**1.430**	**0.237**
REACTOME_ACTIVATED_TLR4_SIGNALLING	**1.428**	**0.108**
REACTOME_UNFOLDED_PROTEIN_RESPONSE	1.423	0.123
REACTOME_ERK_MAPK_TARGETS	1.413	0.243
REACTOME_SIGNALING_BY_FGFR1_FUSION_MUTANTS	1.409	0.251
REACTOME_PHASE1_FUNCTIONALIZATION_OF_COMPOUNDS	1.381	0.250
REACTOME_DIABETES_PATHWAYS	1.380	0.123
REACTOME_NFKB_AND_MAP_KINASES_ACTIVATION_MEDIATED_BY_TLR4_SIGNALING_REPERTOIRE	**1.368**	**0.192**

Strikingly, the GSEA also revealed a significant enrichment of numerous immune-related pathways in A549-ERCC1$^{-/-}$ cells, suggesting a role for ERCC1 in modulating the immune characteristics of NSCLC cells in a cell-autonomous fashion. Indeed, among the top 50 upregulated pathways, we found twenty-five immune-related pathways, including twelve pathways related to immunological signalling, eleven pathways related to pattern recognition receptors (PRR), and two pathways related to antigen presentation (**Table III.2**). The most significantly enriched pathways were type I and II IFN signalling, antigen presentation through MHC Class I, innate immune response, and chemokine and cytokine signalling (**Figure III.2.B**).

GSEA plots interpretation confirmed that type I IFN signalling was significantly enriched in ERCC1-deficient cells compared to isogenic wildtype cells (NES = 2.11; FDR = 0.0057) (**Figure III.3**). Consistent with this enrichment, a number of genes involved in type I IFN response were found upregulated in the A549-ERCC1$^{-/-}$ cells, including several interferon regulatory factors (IRF), which are transcription factors regulating the expression of IFN, and many signalling elements activated in response to IFN. These include for example genes encoding IFN-α/β receptors and members of the signal transducers and activators of transcription (STAT) family of transcription factors (**Table III.3**), but also target genes mediating IFN-induced apoptosis such as *IFI27* and *IFI35*, or involved in IFN-triggered innate immune responses against viral infections such as *OAS1*, *OAS2*, and *MX1*.

Cytokine signalling was also significantly enriched in ERCC1-defective cells (NES = 1.79; FDR = 0.0057) (**Figure III.4**), and consistently, we found an upregulation of several C-C-motif and C-X-C-motif chemokines in those cells. In particular, the lympho-attractant chemokines CCL2, CCL5, CXCL1, CXCL2, CXCL5, CXCL8 and CXCL10 were > 5-fold upregulated in A549-ERCC1$^{-/-}$ cells (FDR < 0.05) (**Table III.3**). Considering the critical immunogenic and lympho-attractant properties of these chemokines (288), this suggested that ERCC1 deficiency might modulate anti-cancer immunity in NSCLC cells.

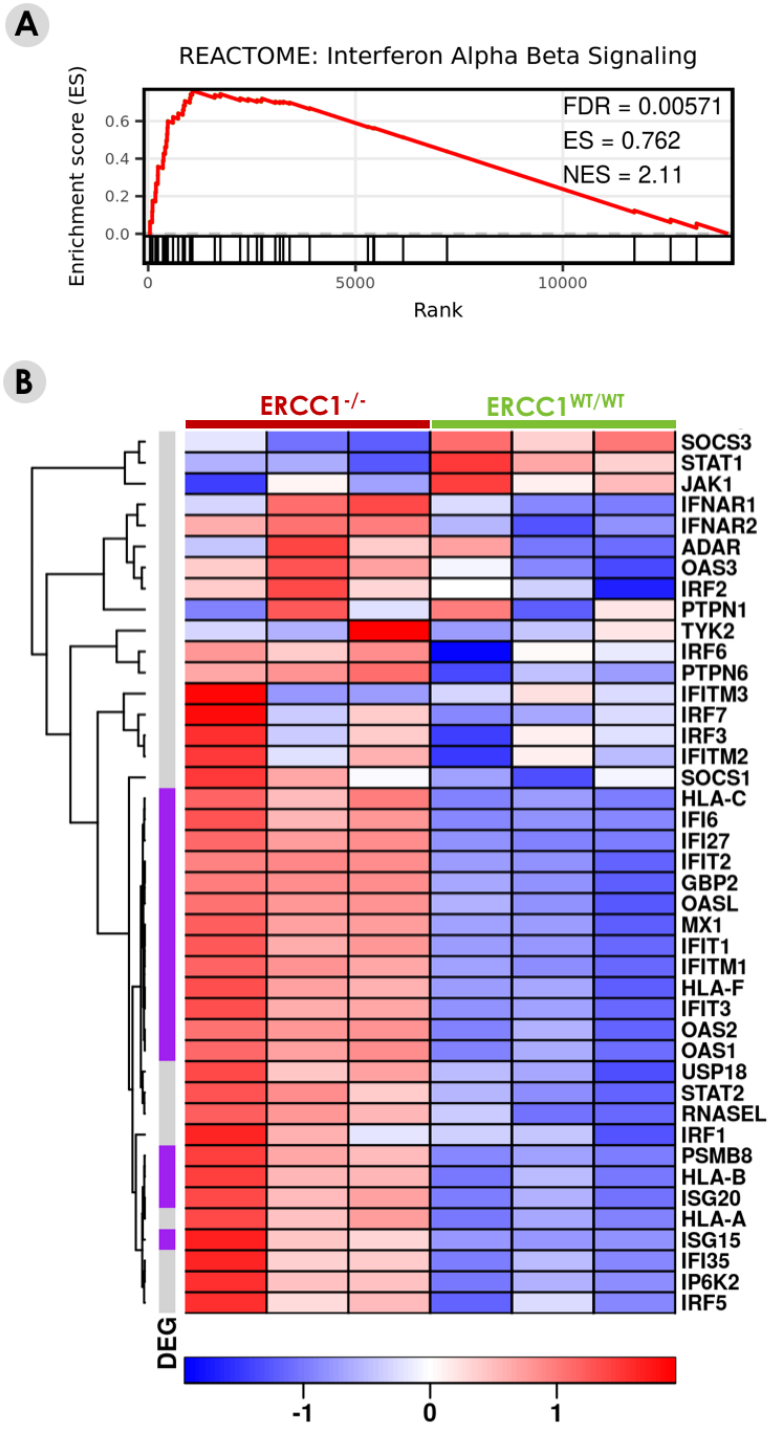

Figure III.3. GSEA of the REACTOME pathway Interferon Alpha Beta Signalling in A549-ERCC1$^{WT/WT}$ compared with A549-ERCC1$^{-/-}$ cells.
A. Enrichment plot generated by GSEA of ranked gene expression data for genes of the REACTOME pathway Interferon Alpha Beta Signalling. **B.** Associated heatmap showing the genes of the pathway, ranked by FDR. N = 3; Heatmap scale is a Z score. Purple, significantly DEGs with FDR < 0.05 and |LFC| > 1; Grey, non-significantly DEGs.

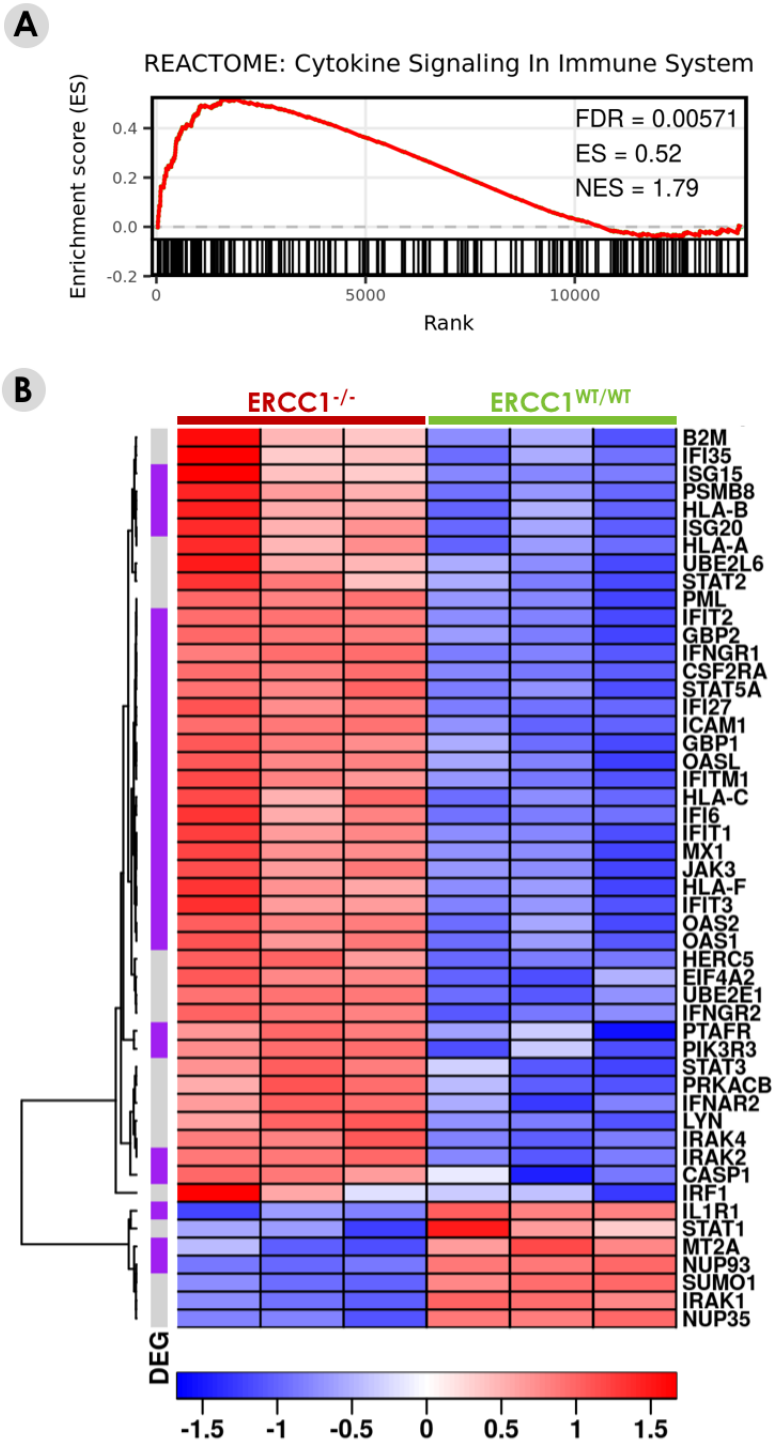

Figure III.4. GSEA of the REACTOME pathway Cytokine Signalling in Immune System in the A549-ERCC1$^{WT/WT}$ compared with A549-ERCC1$^{-/-}$ cells.

A. Enrichment plot generated by GSEA of ranked gene expression data for genes of the REACTOME pathway Cytokine Signalling in Immune System. **B.** Associated heatmap showing the top 50 genes of the pathway, ranked by FDR. N = 3; Heatmap scale is a Z score. Purple, significantly DEGs with FDR < 0.05 and |LFC| > 1; Grey, non-significantly DEGs.

Table III.3. Differential expression analysis of A549-ERCC1$^{-/-}$ cells compared with A549-ERCC1$^{WT/WT}$ cells for various immune-related genes.

Selective table showing differential expression of several IFN-inducible proteins including IFN receptors, and STAT family members, as well as several chemoattractant chemokines, including members of the C-C and C-X-C motif cytokines families.

Genes	***log_2 FC***	***FDR***
IFN receptors		
IFNAR2	0.6988	6.11E-05
IFNGR1	1.5014	1.15E-10
IFNGR2	0.8441	7.54E-08
Signal Transducers and Activators of Transcription (STAT)		
STAT1	-0.6777	1.56E-04
STAT2	0.6025	5.33E-05
STAT3	0.5017	1.26E-04
STAT5A	1.5612	1.01E-08
STAT5B	0.3163	1.40E-02
STAT6	0.9319	1.98E-05
C-C motif cytokines		
CCL2	2.3992	1.01E-08
CCL5	7.4502	4.38E-09
CCL26	1.4605	5.16E-06
C-X-C motif cytokines		
CXCL1	6.7536	3.96E-11
CXCL2	5.3524	7.16E-09
CXCL3	4.9923	2.38E-10
CXCL5	3.2972	1.11E-14
CXCL8	6.0042	5.84E-14
CXCL10	6.0637	3.92E-05
CXCL16	0.7017	1.34E-05

In order to validate that the observed transcriptomic differences were attributable to ERCC1 deficiency in this model, an independent transcriptomic analysis was conducted using RNA-seq in the two other ERCC1-deficient clones (A549-c295 and A549-c375) as well as in the *ERCC1*-heterozygous cell line (herein referred to as A549-ERCC1$^{+/-}$). GSEA revealed a similar enrichment of the type I IFN signalling pathway in both ERCC1-deficient clones compared with the A549-ERCC1$^{WT/WT}$ cell line (NES = 2.54, FDR = 0.0062 for clone 295 and NES = 2.79, FDR = 0.0063 for clone 375), thus confirming our initial observations (**Figure III.5**). In addition, previous genetic characterization by WES of the isogenic ERCC1-deficient clones did not identify mutations in any gene involved in immune signalling (364), suggesting the defect in ERCC1 as the most likely cause of the observed transcriptional dysregulation. Interestingly, the A549-ERCC1$^{+/-}$ cell line also displayed a significant

upregulation of type I IFN signalling (NES = 1.86; FDR = 0.0131) in spite of expressing low levels of ERCC1 (**Figure III.5**), which supports that an altered but not abolished function of ERCC1 is sufficient to trigger this immune-activated phenotype. This is of particular interest since most ERCC1-deficient NSCLC patients display low levels of ERCC1 rather than a total absence of the protein, and supports the translational potential of these observations.

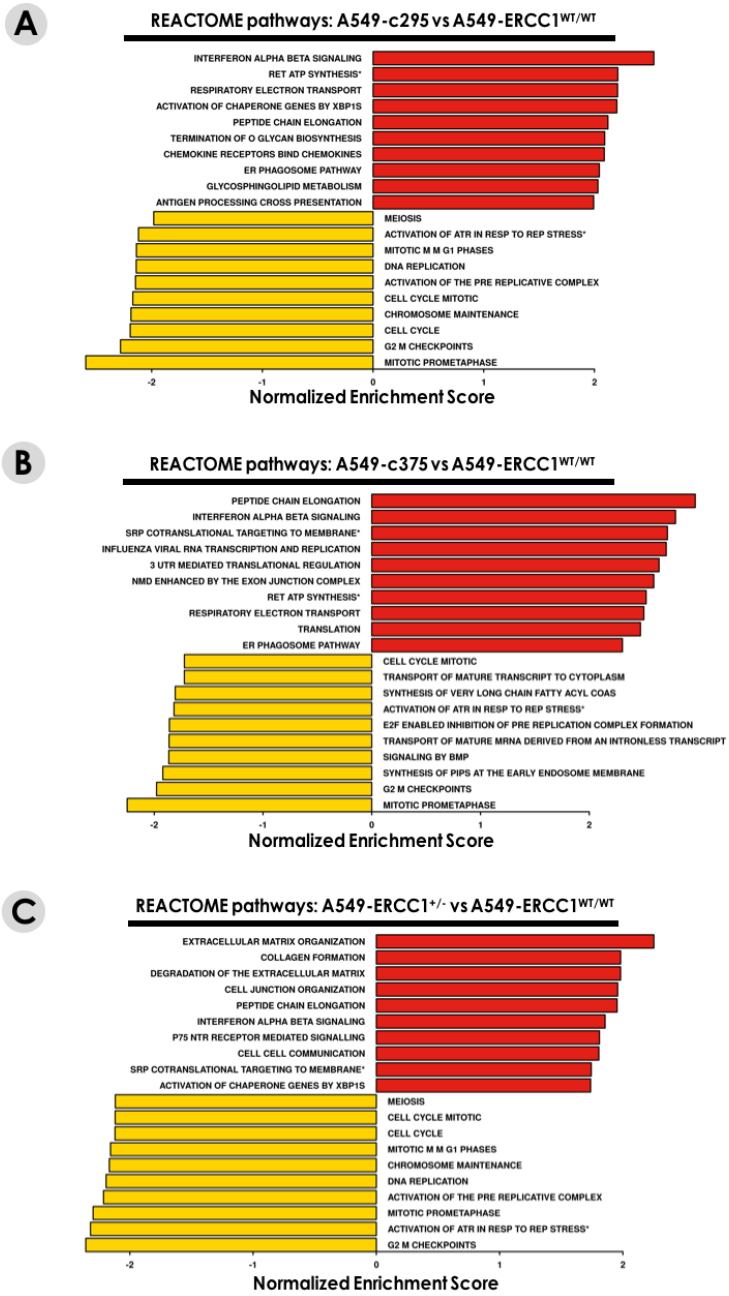

Figure III.5. GSEA of REACTOME pathways in A549-c295 cells (A), A549-c375 cells (B) and A549-ERCC1$^{+/-}$ cells (C) compared with A549-ERCC1$^{WT/WT}$ cells.
Red, top 10 upregulated REACTOME pathways in ERCC1-deficient cells; Yellow, top 10 downregulated REACTOME pathways in ERCC1-deficient cells.

3. Loss of ERCC1 correlates with increased lymphocytic infiltration in NSCLC patients' tumours

In order to investigate the functional effects of this enhanced cell-autonomous immune signalling detected in ERCC1-deficient NSCLC cells, we decided to evaluate the impact of ERCC1 expression levels on markers of activated immunity in NSCLC tumours. T cells infiltration is a well-established marker of activated anti-tumour immunity, which defines the distinctive immunological status of a tumour – "hot, T cell-inflamed" vs "cold, non-T cell inflamed". This characteristic carries a prognostic value in NSCLC (403), and was shown to predict response to ICI in other tumour types (172), highlighting its clinical relevance.

Several groups have linked the presence of CD8+ TILs to the expression of type I IFN signatures in human and mouse tumours (404,405), suggesting the crucial role of IFN signalling in shaping the tumour immune microenvironment. Having observed that ERCC1 deficiency is associated with enhanced type I IFN signalling in NSCLC cells, we hypothesized that ERCC1 expression in tumour cells might influence the levels of TILs in NSCLC tumours.

To test this hypothesis, we conducted a pathological study of the expression of ERCC1 and the levels of TILs in a series of 55 human tumour samples derived from resected lung adenocarcinoma patients (stage I, II and IIIA). ERCC1 status in these tumours was evaluated by IHC as described by Touat and colleagues (379), and TILs were assessed using a semi-quantitative score of coverage based on morphology. The mean coverage percentage of TILs was 18.3 (SD = 1.7) for the ERCC1-high samples (n = 40), whereas it was 26.3 (SD = 3.6) for the ERCC1-low samples (n = 15). Although some degree of overlap was observed between both populations, this difference was statistically significant (P = 0.0265, Mann-Whitney U Test; **Figure III.6**), suggesting that loss of ERCC1 expression in NSCLC tumours associates with increased T cell infiltration. Consistent with our transcriptomic data which identified an enhanced expression of chemotactic chemokines in ERCC1-defective NSCLC cells, these results support the idea that the immune-activated phenotype associated with ERCC1 dysfunction has a functional impact on the TME of NSCLC tumours by driving lymphocytic infiltration.

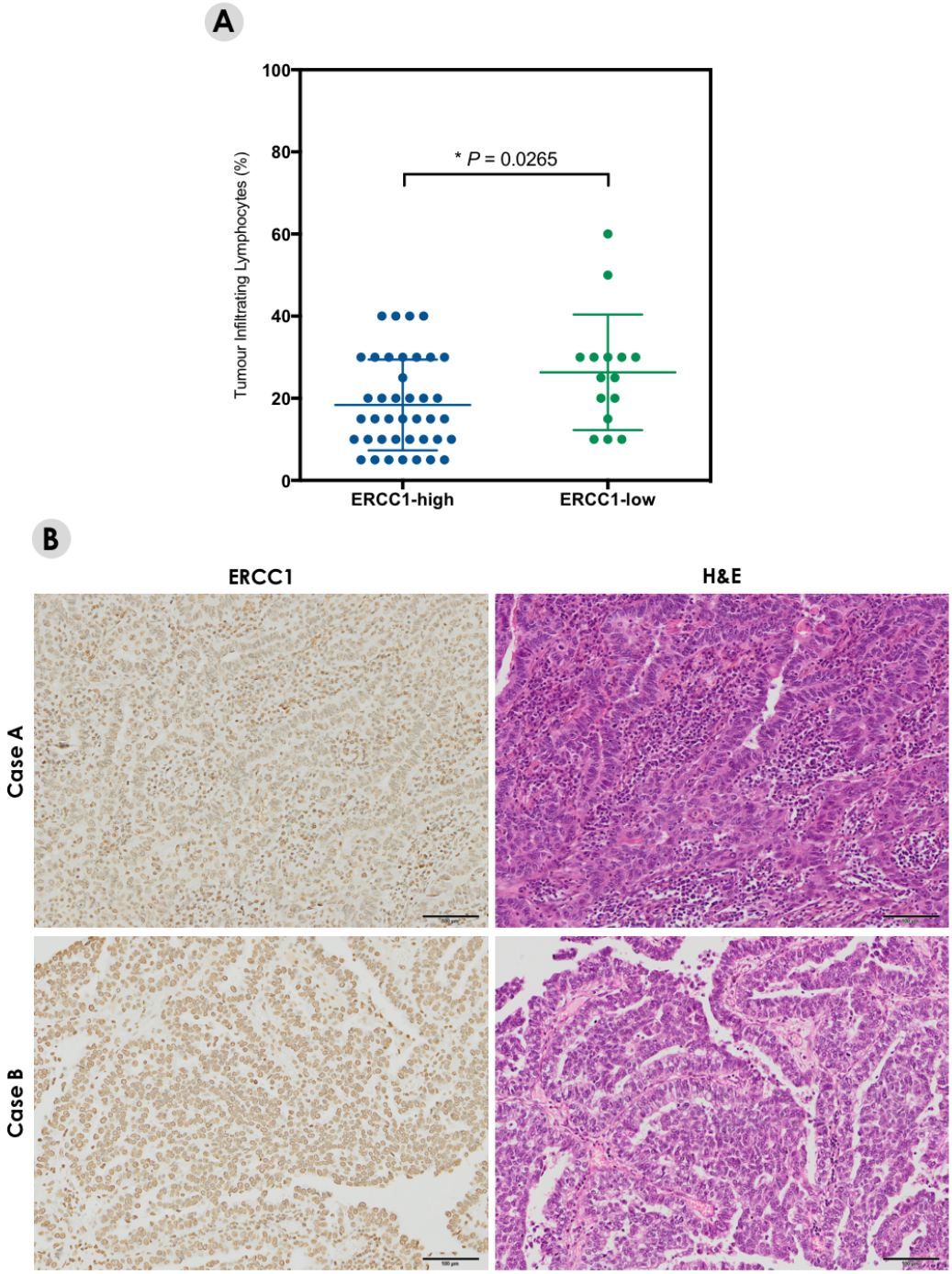

Figure III.6. Low ERCC1 expression correlates with high levels of TILs in human NSCLC tumours.

A. Scatter box plot of ERCC1 protein expression (assessed by IHC staining) and the percentage of TILs (assessed through morphology) in a series of resected human NSCLC adenocarcinoma samples (n = 55). Mann- Whitney U test. **B.** Representative images of ERCC1 and Haematoxylin-Eosin stainings in two surgical specimens of resected lung adenocarcinoma. Case A displays low ERCC1 staining intensity in tumour cells and high stromal TIL density; Case B displays high ERCC1 staining intensity in tumour cells and low stromal TIL density. Scale bar: 50 μm.

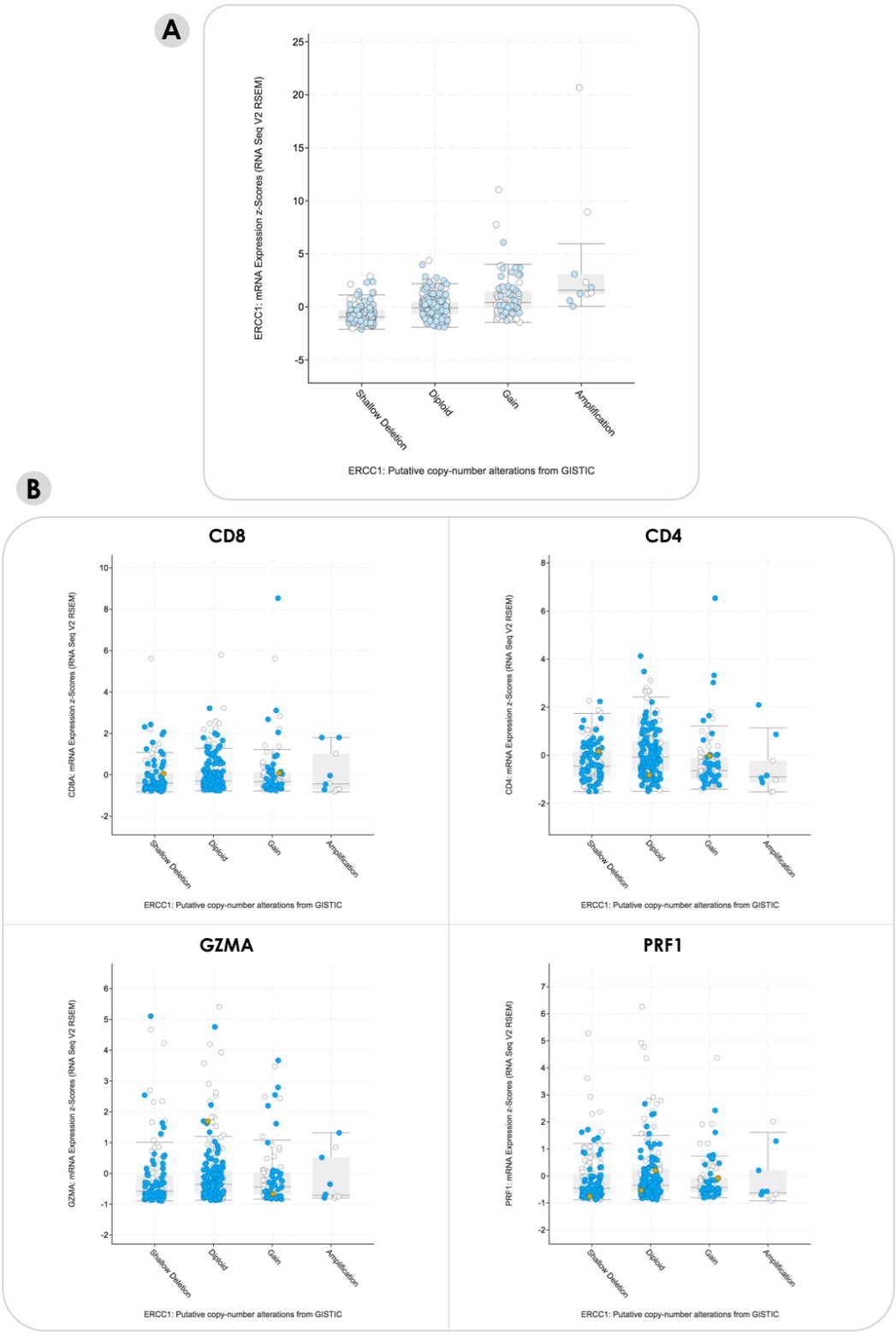

Figure III.7. Evaluation of the correlation between ERCC1 gene copy number and expression of immune-related markers in the TCGA lung adenocarcinoma cohort.
A. Correlation between *ERCC1* gene copy number and mRNA expression. **B.** Absence of correlation between *ERCC1* gene copy number and expression of CD8, CD4, GZMA and PRF1.

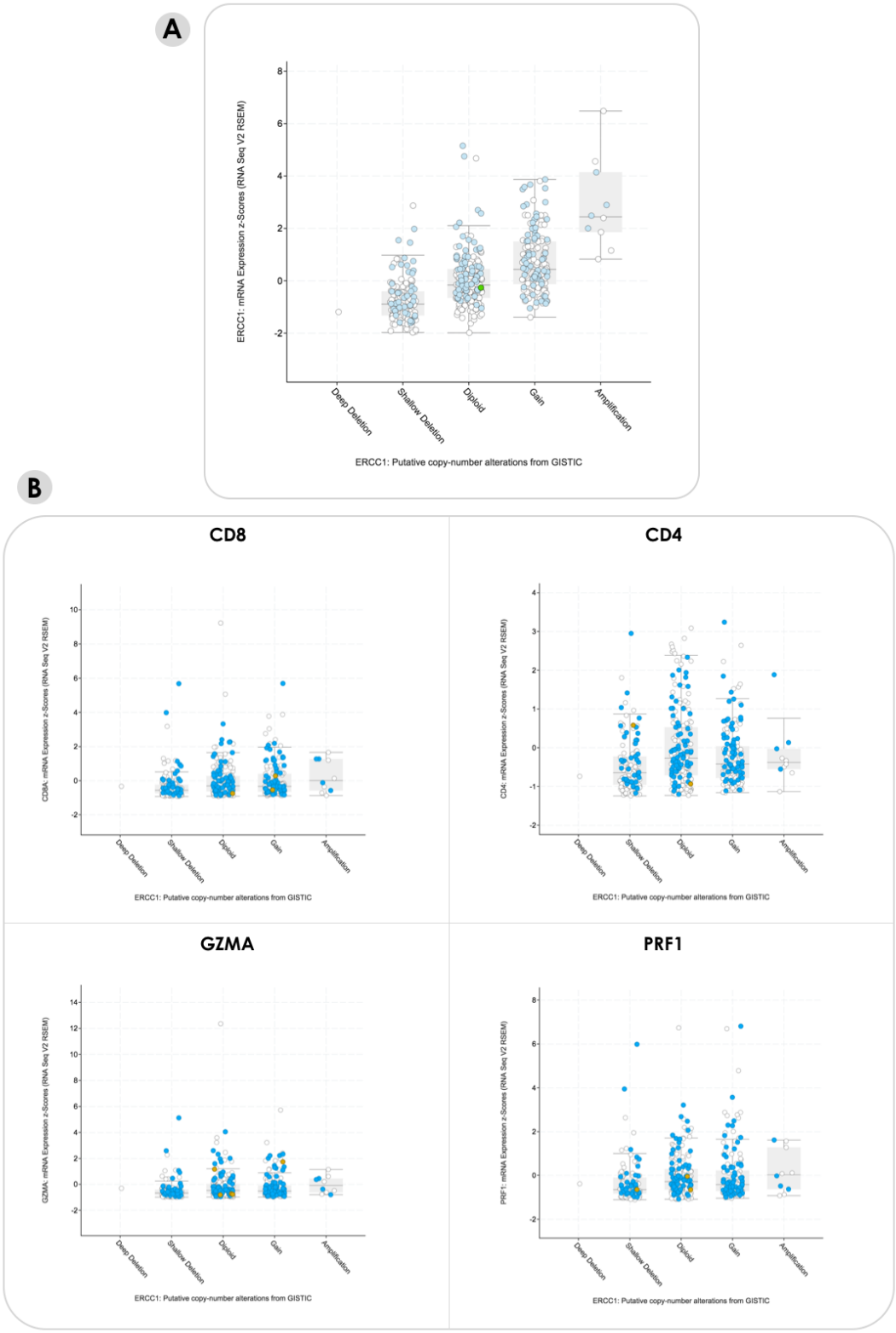

Figure III.8. Evaluation of the correlation between ERCC1 gene copy number and expression of immune-related markers in the TCGA lung squamous cell carcinoma
A. Correlation between *ERCC1* gene copy number and mRNA expression. **B.** Absence of correlation between *ERCC1* gene copy number and expression of CD8, CD4, GZMA and PRF1.

To further evaluate this link between ERCC1 expression and tumour infiltration, we used the cBioPortal platform to retrieve RNA expression data and copy number variation data from two cohorts of NSCLC patients derived from the TCGA: an adenocarcinoma cohort (n = 586) and a squamous-cell carcinoma cohort (n = 511). We found a clear correlation between *ERCC1* gene copy number and mRNA expression in both cohorts (**Figure III.7.A** and **Figure III.8.A**), suggesting that copy number could be used as a surrogate marker of gene expression in the case of ERCC1. We then investigated whether a correlation could be found between *ERCC1* gene copy number and the expression of immune-related markers in those cohorts; we selected *CD8* and *CD4* as lymphocyte-specific markers and Granzyme A (*GZMA*) and Perforin (*PRF1*) as cytotoxicity markers. No differences in expression of any of these genes could be observed according to changes in *ERCC1* gene copy number, suggesting an absence of correlation between these immune-related markers and ERCC1 expression in the TCGA cohorts (**Figure III.7.B** and **Figure III.8.B**). This may be due to several factors: (i) the presence of four closely related ERCC1 isoforms (only one of which is functional); (ii) the absence of equivalence between the direct assessment of TILs by anatomical pathology and the indirect assessment of TME characteristics using immune signatures (406); and (iii) the difference between cohorts (including tumour heterogeneity and tumour stages).

4. ERCC1 dysfunction is associated with higher TMB in human tumours

Tumour genomic instability and DDR defects modulate the anti-cancer immune response by inducing changes in tumour antigenicity. We hypothesized that loss of *ERCC1* gene function, similar to other DDR defects, might favour the accumulation of somatic mutations in the tumour genome, and therefore sought to investigate the possible link between defects in ERCC1 function and TMB. To this aim, we interrogated genomic data from the TCGA dataset and assessed whether deleterious mutations in *ERCC1* would result in higher TMB in human tumours.

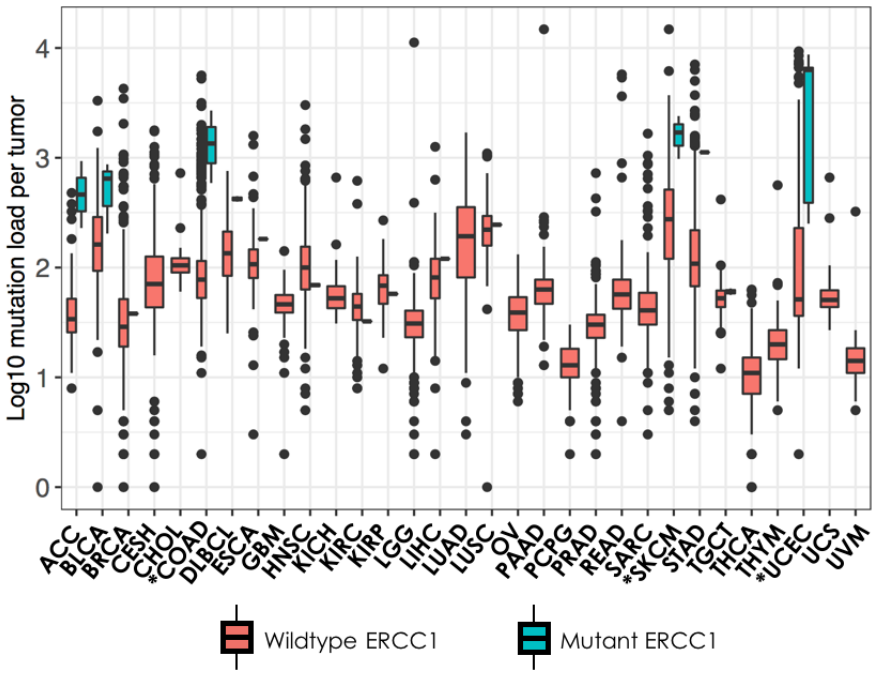

Figure III.9. Deleterious mutations of *ERCC1* are associated with increased TMB in human tumours.

Somatic mutation density observed in tumours of the TCGA database from 31 histotypes, according to the presence or absence of *ERCC1* deleterious mutations. The vertical axis shows $\log_{10}$-valued mutation number in tumours. The horizontal axis shows the TCGA histotype classification. For each histotype, boxplots represent the distribution of TMB values across the cohorts. Red, *ERCC1*-wildtype cohorts; Green, *ERCC1*-mutant cohorts. Cancer types with statistically significant differences between *ERCC1*-wildtype and *ERCC1*-mutant cohorts are indicated by * (Mann-Whitney U test). Abbreviations: ACC, Adrenocortical carcinoma; BLCA, Bladder Urothelial Carcinoma; BRCA, Breast invasive carcinoma; CESC, Cervical squamous cell carcinoma and endocervical adenocarcinoma; CHOL, Cholangiocarcinoma; COAD, Colon adenocarcinoma; DLBCL, Diffuse large B-cell lymphoma; ESCA, Esophageal carcinoma; GBM, Glioblastoma multiforme; HNSC, Head and Neck squamous cell carcinoma; KICH, Kidney Chromophobe; KIRC, Kidney renal clear cell carcinoma; KIRP, Kidney renal papillary cell carcinoma; LGG, Lower Grade Glioma; LIHC, Liver hepatocellular carcinoma; LUAD, Lung adenocarcinoma; LUSC, Lung squamous cell carcinoma; OV, Ovarian serous cystadenocarcinoma; PAAD, Pancreatic adenocarcinoma; PCPG, Pheochromocytoma and Paraganglioma; PRAD, Prostate adenocarcinoma; READ, Rectum adenocarcinoma; SARC, Sarcoma; SKCM, Skin Cutaneous Melanoma; STAD, Stomach adenocarcinoma; TGCT, Testicular Germ Cell Tumors; THCA, Thyroid carcinoma; THYM, Thymoma; UCEC, Uterine Corpus Endometrial Carcinoma; UCS, Uterine Carcinosarcoma; UVM, Uveal Melanoma.

No *ERCC1*-mutant tumour could be identified in the non-small cell lung adenocarcinoma group (LUAD) – which is consistent with literature data that report decreased ERCC1

expression in this histology without genetic alteration (212,374) (**Table III.4**). However, *ERCC1*-mutant samples were identified in uterine corpus endometrial carcinoma (UCEC, 5/242 tumours), colon adenocarcinoma (COAD, 3/353 tumours) and skin cutaneous melanoma (SKCM, 3/361 tumours); all were associated with a significant increase in TMB with a median mutation number of 51.0 vs 6268.0 (P = 0.0015), 78.0 vs 1345.0 (P = 0.0087) and 273.5 vs 1710.0 (P = 0.0079) in *ERCC1*-mutant vs *ERCC1*-wildtype UCEC, COAD and SKCM, respectively (**Figure III.9**). This suggests that deleterious mutations of *ERCC1* in human tumour samples correlate with increased TMB, which might represent an additional determinant of the anti-tumour immune response.

Table III.4. Characteristics of the cohorts used for the pan-cancer analysis of TMB according to *ERCC1* mutation status.

Table displaying the number of *ERCC1*-wildtype and *ERCC1*-mutant tumours per cohort, as well as the P values corresponding to statistically significant differences in TMB between *ERCC1*-wildtype and *ERCC1*-mutant cohorts (Mann-Whitney U test).

Histology	Total number of patients	Number of ERCC1-wildtype patients	Number of ERCC1-mutant patients	P value
ACC	77	75	2	ns
BLCA	391	388	3	ns
BRCA	957	956	1	-
CESC	192	192	0	-
CHOL	35	35	0	-
COAD	353	350	3	0.0087
DLBCL	48	46	2	-
ESCA	180	179	1	-
GBM	148	148	0	-
HNSC	495	493	2	-
KICH	65	65	0	-
KIRC	434	433	1	-
KIRP	161	160	1	-
LGG	510	510	0	-
LIHC	194	193	1	-
LUAD	464	464	0	-
LUSC	169	168	1	-
OV	234	234	0	-
PAAD	146	146	0	-
PCPG	177	177	0	-
PRAD	423	423	0	-
READ	108	108	0	-
SARC	249	249	0	-
SKCM	361	358	3	0.0079
STAD	367	366	1	-
TGCT	133	131	2	-
THCA	398	398	0	-
THYM	119	119	0	-
UCEC	242	237	5	0.0015
UCS	56	56	0	-
UVM	80	80	0	-

Despite this statistically significant increase in TMB associated with deleterious mutations of *ERCC1* in TCGA tumours, this analysis is somewhat limited by the very small number of *ERCC1*-mutant tumours included in each cohort. An ideal approach to validate this link would be to interrogate TCGA datasets for an inverse correlation between the expression of ERCC1 functional isoform (isoform 202) and TMB; however, expression data at the isoform level is currently not available in this dataset.

5. Loss of ERCC1 associates with spontaneous re-expression of STING in isogenic NSCLC cells

Although the above-presented analysis suggests a correlation between *ERCC1* mutation status and TMB, these results do not explain why ERCC1-defective NSCLC cells upregulate various neo-antigen-independent immune signalling pathways, in a cell-autonomous fashion. In other contexts, DDR defects have been linked to innate immune response and type I IFN signalling via cytosolic DNA sensing, notably involving the cGAS/STING pathway (268). In particular, upregulation of the chemotactic chemokines CCL5 and CXCL10 has been observed in the context of BRCA1-deficiency in cellular models of breast cancer, and associated with the activation of a cGAS/STING-mediated type I IFN response. As these chemokines were also found significantly upregulated in ERCC1-deficient cells (**Table III.3**), we hypothesized that loss of ERCC1 might modulate such signals.

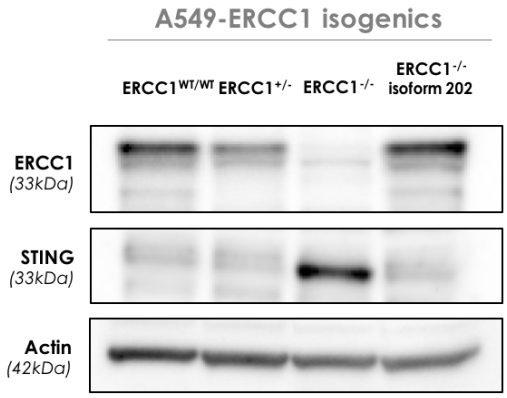

Figure III.10. STING is spontaneously expressed in ERCC1-defective cells.
Western blot illustrating STING protein expression in A549-ERCC1 isogenic cell lines. Proteins were extracted and lysates were probed with the indicated antibodies.

We evaluated the expression of STING, the major effector of the cytosolic DNA sensing pathway, in A549-ERCC1 isogenic cell lines including the A549-ERCC1$^{WT/WT}$, A549-ERCC1$^{+/-}$ and A549-ERCC1$^{-/-}$ cell lines, as well as an A549-ERCC1$^{-/-}$ clone in which a functional isoform of the ERCC1 protein (isoform 202) had been re-expressed through the introduction of a cDNA construct encoding it. Although expression of STING was undetectable by WB in A549-ERCC1$^{WT/WT}$ and A549-ERCC1$^{+/-}$ cells, we found constitutive re-expression of STING in the A549-ERCC1$^{-/-}$ cell line (**Figure III.10**). Consistent with this, STING mRNA levels were > 2.5-fold increased in A549-ERCC1$^{-/-}$ cells (LFC = 1.3769, FDR = 0.0009), and a similar upregulation of STING was also detected in the two other ERCC1-deficient clones (**Table III.5**). Interestingly, we could not detect any STING expression in the A549-ERCC1$^{-/-}$ + isoform 202 cell line, suggesting that modulation of STING expression was a primary effect of ERCC1 deficiency. Of note, cGAS expression was also increased in A549-ERCC1$^{-/-}$ cells compared to A549-ERCC1$^{WT/WT}$ cells (**Table III.5**), suggesting a constitutive activation of the cGAS/STING pathway in A549-ERCC1$^{-/-}$ cells. As activation of the cGAS/STING pathway results in phosphorylation of TBK1, recruitment of IRF3 and eventually type I IFN genes expression (257), these results suggest that the observed transcriptomic profile can be linked to STING activation in A549-ERCC1$^{-/-}$ cells.

Table III.5. Differential expression analysis of A549-ERCC1$^{-/-}$ cells compared with A549-ERCC1$^{WT/WT}$ cells.

Selective table showing differential expression of cGAS and STING in three ERCC1-deficient clones compared to the parental A549-ERCC1$^{WT/WT}$ cell line.

Genes	*log_2 FC*	*FDR*
A549-c216 vs A549-ERCC1$^{WT/WT}$		
STING	1.3769	8.93E-04
CGAS	0.5336	9.82E-03
A549-c295 vs A549-ERCC1$^{WT/WT}$		
STING	0.8462	3.90E-02
CGAS	0.2583	3.26 E-01
A549-c375 vs A549-ERCC1$^{WT/WT}$		
STING	1.0363	1.24E-02
CGAS	0.4951	6.07E-02

Together, our data suggest that ERCC1-defective NSCLC cells are characterized by an enhanced expression of immune signals that shape the TME by driving lymphocytic

infiltration. In particular, loss of ERCC1 stimulates a cancer cell-autonomous type I IFN response associated with the constitutive upregulation of cGAS/STING signalling.

C. Discussion

In this Chapter, we have described an unexpected link between ERCC1 deficiency and activation of specific cancer cell-autonomous immune responses in NSCLC cells. ERCC1-defective cells primarily upregulate key pathways involved in the modulation of innate immune responses, such as type I and type II IFN signalling. Considering the major function of these pathways in orchestrating immune responses through a fine-tuned regulation of the secretion of immunomodulatory signals (9), loss of ERCC1 may constitute an important determinant of anti-tumour immunity in NSCLC cells. The observation that ERCC1-low tumours exhibit increased lymphocytic infiltration compared to ERCC1-high tumours corroborates this notion, and further supports the functional impact of ERCC1 deficiency on the tumour immune microenvironment. Of note, ERCC1-defective cells also display an increased engagement of the antigen presentation machinery (**Figure III.2**, **Table III.2**), which suggests that ERCC1 deficiency may facilitate the recognition of tumour cells by T cells through the enhancement of tumour cells immunogenicity. This overall suggests that loss of ERCC1 in NSCLC tumours might specifically favour the establishment of anti-tumour immune responses in the TME, via modulation of both innate and adaptive immunity.

Interestingly, we observed that ERCC1-defective NSCLC cells present a constitutively high expression of STING compared to their ERCC1-proficient counterparts, suggesting that the immune-activated phenotype of ERCC1-deficient cells may be linked to the upregulation of this DNA sensing pathway effector. In particular, the observation that an ERCC1$^{-/-}$ clone reconstituted with the functional isoform of ERCC1 protein does not express STING supports an ERCC1-dependent reversible modulation of STING expression in this isogenic system. A similar mechanism of reversible expression of STING has recently been described in the context of *LKB1*-mutated, *KRAS*-driven NSCLC (407). In this specific subset of NSCLC, LKB1 loss was shown to result in marked silencing of STING expression, an effect that was

caused by DNMT1-mediated *STING* promoter hypermethylation, and could be reversed following LKB1 reconstitution in STING-low *LKB1*-mutated NSCLC cells. Whether loss of ERCC1 in NSCLC cells triggers a similar epigenetic upregulation of STING is unknown, and would therefore warrant further exploration.

While various DDR defects have been shown to critically contribute to the accumulation of mutations in the tumour genome, only some of them have proven their predictive value as biomarkers of response to anti-PD-(L)1 therapy (121). ERCC1 deficiency has been associated with increased mutation frequency and genomic instability in mice (408), an observation that is consistent with the known roles of ERCC1 in processes that ensure chromosomal stability and maintenance of genome integrity, such as the inter-strand crosslink DNA repair pathway (409) and the resolution of Holliday junction (410). The results of our mutational load analysis in tumours of the TCGA dataset are in line with these published data, and further suggest that ERCC1 dysfunction, *per se*, is sufficient to promote mutagenesis to such an extent that this causes a significant increase in overall TMB. Whether such phenotype relies on the complete abrogation of ERCC1 function or simply on an impaired activity of the protein requires further investigation, and dedicated studies still need to be conducted to identify the threshold of ERCC1 deficiency that is sufficient to cause the observed increase in TMB. Importantly, the levels of somatic mutations found in *ERCC1*-mutated tumours appear to be similar to that measured in other DDR-deficient tumours characterized by a high genomic instability and elevated TNB, such as MMR-deficient tumours – which display an average TMB of 1400-1700 nsSNV per exome (246) – suggesting that ERCC1 dysfunction may also create a tumour mutational landscape that favours the production of new immunogenic neo-antigens. However, whether ERCC1 status itself represents an independent predictive biomarker of response to anti-PD-(L)1 in NSCLC is currently unknown and deserves further investigation.

Chapter IV. PARPi exacerbate cancer cell-autonomous immunity through cGAS/STING in DDR-deficient cells

A. Introduction

PARPi are targeted therapies used for the treatment of DDR-deficient tumours. Although their clinical development has mainly been oriented towards the treatment of *BRCA*-mutated ovarian and breast cancers, several pre-clinical studies have demonstrated the anti-tumour potential of PARPi in other DDR-deficient contexts, including ERCC1-deficient NSCLC (364).

In Chapter III, we have described that ERCC1 deficiency in NSCLC favours the establishment of cancer cell-autonomous immunity through the activation of a type I IFN response associated with constitutive upregulation of STING. Consistent with these observations, several lines of evidence now support that specific DDR defects can activate anti-tumour immunity via cancer cell-autonomous mechanisms independent of neo-antigen production, primarily involving cGAS/STING signalling activation (268) (data presented in details in Chapter I). Furthermore, the induction of DNA damage in cells displaying normal DDR function, via exposure to conventional cytotoxic chemotherapies or IR, has also been shown to trigger cGAS/STING-driven immune responses in various experimental models (263–266). In either case, the elicited immune phenotype involved the secretion of specific chemo-attractant chemokines and resulted in the recruitment of immune effectors to the tumour site.

Knowing that ERCC1-deficient NSCLC cells are characterized by (i) a selective sensitivity to treatment with PARPi and (ii) the activation of specific cell-autonomous immune responses, and considering that various DNA-damaging agents trigger cGAS/STING-mediated innate immune responses, we hypothesized that PARPi could further exacerbate immune

activation in ERCC1-deficient NSCLC cells via stimulation of the cGAS/STING pathway. Our hypothesis is that PARPi, which do not only inhibit the catalytic activity of PARP1, but also trap PARP1 onto the DNA, causing stalled replication forks and subsequent DSBs (349), might specifically favour the formation of cytosolic chromatin fragments (CCF) and in turn trigger cGAS/STING signalling in ERCC1-defective tumour cells.

To test this hypothesis and to characterize the effects of PARPi on cGAS/STING signalling, we developed an experimental methodology that involved (i) evaluating the potential of PARPi to induce formation of CCF; (ii) measuring the activation of cGAS/STING signalling effectors in response to PARPi; (iii) assessing the induction of specific immune responses in the context of PARPi-mediated cGAS/STING activation. For each of these points, we performed a thorough comparison of the effects of PARPi in ERCC1-deficient vs ERCC1-wildtype cells using isogenic NSCLC models. In parallel, we evaluated the validity and specificity of the observed effects in independent DDR-deficient models, including an isogenic TNBC model of *BRCA1*-deficiency. The results of these investigations are presented and discussed in this Chapter.

B. Results

1. PARPi induce formation of CCF in an ERCC1-dependent manner in NSCLC cells

a. Cytoplasmic DNA: a peculiar phenomenon linked to genomic instability

Chromatin is traditionally viewed as a nuclear entity. The presence of chromatin in the cytoplasm of cells is a peculiar phenomenon, which has been associated with specific cellular conditions, such as cellular senescence (411), mitochondrial DNA stress (412), and importantly, neoplasia (413). Cytoplasmic chromatin may take several forms, including free DNA fragments, also known as CCF, and micronuclei. CCF contain genomic DNA, DNA damage markers such as γH2AX, and heterochromatin markers such as H3K9me3 and

H3K27me3, but lack certain euchromatin markers, such as H3K9ac, indicating that CCF are derived from transcriptionally repressed heterochromatin regions and involve the DDR (411). By contrast, micronuclei, which arise from lagging chromosomal DNA and chromatin bridges as a consequence of unresolved genome instability, display chromatin-like structures, and are often heterogeneous in respect to their size, their chromatin condensation level and their possession of a nuclear envelope (414). If this diversity of patterns reflects the relative variety of molecular mechanisms involved in the formation of cytoplasmic DNA, genomic instability remains the common denominator of these mechanisms.

b. Choice of appropriate detection and quantification approaches for the evaluation of cytoplasmic DNA

The detection of cytoplasmic DNA patterns has mainly been achieved through the use of fluorescence-based imaging. Indeed, the detection of nucleic acids can be easily achieved using fluorescence microscopy through the use of various fluorescent dyes, which differ in terms of signal specificity and sensitivity. To evaluate whether PARPi can trigger the formation of CCF or micronuclei, we chose to use PicoGreen®, an extremely sensitive probe with high affinity for dsDNA. This makes it a convenient dye for the detection of cytoplasmic DNA, which is often present in much lower quantity compared to nuclear DNA. PicoGreen® fluorescent staining was coupled with 4',6-diamidino-2-phenylindole (DAPI) staining for the detection of cellular nuclei, and α-tubulin immunostaining for the identification of cytoplasms. We then quantified cytoplasmic PicoGreen® signal via automated high-content fluorescence microscopy, using the Operetta® platform (PerkinElmer).

When working with image-based cell profiling, image analysis usually constitutes a major bottleneck for the generation of reliable and statistically viable data. Here, we chose to develop a customised computational image analysis pipeline, using the Columbus software (PerkinElmer), to quantify the number of CCF in our experiments. This pipeline involved the following steps (**Figure IV.1**): (i) detection of cell nuclei using the blue channel (DAPI staining), allowing the definition of a cell population; (ii) for each cell in the cell population,

detection of cell cytoplasms using the red channel (α-tubulin/AF-647 immunostaining); (iii) for each cell in the cell population, detection of CCF and micronuclei within the cytoplasmic area using the green channel (PicoGreen® staining).

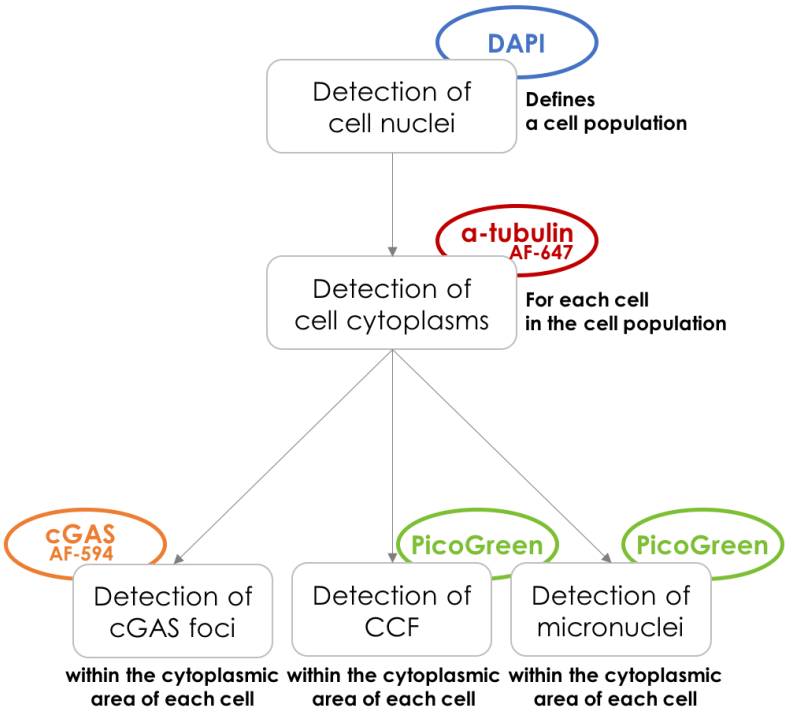

Figure IV.1. Computational image analysis pipeline used for the identification of CCF, micronuclei and cytoplasmic cGAS foci in fluorescence microscopy images.

Both CCF and micronuclei were detected as small regions on the image having a higher intensity than the surrounding cytoplasm. However, based on the observation that micronuclei display much higher intensity compared with CCF, two distinct algorithms with pre-defined intensity parameters were used to differentiate between CCF and micronuclei. The intensity threshold used to detect micronuclei was PicoGreen® staining intensity > 20% higher than that of the surrounding cytoplasm (manufacturer's recommendations). By contrast, detection of CCF was achieved by increasing the detection sensitivity through the assignment of (i) a background correction allowing more sensitive detection of low intensity foci, and (ii) a splitting coefficient enabling separation of joined foci, which resulted in the detection of events displaying an intensity around the sensitivity threshold.

c. Optimization of experimental conditions

In order to evaluate the potential of PARPi to induce formation of CCF in ERCC1-deficient setting, we used the previously described isogenic NSCLC model of ERCC1 deficiency developed in the A549 cell line, as well as another in-house isogenic NSCLC model developed in the H1975 cell line (379). Harbouring an *EGFR* T790M mutation, this cell line has a totally distinct but clinically-relevant background, which makes it an interesting model to study ERCC1-deficiency in NSCLC.

We first assessed the sensitivity of these cell lines to PARPi in short-term viability assays. As previously reported (364), we observed that the A549-ERCC1$^{+/-}$, A549-ERCC1$^{-/-}$ and H1975-ERCC1$^{-/-}$ cell lines displayed enhanced sensitivity to olaparib compared to their ERCC1-proficient counterparts (**Figure IV.2.A**). Consistently, restoration of ERCC1 activity via reintroduction of the functional isoform 202 in A549-ERCC1$^{-/-}$ cells rescued their sensitivity to olaparib. Similar results were obtained in the H1975-ERCC1 isogenic model (**Figure IV.2.B**). We then used these cell viability data to optimize treatment conditions for the evaluation of CCF formation in NSCLC cells exposed to PARPi.

We initially exposed A549- and H1975-ERCC1 isogenic cells to increasing concentrations of two different clinical PARPi, olaparib and rucaparib, and monitored the presence of CCF using IF at different time points (6 hours, 24 h, 48 h, 72 h and 96 h). For each PARPi, we selected concentrations surrounding the SF50 of the parental cell line (dose generating 50% of cell survival in short-term assays, after 5 days of exposure to the drug); we therefore started with a dose corresponding to the SF80 of the wildtype cell line, and subsequently applied a 2-fold increase at each subsequent dose to determine the final dose-range. We determined that the optimal time point for observing the phenotype was 72 hours with the defined dose-range, and thus applied these experimental conditions for every subsequent experiment.

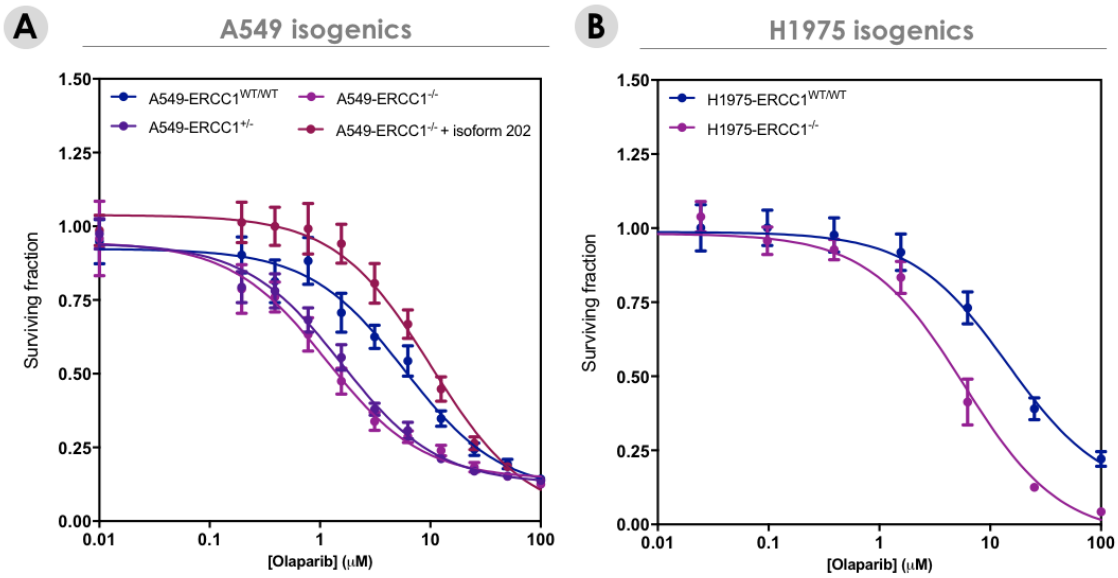

Figure IV.2. ERCC1-deficient cells exhibit enhanced sensitivity to PARPi.
A. Assessment of olaparib cytotoxicity in the A549-ERCC1$^{WT/WT}$, A549-ERCC1$^{+/-}$, A549-ERCC1$^{-/-}$ and A549-ERCC1$^{-/-}$ + isoform 202 cell lines. **B.** Assessment of olaparib cytotoxicity in the H1975-ERCC1$^{WT/WT}$ and H1975-ERCC1$^{-/-}$ cell lines. Cells were treated with a dose range of olaparib and continuously exposed to the drug for 5 days (short-term survival assay). Shown are dose-response curves displaying the mean surviving fractions; Mean ± SD, N=4.

d. PARPi generate CCF in an ERCC1-dependent fashion in A549 cells

We first measured the presence of CCF in A549-ERCC1 isogenic cell lines in the absence of treatment with PARPi, in order to evaluate the impact of ERCC1 deficiency on this phenotype. We observed no statistical difference between the levels of CCF in A549-ERCC1$^{WT/WT}$, A549-ERCC1$^{+/-}$ and A549-ERCC1$^{-/-}$ cells (**Figure IV.3.A** and **Figure IV.3.B**), suggesting that loss of ERCC1 on its own had little effect on the generation of CCF in this model.

We next exposed A549-ERCC1 isogenic cells to increasing concentrations of rucaparib or olaparib, and observed that both PARPi generated a dose-dependent increase in CCF number in A549-ERCC1$^{WT/WT}$, A549-ERCC1$^{+/-}$ and A549-ERCC1$^{-/-}$ cells (**Figure IV.3.A** and **Figure IV.3.C**). Importantly, this effect was significantly enhanced in A549-ERCC1$^{-/-}$ cells

compared to A549-ERCC1$^{WT/WT}$ cells (> 6-fold difference at 10 μM olaparib, *P*=0.0016; > 4-fold difference at 5 μM olaparib, *P*=0.03; two-way ANOVA, *post hoc* Sidak's test). Comparison of CCF levels in PARPi-treated A549-ERCC1$^{+/-}$ and A549-ERCC1$^{WT/WT}$ cells revealed that the heterozygous cell line displayed an intermediate phenotype, also associated with a significant increase in CCF formation compared to the wildtype cell line (> 3-fold difference at 10 μM and 5 μM olaparib, *P*=0.0023 and *P*=0.0384 respectively; two-way ANOVA, *post hoc* Sidak's test). Moreover, introduction of the construct encoding ERCC1 isoform 202 in the A549-ERCC1$^{-/-}$ cell line restored the generation of low levels of CCF in this cell line in response to PARPi (**Figure IV.3.C**).

Together, these results demonstrate that PARPi selectively enhance CCF formation in ERCC1-deficient A549 cells and that ERCC1 expression levels modulate the potential of PARPi to generate CCF in this model. The fact that the heterozygous cell line exhibits increased levels of CCF despite mild expression of ERCC1 suggests that an impaired but not abrogated ERCC1 function is sufficient to allow this selective effect, although the latter appears reduced compared to ERCC1$^{-/-}$ cells. Moreover, the rescue of this phenotype in the context of re-expression of a functional ERCC1 protein in ERCC1$^{-/-}$ cells provides a potent evidence that the observed effects are ERCC1-dependent.

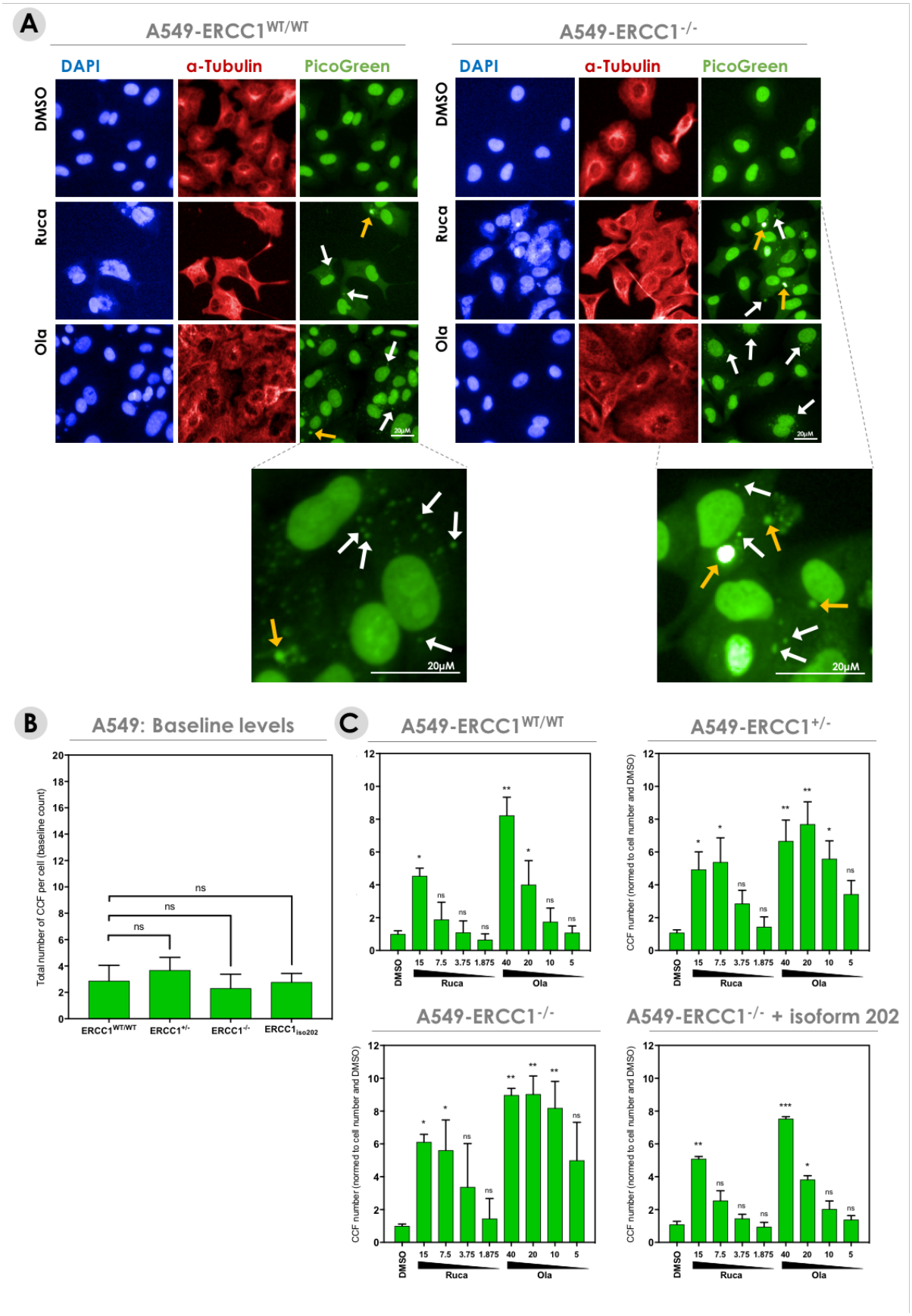
A
A549-ERCC1 WT/WT
A549-ERCC1 -/-
DAPI
α-Tubulin
PicoGreen
DMSO
Ruca
Ola
20μM
B
A549: Baseline levels
Total number of CCF per cell (baseline count)
ns
ERCC1 WT/WT
ERCC1 +/-
ERCC1 -/-
ERCC1 iso202
C
A549-ERCC1 WT/WT
A549-ERCC1 +/-
A549-ERCC1 -/-
A549-ERCC1 -/- + isoform 202
CCF number (normed to cell number and DMSO)
DMSO
15 7.5 3.75 1.875 40 20 10 5
Ruca
Ola

Figure IV.3. PARPi induce formation of CCF in an ERCC1-dependent manner in A549 cells.
A. Representative immunofluorescence images of DMSO-, rucaparib- and olaparib-exposed A549-ERCC1$^{WT/WT}$ and A549-ERCC1$^{-/-}$ cells. Blue, DAPI; Red, α-Tubulin; Green, PicoGreen. Cells were exposed to 15 μM rucaparib or 40 μM olaparib during 72h. White arrows, CCF; Yellow arrows, micronuclei. Scale bar, 20 μm. **B.** Automated quantification of baseline levels of CCF in A549-ERCC1 isogenic cell lines, using Columbus software. Number of CCF per cell is depicted. Mean ± SD, N=3, Kruskal-Wallis test and *post hoc* Dunn's test. **C.** Automated quantification of CCF in A549-ERCC1 isogenic cells exposed to increasing doses of rucaparib or olaparib (μM). Shown are CCF number per cell normalized to DMSO. Mean ± SD, N=3, Kruskal-Wallis test and *post hoc* Dunn's test, relative to DMSO control.

e. PARPi enhance ERCC1-dependent formation of CCF in H1975 cells

Evaluation of basal CCF levels in the H1975-ERCC1 isogenic model revealed that H1975-ERCC1$^{-/-}$ cells displayed a significantly higher number of CCF in the absence of PARPi compared to H1975-ERCC1$^{WT/WT}$ cells (> 2.5-fold difference, P=0.0035; Welch's t-test) (**Figure IV.4.A** and **Figure IV.4.B**). This is in contrast to the A549-ERCC1 isogenic model, and suggests that the distinct genetic background and intrinsic genomic instability of each model may influence the ability of a specific DDR defect, namely ERCC1 deficiency, to promote the formation of CCF. Treatment of H1975-ERCC1$^{WT/WT}$ and H1975-ERCC1$^{-/-}$ cells with PARPi led to a significant increase in CCF levels at high doses (**Figure IV.4.A** and **Figure IV.4.C**), although this increase was much more modest compared to that observed in A549 cells (in the wildtype cell line, 1.5-fold increase with 40 μM olaparib, P=0.04; 1.6-fold increase with 25 μM rucaparib, P=0.0085; Kruskal-Wallis test and *post hoc* Dunn's test). No difference could be observed when comparing H1975-ERCC1$^{-/-}$ and H1975-ERCC1$^{WT/WT}$ cells in their propensity to generate CCF under exposure to PARPi, but considering the difference observed at baseline in these cell lines, the absolute number of CCF generated per cell is certainly higher in H1975-ERCC1$^{-/-}$ cells. These observations are consistent with the phenotype observed in A549 cells, and together, our result support that (i) PARPi generate CCF in a dose-dependent manner in NSCLC cells, and that (ii) these effects are enhanced in the context of ERCC1 deficiency.

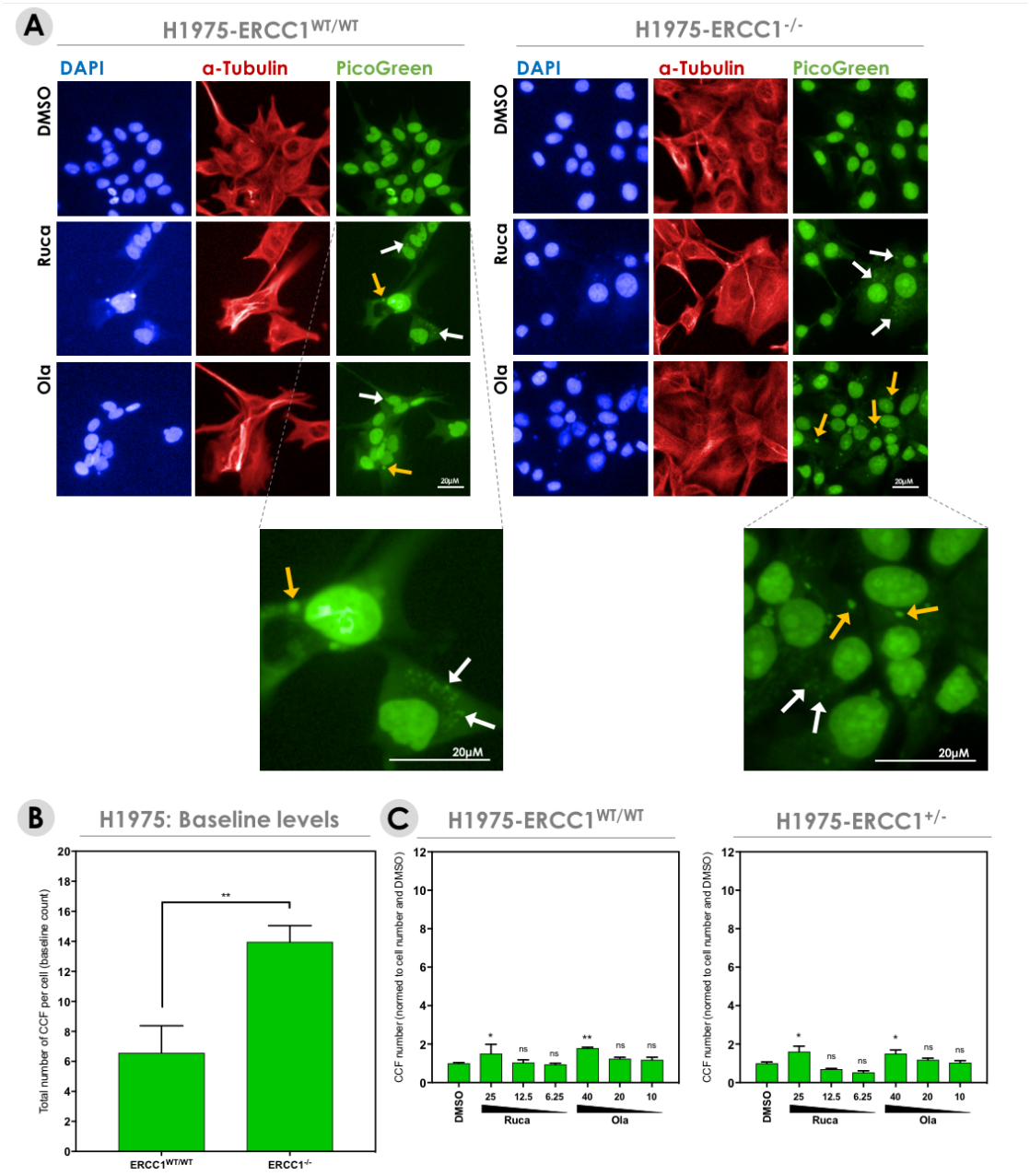

Figure IV.4. PARPi induce formation of CCF in an ERCC1-dependent manner in H1975 cells.

A. Representative immunofluorescence images of DMSO-, rucaparib- and olaparib-exposed H1975-ERCC1$^{WT/WT}$ and H1975-ERCC1$^{-/-}$ cells. Blue, DAPI; Red, α-Tubulin; Green, PicoGreen. Cells were exposed to 25 μM rucaparib or 40 μM olaparib during 72h. White arrows, CCF; Yellow arrows, micronuclei. Scale bar, 20 μm. **B.** Automated quantification of baseline levels of CCF in H1975-ERCC1 isogenic cell lines, using Columbus software. Number of CCF per cell is depicted. Mean ± SD, N=3, unpaired t test with Welch's correction. **C.** Automated quantification of CCF in H1975-ERCC1 isogenic cells exposed to increasing doses of rucaparib or olaparib (μM). Shown are CCF number per cell normalized to DMSO. Mean ± SD, N=3, Kruskal-Wallis test and *post hoc* Dunn's test, relative to DMSO control.

2. PARPi induce formation of CCF in a BRCA1-dependent manner in TNBC cells

In order to study whether increased formation of CCF upon PARPi exposure was specific to ERCC1 defect or a more common phenotype shared with other DDR deficiencies, we extended our experiments to BRCA1-defective tumour cells, which are also profoundly sensitive to PARPi (353). For this purpose, we used recently described isogenic series derived from the *BRCA1*-mutant TNBC cell line SUM149 (376,377).

a. Isogenic TNBC models of BRCA1 deficiency and PARP1-deficiency

The development of isogenic models of BRCA1-deficiency and PARP1-deficiency in the SUM149 cell line was performed at the Institute of Cancer Research by Dr. Amy Dréan and Dr. Stephen Pettitt and colleagues, as described in **Figure IV.5.A**.

The SUM149 cell line is *TP53*-mutated and presents a homozygous frameshift mutation in *BRCA1* (2288delT), which totally inactivates the protein. Thus, the generation of an isogenic model of BRCA1 deficiency in this cell line required the introduction of a mutation in the parental line that would restore the sequence of *BRCA1* gene in frame to allow constitutive re-expression of the protein. This was performed via CRISPR-Cas9 site directed mutagenesis of *BRCA1*. Subsequently, cells were selected upon talazoparib exposure, allowing the isolation of talazoparib-resistant, *BRCA1*-revertant clones. PCR amplification of *BRCA1* and subsequent genotyping of these clones eventually led to the identification and characterization of a validated *BRCA1*-revertant clone.

In addition to this first model, an isogenic model of PARP1 deficiency was generated from the parental SUM149 cell line (which has a wildtype *PARP1* gene). CRISPR-Cas9 site directed mutagenesis was used to insert a loss-of-function mutation in the *PARP1* gene, allowing in this case the generation of PARP1-null clones harbouring talazoparib resistance. Screening of the isolated clones after talazoparib selection led to the identification and characterization of a validated PARP1-null clone.

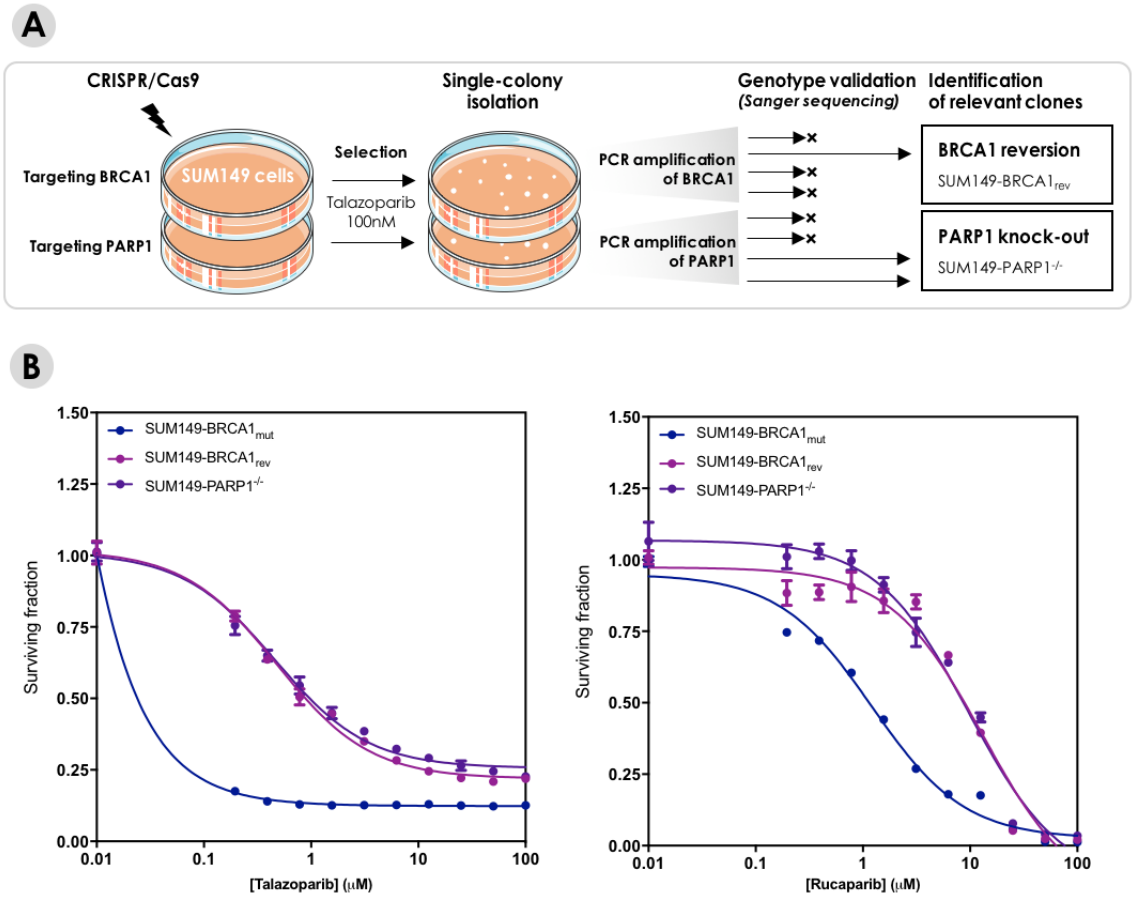

Figure IV.5. Generation of isogenic models of BRCA1-deficiency and PARP1-deficiency in the SUM149 TNBC cell line.

A. Schematic of the generation of *BRCA1*-revertant and PARP1-deficient clones from the parental TNBC cell line SUM149. Full procedures are detailed in Dréan et al. and Pettitt et al. **B.** Assessment of talazoparib and rucaparib cytotoxicity in the SUM149-BRCA1$_{mut}$, SUM149-BRCA1$_{rev}$ and SUM149-PARP1$^{-/-}$ cell lines. Cells were treated with a dose range of talazoparib or rucaparib and continuously exposed to the drug for 5 days (short-term survival assay). Shown are dose-response curves displaying the mean surviving fractions; Mean ± SD, N=4.

These distinct procedures resulted in the development of two isogenic TNBC models of BRCA1 and PARP1 deficiency. These comprise one *BRCA1*-mutant parental line (SUM149-BRCA1$_{mut}$), one *BRCA1*-mutant reverted line which is PARPi-resistant following restoration of the native BRCA1 reading frame and functionality (376) (SUM149-BRCA1$_{rev}$), and one SUM149 cell line with PARPi resistance caused by loss of PARP1 (377) (SUM149-PARP1$^{-/-}$).

Prior to evaluating the effects of PARPi regarding the generation of CCF in these isogenic models, we first assessed the sensitivity of SUM149 isogenic cell lines to PARPi in short-term viability assays. As expected, we revalidated the resistance of SUM149-BRCA1$_{rev}$ and SUM149-PARP1$^{-/-}$ cell lines to talazoparib and rucaparib, while SUM149-BRCA1$_{mut}$ cells displayed exquisite sensitivity to these PARPi (**Figure IV.5.B**).

b. PARPi generate CCF in a BRCA1-dependent fashion in SUM149 cells

To test our hypothesis, we replicated in the SUM149 isogenic models all experiments performed in ERCC1-isogenic NSCLC models, using the exact same experimental conditions and procedures. In the absence of PARPi, we observed that BRCA1-deficient cells (including SUM149-BRCA1$_{mut}$ and SUM149-PARP1$^{-/-}$ cells) displayed a significantly higher number of CCF compared to their BRCA1-proficient counterparts (≈ 10-fold difference, *P*=0.0038, Welch's t-test) (**Figure IV.6.B**). This is consistent with previously reported data (268) which suggest that, by causing an accumulation of unrepaired DSBs in the genome, defects in BRCA1 promote the accumulation of damaged DNA in the cytoplasm following progression through the S-phase of the cell cycle. Interestingly, basal CCF levels were equivalent in SUM149-BRCA1$_{mut}$ and SUM149-PARP1$^{-/-}$ cells, suggesting that the absence of a catalytically active PARP1 has little effect on the spontaneous generation of CCF. Treatment with PARPi resulted in a dose-dependent increase in the number of CCF in both SUM149-BRCA1$_{mut}$ and SUM149-BRCA1$_{rev}$ cells (**Figure IV.6.C**), but this phenotype was significantly enhanced in BRCA1-defective cells (> 2-fold difference at 5 μM olaparib, *P*=0.0001; > 1.5-fold difference at 3 μM rucaparib, *P*=0.0025; two-way ANOVA, *post hoc* Sidak's test). This observation supported that the generation of CCF by PARPi was a BRCA1-dependent process.

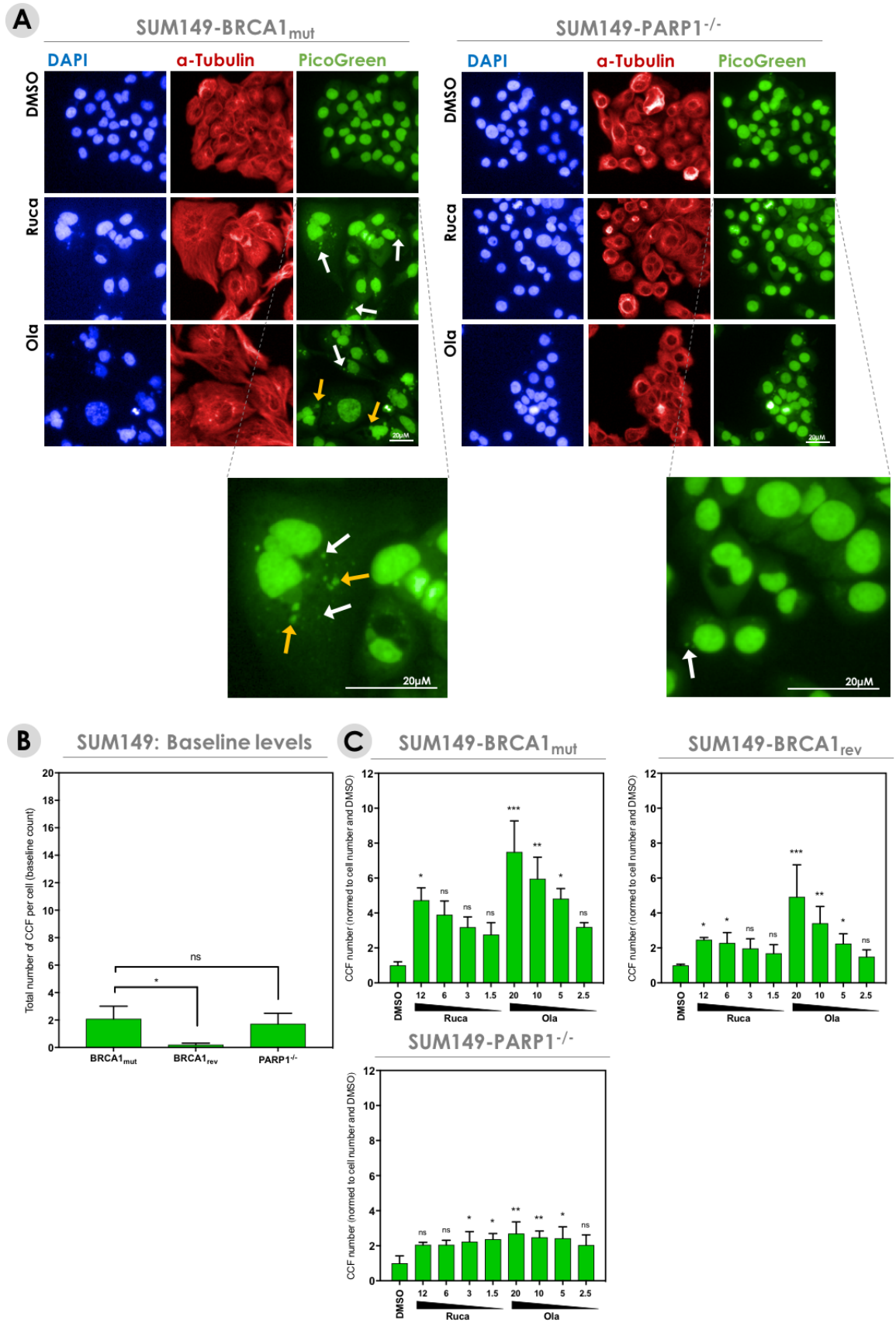
A
SUM149-BRCA1mut
SUM149-PARP1-/-
DAPI
α-Tubulin
PicoGreen
DMSO
Ruca
Ola
20µM
B
SUM149: Baseline levels
Total number of CCF per cell (baseline count)
ns
*
BRCA1mut
BRCA1rev
PARP1-/-
C
SUM149-BRCA1mut
SUM149-BRCA1rev
SUM149-PARP1-/-
CCF number (normed to cell number and DMSO)
DMSO
12
6
3
1.5
20
10
5
2.5
Ruca
Ola

Figure IV.6. PARPi induce formation of CCF in a BRCA1-dependent manner in SUM149 cells.
A. Representative immunofluorescence images of DMSO-, rucaparib- and olaparib-exposed SUM149-BRCA1$_{mut}$ and SUM149-PARP1$^{-/-}$ cells. Blue, DAPI; Red, α-Tubulin; Green, PicoGreen. Cells were exposed to 6 μM rucaparib or 10 μM olaparib during 72h. White arrows, CCF; Yellow arrows, micronuclei. Scale bar, 20 μm. **B.** Automated quantification of baseline levels of CCF in SUM149 isogenic cell lines, using Columbus software. Number of CCF per cell is depicted. Mean ± SD, N=3, unpaired t test with Welch's correction. **C.** Automated quantification of CCF in SUM149-BRCA1 isogenic cells exposed to increasing doses of rucaparib or olaparib (μM). Shown are CCF number per cell normalized to DMSO. Mean ± SD, N=3, Kruskal-Wallis test and *post hoc* Dunn's test, relative to DMSO control.

c. PARPi-mediated formation of CCF results from an on-target effect of PARPi on PARP1

Importantly, while PARPi induced high levels of CCF in SUM149-BRCA1$_{mut}$ cells, treatment of SUM149-PARP1$^{-/-}$ cells with either olaparib or rucaparib in the same conditions did not result in CCF formation (**Figure IV.6.A** and **Figure IV.6.C**), suggesting that this phenotype was dependent on an on-target effect of PARPi on PARP1.

This was further confirmed by the evaluation of the presence of chromatin – that is histone-bound DNA as opposed to naked DNA – in the cytoplasm of SUM149-BRCA1$_{mut}$ and SUM149-PARP1$^{-/-}$ cells, using detection of the protein histone H3. We isolated cytoplasmic and nuclear fractions of PARPi-treated SUM149-BRCA1$_{mut}$ and SUM149-PARP1$^{-/-}$ cells, following a simple biochemical cell fractionation procedure, and subsequently assessed the presence of histone H3 by WB in cytoplasmic and nuclear protein extracts. We used lamin B1 and β-tubulin as purity controls for the cytoplasmic and nuclear fractions respectively, and β-actin as a loading control. We observed a drastic increase in cytoplasmic histone H3 levels in PARPi-treated SUM149-BRCA1$_{mut}$ cells but not SUM149-PARP1$^{-/-}$ cells, while nuclear levels of this protein remained constant in both cell lines (**Figure IV.7**). This further supported the on-target effect of PARPi in generating CCF.

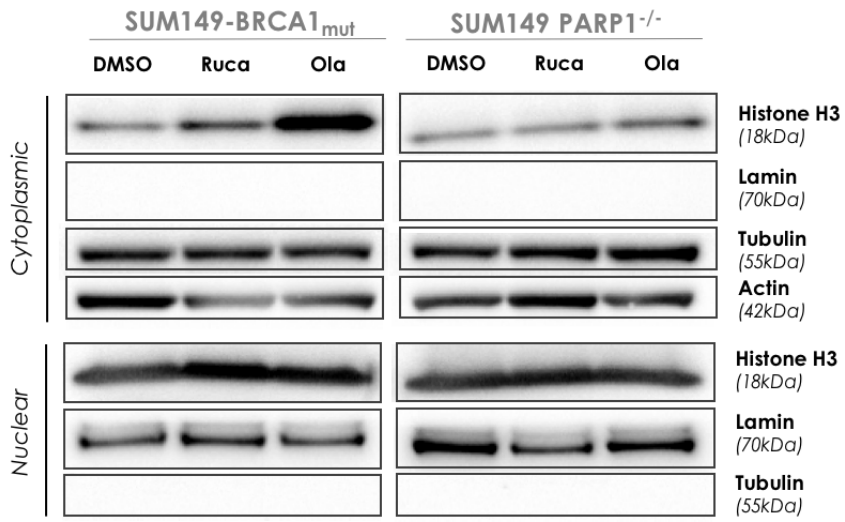

Figure IV.7. PARPi generate cytoplasmic chromatin in SUM149 cells via an on-target effect on PARP1.
Western blot of histone H3 in the nuclear and cytoplasmic fractions of SUM149-BRCA1$_{mut}$ and SUM149-PARP1$^{-/-}$ cells exposed to rucaparib and olaparib during 48h. β-tubulin and lamin B1 are used as fractions purity controls, and β-actin as a loading control.

3. PARPi-mediated generation of CCF is cell cycle-dependent

a. CCF generated by PARPi have micronuclei characteristics

As PARPi cause S-phase-dependent DNA damage, we hypothesized that the observed CCF might, at least in part, be micronuclei (265,266). Micronuclei are signs of genomic or chromosomal instability which have two important characteristics: (i) their formation is cell cycle-dependent – as they arise during anaphase from lagging chromosomes or chromatid bridges following unresolved DNA lesions; (ii) they contain heterochromatin and are replicationally active structures, initially surrounded by a fragile laminar membrane that is eventually easily ruptured (265,415).

To assess whether the CCF generated by PARPi have micronuclei characteristics, we first evaluated the impact of cell cycle blockade on the formation of CCF by PARPi. Therefore, we performed a kinetic experiment by monitoring the formation of CCF at different time points (6 h, 24 h, 48 h) in the presence of PARPi and upon cell cycle blockade in

A549-ERCC1$^{WT/WT}$ cells, using the cell cycle blockers 5-FU and hydroxyurea. We observed that PARPi-mediated formation of CCF was totally abrogated in the context of exposure to 5-FU or hydroxyurea (**Figure IV.8**), suggesting that progression through the cell cycle is required for the generation of CCF by PARPi in this model. These results were further validated with the use of a more specific cell cycle inhibitor, the CDK1 inhibitor (CDK1i) RO-3306, in both A549-ERCC1$^{WT/WT}$ and SUM149-BRCA1$_{mut}$ cells (**Figure IV.9**). These observations support that CCF arise in a cell cycle-dependent manner following treatment with PARPi; furthermore, they suggest that the origin of this phenotype resides in the creation of S-phase-specific DNA damage following the accumulation of stalled or collapsed replication forks that are caused by PARP1 trapping onto the DNA.

To further characterize the CCF generated in the context of exposure to PARPi, we decided to evaluate the presence of micronuclei-associated markers in these structures, such as the heterochromatin marker H3K27me3 and the nuclear membrane marker lamin B1. We performed IF analysis of the co-staining of PicoGreen® with H3K27me3 and lamin B1 in olaparib-treated A549-ERCC1$^{WT/WT}$ and A549-ERCC1$^{-/-}$ cells, and observed the presence of some typical micronuclei structures (**Figure IV.10.A**). Indeed, we found colocalization of CCF with cytoplasmic H3K27me3 foci in both A549-ERCC1$^{WT/WT}$ and A549-ERCC1$^{-/-}$ cells after treatment with olaparib, and consistently observed a dose-dependent increase in the number of H3K27me3 foci in these cell lines (**Figure IV.10.B**). Of note, the levels of generated H3K27me3 foci were significantly higher in A549-ERCC1$^{-/-}$ cells than in A549-ERCC1$^{WT/WT}$ cells (> 10-fold difference at 10 μM olaparib, P=0.0001; > 6-fold difference at 5 μM rucaparib, P=0.0279; two-way ANOVA, *post hoc* Sidak's test), consistent with the previously described enhanced formation of CCF in ERCC1-defective cells. Moreover, we observed the presence of a lamin B1 membrane around some CCF expressing H3K27me3, suggesting that (i) at least some of the generated CCF are most likely to be lamin B1-positive micronuclei; (ii) these may co-exist with other micronuclei structures still containing heterochromatin markers despite loss of the fragile lamin B1 envelope; (iii) the disruption of micronuclei integrity through loss of the lamin B1 envelope may have led to the accumulation of a more heterogeneous population of CCF whose

expression of heterochromatin markers is variable. Thus, the final population of detected CCF comprises a wide variety of structures, ranging from intact micronuclei to much smaller fragments of dsDNA.

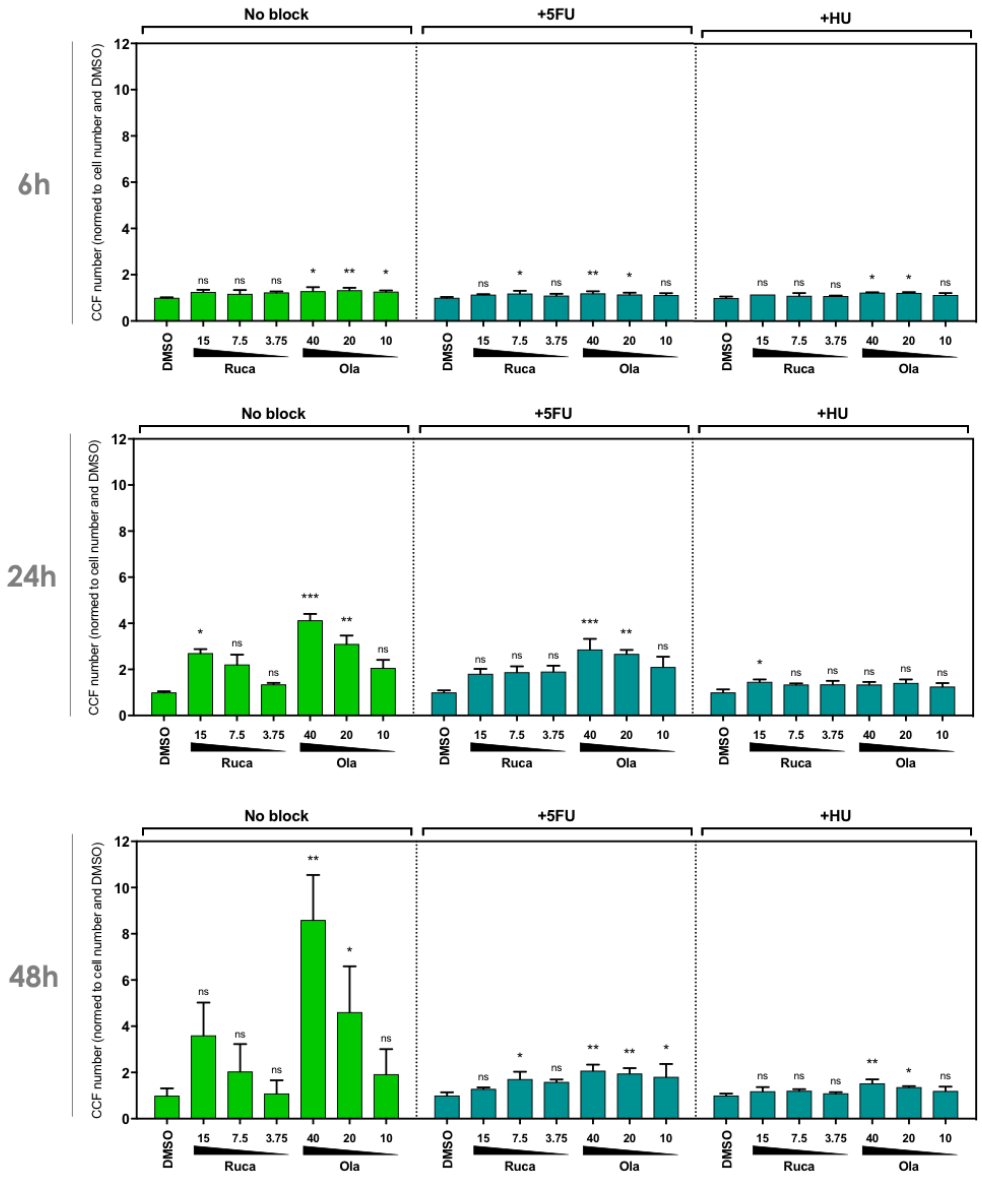

Figure IV.8. The cell cycle blockers 5-FU and hydroxyurea prevent PARPi-mediated formation of CCF in A549 cells.

Automated quantification of CCF at indicated time points in A549-ERCC1$^{WT/WT}$ cells exposed to increasing doses of rucaparib or olaparib (μM) in the presence or absence of the cell cycle blockers 5-FU or hydroxyurea. Number of CCF per cell, counted using Columbus software, are normalized to the DMSO (vehicle). Mean ± SD, N=3, Kruskal-Wallis test and *post hoc* Dunn's test, relative to DMSO control.

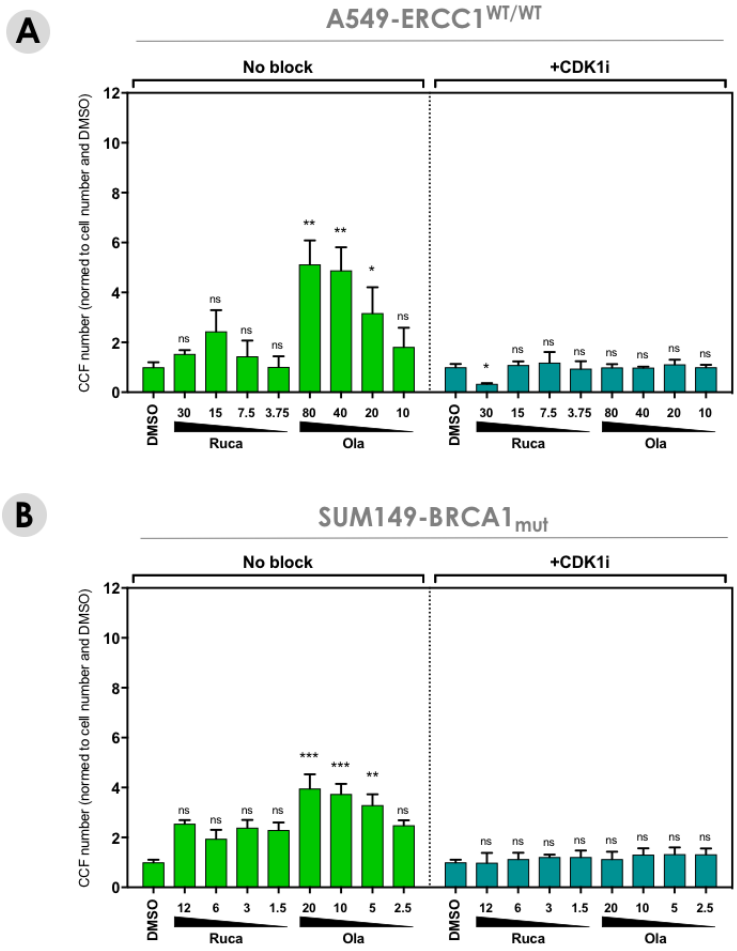

Figure IV.9. The CDK1 inhibitor RO-3306 prevents PARPi-mediated formation of CCF.
Automated quantification of CCF in A549-ERCC1$^{WT/WT}$ (**A**) and SUM149- BRCA1$_{mut}$ (**B**) cells exposed to increasing doses of rucaparib or olaparib (μM) in the presence or absence of the cell cycle blocker RO-3306. Shown are CCF number per cell normalized to DMSO. Mean ± SD, N=3, Kruskal-Wallis test and *post hoc* Dunn's test, relative to DMSO control.

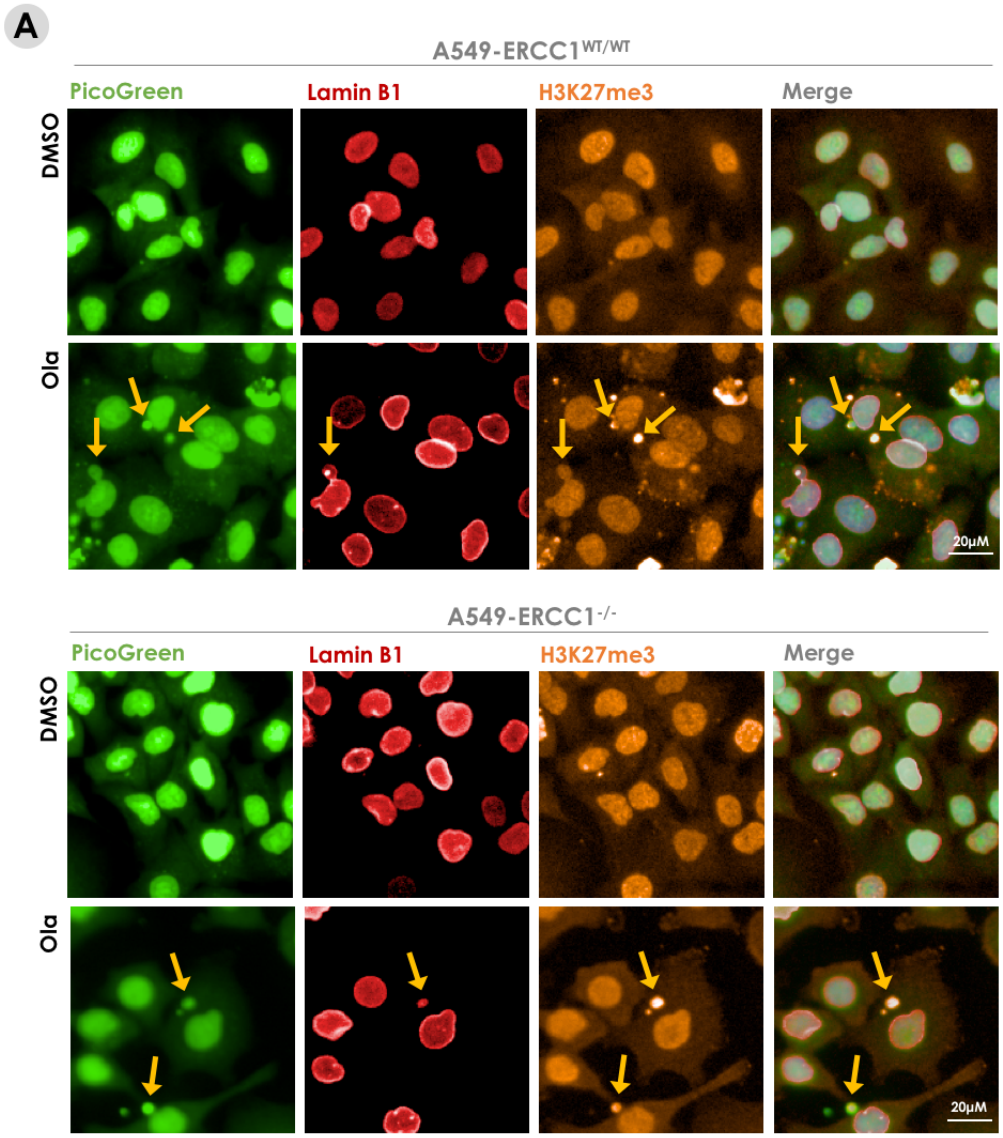
A
A549-ERCC1 WT/WT
PicoGreen
Lamin B1
H3K27me3
Merge
DMSO
Ola
20µM
A549-ERCC1 -/-
PicoGreen
Lamin B1
H3K27me3
Merge
DMSO
Ola
20µM

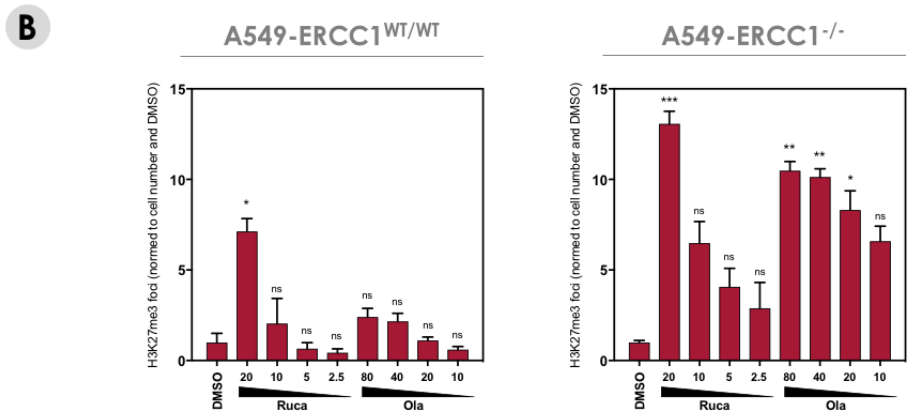
B
A549-ERCC1 WT/WT
A549-ERCC1 -/-
H3K27me3 foci (normed to cell number and DMSO)
DMSO
20
10
5
2.5
80
40
20
10
Ruca
Ola

Figure IV.10. PARPi-induced CCF have micronuclei characteristics.
A. Representative immunofluorescence images of DMSO- and olaparib-exposed A549-ERCC1$^{WT/WT}$ and A549-ERCC1$^{-/-}$ cells. Green, PicoGreen; Red, Lamin B1; Orange, H3K27me3. Cells were exposed to 40 µM olaparib or DMSO during 72h. White arrows, CCF; Yellow arrows, micronuclei. Scale bar, 20 µm. **B.** Automated quantification of cytoplasmic H3K27me3 foci in A549-ERCC1$^{WT/WT}$ and A549-ERCC1$^{-/-}$ cells exposed to increasing doses of rucaparib or olaparib (µM), using Columbus software. Number of H3K27me3 foci per cell normalized to the DMSO of the corresponding cell line is depicted. Mean ± SD, N=3, Kruskal-Wallis test and *post hoc* Dunn's test, relative to DMSO control.

b. PARPi generate dose-dependent formation of micronuclei

In order to appraise the extent of micronuclei generated following treatment with PARPi, we performed an automated quantification of micronuclei using a dedicated pre-defined algorithm in the Columbus software (see Chapter IV, paragraph B.1.b). This quantification revealed baseline patterns similar to that of CCF (**Figure IV.11.A**), as well as a consistent dose-dependent formation of micronuclei upon PARPi exposure, both in ERCC1- and BRCA1-isogenic models (**Figure IV.11.A** and **Figure IV.11.B**). In line with our previous observations on CCF, this effect was more pronounced in A549-ERCC1$^{-/-}$ cells compared with A549-ERCC1$^{WT/WT}$ and in SUM149-BRCA1$_{mut}$ cells compared with SUM149-BRCA1$_{rev}$ cells, suggesting that micronuclei induction is enhanced in ERCC1- and BRCA1-deficient contexts. In addition, the formation of micronuclei was abrogated in the SUM149-PARP1$^{-/-}$ cell line, consistent with an on-target effect of PARPi.

Together, these data support the hypothesis that PARPi exposure promotes the accumulation of CCF, some of which have micronuclei characteristics. This phenotype results from an on-target effect of PARPi on PARP1, is cell cycle-dependent and is enhanced in ERCC1-defective NSCLC cells and other PARPi-sensitive models such as BRCA1-defective TNBC.

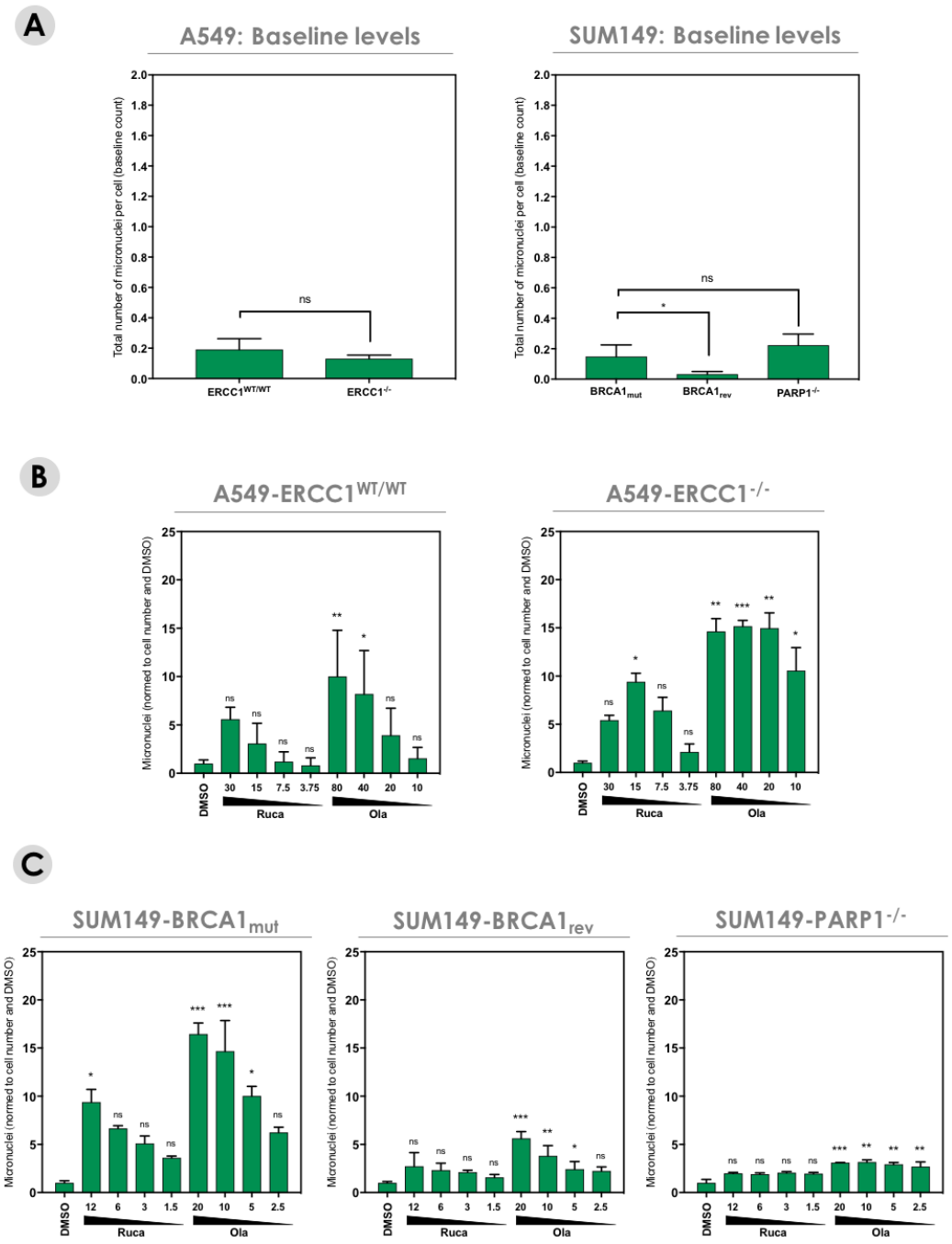

Figure IV.11. PARPi generate dose-dependent formation of micronuclei.

A. Automated quantification of baseline levels of micronuclei in A549 isogenic and SUM149 isogenic cell lines, using Columbus software. Number of micronuclei per cell is depicted. Mean ± SD, N=3, unpaired t test with Welch's correction. **B** and **C.** Automated quantification of micronuclei in A549-ERCC1$^{WT/WT}$ and A549-ERCC1$^{-/-}$ cells (**B**), and SUM149-BRCA1$_{mut}$, SUM149-BRCA1$_{rev}$ and SUM149-PARP1$^{-/-}$ cells (**C**) exposed to increasing doses of rucaparib or olaparib (μM), using Columbus software. Number of micronuclei per cell normalized to the DMSO of the corresponding cell line is depicted. Mean ± SD, N=3, Kruskal-Wallis test and *post hoc* Dunn's test, relative to DMSO control.

4. PARPi-induced CCF are detected by cGAS

cGAS is a very potent sensor of cytoplasmic dsDNA. In the context of micronuclei formation after DNA damage, the rupture of micronuclear envelopes provides a mechanism by which dsDNA is exposed to sensing by cGAS, and consistently, re-localization of cGAS to micronuclei has been observed following exposure to DNA-damaging agents (265,266). Similarly, in cells undergoing senescence, degradation of the nuclear envelope component lamin B1 leads to the formation of CCF that are detected by cGAS (411,416). Along these lines, we hypothesized that the CCF generated following treatment with PARPi may be detected by cGAS, thereby leading to an activation of the cGAS/STING pathway.

a. cGAS mediates the detection of CCF in PARPi-treated NSCLC cells

To investigate whether cGAS senses cytoplasmic DNA following treatment with PARPi, we assessed the ability of cGAS to form foci through re-localization to CCF. We thus performed immunofluorescent staining of cGAS in A549-ERCC1 isogenic cell lines exposed to increasing doses of rucaparib or olaparib. After 72 h of treatment with either of the PARPi, we observed a dose-dependent increase in the number of cytoplasmic cGAS foci in all A549-ERCC1 isogenic cells (**Figure IV.12.A** and **Figure IV.12.C**). Although the number of cGAS foci at baseline did not appear significantly different between ERCC1-proficient and -deficient cell lines (**Figure IV.12.B**), we observed a more intense induction of cGAS foci after treatment with PARPi in A549-ERCC1$^{-/-}$ and A549-ERCC1$^{+/-}$ cells compared to A549-ERCC1$^{WT/WT}$ cells (at 20 µM olaparib, > 6-fold increase in A549-ERCC1$^{-/-}$ and A549-ERCC1$^{+/-}$ cells vs < 3-fold increase in A549-ERCC1$^{WT/WT}$ cells). Moreover, this enhanced formation of cGAS foci in A549-ERCC1$^{-/-}$ cells was impaired by the re-expression of ERCC1 isoform 202, with cGAS foci levels in the A549-ERCC1$^{-/-}$ + isoform 202 cell line similar to that observed in the A549-ERCC1$^{WT/WT}$ cell line (**Figure IV.12.C**). These results suggest that partial or complete loss of ERCC1 is associated with an increased formation of cGAS foci following treatment with PARPi in A549 cells.

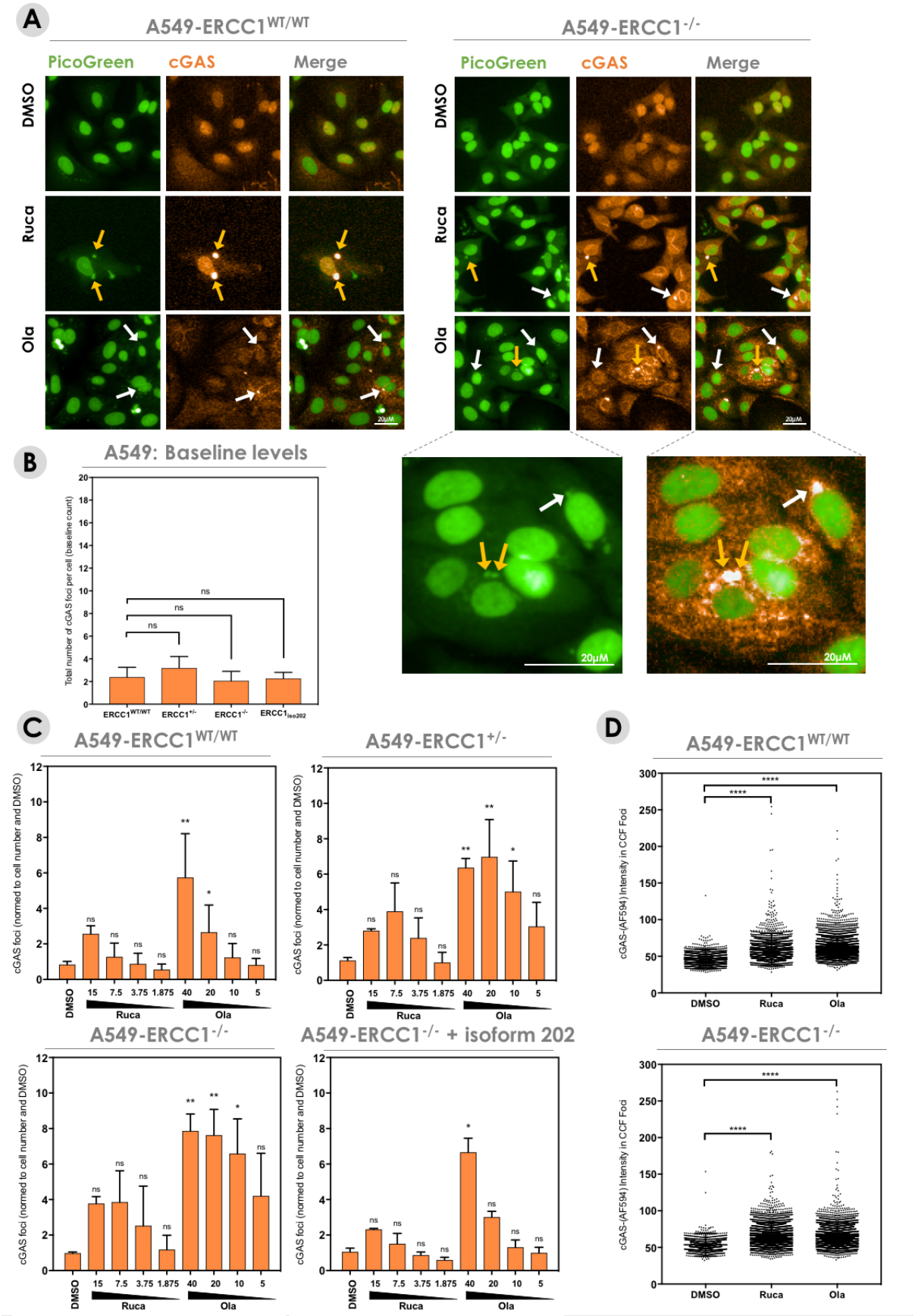
A
A549-ERCC1 WT/WT
A549-ERCC1 -/-
PicoGreen
cGAS
Merge
DMSO
Ruca
Ola
20µM
B
A549: Baseline levels
Total number of cGAS foci per cell (baseline count)
ns
ERCC1 WT/WT
ERCC1 +/-
ERCC1 -/-
ERCC1 Iso202
C
A549-ERCC1 WT/WT
A549-ERCC1 +/-
A549-ERCC1 -/-
A549-ERCC1 -/- + isoform 202
cGAS foci (normed to cell number and DMSO)
15 7.5 3.75 1.875 40 20 10 5
Ruca
Ola
D
A549-ERCC1 WT/WT
A549-ERCC1 -/-
cGAS-(AF594) Intensity in CCF Foci
****

Figure IV.12. PARPi induce formation of cGAS foci in an ERCC1-dependent manner in A549 cells.
A. Representative immunofluorescence images of DMSO-, rucaparib- and olaparib-exposed A549-ERCC1$^{WT/WT}$ and A549-ERCC1$^{-/-}$ cells. Green, PicoGreen; Orange, cGAS. Cells were exposed to 15 μM rucaparib or 40 μM olaparib during 72h. White arrows, CCF; Yellow arrows, micronuclei. Scale bar, 20 μm. **B.** Automated quantification of baseline levels of cytoplasmic cGAS foci in A549-ERCC1 isogenic cell lines, using Columbus software. Number of cytoplasmic cGAS foci per cell is depicted. Mean ± SD, N=3, unpaired t test with Welch's correction. **C.** Automated quantification of cytoplasmic cGAS foci in A549-ERCC1 isogenic cells exposed to increasing doses of rucaparib or olaparib (μM). Shown are cytoplasmic cGAS foci number per cell normalized to DMSO. Mean ± SD, N=3, Kruskal-Wallis test and *post hoc* Dunn's test, relative to DMSO control. **D.** Scatter box plots displaying cytoplasmic cGAS foci intensity for each co-localizing CCF in A549-ERCC1$^{WT/WT}$ and A549-ERCC1$^{-/-}$ cells exposed to DMSO (vehicle), 15 μM rucaparib or 40 μM olaparib. N=3, Kruskal- Wallis test and *post hoc* Dunn's test.

In order to quantify the observed co-localization between CCF and cGAS (**Figure IV.12.A**), we used Columbus software to measure cGAS staining intensity at each CCF location within single images. By pooling the results of three individual images per condition, we were able to compare the level of co-localization between PARPi-treated and DMSO-treated cells. We found, in both A549-ERCC1$^{WT/WT}$ and A549-ERCC1$^{-/-}$ cells, a higher number of CCF harbouring high cGAS staining intensity in rucaparib- and olaparib-treated cells compared with DMSO-treated cells, suggesting an increase in CCF/cGAS co-localization after treatment with PARPi (**Figure IV.12.D**).

To validate our data in an independent model of ERCC1-deficiency, we performed the same analyses in the H1975 isogenic model. Consistent with previous results regarding CCF formation (**Figure IV.4**), we observed, in the absence of PARPi, significantly higher levels of cGAS foci in H1975-ERCC1$^{-/-}$ cells compared with H1975-ERCC1$^{WT/WT}$ cells (P = 0.0279; Welch's t-test, **Figure IV.13.B**), suggesting that the CCF formed as a result of ERCC1 loss trigger re-localization of cytoplasmic cGAS into foci. Quantification of the number of cytoplasmic cGAS foci after PARPi treatment revealed an increased formation of cGAS foci at high doses with rucaparib and olaparib but no significant difference between H1975-ERCC1$^{-/-}$ and H1975-ERCC1$^{WT/WT}$ cells (**Figure IV.13.A** and **Figure IV.13.C**).

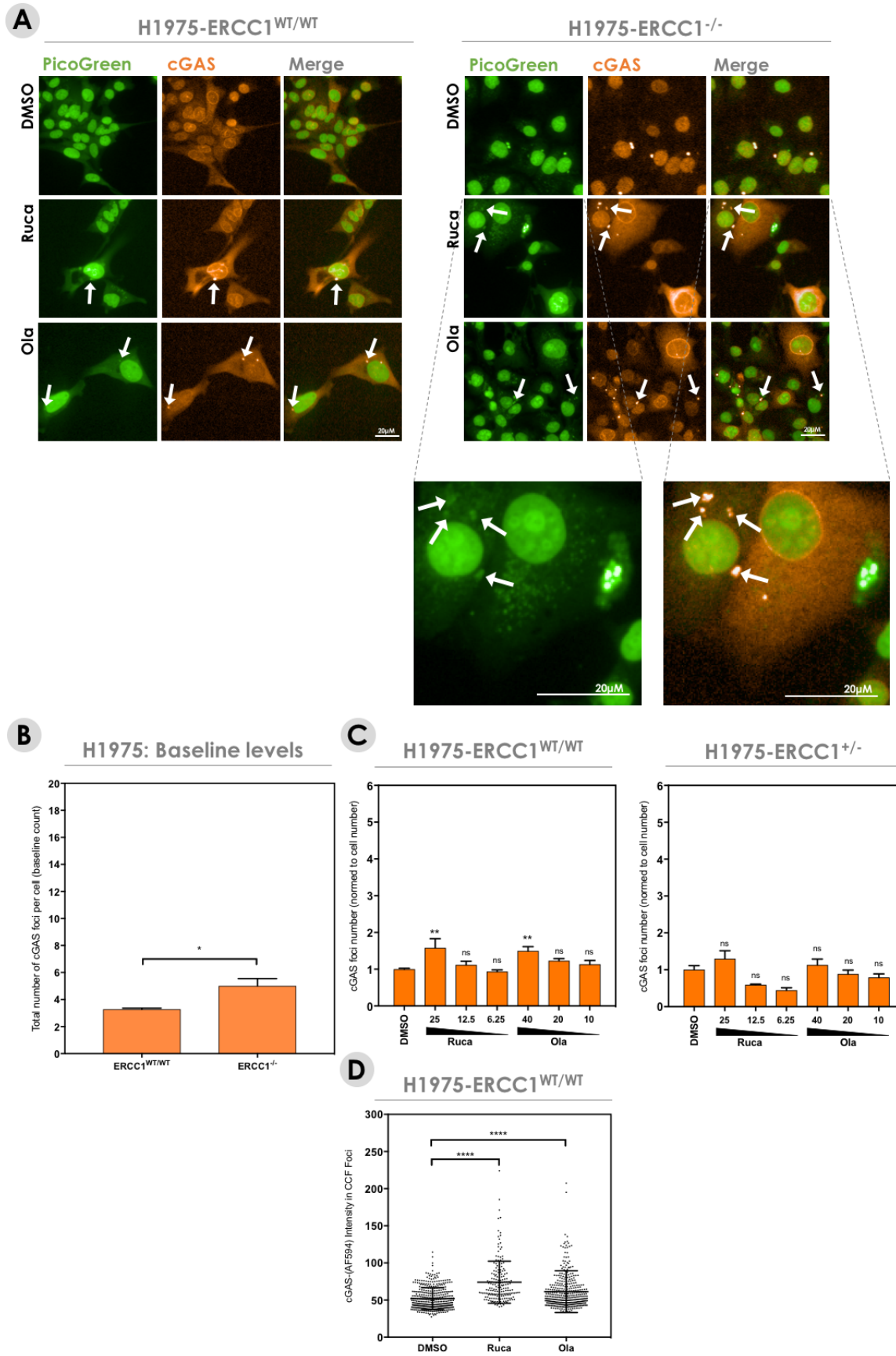
A
H1975-ERCC1WT/WT
H1975-ERCC1-/-
PicoGreen
cGAS
Merge
DMSO
Ruca
Ola
20µM
B
H1975: Baseline levels
Total number of cGAS foci per cell (baseline count)
ERCC1WT/WT
ERCC1-/-
C
H1975-ERCC1WT/WT
H1975-ERCC1+/-
cGAS foci number (normed to cell number)
DMSO
25
12.5
6.25
40
20
10
Ruca
Ola
ns
D
H1975-ERCC1WT/WT
cGAS-(AF594) Intensity in CCF Foci
****

Figure IV.13. PARPi induce formation of cGAS foci in an ERCC1-dependent manner in H1975 cells.
A. Representative immunofluorescence images of DMSO-, rucaparib- and olaparib-exposed H1975-ERCC1$^{WT/WT}$ and H1975-ERCC1$^{-/-}$ cells. Green, PicoGreen; Orange, cGAS. Cells were exposed to 25 µM rucaparib or 40 µM olaparib during 72h. White arrows, CCF; Yellow arrows, micronuclei. Scale bar, 20 µm. **B.** Automated quantification of baseline levels of cytoplasmic cGAS foci in H1975-ERCC1 isogenic cell lines, using Columbus software. Number of cytoplasmic cGAS foci per cell is depicted. Mean ± SD, N=3, unpaired t test with Welch's correction. **C.** Automated quantification of cytoplasmic cGAS foci in H1975-ERCC1 isogenic cells exposed to increasing doses of rucaparib or olaparib (µM). Shown are cytoplasmic cGAS foci number per cell normalized to DMSO. Mean ± SD, N=3, Kruskal-Wallis test and *post hoc* Dunn's test, relative to DMSO control. **D.** Scatter box plot displaying cytoplasmic cGAS foci intensity for each co-localizing CCF in H1975-ERCC1$^{WT/WT}$ cells exposed to DMSO (vehicle), 25 µM rucaparib or 40 µM olaparib. N=3, Kruskal-Wallis test and *post hoc* Dunn's test.

Considering the higher levels of CCF and cytoplasmic cGAS foci at baseline in H1975-ERCC1$^{-/-}$ cells, this suggests that the absolute number of cGAS foci formed after PARPi treatment is higher in ERCC1-deficient cells. Analysis of cGAS staining intensity within CCF revealed a significant increase in cGAS foci/CCF co-localization upon PARPi exposure in H1975-ERCC1$^{WT/WT}$ cells, similar to what was obtained in A549-ERCC1 isogenic cell lines (**Figure IV.13.D**).

Together, these results suggest that the CCF generated by PARPi in NSCLC cells are detected by cGAS. This is reflected by an enhanced formation and re-localization of cytoplasmic cGAS foci to CCF in PARPi-treated cells, a phenotype which appears to be ERCC1-dependent in both A549 and H1975 isogenic models.

b. cGAS mediates the detection of CCF in PARPi-treated TNBC cells

To further evaluate cGAS activation in PARPi-sensitive contexts, we used the previously described isogenic TNBC models of BRCA1 and PARP1 deficiency. Immunofluorescent detection of cGAS in this model revealed that, in the absence of PARPi, SUM149-BRCA1$_{mut}$ cells displayed significantly higher levels of cytoplasmic cGAS foci compared to SUM149-BRCA1$_{rev}$ cells (P = 0.0111; Welch's t-test, **Figure IV.14.B**). This suggested that

the CCF formed as a result of BRCA1 deficiency in SUM149 cells trigger re-localization of cytoplasmic cGAS into foci. In the presence of PARPi, we observed a dose-dependent formation of cytoplasmic cGAS foci in SUM149-BRCA1$_{mut}$ cells, at a higher level than in SUM149- BRCA1$_{rev}$ cells (1.4-fold difference at 20 μM olaparib, $P = 0.0033$; two-way ANOVA post hoc Sidak's test, **Figure IV.14.C**), consistent with the observation that *BRCA1*-mutant cells generate higher levels of CCF when exposed to PARPi. More importantly, no increase in cytoplasmic cGAS foci could be detected in the PARPi-resistant SUM149-PARP1$^{-/-}$ cell line (**Figure IV.14.A** and **Figure IV.14.C**), suggesting that the minimal levels of CCF measured in this cell line were insufficient to trigger cGAS re-localization.

These results support the idea that cGAS detects CCF in SUM149 cells exposed to PARPi. This phenotype is enhanced in BRCA1-deficient cells due to the elevated levels of CCF generated after PARP inhibition, and on the contrary, abrogated in PARP1$^{-/-}$ cells.

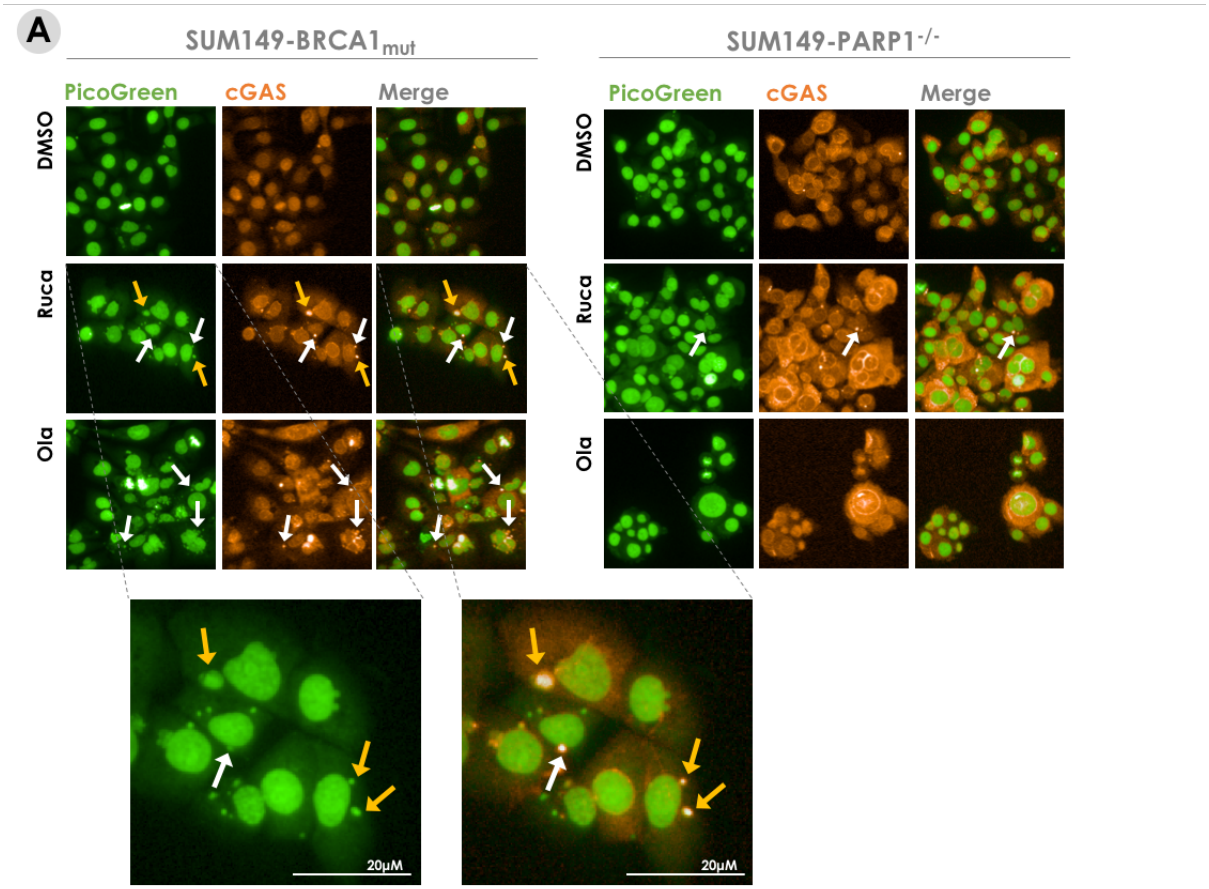

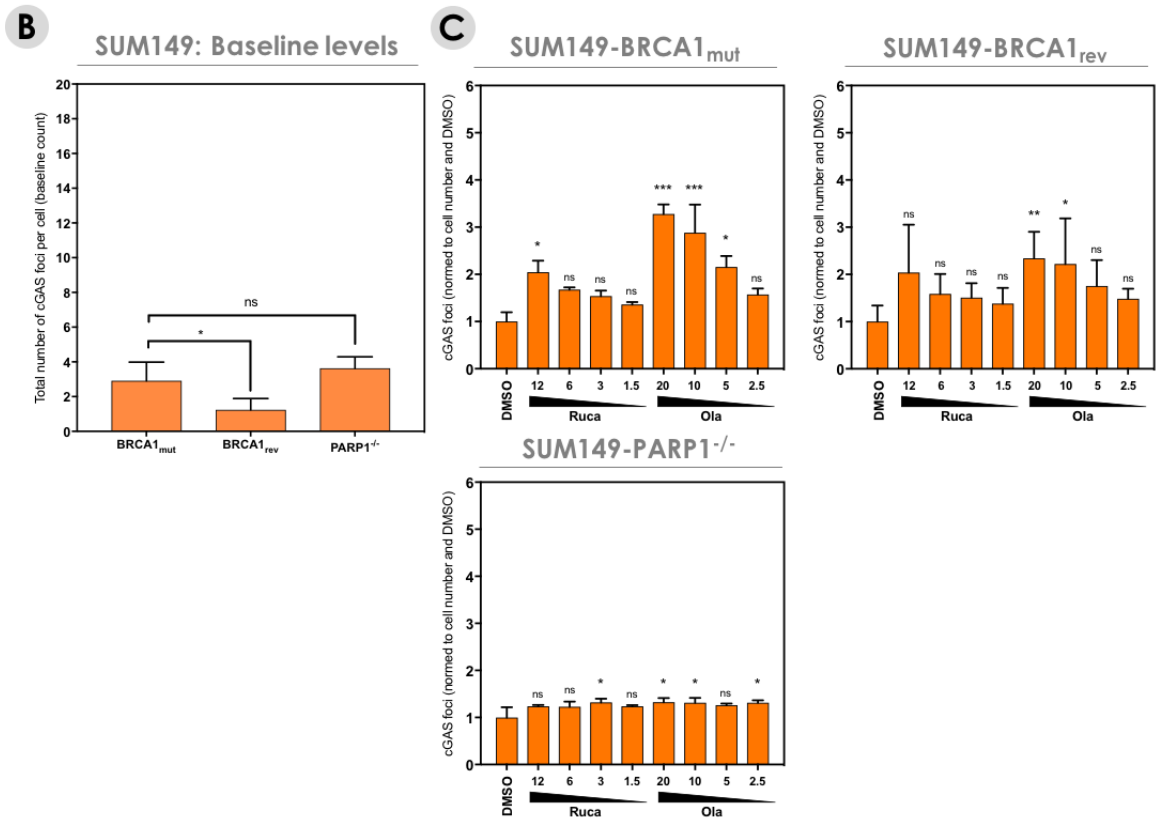

Figure IV.14. PARPi induce formation of cGAS foci in a BRCA1-dependent manner in SUM149 cells.

A. Representative immunofluorescence images of DMSO-, rucaparib- and olaparib-exposed SUM149-BRCA1$_{mut}$ and SUM149-PARP1$^{-/-}$ cells. Green, PicoGreen; Orange, cGAS. Cells were exposed to 6 μM rucaparib or 10 μM olaparib during 72h. White arrows, CCF; Yellow arrows, micronuclei. Scale bar, 20 μm. **B.** Automated quantification of baseline levels of cytoplasmic cGAS foci in SUM149 isogenic cell lines, using Columbus software. Number of cytoplasmic cGAS foci per cell is depicted. Mean ± SD, N=3, unpaired t test with Welch's correction. **C.** Automated quantification of cytoplasmic cGAS foci in SUM149 isogenic cells exposed to increasing doses of rucaparib or olaparib (μM). Shown are cytoplasmic cGAS foci number per cell normalized to DMSO. Mean ± SD, N=3, Kruskal-Wallis test and *post hoc* Dunn's test, relative to DMSO control.

5. PARPi activate cGAS/STING signalling in a DDR-defects-dependent manner

Having observed in various experimental models that the generation of CCF by PARPi triggers cytoplasmic DNA sensing through re-localization of the sensor cGAS to CCF, we next investigated the potential of PARPi to activate cGAS/STING signalling in those models.

Transient activation of the cGAS/STING pathway can be monitored through the analysis of some of its pivotal components. For example, production of the chemical mediator cGAMP is a typical marker associated with cGAS activation, and as such, has been detected in cells transfected with dsDNA, as well as in senescent cells (411). STING also shows hallmarks of activation in the context of cytosolic DNA sensing, including formation of homo-dimers and redistribution into cytoplasmic aggregates. However, the gold-standard approach for monitoring cGAS/STING pathway activation remains the evaluation of its downstream signalling effectors, which include the kinase TBK1 and the transcription factors IRF3, IRF7 and NF-κB. These proteins often undergo phosphorylation as a pattern of activation, which provides a simple and straightforward readout for the evaluation of cGAS/STING signalling status. Therefore, we assessed the phosphorylation of these factors in our models in the context of exposure to PARPi; in the next paragraphs are the results of these investigations.

a. PARPi trigger TBK1 phosphorylation in an ERCC1-dependent manner in NSCLC cells

We first evaluated phosphorylation of TBK1 (pTBK1) in isogenic NSCLC models of ERCC1 deficiency. We exposed A549-ERCC1 isogenic cells to increasing doses of olaparib and monitored TBK1 phosphorylation by WB. We observed a dose-dependent increase in pTBK1 levels in A549-ERCC1$^{-/-}$ cells after olaparib exposure, while TBK1 phosphorylation was almost undetectable in A549-ERCC1$^{WT/WT}$ cells in the same conditions (**Figure IV.15.A**). Interestingly, the A549-ERCC1$^{+/-}$ cell line showed an intermediate phenotype, displaying a slightly more intense phosphorylation of TBK1 than the A549-ERCC1$^{WT/WT}$ cell line at the highest treatment dose (**Figure IV.15.B**). This suggested that the higher levels

of CCF generated in ERCC1-deficient cells – including A549-ERCC1$^{-/-}$ and A549-ERCC1$^{+/-}$ cells – triggered sufficient activation of cGAS to enable cGAMP production, STING homo-dimerization and subsequent phosphorylation of TBK1. Furthermore, the elevated expression of STING exclusively found in A549-ERCC1$^{-/-}$ cells (**Figure III.10**) may provide an additional level of amplification of this signalling cascade, thus leading to an even more enhanced phosphorylation of TBK1 in this cell line. Of note, cGAS protein expression did not appear significantly changed following PARPi treatment in this model, suggesting that its activation depends more on a re-organization of the protein cytoplasmic pools than on a transcriptional upregulation.

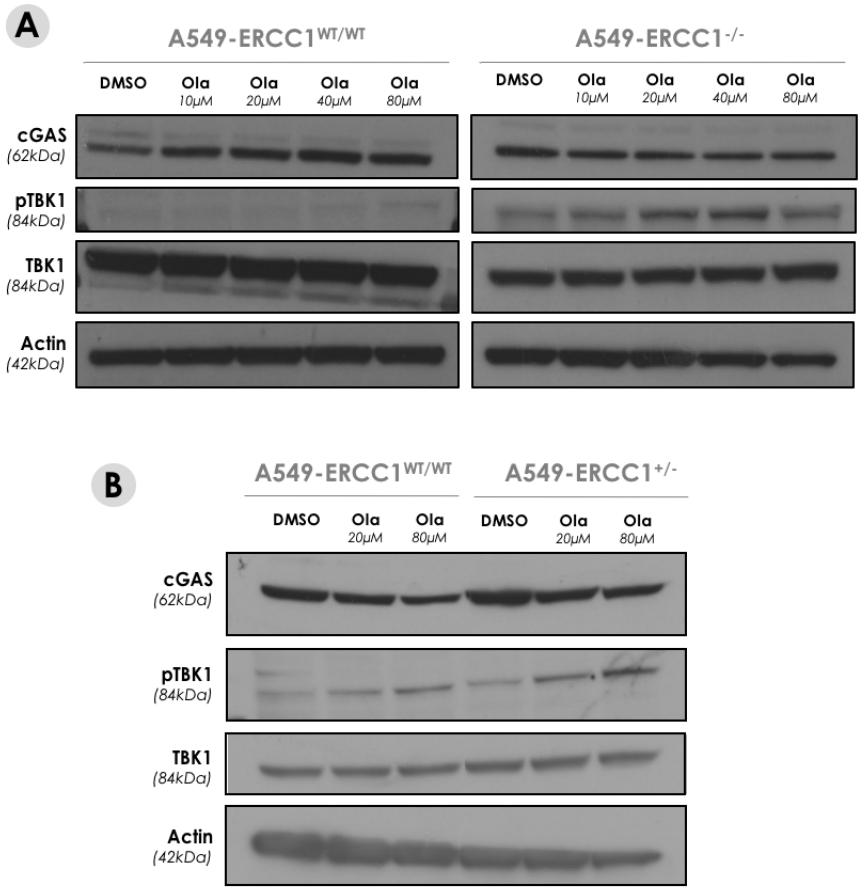

Figure IV.15. PARPi trigger TBK1 phosphorylation in a dose-dependent manner in ERCC1-deficient A549 cells.
A. Western blot of cGAS, pTBK1 and total TBK1 in A549-ERCC1$^{WT/WT}$ and A549-ERCC1$^{-/-}$ cells upon PARPi exposure. Cells were exposed for 48h to DMSO (vehicle) and a dose range of olaparib. Lysates were probed with the indicated antibodies. **B.** Western blot of cGAS, pTBK1 and total TBK1 in A549-ERCC1$^{WT/WT}$ and A549-ERCC1$^{+/-}$ cells upon PARPi exposure. Cells were exposed for 48h to DMSO (vehicle) and 20 μM or 80 μM olaparib. Lysates were probed with the indicated antibodies.

Analysis of pTBK1 levels upon PARPi exposure in H1975-ERCC1 isogenic cell lines revealed patterns similar to that obtained in A549 cells. Indeed, treatment of H1975-ERCC1$^{WT/WT}$ cells with a dose range of rucaparib led to a dose-dependent increase in TBK1 phosphorylation (**Figure IV.16.A**). Importantly, this increase was more pronounced in H1975-ERCC1$^{-/-}$ cells, as illustrated by single-dose treatment assays with either rucaparib or olaparib (**Figure IV.16.B**), and associated with an upregulation of cGAS protein expression.

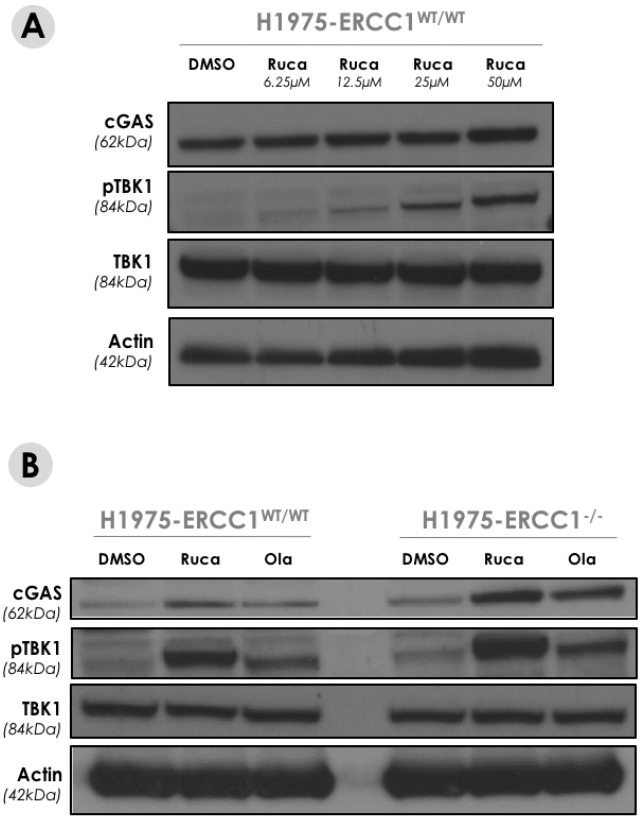

Figure IV.16. PARPi trigger TBK1 phosphorylation in a dose-dependent manner in H1975 cells.

A. Western blot of cGAS, pTBK1 and total TBK1 in H1975-ERCC1$^{WT/WT}$ cells upon PARPi exposure. Cells were exposed for 48h to DMSO (vehicle) and a dose range of rucaparib. Lysates were probed with the indicated antibodies. **B.** Western blot of cGAS, pTBK1 and total TBK1 in H1975-ERCC1$^{WT/WT}$ and H1975-ERCC1$^{+/-}$ cells upon PARPi exposure. Cells were exposed for 48h to DMSO (vehicle) and 25 μM or 40 μM olaparib. Lysates were probed with the indicated antibodies.

Together, these results support that PARPi selectively trigger TBK1 phosphorylation in ERCC1-defective NSCLC cells, suggesting an enhanced activation of the cGAS/STING pathway. Importantly, the expression level of ERCC1 appears to affect the extent of cGAS/STING activation following treatment with PARPi, as indicated by the respectively mild and intense phosphorylation of TBK1 observed in A549-ERCC1$^{+/-}$ and A549-ERCC1$^{-/-}$ cells after exposure to olaparib (**Figure IV.15**). Consistent with the previously described generation of CCF and subsequent detection by cGAS, these effects are dose-dependent, and observed with both rucaparib and olaparib, supporting that they arise from an on-target effect of these agents.

b. cGAS and STING are required for the activation of TBK1 by PARPi

To verify that the phosphorylation of TBK1 observed after treatment with PARPi was a consequence of cGAS-mediated detection of CCF, we decided to assess the potential for small-interfering RNA (siRNA)-mediated silencing of cGAS or STING to abrogate TBK1 phosphorylation. We first transfected A549-ERCC1$^{-/-}$ cells with siRNA targeting cGAS or STING, and subsequently exposed cells to olaparib for 48 h prior to protein extraction. The absence of detection of cGAS and STING proteins by WB confirmed the gene-silencing efficacy of the corresponding siRNAs.

As hypothesized, a decrease in TBK1 phosphorylation levels could be observed upon cGAS or STING siRNA transfection in the A549-ERCC1$^{-/-}$ cell line, as compared with the negative control siRNA (siCTRL) (**Figure IV.17.A**). Moreover, a similar experiment performed in H1975-ERCC1$^{WT/WT}$ cells exposed to rucaparib revealed that, while silencing of either cGAS or STING only moderately decreased PARPi-induced TBK1 phosphorylation, simultaneous silencing of both sensors allowed complete abrogation of pTBK1 (**Figure IV.17.B**).

These results support that cGAS and STING are required for PARPi-mediated phosphorylation of TBK1.

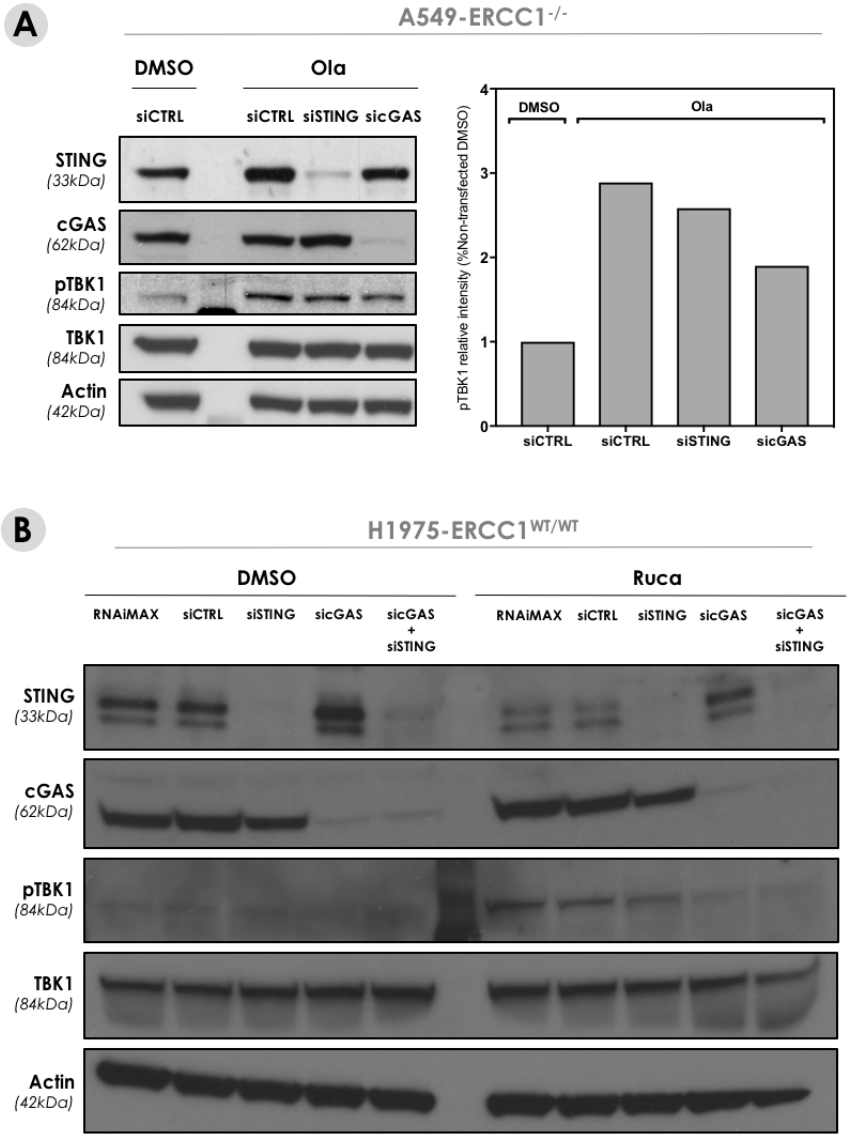

Figure IV.17. PARPi-mediated phosphorylation of TBK1 is dependent on cGAS and STING activity.

A. Western blot of pTBK1 in DMSO- or olaparib-treated A549-ERCC1$^{-/-}$ cells in the context of siRNA silencing of cGAS or STING. Cells were transfected with siCTRL, siSTING or sicGAS, exposed to DMSO (vehicle) or 40 µM olaparib, and lysates were probed with the indicated antibodies. Bar plot: pTBK1/TBK1 intensity was measured for each condition. **B.** Western blot of pTBK1 in DMSO- or rucaparib-treated H1975-ERCC1$^{WT/WT}$ cells in the context of siRNA silencing of cGAS and/or STING. Cells were transfected with siCTRL, siSTING, sicGAS or siSTING+sicGAS, exposed to DMSO (vehicle) or 25 µM rucaparib, and lysates were probed with the indicated antibodies.

c. *Progression through the cell cycle is required for PARPi-mediated TBK1 activation*

Because our previous observations showed cell cycle-dependency of CCF formation (**Figure IV.8** and **Figure IV.9**), we hypothesized that the activation of cGAS/STING by PARPi would be cell cycle-dependent. We thus monitored TBK1 phosphorylation upon cell cycle blockade by CDK1i in PARPi-treated H1975-ERCC1$^{WT/WT}$ cells. Although CDK1i itself appeared to increase baseline pTBK1 levels, we could detect an abrogation of the previously observed increase in TBK1 phosphorylation upon PARPi exposure (**Figure IV.18**), suggesting that the absence of formation of CCF in cells subjected to cell cycle-blockade impairs cGAS/STING activation.

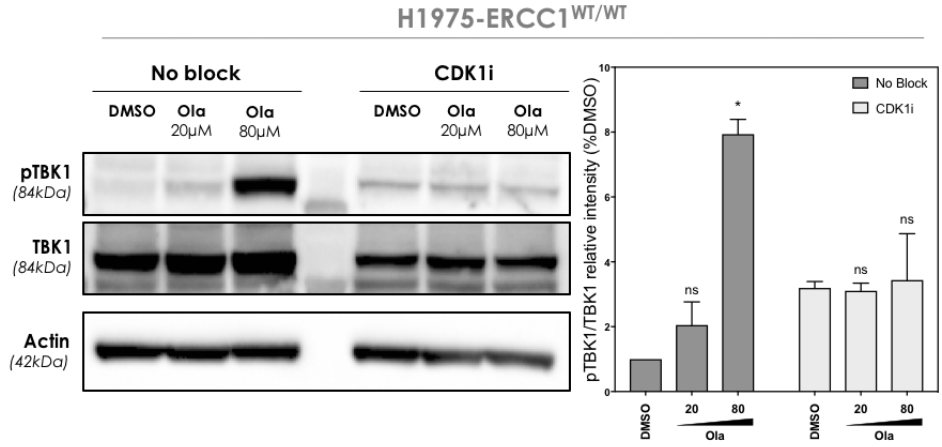

Figure IV.18. PARPi-mediated phosphorylation of TBK1 is cell cycle-dependent.
Western blot of pTBK1 in DMSO- or olaparib-treated H1975-ERCC1$^{WT/WT}$ cells upon cell-cycle blockade. Cells were exposed to DMSO, 20 μM or 80 μM olaparib in the presence or absence of the cell cycle blocker CDK1i RO-3306. Lysates were probed with the indicated antibodies. Bar plot: pTBK1/TBK1 intensity was measured for each condition and normalized to DMSO. Mean ± SD, N = 3, Kruskal-Wallis test and *post hoc* Dunn's test, relative to DMSO control.

d. PARPi trigger TBK1 phosphorylation and downstream STING signalling in a BRCA1-dependent manner in TNBC cells

To further characterize the activation of the cGAS/STING pathway in the context of PARPi exposure, we evaluated pTBK1 in the SUM149-BRCA1 isogenic TNBC model. Consistent with results obtained in the NSCLC models, we found a dose-dependent increase of pTBK1 upon PARPi exposure in SUM149-BRCA1$_{mut}$ but not SUM149-BRCA1$_{rev}$ cells (**Figure IV.19.A**), suggesting that this phenotype was conditioned by the presence of a defect in *BRCA1*. To further confirm these results, we studied the activation of several downstream effectors of the cGAS/STING pathway in this model, including IRF3, IRF7 and NF-κB. Detection of the phosphorylated forms of these proteins by WB revealed a clear phosphorylation of IRF3 and IRF7 in SUM149-BRCA1$_{mut}$ cells treated with olaparib, whereas pIRF3 and pIRF7 were scarcely detectable in SUM149-BRCA1$_{rev}$ cells (**Figure IV.19.B**). Similarly, a dose-dependent phosphorylation of the p65 NF-κB subunit could be detected in both SUM149-BRCA1$_{mut}$ and SUM149-BRCA1$_{rev}$ cells, but appeared enhanced in SUM149-BRCA1$_{mut}$ cells.

These results suggest that PARPi selectively enhance cGAS/STING pathway activation in BRCA1-deficient cells. This is in line with previously reported data showing, in various experimental models of TNBC, that cGAS/STING signalling is active in cells harbouring a *BRCA1* mutation but not in their isogenic counterparts re-expressing a functional BRCA1 protein (268).

Collectively, our data support the notion that PARPi-induced CCF activate cGAS/STING signalling, and that this effect, found in various histological types, relies on the presence of specific DDR defects such as ERCC1 deficiency in NSCLC and BRCA1 deficiency in TNBC.

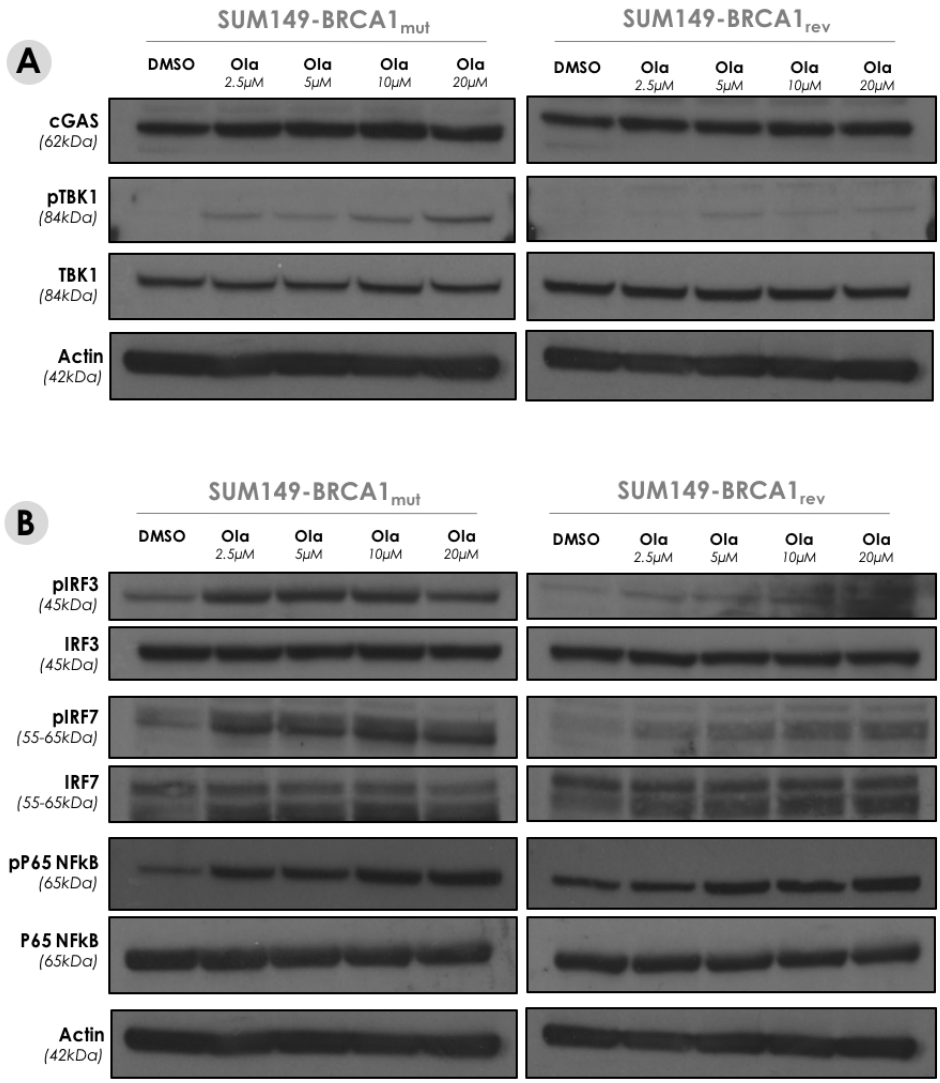

Figure IV.19. PARPi trigger TBK1 phosphorylation in a dose-dependent manner in *BRCA1*-mutated SUM149 cells.

A. Western blot of cGAS, pTBK1 and total TBK1 in SUM149-BRCA1$_{mut}$ and SUM149-BRCA1$_{rev}$ cells upon PARPi exposure. Cells were exposed for 48h to DMSO (vehicle) and a dose range of olaparib. Lysates were probed with the indicated antibodies. **B.** Western blot showing phosphorylation levels of several downstream STING signaling effectors in SUM149-BRCA1$_{mut}$ and SUM149-BRCA1$_{rev}$ cells exposed to DMSO (vehicle) or a dose range of olaparib for 48h. Lysates were probed with the indicated antibodies.

e. Specificity of activation of the cGAS/STING pathway by PARPi

Cytoplasmic DNA is an important molecular pattern, alternately considered as a DAMP or a pathogen-associated molecular pattern (PAMP) according to the type of stress that has initiated its formation. To cope with this typical "danger signal", cells have evolved to develop a series of cytoplasmic DNA sensing pathways implicated in the activation of appropriate cellular responses (417). The cGAS/STING pathway has a pivotal function in this respect, but other biological pathways, collectively known as PRR, have also been involved in cytoplasmic DNA sensing. These include the TLR and RIG-1-like receptors (RLR) pathways (418,419), as well as several independent cytosolic DNA sensors such as DAI (420) and IFI16 (421).

To assess whether the stimulating effects of PARPi were private to the cGAS/STING pathway, or shared with other cytoplasmic DNA sensors, we monitored the activation of TLR and RLR signalling after PARPi exposure in our models. We observed no activation of the RLR effectors RIG-1 and MDA-5, nor of the independent sensor IFI16 in NSCLC cells exposed to increasing doses of olaparib, while IFN-γ, a canonical inducer of these pathways, triggered their upregulation (**Figure IV.20.A**). Similarly, no activation of the endosomal sensor TLR9 or any of its signalling effectors could be detected upon PARPi exposure (**Figure IV.20.B**) in either of the NSCLC cell lines tested. These results suggested that the detection of CCF following exposure to PARPi was relatively specific to the cGAS/STING pathway.

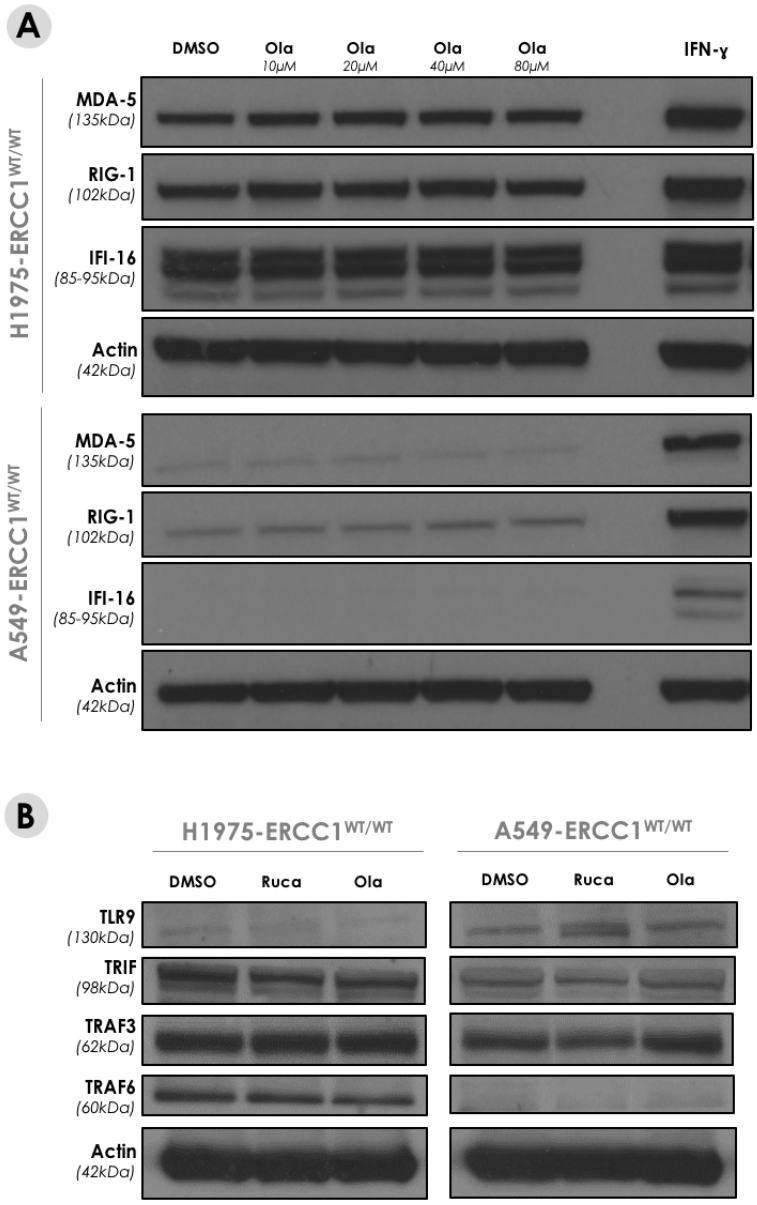

Figure IV.20. PARPi do not trigger RLR or TLR signalling pathways activation in NSCLC cells.

Western blot showing protein expression of several RLR (**A**) or TLR (**B**) effectors in A549-ERCC1$^{WT/WT}$ and H1975-ERCC1$^{WT/WT}$ cells exposed to DMSO (vehicle) or a dose range of olaparib for 48h. Lysates were probed with the indicated antibodies and IFN-γ was used as a positive control of activation.

6. Activation of cGAS/STING by PARPi triggers secretion of CCL5 in a DDR-defects-dependent manner

By mediating the activation of (i) type I IFN signalling through IRF3/IRF7 and (ii) pro-inflammatory signalling through NF-κB, the cGAS/STING pathway elicits effective immunity in response to DNA damage-induced genomic instability (257). As previously described, these cGAS/STING-mediated immune phenotypes have been reported in the context of DDR deficiency and following exposure to S-phase-dependent DNA-damaging agents or IR (263,265,266,268). In particular, DDR-related type I IFN responses were associated with the production of IFN-β, as well as the secretion of specific chemotactic chemokines, including CCL5 and CXCL10. Therefore, we hypothesized that PARPi might enhance the production of IFN-stimulated chemokines in a cGAS/STING-dependent manner in our models, especially in ERCC1- and BRCA1-deficient cells.

CCL5 is a member of the C-C-motif family of chemokines. Also known as regulated upon activation, normally T-cell expressed, and secreted (RANTES), CCL5 has been shown to bind to several receptors including CCR1, CCR3, CCR4, and CCR5. Expressed by T cells, macrophages and endothelial cells, CCL5 has also been reported to be produced by cancer cells or non-malignant stromal cells at primary and metastatic sites (422). Although CCL5 has been associated with both pro-tumoural and anti-tumoural processes (423), its involvement in the recruitment of immune effectors to the tumour site is incontrovertible. In addition, cGAS/STING-dependent secretion of CCL5 has been observed as a consequence of DDR defects in TNBC cells and has been associated with immune cells chemotaxis in *in vitro* assays (268), suggesting that this chemokine has a predominant role in driving lymphocytic infiltration in DDR-deficient tumours.

We thus primarily sought to assess the production of CCL5 in our isogenic models of DDR-deficient NSCLC and TNBC. To evaluate the cell-autonomous production of CCL5 and other chemokines in response to PARPi, we used two distinct and complementary experimental strategies including: (i) the assessment of chemokines transcriptional levels using quantitative reverse transcription polymerase chain reaction (RT-qPCR) and (ii) the

assessment of chemokines secretion levels in cells supernatants using Enzyme-Linked Immunosorbent Assay (ELISA).

a. ERCC1-deficient NSCLC cells secrete CCL5 in response to PARPi

We first assessed the secretion of CCL5 in culture supernatants from A549-ERCC1 isogenic cells exposed to a dose range of olaparib. To assess the implication of cGAS/STING signalling in this secretion, we transfected cells prior to treatment with a combination of siRNAs targeting cGAS and STING, or a negative control siRNA. Supernatants were collected after 72 h of culture, and subjected to ELISA detection using a commercially-available kit.

While no secretion of CCL5 could be detected in A549-ERCC1$^{WT/WT}$ or A549-ERCC1$^{+/-}$ cells after olaparib exposure, we observed a significant dose-dependent increase in extracellular levels of CCL5 in the A549-ERCC1$^{-/-}$ cell line (**Figure IV.21**). Importantly, depletion of STING and cGAS by siRNA resulted in a substantial decrease of CCL5 secretion in this cell line, suggesting that cGAS/STING signalling activation might be involved in this process. Furthermore, exposure of the A549-ERCC1$^{-/-}$ + isoform 202 cell line to olaparib did not trigger CCL5 secretion, supporting the notion that a defect in ERCC1 is required to trigger CCL5 secretion in response to PARPi in this model. Consistent with these observations, RT-qPCR analyses revealed that baseline *CCL5* expression levels were 12-fold higher in A549-ERCC1$^{-/-}$ cells compared to A549-ERCC1$^{WT/WT}$ cells (**Figure IV.22.A**), and significantly depleted in the presence of siRNA targeting STING. Interestingly, *CCL5* transcription was induced by PARPi in both A549-ERCC1$^{WT/WT}$ and A549-ERCC1$^{-/-}$ cells (**Figure IV.22.B**), suggesting that the undetectable levels of CCL5 protein found in the wildtype cell line were due to an extremely low basal expression of *CCL5* gene in this cell line.

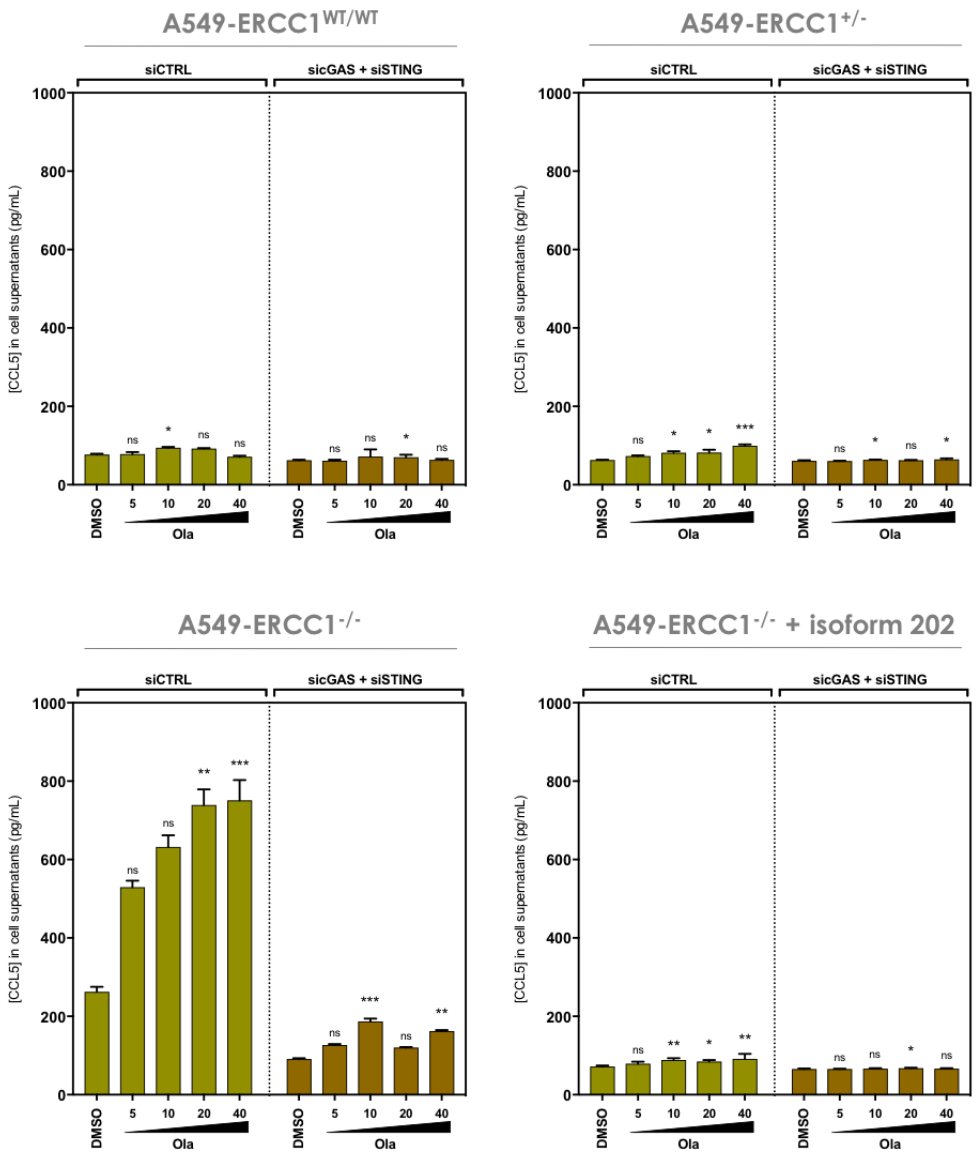

Figure IV.21. PARPi trigger CCL5 secretion via cGAS/STING in ERCC1-deficient A549 cells.

Quantitative analysis of CCL5 secretion in A549-ERCC1 isogenic cells supernatants upon olaparib exposure, in the presence or absence of cGAS/STING silencing by siRNA. Cells were transfected with siCTRL or sicGAS + siSTING and treated for 72h with DMSO or a dose range of olaparib (μM). Supernatants were collected and analysed by ELISA for detection of CCL5. Shown are CCL5 concentrations; Mean ± SD, N=4, Kruskal-Wallis test and *post hoc* Dunn's test, relative to DMSO control.

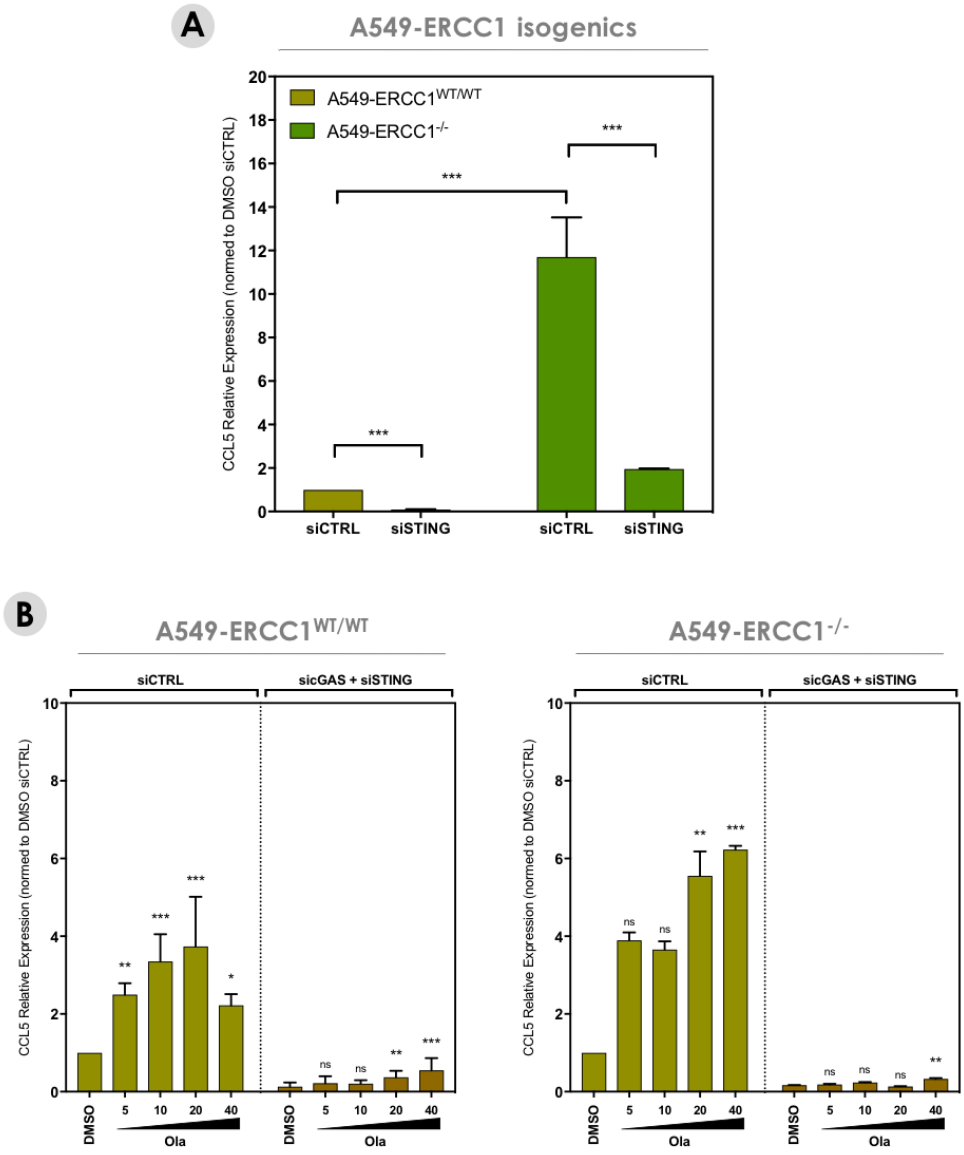

Figure IV.22. PARPi activate CCL5 transcription via cGAS/STING in A549 cells.
A. RT-qPCR analysis of RNA isolated from A549-ERCC1$^{WT/WT}$ and A549-ERCC1$^{-/-}$ cells, in the presence or absence of STING silencing by siRNA. Cells were transfected with siCTRL or siSTING. CCL5 mRNAs were analyzed relative to GAPDH (to control for cDNA quantity). Shown are arbitrary units of gene expression, normalized to A549-ERCC1$^{WT/WT}$ DMSO-treated control. Mean ± SD, N=12, two-way ANOVA test. **B.** RT-qPCR analysis of RNA isolated from olaparib-exposed A549-ERCC1$^{WT/WT}$ and A549-ERCC1$^{-/-}$ cells, in the presence or absence of cGAS/STING silencing by siRNA. Cells were transfected with siCTRL or sicGAS + siSTING and treated for 72h with DMSO or a dose range of olaparib (μM). CCL5 mRNAs were analyzed relative to GAPDH (to control for cDNA quantity). Shown are arbitrary units of gene expression, normalized to DMSO-treated control. Mean ± SD, N=4, Kruskal-Wallis test and *post hoc* Dunn's test, relative to DMSO control.

Together, these results suggest that PARPi selectively promote CCL5 secretion in ERCC1-deficient NSCLC cells. The observation that A549-ERCC1$^{-/-}$ cells exhibit higher CCL5 baseline expression levels compared to A549-ERCC1$^{WT/WT}$ cells is consistent with our RNA-seq data showing the spontaneous activation of a type I IFN response in ERCC1-deficient cells (**Figure III.3**), and reinforces the notion that loss of ERCC1 in NSCLC cells drives cell-autonomous expression of specific immune signals. In addition, the induction of CCL5 expression by PARPi is dose-dependent and exclusively found in A549-ERCC1$^{-/-}$ cells, consistent with the previously observed dose-dependent activation of cGAS/STING signalling following exposure to PARPi in this cell line (**Figure IV.15**). Furthermore, the fact that the A549-ERCC1$^{+/-}$ cell line does not exhibit CCL5 secretion upon exposure to PARPi while cGAS/STING is activated, suggests that the level of activation of cGAS/STING signalling is important in determining CCL5 secretion.

b. BRCA1-deficient TNBC cells secrete CCL5 in response to PARPi

To extend these investigations of the potential of PARPi to augment chemokine signalling, we studied CCL5 and IFN-β production in the independent isogenic model of BRCA1-deficient TNBC cells. RT-qPCR analyses of *CCL5* and *IFNB1* mRNA levels revealed a dose-dependent increase in the transcription of both genes following exposure to olaparib in SUM149-BRCA1$_{mut}$ but not SUM149-BRCA1$_{rev}$ cells (**Figure IV.23.A** and **Figure IV.23.B**). In the SUM149-BRCA1$_{mut}$ cell line, we found a substantial reduction of the PARPi-induced expression of both chemokines following transfection with siRNAs targeting STING and cGAS, compatible with an involvement of the cGAS/STING pathway in this induction. Consistent with these observations, SUM149-BRCA1$_{mut}$ cells, but not SUM149-BRCA1$_{rev}$ cells, displayed enhanced secretion of CCL5 – as detected by ELISA – following treatment with olaparib, a phenotype that was reduced upon co-depletion of STING and cGAS (**Figure IV.24.A**). Interestingly, no secretion of IFN-β could be detected in either of the isogenic SUM149 cell lines upon treatment with olaparib (**Figure IV.24.B**), suggesting that the levels of expression of *IFNB1*, although induced by olaparib in SUM149-BRCA1$_{mut}$ cells, were not sufficient to enable detection of the corresponding secreted protein in cells supernatants.

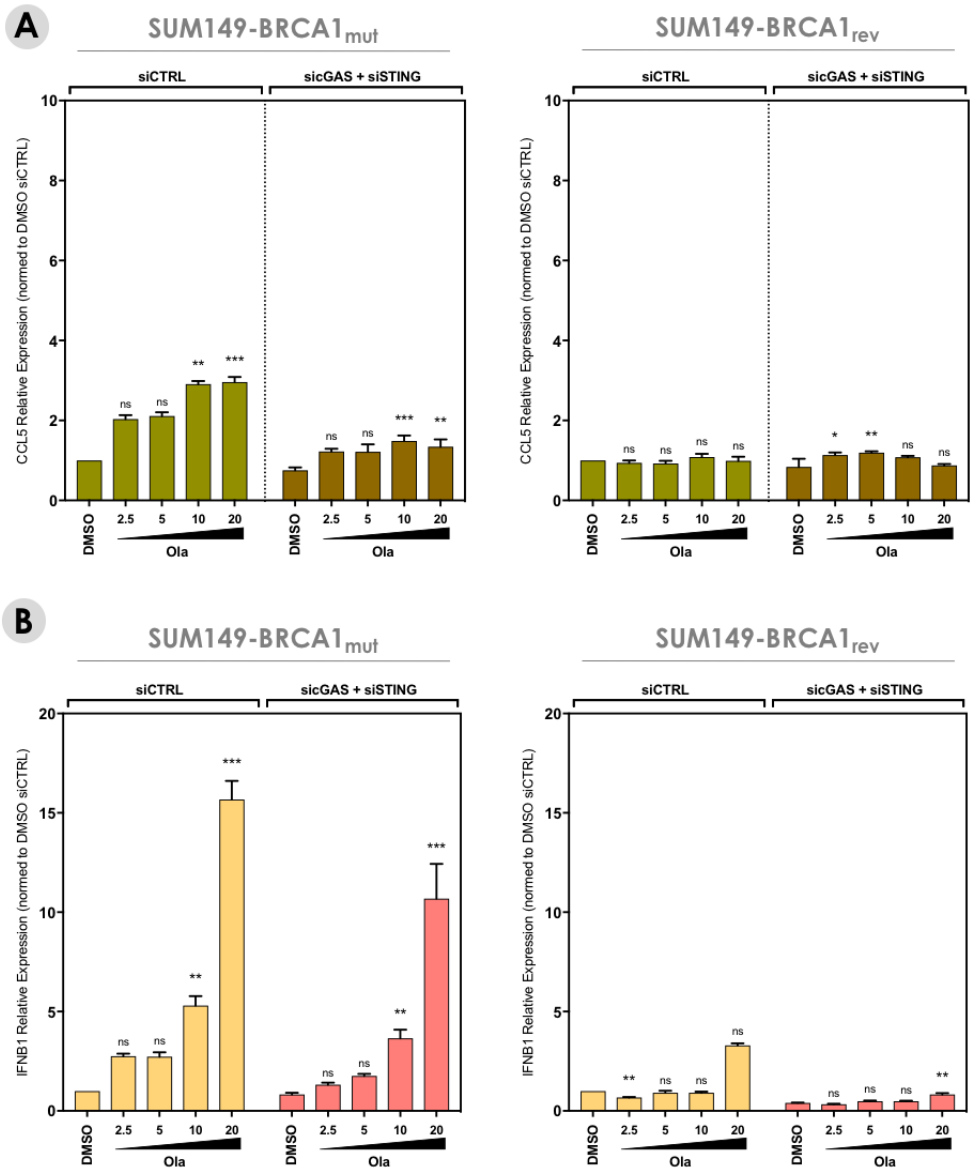

Figure IV.23. PARPi induce *CCL5* and *IFNB1* transcription in BRCA1-mutated SUM149

RT-qPCR analysis of RNA isolated from olaparib-exposed SUM149-BRCA1$_{mut}$ and SUM149-BRCA1$_{rev}$ cells, in the presence or absence of cGAS/STING silencing by siRNA. Cells were transfected with siCTRL or sicGAS + siSTING and treated for 72h with DMSO or a dose range of olaparib (µM). *CCL5* (**A**) or *IFNB1* (**B**) mRNAs were analyzed relative to GAPDH (to control for cDNA quantity). Shown are arbitrary units of gene expression, normalized to DMSO-treated control. Mean ± SD, N=4, Kruskal- Wallis test and *post hoc* Dunn's test, relative to DMSO control.

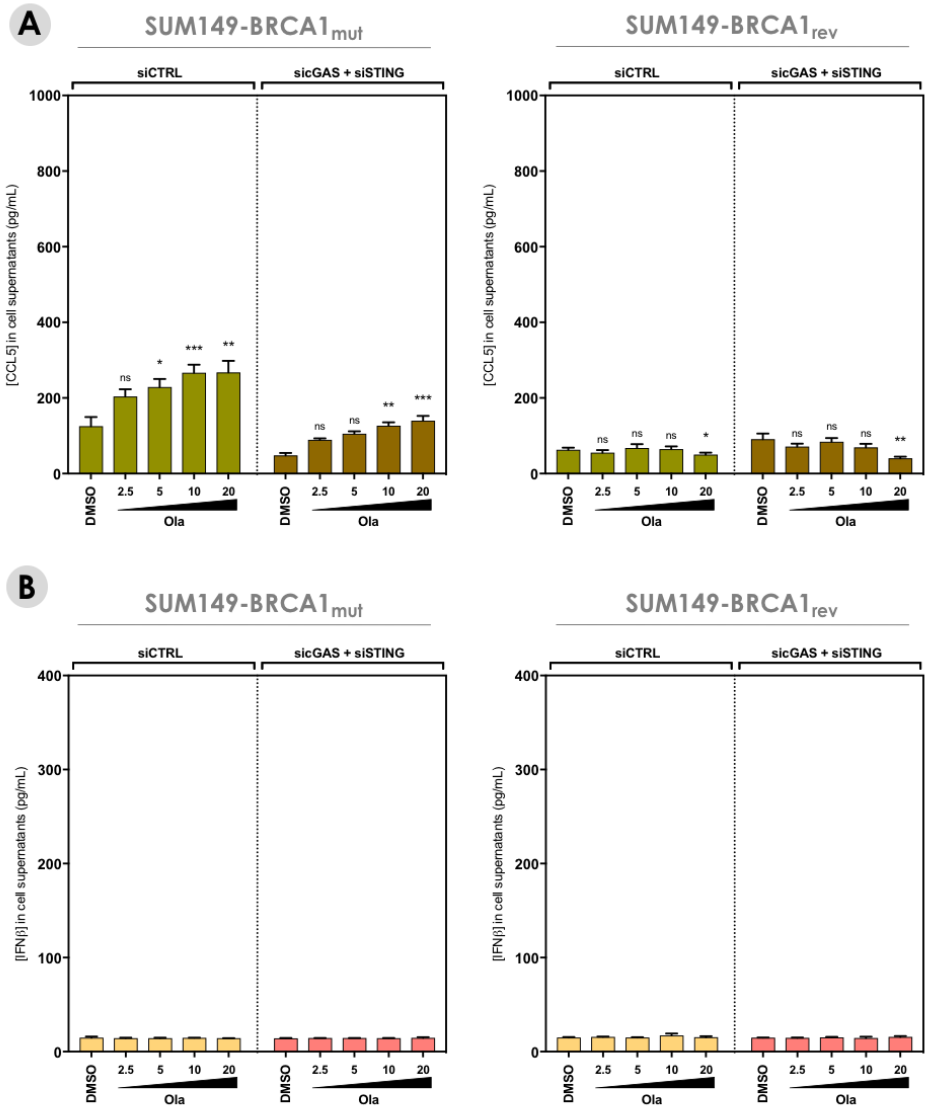

Figure IV.24. PARPi induce secretion of CCL5 but not IFN-β in *BRCA1*-mutated SUM149 cells.

A. Quantitative analysis of CCL5 secretion in SUM149-BRCA1$_{mut}$ and SUM149-BRCA1$_{rev}$ cells supernatants upon olaparib exposure, in the presence or absence of cGAS/STING silencing by siRNA. Cells were transfected with siCTRL or sicGAS + siSTING and treated for 72h with DMSO or a dose range of olaparib (µM). Supernatants were collected and analysed by ELISA for detection of CCL5. Shown are CCL5 concentrations; Mean ± SD, N=4, Kruskal-Wallis test and *post hoc* Dunn's test, relative to DMSO control. **B.** Quantitative analysis of IFN-β secretion in SUM149-BRCA1$_{mut}$ and SUM149-BRCA1$_{rev}$ cells supernatants upon olaparib exposure, in the presence or absence of cGAS/STING silencing by siRNA. Cells were transfected with siCTRL or sicGAS + siSTING and treated for 72h with DMSO or a dose range of olaparib (µM). Supernatants were collected and analysed by ELISA for detection of IFN-β. Shown are IFN-β concentrations; Mean ± SD, N=4, Kruskal-Wallis test and *post hoc* Dunn's test, relative to DMSO control.

Together, these results support that in the context of specific DDR defects such as ERCC1-deficiency in NSCLC or BRCA1-deficiency in TNBC, PARPi induce the expression of several type I IFN chemokines, including IFN-β and CCL5. These effects are dose-dependent and conditioned by the activation of the cGAS/STING pathway.

7. PARPi activate type I IFN signalling in ERCC1-deficient cells

To comprehensively characterize cell-autonomous immunomodulation induced by PARPi, we decided to evaluate, on a broad basis, the activation of immune signals in NSCLC exposed to PARPi. To this aim, we performed RNA-seq on A549-ERCC1$^{WT/WT}$ and A549-ERCC1$^{-/-}$ cells exposed to talazoparib (the most potent and specific clinical PARPi) for 48 h. Differential expression analysis and GSEA were performed on RNA-seq data to investigate pathway enrichment between talazoparib-treated and vehicle-treated cells.

GSEA using the REACTOME pathway database revealed, as expected, a significant downregulation of many pathways involved in cell cycle regulation, DNA replication and DNA repair in talazoparib-treated A549-ERCC1$^{-/-}$ cells, notably HR-mediated DSB repair, transcription-coupled NER, and the Fanconi anemia pathway (**Table IV.1**). This is consistent with the known effects of PARPi in preventing HR-mediated repair of DSBs in the absence of ERCC1. GSEA also revealed a significant upregulation of several immune-related pathways in talazoparib-treated A549-ERCC1$^{-/-}$ cells (**Table IV.2**) but not A549-ERCC1$^{WT/WT}$ (**Table IV.3**). Importantly, the most upregulated pathways found in A549-ERCC1$^{-/-}$ cells following exposure to talazoparib were type I and type II IFN signalling. Consistent with this, GSEA plots interpretation revealed a significant enrichment of type I IFN signalling in talazoparib-treated A549-ERCC1$^{-/-}$ cells compared with DMSO-treated cells (NES = 2.12, FDR = 0.0018; **Figure IV.25**). This upregulation was also observed in the A549-ERCC1$^{WT/WT}$ cell line, but the corresponding enrichment was more modest in this latter cell line (NES = 1.64, FDR = 0.0314; **Figure IV.26**), further highlighting the role of ERCC1 deficiency in potentiating PARPi-mediated type I IFN signalling induction.

Table IV.1. GSEA of REACTOME pathways in talazoparib-treated A549-ERCC1$^{-/-}$ cells compared with DMSO-treated A549-ERCC1$^{-/-}$ cells.

Shown are the top 50 downregulated REACTOME pathways in talazoparib-treated A549-ERCC1$^{-/-}$ cells. Pathways highlighted in forest green relate to cell cycle; pathways highlighted in light green relate to DNA replication; pathways highlighted in dark green relate to DNA repair.

REACTOME pathways	*NES*	*FDR*
REACTOME_CELL_CYCLE_MITOTIC	**-2.915**	**0.002**
REACTOME_CELL_CYCLE	**-2.876**	**0.002**
REACTOME_DNA_REPLICATION	**-2.873**	**0.002**
REACTOME_MITOTIC_M_M_G1_PHASES	**-2.866**	**0.002**
REACTOME_MITOTIC_PROMETAPHASE	**-2.625**	**0.002**
REACTOME_M_G1_TRANSITION	**-2.592**	**0.002**
REACTOME_G2_M_CHECKPOINTS	**-2.566**	**0.002**
REACTOME_MITOTIC_G1_G1_S_PHASES	**-2.552**	**0.002**
REACTOME_SYNTHESIS_OF_DNA	**-2.536**	**0.002**
REACTOME_G1_S_TRANSITION	**-2.510**	**0.002**
REACTOME_S_PHASE	**-2.498**	**0.002**
REACTOME_CHROMOSOME_MAINTENANCE	**-2.487**	**0.002**
REACTOME_ACTIVATION_OF_ATR_IN_RESPONSE_TO_REPLICATION_STRESS	**-2.482**	**0.002**
REACTOME_CELL_CYCLE_CHECKPOINTS	**-2.477**	**0.002**
REACTOME_ACTIVATION_OF_THE_PRE_REPLICATIVE_COMPLEX	**-2.450**	**0.002**
REACTOME_DNA_STRAND_ELONGATION	**-2.408**	**0.002**
REACTOME_ASSEMBLY_OF_THE_PRE_REPLICATIVE_COMPLEX	**-2.344**	**0.002**
REACTOME_PROCESSING_OF_CAPPED_INTRON_CONTAINING_PRE_MRNA	**-2.312**	**0.002**
REACTOME_MITOTIC_G2_G2_M_PHASES	**-2.303**	**0.002**
REACTOME_E2F_MEDIATED_REGULATION_OF_DNA_REPLICATION	**-2.266**	**0.002**
REACTOME_MRNA_PROCESSING	**-2.265**	**0.002**
REACTOME_REGULATION_OF_MITOTIC_CELL_CYCLE	**-2.241**	**0.002**
REACTOME_KINESINS	-2.230	0.002
REACTOME_DNA_REPAIR	**-2.204**	**0.002**
REACTOME_EXTENSION_OF_TELOMERES	-2.204	0.002
REACTOME_TELOMERE_MAINTENANCE	-2.162	0.002
REACTOME_ORC1_REMOVAL_FROM_CHROMATIN	-2.155	0.002
REACTOME_MRNA_SPLICING	-2.150	0.002
REACTOME_G0_AND_EARLY_G1	**-2.119**	**0.002**
REACTOME_LAGGING_STRAND_SYNTHESIS	**-2.117**	**0.002**
REACTOME_FANCONI_ANEMIA_PATHWAY	**-2.112**	**0.002**
REACTOME_DEPOSITION_OF_NEW_CENPA_CONTAINING_NUCLEOSOMES_AT_THE_CENTROMERE	-2.099	0.002
REACTOME_G1_S_SPECIFIC_TRANSCRIPTION	-2.070	0.002
REACTOME_RECRUITMENT_OF_MITOTIC_CENTROSOME_PROTEINS_AND_COMPLEXES	-2.068	0.002
REACTOME_MEIOSIS	-2.052	0.002
REACTOME_TRANSPORT_OF_MATURE_TRANSCRIPT_TO_CYTOPLASM	-2.033	0.002
REACTOME_TRANSCRIPTION_COUPLED_NER_TC_NER	**-2.028**	**0.002**
REACTOME_LOSS_OF_NLP_FROM_MITOTIC_CENTROSOMES	-2.010	0.002
REACTOME_CYCLIN_A_B1_ASSOCIATED_EVENTS_DURING_G2_M_TRANSITION	**-2.007**	**0.002**
REACTOME_UNWINDING_OF_DNA	**-2.003**	**0.002**
REACTOME_GLUCOSE_TRANSPORT	-1.990	0.002
REACTOME_ASSOCIATION_OF_LICENSING_FACTORS_WITH_THE_PRE_REPLICATIVE_COMPLEX	-1.990	0.002
REACTOME_INTERACTIONS_OF_VPR_WITH_HOST_CELLULAR_PROTEINS	-1.979	0.002
REACTOME_HOMOLOGOUS_RECOMBINATION_REPAIR_OF _DOUBLE_STRAND_BREAKS	**-1.975**	**0.002**
REACTOME_DOUBLE_STRAND_BREAK_REPAIR	**-1.975**	**0.002**
REACTOME_NEP_NS2_INTERACTS_WITH_THE_CELLULAR_EXPORT_MACHINERY	-1.968	0.002
REACTOME_APC_C_CDC20_MEDIATED_DEGRADATION_OF_MITOTIC_PROTEINS	-1.968	0.002
REACTOME_APC_C_CDH1_MEDIATED_DEGRADATION_OF_CDC20_AND_OTHER_APC_C_CDH1_TARGETED_PROTEINS_IN_LATE_MITOSIS_EARLY_G1	**-1.958**	**0.002**
REACTOME_CDC6_ASSOCIATION_WITH_THE_ORC_ORIGIN_COMPLEX	-1.957	0.002

Table IV.2. GSEA of REACTOME pathways in talazoparib-treated A549-ERCC1$^{-/-}$ cells compared with DMSO-treated A549-ERCC1$^{-/-}$ cells.

Shown are the top 50 upregulated REACTOME pathways in talazoparib-treated A549-ERCC1$^{-/-}$ cells. Pathways highlighted in orange relate to immune signaling; pathways highlighted in yellow relate to antigen presentation; pathways highlighted in red relate to PRR signaling.

REACTOME pathways	*NES*	*FDR*
REACTOME_INTERFERON_GAMMA_SIGNALING	**2.149**	**0.002**
REACTOME_INTERFERON_ALPHA_BETA_SIGNALING	**2.123**	**0.002**
REACTOME_COMPLEMENT_CASCADE	**1.863**	**0.006**
REACTOME_PEPTIDE_CHAIN_ELONGATION	1.845	0.002
REACTOME_INNATE_IMMUNE_SYSTEM	**1.834**	**0.002**
REACTOME_REGULATION_OF_COMPLEMENT_CASCADE	**1.807**	**0.007**
REACTOME_NUCLEOTIDE_BINDING_DOMAIN_LEUCINE_RICH_REPEAT_CONTAINING_RECEPTOR_NLR	1.787	0.002
REACTOME_NEGATIVE_REGULATORS_OF_RIG_I_MDA5_SIGNALING	**1.783**	**0.004**
REACTOME_PI3K_EVENTS_IN_ERBB4_SIGNALING	1.745	0.006
REACTOME_ENDOSOMAL_SORTING_COMPLEX_REQUIRED_FOR_TRANSPORT_ESCRT	1.745	0.017
REACTOME_SRP_DEPENDENT_COTRANSLATIONAL_PROTEIN_TARGETING_TO_MEMBRANE	1.736	0.003
REACTOME_RIG_I_MDA5_MEDIATED_INDUCTION_OF_IFN_ALPHA_BETA_PATHWAYS	**1.720**	**0.008**
REACTOME_3_UTR_MEDIATED_TRANSLATIONAL_REGULATION	1.704	0.003
REACTOME_IMMUNOREGULATORY_INTERACTIONS_BETWEEN_LYMPHOID_AND_NONLYMPHOID_CELL	1.701	0.026
REACTOME_ANTIGEN_PRESENTATION_FOLDING_ASSEMBLY_AND_PEPTIDE_LOADING_CLASS_I_MHC	**1.691**	**0.033**
REACTOME_LATENT_INFECTION_OF_HOMO_SAPIENS_WITH_MYCOBACTERIUM_TUBERCULOSIS	1.685	0.036
REACTOME_NOD1_2_SIGNALING_PATHWAY	1.679	0.030
REACTOME_TRANSLATION	1.670	0.003
REACTOME_G_ALPHA_Q_SIGNALLING_EVENTS	1.660	0.008
REACTOME_EXTRINSIC_PATHWAY_FOR_APOPTOSIS	1.658	0.043
REACTOME_CHONDROITIN_SULFATE_DERMATAN_SULFATE_METABOLISM	1.656	0.033
REACTOME_IL_3_5_AND_GM_CSF_SIGNALING	**1.645**	**0.040**
REACTOME_PEPTIDE_LIGAND_BINDING_RECEPTORS	**1.644**	**0.030**
REACTOME_AKT_PHOSPHORYLATES_TARGETS_IN_THE_CYTOSOL	1.640	0.051
REACTOME_TRAF6_MEDIATED_IRF7_ACTIVATION	**1.620**	**0.068**
REACTOME_BOTULINUM_NEUROTOXICITY	**1.612**	**0.072**
REACTOME_PI3K_EVENTS_IN_ERBB2_SIGNALING	1.603	0.047
REACTOME_MEMBRANE_TRAFFICKING	1.601	0.007
REACTOME_ENERGY_DEPENDENT_REGULATION_OF_MTOR_BY_LKB1_AMPK	1.600	0.076
REACTOME_REGULATION_OF_AMPK_ACTIVITY_VIA_LKB1	1.587	0.089
REACTOME_SIGNALING_BY_ILS	1.576	0.017
REACTOME_IL_RECEPTOR_SHC_SIGNALING	1.566	0.099
REACTOME_INTRINSIC_PATHWAY_FOR_APOPTOSIS	1.552	0.085
REACTOME_PIP3_ACTIVATES_AKT_SIGNALING	1.551	0.085
REACTOME_NUCLEAR_SIGNALING_BY_ERBB4	1.550	0.094
REACTOME_CLASS_A1_RHODOPSIN_LIKE_RECEPTORS	1.546	0.048
REACTOME_GAB1_SIGNALOSOME	1.541	0.084
REACTOME_CELL_JUNCTION_ORGANIZATION	1.538	0.065
REACTOME_PROTEOLYTIC_CLEAVAGE_OF_SNARE_COMPLEX_PROTEINS	1.533	0.121
REACTOME_TRAFFICKING_OF_AMPA_RECEPTORS	1.531	0.112
REACTOME_TRAF3_DEPENDENT_IRF_ACTIVATION_PATHWAY	**1.524**	**0.135**
REACTOME_NFKB_ACTIVATION_THROUGH_FADD_RIP1_PATHWAY_MEDIATED_BY_CASPASE_8_AND10	**1.520**	**0.135**
REACTOME_NEUROTRANSMITTER_RELEASE_CYCLE	1.515	0.130
REACTOME_CELL_CELL_COMMUNICATION	1.511	0.039
REACTOME_INFLAMMASOMES	1.507	0.135
REACTOME_FORMATION_OF_THE_TERNARY_COMPLEX_AND_SUBSEQUENTLY_THE_43S_COMPLEX	1.495	0.085
REACTOME_PI3K_AKT_ACTIVATION	1.487	0.130
REACTOME_REGULATION_OF_INSULIN_GROWTH_FACTOR_IGF_ACTIVITY_BY_IGF_BINDING_PROTEINS	1.487	0.156
REACTOME_INSULIN_RECEPTOR_RECYCLING	1.487	0.152

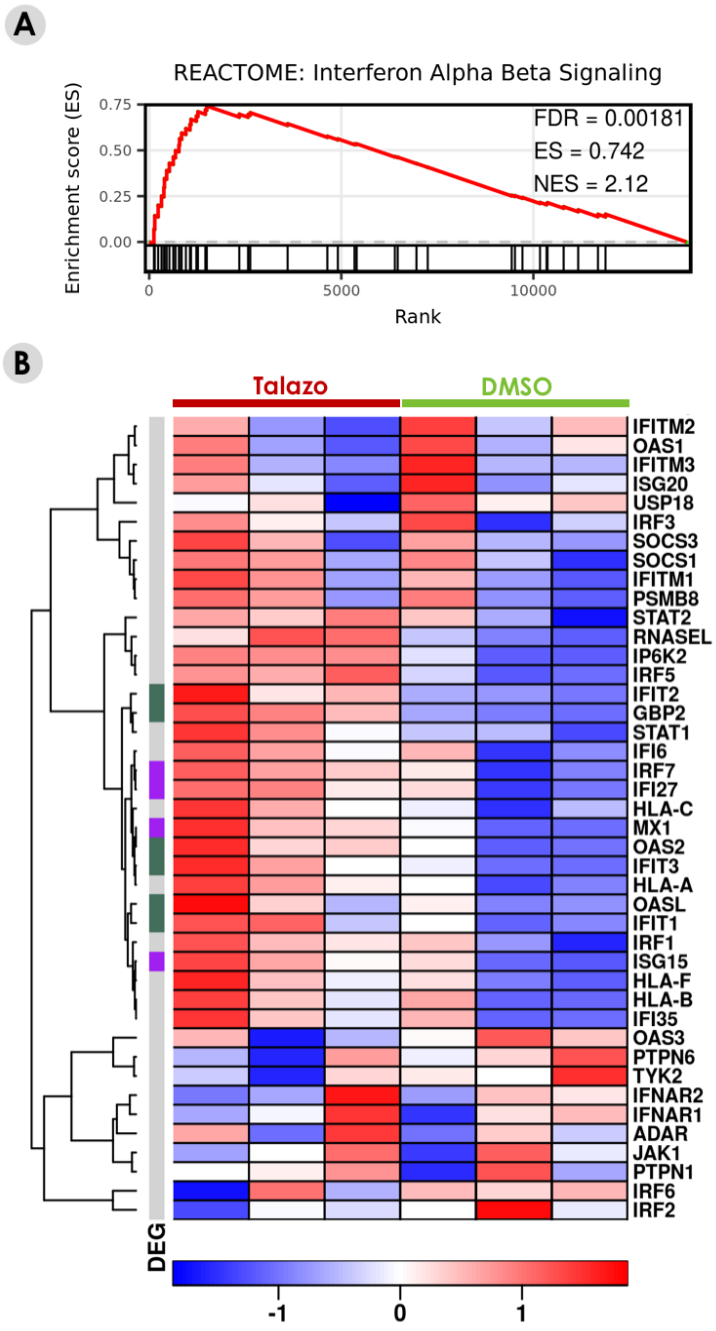

Figure IV.25. GSEA of the REACTOME pathway Interferon Alpha Beta Signalling in talazoparib- vs DMSO- treated A549-ERCC1$^{-/-}$ cells.

A. Enrichment plot generated by GSEA of ranked gene expression data for genes of the REACTOME pathway Interferon Alpha Beta Signalling. **B.** Associated heatmap showing the genes of the pathway, ranked by FDR. N = 3; Heatmap scale is a Z score. Purple, significantly DEGs with FDR < 0.05 and |LFC| > 1; Green, significantly DEGs with FDR < 0.05 and |LFC| > 0.58; Grey, non-significantly DEGs.

Table IV.3. GSEA of REACTOME pathways in talazoparib-treated A549-ERCC1$^{WT/WT}$ cells compared with DMSO-treated A549-ERCC1$^{WT/WT}$ cells.

Shown are the top 50 upregulated REACTOME pathways in talazoparib-treated A549-ERCC1$^{WT/WT}$ cells. Pathways highlighted in orange relate to immune signaling; pathways highlighted in yellow relate to antigen presentation.

REACTOME pathways	*NES*	*FDR*
REACTOME_PEPTIDE_CHAIN_ELONGATION	2.261	0.002
REACTOME_SRP_DEPENDENT_COTRANSLATIONAL_PROTEIN_TARGETING_TO_MEMBRANE	2.151	0.002
REACTOME_RESPIRATORY_ELECTRON_TRANSPORT_ATP_SYNTHESIS_BY_CHEMIOSMOTIC_COUPLING	2.026	0.002
REACTOME_INFLUENZA_VIRAL_RNA_TRANSCRIPTION_AND_REPLICATION	2.026	0.002
REACTOME_RESPIRATORY_ELECTRON_TRANSPORT	1.944	0.002
REACTOME_3_UTR_MEDIATED_TRANSLATIONAL_REGULATION	1.938	0.002
REACTOME_TRANSLATION	1.866	0.002
REACTOME_LATENT_INFECTION_OF_HOMO_SAPIENS_WITH_MYCOBACTERIUM_TUBERCULOSIS	**1.848**	**0.004**
REACTOME_BIOLOGICAL_OXIDATIONS	1.833	0.004
REACTOME_PHASE_II_CONJUGATION	1.800	0.007
REACTOME_NEUROTRANSMITTER_RELEASE_CYCLE	1.765	0.011
REACTOME_NONSENSE_MEDIATED_DECAY_ENHANCED_BY_THE_EXON_JUNCTION_COMPLEX	1.762	0.005
REACTOME_TRAFFICKING_OF_AMPA_RECEPTORS	1.750	0.006
REACTOME_TCA_CYCLE_AND_RESPIRATORY_ELECTRON_TRANSPORT	1.741	0.005
REACTOME_MEMBRANE_TRAFFICKING	1.719	0.006
REACTOME_PEROXISOMAL_LIPID_METABOLISM	1.708	0.017
REACTOME_INSULIN_RECEPTOR_RECYCLING	1.700	0.022
REACTOME_GLUTATHIONE_CONJUGATION	1.687	0.023
REACTOME_ENDOSOMAL_SORTING_COMPLEX_REQUIRED_FOR_TRANSPORT_ESCRT	1.686	0.022
REACTOME_GLUTAMATE_NEUROTRANSMITTER_RELEASE_CYCLE	1.674	0.022
REACTOME_INTERFERON_ALPHA_BETA_SIGNALING	**1.642**	**0.031**
REACTOME_CLASS_A1_RHODOPSIN_LIKE_RECEPTORS	1.642	0.014
REACTOME_TRANSFERRIN_ENDOCYTOSIS_AND_RECYCLING	1.600	0.065
REACTOME_EXTRACELLULAR_MATRIX_ORGANIZATION	1.579	0.058
REACTOME_FORMATION_OF_THE_TERNARY_COMPLEX_AND_SUBSEQUENTLY_THE_43S_COMPLEX	1.576	0.040
REACTOME_BOTULINUM_NEUROTOXICITY	1.570	0.083
REACTOME_COMPLEMENT_CASCADE	**1.535**	**0.114**
REACTOME_RESPONSE_TO_ELEVATED_PLATELET_CYTOSOLIC_CA2_	1.533	0.052
REACTOME_TRANSMISSION_ACROSS_CHEMICAL_SYNAPSES	1.530	0.020
REACTOME_CELL_CELL_JUNCTION_ORGANIZATION	1.530	0.092
REACTOME_SYNTHESIS_OF_BILE_ACIDS_AND_BILE_SALTS	1.528	0.113
REACTOME_EXTRINSIC_PATHWAY_FOR_APOPTOSIS	1.522	0.110
REACTOME_NEURONAL_SYSTEM	1.521	0.014
REACTOME_BILE_ACID_AND_BILE_SALT_METABOLISM	1.505	0.139
REACTOME_IL_RECEPTOR_SHC_SIGNALING	1.505	0.140
REACTOME_SPHINGOLIPID_METABOLISM	1.504	0.065
REACTOME_PROTEOLYTIC_CLEAVAGE_OF_SNARE_COMPLEX_PROTEINS	1.494	0.146
REACTOME_PEPTIDE_LIGAND_BINDING_RECEPTORS	**1.485**	**0.113**
REACTOME_ABC_FAMILY_PROTEINS_MEDIATED_TRANSPORT	1.479	0.159
REACTOME_IMMUNOREGULATORY_INTERACTIONS_BETWEEN_LYMPHOID_AND_NONLYMPHOID_CELL	**1.469**	**0.160**
REACTOME_GAP_JUNCTION_TRAFFICKING	1.466	0.176
REACTOME_AKT_PHOSPHORYLATES_TARGETS_IN_THE_CYTOSOL	1.462	0.180
REACTOME_IRON_UPTAKE_AND_TRANSPORT	1.461	0.160
REACTOME_SYNTHESIS_OF_BILE_ACIDS_AND_BILE_SALTS_VIA_7ALPHA_HYDROXYCHOLESTEROL	1.459	0.176
REACTOME_FORMATION_OF_ATP_BY_CHEMIOSMOTIC_COUPLING	1.458	0.185
REACTOME_CELL_JUNCTION_ORGANIZATION	1.458	0.117
REACTOME_NEUROTRANSMITTER_RECEPTOR_BINDING_AND_DOWNSTREAM_TRANSMISSION	1.456	0.076
REACTOME_TIGHT_JUNCTION_INTERACTIONS	1.449	0.185
REACTOME_COLLAGEN_FORMATION	1.448	0.172

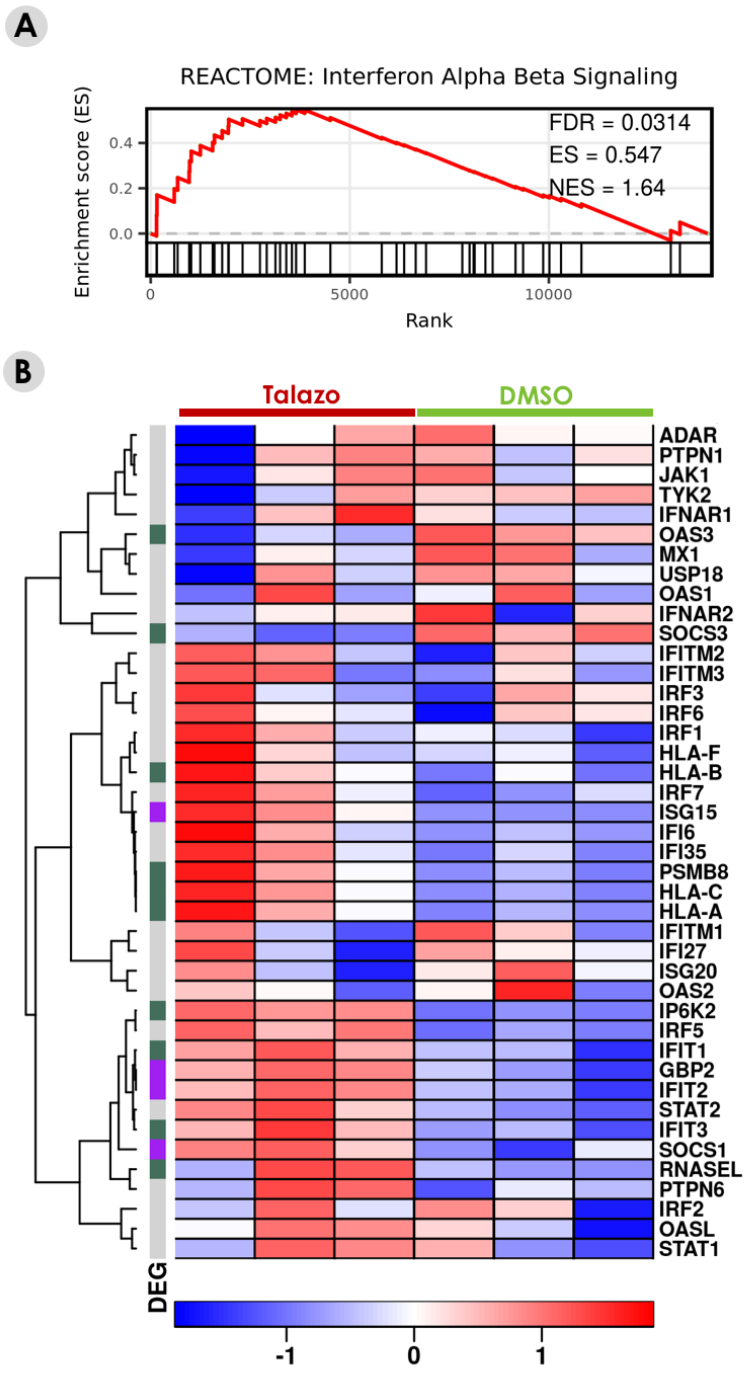

Figure IV.26. GSEA of the REACTOME pathway Interferon Alpha Beta Signalling in talazoparib- vs DMSO- treated A549-ERCC1$^{WT/WT}$ cells.
A. Enrichment plot generated by GSEA of ranked gene expression data for genes of the REACTOME pathway Interferon Alpha Beta Signalling. **B.** Associated heatmap showing the genes of the pathway, ranked by FDR. N = 3; Heatmap scale is a Z score. Purple, significantly DEGs with FDR < 0.05 and |LFC| > 1; Green, significantly DEGs with FDR < 0.05 and |LFC| > 0.58; Grey, non-significantly DEGs.

Together, these data support the hypothesis that PARPi specifically activate, in a cell-autonomous fashion in NSCLC cells, a type I IFN immune response that is enhanced in the context of ERCC1 deficiency, and can be linked to cGAS/STING activation and CCL5 secretion in our models.

8. PARPi exert immunomodulatory properties *in vivo*

To further assess the cell-autonomous immunomodulatory potential of PARPi, we decided to test the ability of these agents to generate tumour-intrinsic immunity *in vivo*. Indeed, if *in vitro* models provide convenient experimental platforms for investigating the properties and mechanisms of action of anti-cancer drugs, especially in "genetically-controlled" conditions such as in isogenic systems, these have obvious limitations owing to their inability to model the complexity of a tumour in terms of histological features, genetic heterogeneity, and cellular interactions within the tumour mass. In our case, testing the effects of PARPi in a relevant model *in vivo* would allow to evaluate the validity and translatability of our *in vitro* data regarding the potential of these drugs to generate cell-autonomous immune responses in cancer cells.

a. Experimental approach

Several experimental approaches may be utilized to test the immunomodulatory potential of anti-cancer drugs *in vivo*. Most approaches in immuno-oncology have involved the use of syngeneic mouse models, which have the advantage to faithfully recapitulate the interactions between the tumour and an intact host immune system, through the inoculation of immortalized mouse cancer cells into an inbred immunocompetent mouse strain of the same genetic background – thus creating an immunocompetent model in which tumour rejection cannot occur. Such models are ideal for the evaluation and monitoring of anti-cancer immune responses under treatment. By contrast, patient-derived xenograft (PDX) models, which arise from the subcutaneous or orthotopic implantation of fresh human tumour tissues into immuno-deficient mice, provide a convenient platform for

studying tumour-autonomous immune phenotypes elicited by specific therapeutic agents. As PDXs appear to recapitulate many aspects of the original patient tumour, except tumour-immune interactions, they constitute accurate model systems reflecting the complex biological evolution of human tumours, and as such often serve as a useful predictive platform for therapeutic outcomes. Therefore, we thought that, by capturing gene expression data in tumour tissue extracted from relevant PDX models treated with PARPi, we could evaluate the tumour-intrinsic immunomodulatory properties of PARPi *in vivo*.

For this experiment, the selection of a PDX model that would best match the models used in our *in vitro* study was important. Thus, in the absence of available PDX models of ERCC1-deficient NSCLC, we decided to use PDX models of *BRCA1*-mutant TNBC; these were kindly provided by Prof Andrew Tutt (Guy's and St. Thomas's Research Tissue and Data Bank, London) thanks to his existing collaboration with Prof. Chris Lord at the Institute of Cancer Research. We used two independent PDX models of *BRCA1*-mutant TNBC: (i) the BTBC456 model originating from a treatment-naïve, *BRCA1*-mutation carrier patient with confirmed LOH in the primary tumour and PDX; and (ii) the BX102 model derived from a treatment-naïve patient with unknown BRCA status (testing was declined), whose PDX subsequently revealed to have a *BRCA1* mutation.

To assess the effects of PARPi and subsequently evaluate cancer cell-autonomous immunomodulation in these two PDX models, a therapeutic assay was conducted with PDX-bearing mice. BTBC456 or BX102 tumours were implanted orthotopically into the mammary fat pad of immuno-deficient NOD/SCID/IL2rg$^{-/-}$ (NSG) host mice, and once tumours were palpable, mice were randomly assigned to vehicle or olaparib treatment groups (100mg/kg daily). At the time they reached a diameter greater than 12mm in the vehicle group, tumours were harvested, formalin fixed, and processed for paraffin embedding. Subsequently, RNA was extracted from tissue sections of 2-4 tumours from each treatment group, and subjected to immune gene expression profiling using the Nanostring® technology (**Figure IV.27.A**).

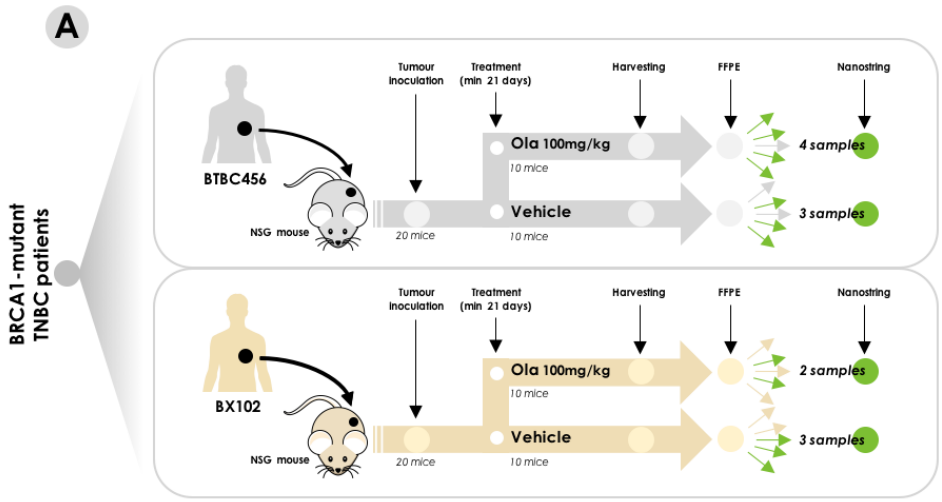
A
BRCA1-mutant TNBC patients
BTBC456
NSG mouse
Tumour inoculation
Treatment (min 21 days)
Harvesting
FFPE
Nanostring
Ola 100mg/kg
10 mice
Vehicle
10 mice
20 mice
4 samples
3 samples
BX102
NSG mouse
Tumour inoculation
Treatment (min 21 days)
Harvesting
FFPE
Nanostring
Ola 100mg/kg
10 mice
Vehicle
10 mice
20 mice
2 samples
3 samples

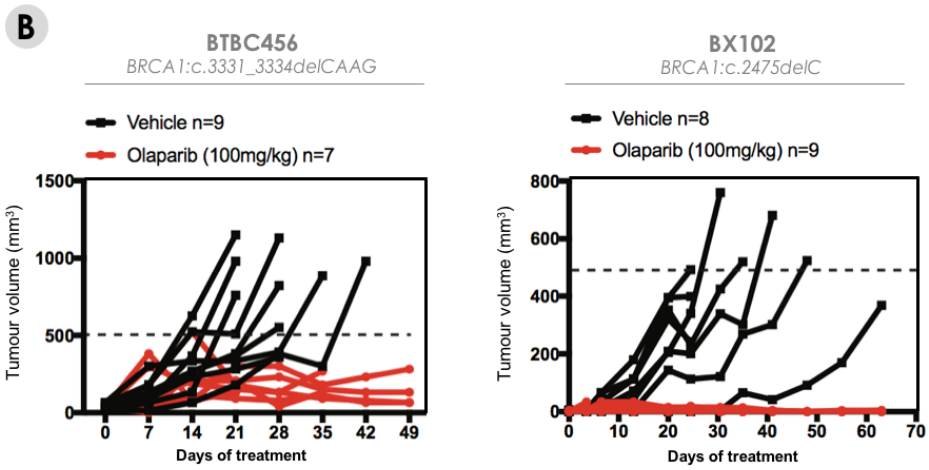
B
BTBC456
BRCA1:c.3331_3334delCAAG
Vehicle n=9
Olaparib (100mg/kg) n=7
Tumour volume (mm³)
Days of treatment
BX102
BRCA1:c.2475delC
Vehicle n=8
Olaparib (100mg/kg) n=9
Tumour volume (mm³)
Days of treatment

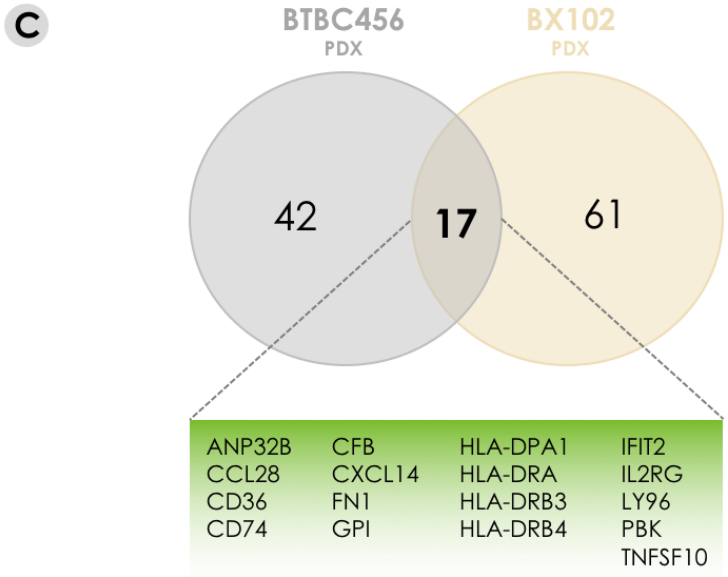
C
BTBC456
PDX
BX102
PDX
42
17
61
ANP32B
CCL28
CD36
CD74
CFB
CXCL14
FN1
GPI
HLA-DPA1
HLA-DRA
HLA-DRB3
HLA-DRB4
IFIT2
IL2RG
LY96
PBK
TNFSF10

Figure IV.27.Experimental details of the Nanostring® analysis of BTBC456 and BX102 tumours.
A. Schematic of the *in vivo* experiment that has been performed to generate olaparib-treated BTBC456 and BX102 tumours. **B.** Therapeutic response to olaparib treatment in mice bearing BTBC456 or BX102 tumours. BTBC456 group: PDX tumour fragments were transplanted into 16 recipient mice; once tumours had established, animals were treated with either drug vehicle or olaparib (100 mg/kg daily, n=9 for the vehicle-treated cohort and n=7 for the olaparib-treated cohort). Tumour volumes after the initiation of treatment are shown. BX102 group: PDX tumour fragments were transplanted into 17 recipient mice; once tumours had established, animals were treated with either drug vehicle or olaparib (100 mg/kg daily, n=8 for the vehicle-treated cohort and n=9 for the olaparib-treated cohort). Tumour volumes after the initiation of treatment are shown. **C.** Venn diagram depicting the number of significantly differentially expressed genes in olaparib-treated PDXs compared with vehicle-treated PDXs in BTBC456 and BX102 models. Threshold for differential expression was |LFC| > 1 and threshold for significance was FDR < 0.1. The significantly DEGs found in common between both PDXs are indicated below.

For mice of both models, tumour shrinkage was observed after treatment with olaparib, highlighting the exquisite sensitivity of these PDX models to PARPi, and confirming their clinical relevance (**Figure IV.27.B**).

b. Genetic characteristics of the PDX models

WES was performed on both PDX models, and used to identify their inherent genetic alterations. The BTBC456 model was characterized by the *BRCA1* mutation c.3331_3334delCAAG associated with an inactivating mutation in *TP53*, and revealed to have amplification or mutations in a number of oncogenes including *HRAS*, *KIT* and *PIK3CA* (**Table IV.4**). Interestingly, this model also exhibited amplification of the *MB21D1* gene encoding for the cytosolic DNA sensor cGAS, as well as of the *IRF7* gene, suggesting that BTBC456 tumours might be more likely to activate cGAS/STING signalling in response to cytosolic DNA sensing.

Table IV.4. Genetic characteristics of the BTBC456 PDX model.

Selective table showing copy-number alterations and mutation data extracted from WES of the BTBC456 model for the main oncogenes, tumour suppressors, DDR- and immune-related genes.

Gene family	*Gene*	*Copy number alteration*	*Mutation*	*Mutation type*
Oncogenes	BCL3	AMP		
	CBLC	AMP		
	CCND2	AMP		
	CCND3	AMP		
	ETV6	AMP		
	FGFR3	AMP		
	HRAS	AMP		
	KIT		MUT	N/A
	PIK3CA		MUT	N/A
Non-DDR tumour suppressors	CARS		P10A	Missense
	CDKN1B	AMP		
	CDK8		H235Y	Missense
	CDK17		G78A	Missense
	TP53		A189fs	Frameshift
DDR genes	BRCA1		Germline MUT	
	PARP11	AMP		
	POLH		MUT	N/A
	POLN	AMP		
	RAD52	AMP		
Immune-related genes	IRF7	AMP		
	MB21D1	AMP		

Table IV.5. Genetic characteristics of the BX102 PDX model.

Selective table showing copy-number alterations and mutation data extracted from WES of the BX102 model for the main oncogenes, tumour suppressors, DDR- and immune-related genes.

Gene family	*Gene*	*Copy number alteration*	*Mutation*	*Mutation type*
Oncogenes	BCL2	DEL		
	ETV6		G38A	Missense
	FGFR1	DEL		
	FUS		MUT	N/A
	MYC	AMP		
	NUP214		P1607fs	Frameshift
	PIK3CA		MUT	N/A
	SS18		MUT	N/A
Non-DDR tumour suppressors	APC		R1171H	Missense
	BMPR1A		I165V	Missense
	CDK8		H235Y	Missense
	EXT1	AMP		
	FBXW7	DEL		
	NOTCH1		A882T	Missense
	SDHB	AMP		
	SMARCA2	DEL		
	SMARCA4		A1423A	Splice Region
	TNFAIP3	DEL		
	TP53		MUT	
	WRN	DEL		
DDR genes	ATM		R1575H	Missense
	BRCA1		Germline MUT	
	CHEK1	AMP		
	MSH3		K383fs	Frameshift
	PARP9		C646*	Non-sense
	PARP10	AMP		
	XPF	DEL	MUT	Splice Region
	RAD50	DEL		
	RAD51	DEL		
	POLG		V185E	Missense
	SPO11	DEL		
	FANCB	DEL		
	TP53BP1	DEL		
Immune-related genes	IRF1	DEL		
	IRF2	DEL		
	JAK2	DEL		
	IFNA21	DEL		
	IFNA16	DEL		
	IFNA7	DEL		
	IFNA14	DEL		

Gene family	*Gene*	*Copy number alteration*	*Mutation*	*Mutation type*
Immune-related genes	IFNA5	DEL		
	IFNA6	DEL		
	IFNA13	DEL		
	IFNA2	DEL		
	IFNA8	DEL		
	IFNA1	DEL		
	IFNB1	DEL		
	IFNGR1	DEL		
	IFNW1	DEL		
	HLA-A		K292E	Missense
	HLA-DRB5		T214fs	Frameshift
	CXCL14	DEL		
	IL1RAPL2	DEL		
	IL2RG	DEL		
	IL3	DEL		
	IL3RA	DEL		
	IL4	DEL		
	IL5	DEL		
	IL6ST	DEL		
	IL7R		I121fs	Frameshift
	IL9	DEL		
	IL11RA		R395Q	Missense
	IL13	DEL		
	IL17RA	DEL		
	IL17D		E111A	Missense
	IL20RA	DEL		
	IL22RA2	DEL		
	IL31RA	DEL	MUT	Splice Region
	IL33	DEL		
	TLR2	DEL		
	TLR3	DEL		
	TLR7	DEL		
	TLR8	DEL		

The BX102 model was characterized by the *BRCA1* mutation c.2475delC associated with an inactivating mutation in *TP53*, and showed amplification or mutation of the oncogenes *MYC* and *PIK3CA* (**Table IV.5**). Interestingly, this model also displayed mutations or deletions in a number of other important DNA repair proteins including *ATM*, *XPF*, *RAD50*, *RAD51*, and *MSH3*, that might participate to increase the sensitivity of BX102 tumours to PARPi. In addition, this PDX model appeared to have a deletion of a whole region of chromosome 9 surrounding the *IFNB1* and *IFNA1* genes loci, suggesting an impaired activation of IFN responses in BX102 tumours.

c. Verification of the tissue specificity of the Nanostring® assay

The Nanostring® nCounter technology is a novel gene expression profiling system which offers advantages over current methods including digital output of data and direct mRNA measurement without enzymatic reaction (424). mRNA expression levels from FFPE tissue samples, which are often degraded, can be evaluated using the nCounter system because of increased sensitivity, reproducibility and technical robustness compared to other transcriptomic approaches (425) – low-abundance mRNAs can indeed be detected with a greater sensitivity than using microarray-based approaches (426). Considering these advantages, the Nanostring® technology appeared as an appropriate method for performing gene expression profiling of our PDX tumour samples. To specifically characterize the expression of immune signals in these samples, we chose to use the nCounter® PanCancer immune profiling panel, which comprises a set of 770 immune-related genes whose expression can be profiled in a single multiplexed gene expression analysis.

Table IV.6. Genes of the nCounter® PanCancer immune panel whose probe sequence has shown alignment with the mouse genome.

AKT3	CXCR4	MAP2K1	TBX21
ALCAM	CYFIP2	MAP3K5	THBS1
APP	CYLD	MAP3K7	TMEFF2
ATF2	DPP4	MAPK1	TNFSF8
ATG7	EGR1	MAPKAPK2	UBC
BATF	EP300	MEF2C	VEGFA
BCL2	EWSR1	MIF	AGK
BCL2L1	FEZ1	MS4A1	CNOT10
BTK	FOXJ1	NCAM1	CNOT4
C3AR1	HLA-DQB1	NFATC3	EDC3
C5	IGF1R	NFKBIA	HPRT1
CCR2	IL13RA1	NOD2	MTMR14
CD24	IL17RB	POU2F2	NOL7
CD37	IL34	PSMB7	SDHA
CHUK	ILF3	REPS1	TBP
CLEC5A	ITGA1	SH2D1A	TLK2
CSF1	ITGB2	SPA17	TRIM39
CTSH	LGALS3	STAT6	TUBB
CXCL12	MAF	SYK	ZNF143

Because PDX tumours were extracted from mice and contamination with mouse tissue may create concern by introducing a major bias in the analysis, we first decided to evaluate the level of cross-reactivity of the Nanostring® assay for mouse tissue. To do this, we retrieved sequence data from the 770 probes of the nCounter® PanCancer immune panel, and aligned them to the mouse genome using the online-available nucleotide basic local alignment search tool (BLASTn). Among the 770 probes profiled, we found 76 probes aligning to the mouse genome (**Table IV.6**), that is, a percentage of cross-reactivity of approximately 10%.

Therefore, these 76 genes were removed from the analysis of gene expression data generated by Nanostring® in our experiment, leaving the opportunity of reliably profiling the expression of the other 694 immune-related genes of the panel.

d. PARPi-treated tumours exhibit enhanced expression of type I IFN genes

Differential expression analysis of the Nanostring® data revealed that, among the 694 profiled genes, 59 and 78 were significantly differentially expressed between olaparib-treated and vehicle-treated PDXs in the BTBC456 and BX102 groups respectively (**Figure IV.27.C**); 17 genes were found commonly differentially expressed between the two models, among which four genes encoded components of the MHC class II.

In olaparib-treated BTBC456 PDXs, we found a significant upregulation of twelve genes involved in antigen presentation (fold-change (FC) > 2, FDR < 0.1) including several components of MHC class I (namely *HLA-B* and *HLA-C*) and MHC class II (*HLA-DPA1*, *HLA-DPB1*, *HLA-DMA*, *HLA-DMB*, *HLA-DRA*, *HLA-DRB3*, *HLA-DRB4* and *CD74*), as well as genes encoding proteins that mediate peptide degradation such as *CTSS* (**Figure IV.28**). More interestingly, we also found a significant upregulation of eight genes involved in type I IFN signalling (FC > 2.5, FDR < 0.1) – including *IFI27*, *IFI35*, *IFIT1*, *IFIT2*, *IFITM1*, *ISG15*, *MX1* and *NLRC5* – and increased expression of the lympho-attractant chemokines CCL5 and CCL28 (FC = 2.66, FDR = 0.005 and FC = 5.51, FDR < 0.0001 respectively). This suggested that treatment of mice bearing BTBC456 PDX tumours with olaparib triggered cancer cell-

autonomous activation of a type I IFN response *in vivo*, associated with the upregulation of chemotactic chemokines.

In olaparib-treated BX102 PDXs, we found upregulation of several genes encoding components of MHC class II (*HLA-DPA1*, *HLA-DRA*, *HLA-DRB3*, *HLA-DRB4* and *CD74*), consistent with what was observed in the BTBC456 model (**Figure IV.29**). However, despite a significant increase in expression of several chemotactic chemokines including CCL7 (FC = 2.22, FDR = 0.01), CCL19 (FC = 3.02, FDR = 0.001), CCL21 (FC = 4.08, *P* = 0.009), CXCL13 (FC = 4.21, FDR = 0.0001) and CXCL14 (FC = 4.58, FDR = 0.002), we did not observe any significant upregulation of genes involved in type I IFN signalling after treatment with olaparib in this model.

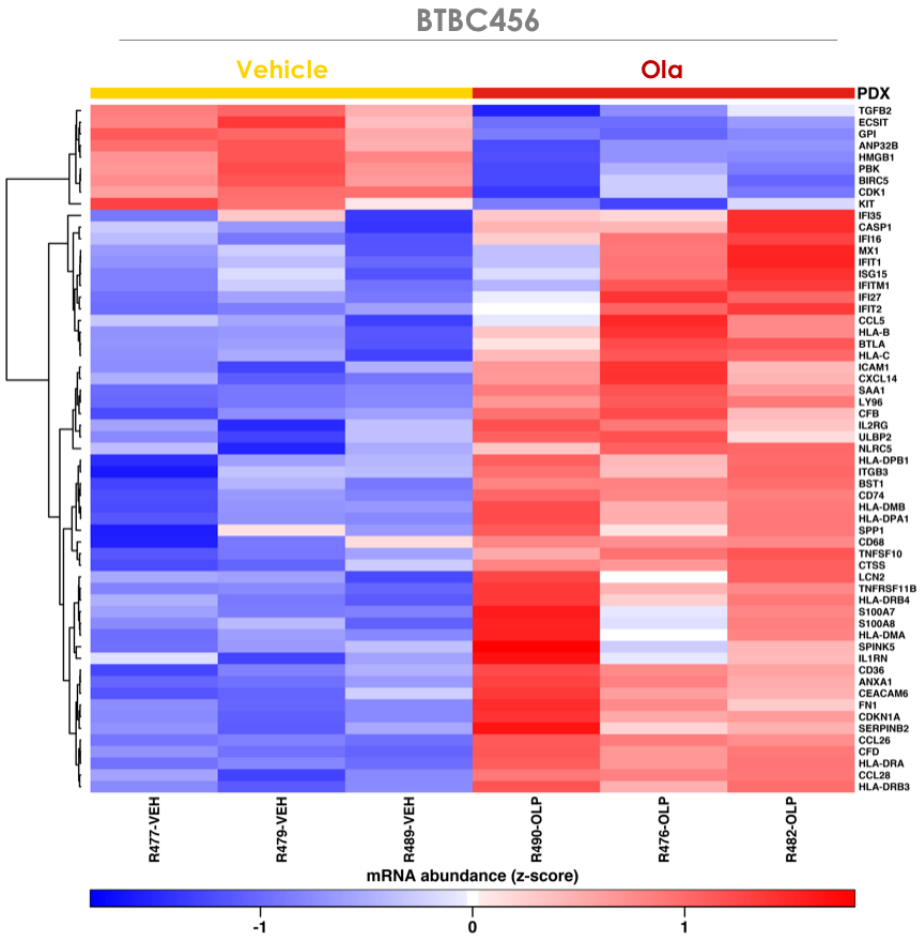

Figure IV.28. Heatmap showing all significantly differentially expressed genes in olaparib-treated vs vehicle-treated BTBC456 tumours.
N = 3; Heatmap scale is a Z score. Threshold for differential expression was |LFC| > 1 and threshold for significance was FDR < 0.1.

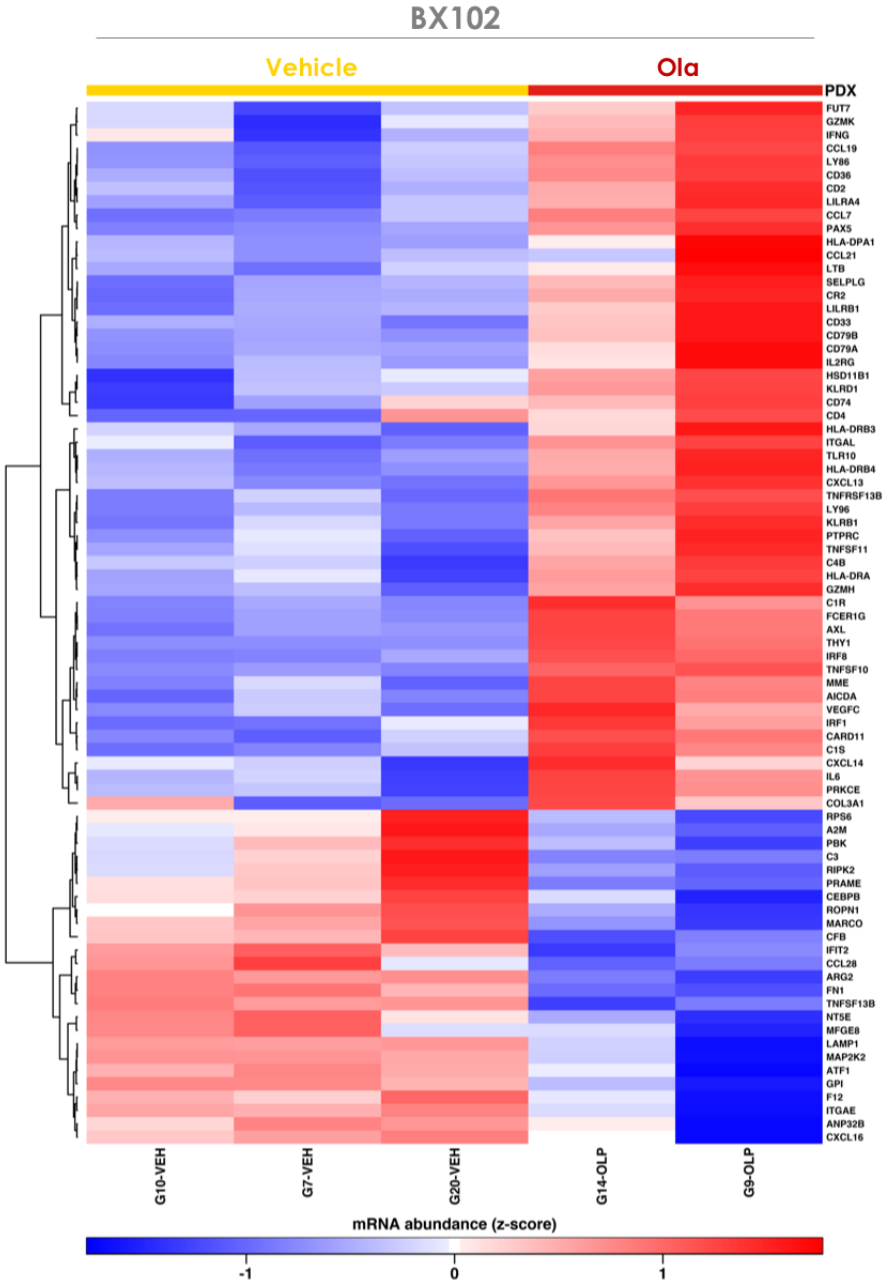

Figure IV.29. Heatmap showing all significantly differentially expressed genes in olaparib-treated vs vehicle-treated BX102 tumours.
N = 3; Heatmap scale is a Z score. Threshold for differential expression was |LFC| > 1 and threshold for significance was FDR < 0.1.

These differences observed between the expression data of the two PDX models may be explained by their inherent genetic characteristics. Indeed, if the BTBC456 model probably carries an enhanced potential for cGAS/STING-mediated type I IFN signalling activation

due to amplification of the *MB21D1* gene, it is reasonable to assume that, by contrast, the BX102 model might be unresponsive to such signals because of the deletion of *IFNA1*, *IFNB1* and many other IFN-related genes.

e. *PARPi upregulate MHC components in NSCLC cell lines* in vitro

To assess whether the upregulation of MHC components upon PARPi treatment observed in both PDXs would also operate in NSCLC models, we measured expression of HLA-ABC, the major components of MHC class I, in A549-ERCC1$^{WT/WT}$ and H1975-ERCC1$^{WT/WT}$ cell lines exposed to PARPi and/or IFN-γ (used as a positive control of activation) for 48 h. Flow cytometry analysis of HLA-ABC staining on these cells revealed an upregulation of HLA-ABC expression upon treatment with the PARPi talazoparib or niraparib, consistent with results obtained *in vivo* (**Figure IV.30**). This suggested that PARPi may directly modulate tumour immunogenicity by increasing cell-surface expression of MHC class I components, both *in vitro* and *in vivo*.

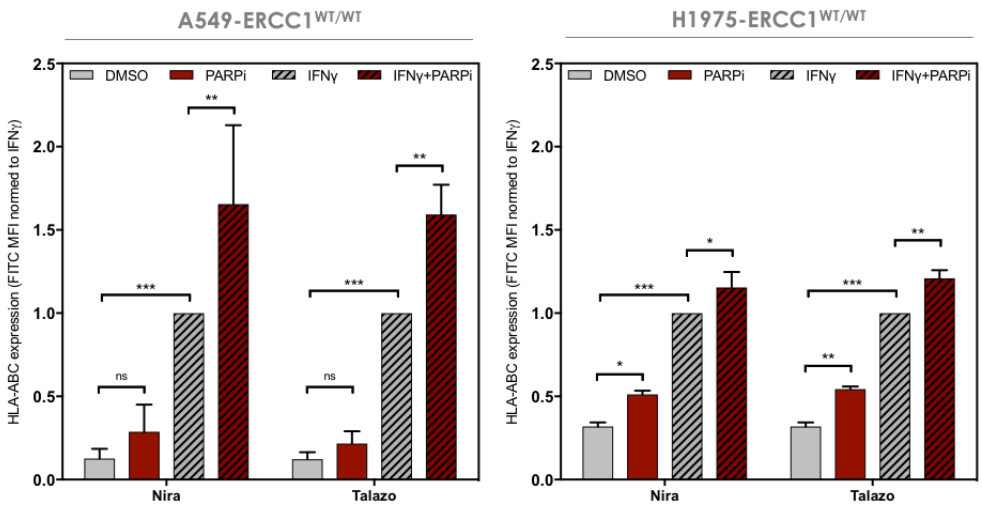

Figure IV.30. PARPi induce cell-surface expression of MHC class I components in NSCLC cells.
Quantification of HLA-ABC cell surface expression by flow cytometry in A549-ERCC1$^{WT/WT}$ and H1975-ERCC1$^{WT/WT}$ cells upon PARPi exposure, in the presence or absence of IFN-γ. Cells were treated for 48h with DMSO, 10 µM niraparib, 3 µM talazoparib, and/or 500 U/mL IFN-γ. MFI ± SD, N = 3, two-way ANOVA and post hoc Tukey's test.

C. Discussion

In this Chapter, we have described how PARPi trigger cell-autonomous activation of immune signalling in cancer cells. Using a unique combination of isogenic models of *ERCC1*-deficient NSCLC and *BRCA1*-deficient TNBC, we found that PARPi generate cytosolic DNA in a cell cycle- and DNA repair defect-dependent fashion, which in turn activates cGAS/STING signalling and elicits specific tumour cell-intrinsic immune responses in DDR-deficient cells. These results obtained *in vitro* are corroborated with the activation of cell-autonomous immunity *in vivo* in two distinct PDX models of *BRCA1*-mutated TNBC exposed to PARPi.

Although several scenarios may explain our findings, we propose the following model to describe our observations (**Figure IV.31**). DSB repair-proficient cells, such as wildtype *ERCC1* and *BRCA1* cells, adequately repair endogenous DNA lesions. PARPi exposure causes DNA damage, mostly initiated by PARP1 itself trapped onto the DNA at sites of spontaneous SSBs. Trapped-PARP1 generates stalled replication forks and subsequent DSBs during DNA replication. In DSB repair-proficient cells, trapped-PARP1 lesions can be adequately excised, a process which is likely to be orchestrated by ERCC1 (364). Following excision, BRCA1-mediated repair of DSBs occurs through HR, and replication restarts. Residual unrepaired lesions cause minimal formation of CCF, which are insufficient to trigger cGAS/STING signaling (**Figure IV.31.A-D**). By contrast, DSB repair-deficient cells, such as ERCC1$^{-/-}$ and *BRCA1*-mutated cells are exposed to increased levels of endogenous DNA damage, which are further enhanced upon exposure to PARPi. In ERCC1$^{-/-}$ cells, trapped-PARP1 lesions cannot be appropriately resolved (364), which prevents the subsequent processing of DSBs through HR (**Figure IV.31.E** and **Figure IV.31.F**). In *BRCA1*-mutated cells, several steps of HR are disabled and HR-mediated DSB repair cannot occur (349) (**Figure IV.31.I** and **Figure IV.31.J**). In either case, this results in the accumulation of stalled replication forks, subsequent DSBs and unrepaired DNA lesions which eventually cause increased micronuclei formation and CCF generation (**Figure IV.31.G** and **Figure IV.31.K**). These are detected by cGAS, which activates the

STING/pTBK1/pIRF3 cascade and results in a type I IFN response characterized by the secretion of CCL5 and other chemotactic cytokines (**Figure IV.31.H** and **Figure IV.31.L**).

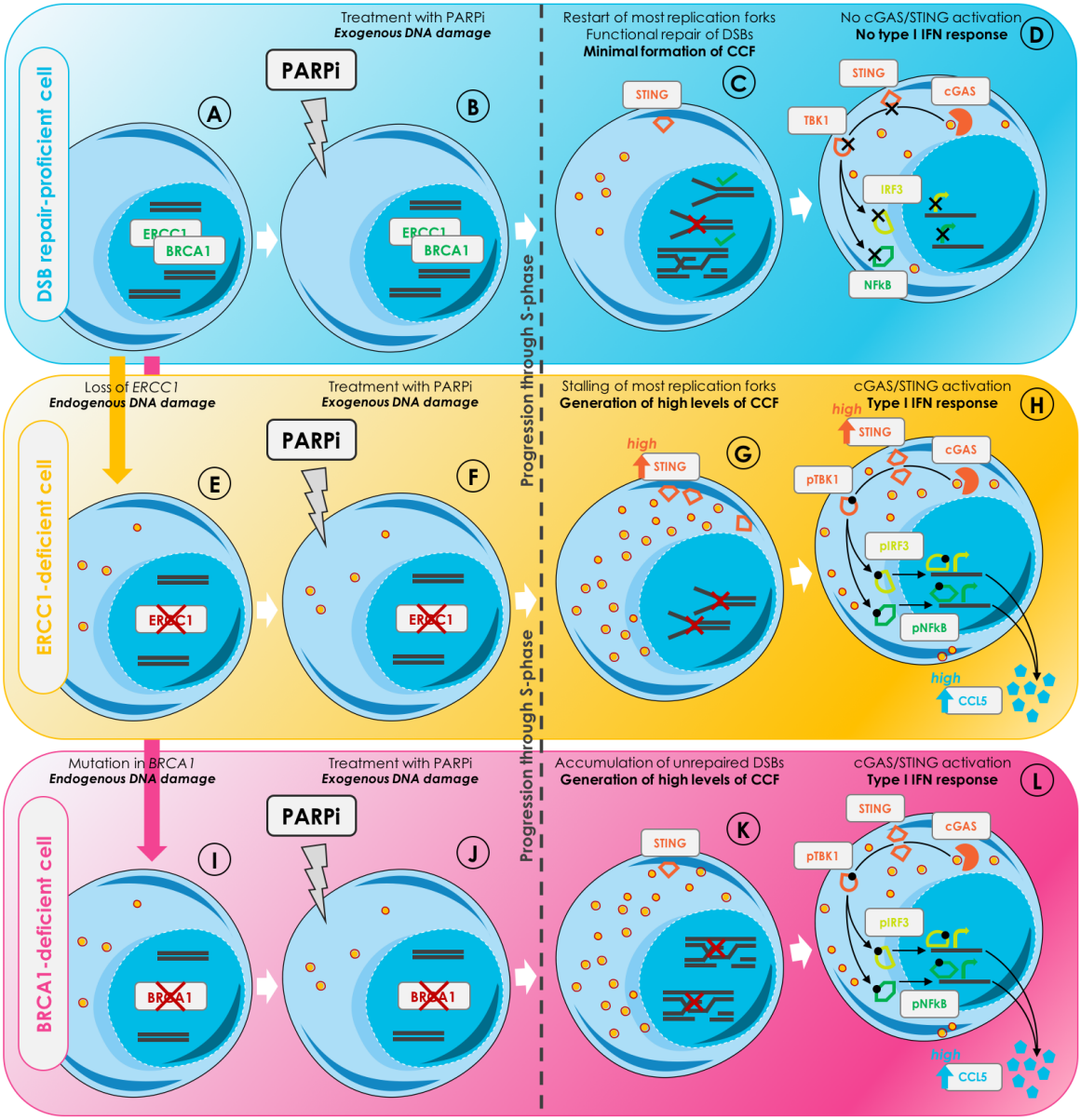

Figure IV.31. A proposed model to explain cGAS/STING activation following PARPi exposure in tumour cells harbouring DDR defects.

Our data support that clinical PARPi can induce cytosolic DNA, which is at least in part in the form of micronuclei, and subsequently activates cGAS/STING signalling. However, the exact mechanism underlying this formation of cytosolic DNA remains unclear. Our

observation that CCF accumulation is abrogated in PARP1-null cells supports a direct on-target effect of these drugs, which is mostly mediated by their PARP-trapping potential. Therefore, it is reasonable to assume that both trapped-PARP and additional unrepaired DNA lesion, by generating stalled replication forks, allow formation of ssDNA fragments via rupture of the nascent DNA during replication or dsDNA fragments as a result of DSBs. Both eventually accumulate in the cytosol. However, whereas ssDNA – which can form internal duplex structures – and short dsDNA fragments presumably provide a direct substrate for cGAS in the form of CCF, large dsDNA fragments most probably accumulate in the form of micronuclei, that are at some point detected by cGAS upon degradation of their fragile lamin membrane. Our data suggest that both CCF and micronuclei co-exist in cells exposed to PARPi, but which form of cytosolic DNA triggers the strongest cGAS/STING activation remains unknown. Whether this heterogeneity in cytosolic DNA forms could be controlled in the context of DNA damage induction to optimize cytosolic DNA sensing by cGAS would deserve further investigation for optimal therapeutic exploitation.

The cGAS/STING pathway is a very potent inducer of innate immune responses. Although our model is consistent with the cancer cell-autonomous activation of a type I IFN response consequent to PARP inhibition in DDR-deficient cells, it does not explain why PARPi appear to modulate other immune signals in a tumour cell-intrinsic manner, such as for example the expression of MHC components that has been observed both *in vitro* and *in vivo* in DDR-proficient and -deficient models. This might result from downstream and late effects of type I IFN signalling activation, but also suggests that PARPi may directly affect other immune signalling pathways in cancer cells; this potential may either result from the various effects of PARPi on PARP proteins – i.e. inhibition of their catalytic activity and PARP trapping mechanisms –, or could alternatively be a consequence of specific off-target effects of these agents. Indeed, recent studies have evidenced the existence of other biological targets of PARPi (427), raising the possibility that the immunomodulatory potential of these drugs may partly originate from effects on some of their secondary targets. Further investigation would be required to characterize these effects and identify relevant correlates of activation of immune responses in cancer cells.

Chapter V. PARPi modulate PD-L1 expression in tumour cells

A. Introduction

Among all immune checkpoints, the PD-1/PD-L1 axis has raised considerable interest over the past years because of its proven value as a therapeutic target for IO. At present, more than 1,000 clinical trials are evaluating anti-PD-(L)1 therapies in a wide range of histologies, and several of these agents have already been approved for treatment of several cancers including NSCLC, melanoma, RCC, UBC, HNSCC, Hodgkin lymphoma, HCC, and MSI-high or MMR-deficient solid tumours. Along this fast-paced clinical development of anti-PD-(L)1 agents, PD-L1 expression in tumour cells has undergone extensive assessment with respect to its value as a predictive biomarker of response to these therapies. As shown in a number of cancer types, patients with PD-L1-positive tumours have a higher ORR and improved PFS and OS compared with PD-L1-negative subgroups (115,118,136,428,429). Thus, PD-L1 expression in tumour cells has emerged as an important parameter influencing the outcome of anti-PD-(L)1 therapy in patients, and an increasing number of studies have focused on deciphering the mechanisms that regulate PD-L1 expression in human tumours.

To date, the complex regulatory network that determines PD-L1 levels in tumour cells can be broken down into five major components that involve:

(1) Genetic alterations at the PD-L1 locus. Both amplifications and translocations have been shown to increase PD-L1 expression in several tumour types. These include for example Hodgkin lymphoma and NSCLC in which 9p copy number amplifications have been reported to correlate with increased expression of PD-L1 (430,431), and primary mediastinal large B-cell lymphoma in which specific genomic rearrangements were shown to induce PD-L1 (432).

(2) Inflammatory signalling. A number of soluble factors produced by immune cells have been described to induce PD-L1 in tumour cells. In particular, the secretion of IFN-γ by

activated lymphocytes frequently drives PD-L1 expression in human tumours, and previous studies have demonstrated the existence of a correlation between PD-L1 expression and levels of CD8+ T cells in the tumour stroma (433). Other cytokines are also known to modulate tumour PD-L1 expression such as IFN-α and IFN-β, TNF-α, IL-4, IL-17, as well as several PRR such as TLR3 and TLR4 (434).

(3) Aberrant oncogenic signalling. Several oncogenic pathways have been shown to contribute to tumour outgrowth by driving PD-L1 expression (see Chapter I, paragraph A.3.b) (434).

(4) miRNA-mediated regulation. A number of miRNAs have been shown to regulate PD-L1 expression via direct binding to PD-L1 mRNA or through indirect modulation of the expression of other PD-L1 regulators (434).

(5) Post-translational modulation. Positive regulators of PD-L1 expression have also been identified at the protein level: for example, the chemokine-like factor superfamily members 4 and 6 (CMTM4/6) have been found to increase PD-L1 expression in various histologies (435,436). These proteins are thought to bind to PD-L1 and increase its half-life, presumably by preventing ubiquitination and lysosomal degradation during protein recycling. Other known PD-L1 protein regulators include CDK4, GSK3-β, B3GNT3 and CSN5 (434).

Beyond these endogenous factors influencing PD-L1 expression in tumour cells, transient upregulation of PD-L1 has been observed in the context of DNA damage induction or impaired DDR. In particular, certain chemotherapeutic regimens have been shown to upregulate PD-L1 in solid tumours and haematological malignancies (301,437), and S phase-specific DNA damaging agents such as cisplatin have been identified as potent PD-L1 inducers in patients (438). Consistently, pre-clinical studies have established the potential of cisplatin to promote PD-L1 upregulation in cancer cells *in vitro* and *in vivo* (268,439,440). Similarly, the induction of specific DDR defects in cancer cell lines – via siRNA silencing of DDR genes, such as *BRCA1* – has been associated with transient upregulation of PD-L1 (268), suggesting a direct link between PD-L1 expression and the DDR. If the biological mechanisms underlying this link are currently poorly understood,

some studies have suggested that activation of the cGAS/STING pathway following S phase-specific DNA damage might be involved (268).

These recently reported data prompted us to investigate the potential of PARPi to modulate PD-L1 expression in cancer cells in the context of functional and dysfunctional DDR. Because our previous data suggested mostly activation of type I IFN signalling through cGAS/STING in response to PARPi, but also activation of type II IFN signalling (Chapter IV), we hypothesized that PARPi may synergize with IFN-γ to induce PD-L1 expression in a DDR defects- and cGAS/STING-dependent manner in cancer cells.

To test this hypothesis, we developed an experimental strategy that comprised: (i) directly measuring PD-L1 expression at the transcriptional level and at the cell surface in NSCLC cells exposed *in vitro* to various clinical PARPi alone, and in combination with IFN-γ; (ii) comparing PD-L1 expression following exposure to PARPi (+/- IFN-γ) in ERCC1-proficient and -deficient NSCLC models; (iii) assessing the involvement of cGAS/STING signalling in the observed phenotypes. In this Chapter are described and discussed the results of this investigation.

B. Results

1. PARPi synergise with IFN-γ to induce PD-L1 expression in NSCLC cells

Cell-surface expression of PD-L1 is defined by an elevated heterogeneity across cancer patients, including NSCLC patients (441), and is known to be influenced by driver genes mutation status. In NSCLC, mutations of *EGFR* were found associated with enhanced expression of PD-L1 in patients tumours (442). To take this variability of expression into account in our study, we decided to use two different NSCLC cell lines characterized by distinct basal PD-L1 expression: the *EGFR*-mutated H1975 cell line which expresses high levels of PD-L1 and the *KRAS*-mutated A549 cell line which, in comparison, expresses low levels of PD-L1 (443). In addition, the choice of these models allowed us to evaluate the

impact of ERCC1 deficiency on the modulation of PD-L1 expression by PARPi, by using the available isogenic ERCC1-deficient A549 and H1975 cell lines.

a. Experimental approach and controls

We exposed A549-ERCC1$^{WT/WT}$ and H1975-ERCC1$^{WT/WT}$ cells to SF50 doses of the clinical PARPi rucaparib, talazoparib and niraparib during 48 h, in the presence or absence of IFN-γ, and monitored cell surface PD-L1 expression using flow cytometry.

In order to avoid potential biases induced by the detection of intracellular PD-L1 in cells displaying loss of plasma membrane integrity following PARPi-mediated apoptosis, we used propidium iodide (PI) as a viability marker and measured PD-L1 expression in viable cells only. Thus, our gating strategy involved two simple steps (**Figure V.1.A**): (i) doublet discrimination via plotting of the height vs area parameters of the forward scatter (FSC) and subsequent exclusion of events characterized by a height/area disproportion; (ii) necrotic cells discrimination via exclusion of PI-positive cells. Following these gating steps, we measured the mean fluorescence intensity (MFI) of PD-L1 staining in the selected population for each experimental condition and used an isotype control antibody to identify background staining and control for the specificity of PD-L1 staining. The MFI corresponding to staining with the isotype control antibody was much lower compared to that of the PD-L1 antibody, supporting the binding specificity of PD-L1 antibody to its target (**Figure V.1.B**). Moreover, no differences in MFI could be detected between experimental conditions for the isotype control staining, thus confirming the validity of the assay.

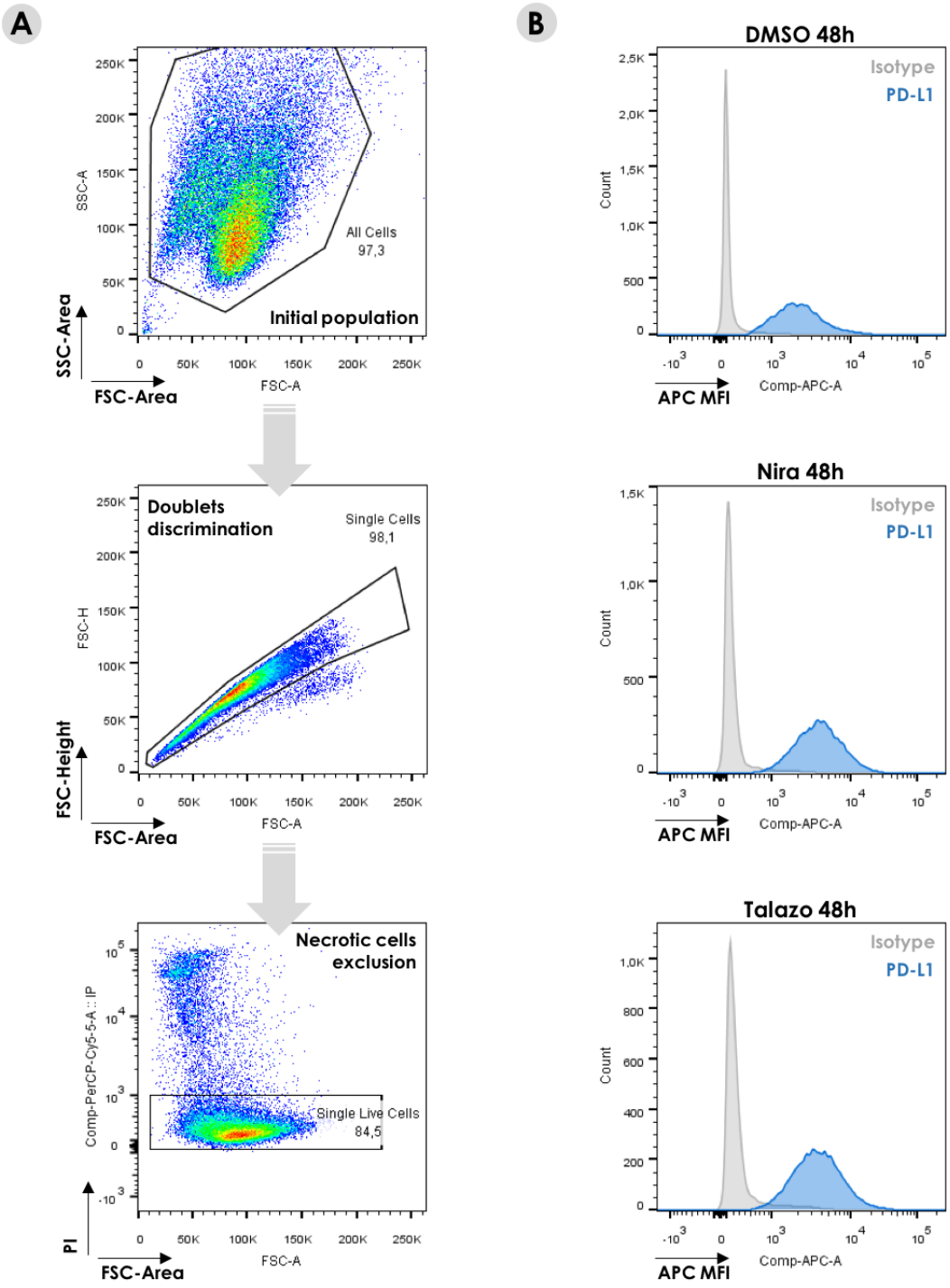

Figure V.1. Details of the flow cytometry analysis used to detect PD-L1 cell surface expression in NSCLC cells.

A. Gating strategy used to isolate a population of live single cells within talazoparib-treated H1975-ERCC1$^{WT/WT}$ cells. Flow cytometry dot plots represent the regions selected for each discrimination step. **B.** Flow cytometry histogram plots showing the allophycocyanin (APC) MFI associated with the isotype control and PD-L1 stainings in DMSO- and PARPi-treated cells.

b. Several clinical PARPi potentiate IFN-γ-mediated PD-L1 upregulation in NSCLC cells

In the A549-ERCC1$^{WT/WT}$ cell line – expressing low levels of PD-L1 at baseline –, we measured no significant induction of PD-L1 expression with PARPi alone (**Figure V.2.A**), although a tendency towards induction could be observed. By contrast, a significant upregulation of PD-L1 could be detected in the H1975-ERCC1$^{WT/WT}$ cell line after treatment with either rucaparib, talazoparib or niraparib as monotherapy (≈ 2-fold increase; P = 0.0002, P = 0.002, P = 0.0005 respectively, two-way ANOVA and *post hoc* Tukey's test; **Figure V.2.B**). Interestingly, co-treatment of PARPi plus IFN-γ was synergistic and could potentiate the induction of PD-L1 expression in both A549-ERCC1$^{WT/WT}$ and H1975-ERCC1$^{WT/WT}$ cells (**Figure V.2.A** and **Figure V.2.B**) – i.e. PD-L1 induction following combined treatment of PARPi plus IFN-γ was greater than the sum of the individual inductions obtained with these agents alone.

These results suggest that PARPi have an inherent potential to induce cell surface PD-L1 expression in NSCLC cells. This potential is enhanced in the context of constitutively high PD-L1 expression levels, and allows potentiation of IFN-γ-driven PD-L1 induction.

c. PARPi-mediated PD-L1 upregulation is dose-dependent, specific, and results from an on-target effect of PARPi

To further characterize this potential of PARPi to induce PD-L1 expression in cancer cells, we first sought to evaluate whether the observed phenotype was dose-dependent. To do this, we exposed A549-ERCC1$^{WT/WT}$ and H1975-ERCC1$^{WT/WT}$ cells to a dose range of talazoparib in the presence or absence of IFN-γ, and monitored PD-L1 expression by flow cytometry. We observed that, regardless of the presence of IFN-γ, there was a dose-dependent induction of PD-L1 expression in both A549-ERCC1$^{WT/WT}$ and H1975-ERCC1$^{WT/WT}$ cells following talazoparib treatment (**Figure V.3**).

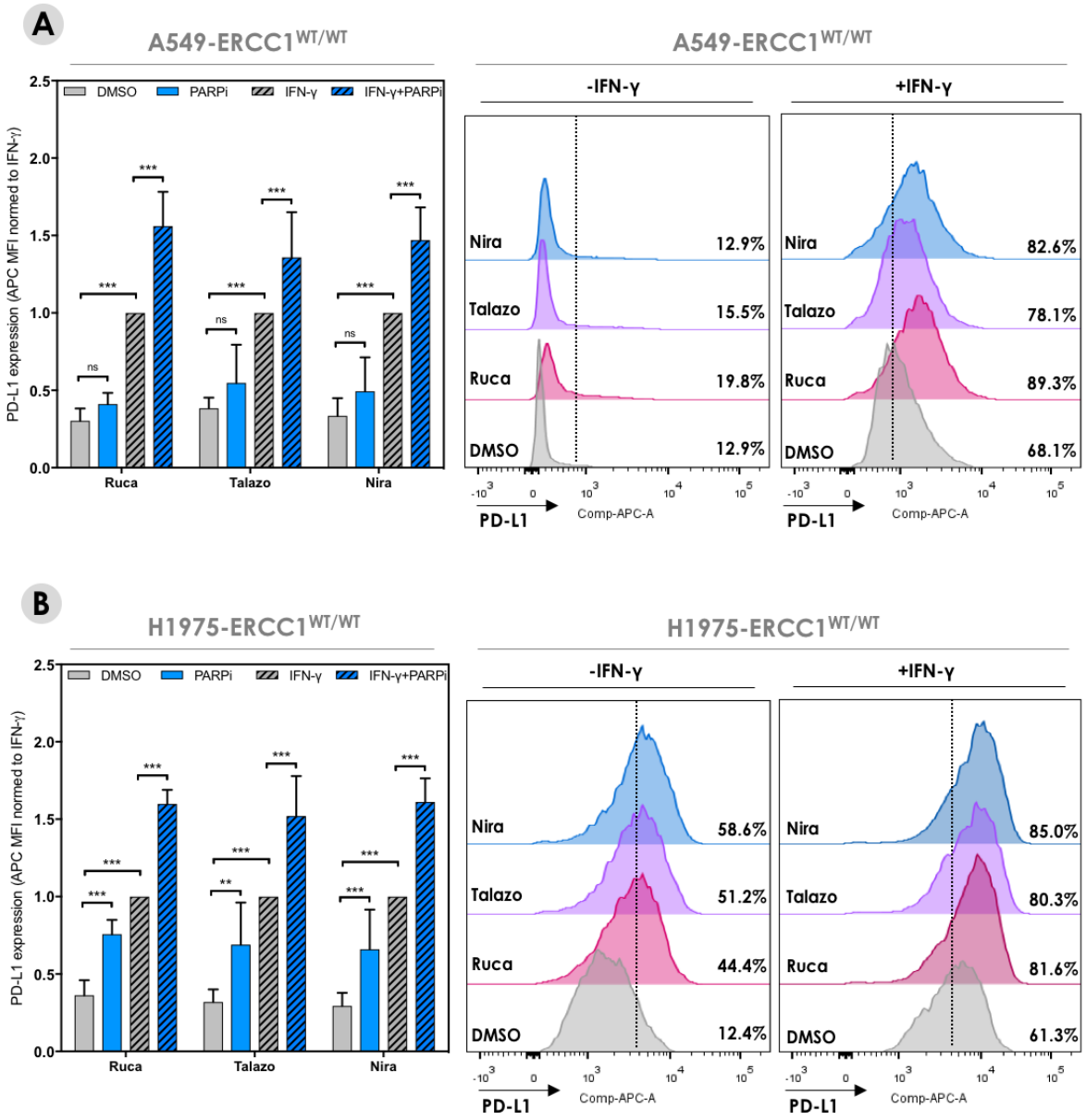

Figure V.2. PARPi synergize with IFN-γ to induce PD-L1 cell surface expression in NSCLC cells.

Quantification of PD-L1 cell surface expression by flow cytometry in A549-ERCC1$^{WT/WT}$ (**A**) and H1975-ERCC1$^{WT/WT}$ cells (**B**) upon PARPi and IFN-γ exposure. Cells were treated for 48h with DMSO, 15 µM Ruca, 3 µM Talazo, 10 µM Nira, and/or 500 U/mL IFN-γ. MFI ± SD normalized to IFN-γ; N = 3, two-way ANOVA and *post hoc* Tukey's test. Next to the bar graphs are displayed the corresponding flow cytometry histograms; shown is the percentage of PD-L1-positive cells.

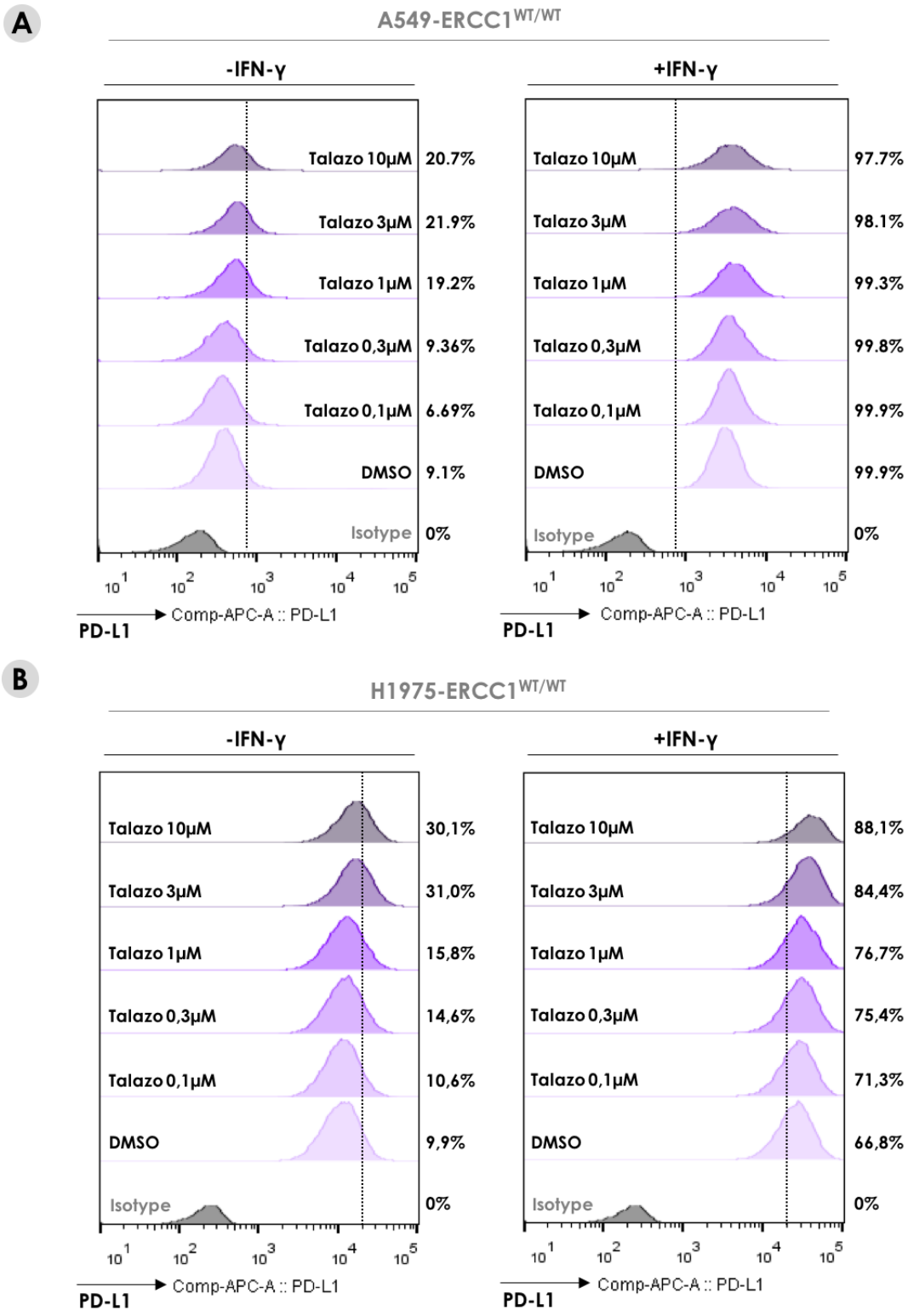

Figure V.3. PARPi-mediated induction of PD-L1 is dose-dependent.

Representative flow cytometry histograms showing PD-L1 expression in talazoparib-treated A549-ERCC1$^{WT/WT}$ (**A**) and H1975-ERCC1$^{WT/WT}$ cells (**B**), in the presence or absence of IFN-γ. Cells were treated with DMSO, or a dose range of talazoparib, in combination or not with 500 U/mL IFN-γ. Shown is the percentage of PD-L1-positive cells.

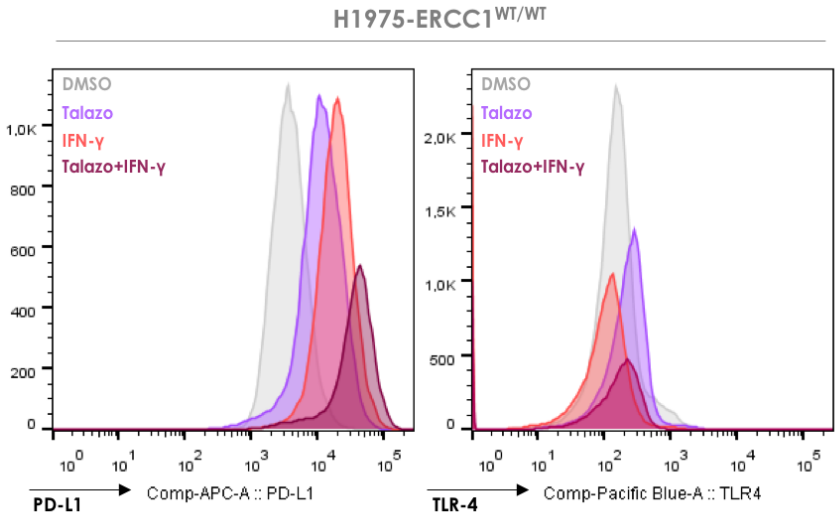

Figure V.4. PARPi induce cell surface expression of PD-L1 but not TLR4 in H1975 cells. Representative flow cytometry histograms showing PD-L1 and TLR4 expression in H1975-ERCC1$^{WT/WT}$ cells upon PARPi exposure, in the presence or absence of IFN-γ. Cells were treated with DMSO, 3 μM Talazo, 500 U/mL IFN-γ or both.

We next sought to verify the specificity of PARPi-mediated PD-L1 induction, by evaluating the membrane expression of other cell surface markers. For this analysis, we chose TLR4, an immune-related cell surface PRR which has been described to be positively correlated with PD-L1 expression in NSCLC samples (444). No TLR4 induction could be detected upon treatment with talazoparib (**Figure V.4**), suggesting that PD-L1 induction by PARPi might be relatively specific.

Finally, we decided to evaluate whether the induction of PD-L1 by PARPi was attributable to an on-target effect of these agents. To do this, we used the previously described isogenic model of PARP1 deficiency developed in the SUM149 cell line. We exposed SUM149-BRCA1$_{mut}$ (PARP1$^{+/+}$) and SUM149-PARP1$^{-/-}$ cells to talazoparib and/or IFN-γ for 48 h, and monitored the expression PD-L1 by flow cytometry. Although a significant synergy between talazoparib and IFN-γ could be observed in the parental SUM149-BRCA1$_{mut}$ cell line, this effect was completely abrogated in the SUM149-PARP1$^{-/-}$ cell line, where only IFN-γ could induce cell surface PD-L1 (**Figure V.5**). These results suggested that PARP1 is required for PARPi-mediated PD-L1 induction, supporting the hypothesis of an on-target effect of these drugs in the generation of this phenotype.

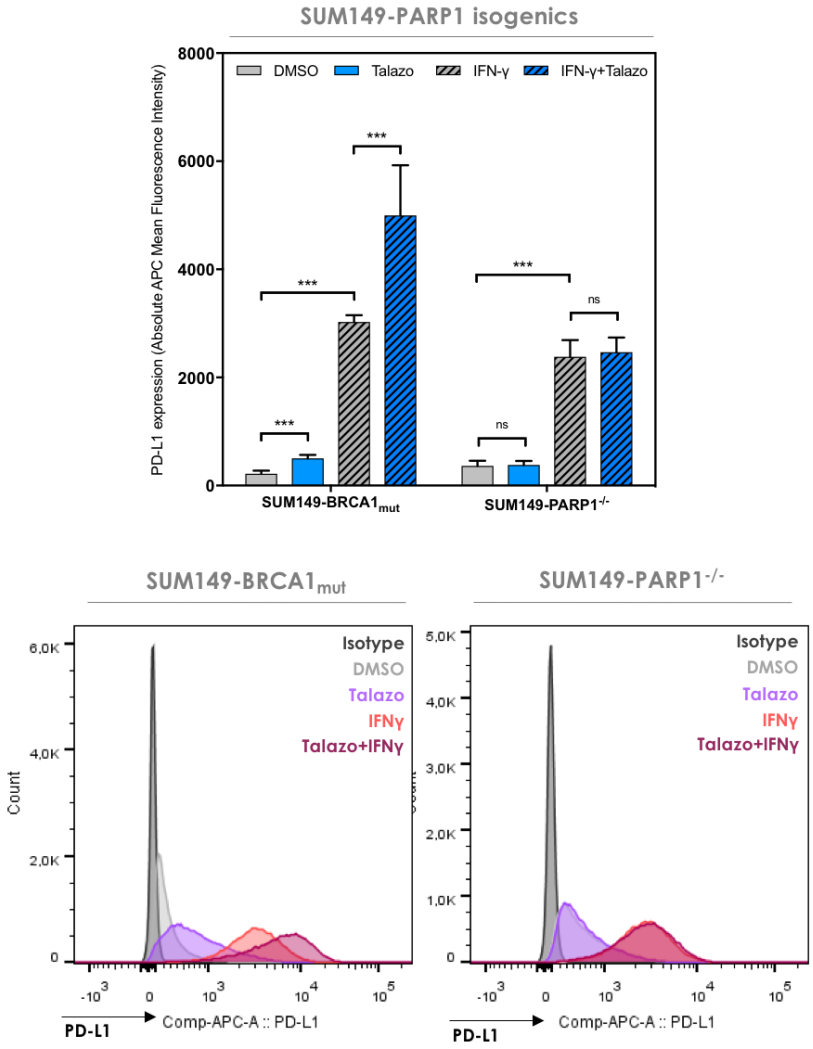

Figure V.5. PD-L1 induction results from an on-target effect of PARPi on PARP1. Quantification of PD-L1 cell surface expression by flow cytometry in SUM149-BRCA1$_{mut}$ and SUM149-PARP1$^{-/-}$ cells treated for 48h with DMSO, 3 µM Talazo, and/or 500 U/mL IFN-γ. MFI ± SD; N = 3, two-way ANOVA and *post hoc* Tukey's test. The corresponding flow cytometry histograms are displayed at the bottom of the graph.

d. PARPi induce PD-L1 expression in patient-derived NSCLC cells

To further corroborate the potential of PARPi to induce PD-L1 expression in cancer cells, we next sought to assess whether the mechanisms observed in cell lines would also operate in patients. To this aim, we collected fresh cells from a NSCLC patient's pleural effusion sample and exposed them *in vitro* to PARPi and IFN-γ. For this experiment, we used niraparib at a concentration of 10 µM (similar dose to that used in cancer cell lines) and

treated the patient's cells for 48 h, prior to flow cytometry analysis. Epithelial cell adhesion molecule (EpCAM) was used as a marker of tumour cells, and accordingly, an additional step of exclusion of EpCAM-negative cells was added to the gating protocol. Eventually, PD-L1 cell-surface expression was quantified in EpCAM-positive cells exclusively. This revealed an increased expression of PD-L1 upon niraparib exposure in the patient's tumour cells, which was again enhanced in the presence of IFN-γ (**Figure V.6**), consistent with our findings on cancer cell lines.

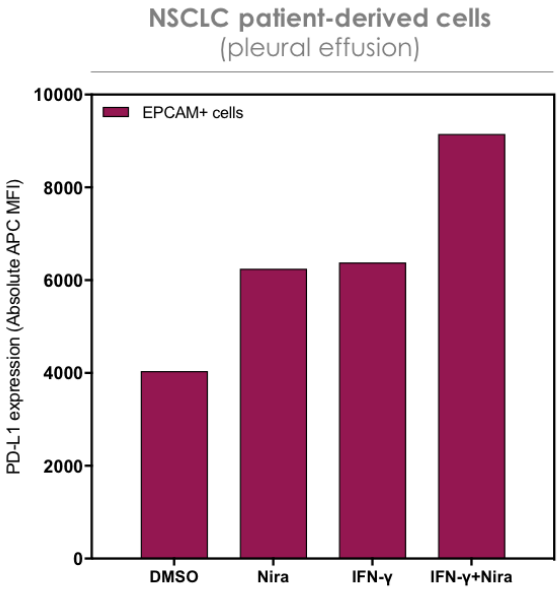

Figure V.6. PARPi induce PD-L1 expression in patient-derived tumour cells.
Quantification of PD-L1 cell surface expression by flow cytometry in the EpCAM-positive cells of a pleural effusion sample upon PARPi and/or IFN-γ exposure. Cells were treated *in vitro* for 48h with DMSO, 10 μM Nira, 500 U/mL IFNγ or both. MFI of a single PD-L1 staining is shown.

Together, our results strongly support that PARPi promote PD-L1 expression in a cell-autonomous fashion in NSCLC cells. This effect is dose-dependent, specific, and potentiated by the addition of IFN-γ. Furthermore, the observation that PD-L1 is not induced in PARP1$^{-/-}$ cells in response to PARPi suggests that PD-L1 induction results from an on-target effect of PARPi on PARP1. These results are in line with previously published data showing that PARPi mediate upregulation of PD-L1 in BRCA1-deficient breast cancer models (445).

2. ERCC1 deficiency exacerbates PARPi-mediated PD-L1 upregulation

Because some DDR defects have been associated with upregulation of PD-L1 in cancer cells (268), we hypothesized that ERCC1 deficiency might potentiate PARPi-mediated induction of PD-L1 expression in NSCLC cells. To test this hypothesis, we exposed A549- and H1975-ERCC1 isogenic cell lines to PARPi, and measured the expression of PD-L1 at the transcriptional level using RT-qPCR and at the cell surface level using flow cytometry. In the A549 model, although we observed little induction of cell-surface PD-L1 and no significant difference between A549-ERCC1$^{WT/WT}$ and A549-ERCC1$^{-/-}$ with talazoparib as monotherapy, we detected, in the presence of IFN-γ, a significantly enhanced upregulation of PD-L1 following talazoparib treatment in ERCC1-deficient cells compared to ERCC1-wildtype cells (**Figure V.7.A**). Similar results were obtained in the H1975 model, where a significantly higher expression of PD-L1 was systematically found in ERCC1-deficient cells. Likewise, analysis of PD-L1 mRNAs by RT-qPCR in talazoparib- or rucaparib-treated A549-ERCC1 isogenic cell lines revealed an increased transcription of *PD-L1* in A549-ERCC1$^{-/-}$ compared to A549-ERCC1$^{WT/WT}$ cells (**Figure V.7.B**).

These data support the notion that ERCC1-deficient cells harbour higher basal expression of PD-L1 and are more likely to induce cell surface PD-L1 expression in response to PARPi and IFN-γ. At the transcriptional level, this is reflected by an activation of *PD-L1* transcription upon PARPi and IFN-γ exposure, which is enhanced in the context of ERCC1 deficiency, suggesting that the cancer cell DDR status influences this phenomenon.

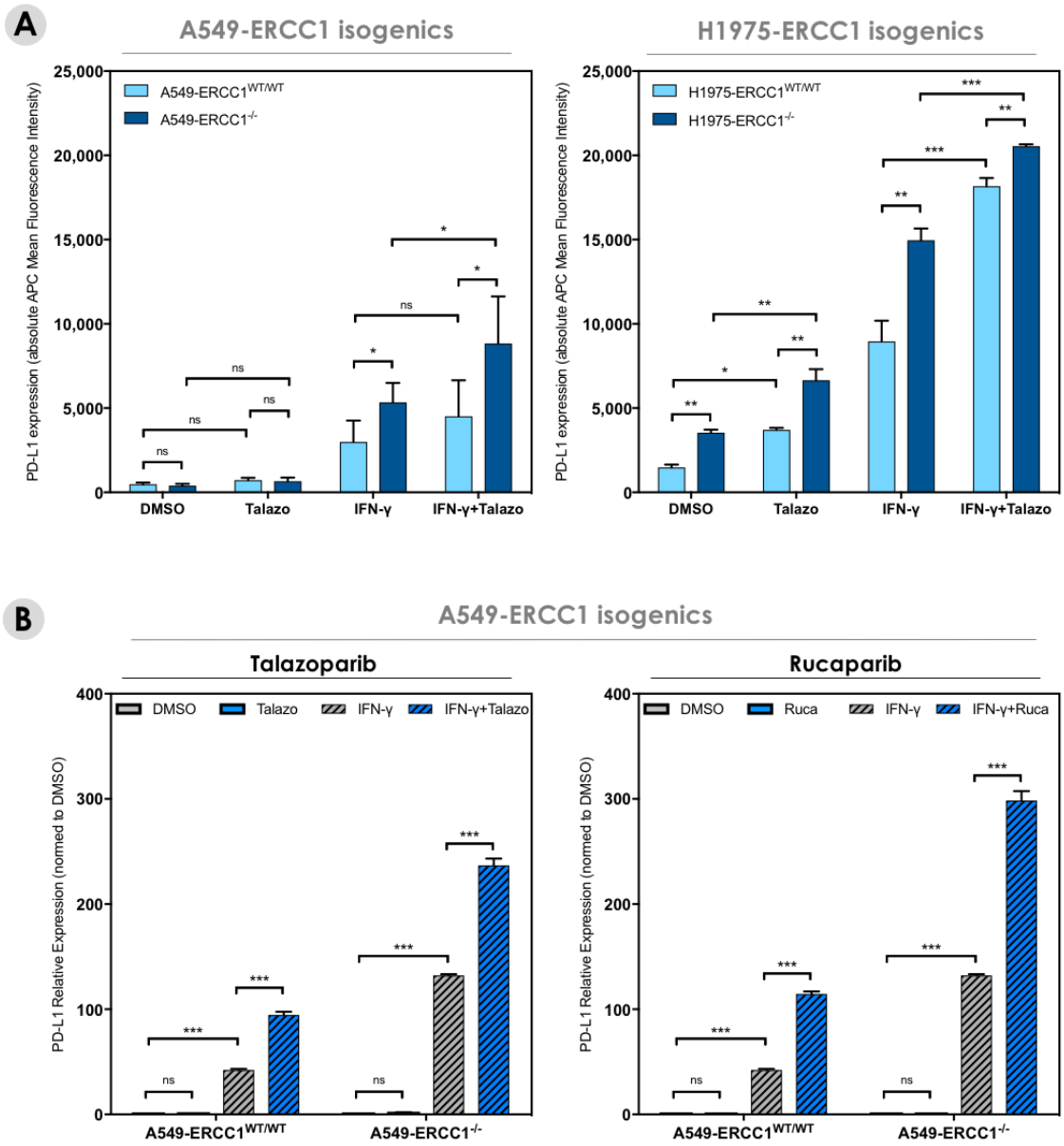

Figure V.7. ERCC1-deficient cells present an enhanced potential to induce PD-L1 expression in response to PARPi and IFN-γ.

A. Quantification of PD-L1 cell surface expression by flow cytometry in A549-ERCC1$^{WT/WT}$, A549-ERCC1$^{-/-}$, H1975-ERCC1$^{WT/WT}$ and H1975-ERCC1$^{-/-}$ cells treated for 48h with DMSO, 3 µM Talazo, and/or 500 U/mL IFN-γ. MFI ± SD; N = 3, two-way ANOVA and *post hoc* Tukey's test. **B.** RT-qPCR analysis of RNA isolated from A549-ERCC1$^{WT/WT}$ and A549-ERCC1$^{-/-}$ cells exposed to PARPi and/or IFN-γ. Cells were treated for 48h with DMSO, 3 µM Talazo or 13.5 µM Ruca, and/or 500 U/mL IFN-γ. PD-L1 mRNAs were analysed relative to GAPDH (to control for cDNA quantity). Shown are arbitrary units of gene expression, normalized to A549- ERCC1$^{WT/WT}$ DMSO-treated control. Mean ± SD, N=4, two-way ANOVA and *post hoc* Tukey's test.

3. PARPi-mediated PD-L1 upregulation is independent from cGAS/STING signalling activation

As previously published data showed that PD-L1 can be induced by type I IFN (446), we hypothesized that the upregulation of PD-L1 observed upon PARPi exposure might occur via cGAS/STING-mediated activation of type I IFN signalling.

To assess the implication of cGAS/STING signalling in the upregulation of PD-L1 by PARPi, we transfected NSCLC cells with siRNAs targeting cGAS, STING, TBK1, IRF3, or a negative control siRNA, and evaluated PD-L1 expression by flow cytometry after 48 h of exposure to talazoparib and/or IFN-γ. In the H1975-ERCC1$^{WT/WT}$ cell line, transfection with the negative control siRNA and subsequent treatment with talazoparib led to a significant induction of cell surface PD-L1 expression, regardless of the presence IFN-γ, which was consistent with our previous observations. Transfection with any of the siRNAs targeting the cGAS/STING pathway also yielded induction of PD-L1 expression after treatment with talazoparib (**Figure V.8.A**), although this latter appeared to be reduced compared to that obtained in the control siRNA condition. Similarly, analysis of cell surface PD-L1 expression in the same conditions in A549-ERCC1$^{WT/WT}$ and A549-ERCC1$^{-/-}$ cells revealed no obvious abrogation of talazoparib-mediated PD-L1 upregulation upon transfection with siRNAs targeting the cGAS/STING pathway, and a highly variable effect according to the protein depleted (**Figure V.8.B**).

Together, these results suggest that PD-L1 upregulation by PARPi in NSCLC cells cannot be directly attributed to cGAS/STING signalling activation. In particular, the fact that ERCC1-deficient cells still upregulate PD-L1 in response to PARPi while cGAS/STING effectors are depleted suggests that, in this context, DNA damage-associated cGAS/STING signalling activation may not drive PD-L1 expression. This is contradictory to previously published data showing that cisplatin-mediated PD-L1 upregulation was cGAS/STING-dependent in breast cancer cell lines (268), and further supports the involvement of other immune signalling pathways in the modulation of PD-L1 expression by PARPi.

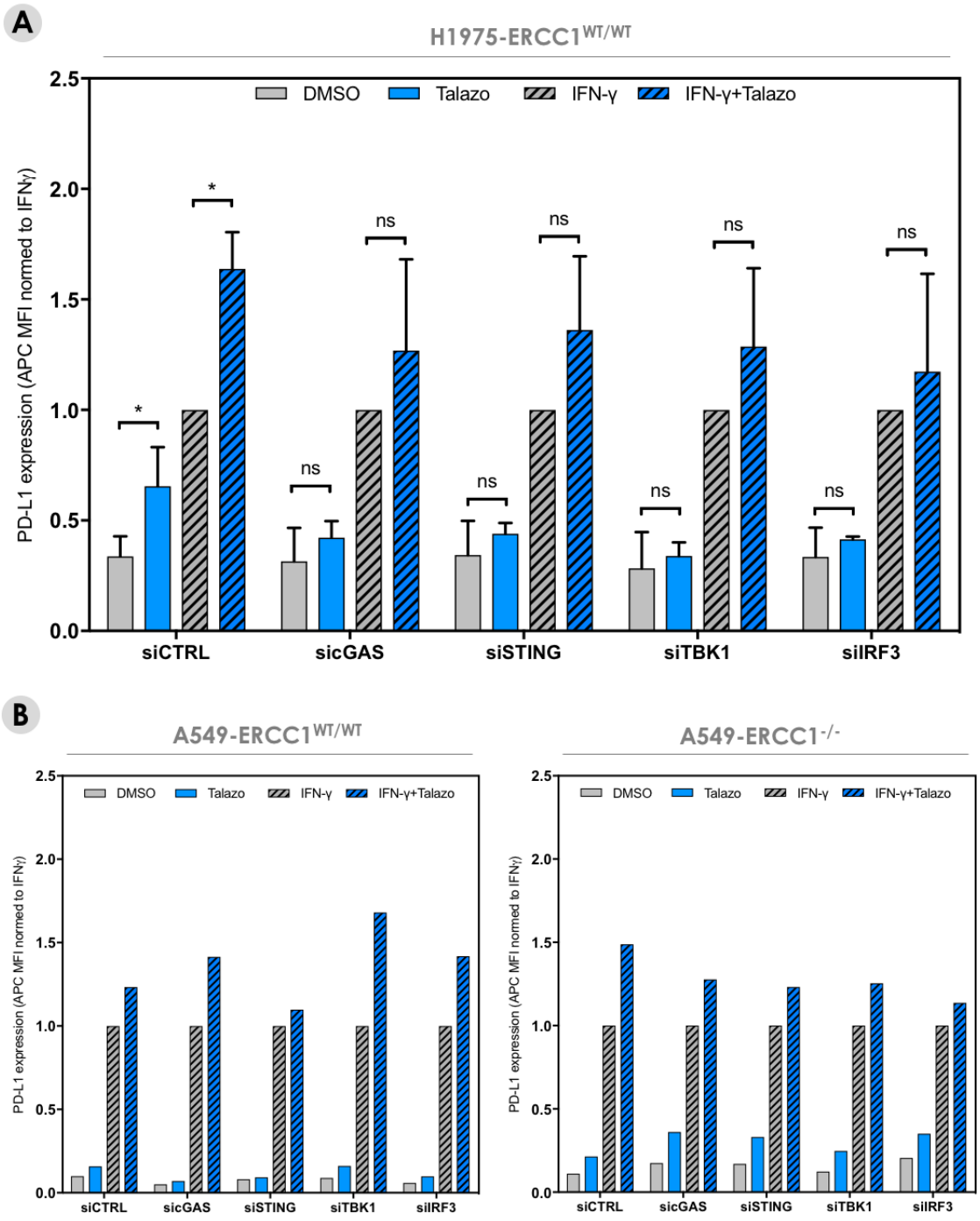

Figure V.8. PARPi does not induce PD-L1 expression via cGAS/STING signalling activation.

Quantification of PD-L1 cell surface expression by flow cytometry in H1975- ERCC1$^{WT/WT}$ (**A**), A549-ERCC1$^{WT/WT}$ and A549-ERCC1$^{-/-}$ cells (**B**) upon PARPi and IFN-γ exposure, in the presence or absence of cGAS/STING silencing by siRNA. Cells were transfected with siCTRL, sicGAS, siSTING, siTBK1 or siIRF3 and treated for 48 h with DMSO, 3 µM talazoparib, and/or 500 U/mL IFN-γ. MFI ± SD normalized to IFN-γ, N = 2, two-way ANOVA and *post hoc* Tukey's test (**A**) or MFI normalized to IFN-γ, N = 1 (**B**).

4. PARP1 activity is linked to PD-L1 expression in cancer cells

As PARPi have a dual mechanism of action (i.e. inhibition of the PARylation catalytic activity of PARP1 and PARP1 trapping), we also sought to evaluate whether PARylation levels or PARP1 expression would correlate with PD-L1 expression in human tumour samples. To this aim, we performed immunostaining of PAR, PARP1 and PD-L1 in a series of 49 resected stage I/II NSCLC samples. PAR and PARP1 expression were assessed on tumour cells using a semi-quantitative H-score; PD-L1 level was scored on immune cells and tumour cells using a methodology validated in complementary and companion assays in NSCLC (381). Although no correlation was found between PARP1 and PD-L1 expression in tumour cells (**Figure V.9.A**), a significant inverse correlation was identified between PAR and PD-L1 levels on tumour cells (mean PARylation H-score of 100 in PD-L1-low vs 60 in PD-L1-high cases; $P = 0.003$; Mann-Whitney U test; **Figure V.9.B** and **Figure V.10.C**), consistent with a previous report in breast cancer specimens (445). No correlation was found between PAR/PARP1 levels and PD-L1 expression on immune cells (**Figure V.10**).

To further investigate this link between PARP1 activity and expression of PD-L1, we evaluated basal PD-L1 levels in the SUM149-PARP1 isogenic model. We observed a significantly enhanced expression of PD-L1 in the SUM149-PARP1$^{-/-}$ cell line at baseline compared to the parental line (**Figure V.11.A** and **Figure V.11.B**), while other immune-related cell surface markers such as the MHC class I components HLA-ABC did not appear significantly changed.

Together, these results support a link between PARP1 PARylation activity and PD-L1 expression in cancer cells. Cell surface PD-L1 expression is constitutively increased in cells harbouring low or defective PARP1 activity, a phenotype that is apparently distinct from the transient induction of PD-L1 observed following exposure to PARPi. What exact mechanisms underlie this phenotype and how it could be therapeutically exploited warrants further exploration.

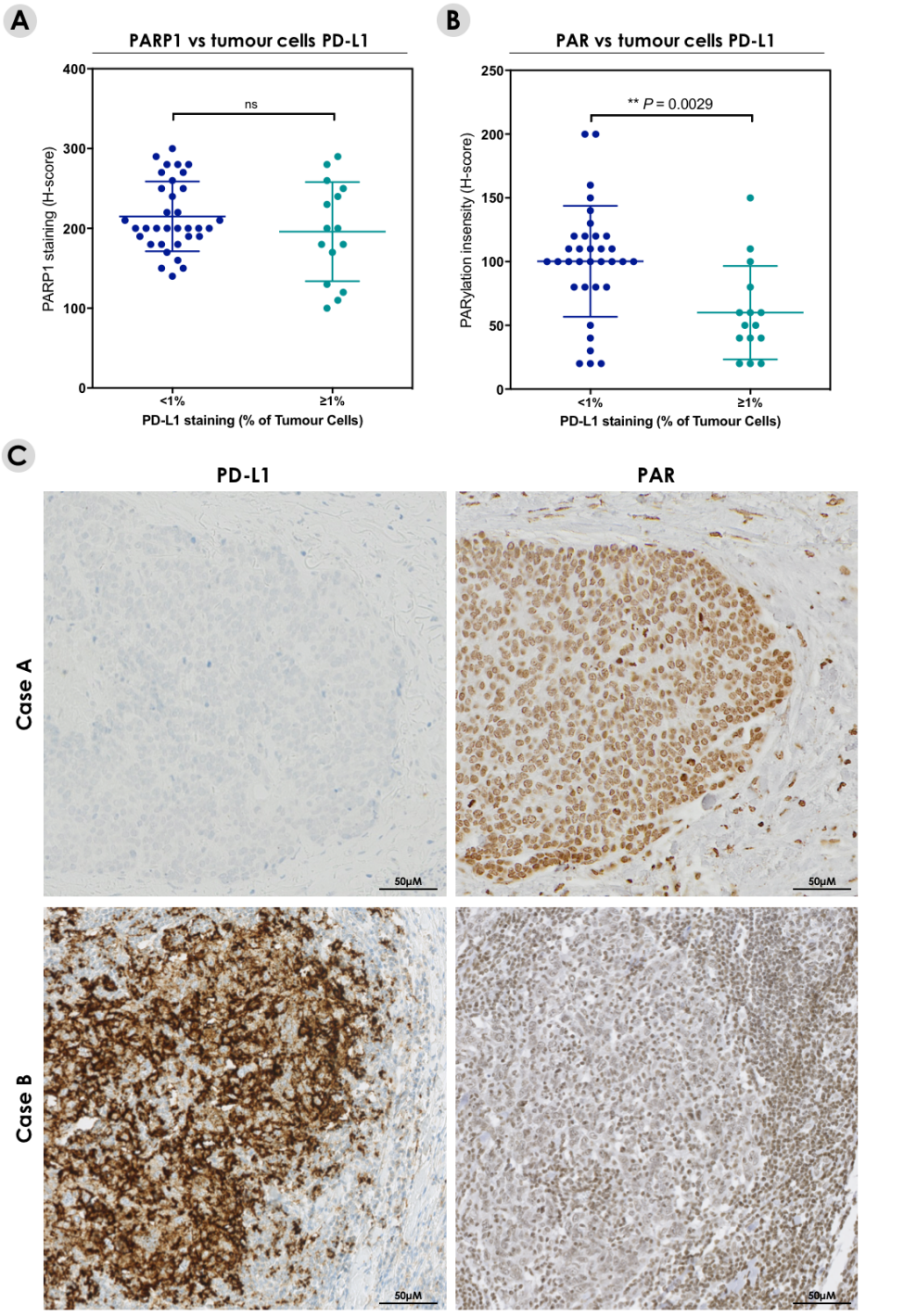

Figure V.9. Low PARylation levels correlate with high PD-L1 expression in human NSCLC tumours.

A and **B.** Scatter box plots depicting PARP1 (**A**) or PARylation (**B**) levels and tumour cell expression of PD-L1 (as assessed by IHC) in a series of resected stage I/II NSCLC (invasive adenocarcinomas and squamous cell carcinomas) samples (n = 49). Mann-Whitney U test. **C.** Representative images of PAR and PD-L1 IHC stainings in surgical specimens of NSCLC. Case A displays low PD-L1 staining in tumour cells and high PARylation levels; Case B displays high PD-L1 staining in tumour cells and low PARylation levels. Scale bar, 50 µm.

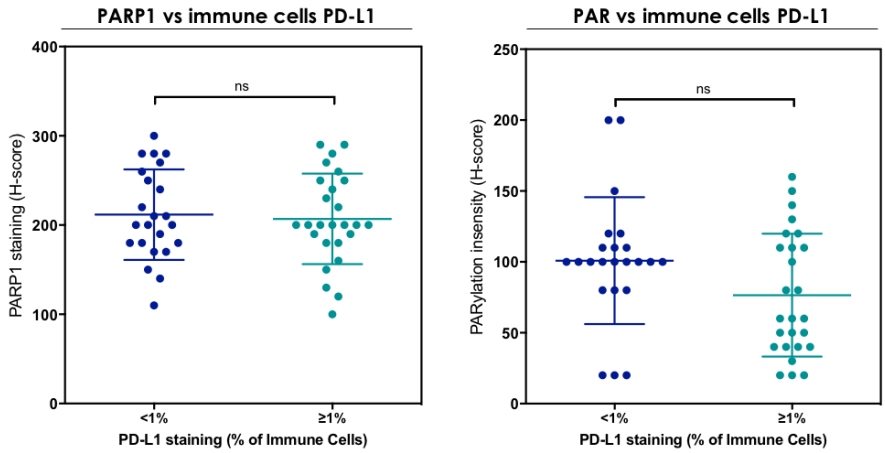

Figure V.10. PARP1 expression and PARylation levels in tumour cells do not correlate with PD-L1 expression in immune cells in human NSCLC tumours.
Scatter box plots depicting tumour PARP1 or PARylation levels and immune cells expression of PD-L1 (as assessed by IHC) in a series of resected stage I/II NSCLC (invasive adenocarcinomas and squamous cell carcinomas) samples (n = 49). Mann-Whitney U test.

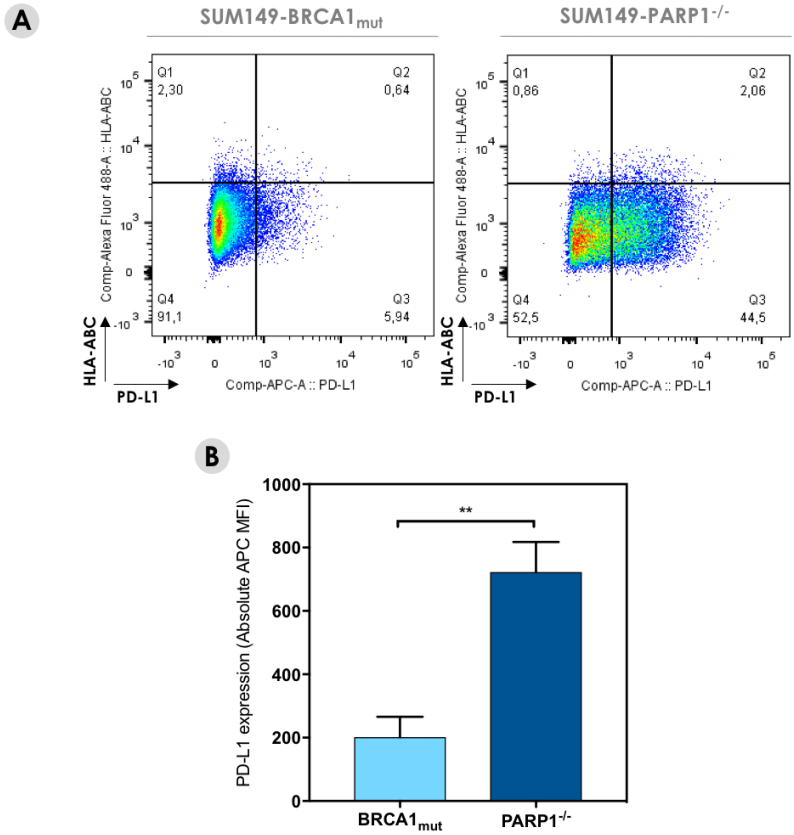

Figure V.11. PARP1-deficient SUM149 cells express higher baseline expression levels of PD-L1 compared to their PARP1-wildtype isogenic counterparts.
A. Representative flow cytometry dot plots showing basal PD-L1 and HLA-ABC expression in SUM149-BRCA1$_{mut}$ and SUM149-PARP1$^{-/-}$ cell lines. **B.** Quantification of PD-L1 cell surface expression by flow cytometry in SUM149-BRCA1$_{mut}$ and SUM149-PARP1$^{-/-}$ cell lines. MFI ± SD; N = 3, Welch's t test.

C. Discussion

In this Chapter, we describe another immunomodulatory effect of PARPi involving the induction of PD-L1 expression in cancer cells. Our data support that exposure to PARPi activates *PD-L1* transcription and results in the upregulation of PD-L1 levels at the cell surface. This phenotype is dose-dependent, potentiated by the addition of IFN-γ, and abrogated in the absence of PARP1, suggesting an on-target effect of PARPi. More importantly, ERCC1 deficiency appears to enhance this phenotype, which supports an involvement of the DDR in PARPi-mediated PD-L1 modulation.

Recent studies have investigated the link between PD-L1 expression and the DDR. In particular, recent evidence suggests that PD-L1 expression in cancer cells is regulated by the function of key DSB repair pathways effectors such as BRCA2, PALB2 and Ku70/80 (447). It was shown that PD-L1 is upregulated in response to exogenous DNA damage-induced DSBs, especially in the context of BRCA2 or Ku70/80 depletion, and that this induction is dependent on the activation of the checkpoint kinase 1 (CHK1). Indeed, CHK1 activation has been linked to the activation of JAK/STAT pathway effectors including STAT1 and STAT3, and importantly, of the downstream transcription factor IFR1 which was previously shown to regulate PD-L1 expression in response to IFN-γ (446). Mechanistically, in the presence of DSBs, the defect in BRCA2 is thought to sustain CHK1 activation by blocking HR repair at the step of RAD51 loading; similarly, lack of the Ku complex is thought to promote CHK1 activation by preventing NHEJ and favouring a repair switch towards HR. Lack of PALB2, a protein mediating the recruitment of BRCA2 to the chromatin, has also been shown to enhance PD-L1 expression in response to DSBs, but interestingly, the absence of other important DSB repair components such as BRCA1 did not trigger such phenotype, because of a failure to activate the CHK1 signal. Thus, the repair of DSBs *per se* is not a factor regulating PD-L1 expression in cancer cells, but the activation of CHK1 following DSB repair initiation is a critical step leading to the upregulation of PD-L1.

ERCC1-deficient cells have been shown to undergo major cell cycle disruption in response to PARPi (364). Indeed, if both ERCC1-deficient and -proficient cells exhibit a G2/M arrest in response to PARPi exposure, this arrest is much more profound and prolonged in ERCC1-

deficient cells. Thus, it is reasonable to assume that in these conditions, CHK1 is sustainably activated following PARP inhibition, and that this signalling promotes a substantial induction of PD-L1 expression in ERCC1-deficient cells. Whether such signalling is also activated – although to a lesser extent – in ERCC1-proficient cells in response to PARPi remains unknown, and further investigation would be needed to precisely define the activation threshold of CHK1 required for subsequent PD-L1 upregulation. Although it is unclear whether the transient upregulation of PD-L1 is a clinically relevant mechanism that could be exploited for the use of anti-PD-(L)1 agents, these elements provide a novel mechanistic insight into the DDR-associated upregulation of PD-L1.

IFN-γ is a very potent inducer of PD-L1 expression in cancer cells. The observation that PARPi synergize with IFN-γ to induce higher levels of PD-L1 suggests an interaction between the mechanisms leading to PD-L1 induction in response to these agents. To explore this interaction, we studied the activation of the JAK/STAT pathway in ERCC1-wildtype cells following PARPi exposure. We assessed the phosphorylation of STAT1 as a major pattern of activation of JAK/STAT signalling in A549-ERCC1$^{WT/WT}$ cells exposed to PARPi and/or IFN-γ. Western blot detection of pSTAT1 revealed that, although PARPi as monotherapy did not induce STAT1 phosphorylation, an enhanced STAT1 phosphorylation was generated following combination treatment of PARPi plus IFN-γ, compared to IFN-γ alone (**Figure V.12**). This suggested a potentiation of IFN-γ-mediated stimulation of the JAK/STAT pathway by PARPi. Interestingly, this effect was abrogated upon cell cycle blockade with the CDK1i RO-3306, suggesting that progression through the cell cycle is required for the potentiation of STAT signalling by PARPi. This supports the hypothesis that CHK1-independent mechanisms might also drive PD-L1 upregulation in response to PARPi in ERCC1-proficient cells.

Finally, some studies have highlighted the fact that, in response to DNA damage, the magnitude of PD-L1 upregulation between mRNA and protein levels was not always perfectly matched (447). Because post-translational modifications such as ubiquitination are known to control PD-L1 expression (448,449), and multiple ubiquitin ligases are activated through PARylation (450,451), it is possible that PD-L1 levels are sustained as a consequence of impaired ubiquitin ligases-mediated degradation of PD-L1 in response to

PARPi. Alternatively, as various ubiquitin ligases and deubiquitinating enzymes are also activated following DSBs (452), PD-L1 expression may be fine-tuned by these post-translational modifications depending on the cellular situation after DNA damage. Additional studies are required to dissect the complex post-translational regulation of PD-L1 expression after DNA damage.

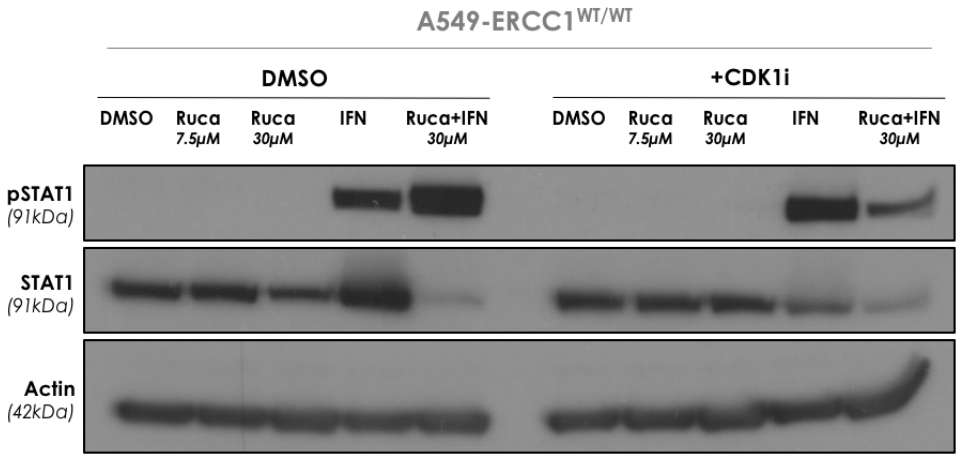

Figure V.12. PARPi potentiate IFN-γ-mediated phosphorylation of STAT1 in normally cycling ERCC1-proficient cells.

Western blot of pSTAT1 in A549-ERCC1$^{WT/WT}$ cells under rucaparib and IFN-γ exposure, in the context of cell cycle blockade. Cells were treated for 48h with DMSO, 7.5 μM rucaparib, 30 μM rucaparib, 500 U/mL IFN-γ or a combination of rucaparib and IFN-γ, in the presence or absence of the cell cycle blocker CDK1i RO-3306. Lysates were probed with the indicated antibodies.

Chapter VI. PARPi generate immunogenic cell death

A. Introduction

In the previous Chapters, we have described how PARPi modulate various aspects of cancer cell-autonomous immunity by mediating activation or stimulation of key immune-related signalling pathways in cancer cells, such as the cGAS/STING and JAK/STAT pathways. Of note, these effects are dependent on the presence of specific DDR defects in cancer cells, and in particular, loss of ERCC1 in NSCLC and mutations of *BRCA1* in TNBC have been found to enhance the immunological potential of PARPi. In these molecular contexts, the use of PARPi at clinically relevant doses is known to trigger cancer cell death through synthetic lethality (353,364). Whether the mechanisms leading to PARPi-mediated immunomodulation and PARPi-mediated cell death are independent, or rather proceed cooperatively to elicit an immunogenic form of cell death is currently unknown.

ICD has been defined as a functionally peculiar form of regulated cell death that is sufficient to activate an adaptive immune response specific for endogenous (cellular) or exogenous (viral) antigens expressed by dying cells (453). ICD can be initiated by a relatively restricted set of stimuli including viral infection, hypericin-based photodynamic therapy, and importantly, exposure to various DNA-damaging agents including some FDA-approved chemotherapeutics (e.g. anthracyclines) as well as specific forms of IR. As previously described in Chapter I, these agents have been shown to trigger the timely release of a series of DAMPs, which can be sensed as danger signals by innate and adaptive components of the immune system through PRR recognition, and that subsequently stimulate the activation of an immune response generally associated with the establishment of immunological memory (454). To date, six DAMPs have been mechanistically linked to the elicitation of ICD: (i) CALR exposure (280), (ii) ATP secretion (285), (iii) HMGB1 release

(294), (iv) type I IFN response induction (288), (v) release of cancer cell-derived nucleic acids (455), and (vi) ANXA1 excretion (295).

We previously showed that PARPi stimulate a cancer cell-autonomous type I IFN response through cytosolic DNA formation and cGAS/STING activation. Knowing that some conventional cytotoxic agents also trigger such phenotype (288,456), and have besides proven to be potent ICD inducers as they produce other critical DAMPs, we hypothesized that PARPi might similarly elicit ICD of cancer cells.

To test our hypothesis, we used an experimental approach that involved (i) the detection of surrogate markers of ICD *in vitro*, including eIF2α phosphorylation, CALR exposure, LC3 activation, ATP secretion and HMGB1 release, in DDR-proficient NSCLC cells exposed to various clinical PARPi, and (ii) the *in vivo* evaluation of PARPi potential to activate adaptive immunity in immunocompetent hosts via implementation of a vaccination assay in a syngeneic mouse model of ectopic colon carcinoma classically used for ICD assessment. This Chapter describes and further discusses the results of this investigation.

B. Results

1. *In vitro* detection of ICD: study design and experimental choices

Using the previously described NSCLC models A549 and H1975, we focused our analyses on the ERCC1$^{WT/WT}$ cell lines in order to assess the ICD-inducing potential of PARPi in conditions where synthetic lethality is not at stake. We selected four different clinical PARPi carrying distinct pharmacological properties in terms of PARP catalytic inhibition activity, PARP trapping potency and off-target effects (**Figure VI.1.A**): (i) rucaparib, which has a high PARP inhibition activity, low PARP trapping potency and multiple off-target effects; (ii) talazoparib, which is very potent in terms of PARP inhibition and PARP trapping, and has very few off-target effects; (iii) olaparib, which carries an intermediate PARP inhibition activity and PARP trapping potency and has no off-target effects; (iv) veliparib, which has a relatively low PARP inhibition activity, no PARP trapping potency, and few off-target effects.

A

PARPi	Ruca	Talazo	Ola	Veli
PARP catalytic inhibition	+++	+++	+	+
PARP trapping potency	+	+++	+	None
Off-target effects	+++	+	None	+

B

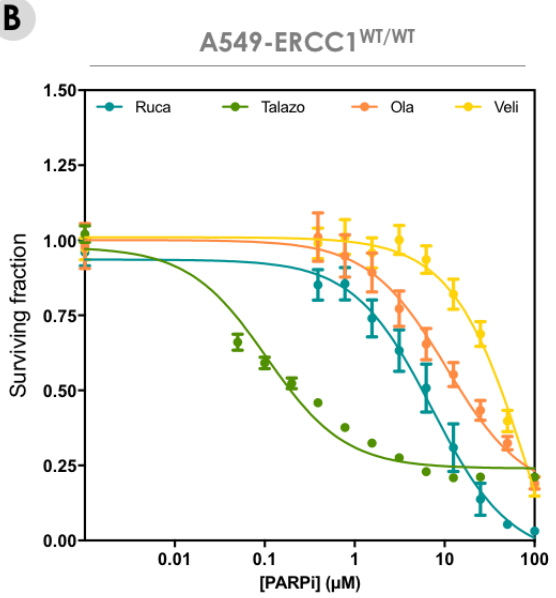

A549	Ruca	Talazo	Ola	Veli
SF50	7μM	0.6μM	15μM	42μM
SF20	21μM	6μM	100μM	92μM

C

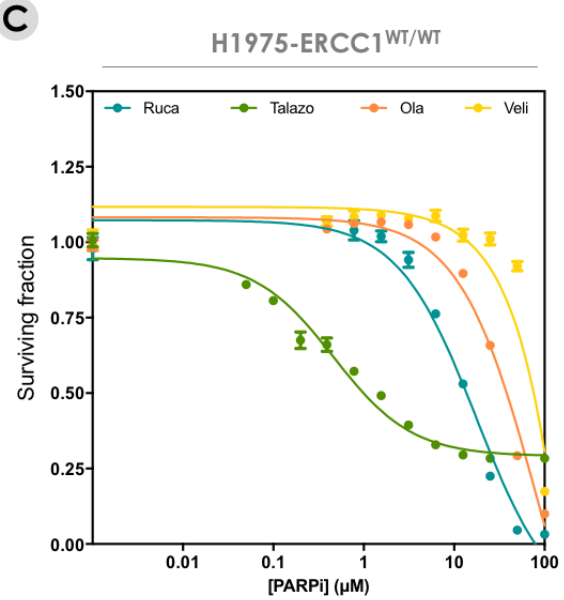

H1975	Ruca	Talazo	Ola	Veli
SF50	16μM	1μM	38μM	76μM
SF20	45μM	12μM	75μM	112μM

Figure VI.1. PARPi have distinct pharmacological properties and exert different cytotoxic effects in NSCLC cell lines.

A. Pharmacological properties of PARPi in terms of PARP catalytic inhibition activity, PARP trapping potency and extent of off-target effects. **B** and **C.** Assessment of PARPi cytotoxicity in A549-ERCC1$^{WT/WT}$ (**A**) and H1975-ERCC1$^{WT/WT}$ (**B**) cells. Cells were treated with a dose range of rucaparib, talazoparib, olaparib or veliparib and continuously exposed to the drug for 5 days (short-term survival assay). Shown are dose-response curves displaying the mean surviving fractions; Mean ± SD, N=4.

We initially performed short-term survival assays on A549-ERCC1$^{WT/WT}$ and H1975-ERCC1$^{WT/WT}$ cells individually exposed to rucaparib, talazoparib, olaparib or veliparib in order to evaluate the degree of sensitivity of these cell lines to the PARPi tested. Determination of the SF50 and SF20 values for each of these agents revealed substantial differences in sensitivity between the PARPi in both cell lines **(Figure VI.1.B** and **Figure VI.1.C**), consistent with previously published data (355,457).

We subsequently sought to develop a rationale experimental pipeline for the assessment of surrogate markers of ICD *in vitro* in response to PARPi. Based on the existing literature, and with the precious help of Dr. Isabelle Martins in Guido Kroemer's lab (INSERM U1138, Centre de Recherche des Cordeliers, Paris), we adapted standardized protocols originally used for the detection of ICD in cells exposed to chemotherapy (454), to the assessment of PARPi in our cell lines. We optimized treatment conditions, including doses and timing of exposure, for each PARPi in both A549 and H1975 cell lines, and finally established the following experimental procedure (**Figure VI.2**):

(1) ER stress is usually initiated after a short exposure to ICD inducers, thereby leading to an early expression of ER stress markers such as eIF2α phosphorylation and CALR exposure (458). In the case of PARPi, our optimizations revealed that the ideal timing for observing these DAMPs was 24 h to 48 h following exposure to the drugs. We thus decided to assess eIF2α phosphorylation via western blotting and CALR exposure via immunocytochemistry (ICC) or flow cytometry at these time points.

(2) Autophagy is required for and precedes ATP secretion, a phenotype frequently reported to appear from 48 h after exposure to ICD inducers (286), but not before. We thus evaluated ATP secretion after 48 h of exposure to PARPi and activation of the key autophagy marker LC3 via western blotting or ICC at 24 h.

(3) The passive release of HMGB1 is a belated marker of ICD, usually associated with late apoptosis or secondary necrosis (289,294). We monitored the onset of apoptosis through detection of phosphatidyl-serine (PS) exposure using flow cytometry with Annexin-V/7-aminoactinomycin D (7-AAD) staining after 48 h of exposure to PARPi, and assessed the release of HMGB1 through ELISA detection or ICC at 72 h.

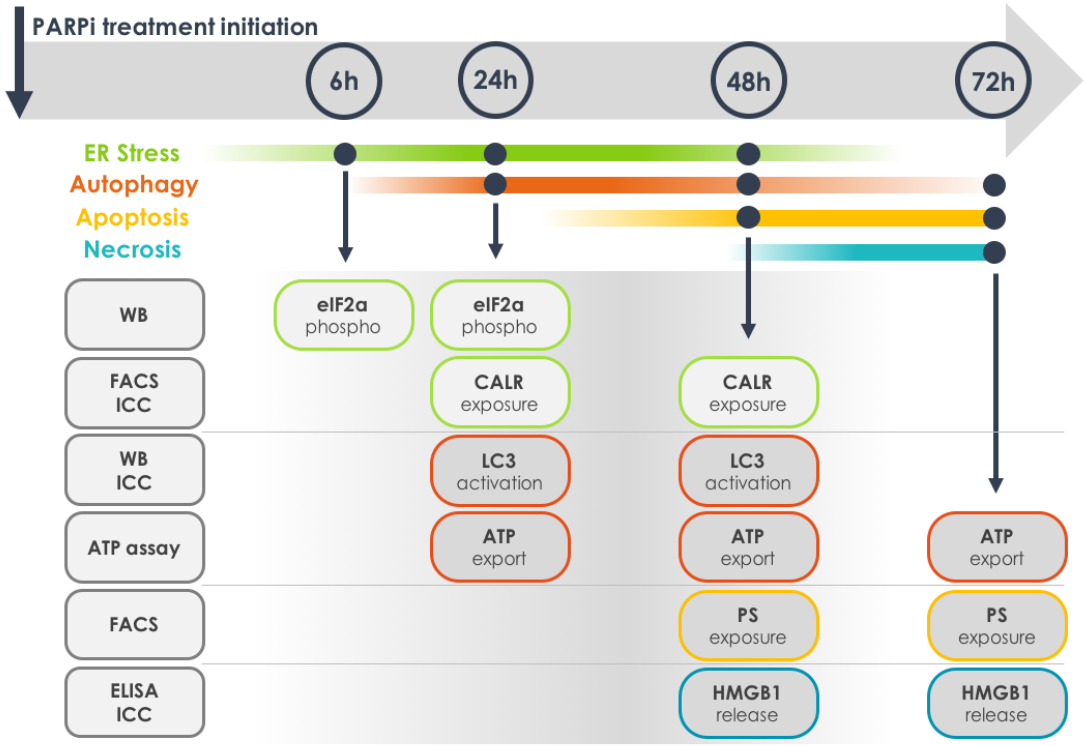

Figure VI.2. Diagram depicting the experimental pipeline developed for the evaluation of ICD in response to PARPi in NSCLC cell lines.
Cells undergoing ICD are sequentially exposed to diverse stresses including ER stress (green), autophagy (orange), apoptosis (yellow) and necrosis (blue). This pipeline allows the timely detection of successive ICD-related DAMPs as they are elicited by PARPi. DAMPs are indicated in the round-shaped boxes at the bottom of the diagram, with coloured borders corresponding to the cellular stress from which they individually arise. On the left-hand side of the diagram are grey rounded rectangles indicating the experimental techniques used for detection of the corresponding DAMPs. Abbreviations: ELISA, enzyme-linked immunosorbent assay; FACS, fluorescence-activated cell sorting (flow cytometry); ICC, immunocytochemistry; PS, phosphatidyl-serine; WB, western blot.

For each of these experiments, we exposed A549-ERCC1$^{WT/WT}$ and H1975-ERCC1$^{WT/WT}$ cells to SF50 and SF20 doses of PARPi – as determined after 5 days of exposure to the drugs in the previously presented short-term survival assays (**Figure VI.1.B** and **Figure VI.1.C**).

2. PARPi generate apoptosis of NSCLC cells

By definition, candidate drugs must be cytotoxic and provoke cell death to a certain extent to be considered as *bona fide* ICD inducers. Notably, activation of apoptosis has been

described as a hallmark of ICD which actively participates to the expression of key DAMPs including ATP secretion, which requires caspase-mediated cleavage of PANX1 channels (459,460), and HMGB1 release, which relies on the post-apoptotic (necrotic) disruption of cellular plasma membranes (286,294).

We thus first assessed the ability of PARPi to induce apoptotic cell death in NSCLC cells. Several assays are commercially available to monitor apoptosis-associated parameters, including early-stage loss of mitochondrial transmembrane potential, caspase activation, and end-stage externalization of PS. Here, we assessed PS exposure because this molecular event is a characteristic marker of caspase-dependent apoptosis (461). We used flow cytometry and phycoerythrin (PE)-conjugated Annexin-V staining for detection of PS exposure, and further monitored plasma membrane permeabilization using the fluorescent DNA stain 7-AAD – which only accumulates in cells with permeabilized plasma membranes.

Flow cytometry analysis of NSCLC cells exposed to PARPi for 48 h revealed a dose-dependent increase in PS externalization and plasma membrane permeabilization with all four PARPi in both A549-ERCC1$^{WT/WT}$ and H1975-ERCC1$^{WT/WT}$ cells (**Figure VI.3** and **Figure VI.4**), supporting an induction of apoptosis and secondary necrosis in these conditions. Interestingly, there were substantial differences between the PARPi tested – although relative concentrations were equivalent: while talazoparib, olaparib and veliparib only triggered a mild induction of cell death, rucaparib generated high levels of cell death in both cell lines (> 80% lethality in A549-ERCC1$^{WT/WT}$ and > 70% lethality in H1975-ERCC1$^{WT/WT}$ after 48 h of exposure to the SF20 dose). Of note, cell death in rucaparib-treated cells appeared to be predominantly associated with apoptosis, as a significant proportion of dying cells were apoptotic after 48 h of exposure to the SF20 dose (cells enduring PS externalization represented 74.3% and 53.4% of dying cells in A549-ERCC1$^{WT/WT}$ and H1975-ERCC1$^{WT/WT}$ populations respectively). These results suggested that the PARPi tested have different kinetics of apoptotic cell death induction, with rucaparib being the most potent inducer of apoptosis at early time points.

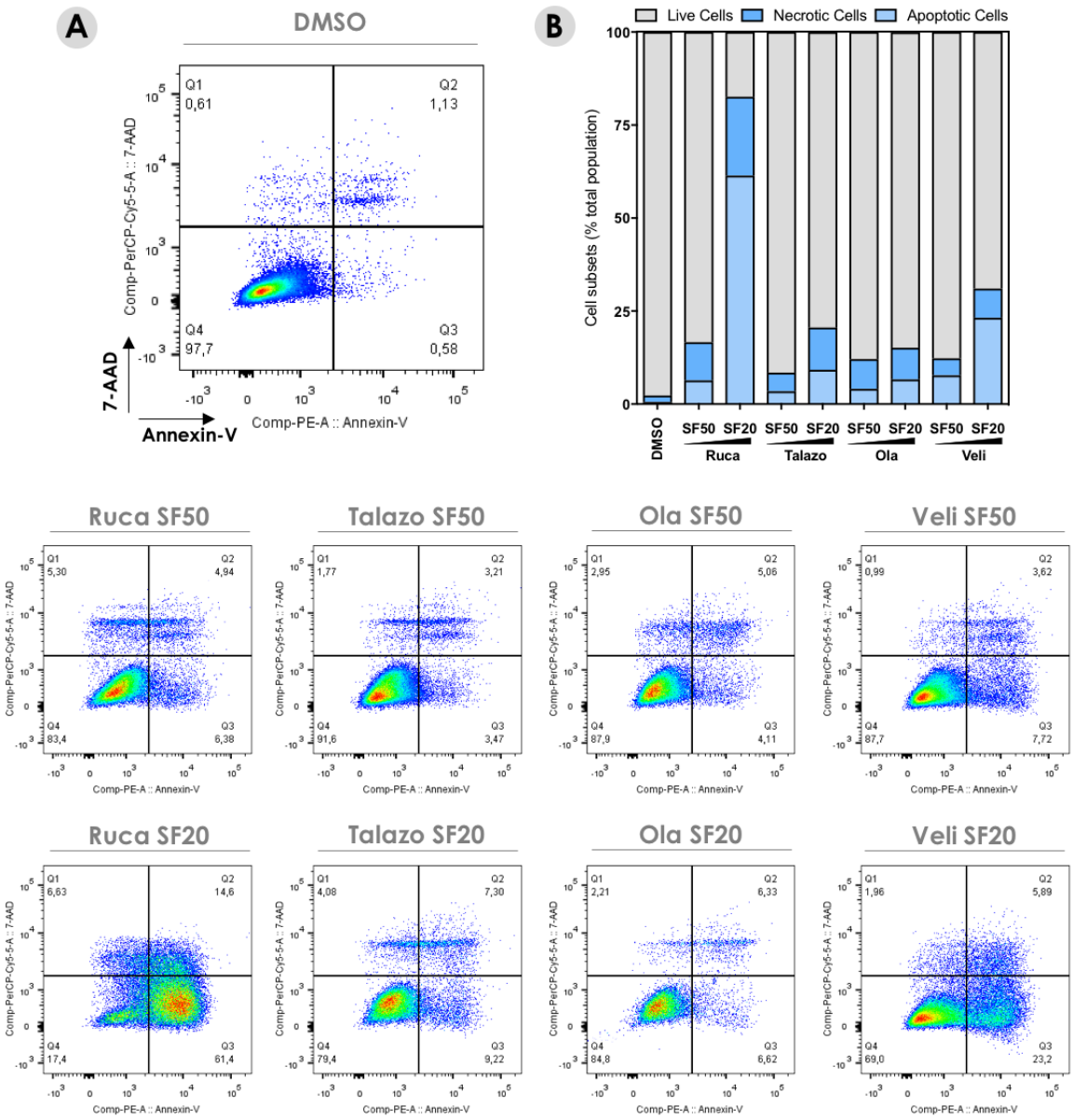

Figure VI.3. PARPi induce apoptosis and subsequent secondary necrosis in A549-ERCC1$^{WT/WT}$ cells.

A. Representative flow cytometry dot plots showing Annexin-V and 7-AAD staining intensities in A549-ERCC1$^{WT/WT}$ cells exposed to PARPi. Cells were treated for 48 h with DMSO or SF50/SF20 doses of rucaparib, talazoparib, olaparib or veliparib, and subsequently co-stained for flow cytometry detection of plasma membrane integrity (using 7-AAD) and phosphatidyl-serine exposure (using PE-conjugated Annexin-V). **B.** Quantification of the levels of apoptosis and necrosis in A549-ERCC1$^{WT/WT}$ cells exposed to PARPi. The percentages of live, apoptotic and necrotic cells were calculated from the dot plots displayed in **A**, with live cells corresponding to cells in gate Q4, apoptotic cells corresponding to cells in gate Q3, and necrotic cells corresponding to cells in gate Q1+Q2.

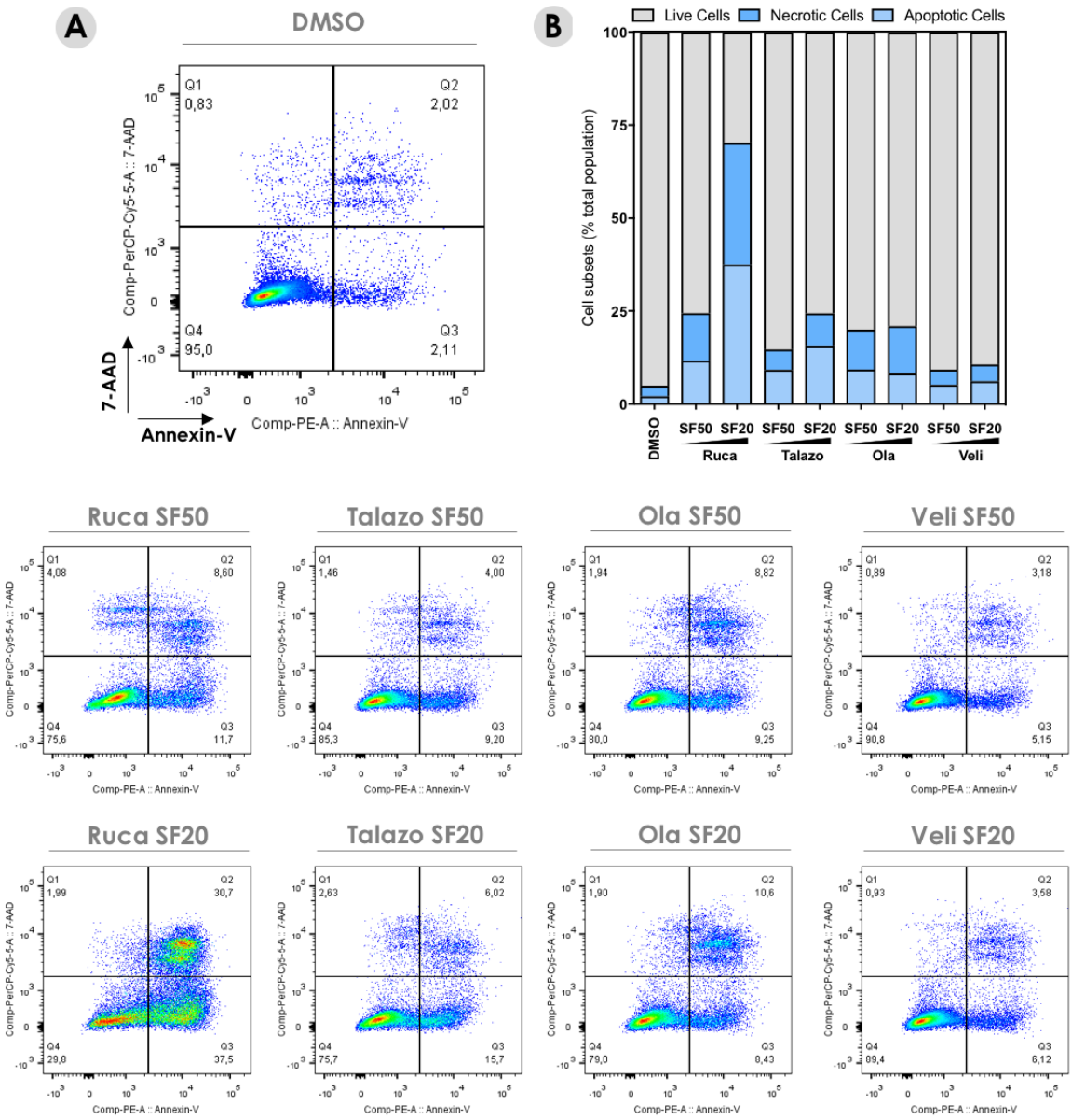

Figure VI.4. PARPi induce apoptosis and subsequent secondary necrosis in H1975-ERCC1$^{WT/WT}$ cells.

A. Representative flow cytometry dot plots showing Annexin-V and 7-AAD staining intensities in H1975-ERCC1$^{WT/WT}$ cells exposed to PARPi. Cells were treated for 48 h with DMSO or SF50/SF20 doses of rucaparib, talazoparib, olaparib or veliparib, and subsequently co-stained for flow cytometry detection of plasma membrane integrity (using 7-AAD) and phosphatidyl-serine exposure (using PE-conjugated Annexin-V). **B.** Quantification of the levels of apoptosis and necrosis in H1975-ERCC1$^{WT/WT}$ cells exposed to PARPi. The percentages of live, apoptotic and necrotic cells were calculated from the dot plots displayed in **A**, with live cells corresponding to cells in gate Q4, apoptotic cells corresponding to cells in gate Q3, and necrotic cells corresponding to cells in gate Q1+Q2.

3. PARPi induce ER stress in NSCLC cells

ER stress is a pivotal marker of ICD, which derives from the accumulation of unfolded proteins in the ER and is associated with an evolutionarily conserved mechanism of adaptation called the UPR, which aims to restore the ER-associated protein folding capacity by increasing ER volume and expression of ER chaperones, as well as transiently attenuating protein translation (462). The UPR signals through three ER stress sensors, namely, inositol-requiring enzyme 1 alpha (IRE1α), protein kinase R-like ER kinase (PERK), and activating transcription factor 6 (ATF6); however, although all three branches of the UPR are activated in response to ICD inducers, only PERK activation is known to be mandatory for ICD. Indeed, PERK is required for the inactivating phosphorylation of eIF2α and subsequent pre-apoptotic exposure of ER chaperones, such as CALR and ERp57, at the plasma membrane (458). Importantly, CALR/ERp57 exposure occurs independently and upstream of apoptosis or necrosis, as part of a specific danger-signalling system connected to ER stress (280). Thus, agents that trigger cell death but are intrinsically unable to promote ER stress usually fail to engage ICD. This is for example the case of cisplatin, which differs from its derivative oxaliplatin in its ability to trigger the UPR and the consequent translocation of CALR to the outer leaflet of the plasma membrane of dying cells (278). Remarkably, the exogenous co-provision of a UPR-inducer (e.g. thapsigargin or tunicamycin) was shown to efficiently restore the immunogenicity of cell death in response to cisplatin (463), demonstrating the critical role of ER stress in mediating ICD.

To assess the ability of PARPi to trigger ER stress, we evaluated eIF2α phosphorylation and CALR exposure in PARPi-treated NSCLC cells. eIF2α phosphorylation was measured via western blotting, and CALR exposure was detected using two complementary cell-based approaches involving the techniques of ICC and flow cytometry.

a. Rucaparib induces phosphorylation of the ER factor eIF2α

We exposed A549-ERCC1$^{WT/WT}$ and H1975-ERCC1$^{WT/WT}$ cells to SF50 and SF20 doses of rucaparib, talazoparib, olaparib or veliparib for 24 h, and subsequently measured eIF2α phosphorylation by WB. This analysis revealed a dose-dependent increase of peIF2α upon

rucaparib exposure (**Figure VI.5**); the effects of the three other PARPi on this protein were in comparison much more modest.

These results suggest that rucaparib induces ER stress in NSCLC cell lines, while talazoparib, olaparib and veliparib might not carry such properties. Therefore, we primarily assessed rucaparib, but also talazoparib (as the most specific PARPi) for their ability to trigger CALR exposure.

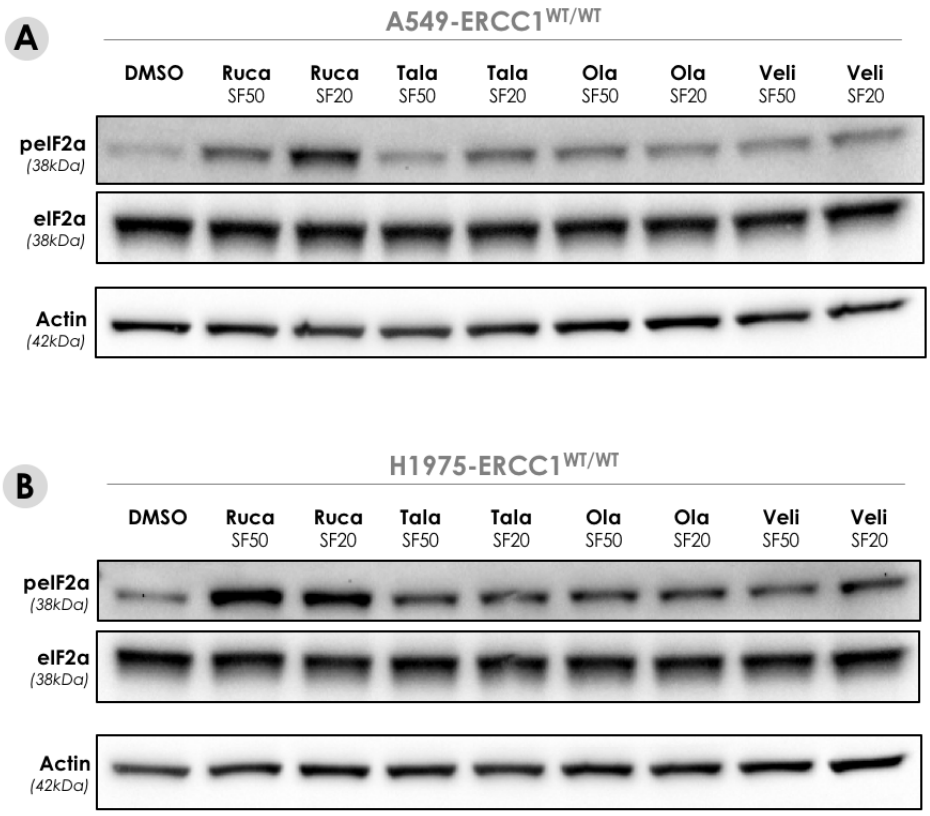

Figure VI.5. Rucaparib induces intense phosphorylation of eIF2α in A549-ERCC1$^{WT/WT}$ and H1975-ERCC1$^{WT/WT}$ cells.
Western blot of peIF2α and total eIF2α in A549-ERCC1$^{WT/WT}$ (**A**) and H1975-ERCC1$^{WT/WT}$ (**B**) cells upon PARPi exposure. Cells were exposed for 24h to DMSO (vehicle) or SF50/SF20 doses of rucaparib, talazoparib, olaparib or veliparib. Lysates were probed with the indicated antibodies.

b. Rucaparib and talazoparib trigger CALR exposure

Because CALR exposure is a transient and precarious phenomenon, its detection can be laborious and hampered by a lack of reproducibility due to the introduction of experimental biases. Most published studies have used flow cytometry to detect CALR translocation to the plasma membrane surface, as well as image-based techniques such as IF, or IHC in the case of detection on tumour tissue. In our study, we first sought to visualize this phenotype using ICC, by adapting a previously described IHC protocol developed on series of human NSCLC tumours (464).

We thus exposed A549-ERCC1$^{WT/WT}$ cells to SF20 doses of the PARPi rucaparib and talazoparib for 48 h, and used the known ICD inducer nocodazole (NCZ) as positive control for the experiment. We subsequently fixed cells and prepared paraffin-embedded cell suspensions using a commercially-available cytoblock preparation kit. We then generated cytoblock sections and performed ICC staining of CALR on these sections using the protocol described in Fucikova *et al*. These analyses revealed that, whereas control (DMSO-treated) cells exhibited a homogeneous cytoplasmic staining of CALR, rucaparib- and talazoparib-treated cells displayed a clear membrane reinforcement of the staining, characteristic of an exposure of CALR at the plasma membrane (**Figure VI.6.A**).

Interestingly, while CALR staining was clearly located at the membrane in rucaparib-treated cells, talazoparib-treated cells were rather characterized by an increase in cytoplasmic staining of regions in close vicinity to the plasma membrane, suggesting that the translocation of CALR in these cells was not fully completed at the time of fixation. Manual quantification of the percentage of cells displaying a membrane staining of CALR (herein referred to as ecto-CALR-positive cells) revealed a comparable increase in conditions treated with rucaparib, talazoparib and the positive control NCZ, supporting the relevance of these observations.

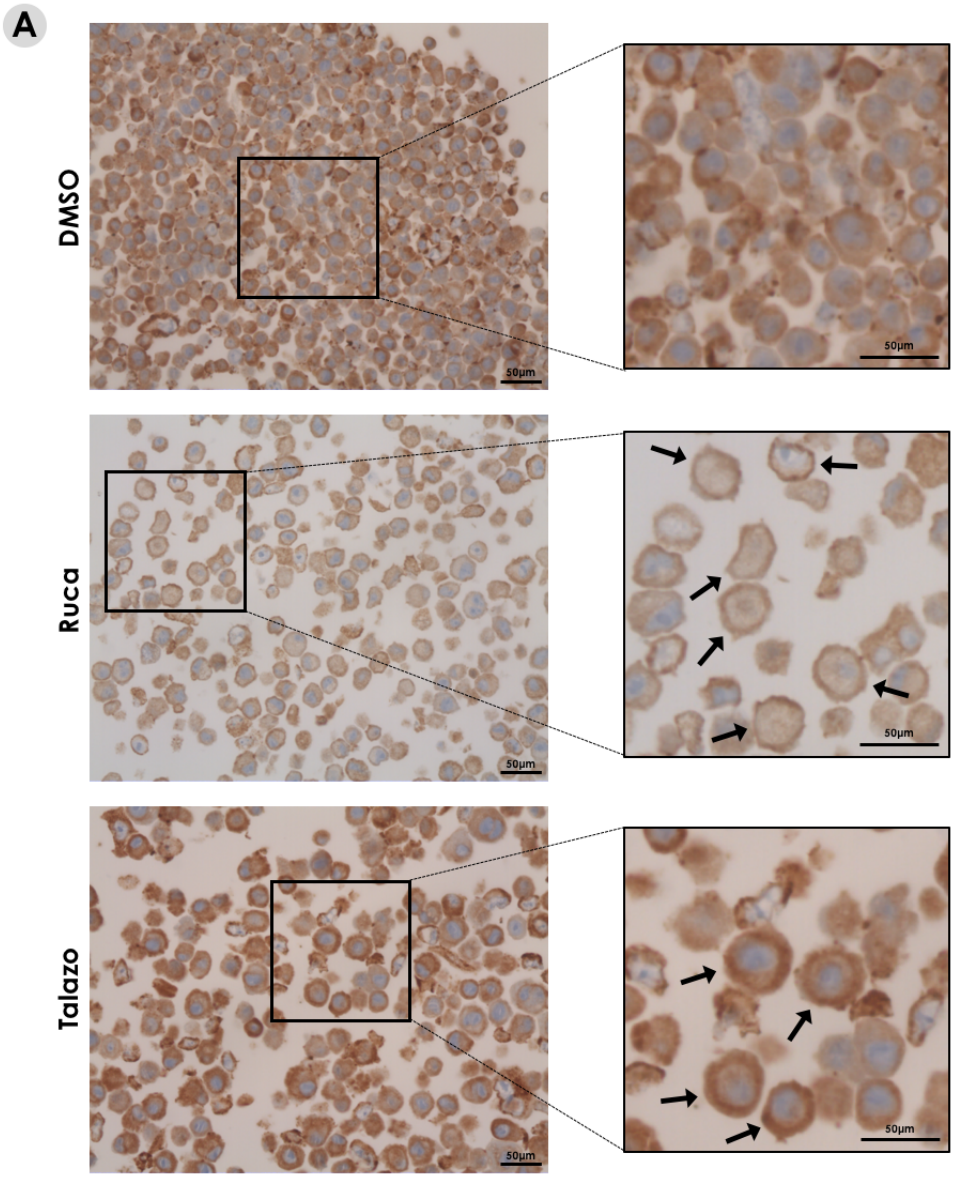
A
DMSO
Ruca
Talazo
50µm

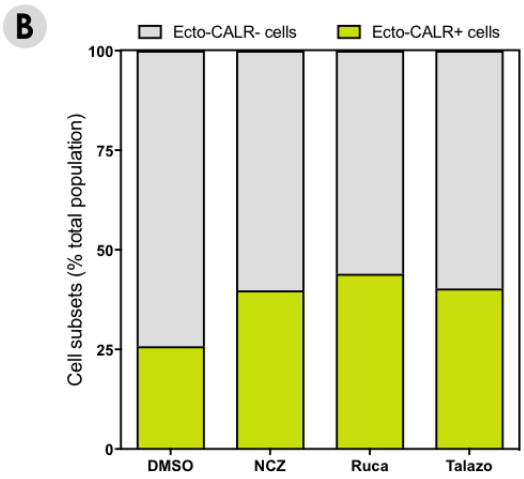
B
Ecto-CALR- cells
Ecto-CALR+ cells
Cell subsets (% total population)
100
75
50
25
0
DMSO
NCZ
Ruca
Talazo

Figure VI.6. PARPi rucaparib and talazoparib induce CALR exposure in A549-ERCC1$^{WT/WT}$ cells.
A. Representative images of CALR ICC staining in PARPi-treated A549-ERCC1$^{WT/WT}$ cells. Cells were treated with DMSO or SF20 doses of rucaparib and talazoparib for 48 h. Scale bar: 50µm. **B.** Manual quantification of the number of ecto-CALR-positive cells in A549-ERCC1$^{WT/WT}$ populations exposed to DMSO, SF20 doses of rucaparib and talazoparib or 200µM NCZ for 48 h. Shown are the percentages of ecto-CALR-positive and ecto-CALR-negative cells within the total population; N=1.

To further confirm these results, we sought to evaluate CALR exposure by flow cytometry in A549-ERCC1$^{WT/WT}$ cells exposed to PARPi, using an indirect staining with a CALR-directed primary antibody and an AF-488-conjugated secondary antibody. For this experiment, we selected talazoparib which displays minimal autofluorescent properties compared to rucaparib.

Treatment of A549-ERCC1$^{WT/WT}$ cells with SF50 and SF20 doses of talazoparib led to a significantly enhanced (but not dose-dependent) exposure of CALR at the cell surface, as assessed by the increased proportion of ecto-CALR-positive cells measured in talazoparib-treated cells (**Figure VI.7.A** and **Figure VI.7.B**), and the augmentation of AF-488 MFI in these conditions (**Figure VI.7.C**). Of note, talazoparib appeared to induce higher levels of CALR exposure than the positive control NCZ, thus giving an order of magnitude of the extent of this induction.

Together, these data suggest that the PARPi rucaparib and talazoparib trigger ER stress to a sufficient threshold level to allow CALR translocation and exposure to NSCLC cells plasma membrane. This is consistent with the induction of eIF2α phosphorylation observed in rucaparib-treated cells, and to a lesser extent in talazoparib-treated cells.

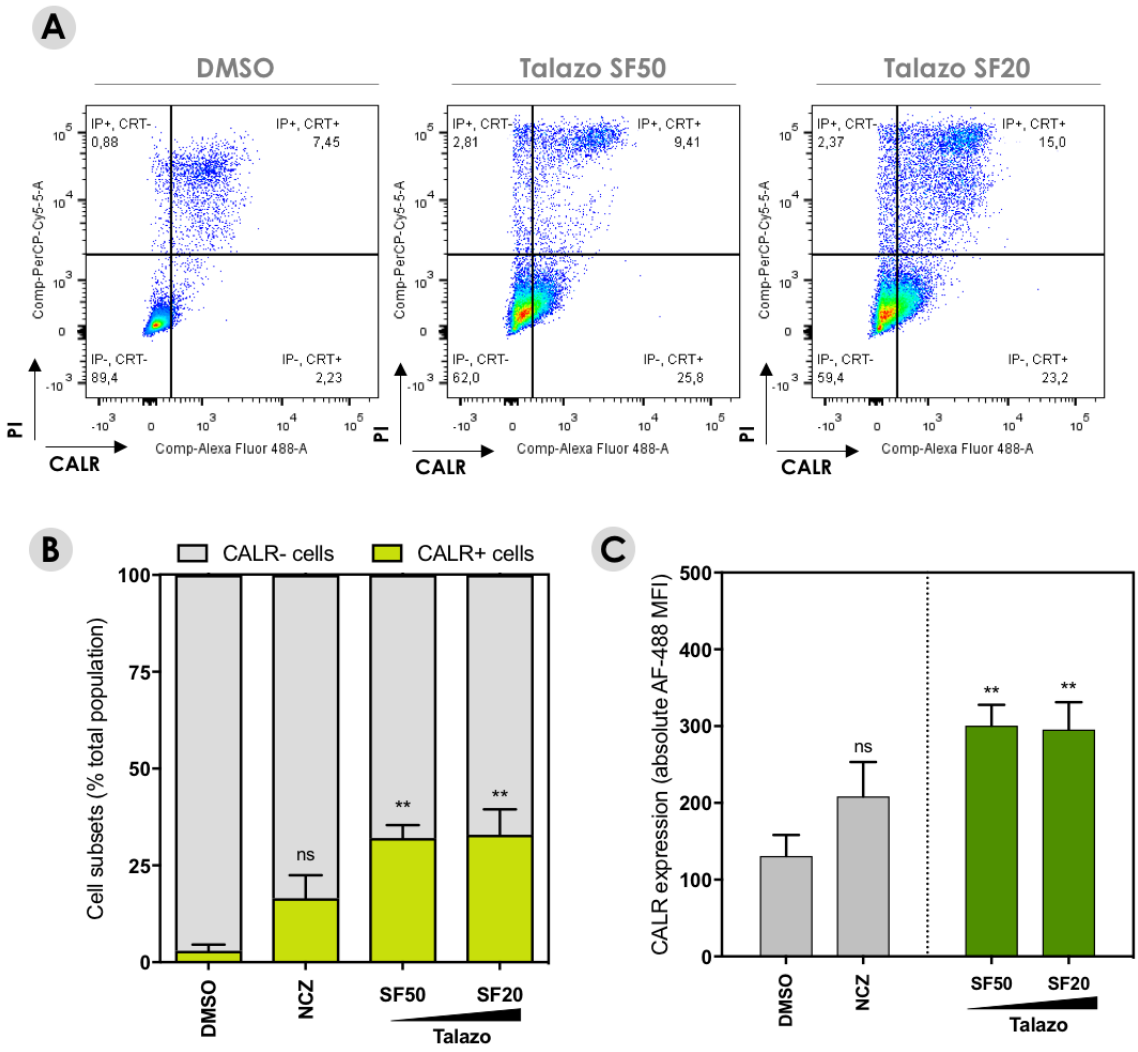

Figure VI.7. A549-ERCC1$^{WT/WT}$ cells undergo CALR exposure in response to treatment with talazoparib.

A. Representative flow cytometry dot plots showing AF-488-CALR and PI staining intensities in A549-ERCC1$^{WT/WT}$ cells exposed to talazoparib. Cells were treated for 48 h with DMSO or SF50/SF20 doses of talazoparib. **B.** Quantification of the number of ecto-CALR-positive cells in A549-ERCC1$^{WT/WT}$ populations exposed to DMSO, SF50/SF20 doses of talazoparib or 200μM NCZ for 48h. Ecto-CALR-positive cells correspond to PI-negative/CALR-positive cells. N = 3, Kruskal-Wallis test and *post hoc* Dunn's test, relative to DMSO control. **C.** Quantification of CALR cell surface expression by flow cytometry in A549-ERCC1$^{WT/WT}$ cells treated for 48h with DMSO, SF50/SF20 doses of talazoparib or 200μM NCZ. MFI ± SD; N = 3, Kruskal-Wallis test and *post hoc* Dunn's test, relative to DMSO control.

4. PARPi stimulate autophagy and promote ATP secretion in NSCLC cells

The molecular processes whereby ICD inducers stimulate the active secretion of ATP by dying cells have been thoroughly studied, and an unexpected complexity has been revealed in the mechanisms underpinning this phenomenon. If initial studies have evidenced the critical role of autophagy in promoting ATP secretion (285,465), the involvement of apoptosis has later been demonstrated, with the description of a role for caspase 3 in mediating constitutive activation of ATP channels through PANX1 cleavage (466). Therefore, although induction of autophagy alone may result in the secretion of ATP (467), this phenotype is significantly enhanced when apoptosis occurs simultaneously (285,468). Conversely, while the caspase-induced formation of truncated PANX1 channels increases the permeability of plasma membranes in both wildtype and autophagy-deficient cells, ATP can only be efficiently released by the former, supporting that the sole presence of open PANX1 channels is not sufficient for the effective secretion of ATP (286).

In line with this model, a substantial fraction of intracellular ATP is present in cytoplasmic vesicles rather than in the cytosol, explaining why it cannot diffuse freely through open PANX1 channels. ATP-containing vesicles comprise lysosomal markers such as lysosomal-associated membrane protein 1 (LAMP1), and in response to ICD inducers, a majority of these vesicles re-localize to LC3-positive autophagosomes and autolysosomes (286). Subsequently, LAMP1 exposure at the cell surface occurs concurrently with PS externalization, suggesting that lysosomes fuse with the plasma membrane during apoptosis, thereby strongly contributing to ICD-associated ATP secretion (469). Interestingly, while pharmacological inhibition of caspases and knockdown of PANX1 prevent LAMP1 from translocating to the plasma membrane, the depletion of essential autophagic factors such as ATG5, ATG7 or BCN1 fails to affect LAMP1 translocation, meaning that apoptosis but not autophagy is required for lysosomal exocytosis (286). Thus, in response to ICD inducers, autophagy appears to facilitate the formation of ATP-containing vesicles in the cytosol, yet being dispensable for their exocytosis.

Beyond apoptosis-mediated membrane permeabilization and lysosomal exocytosis, apoptotic blebbing of the plasma membrane has also been shown to critically mediate ICD-

associated ATP secretion (286). This ultimate process may constitute the very last step of the molecular cascade mediating ATP release in response to ICD inducers, operating downstream of PANX1 channel opening, autophagy and LAMP1 translocation.

ATP secretion is thus orchestrated by a complex interplay between multiple molecules that are essential for apparently distinct cellular processes including autophagy, lysosomal exocytosis, apoptosis, membrane blebbing and plasma membrane permeabilization. These processes are activated in tumour cells undergoing ICD in response to a large panel of cytotoxic agents (470). Here, we evaluated the potential of PARPi to activate autophagy and promote ATP secretion in NSCLC cells.

a. ATP is secreted in response to rucaparib exposure

In order to assess ATP secretion in response to PARPi, we evaluated intracellular and extracellular ATP levels using a luminescent-based titration technique. We exposed A549-ERCC1$^{WT/WT}$ and H1975-ERCC1$^{WT/WT}$ cells to increasing doses of the PARPi rucaparib, talazoparib, olaparib or veliparib for 48 h, and used the known ICD inducer mitoxantrone (MTX) as positive control for the experiment. We then performed titrations on ATP extracts (for intracellular ATP) or culture supernatants (for extracellular ATP) from these cells, using commercially-available kits. In both A549-ERCC1$^{WT/WT}$ and H1975-ERCC1$^{WT/WT}$ cell lines, we found that intracellular ATP levels were depleted in a dose-dependent manner following exposure to all four PARPi (**Figure VI.8.A** and **Figure VI.9.A**). The extent of this depletion appeared to be similar to that obtained in MTX-treated cells when cells were exposed to the highest dose (SF20) of PARPi (≈ 5-fold decrease in A549-ERCC1$^{WT/WT}$ cells and ≈ 2.5-fold decrease in H1975-ERCC1$^{WT/WT}$ cells). While all PARPi induced a decrease in intracellular ATP levels, only rucaparib was found to cause an increase in extracellular ATP levels in both A549-ERCC1$^{WT/WT}$ and H1975-ERCC1$^{WT/WT}$ cells (**Figure VI.8.B** and **Figure VI.9.B**; > 4-fold increase in A549-ERCC1$^{WT/WT}$ and > 6-fold increase in H1975-ERCC1$^{WT/WT}$ cells exposed to rucaparib at the SF20 dose). These results suggested differences between rucaparib and the other PARPi with regard to ATP secretion in NSCLC cells.

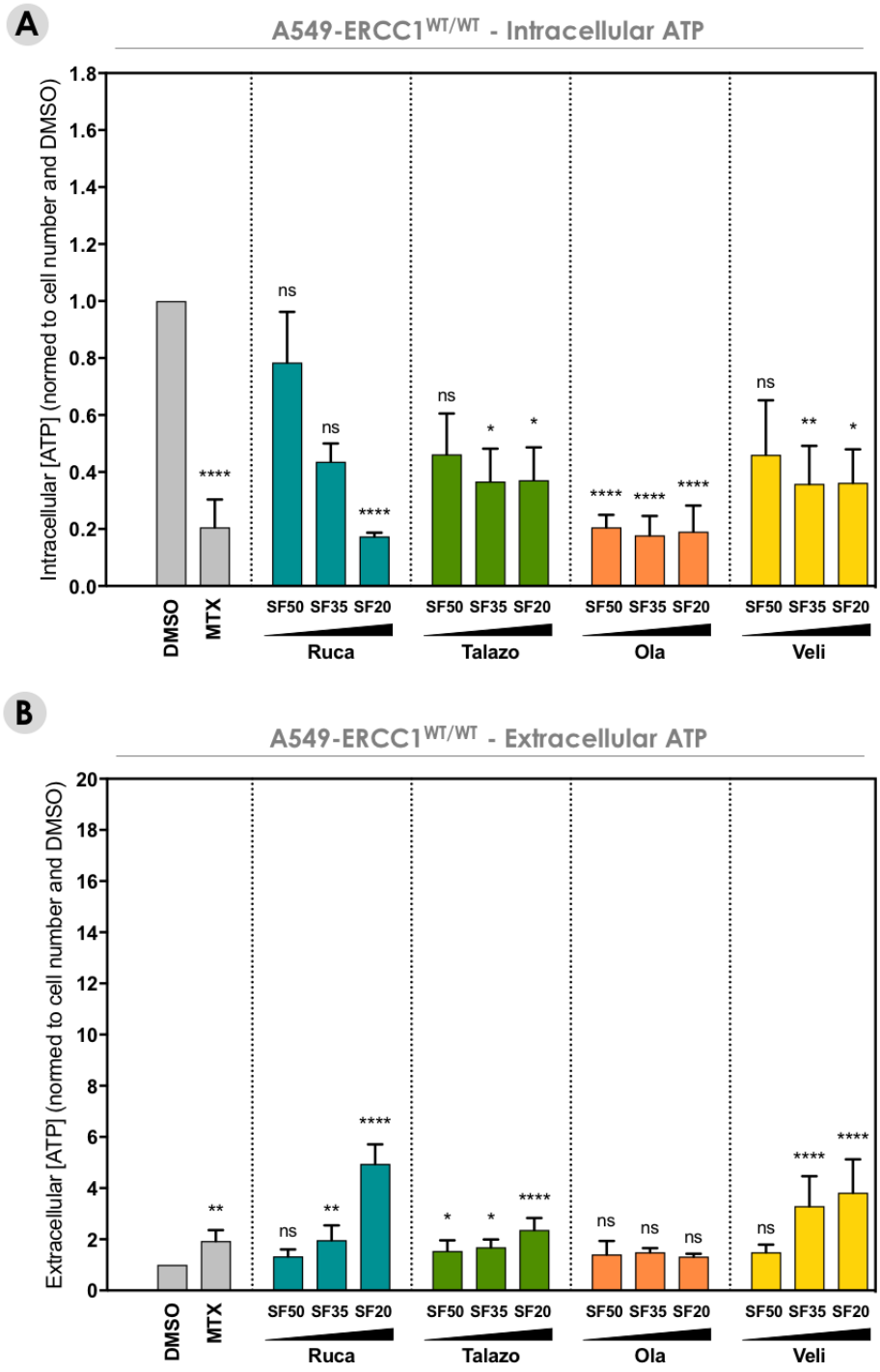

Figure VI.8. Rucaparib triggers ATP secretion in A549-ERCC1$^{WT/WT}$ cells.

Quantitative analysis of intracellular (**A**) and extracellular (**B**) ATP concentrations in A549-ERCC1$^{WT/WT}$ cells. Cells were exposed to DMSO, 2µM MTX, or SF50/SF35/SF20 doses of rucaparib, talazoparib, olaparib and veliparib for 48h. ATP was titrated in cellular ATP extracts (**A**) and culture supernatants (**B**). Shown are ATP concentrations normalized to cell number and DMSO. Mean ± SD, N=3, Kruskal-Wallis test and *post hoc* Dunn's test, relative to DMSO control.

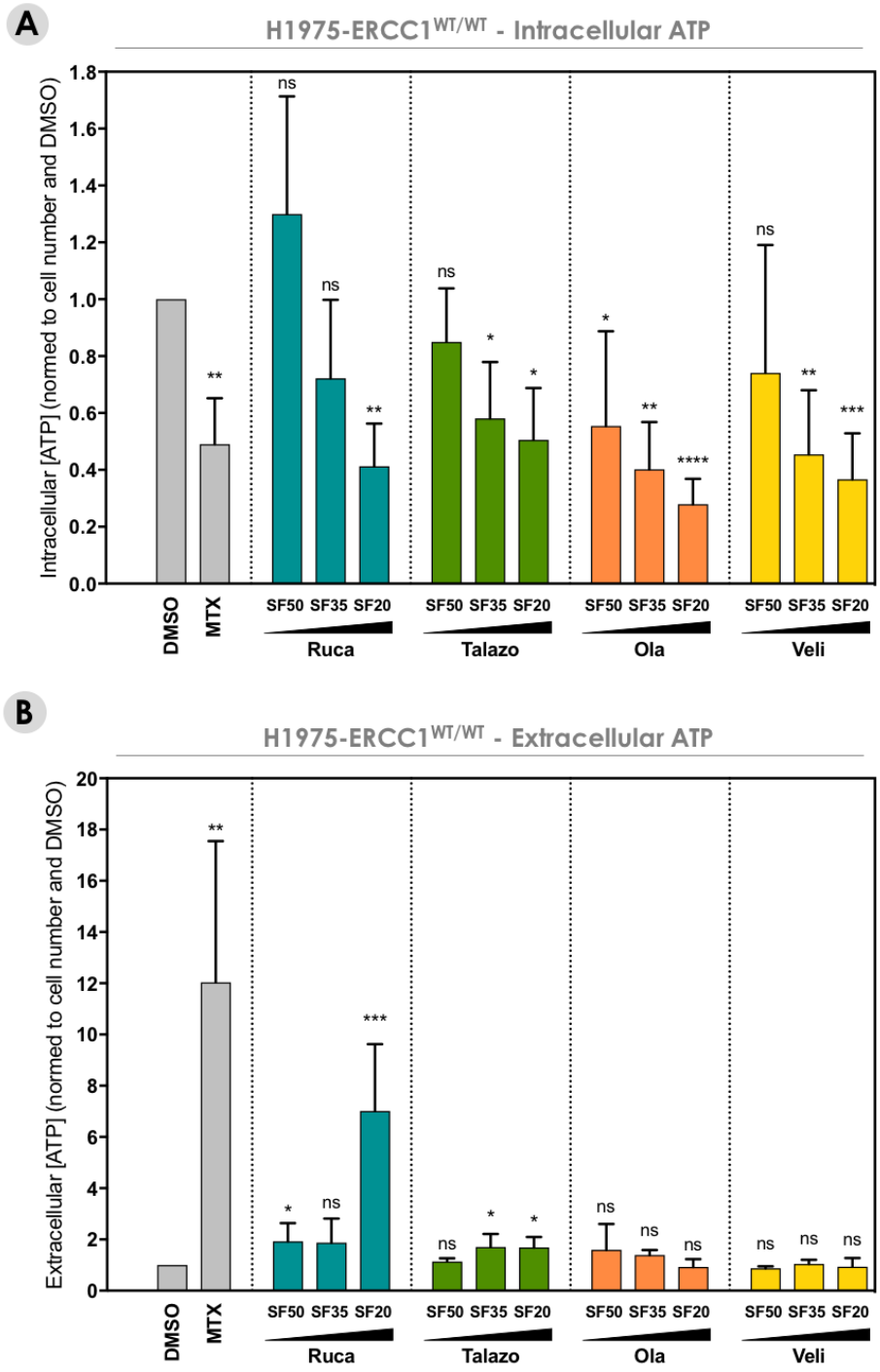

Figure VI.9. Rucaparib triggers ATP secretion in H1975-ERCC1$^{WT/WT}$ cells.

Quantitative analysis of intracellular (**A**) and extracellular (**B**) ATP concentrations in H1975-ERCC1$^{WT/WT}$ cells. Cells were exposed to DMSO, 2µM MTX, or SF50/SF35/SF20 doses of rucaparib, talazoparib, olaparib and veliparib for 48h. ATP was titrated in cellular ATP extracts (**A**) and culture supernatants (**B**). Shown are ATP concentrations normalized to cell number and DMSO. Mean ± SD, N=3, Kruskal-Wallis test and *post hoc* Dunn's test, relative to DMSO control.

b. Rucaparib and talazoparib trigger LC3 activation

To further investigate the molecular mechanisms involved in ATP secretion after exposure to PARPi, we decided to evaluate whether rucaparib or talazoparib would activate autophagy in NSCLC cells. To do this, we first performed ICC staining of LC3 in A549-ERCC1$^{WT/WT}$ cells treated for 48 h with SF20 doses of these PARPi or the positive control NCZ, following a previously described protocol used in series of FFPE human surgical specimens (471). This analysis revealed that, in contrast with DMSO-treated cells which displayed a diffuse cytoplasmic distribution of LC3, rucaparib- and talazoparib-treated cells exhibited foci-like structures in their cytoplasm (**Figure VI.10.A**), indicative of a redistribution of LC3 to autophagosomal membranes. This phenotype is characteristic of an activation of autophagy, in which the previously non-activated form of LC3 (LC3-I), evenly distributed throughout the cytoplasm, conjugates with lipid phosphatidylethanolamine and is subsequently recruited via its lipid moiety to autophagosome membranes, hence forming LC3-decorated autophagic puncta. This activated form of LC3 is referred to as LC3-II. Manual quantification of the number of LC3-II-positive cells (i.e. cells displaying more than 5 cytoplasmic LC3 puncta) showed an increase after treatment with rucaparib, talazoparib and NCZ (**Figure VI.10.B**). Strikingly, 97.6% of cells were LC3-II-positive in the rucaparib-treated condition, suggesting a massive activation of autophagy in response to this PARPi. Consistently, we found a significant increase in the number of LC3 puncta per cells in rucaparib-treated cells compared to DMSO-treated cells (**Figure VI.10.C**, mean puncta/cell = 31 in rucaparib-treated cells vs 6 in DMSO-treated cells, $P < 0.0001$), and to a lesser extent in talazoparib-treated cells (mean puncta/cell = 18 in talazoparib-treated cells vs 6 in DMSO-treated cells, $P = 0.0039$).

To further confirm this activation of autophagy after exposure to PARPi, we performed western blotting of LC3-I and LC3-II on proteins extracts from A549-ERCC1$^{WT/WT}$ and H1975-ERCC1$^{WT/WT}$ cells exposed for 48 h with SF50 and SF20 doses of rucaparib, talazoparib, olaparib and veliparib. Consistent with our previous observations, we detected an intense and dose-dependent increase of the levels of LC3-II in cells exposed to rucaparib, but not in cells exposed to the other PARPi (**Figure VI.11.A** and **Figure VI.11.B**).

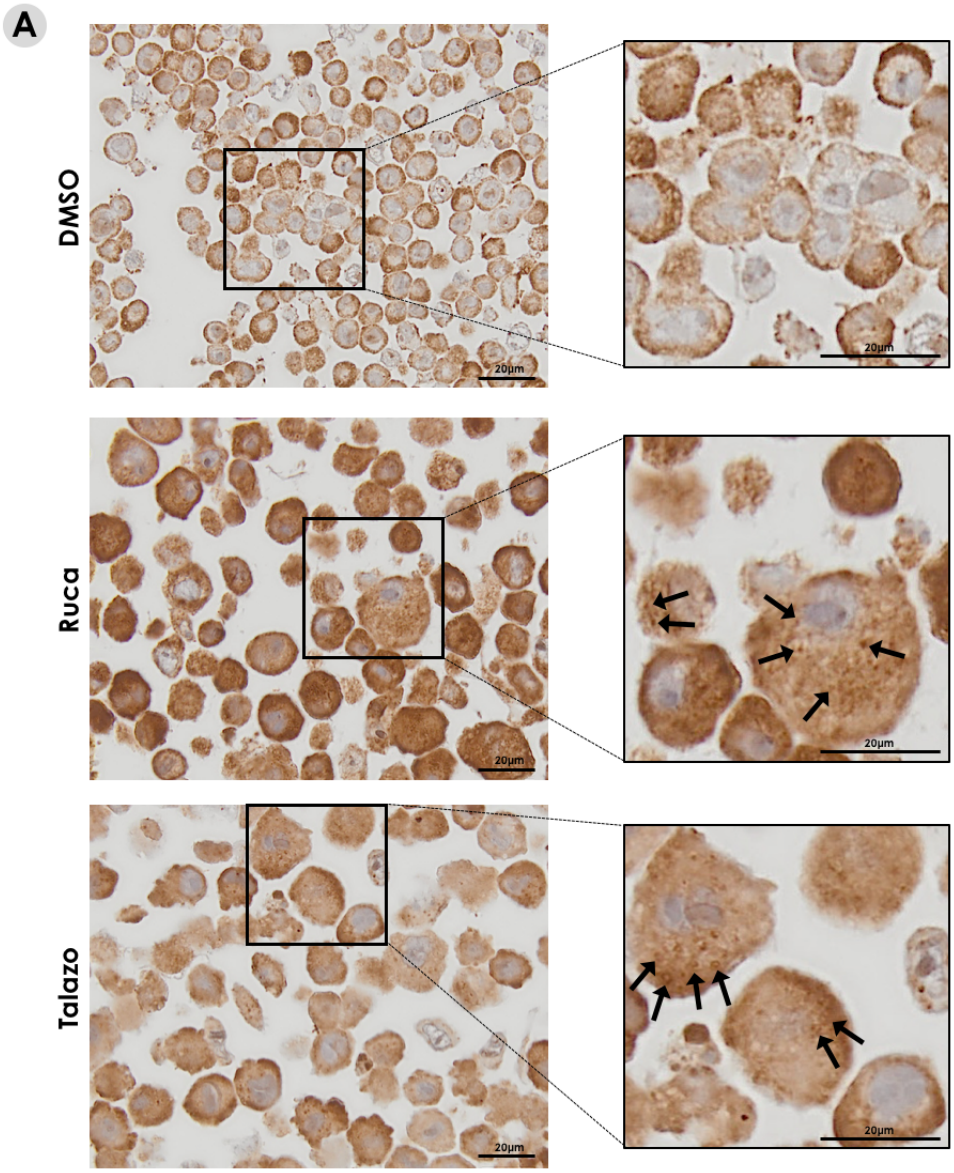
A
DMSO
Ruca
Talazo
20µm

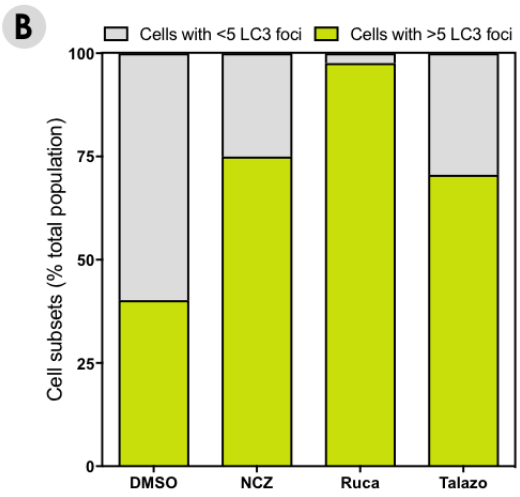
B
Cells with <5 LC3 foci
Cells with >5 LC3 foci
Cell subsets (% total population)
100
75
50
25
0
DMSO
NCZ
Ruca
Talazo

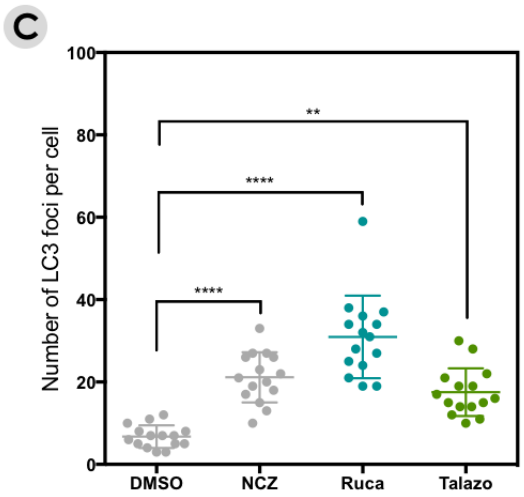
C
Number of LC3 foci per cell
100
80
60
40
20
0
**
****
****
DMSO
NCZ
Ruca
Talazo

Figure VI.10. Rucaparib and talazoparib promote the formation of LC3-decorated autophagic puncta in A549-ERCC1$^{WT/WT}$ cells.
A. Representative images of LC3 ICC staining in PARPi-treated A549-ERCC1$^{WT/WT}$ cells. Cells were treated with DMSO or SF20 doses of rucaparib and talazoparib for 48 h. Scale bar: 20µm. **B.** Manual quantification of the number of LC3-II-positive cells in A549-ERCC1$^{WT/WT}$ populations exposed to DMSO, SF20 doses of rucaparib and talazoparib or 200µM NCZ for 48 h. Shown are the percentages of LC3-II-positive and LC3-II-negative cells within the total population; N=1. **C.** Manual quantification of the number of LC3 puncta per cell in A549-ERCC1$^{WT/WT}$ populations exposed to DMSO, SF20 doses of rucaparib and talazoparib or 200µM NCZ for 48 h. Shown is the total number of LC3 puncta per cell in a restricted population of 15 cells; N=1. Kruskal-Wallis test and *post hoc* Dunn's test, relative to DMSO control.

Together, our results suggest that rucaparib efficiently triggers autophagy and ATP secretion in NSCLC cells. This is in contrast with the three other PARPi tested, which, in the same conditions, are unable to stimulate ATP secretion in NSCLC cells, despite a possible potential to activate autophagy.

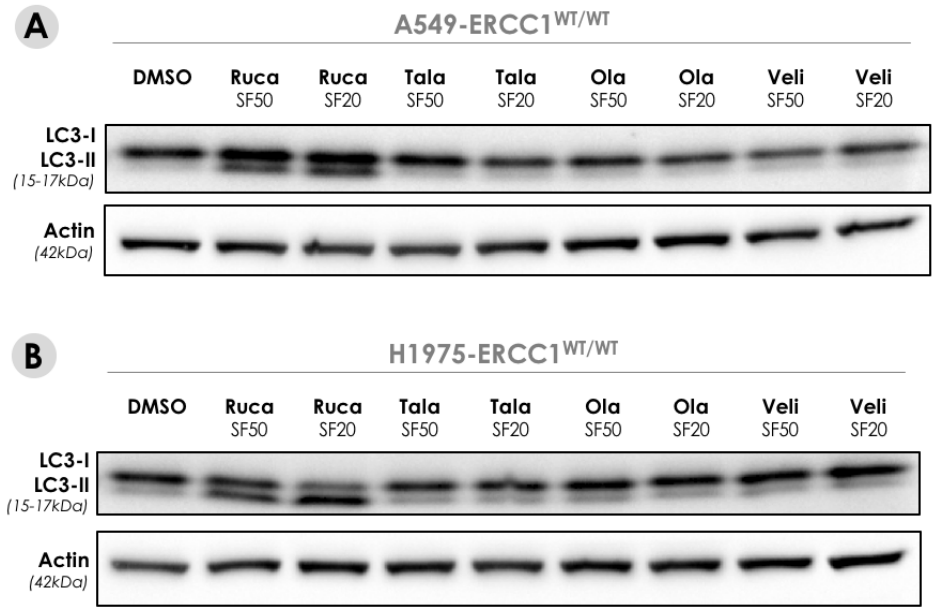

Figure VI.11. Rucaparib triggers LC3 activation in NSCLC cells.
Western blot of LC3 in A549-ERCC1$^{WT/WT}$ (**A**) and H1975-ERCC1$^{WT/WT}$ (**B**) cells upon PARPi exposure. Cells were exposed for 48h to DMSO (vehicle) or SF50/SF20 doses of rucaparib, talazoparib, olaparib or veliparib. Lysates were probed with the indicated antibodies.

5. PARPi generate HMGB1 release in NSCLC cells

HMGB1 is a nuclear factor involved in epigenetic processes such as chromatin remodelling. It is also a highly mobile protein, sometimes termed "alarmin", that can be actively secreted from inflammatory cells (472) or passively released as a soluble molecule from necrotic cells (289) to signal tissue injury and initiate inflammatory responses through binding to RAGE, and the PRR TLR2 or TLR4 (473–475). Exposure of tumour cells to various ICD inducers has been shown to cause the late release of HMGB1 in the extracellular medium (294). Although this process was shown to be dependent on the apoptotic activation of caspases, which presumably facilitates the exodus of HMGB1 from the nucleus, the precise molecular mechanisms leading to HMGB1 release in the context of ICD remain unclear.

To evaluate the potential of PARPi to provoke HMGB1 release in NSCLC cells, we first assessed the nucleo-cytoplasmic translocation of HMGB1 by ICC in response to PARPi, following a previously described protocol used for the detection of HMGB1 in breast cancer tumour archival samples (476). We exposed A549-ERCC1$^{WT/WT}$ cells to SF20 doses of the PARPi rucaparib and talazoparib for 48 h, and subsequently performed HMGB1 staining on FFPE cell suspensions (NCZ was used as a positive control for the experiment).

This analysis revealed that, whereas DMSO-treated cells mostly displayed a nuclear staining of HMGB1 but no cytoplasmic staining, rucaparib- and talazoparib-treated cells were characterized by a reduced intensity of HMGB1 nuclear staining associated with an enhanced intensity of HMGB1 cytoplasmic staining (**Figure VI.12.A**). Consistent with these observations, our manual quantification revealed a substantial increase in the proportion of cells exhibiting HMGB1 cytoplasmic staining (cyto-HMGB1-positive cells) in rucaparib-, talazoparib- and NCZ-treated conditions compared with the DMSO-treated condition (**Figure VI.12.B**). Again, this effect appeared to be more pronounced in cells exposed to rucaparib compared to cells exposed to talazoparib, with the percentage of cyto-HMGB1-positive cells being comparable in cells exposed to rucaparib and NCZ. These data suggested a translocation of HMGB1 from the nucleus to the cytoplasm in response to PARPi.

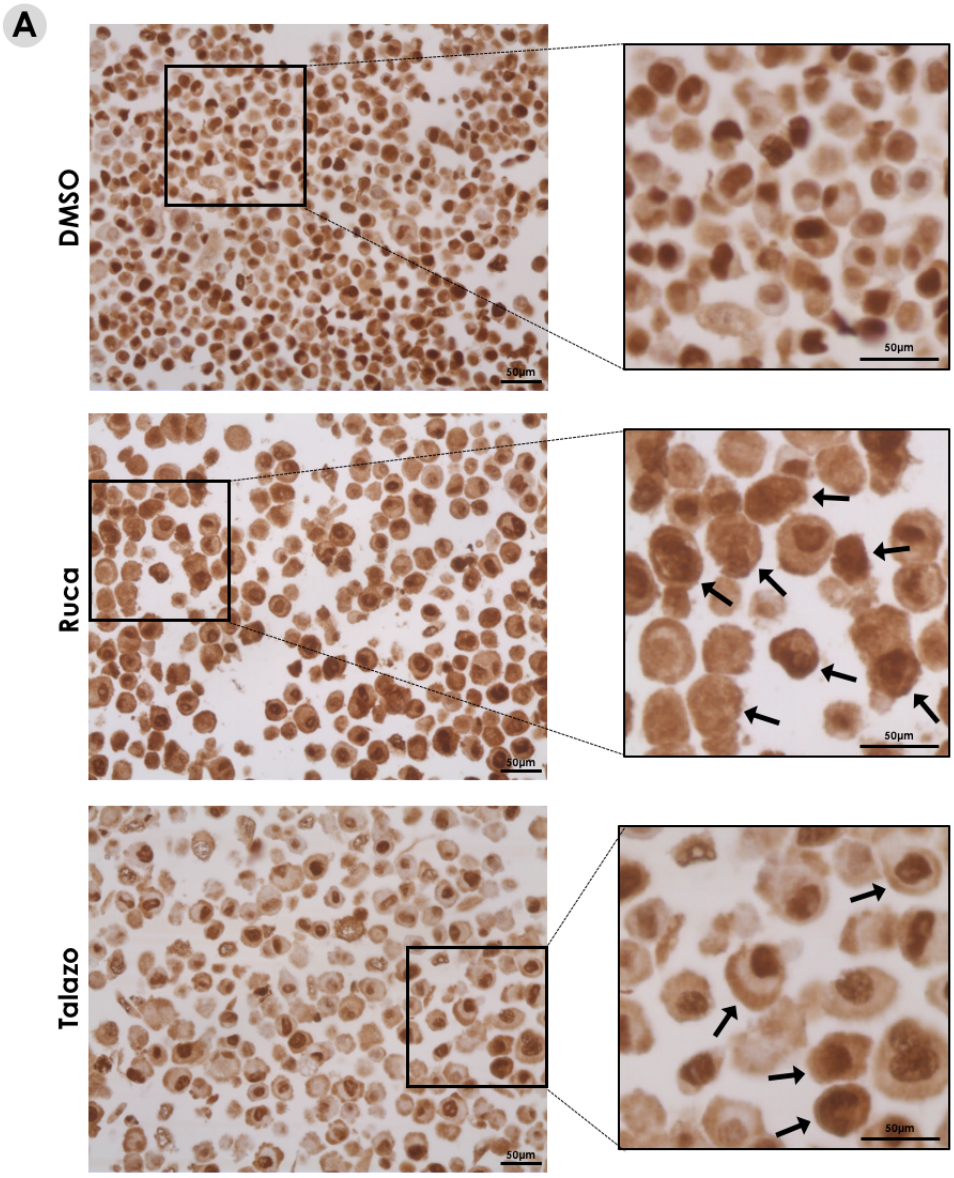
A
DMSO
Ruca
Talazo
50µm

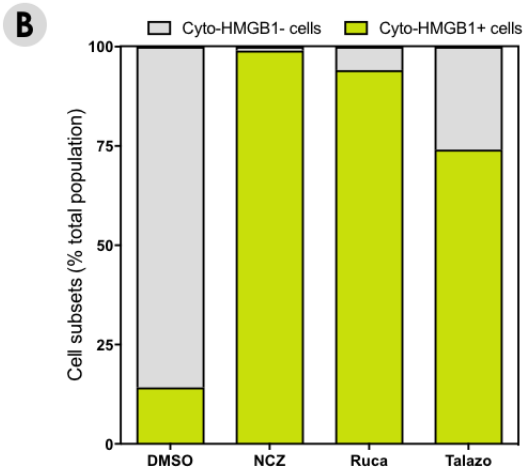
B
Cyto-HMGB1- cells
Cyto-HMGB1+ cells
Cell subsets (% total population)
100
75
50
25
0
DMSO
NCZ
Ruca
Talazo

Figure VI.12. Rucaparib and talazoparib trigger HMGB1 nucleo-cytoplasmic translocation in A549-ERCC1$^{WT/WT}$ cells.
A. Representative images of HMGB1 ICC staining in PARPi-treated A549-ERCC1$^{WT/WT}$ cells. Cells were treated with DMSO or SF20 doses of rucaparib and talazoparib for 48 h. Scale bar: 50µm. **B.** Manual quantification of the number of cyto-HMGB1-positive cells in A549-ERCC1$^{WT/WT}$ populations exposed to DMSO, SF20 doses of rucaparib and talazoparib or 200µM NCZ for 48 h. Shown are the percentages of cyto-HMGB1-positive and cyto-HMGB1-negative cells within the total population; N=1.

To further assess whether this nucleo-cytoplasmic translocation of HMGB1 would result in release of the protein in the extracellular medium, we measured HMGB1 protein levels in cells supernatants using ELISA. We exposed A549-ERCC1$^{WT/WT}$ and H1975-ERCC1$^{WT/WT}$ cells to SF50 and SF20 doses of PARPi and collected cells supernatants after 48 h of exposure to the drugs. Exposure to MTX in the same conditions was used as a positive control for the release of HMGB1. In both cell lines, we measured a significant increase in HMGB1 extracellular concentrations after exposure to MTX and rucaparib at the SF20 dose (**Figure VI.13**; 7.53 ± 1.77 ng/mL in DMSO-treated vs 30.88 ± 3.95 ng/mL in rucaparib-treated A549-ERCC1$^{WT/WT}$ cells, $P < 0.0001$; 11.23 ± 0.63 ng/mL in DMSO-treated vs 20.15 ± 7.88 ng/mL in rucaparib-treated H1975-ERCC1$^{WT/WT}$ cells, $P = 0.0002$; Kruskal-Wallis test and *post hoc* Dunn's test). By contrast, no significant increase in extracellular HMGB1 could be detected in response to the three other PARPi.

Together, these results suggest that rucaparib but not talazoparib, olaparib or veliparib trigger HMGB1 release in NSCLC cells. This is consistent with data regarding apoptosis, which showed a significant induction of apoptotic cell death in cells exposed to rucaparib for 48 h, a phenotype that was not observed (at least to such extent) in cells exposed to the three other PARPi.

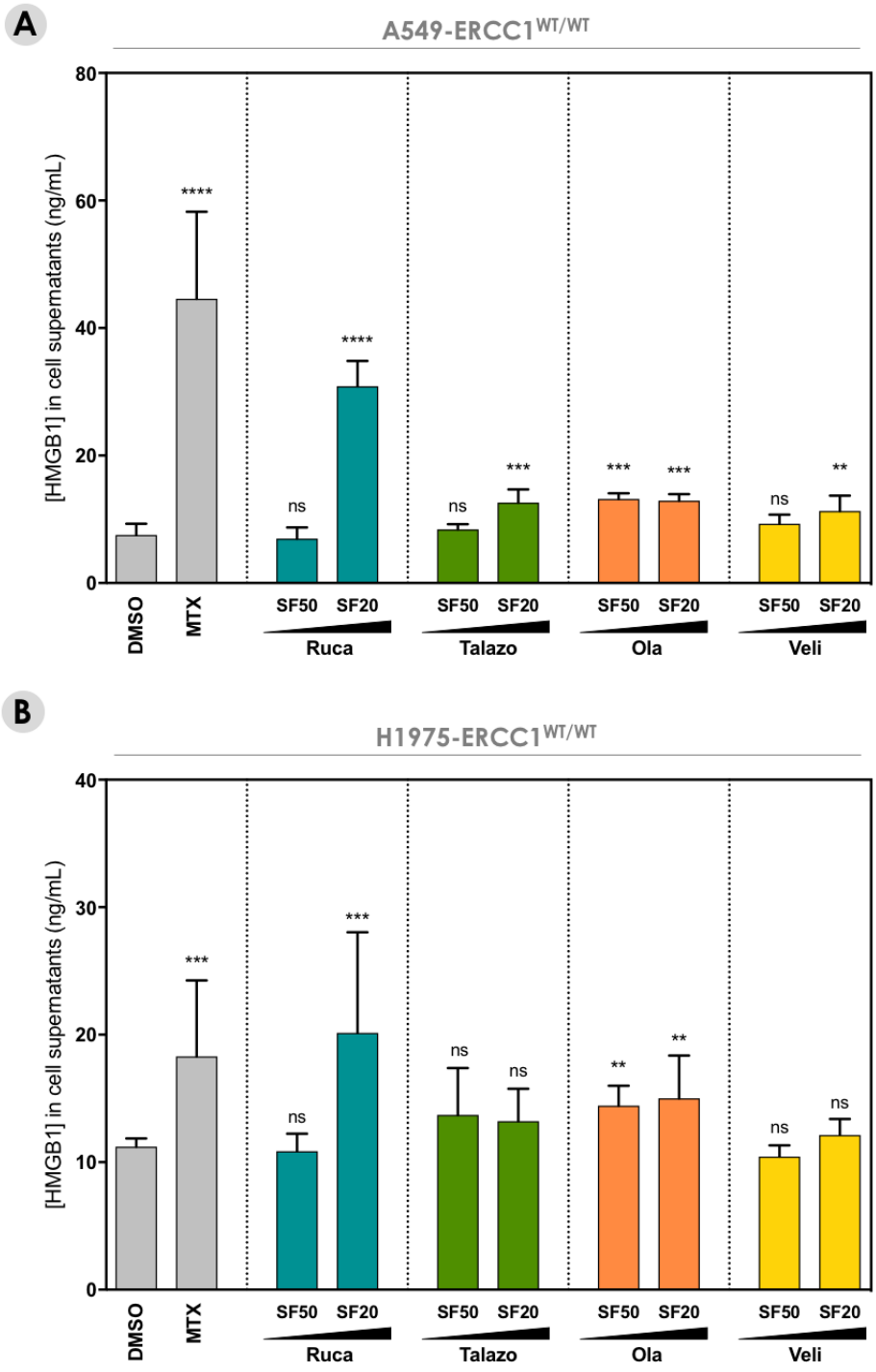

Figure VI.13. HMGB1 is released in response to rucaparib in NSCLC cells.
Quantitative analysis of HMGB1 secretion in A549-ERCC1$^{WT/WT}$ (**A**) and H1975-ERCC1$^{WT/WT}$ (**B**) cells exposed to PARPi. Cells were treated with DMSO, 2μM MTX, or SF50/SF20 doses of rucaparib, talazoparib, olaparib and veliparib for 48h. Supernatants were collected and analysed by ELISA for detection of HMGB1. Shown are HMGB1 concentrations; Mean ± SD, N=3, Kruskal-Wallis test and *post hoc* Dunn's test, relative to DMSO control.

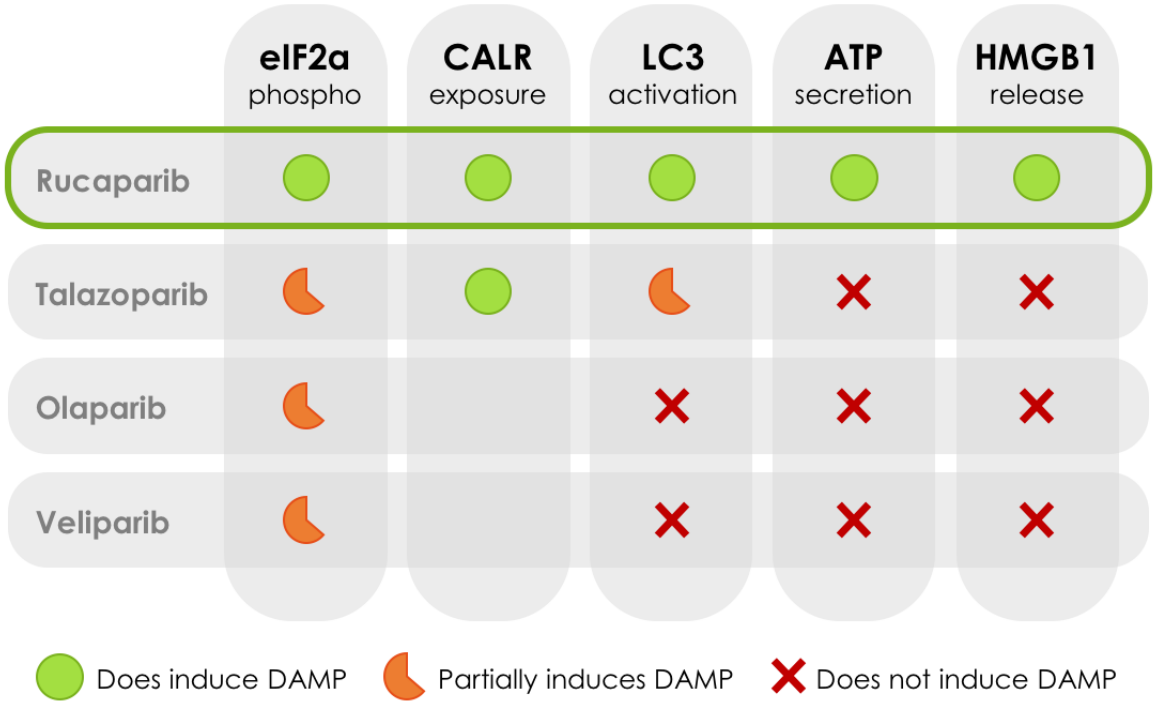

Figure VI.14. Schematic of the differential induction of ICD-associated DAMPs by PARPi in NSCLC cells.

In a nutshell, our *in vitro* data point towards the conclusion that PARPi have a differential ability to induce the key manifestations of ICD in NSCLC cells (**Figure VI.14**). More precisely, we found that rucaparib has a definite potential to trigger eIF2α phosphorylation, induce CALR exposure, activate LC3, induce ATP secretion, and promote HMGB1 release in a setting where high levels of apoptosis are generated. By contrast, talazoparib, olaparib and veliparib display variable potencies to induce these DAMPs, and lower levels of apoptosis are generated in similar experimental conditions. Therefore, rucaparib might carry a specific potential to activate ICD, which is apparently not shared with other PARPi. To further investigate these properties, we sought to evaluate the ICD-inducing potential of rucaparib *in vivo*.

6. *In vivo* study of the potential of rucaparib to generate ICD

To date, the gold-standard approach to evaluate the ability of a specific agent to cause *bona fide* ICD relies on vaccination assays (454). This procedure (described in details in Chapter I) has been overall successful in identifying potent ICD inducers, and, as a reference, murine cells succumbing to prototypic ICD inducers such as doxorubicin or MTX effectively vaccinate 80% of mice (280). As a confirmatory assay, putative ICD inducers can be assessed for their ability to mediate immune-dependent therapeutic effects against established neoplastic lesions (454). In this experimental setup, subcutaneous or orthotopic tumours are established in both immunocompetent and immunodeficient animals, and tumour-bearing mice are treated with the agent under evaluation. In such configuration, *bona fide* ICD inducers typically mediate optimal therapeutic effects in immunocompetent mice, but not in their immunodeficient counterparts (280,477). These experimental systems, despite being limited by the relatively restricted number of syngeneic tumour models that are currently available, present the advantage of providing a simple and reliable readout of the potential of a given compound to activate memory immune responses against tumours through ICD *in vivo*.

Because therapeutic assays cannot be employed alone to determine the capacity of a specific agent to cause ICD (454) while vaccination assays are commonly used for this purpose, we decided to set up a pilot vaccination assay to evaluate rucaparib as an ICD inducer *in vivo*.

a. *Design of a pilot vaccination assay*

For this experiment, we chose to work with a model which has repeatedly been used in the literature to assess ICD through vaccination assays (277,285,294,478): the BALB/c mouse-derived colon carcinoma cell line CT26.

We first assessed the cytotoxicity of rucaparib in this cell line using *in vitro* short-term survival assays, and observed that CT26 cells were markedly resistant to rucaparib as well as to other PARPi (**Figure VI.15**; SF50 of rucaparib ≈ 70 μM). Therefore, we selected relatively high doses of rucaparib for the *in vitro* pre-treatment of CT26 cells in the

vaccination assay, in order to generate cell death to a sufficient level to (i) ensure the induction of the key DAMPs associated with ICD and (ii) prevent pre-treated cells to progress into neoplastic lesions once inoculated in mice (vaccination).

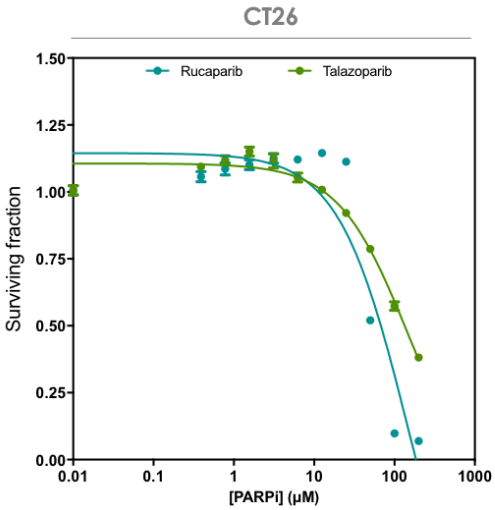

CT26	Ruca	Talazo
SF50	68µM	133µM
SF20	126µM	N.R.

Figure VI.15. Cytotoxic effects of PARPi in CT26 cells.
Cells were treated with a dose range of rucaparib or talazoparib and continuously exposed to the drug for 5 days (short-term survival assay). Shown are dose-response curves displaying the mean surviving fractions; Mean ± SD, N=4.

We designed a pilot vaccination assay comprising 20 mice distributed into four independent pre-treatment arms (**Figure VI.16**):

- **One DMSO-pre-treatment arm:** 5 mice inoculated at day 0 with $3x10^6$ CT26 cells pre-treated *in vitro* with DMSO (rucaparib vehicle).
- **One MTX-pre-treatment arm:** 5 mice inoculated at day 0 with $3x10^6$ CT26 cells pre-treated *in vitro* with 2 µM MTX for 48 h (positive control).
- **Two rucaparib-pre-treatment arms:** 10 mice inoculated at day 0 with $3x10^6$ CT26 cells pre-treated *in vitro* with 70 µM or 90 µM rucaparib for 48 h (5 mice for each concentration).

One week after the first injection, all 20 mice were re-challenged with $5x10^5$ live CT26 cells, and subsequently monitored for the appearance of subcutaneous tumours for 28 days.

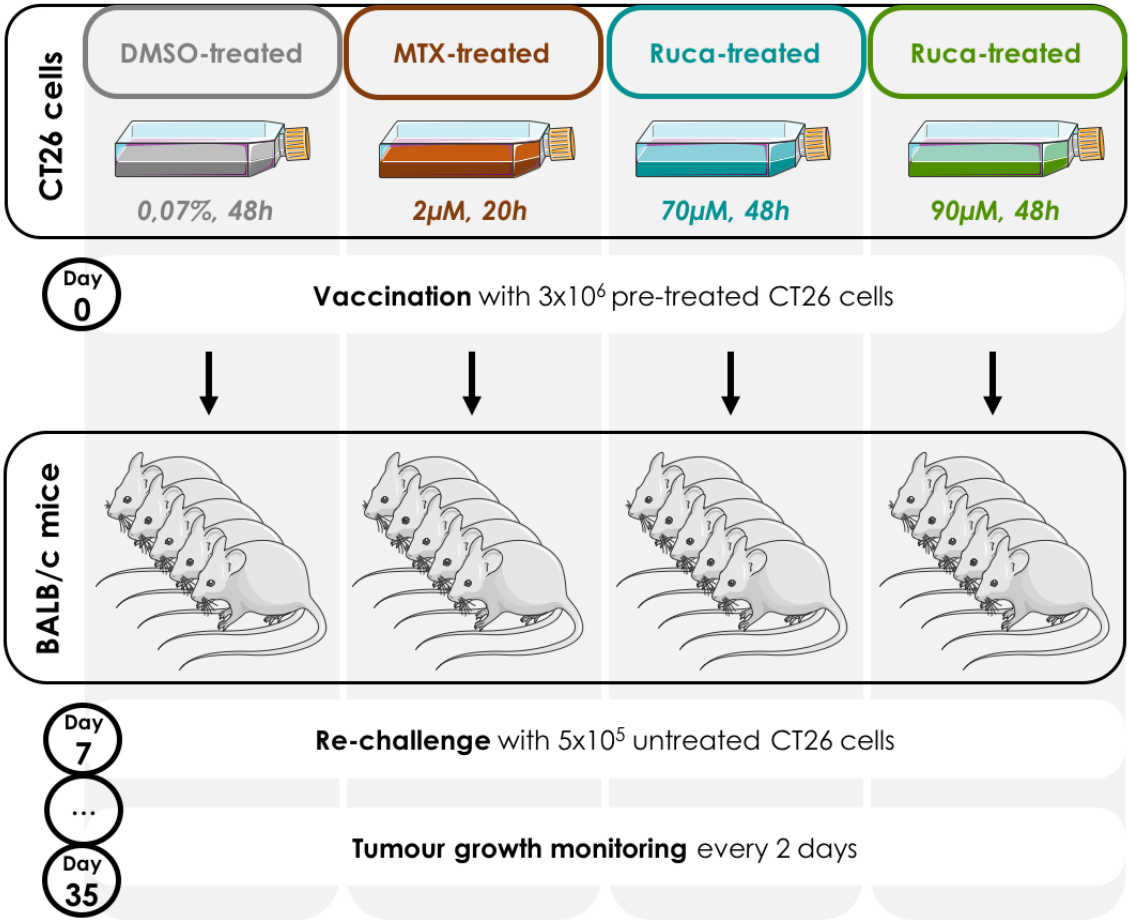

Figure VI.16. Schematic of the pilot vaccination assay designed to evaluate the potential of rucaparib to trigger ICD *in vivo*.

b. Vaccination assay: results

Prior to their injection in mice, *in vitro* pre-treated CT26 cells were analysed by flow cytometry to assess the proportion of live, apoptotic and necrotic fractions in the injection suspension. The previously used Annexin-V/7-AAD staining was performed and the percentage of cell death was measured and compared between DMSO- and rucaparib-treated conditions. We detected approximately 79% and 85% of cell death in cells exposed to 70 µM and 90 µM rucaparib respectively, while DMSO-treated cells only displayed 13% of cell death (**Figure VI.17.A** and **Figure VI.17.B**). Moreover, western blot analysis of peIF2α and LC3 on proteins extracted from DMSO- and rucaparib-treated CT26 cells revealed an intense and dose-dependent increase in eIF2α phosphorylation and LC3

activation after exposure to rucaparib (**Figure VI.17.C**). Together, these analyses confirmed the induction of apoptotic cell death, ER stress and autophagy in CT26 cells exposed to rucaparib at the chosen doses, thus providing adequate conditions for moving forward with the vaccination assay.

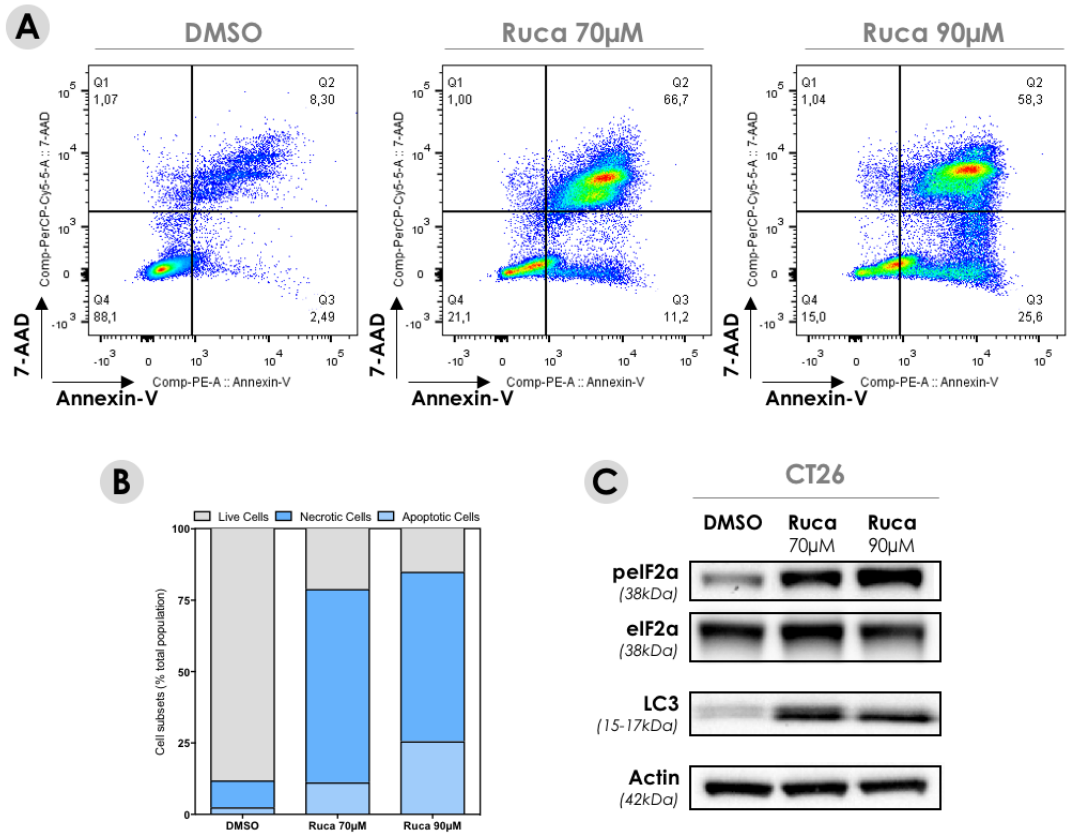

Figure VI.17. Rucaparib induces apoptosis, ER stress and autophagy in CT26 cells. **A.** Representative flow cytometry dot plots showing Annexin-V and 7-AAD staining intensities in CT26 cells exposed to PARPi. Cells were treated for 48h with DMSO, 70µM or 90µM rucaparib, and subsequently co-stained for flow cytometry detection of plasma membrane integrity (using 7-AAD) and phosphatidyl-serine exposure (using PE-conjugated Annexin-V). **B.** Quantification of the levels of apoptosis and necrosis in CT26 cells exposed to PARPi. The percentages of live, apoptotic and necrotic cells were calculated from the dot plots displayed in **A**, with live cells corresponding to cells in gate Q4, apoptotic cells corresponding to cells in gate Q3, and necrotic cells corresponding to cells in gate Q1+Q2. **C.** Western blot of peIF2α, total eIF2α and LC3 in CT26 cells upon PARPi exposure. Cells were treated with DMSO, 70µM or 90µM rucaparib for 48h. Lysates were probed with the indicated antibodies.

Tumour growth monitoring of mice re-challenged with live CT26 cells one week after vaccination revealed, as expected, the appearance of tumours in all mice of the DMSO-pre-treatment group (**Figure VI.18**). By contrast, only three of five mice in the MTX-pre-treatment group displayed established and growing tumours, confirming the validity of the positive control. Disappointingly, in both rucaparib-pre-treatment groups, all mice eventually developed neoplastic lesions at the site of re-injection, although a delay could be observed in comparison with the DMSO-pre-treatment group. This indicated that vaccination of mice with cells succumbing rucaparib-induced ICD was inefficient in protecting them against a second tumour challenge, at least in the conditions of this assay.

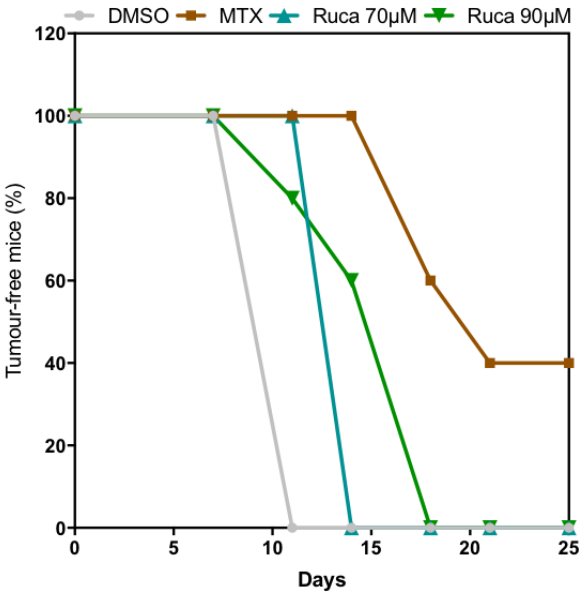

Figure VI.18. Rucaparib does not protect syngeneic mice against CT26 tumours.
BALB/c mice were immunized with CT26 tumour cells treated with DMSO, 2μM MTX, or 70μM/90μM rucaparib, and subsequently re-challenged with live CT26 cells a week later. The percentage of tumour-free mice is indicated; N=1.

Importantly, a large proportion of mice in both rucaparib-pre-treatment groups showed the presence of malignant lesions at the primary injection site (vaccination site), indicating that a sufficient number of rucaparib-pre-treated cells were still able to develop into established tumours once inoculated in the animals. This suggests that the selected doses did not trigger sufficient levels of cell death to prevent the development of tumours at the vaccination site. CT26 cells were very resistant to PARPi and the use of a more sensitive

syngeneic murine model – e.g. MCA205 fibrosarcoma cell line, also commonly used for the detection of ICD *in vivo*, or TC1 lung tumour cell line, which would provide a more consistent model with regard to our *in vitro* investigations – will be considered for future experiments.

C. Discussion

In this Chapter, we have described another aspect of the immunomodulatory potential of PARPi, that is, the ability – at least for some of them – to trigger ICD. In particular, we observed that rucaparib induces the key manifestations of ICD *in vitro*, including apoptotic cell death, eIF2α phosphorylation, CALR exposure, LC3 activation, ATP secretion, and HMGB1 release. Importantly, these DAMPs appear to be triggered in a timely fashion between 24 h and 48 h of exposure to SF20 doses of rucaparib in both NSCLC models, indicating that the induction of ICD might be favoured in this setting due to the concurrent release of these endogenous adjuvants. In similar treatment conditions, talazoparib, olaparib and veliparib were unable to induce most of these DAMPs, suggesting a specificity of activation of ICD in the context of exposure to rucaparib.

These discrepancies observed over the capacity of different PARPi to generate ICD-associated DAMPs may be explained by several factors:

(1) From our data, it is clear that the PARPi tested have a differential potential to induce apoptosis in NSCLC cells. As assessed after 48 h of exposure, the generation of apoptosis was significantly greater in response to rucaparib than in response to the three other PARPi. This may selectively favour the production of apoptosis-dependent DAMPs such as ATP secretion and HMGB1 release. Whether such signals could be elicited at higher doses or later time points with talazoparib, olaparib or veliparib remains to be formally tested, but we can assume that adjusted conditions of cell death would facilitate ATP secretion and HMGB1 release in cells exposed to these PARPi.

(2) The PARPi tested appear to have an intrinsically distinct potential to trigger ER stress and autophagy in our models. This may explain why ATP secretion, which is in part caused by an autophagy-dependent process, is observed only in response to rucaparib, which markedly induces eIF2α phosphorylation and LC3 activation. Indeed, as ATP in the extracellular medium is actively degraded by specific enzymes present at the tumour cell surface, such as the ecto-5'-nucleotidases CD39 and CD73 which catalyse ATP phospho-hydrolysis (479,480), a sustained secretion of ATP may be needed to allow the extracellular accumulation of this nucleotide and its subsequent biochemical detection. Thus, although all PARPi may induce ATP secretion to a certain extent – as evidenced by the dose-dependent decrease in intracellular ATP concentrations after exposure to all four PARPi –, it is likely that this secretion is not sufficiently sustained in cells exposed to talazoparib, olaparib or veliparib because autophagy is not activated.

(3) The four PARPi assessed in this study carry distinct pharmacological properties in terms of PARP catalytic inhibition activity, PARP trapping potency and off-target effects. Based on our observations, we can reasonably hypothesize that the potential of PARPi to induce ICD does not rely on their inherent PARP catalytic inhibition activity or PARP trapping potency – as talazoparib, olaparib and veliparib have distinct properties in this regard while being all unable to trigger ICD. Conversely, their respective off-target effects may greatly influence this potential. Interestingly, rucaparib (which is the only PARPi displaying ICD-inducing properties in our study) is the agent that has the most off-target effects compared to the other PARPi. In particular, rucaparib has been shown to inhibit a number of protein kinases including *PIM1, PIM2, PRKD2, DYRK1A, CDK1, CDK9, HIPK2, CK2,* and *ALK* (481). Of note, pharmacological inhibition of PIM kinases by small molecule inhibitors has been linked to the induction of the UPR and subsequent ER stress (482), as well as to the activation of autophagy (483), raising the possibility that rucaparib-mediated PIM1/2 inhibition may cause an enhanced generation of the DAMPs associated with these stresses. Overall, further investigation of the impact of these off-target effects would be needed to fully characterize the determinants of rucaparib potential to induce ICD.

In conclusion, rucaparib is a putative ICD inducer which carries a specific potential to activate the crucial DAMPs associated with this peculiar cell death modality. Now, the implementation of adequate *in vivo* assays (including optimized vaccination assays and confirmatory therapeutic assays in immunodeficient vs immunocompetent animals) will be key to fully reveal the potential of this PARPi to trigger ICD.

Chapter VII. Final discussion and perspectives

DDR deficiency is an important hallmark of cancer that participates to tumour development by promoting genomic instability. This hallmark has been exploited as a therapeutic opportunity in cancer treatment for more than 50 years with the use of conventional cytotoxic chemotherapies, in an "unselected" fashion. More recently, the description of synthetic lethal relationships, such as BRCA deficiency/PARP inhibition, has opened the path for exploiting DDR deficiency in more "selected" and molecularly-targeted approaches. Such successful approaches have led to the accelerated approval of the PARPi olaparib (2014) (359) and rucaparib (2016) (484) for the treatment of germline *BRCA*-mutant advanced ovarian cancer, and since January 2018, for the treatment of germline *BRCA*-mutant metastatic breast cancer (olaparib) (361). In addition, the involvement of PARP in other synthetic lethal interactions, such as ERCC1-deficiency in NSCLC (364) or ARID1A-deficiency in multiple tumour types (365), has also been described. These recent advances support the importance of PARPi in the therapeutic armamentarium against cancer, and further establish the significance and broad applicability of synthetic lethal approaches.

Alongside this progress, the advent of immune-based therapies has brought outstanding benefit in the treatment of many cancers. In particular, anti-PD-(L)1 therapies have allowed significant survival improvements in several aggressive diseases in oncology, notably melanoma, NSCLC, clear cell RCC, Merkel cell carcinoma, UBC and tumours harbouring high MSI. Despite these encouraging results, only a minority of patients respond to these therapies (15-45% according to the histology) and therefore, the identification of rationale combinations that would permit increasing the proportion of patients who benefit from ICI is currently an active area of clinical research.

Recent discoveries regarding the impact of genomic instability and DDR defects on the response to anti-PD-(L)1 therapies have encouraged the development of combinations with

chemotherapeutic regimens. This strategy has demonstrated exceptional efficacy, as illustrated by very recent results of the large phase III trial KeyNote-189, which has reported unprecedented improvements in OS and PFS when using pembrolizumab and platinum-doublet in first-line therapy in NSCLC (129). Along similar lines, an increasing number of combinatorial clinical trials are being developed to evaluate anti-PD-(L)1 agents in combination with DDR-targeted therapies, especially PARPi (**Table VII.1**).

In a context where very little is known about the immunomodulatory properties of PARPi and their interaction with cells of the immune system, the objective of this PhD project was to investigate the molecular mechanisms that may influence anti-tumour immunity in response to PARPi, with the aim of building a robust scientific rationale for the ongoing and upcoming clinical trials evaluating such combinations.

Table VII.1. Summary of the ongoing clinical trials evaluating PARPi plus anti-PD-(L)1 agents for the treatment of cancer.

For each clinical trial, the PARPi and anti-PD-(L)1 tested are indicated, along with the cancer types involved and the corresponding indications. Data cut-off: October 2018.

PARPi	ICI	Histology	Indication	Phase	NCT
Olaparib	Durvalumab	Breast Gastric Ovarian SCLC	3rd line 2nd line Platinum-sensitive 2nd line	I/II	NCT02734004
Olaparib	Durvalumab	NSCLC SCLC TNBC Ovarian CRC mCRPC	2nd line or higher 2nd line or higher < 3 prior lines Platinum-resistant 3rd line	I/II	NCT02484404
Olaparib	Durvalumab +Tremelimumab	Ovarian	BRCA-mutated (germline)	I/II	NCT02953457
Olaparib	Durvalumab	TNBC	< 2 prior lines	I	NCT03544125
Olaparib	Durvalumab	Breast		I/II	NCT03594396
Olaparib	Durvalumab	UBC	Platinum-ineligible	II	NCT03459846
Olaparib	Atezolizumab	TNBC	BRCA-mutated (germline)	II	NCT02849496

PARPi	ICI	Histology	Indication	Phase	NCT
Rucaparib	Nivolumab	mCRPC Endometrial	Any prior therapy allowed Any prior therapy allowed	I/II	NCT03572478
Rucaparib	Nivolumab	Ovarian	Platinum-sensitive	III	NCT03522246
Rucaparib	Nivolumab	mCRPC		II	NCT03338790
Niraparib	Pembrolizumab	NSCLC	PD-L1-positive	II	NCT03308942
Niraparib	Pembrolizumab	Breast Ovarian	< 3 prior lines < 4 prior lines	I/II	NCT02657889
Niraparib	Nivolumab	Pancreatic	Platinum-sensitive	I	NCT03404960
Niraparib	Atezolizumab	Ovarian	< 2 prior lines	III	NCT03598270
Veliparib +platinum	Nivolumab	NSCLC	1st line metastatic	II	NCT02944396
Veliparib	Nivolumab	Advanced solid tumours	Refractory to standard therapy	I	NCT03061188
Veliparib +chemotherapy	Pembrolizumab	Rectal		II	NCT02921256
Talazoparib	Avelumab	Advanced solid tumours		II	NCT03330405
Talazoparib	Avelumab	Advanced solid tumours	BRCA- or ATM-mutated	II	NCT03565991
Talazoparib	Avelumab	Ovarian		III	NCT03642132
Talazoparib	Avelumab	Advanced solid tumours	RAS-mutated	II	NCT03637491
BGB-290	BGB-A317	Advanced solid tumours	2nd line or higher	I	NCT02660034

A. Critical findings presented in this thesis

In the present study, we developed a tumour cell-based approach to investigate the immunomodulatory properties of PARPi in various histological and molecular contexts, including DDR-deficient and -proficient NSCLC and TNBC. We took advantage of a unique combination of *in vitro* isogenic systems of ERCC1-defective NSCLC, *BRCA1*-mutant and PARPi-sensitive or PARPi-resistant TNBC to study diverse aspects of the immunological

potential of PARPi, notably their ability (i) to activate cGAS/STING-mediated cancer cell-intrinsic immune responses, (ii) to modulate IFN signalling and PD-L1 expression in cancer cells, and (iii) to trigger an immunogenic form of tumour cell death.

The main findings of our work are as follows:

(1) Loss of ERCC1 in NSCLC results in an immunological phenotype characterized by the transcriptional upregulation of type I IFN and cytokine signalling in tumour cells, and correlated with an enhanced T cell infiltration in NSCLC patient tumours.

(2) This phenotype can be linked to the constitutive reactivation of the cGAS/STING pathway in ERCC1-deficient cells, as ERCC1 loss results in marked re-expression of STING in NSCLC cells.

(3) cGAS/STING signalling activation can be selectively triggered by several clinical PARPi in DDR-deficient contexts, such as ERCC1-defective NSCLC and *BRCA1*-mutant TNBC.

(4) Exposure to PARPi causes cell cycle-dependent accumulation of cytosolic DNA in the form of CCF or micronuclei; these patterns are detected by cGAS and activate a signalling cascade involving STING, TBK1, IRF3 and NF-κB, which eventually results in a type I IFN response and the secretion of chemotactic chemokines, such as CCL5.

(5) These effects are on-target, and critically conditioned by the presence of endogenous DDR defects in cancer cells, as indicated by the suppression of cGAS/STING-mediated cytokine production in response to PARPi in *ERCC1*-rescued NSCLC cells and *BRCA1*-reverted TNBC cells.

(6) Consistent with these *in vitro* data, olaparib exerts immunomodulatory properties at clinically-relevant doses *in vivo* in PDX models of *BRCA1*-mutant breast cancer, which supports the translational utility of our findings.

(7) PARPi induce transcriptional upregulation and enhanced cell surface expression of PD-L1 in cancer cells. This induction is exacerbated in ERCC1-deficient NSCLC cells, and results from the dose-dependent and on-target effects of PARPi on PARP1.

(8) PARPi further potentiate IFN-γ-mediated PD-L1 upregulation through stimulation of the JAK/STAT pathway, which suggests that PARPi might endogenously, or via IFN-γ-mediated autocrine and paracrine circuitries, influence the signalling networks controlling PD-L1 expression.

(9) Rucaparib is a potent inducer of all the key molecular manifestations of ICD, including the ER stress-dependent exposure of CALR at the tumour cell surface, the autophagy- and apoptosis-mediated secretion of ATP, and the necrosis-associated release of HMGB1 in the extracellular milieu.

In this ultimate Chapter, we discuss biological and clinical implications of our findings, as well as future directions to further develop our research.

B. Mechanisms controlling cytosolic DNA accumulation in response to PARPi

In Chapter IV of this thesis, we showed that PARPi trigger a cell-autonomous type I IFN response through activation of the cGAS/STING pathway in cancer cells, a phenotype that is associated with the accumulation of cytosolic DNA in response to PARPi. If one can easily speculate that in DDR-deficient contexts, PARP inhibition causes toxic DNA lesions that favour formation of CCF, the mechanisms leading to this shedding of DNA into the cytosol remain mostly unclear. Several studies have suggested an important role for factors that control DNA end resection and resolution of DNA joint molecules, such as the structure-specific endonuclease MUS81 (485) which mediates cleavage of DNA structures at stalled replication forks, and the BLM helicase and EXO1 exonuclease (263) which both participate to the resolution of Holliday junctions (486). A suggested mechanism to explain such link is that the repair activity of these enzymes creates DNA fragments that eventually accumulate in the cytosol. Indeed, MUS81-mediated replication fork processing involves the cleavage of potentially detrimental DNA structures (487), which implies that DNA fragments are generated as by-products of MUS81 activity. Comparably, in the setting of DSB repair in response to DNA-damaging agents, the nuclease activity of MRE11 is required to initiate resection of dsDNA ends into 3′ ssDNA overhangs. One of the pathways controlling this process involves the 5′-to-3′ exonuclease activity of EXO1, acting in concert with the DNA-unwinding activity of BLM helicase (488), and was shown to generate 3′ overhang resection

products of several thousand nucleotides, thus promoting the formation of free DNA fragments that presumably subsequently accumulate in the cytosol.

ERCC1/XPF is also an important DNA repair mediator displaying an exonuclease activity, which acts in the NER and inter-strand crosslink repair pathways (489), and interestingly, is also known to participate to the resolution of Holliday junctions (410). In the context of ERCC1 deficiency, cells have a decreased potential to repair toxic DNA lesions, notably PARP trapping lesions, which are thought to be particularly persistent in the absence of ERCC1-mediated excision (364). Our data support that exposure of ERCC1-deficient cells to non-lethal doses of PARPi (at early time points) selectively trigger the enhanced production of cytosolic DNA fragments. One hypothesis that could explain this phenotype may be the activation of alternative repair mechanisms that favour the production of DNA fragments and their accumulation in the cytosol. For example, MUS81 nuclease activity could be involved in the resolution of PARP trapping lesions in the absence of ERCC1, as this enzyme is essential for replication fork restart under replication stress elicited by exogenous treatments (490,491) and endogenous DDR defects (492). Alternatively, late-stage replication intermediates caused by PARP trapping that persist until mitosis may be cleared by MUS81 or other resolvases, including the BLM-TopoIIIα-RMI1-RMI2 (BTR) complex (493,494), which also favours DNA fragments production. One way to test these hypotheses could be to monitor, in our ERCC1-deficient models, the formation of CCF in response to PARPi after depletion (by CRISPR or siRNA targeting) of MUS81 or other DDR-associated resolvases.

If the molecular mechanisms leading to the generation of DNA fragments in response to DNA damage are unclear, those involved in the translocation of these fragments in the cytosol are even more obscure. The presence of free cytosolic DNA fragments has been reported as a result of intrinsic DDR defects or induced DNA damage (263,269,495). Few studies have described an active nuclear DNA export process in response to DNA-damaging agents, involving nuclear DNA bud formation and detachment of chromatin from the nucleus into the cytosol through unusual thread-like structures that are first connected to the nucleus and then fragmented in the cytosol (496). Other lines of evidence suggest that cytoplasmic DNA originating from genomic instability is mainly present in the

form of micronuclei (265,266). For instance, centromere-deficient chromosome fragments, which originate from the error-prone NHEJ repair pathway, are unable to segregate normally and form micronuclei outside the newly formed nucleus. Similarly, whole chromosomes left behind by the spindle because of centromere hypomethylation or kinetochore dysfunction also end up as micronuclei after mitosis (497). Considering the cell cycle-dependency of CCF formation in our study, it is likely that these fragments arise as micronuclei following exposure to PARPi. Of note, if micronuclei presenting an intact nuclear membrane do not constitute substrates for DNA-sensing machineries, ruptured micronuclei, by contrast, are potent inducers of the cGAS/STING pathway as chromosomal DNA becomes accessible to cGAS (265,266,416,498,499). Finally, in the context of cellular senescence, the accumulation of CCF was shown to result from loss of the nuclear lamina protein lamin B1, leading to compromised integrity of the nuclear envelope (411,500). This process was mediated by the active degradation of lamin B1 involving the autophagic factor LC3 in cells exposed to oncogenic insults (501), and associated with the release of CCF. Whether a similar mechanism could operate in our models upon exposure to PARPi warrants further exploration.

Overall, identifying the factors that may impair cGAS-mediated cytosolic DNA sensing would be key in order to optimize cGAS/STING signalling activation in response to PARPi. While we previously discussed the possible impact of the heterogeneity in cytosolic DNA forms (i.e. CCF vs micronuclei), another important factor that should be anticipated is the presence of cytoplasmic exonucleases which actively degrade DNA as it accumulates in the cytosol. For example, the lysosomal nuclease DNASE2 was shown to be involved in the degradation of cytosolic DNA in lysosomes (496). Consistently, elevated levels of cytosolic DNA were found in DNASE2-deficient cells, and this has been associated with an inflammatory phenotype that could be attributed to cGAS/STING activation. This example is characteristic of deficiencies in DNA-degrading nucleases that lead to self-DNA accumulation and induction of autoimmunity in mice as well as in monogenic and polygenic human diseases. Other instances include the generally lethal disorders Aicardi-Goutières syndrome and severe systemic lupus erythematosus which have been linked to defects in the cytosolic exonuclease TREX1 (502,503). Very interestingly, a recent study has

demonstrated that TREX1 is induced in different cancer cells exposed to IR, and that this induction attenuates their immunogenicity by degrading cytosolic DNA accumulated upon irradiation (456). This effect could be avoided by exposing cells to reduced doses of IR, which appeared to prevent TREX1 upregulation while sustaining the accumulation of cytosolic DNA. Importantly, this adapted treatment schedule allowed the amplification of cGAS/STING-mediated immune responses and subsequent priming of CD8+ T cells mediating systemic tumour rejection (abscopal effect) in the context of combination with ICI. Thus, TREX1 is a key upstream regulator of IR-driven anti-tumour immunity, which may have a broader significance in the context of treatment with other DNA-damaging and DDR-targeted therapies. Evaluating the effects of DDR deficiencies and PARPi exposure on TREX1 expression or activation would therefore deserve further investigation.

Lastly, the study of human interferonopathies, such as the Aicardi-Goutières syndrome which is characterized by constitutive activation of the cGAS/STING pathway and chronic upregulation of type I IFN, has recently shed a new light on the possible mechanisms regulating cytosolic DNA accumulation under genotoxic stress conditions (504). In particular, recent discoveries have uncovered a key role for several DDR-interacting factors, frequently mutated in Aicardi-Goutières syndrome such as SAMHD1 and RNase H2, in the regulation of cGAS/STING signalling activation. SAMHD1 is a deoxynucleoside triphosphate (dNTP) hydrolase that depletes intracellular dNTP pools in non-cycling cells, and plays a major role in DSB repair by promoting MRE11-mediated resection of DNA ends (505). SAMHD1 specifically acts at stalled replication forks to facilitate degradation of nascent DNA, a function that activates the ATR/CHK1 checkpoint and allows replication to restart. Consistently, SAMHD1 deficiency was shown to induce a significant level of replication stress which triggers the release of ssDNA fragments from stalled replication forks; the accumulation of these fragments in the cytosol was associated with activation of cGAS/STING-induced IFN responses (506). Similarly, mutations in RNase H2 – a protein involved in the removal of ribonucleotides misincorporated into DNA during replication and in the resolution of co-transcriptional RNA:DNA hybrids (507) – were shown to cause spontaneous replication stress, and were associated with immunogenic micronuclei formation (498) and cGAS/STING activation (508). SAMHD1 and RNase H2 are thus

important regulators of the inflammatory response to replication stress that protect cells from chronic inflammation by preventing DNA fragments synthesis. As mutations in SAMHD1 have been described in several cancers (509), and RNase H2 mutations have recently been associated with increased sensitivity to PARPi (510), both factors may represent interesting biomarkers to predict the immunological potential of PARPi therapy.

C. Biological implications of PARPi-mediated stimulation of the cGAS/STING pathway

1. Immunological impact of cGAS/STING signalling activation

Effective anti-tumour immunity relies on cross-presentation of tumour antigens by APCs to CD8+ T lymphocytes. In this respect, type I IFN signals elicited by innate immune sensors are crucial as they promote the activation and function of APCs (405,511), and it has now become clear that the DDR-induced cGAS/STING pathway in tumour cells largely contributes to this process (512). In line with this notion, our study demonstrates that DDR defects in cancer cells exacerbate cytosolic DNA formation and induction of a cGAS/STING-mediated cell-autonomous type I IFN response upon exposure to PARPi. Importantly, activation of the cGAS/STING pathway in APCs also critically participates to the priming of CD8+ T cells. Indeed, tumour cell-derived DNA triggers the production of type I IFN in CD11c+ tumour-infiltrating DCs via cGAS/STING, thereby priming cytotoxic T lymphocytes specific for tumour-associated antigens (260). Likewise, cGAS-mediated DNA sensing was shown to be required for DCs-mediated cross-presentation of tumour-associated antigens to CD8+ T cells in the context of immune checkpoint blockade (274). To date, the effects of PARPi on these immune cells populations are unknown, and whether exposure to PARPi could facilitate anti-tumour immune responses via stimulation of APCs or effector T cells would deserve further investigation. In addition, whether cancer cell-autonomous immunity elicited by PARPi would effectively participate to tumour rejection remains to be formally tested in relevant immunocompetent models *in vivo*, yet our results suggest that PARPi may serve as potent adjuvant "immune therapies" in appropriately-selected populations.

2. Deleterious effects of chronic cGAS/STING pathway activation

Chromosomal instability and micronuclei formation have recently been linked to invasion and metastasis through chronic activation of the cGAS/STING pathway and downstream non-canonical NFκB signalling (270). Indeed, chromosomally unstable cancer cells have been shown to sustain activation of the inflammatory STING-dependent NF-kB signalling, while largely suppressing type I IFN signalling through multiple mechanisms (271). This chronic activation of NF-kB leads to the senescence-associated secretory phenotype (SASP) and mediates cellular migration and distant metastasis (270,513,514). STING itself, type I IFN signalling, and important components of the non-canonical NFκB signalling – including NFκB1, NFκB2 and RELB – were constitutively upregulated in our A549-ERCC1$^{-/-}$ models. Although this phenotype is certainly beneficial in the context of type I IFN-mediated stimulation of autocrine or paracrine circuits underlying cancer immunosurveillance (515), it may also have deleterious effects in the chronic setting due to altered innate immune function (516). Indeed, chronic type I IFN signalling has been associated with immunosuppression via inhibition of specific CD8+ T cells responses and accumulation of MDSC (517), and may even favour tumour progression in specific DDR-deficient contexts, such as *ATM*-associated hematologic malignancies (518). Which balance between cGAS/STING signalling activation and inhibition is optimal for anti-tumour immune control requires further exploration.

D. Potential determinants of cancer cell-autonomous immune responses elicited by PARPi

1. Epigenetic determinants of cGAS/STING-mediated immune responses

In Chapter III of this thesis, we described that NSCLC cells re-express STING upon loss of ERCC1; this phenotype was reversed when a functional isoform of ERCC1 had been reintroduced in ERCC1-deficient cells, suggesting a fully reversible and potentially epigenetic silencing of *STING* in ERCC1-proficient cells. In line with this hypothesis, an

emerging body of data now supports that various epigenetic processes are involved in the repression of cGAS/STING-mediated immune responses. Recent studies have reported recurrent suppression of *cGAS* or *STING* expression through promoter hypermethylation in many human cancers, a phenomenon that was associated with impaired cytokine production in the context of exposure to DNA damage (519–521). Insensitivity to cytosolic DNA sensing has also been described in *LKB1*-mutated NSCLC as a result of *STING* promoter hypermethylation (407), and was proposed to be a mechanism of primary resistance to immune checkpoint blockade. Other epigenetic processes may also participate to STING suppression, such as removal of the H3K4me3 mark from the *STING* locus by lysine (K)-specific demethylases 5B and 5C (KDM5B/C) (522). These recent lines of evidence suggest that epigenetic deregulation of STING signalling is an important mechanism controlling tumour-intrinsic immunity in response to DNA damage, which could be therapeutically exploited to enhance the effects of immunomodulatory agents such as PARPi.

2. Multiple DDR defects might trigger tumour cell-intrinsic immunity

Although our study focused on ERCC1 deficiency, we can hypothesize that our findings may be applicable to other DDR defects found at a lower frequency in NSCLC. For example, *BRCA1*, *BRCA2*, *ATM* or *MSH2*, mutated in 5%, 6%, 9% and 3% of NSCLC cases respectively (523), have also been associated with PARPi sensitivity and type I IFN signature (268,269,362,524,525). Similarly, defects in *RAD51* have been associated with cGAS/STING activation and type I IFN signalling (526,527), and it is thus reasonable to assume that other HR defects, frequently mutated in breast or ovarian cancers (such as *PALB2*, *BARD1*, *BRIP1* or *RAD50*, see **Table I.3**) may be associated with a similar phenotype in these histologies. Interestingly, Teo et al. recently reported that somatic DDR alterations that were associated with improved clinical outcomes in platinum-treated patients with advanced UBC (528), also correlated with longer PFS and OS upon anti-PD-(L)1 therapy (256). In this study, authors reported that 25% of patients presented tumours with alterations in DDR genes, the most commonly altered genes being *ATM, POLE, BRCA2, ERCC2, FANCA* and *MSH6*.

These observations suggest that the interplay between DDR deficiency, platinum- or PARPi-sensitivity and anti-cancer immune response operates in several tumour types and can involve multiple DDR defects.

E. Challenges in exploiting PARPi potential to induce ICD

In Chapter VI of this thesis, we have described how rucaparib elicits an immunogenic form of cancer cell death by inducing key DAMPs involved in the stimulation of innate and adaptive immune effectors. However, the immunogenicity of cell death relies on the contribution of two distinct biological parameters: the antigenicity provided by neo-epitopes, and the adjuvanticity conferred by specific DAMPs (276). Although our data suggest a potential for rucaparib to increase the adjuvanticity of dying cancer cells as they emit ICD-associated DAMPs, nothing indicates that these cells display an enhanced antigenicity as a result of rucaparib treatment. To our knowledge, no solid studies have currently been conducted to assess the modulation of TNB in response to PARPi, and although such analyses have been performed in the context of exposure to DNA-damaging agents, these have for now failed to demonstrate a substantial contribution of DNA damage-induced mutagenesis to predicted neo-antigens expression (529). In the face of this lack of evidence, and considering the importance of TMB/TNB as predictive biomarkers of response to anti-PD-(L)1, it will be key to evaluate the impact of PARPi treatment on these parameters. In the context of ICD, incorporating lessons learnt from the immunological impact of endogenous DDR defects will certainly guide the identification of molecular subtypes in which the immunogenic potential of PARPi-induced cell death will be optimal. DDR-deficient tumours, which inherently exhibit elevated TMB/TNB and display enhanced sensitivity to PARPi, may therefore constitute favourable environments for exploiting PARPi potential to induce ICD. In particular, we can reasonably assume that the immunogenicity of cell death elicited by rucaparib might be enhanced in ERCC1-deficient contexts because: (i) ERCC1-deficient tumour cells are more sensitive to PARPi (364) and might, as such, carry an augmented capacity to emit ICD-associated DAMPs in response to rucaparib (adjuvanticity); (ii) ERCC1-deficient cells exhibit high genomic instability and elevated TMB

(408) – a result corroborated by our analysis of TCGA datasets showing a higher mutation frequency in *ERCC1*-mutant tumours –, which suggests that they might intrinsically express higher levels of neo-antigens (antigenicity). Together, these elements may favour the activation of ICD-driven adaptive immune responses in ERCC1-deficient tumours exposed to rucaparib. Similar mechanisms could be involved in *BRCA1/2*-mutant tumours. These hypotheses need to be formally investigated in future studies, and the ability of rucaparib to drive *bona fide* ICD in such contexts must be assessed *in vivo* in appropriate mouse models.

If a judicious molecular selection of patients is crucial to best exploit the immunostimulatory potential of PARPi for their benefit, the identification of an optimal therapeutic window is also key in the course of clinical implementation. In this regard, the selection of a relevant dose, treatment schedule and route of administration is particularly important to optimize treatment efficacy. In the context of ICD, elevated doses of drugs have overall been used in vaccination and therapeutic assays *in vivo* to elicit the intended effects (278,454), and intra-tumour administration has often been chosen in therapeutic assays to avoid the systemic toxicities associated with chemotherapeutic treatments (277). In our study, we also tested relatively high doses of PARPi to evaluate the capacity of these compounds to induce ICD. In the case of rucaparib, although elevated doses did trigger all the key manifestations of ICD *in vitro*, these appeared not to be appropriate for the induction of ICD in vaccination assays *in vivo*. A reason for this discrepancy might be that, in the conditions of the assay, such doses were not cytotoxic enough to prevent the development of neoplastic lesions at the vaccination site, or on the contrary, that they induced too much cytotoxicity so that the fraction of dying cells (cells actually succumbing to apoptosis, as opposed to already dead cells which are no longer immunogenic) was excessively low, thereby hindering the establishment of protective immunity. In the first situation, the lack of cytotoxicity induced by the assayed agent can be virtually corrected by the addition of a potent non-immunogenic cytotoxic agent (such as cisplatin or mitomycin C) which serves as a blocker to neoplastic development (477). In the second situation, a refined optimization of the pre-treatment dose and timing is required to ensure the injection of a vaccination mixture containing an optimal proportion of dying tumour cells. Naturally, if these procedures are

applicable in the artificial setting of a vaccination assay, their clinical relevance is quite limited as similar strategies cannot be employed in patients. Therefore, working with clinically-relevant doses of PARPi in appropriately-selected molecular contexts would be our best chance to guarantee the translational applicability of these pre-clinical findings. Such approach will be launched soon in ERCC1-deficient and *BRCA1*-mutant syngeneic models of NSCLC/TNBC.

Finally, in a context where immunogenic chemotherapies have proven their capacity to sensitize tumours to immune checkpoint blockade (304), the ICD-inducing potential of PARPi could be readily exploited in combination with anti-PD-(L)1 therapy. Further pre-clinical work in appropriate immunocompetent mouse models would allow investigating the relevance of such strategy.

F. Complementary approaches to assess the immunomodulatory properties of PARPi

In our study, we developed a tumour cell-based approach to study the impact of PARPi on immunological signalling in cancer cells. The use of genetically-controlled isogenic systems allowed us to identify important determinants of PARPi-mediated cancer cell-autonomous immunity, and to dissect the biological mechanisms controlling this immunological potential of PARPi in specific molecular contexts. Despite these advantages, our methodology has concealed important aspects classically investigated in immuno-oncology research approaches, including the formal assessment of (i) the activation of local and systemic immune responses involving innate and/or adaptive immune effectors, (ii) the involvement of these immune responses in the anti-tumour efficacy of PARPi as monotherapy and in combination with ICI, and (iii) the direct impact of PARPi on immune cells function. If the use of syngeneic immunocompetent mouse models would most likely suffice to address some of these limitations, the implementation of complementary patient-based approaches would definitely be beneficial with a view to integrate, in the

experimental setting, the complex functional interactions characterizing human tumours and their immune micro-environment.

Such complementary approaches, involving the *ex vivo* culture of dissociated human tumours, are being developed at Gustave Roussy in the laboratories of Pr. Laurence Zitvogel and Dr. Aurélien Marabelle (530). In particular, the "*in sitro*" technique, which consists in the *in vitro* culture of dissociated tumour tissue, allows the monitoring of immune parameters under treatment, such as the nature and functionality of the immune infiltrate, the expression of cell surface markers on tumour and immune cells, or the secretion of chemokines and cytokines in culture supernatants. This type of assay often allows the simultaneous evaluation of several of these parameters in multiple experimental conditions, thereby offering an opportunity to generate a comprehensive picture of the tumour-immune dynamics at baseline and under various treatment conditions. Transcriptomics may also guide the estimation of immune cell content in tumour tissue (406,531). However, several hurdles currently limit the implementation of this kind of approach: (i) depending on the cancer type, tumour material is not always available, restricting these assays to the study of some histologies; (ii) a fine-tuned optimization of culture and treatment conditions is required to ensure reliability and consistency in the readouts; (iii) such assays are impeded by a lack of reproducibility and a high inter-patients variability which hampers the interpretation of experimental data; (iv) the assessment of a wide panel of parameters can be labour-intense and expensive due to the use of antibody-based techniques (flow cytometry, ELISA). Although these limitations constitute major challenges for implementing the "*in sitro*" approach on a routine basis, such assays could be easily performed to study the immunomodulatory properties of PARPi alone and in combination with ICI in NSCLC tumours.

The organotypic culture of tumour slices could also be an interesting complementary approach to our study (532). This *in situ* technique has the advantage of preserving cell-cell interactions within the tumour tissue, and could therefore constitute a useful platform for monitoring changes in the tumour immune micro-environment induced by exposure to PARPi.

G. Clinical implications of the immunological potential of PARPi

Despite significant improvements in outcome brought by the advent of anti-PD-(L)1 therapies, NSCLC still represents the leading cause of cancer-related death. Limited efficacy of these agents has also been observed in TNBC so far (533). Only a minority of patients currently benefits from ICI, and strategies to turn "cold" tumours into "hot" tumours are actively investigated. Our observation that PARPi trigger cGAS/STING signalling and favour secretion of lympho-attractant chemokines such as CCL5 in *BRCA1*-mutant TNBC and ERCC1-deficient NSCLC suggests that combining PARPi and ICI could be beneficial in these histotypes. In line with our findings, preclinical data evaluating rucaparib in combination with anti-PD-(L)1 in syngeneic models of ovarian cancer have suggested a possible role for PARPi in promoting tumour lymphocytic infiltration, and increased benefit compared to anti-PD(L)1 monotherapies in *BRCA1*-mutated tumours (370). Importantly, recent data from the large randomized double-bind phase III study Keynote 189 evaluating the combination of pembrolizumab and platinum-based chemotherapy in first-line metastatic NSCLC has reported impressive benefits in PFS and OS (hazard ratio for death = 0.49; 95% confidence interval, 0.38 to 0.64; $P < 0.001$) (129). These results were practice-changing, setting up the frame for recommending anti-PD-(L)1 therapy in combination with a platinum-based doublet chemotherapy in first-line advanced NSCLC. Interestingly and contrary to previous studies evaluating anti-PD-(L)1 monotherapy, this benefit was observed across all subgroups and was independent from baseline PD-L1 tumour expression score, suggesting that other tumour characteristics – such as the DDR status – might play a role in response to this combination. Because platinum-sensitivity is a relevant phenotypical biomarker of sensitivity to PARPi (534), this suggests that PARPi – which are much better tolerated and do not have severe bone marrow toxicity – might represent an interesting alternative or complement (in the maintenance setting) to platinum-based chemotherapy in combination with anti-PD-(L)1 agents in NSCLC. Similarly, *BRCA1*-mutant TNBC might benefit from combining PARPi with ICI. Clinical trials addressing this question are underway.

In particular, an upcoming Gustave Roussy-promoted phase II trial will evaluate the efficacy of rucaparib plus atezolizumab (anti-PD-L1) in patients with DDR-deficient advanced solid tumours including but not restricted to NSCLC, UBC, HNSCC, mCRPC and biliary tract carcinoma. This academy-sponsored, industry-funded trial will include 164 patients in total from 6 centres, and is due to start at the end of 2018. Patients will be selected on the basis of (i) a molecular screening of their DDR status using an in-house DDR genes panel developed at Gustave Roussy (*ATM, BARD1, BRCA1, BRCA2, BRIP1, CDK12, CHEK2, PALB2, RAD51C, RAD51D, FANCA, NBN, RAD51, RAD54L*), or (ii) a phenotypical screening based on platinum sensitivity. Patients will be enrolled concomitantly into the different exploratory cohorts, and treatment will consist of a rucaparib monotherapy priming phase lasting 21 days, followed by a combination phase during which atezolizumab will be administered every 21 days. Disease will be assessed every 2 cycles (6 weeks) by computed tomography scan.

The primary objective of the trial will be to evaluate the anti-tumour activity of atezolizumab and rucaparib in patients with selected advanced solid tumours as measured by the ORR at 12 weeks according to Response Evaluation Criteria in Solid Tumours version 1.1 (RECIST 1.1) or Prostate Cancer Clinical Trials Working Group 3 (PCWG3) for mCRPC. Secondary objectives in terms of efficacy will be: (i) to describe the disease control rate (DCR) at 12, 18 and 24 weeks, the ORR at 18 and 24 weeks, the duration of response (DOR), best overall response rate (BORR), PFS, time to progression (TTP), and percentage of change from baseline in tumour size at 12, 18 and 24 weeks according to RECIST 1.1 or PCWG3 and according to immune-related RECIST; (ii) to evaluate the OS. Translational exploratory objectives will be: (i) to explore the relationship between the tumour DNA repair deficiency, defined as bi-allelic loss-of-function alteration (mutation and/or deletion) in at least one of the genes of the Gustave Roussy DDR genes panel, and measures of efficacy; (ii) to explore the relationship between immune-related biomarkers (including but not limited to tumour tissue PD-L1 expression by IHC, RNA gene expression profiling and DNA mutation analysis) and measures of efficacy; (iii) to evaluate the relationship between the DDR status (including but not limited to mutation of interest and γH2AX/RAD51 foci formation) and measures of efficacy; (iv) to explore the relationship between immune-related biomarkers and DNA

repair-related biomarkers, and their modification on treatment; (v) to assess whether the identified biomarkers of interest are private to each tumour type or shared across histologies. Quality of life according to the EORTC Quality of Life Questionnaire (QLQ-C30) will also be evaluated.

This clinical trial will not only inform an understanding of the clinical responses to rucaparib plus atezolizumab combinatorial therapy, but also provide insight into the histological contexts in which the combination might be best efficient, allow evaluation of the relevance of a PARPi priming phase schedule prior to combination, and ultimately enable assessment of the role of specific DDR defects as potential predictive biomarkers of response to this combination. In parallel to this study, other clinical trials evaluating distinct combinations of PARPi with anti-PD-(L)1 will also give valued data regarding the efficacy and tolerability of this therapeutic strategy in various histological and molecular contexts.

H. Final conclusion

In this study, we have shown that several clinical PARPi, including the currently licensed rucaparib, olaparib and talazoparib, elicit immunomodulatory effects in a cell-autonomous fashion in cancer cells. These effects were observed in multiple isogenic models of DDR deficiency, tumour cell lines from distinct histological origins, fresh and archived NSCLC tumour samples, and two different PDX models of *BRCA1*-defective breast cancer.

This work provides a scientific rationale for combining PARPi with anti-PD-(L)1 therapy in molecularly-selected DDR-deficient populations. While several clinical trials are currently assessing this combination in *BRCA1/2*-mutant breast or ovarian cancers, other histologies, such as NSCLC in which anti-PD-(L)1 therapies have already shown impressive results, might also benefit from such association. Basket clinical trials will be launched soon to explore this question.

References

1. Ehrlich P. Ueber Den Jetzigen Stand Der Karzinomforschung. Ned Tijdschr voor Geneeskd. 1909;
2. BURNET M. Cancer; a biological approach. I. The processes of control. Br Med J. 1957;1:779–86.
3. Burnet FM. Immunological Surveillance in Neoplasia. Immunol Rev. 1971;
4. Old LJ, Boyse EA. Immunology of Experimental Tumors. Annu Rev Med. 1964;
5. Stutman O. Tumor development after 3-methylcholanthrene in immunologically deficient athymic-nude mice. Science (80-). 1974;
6. Stutman O. Chemical carcinogenesis in nude mice: Comparison between nude mice from homozygous matings and heterozygous matings and effect of age and carcinogen dose. J Natl Cancer Inst. 1979;
7. Shankaran V, Ikeda H, Bruce AT, White JM, Swanson PE, Old LJ, et al. IFNγ, and lymphocytes prevent primary tumour development and shape tumour immunogenicity. Nature. 2001;
8. Dunn GP, Bruce AT, Ikeda H, Old LJ, Schreiber RD. Cancer immunoediting: From immunosurveillance to tumor escape. Nat Immunol. 2002;
9. Parker BS, Rautela J, Hertzog PJ. Antitumour actions of interferons: Implications for cancer therapy. Nat Rev Cancer. 2016;
10. Matsushita H, Vesely MD, Koboldt DC, Rickert CG, Uppaluri R, Magrini VJ, et al. Cancer exome analysis reveals a T-cell-dependent mechanism of cancer immunoediting. Nature. 2012;
11. O'Sullivan T, Saddawi-Konefka R, Vermi W, Koebel CM, Arthur C, White JM, et al. Cancer immunoediting by the innate immune system in the absence of adaptive immunity. J Exp Med. 2012;
12. Dunn GP, Koebel CM, Schreiber RD. Interferons, immunity and cancer immunoediting. Nat Rev Immunol. 2006;
13. Takeda K, Nakayama M, Hayakawa Y, Kojima Y, Ikeda H, Imai N, et al. IFN-γ is required for cytotoxic T cell-dependent cancer genome immunoediting. Nat Commun. 2017;
14. Williams MJ, Werner B, Barnes CP, Graham TA, Sottoriva A. Identification of neutral tumor evolution across cancer types. Nat Genet. 2016;
15. Efremova M, Rieder D, Klepsch V, Charoentong P, Finotello F, Hackl H, et al. Targeting immune checkpoints potentiates immunoediting and changes the dynamics of tumor evolution. Nat Commun. 2018;

16. Chen DS, Mellman I. Oncology meets immunology: The cancer-immunity cycle. Immunity. 2013;

17. Hanahan D, Weinberg RA. Hallmarks of cancer: The next generation. Cell. 2011;

18. Heemskerk B, Kvistborg P, Schumacher TNM. The cancer antigenome. EMBO J. Nature Publishing Group; 2013;32:194–203.

19. Coulie PG, Van Den Eynde BJ, Van Der Bruggen P, Boon T. Tumour antigens recognized by T lymphocytes: At the core of cancer immunotherapy. Nat Rev Cancer. 2014;

20. Johnsen AK, Templeton DJ, Sy M, Harding C V. Deficiency of transporter for antigen presentation (TAP) in tumor cells allows evasion of immune surveillance and increases tumorigenesis. J Immunol. 1999;

21. Tripathi SC, Peters HL, Taguchi A, Katayama H, Wang H, Momin A, et al. Immunoproteasome deficiency is a feature of non-small cell lung cancer with a mesenchymal phenotype and is associated with a poor outcome. Proc Natl Acad Sci. 2016;

22. Angell TE, Lechner MG, Jang JK, LoPresti JS, Epstein AL. MHC class I loss is a frequent mechanism of immune escape in papillary thyroid cancer that is reversed by interferon and selumetinib treatment in Vitro. Clin Cancer Res. 2014;

23. Khong HT, Restifo NP. Natural selection of tumor variants in the generation of "tumor escape" phenotypes. Nat Immunol. 2002;

24. D'Urso CM, Wang Z, Cao Y, Tatake R, Zeff RA, Ferrone S. Lack of HLA class I antigen expression by cultured melanoma cells FO-1 due to a defect in B2m gene expression. J Clin Invest. 1991;

25. Restifo NP, Marincola FM, Kawakami Y, Taubenberger J, Yannelli JR, Rosenberg SA. Loss of functional beta2-microglobulin in metastatic melanomas from five patients receiving immunotherapy. J Natl Cancer Inst. 1996;

26. Sucker A, Zhao F, Real B, Heeke C, Bielefeld N, Maßen S, et al. Genetic evolution of T-cell resistance in the course of melanoma progression. Clin Cancer Res. 2014;

27. Gettinger S, Choi J, Hastings K, Truini A, Datar I, Sowell R, et al. Impaired HLA class I antigen processing and presentation as a mechanism of acquired resistance to immune checkpoint inhibitors in lung cancer. Cancer Discov. 2017;

28. Yoshihama S, Roszik J, Downs I, Meissner TB, Vijayan S, Chapuy B, et al. NLRC5/MHC class I transactivator is a target for immune evasion in cancer. Proc Natl Acad Sci. 2016;

29. Ozcan M, Janikovits J, von Knebel Doeberitz M, Kloor M. Complex pattern of immune evasion in MSI colorectal cancer. Oncoimmunology. 2018;

30. Davoli T, Uno H, Wooten EC, Elledge SJ. Tumor aneuploidy correlates with markers of immune evasion and with reduced response to immunotherapy. Science (80-). 2017;

31. Chabanon RM, Pedrero M, Lefebvre C, Marabelle A, Soria JC, Postel-Vinay S.

Mutational landscape and sensitivity to immune checkpoint blockers. Clin Cancer Res. 2016;22:4309–21.

32. Zhu J, Powis De Tenbossche CG, Cané S, Colau D, Van Baren N, Lurquin C, et al. Resistance to cancer immunotherapy mediated by apoptosis of tumor-infiltrating lymphocytes. Nat Commun. 2017;

33. Horton BL, Williams JB, Cabanov A, Spranger S, Gajewski TF. Intratumoral CD8+ T-Cell Apoptosis is a Major Component of T Cell Dysfunction and Impedes Anti-Tumor Immunity. Cancer Immunol Res. 2017;

34. Weiskopf K, Jahchan NS, Schnorr PJ, Cristea S, Ring AM, Maute RL, et al. CD47-blocking immunotherapies stimulate macrophage-mediated destruction of small-cell lung cancer. J Clin Invest. 2016;

35. Jaiswal S, Jamieson CHM, Pang WW, Park CY, Chao MP, Majeti R, et al. CD47 Is Upregulated on Circulating Hematopoietic Stem Cells and Leukemia Cells to Avoid Phagocytosis. Cell. 2009;

36. Tauriello DVF, Palomo-Ponce S, Stork D, Berenguer-Llergo A, Badia-Ramentol J, Iglesias M, et al. TGFβ drives immune evasion in genetically reconstituted colon cancer metastasis. Nature. 2018;

37. Kim R, Emi M, Tanabe K, Arihiro K. Tumor-driven evolution of immunosuppressive networks during malignant progression. Cancer Res. 2006;

38. Spranger S, Gajewski TF. Impact of oncogenic pathways on evasion of antitumour immune responses. Nat Rev Cancer. 2018;

39. Kearney CJ, Vervoort SJ, Hogg SJ, Ramsbottom KM, Freeman AJ, Lalaoui N, et al. Tumor immune evasion arises through loss of TNF sensitivity. Sci Immunol. 2018;

40. Katlinski K V., Gui J, Katlinskaya Y V., Ortiz A, Chakraborty R, Bhattacharya S, et al. Inactivation of Interferon Receptor Promotes the Establishment of Immune Privileged Tumor Microenvironment. Cancer Cell. 2017;

41. Liu Y, Cao X. Immunosuppressive cells in tumor immune escape and metastasis. J Mol Med. 2015;

42. Facciabene A, Motz GT, Coukos G. T-Regulatory cells: Key players in tumor immune escape and angiogenesis. Cancer Res. 2012.

43. Highfill SL, Cui Y, Giles AJ, Smith JP, Zhang H, Morse E, et al. Disruption of CXCR2-mediated MDSC tumor trafficking enhances anti-PD1 efficacy. Sci Transl Med. 2014;

44. Umansky V, Blattner C, Gebhardt C, Utikal J. The Role of Myeloid-Derived Suppressor Cells (MDSC) in Cancer Progression. Vaccines. 2016;

45. Pardoll DM. The blockade of immune checkpoints in cancer immunotherapy. Nat Rev Cancer. 2012;

46. Topalian SL, Drake CG, Pardoll DM. Immune checkpoint blockade: A common denominator approach to cancer therapy. Cancer Cell. 2015;27:451–61.

47. Chen DS, Irving BA, Hodi FS. Molecular pathways: Next-generation immunotherapy-

inhibiting programmed death-ligand 1 and programmed death-1. Clin Cancer Res. 2012;

48. Dong H, Strome SE, Salomao DR, Tamura H, Hirano F, Flies DB, et al. Tumor-associated B7-H1 promotes T-cell apoptosis: a potential mechanism of immune evasion. Nat Med. 2002;8:793–800.

49. Akbay EA, Koyama S, Carretero J, Altabef A, Tchaicha JH, Christensen CL, et al. Activation of the PD-1 pathway contributes to immune escape in EGFR-driven lung tumors. Cancer Discov. American Association for Cancer Research; 2013;3:1355–63.

50. Kim MH, Kim CG, Kim S-K, Shin SJ, Choe EA, Park S-H, et al. YAP-induced PD-L1 expression drives immune evasion in BRAFi-resistant melanoma. Cancer Immunol Res. 2018;

51. Juneja VR, McGuire KA, Manguso RT, LaFleur MW, Collins N, Haining WN, et al. PD-L1 on tumor cells is sufficient for immune evasion in immunogenic tumors and inhibits CD8 T cell cytotoxicity. J Exp Med. 2017;

52. Wischhusen J, Jung G, Radovanovic I, Beier C, Steinbach JP, Rimner A, et al. Identification of CD70-mediated apoptosis of immune effector cells as a novel immune escape pathway of human glioblastoma. Cancer Res. 2002;

53. Junker K, Hindermann W, von Eggeling F, Diegmann J, Haessler K, Schubert J. CD70: a new tumor specific biomarker for renal cell carcinoma. J Urol. 2005;

54. Yang J, Zhu L, Cai Y, Suo J, Jin J. Role of downregulation of galectin-9 in the tumorigenesis of gastric cancer. Int J Oncol. 2014;

55. Martin-Orozco N, Li Y, Wang Y, Liu S, Hwu P, Liu YJ, et al. Melanoma cells express ICOS ligand to promote the activation and expansion of T-regulatory cells. Cancer Res. 2010;

56. Kataoka K, Shiraishi Y, Takeda Y, Sakata S, Matsumoto M, Nagano S, et al. Aberrant PD-L1 expression through 3′-UTR disruption in multiple cancers. Nature. 2016;

57. Coelho MA, de Carné Trécesson S, Rana S, Zecchin D, Moore C, Molina-Arcas M, et al. Oncogenic RAS Signaling Promotes Tumor Immunoresistance by Stabilizing PD-L1 mRNA. Immunity. 2017;

58. Casey SC, Tong L, Li Y, Do R, Walz S, Fitzgerald KN, et al. MYC regulates the antitumor immune response through CD47 and PD-L1. Science (80-). 2016;

59. Lastwika KJ, Wilson W, Li QK, Norris J, Xu H, Ghazarian SR, et al. Control of PD-L1 expression by oncogenic activation of the AKT-mTOR pathway in non-small cell lung cancer. Cancer Res. 2016;

60. An G, Acharya C, Feng X, Wen K, Zhong M, Zhang L, et al. Osteoclasts promote immune suppressive microenvironment in multiple myeloma: Therapeutic implication. Blood. 2016;

61. Hsu JM, Xia W, Hsu YH, Chan LC, Yu WH, Cha JH, et al. STT3-dependent PD-L1 accumulation on cancer stem cells promotes immune evasion. Nat Commun. 2018;

62. Sasidharan Nair V, El Salhat H, Taha RZ, John A, Ali BR, Elkord E. DNA methylation

and repressive H3K9 and H3K27 trimethylation in the promoter regions of PD-1, CTLA-4, TIM-3, LAG-3, TIGIT, and PD-L1 genes in human primary breast cancer. Clin Epigenetics. 2018;

63. Chen LL, Gibbons DL, Goswami S, Cortez MA, Ahn Y-H, Byers L a, et al. Metastasis is regulated via microRNA-200/ZEB1 axis control of tumour cell PD-L1 expression and intratumoral immunosuppression. Nat Commun. 2014;5:5241.

64. Taube JM, Anders RA, Young GD, Xu H, Sharma R, McMiller TL, et al. Colocalization of inflammatory response with B7-h1 expression in human melanocytic lesions supports an adaptive resistance mechanism of immune escape. Sci Transl Med. 2012;4:127ra37.

65. Spranger S, Spaapen RM, Zha Y, Williams J, Meng Y, Ha TT, et al. Up-regulation of PD-L1, IDO, and Tregs in the melanoma tumor microenvironment is driven by CD8+ T cells. Sci Transl Med. 2013;

66. Coley WB. The treatment of malignant tumors by repeated inoculations of erysipelas. With a report of ten original cases. 1893. Am J Med Sci. 1893;

67. Old LJ, Clarke DA, Benacerraf B. Effect of bacillus calmette-guérin infection on transplanted tumours in the mouse. Nature. 1959;

68. Morton DL, Eilber FR, Joseph WL, Wood WC, Trahan E, Ketcham AS. Immunological factors in human sarcomas and melanomas: a rational basis for immunotherapy. Ann Surg. 1970;

69. Isaacs A, Lindenmann J. Virus Interference: I. The Interferon. Proc R Soc London. 1957;

70. Paucker K, Cantell K, Henle W. Quantitative studies on viral interference in suspended L cells. III. Effect of interfering viruses and interferon on the growth rate of cells. Virology. 1962;

71. Gresser I, Bourali C, Lévy JP, Fontaine-Brouty-Boyé D, Thomas MT. Increased survival in mice inoculated with tumor cells and treated with interferon preparations. Proc Natl Acad Sci U S A. 1969;

72. Kirkwood JM, Ernstoff MS, Davis CA, Reiss M, Ferraresi R, Rudnick SA. Comparison of intramuscular and intravenous recombinant alpha-2 interferon in melanoma and other cancers. Ann Intern Med. 1985;

73. Lotze MT, Chang AE, Seipp CA, Simpson C, Vetto JT, Rosenberg SA. High-Dose Recombinant Interleukin 2 in the Treatment of Patients With Disseminated Cancer: Responses, Treatment-Related Morbidity, and Histologic Findings. JAMA J Am Med Assoc. 1986;

74. Grimm EA, Mazumder A, Zhang HZ, Rosenberg SA. Lymphokine-activated killer cell phenomenon. Lysis of natural killer-resistant fresh solid tumor cells by interleukin 2-activated autologous human peripheral blood lymphocytes. J Exp Med. 1982;

75. Rosenberg SA, Lotze MT, Muul LM, Leitman S, Chang AE, Ettinghausen SE, et al. Observations on the systemic administration of autologous lymphokine-activated

killer cells and recombinant interleukin-2 to patients with metastatic cancer. N Engl J Med. 1985;

76. Rosenberg SA, Packard BS, Aebersold PM, Solomon D, Topalian SL, Toy ST, et al. Use of tumor-infiltrating lymphocytes and interleukin-2 in the immunotherapy of patients with metastatic melanoma: a preliminary report. N Engl J Med. 1988;

77. Köhler G, Milstein C. Continuous cultures of fused cells secreting antibody of predefined specificity. Nature. 1975;

78. Miller RA, Maloney DG, Warnke R, Levy R. Treatment of B-Cell Lymphoma with Monoclonal Anti-Idiotype Antibody. N Engl J Med. 1982;

79. Eiermann W. Trastuzumab combined with chemotherapy for the treatment of HER2-positive metastatic breast cancer: pivotal trial data. Ann Oncol. 2001;

80. Yang JC, Haworth L, Sherry RM, Hwu P, Schwartzentruber DJ, Topalian SL, et al. A randomized trial of bevacizumab, an anti-vascular endothelial growth factor antibody, for metastatic renal cancer. N Engl J Med. 2003;

81. Jonker DJ, O'Callaghan CJ, Karapetis CS, Zalcberg JR, Tu D, Au H-J, et al. Cetuximab for the treatment of colorectal cancer. N Engl J Med. 2007;

82. Bonner JA, Harari PM, Giralt J, Azarnia N, Shin DM, Cohen RB, et al. Radiotherapy plus Cetuximab for Squamous-Cell Carcinoma of the Head and Neck. N Engl J Med. 2006;

83. Brunet J-F, Denizot F, Luciani M-F, Roux-Dosseto M, Suzan M, Mattei M-G, et al. A new member of the immunoglobulin superfamily—CTLA-4. Nature. 1987;

84. Nishimura H, Nose M, Hiai H, Minato N, Honjo T. Development of lupus-like autoimmune diseases by disruption of the PD-1 gene encoding an ITIM motif-carrying immunoreceptor. Immunity. 1999;

85. Wang S, Bajorath J, Flies DB, Dong H, Honjo T, Chen L. Molecular Modeling and Functional Mapping of B7-H1 and B7-DC Uncouple Costimulatory Function from PD-1 Interaction. J Exp Med. 2003;

86. Smith MR. Rituximab (monoclonal anti-CD20 antibody): Mechanisms of action and resistance. Oncogene. 2003;

87. Park SG, Jiang Z, Mortenson ED, Deng L, Radkevich-Brown O, Yang X, et al. The therapeutic effect of anti-HER2/neu antibody depends on both innate and adaptive immunity. Cancer Cell. 2010;

88. Heiss MM, Murawa P, Koralewski P, Kutarska E, Kolesnik OO, Ivanchenko V V., et al. The trifunctional antibody catumaxomab for the treatment of malignant ascites due to epithelial cancer: Results of a prospective randomized phase II/III trial. Int J Cancer. 2010;

89. Gökbuget N, Dombret H, Bonifacio M, Reichle A, Graux C, Faul C, et al. Blinatumomab for minimal residual disease in adults with B-precursor acute lymphoblastic leukemia. Blood. 2018;

90. Kantarjian H, Stein A, Gökbuget N, Fielding AK, Schuh AC, Ribera J-M, et al.

Blinatumomab versus Chemotherapy for Advanced Acute Lymphoblastic Leukemia. N Engl J Med. 2017;

91. Lotze MT, Grimm EA, Mazumder A, Strausser JL, Rosenberg SA. Lysis of fresh and cultured autologous tumor by human lymphocytes cultured in T-cell growth factor. Cancer Res. 1981;

92. Lu PH, Negrin RS. A novel population of expanded human CD3+CD56+ cells derived from T cells with potent in vivo antitumor activity in mice with severe combined immunodeficiency. J Immunol. 1994;

93. Mule J, Shu S, Schwarz S, Rosenberg S. Adoptive immunotherapy of established pulmonary metastases with LAK cells and recombinant interleukin-2. Science (80-). 1984;

94. Parkhurst MR, Riley JP, Dudley ME, Rosenberg SA. Adoptive transfer of autologous natural killer cells leads to high levels of circulating natural killer cells but does not mediate tumor regression. Clin Cancer Res. 2011;

95. Gao X, Mi Y, Guo N, Xu H, Xu L, Gou X, et al. Cytokine-Induced killer cells as pharmacological tools for cancer immunotherapy. Front Immunol. 2017;

96. June CH, O'Connor RS, Kawalekar OU, Ghassemi S, Milone MC. CAR T cell immunotherapy for human cancer. Science (80-). 2018;

97. Kershaw MH, Westwood JA, Darcy PK. Gene-engineered T cells for cancer therapy. Nat Rev Cancer. 2013;

98. Brentjens RJ, Davila ML, Riviere I, Park J, Wang X, Cowell LG, et al. CD19-targeted T cells rapidly induce molecular remissions in adults with chemotherapy-refractory acute lymphoblastic leukemia. Sci Transl Med. 2013;

99. Neelapu SS, Locke FL, Bartlett NL, Lekakis LJ, Miklos DB, Jacobson CA, et al. Axicabtagene Ciloleucel CAR T-Cell Therapy in Refractory Large B-Cell Lymphoma. N Engl J Med. 2017;

100. Dranoff G, Jaffee E, Lazenby A, Golumbek P, Levitsky H, Brose K, et al. Vaccination with irradiated tumor cells engineered to secrete murine granulocyte-macrophage colony-stimulating factor stimulates potent, specific, and long-lasting anti-tumor immunity. Proc Natl Acad Sci. 1993;

101. Schwartzentruber DJ, Lawson DH, Richards JM, Conry RM, Miller DM, Treisman J, et al. gp100 Peptide Vaccine and Interleukin-2 in Patients with Advanced Melanoma. N Engl J Med. 2011;

102. Gérard C, Baudson N, Ory T, Louahed J. Tumor mouse model confirms MAGE-A3 cancer immunotherapeutic as an efficient inducer of long-lasting anti-tumoral responses. PLoS One. 2014;

103. Lemoine FM, Cherai M, Giverne C, Dimitri D, Rosenzwajg M, Trebeden-Negre H, et al. Massive expansion of regulatory T-cells following interleukin 2 treatment during a phase I-II dendritic cell-based immunotherapy of metastatic renal cancer. Int J Oncol. 2009;

104. Kantoff PW, Higano CS, Shore ND, Berger ER, Small EJ, Penson DF, et al. Sipuleucel-T Immunotherapy for Castration-Resistant Prostate Cancer. N Engl J Med. 2010;

105. Lamm DL, Blumenstein BA, Crawford ED, Montie JE, Scardino P, Grossman HB, et al. A Randomized Trial of Intravesical Doxorubicin and Immunotherapy with Bacille Calmette–Guérin for Transitional-Cell Carcinoma of the Bladder. N Engl J Med. 1991;

106. Schölch S, Rauber C, Tietz A, Rahbari NN, Bork U, Schmidt T, et al. Radiotherapy combined with TLR7/8 activation induces strong immune responses against gastrointestinal tumors. Oncotarget. 2015;

107. Iribarren K, Bloy N, Buqué A, Cremer I, Eggermont A, Fridman WH, et al. Trial Watch: Immunostimulation with Toll-like receptor agonists in cancer therapy. Oncoimmunology. 2016;

108. Negrier S, Escudier B, Lasset C, Douillard J-Y, Savary J, Chevreau C, et al. Recombinant Human Interleukin-2, Recombinant Human Interferon Alfa-2a, or Both in Metastatic Renal-Cell Carcinoma. N Engl J Med. 1998;

109. Topalian SL, Taube JM, Anders RA, Pardoll DM. Mechanism-driven biomarkers to guide immune checkpoint blockade in cancer therapy. Nat Rev Cancer. 2016;

110. Weber JS, O'Day S, Urba W, Powderly J, Nichol G, Yellin M, et al. Phase I/II study of ipilimumab for patients with metastatic melanoma. J Clin Oncol. 2008;

111. Hodi FS, O'Day SJ, McDermott DF, Weber RW, Sosman JA, Haanen JB, et al. Improved survival with ipilimumab in patients with metastatic melanoma. N Engl J Med. 2010;363:711–23.

112. Ribas A, Kefford R, Marshall MA, Punt CJA, Haanen JB, Marmol M, et al. Phase III randomized clinical trial comparing tremelimumab with standard-of-care chemotherapy in patients with advanced melanoma. J Clin Oncol. 2013;

113. Topalian SL, Hodi FS, Brahmer JR, Gettinger SN, Smith DC, McDermott DF, et al. Safety, activity, and immune correlates of anti-PD-1 antibody in cancer. N Engl J Med. 2012;366:2443–54.

114. Robert C, Soria JC, Eggermont AMM. Drug of the year: Programmed Death-1 receptor/Programmed Death-1 Ligand-1 receptor monoclonal antibodies. Eur J Cancer. 2013;49:2968–71.

115. Robert C, Schachter J, Long G V, Arance A, Grob JJ, Mortier L, et al. Pembrolizumab versus Ipilimumab in Advanced Melanoma. N Engl J Med. 2015;372:2521–32.

116. Robert C, Long G V., Brady B, Dutriaux C, Maio M, Mortier L, et al. Nivolumab in previously untreated melanoma without BRAF mutation. N Engl J Med. 2015;372:320–30.

117. Brahmer JR, Rodríguez-Abreu D, Robinson AG, Hui R, Csőszi T, Fülöp A, et al. Health-related quality-of-life results for pembrolizumab versus chemotherapy in advanced, PD-L1-positive NSCLC (KEYNOTE-024): a multicentre, international, randomised, open-label phase 3 trial. Lancet Oncol. 2017;

118. Borghaei H, Paz-Ares L, Horn L, Spigel DR, Steins M, Ready NE, et al. Nivolumab

versus Docetaxel in Advanced Nonsquamous Non-Small-Cell Lung Cancer. N Engl J Med. 2015;373:1627–39.

119. Ferris RL, Blumenschein G, Fayette J, Guigay J, Colevas AD, Licitra L, et al. Nivolumab for Recurrent Squamous-Cell Carcinoma of the Head and Neck. N Engl J Med. 2016;

120. Motzer RJ, Escudier B, McDermott DF, George S, Hammers HJ, Srinivas S, et al. Nivolumab versus Everolimus in Advanced Renal-Cell Carcinoma. N Engl J Med. 2015;1803–13.

121. Le DT, Uram JN, Wang H, Bartlett BR, Kemberling H, Eyring AD, et al. PD-1 Blockade in Tumors with Mismatch-Repair Deficiency. N Engl J Med. 2015;372:2509–20.

122. Bellmunt J, de Wit R, Vaughn DJ, Fradet Y, Lee J-L, Fong L, et al. Pembrolizumab as Second-Line Therapy for Advanced Urothelial Carcinoma. N Engl J Med. 2017;

123. Shitara K, Özgüroğlu M, Bang YJ, Bartolomeo M Di, Mandalà M, Ryu MH, et al. Pembrolizumab versus paclitaxel for previously treated, advanced gastric or gastro-oesophageal junction cancer (KEYNOTE-061): a randomised, open-label, controlled, phase 3 trial. Lancet. 2018;

124. Frenel JS, Le Tourneau C, O'Neil B, Ott PA, Piha-Paul SA, Gomez-Roca C, et al. Safety and efficacy of pembrolizumab in advanced, programmed death ligand 1-positive cervical cancer: Results from the phase IB KEYNOTE-028 trial. J Clin Oncol. 2017.

125. Kaufman HL, Russell J, Hamid O, Bhatia S, Terheyden P, D'Angelo SP, et al. Avelumab in patients with chemotherapy-refractory metastatic Merkel cell carcinoma: a multicentre, single-group, open-label, phase 2 trial. Lancet Oncol. 2016;

126. Moskowitz CH, Zinzani PL, Fanale MA, Armand P, Johnson NA, Radford JA, et al. Pembrolizumab in Relapsed/Refractory Classical Hodgkin Lymphoma: Primary End Point Analysis of the Phase 2 Keynote-087 Study. Blood. 2016;

127. Gettinger S, Horn L, Jackman D, Spigel D, Antonia S, Hellmann M, et al. Five-year follow-up of nivolumab in previously treated advanced non–small-cell lung cancer: Results from the CA209-003 study. J Clin Oncol. 2018;

128. Reck M, Rodríguez-Abreu D, Robinson AG, Hui R, Csőszi T, Fülöp A, et al. Pembrolizumab versus Chemotherapy for PD-L1–Positive Non–Small-Cell Lung Cancer. N Engl J Med. 2016;

129. Gandhi L, Rodríguez-Abreu D, Gadgeel S, Esteban E, Felip E, De Angelis F, et al. Pembrolizumab plus Chemotherapy in Metastatic Non–Small-Cell Lung Cancer. N Engl J Med. 2018;

130. Langer CJ, Gadgeel SM, Borghaei H, Papadimitrakopoulou VA, Patnaik A, Powell SF, et al. Carboplatin and pemetrexed with or without pembrolizumab for advanced, non-squamous non-small-cell lung cancer: a randomised, phase 2 cohort of the open-label KEYNOTE-021 study. Lancet Oncol. 2016;

131. Herbst RS, Baas P, Kim DW, Felip E, Pérez-Gracia JL, Han JY, et al. Pembrolizumab versus docetaxel for previously treated, PD-L1-positive, advanced non-small-cell lung cancer (KEYNOTE-010): A randomised controlled trial. Lancet. 2015;

132. Garon EB, Rizvi NA, Hui R, Leighl N, Balmanoukian AS, Eder JP, et al. Pembrolizumab for the treatment of non-small-cell lung cancer. N Engl J Med. 2015;372:2018–28.

133. Hellmann MD, Ciuleanu T-E, Pluzanski A, Lee JS, Otterson GA, Audigier-Valette C, et al. Nivolumab plus Ipilimumab in Lung Cancer with a High Tumor Mutational Burden. N Engl J Med. 2018;

134. Brahmer J, Reckamp K, Baas P, Crinò L, Eberhardt W, Poddubskaya E, et al. Nivolumab versus Docetaxel in Advanced Squamous-Cell Non-Small-Cell Lung Cancer. N Engl J Med. 2015;

135. Socinski MA, Jotte RM, Cappuzzo F, Orlandi F, Stroyakovskiy D, Nogami N, et al. Atezolizumab for First-Line Treatment of Metastatic Nonsquamous NSCLC. N Engl J Med. 2018;

136. Fehrenbacher L, Spira A, Ballinger M, Kowanetz M, Vansteenkiste J, Mazieres J, et al. Atezolizumab versus docetaxel for patients with previously treated non-small-cell lung cancer (POPLAR): a multicentre, open-label, phase 2 randomised controlled trial. Lancet. 2016;

137. Rittmeyer A, Barlesi F, Waterkamp D, Park K, Ciardiello F, von Pawel J, et al. Atezolizumab versus docetaxel in patients with previously treated non-small-cell lung cancer (OAK): a phase 3, open-label, multicentre randomised controlled trial. Lancet. 2017;

138. Antonia SJ, Villegas A, Daniel D, Vicente D, Murakami S, Hui R, et al. Overall Survival with Durvalumab after Chemoradiotherapy in Stage III NSCLC. N Engl J Med. 2018;

139. Barlesi F, Vansteenkiste J, Spigel D, Ishii H, Garassino M, de Marinis F, et al. Avelumab versus docetaxel in patients with platinum-treated advanced non-small-cell lung cancer (JAVELIN Lung 200): an open-label, randomised, phase 3 study. Lancet Oncol. 2018;

140. Postow MA, Chesney J, Pavlick AC, Robert C, Grossmann K, McDermott D, et al. Nivolumab and Ipilimumab versus Ipilimumab in Untreated Melanoma. N Engl J Med. 2015;

141. Larkin J, Chiarion-Sileni V, Gonzalez R, Grob JJ, Cowey CL, Lao CD, et al. Combined Nivolumab and Ipilimumab or Monotherapy in Untreated Melanoma. N Engl J Med. 2015;

142. Mezquita L, Planchard D. Durvalumab for the treatment of non-small cell lung cancer. Expert Rev Respir Med. 2018;

143. Stauss HJ, Van Waes C, Fink MA, Starr B, Schreiber H. Identification of a unique tumor antigen as rejection antigen by molecular cloning and gene transfer. J Exp Med. 1986;

144. Yadav M, Jhunjhunwala S, Phung QT, Lupardus P, Tanguay J, Bumbaca S, et al. Predicting immunogenic tumour mutations by combining mass spectrometry and exome sequencing. Nature. 2014;

145. Gubin MM, Zhang X, Schuster H, Caron E, Ward JP, Noguchi T, et al. Checkpoint

blockade cancer immunotherapy targets tumour-specific mutant antigens. Nature. 2014;515:577–81.

146. Robbins PF, Lu YC, El-Gamil M, Li YF, Gross C, Gartner J, et al. Mining exomic sequencing data to identify mutated antigens recognized by adoptively transferred tumor-reactive T cells. Nat Med. 2013;

147. Linnemann C, Van Buuren MM, Bies L, Verdegaal EME, Schotte R, Calis JJA, et al. High-throughput epitope discovery reveals frequent recognition of neo-antigens by CD4+T cells in human melanoma. Nat Med. 2015;

148. Schumacher TN, Schreiber RD. Neoantigens in cancer immunotherapy. Science (80-). 2015;348:69–74.

149. Snyder A, Makarov V, Merghoub T, Yuan J, Zaretsky JM, Desrichard A, et al. Genetic Basis for Clinical Response to CTLA-4 Blockade in Melanoma. N Engl J Med. 2014;2189–99.

150. Van Allen EM, Miao D, Schilling B, Shukla SA, Blank C, Zimmer L, et al. Genomic correlates of response to CTLA-4 blockade in metastatic melanoma. Science (80-). 2015;350:207–11.

151. Rizvi NA, Hellmann MD, Snyder A, Kvistborg P, Makarov V, Havel JJ, et al. Cancer immunology. Mutational landscape determines sensitivity to PD-1 blockade in non-small cell lung cancer. Science (80-). 2015;

152. Van Rooij N, Van Buuren MM, Philips D, Velds A, Toebes M, Heemskerk B, et al. Tumor exome analysis reveals neoantigen-specific T-cell reactivity in an ipilimumab-responsive melanoma. J Clin Oncol. 2013;31:439–42.

153. Hugo W, Zaretsky JM, Sun L, Song C, Moreno BH, Hu-Lieskovan S, et al. Genomic and Transcriptomic Features of Response to Anti-PD-1 Therapy in Metastatic Melanoma. Cell. 2016;

154. Ansell SM, Lesokhin AM, Borrello I, Halwani A, Scott EC, Gutierrez M, et al. PD-1 Blockade with Nivolumab in Relapsed or Refractory Hodgkin's Lymphoma. N Engl J Med. 2014;1–9.

155. McGranahan N, Furness AJS, Rosenthal R, Ramskov S, Lyngaa R, Saini SK, et al. Clonal neoantigens elicit T cell immunoreactivity and sensitivity to immune checkpoint blockade. Science (80-). 2016;

156. Taube JM, Klein A, Brahmer JR, Xu H, Pan X, Kim JH, et al. Association of PD-1, PD-1 ligands, and other features of the tumor immune microenvironment with response to anti-PD-1 therapy. Clin Cancer Res. 2014;20:5064–74.

157. Passiglia F, Bronte G, Bazan V, Natoli C, Rizzo S, Galvano A, et al. PD-L1 expression as predictive biomarker in patients with NSCLC: a pooled analysis. Oncotarget. 2016;

158. Maleki Vareki S, Garrigós C, Duran I. Biomarkers of response to PD-1/PD-L1 inhibition. Crit Rev Oncol Hematol. 2017;

159. Khunger M, Hernandez A V., Pasupuleti V, Rakshit S, Pennell NA, Stevenson J, et al. Programmed Cell Death 1 (PD-1) Ligand (PD-L1) Expression in Solid Tumors As a

Predictive Biomarker of Benefit From PD-1/PD-L1 Axis Inhibitors: A Systematic Review and Meta-Analysis. JCO Precis Oncol. 2017;

160. Patel SP, Kurzrock R. PD-L1 Expression as a Predictive Biomarker in Cancer Immunotherapy. Mol Cancer Ther. 2015;14:847–56.

161. Kerr KM, Tsao M-S, Nicholson AG, Yatabe Y, Wistuba II, Hirsch FR. Programmed Death-Ligand 1 Immunohistochemistry in Lung Cancer: In what state is this art? J Thorac Oncol. 2015;10:985–9.

162. Madore J, Vilain RE, Menzies AM, Kakavand H, Wilmott JS, Hyman J, et al. PD-L1 expression in melanoma shows marked heterogeneity within and between patients: Implications for anti-PD-1/PD-L1 clinical trials. Pigment Cell Melanoma Res. 2015;28:245–53.

163. MacMicking JD. Interferon-inducible effector mechanisms in cell-autonomous immunity. Nat Rev Immunol. 2012;12:367–82.

164. Klemm F, Joyce JA. Microenvironmental regulation of therapeutic response in cancer. Trends Cell Biol. 2015;

165. Binnewies M, Roberts EW, Kersten K, Chan V, Fearon DF, Merad M, et al. Understanding the tumor immune microenvironment (TIME) for effective therapy. Nat Med. 2018;

166. Huh JW, Lee JH, Kim HR. Prognostic significance of tumor-infiltrating lymphocytes for patients with colorectal cancer. Arch Surg. 2012;

167. Thomas NE, Busam KJ, From L, Kricker A, Armstrong BK, Anton-Culver H, et al. Tumor-infiltrating lymphocyte grade in primary melanomas is independently associated with melanoma-specific survival in the population-based genes, environment and melanoma study. J Clin Oncol. 2013;

168. Zeng D-Q, Yu Y-F, Ou Q-Y, Li X-Y, Zhong R-Z, Xie C-M, et al. Prognostic and predictive value of tumor-infiltrating lymphocytes for clinical therapeutic research in patients with non-small cell lung cancer. Oncotarget. 2016;

169. Gajewski TF, Louahed J, Brichard VG. Gene signature in melanoma associated with clinical activity a potential clue to unlock cancer immunotherapy. Cancer J. 2010;

170. Sullivan RJ, Hoshida Y, Brunet J, Tahan S, Aldridge J, Kwabi C, et al. A single center experience with high-dose (HD) IL-2 treatment for patients with advanced melanoma and pilot investigation of a novel gene expression signature as a predictor of response. J Clin Oncol. 2009;

171. Hamid O, Schmidt H, Nissan A, Ridolfi L, Aamdal S, Hansson J, et al. A prospective phase II trial exploring the association between tumor microenvironment biomarkers and clinical activity of ipilimumab in advanced melanoma. J Transl Med. 2011;

172. Tumeh PC, Harview CL, Yearley JH, Shintaku IP, Taylor EJM, Robert L, et al. PD-1 Blockade Induces Responses by Inhibiting Adaptive Immune Resistance. Nature. 2015;515:568–71.

173. Hu-Lieskovan S, Goldman J, Han M, Zaretsky J, Shintaku I, Wolf B, et al. High

intratumoral T-cell infiltration correlated with mutational load and response to pembrolizumab in non-small cell lung cancer. [abstract]. Proc 16th World Conf Lung Cancer; 6-9 Sept 2015; Denver, USA, 2015; Abstr nr ORAL3105.

174. Gibney GT, Weiner LM, Atkins MB. Predictive biomarkers for checkpoint inhibitor-based immunotherapy. Lancet Oncol. 2016;

175. Spranger S, Luke JJ, Bao R, Zha Y, Hernandez KM, Li Y, et al. Density of immunogenic antigens does not explain the presence or absence of the T-cell–inflamed tumor microenvironment in melanoma. Proc Natl Acad Sci. 2016;

176. Rooney MS, Shukla SA, Wu CJ, Getz G, Hacohen N. Molecular and genetic properties of tumors associated with local immune cytolytic activity. Cell. Elsevier Inc.; 2015;160:48–61.

177. Tang H, Wang Y, Chlewicki LK, Zhang Y, Guo J, Liang W, et al. Facilitating T Cell Infiltration in Tumor Microenvironment Overcomes Resistance to PD-L1 Blockade. Cancer Cell. 2016;

178. Mazzaschi G, Madeddu D, Falco A, Bocchialini G, Goldoni M, Sogni F, et al. Low PD-1 expression in cytotoxic CD8+ tumor-Infiltrating lymphocytes confers an immune-privileged tissue microenvironment in NSCLC with a prognostic and predictive value. Clin Cancer Res. 2018;

179. Koyama S, Akbay EA, Li YY, Herter-Sprie GS, Buczkowski KA, Richards WG, et al. Adaptive resistance to therapeutic PD-1 blockade is associated with upregulation of alternative immune checkpoints. Nat Commun. 2016;

180. Newman AM, Liu CL, Green MR, Gentles AJ, Feng W, Xu Y, et al. Robust enumeration of cell subsets from tissue expression profiles. Nat Methods. 2015;

181. Aran D, Hu Z, Butte AJ. xCell: Digitally portraying the tissue cellular heterogeneity landscape. Genome Biol. 2017;

182. Bindea G, Mlecnik B, Tosolini M, Kirilovsky A, Waldner M, Obenauf A, et al. Spatiotemporal Dynamics of Intratumoral Immune Cells Reveal the Immune Landscape in Human Cancer. Immunity. 2013;

183. Ji RR, Chasalow SD, Wang L, Hamid O, Schmidt H, Cogswell J, et al. An immune-active tumor microenvironment favors clinical response to ipilimumab. Cancer Immunol Immunother. 2012;

184. Ribas A, Robert C, Hodi FS, Wolchok JD, Joshua AM, Hwu WJ, et al. Association of response to programmed death receptor 1 (PD-1) blockade with pembrolizumab (MK-3475) with an interferon-inflammatory immune gene signature. J Clin Oncol. 2015;

185. Johnson DB, Estrada M V., Salgado R, Sanchez V, Doxie DB, Opalenik SR, et al. Melanoma-specific MHC-II expression represents a tumour-autonomous phenotype and predicts response to anti-PD-1/PD-L1 therapy. Nat Commun. 2016;

186. Weide B, Martens A, Hassel JC, Berking C, Postow MA, Bisschop K, et al. Baseline biomarkers for outcome of melanoma patients treated with pembrolizumab. Clin

Cancer Res. 2016;

187. Herbst RS, Soria J-C, Kowanetz M, Fine GD, Hamid O, Gordon MS, et al. Predictive correlates of response to the anti-PD-L1 antibody MPDL3280A in cancer patients. Nature. Nature Publishing Group; 2014;515:563–7.

188. Postow MA, Manuel M, Wong P, Yuan J, Dong Z, Liu C, et al. Peripheral T cell receptor diversity is associated with clinical outcomes following ipilimumab treatment in metastatic melanoma. J Immunother Cancer. 2015;

189. Tanneau I, Nondé A, Courtier A, Parmentier G, Noël M, Grivès A, et al. ImmunTraCkeR® as a reliable TCR repertoire profiling tool to understand immune response and to explore immunotherapy biomarkers. J Immunother Cancer. 2013;

190. Powles T, Eder JP, Fine GD, Braiteh FS, Loriot Y, Cruz C, et al. MPDL3280A (anti-PD-L1) treatment leads to clinical activity in metastatic bladder cancer. Nature. 2014;515:558–62.

191. Kamphorst AO, Pillai RN, Yang S, Nasti TH, Akondy RS, Wieland A, et al. Proliferation of PD-1+ CD8 T cells in peripheral blood after PD-1-targeted therapy in lung cancer patients. Proc Natl Acad Sci U S A. 2017;

192. Choueiri TK, Fishman M, Escudier B, McDermott DF, Drake CG, Kluger HM, et al. Immunomodulatory Activity of Nivolumab in Metastatic Renal Cell Carcinoma. Clin Cancer Res. 2016;

193. Church SE, Galon J. Tumor Microenvironment and Immunotherapy: The Whole Picture Is Better Than a Glimpse. Immunity. 2015. page 631–3.

194. Choueiri TK, Fishman MN, Escudier B, Stadler WM, Chasalow S, Ross-Macdonald P, et al. Biomarker results from a clinical trial of nivolumab in patients (pts) with metastatic renal cell carcinoma (mRCC) (CA209-009): Gene expression, serum profiling for immune markers, and multiplex tissue immunohistochemistry (IHC). [abstract]. Proc 106th Annu Meet Am Assoc Cancer Res 18-22 Apr 2015; Philadelphia, USA, 2015; Abstr nr 1306.

195. Cona MS, Torri V, Di Nicola M, Garassino M, Del Vecchio M, Cresta S, et al. Baseline LDH serum level as predictive value of activity in patients treated with anti PD-1 and PDL-1 monoclonal antibodies. [abstract]. Proc 107th Annu Meet Am Assoc Cancer Res 16-20 Apr 2016; New Orleans, USA, 2016; Abstr nr 3943.

196. Paulos CM, Wrzesinski C, Kaiser A, Hinrichs CS, Chieppa M, Cassard L, et al. Microbial translocation augments the function of adoptively transferred self/tumor-specific CD8+ T cells via TLR4 signaling. J Clin Invest. 2007;

197. Sivan A, Corrales L, Hubert N, Williams JB, Aquino-Michaels K, Earley ZM, et al. Commensal Bifidobacterium promotes antitumor immunity and facilitates anti-PD-L1 efficacy. Science (80-). 2015;

198. Iida N, Dzutsev A, Stewart CA, Smith L, Bouladoux N, Weingarten RA, et al. Commensal bacteria control cancer response to therapy by modulating the tumor microenvironment. Science (80-). 2013;

199. Viaud S, Saccheri F, Mignot G, Yamazaki T, Daillère R, Hannani D, et al. The intestinal microbiota modulates the anticancer immune effects of cyclophosphamide. Science (80-). 2013;

200. Gopalakrishnan V, Spencer CN, Nezi L, Reuben A, Andrews MC, Karpinets T V., et al. Gut microbiome modulates response to anti-PD-1 immunotherapy in melanoma patients. Science (80-). 2018;

201. Routy B, Le Chatelier E, Derosa L, Duong CPM, Alou MT, Daillère R, et al. Gut microbiome influences efficacy of PD-1-based immunotherapy against epithelial tumors. Science (80-). 2018;

202. Matson V, Fessler J, Bao R, Chongsuwat T, Zha Y, Alegre ML, et al. The commensal microbiome is associated with anti-PD-1 efficacy in metastatic melanoma patients. Science (80-). 2018;

203. Chen DS, Mellman I. Elements of cancer immunity and the cancer-immune set point. Nature. 2017.

204. Alexandrov LB, Nik-Zainal S, Wedge DC, Aparicio S a JR, Behjati S, Biankin A V, et al. Signatures of mutational processes in human cancer. Nature. 2013;500:415–21.

205. Pfeifer GP, You Y-H, Besaratinia A. Mutations induced by ultraviolet light. Mutat Res. 2005;571:19–31.

206. Pleasance ED, Stephens PJ, O'Meara S, McBride DJ, Meynert A, Jones D, et al. A small-cell lung cancer genome with complex signatures of tobacco exposure. Nature. 2010;463:184–90.

207. Helleday T, Eshtad S, Nik-Zainal S. Mechanisms underlying mutational signatures in human cancers. Nat Rev Genet. 2014;15:585–98.

208. Lord CJ, Ashworth A. The DNA damage response and cancer therapy. Nature. 2012;481:287–94.

209. Bartkova J, Rezaei N, Liontos M, Karakaidos P, Kletsas D, Issaeva N, et al. Oncogene-induced senescence is part of the tumorigenesis barrier imposed by DNA damage checkpoints. Nature. 2006;

210. Halazonetis TD, Gorgoulis VG, Bartek J. An Oncogene-Induced DNA Damage Model for Cancer Development. Science (80-). 2008;

211. O'Sullivan CC, Moon DH, Kohn EC, Lee J, Sullivan CCO, Moon DH, et al. Beyond Breast and Ovarian Cancers: PARP Inhibitors for BRCA Mutation-Associated and BRCA-Like Solid Tumors. Front Oncol. 2014;4:42.

212. Postel-Vinay S, Vanhecke E, Olaussen K a., Lord CJ, Ashworth A, Soria J-C. The potential of exploiting DNA-repair defects for optimizing lung cancer treatment. Nat Rev Clin Oncol. Nature Publishing Group; 2012;9:144–55.

213. Huang QM, Tomida S, Masuda Y, Arima C, Cao K, Kasahara TA, et al. Regulation of DNA polymerase POLD4 influences genomic instability in lung cancer. Cancer Res. 2010;70:8407–16.

214. The Cancer Genome Atlas Network, Creighton CJ, Morgan M, Gunaratne PH,

Wheeler D a., Gibbs R a., et al. Comprehensive molecular characterization of clear cell renal cell carcinoma. Nature. 2013;499:43–9.

215. Feng C, Ding G, Jiang H, Ding Q, Wen H. Loss of MLH1 confers resistance to PI3Kβ inhibitors in renal clear cell carcinoma with SETD2 mutation. Tumor Biol. 2015;36:3457–64.

216. Yoo KH, Won KY, Lim S-J, Park Y-K, Chang S-G. Deficiency of MSH2 expression is associated with clear cell renal cell carcinoma. Oncol Lett. 2014;8:2135–9.

217. Nickerson ML, Dancik GM, Im KM, Edwards MG, Turan S, Brown J, et al. Concurrent alterations in TERT, KDM6A, and the BRCA pathway in bladder cancer. Clin Cancer Res. 2014;20:4935–48.

218. Plimack ER, Dunbrack RL, Brennan TA, Andrake MD, Zhou Y, Serebriiskii IG, et al. Defects in DNA Repair Genes Predict Response to Neoadjuvant Cisplatin-based Chemotherapy in Muscle-invasive Bladder Cancer. Eur Urol. 2015;68:959–67.

219. Mullane SA, Werner L, Guancial EA, Lis RT, Stack EC, Loda M, et al. Expression Levels of DNA Damage Repair Proteins Are Associated With Overall Survival in Platinum-Treated Advanced Urothelial Carcinoma. Clin Genitourin Cancer. 2015;

220. Bai S, Nunez AL, Wei S, Ziober A, Yao Y, Tomaszewski JE, et al. Microsatellite instability and TARBP2 mutation study in upper urinary tract urothelial carcinoma. Am J Clin Pathol. 2013;139:765–70.

221. Weinstein JN, Akbani R, Broom BM, Wang W, Verhaak RGW, McConkey D, et al. Comprehensive molecular characterization of urothelial bladder carcinoma. Nature. Nature Publishing Group; 2014;507:315–22.

222. Stoepker C, Ameziane N, van der Lelij P, Kooi IE, Oostra AB, Rooimans MA, et al. Defects in the fanconi anemia pathway and chromatid cohesion in head-and-neck cancer. Cancer Res. 2015;0008-5472.CAN-15-0528-.

223. Lee JM, Ledermann JA, Kohn EC. PARP inhibitors for BRCA1/2 mutation-associated and BRCA-like malignancies. Ann Oncol. 2014;25:32–40.

224. Burgess M, Puhalla S. BRCA 1/2-Mutation Related and Sporadic Breast and Ovarian Cancers: More Alike than Different. Front Oncol. 2014;4:19.

225. Walsh T, Casadei S, Lee MK, Pennil CC, Nord AS, Thornton AM, et al. Mutations in 12 genes for inherited ovarian, fallopian tube, and peritoneal carcinoma identified by massively parallel sequencing. Proc Natl Acad Sci U S A. 2011;108:18032–7.

226. Bryant C, Rawlinson R, Massey AJ. Chk1 inhibition as a novel therapeutic strategy for treating triple-negative breast and ovarian cancers. BMC Cancer. 2014;14:570.

227. Bass AJ, Thorsson V, Shmulevich I, Reynolds SM, Miller M, Bernard B, et al. Comprehensive molecular characterization of gastric adenocarcinoma. Nature. Nature Publishing Group; 2014;513:202–9.

228. Hewish M, Lord CJ, Martin S a, Cunningham D, Ashworth A. Mismatch repair deficient colorectal cancer in the era of personalized treatment. Nat Rev Clin Oncol. Nature Publishing Group; 2010;7:197–208.

229. Miquel C, Jacob S, Grandjouan S, Aime A, Viguier J, Sabourin JC, et al. Frequent alteration of DNA damage signalling and repair pathways in human colorectal cancers with microsatellite instability. Oncogene. 2007;26:5919–26.

230. Muzny D, Bainbridge M, Chang K, Dinh H, Drummond J, Fowler G, et al. Comprehensive molecular characterization of human colon and rectal cancer. Nature. Nature Publishing Group; 2012;487:330–7.

231. Wang Y, Hong Y, Li M, Long J, Zhao YP, Zhang JX, et al. Mutation inactivation of Nijmegen breakage syndrome gene (NBS1) in hepatocellular carcinoma and intrahepatic cholangiocarcinoma. PLoS One. 2013;8.

232. Hinrichsen I, Kemp M, Peveling-Oberhag J, Passmann S, Plotz G, Zeuzem S, et al. Promoter methylation of MLH1, PMS2, MSH2 and p16 is a phenomenon of advanced-stage HCCs. PLoS One. 2014;9.

233. Wani Y, Notohara K, Tsukayama C, Okada S. Reduced expression of hMLH1 and hMSH2 gene products in high-grade hepatocellular carcinoma. Acta Med Okayama. 2001;55:65–71.

234. Moy AP, Shahid M, Ferrone CR, Borger DR, Zhu AX, Ting D, et al. Microsatellite instability in gallbladder carcinoma. Virchows Arch. 2015;466:393–402.

235. Abraham SC, Lee JH, Boitnott JK, Argani P, Furth EE, Wu TT. Microsatellite instability in intraductal papillary neoplasms of the biliary tract. Mod Pathol. 2002;15:1309–17.

236. Mateo J, Carreira S, Sandhu S, Miranda S, Mossop H, Perez-Lopez R, et al. DNA-Repair Defects and Olaparib in Metastatic Prostate Cancer. N Engl J Med. 2015;373:1697–708.

237. Abeshouse A, Ahn J, Akbani R, Ally A, Amin S, Andry CD, et al. The Molecular Taxonomy of Primary Prostate Cancer. Cell. 2015;163:1011–25.

238. Howitt BE, Shukla S a., Sholl LM, Ritterhouse LL, Watkins JC, Rodig S, et al. Association of Polymerase e-Mutated and Microsatellite-Instable Endometrial Cancers With Neoantigen Load, Number of Tumor-Infiltrating Lymphocytes, and Expression of PD-1 and PD-L1. JAMA Oncol. 2015;1–5.

239. Network CGAR, Institute GSCB, Getz G, Gabriel SB, Cibulskis K, Lander E, et al. Integrated genomic characterization of endometrial carcinoma. Nature. 2013;497:67–73.

240. Rustgi AK. Familial pancreatic cancer: Genetic advances. Genes Dev. 2014. page 1–7.

241. Riazy M, Kalloger SE, Sheffield BS, Peixoto RD, Li-Chang HH, Scudamore CH, et al. Mismatch repair status may predict response to adjuvant chemotherapy in resectable pancreatic ductal adenocarcinoma. Mod Pathol. 2015;28:1383–9.

242. Kelderman S, Schumacher TN, Kvistborg P. Mismatch Repair-Deficient Cancers Are Targets for Anti-PD-1 Therapy. Cancer Cell. 2015.

243. Smyrk TC, Watson P, Kaul K, Lynch HT. Tumor-infiltrating lymphocytes are a marker for microsatellite instability in colorectal carcinoma. Cancer. 2001;

244. Galon J, Costes A, Sanchez-Cabo F, Kirilovsky A, Mlecnik B, Lagorce-Pagès C, et al. Type, density, and location of immune cells within human colorectal tumors predict clinical outcome. Science (80-). 2006;

245. Llosa NJ, Cruise M, Tam A, Wicks EC, Hechenbleikner EM, Taube JM, et al. The vigorous immune microenvironment of microsatellite instable colon cancer is balanced by multiple counter-inhibitory checkpoints. Cancer Discov. 2015;

246. Le DT, Durham JN, Smith KN, Wang H, Bartlett BR, Aulakh LK, et al. Mismatch repair deficiency predicts response of solid tumors to PD-1 blockade. Science (80-). 2017;

247. Rayner E, Van Gool IC, Palles C, Kearsey SE, Bosse T, Tomlinson I, et al. A panoply of errors: Polymerase proofreading domain mutations in cancer. Nat. Rev. Cancer. 2016.

248. Van Gool IC, Eggink FA, Freeman-Mills L, Stelloo E, Marchi E, De Bruyn M, et al. POLE proofreading mutations elicit an antitumor immune response in endometrial cancer. Clin Cancer Res. 2015;

249. Mehnert JM, Panda A, Zhong H, Hirshfield K, Damare S, Lane K, et al. Immune activation and response to pembrolizumab in POLE-mutant endometrial cancer. J Clin Invest. 2016;

250. Johanns TM, Miller CA, Dorward IG, Tsien C, Chang E, Perry A, et al. Immunogenomics of hypermutated glioblastoma: A patient with germline POLE deficiency treated with checkpoint blockade immunotherapy. Cancer Discov. 2016;

251. Clarke B, Tinker A V., Lee CH, Subramanian S, Van De Rijn M, Turbin D, et al. Intraepithelial T cells and prognosis in ovarian carcinoma: Novel associations with stage, tumor type, and BRCA1 loss. Mod Pathol. 2009;

252. McAlpine JN, Porter H, Köbel M, Nelson BH, Prentice LM, Kalloger SE, et al. BRCA1 and BRCA2 mutations correlate with TP53 abnormalities and presence of immune cell infiltrates in ovarian high-grade serous carcinoma. Mod Pathol. 2012;

253. Strickland KC, Howitt BE, Shukla SA, Rodig S, Ritterhouse LL, Liu JF, et al. Association and prognostic significance of BRCA1/2-mutation status with neoantigen load, number of tumor-infiltrating lymphocytes and expression of PD-1/PD-L1 in high grade serous ovarian cancer. Oncotarget. 2016;

254. Wu YM, Cieślik M, Lonigro RJ, Vats P, Reimers MA, Cao X, et al. Inactivation of CDK12 Delineates a Distinct Immunogenic Class of Advanced Prostate Cancer. Cell. 2018;

255. Boudadi K, Suzman DL, Anagnostou V, Fu W, Luber B, Wang H, et al. Ipilimumab plus nivolumab and DNA-repair defects in AR-V7-expressing metastatic prostate cancer. Oncotarget. 2018;

256. Teo MY, Seier K, Ostrovnaya I, Regazzi AM, Kania BE, Moran MM, et al. Alterations in DNA damage response and repair genes as potential marker of clinical benefit from PD-1/PD-L1 blockade in advanced urothelial cancers. J Clin Oncol. 2018;

257. Chen Q, Sun L, Chen ZJ. Regulation and function of the cGAS-STING pathway of cytosolic DNA sensing. Nat. Immunol. 2016.

258. Ahn J, Barber GN. Self-DNA, STING-dependent signaling and the origins of autoinflammatory disease. Curr. Opin. Immunol. 2014.

259. Ahn J, Xia T, Konno H, Konno K, Ruiz P, Barber GN. Inflammation-driven carcinogenesis is mediated through STING. Nat Commun. 2014;

260. Woo SR, Fuertes MB, Corrales L, Spranger S, Furdyna MJ, Leung MYK, et al. STING-dependent cytosolic DNA sensing mediates innate immune recognition of immunogenic tumors. Immunity. 2014;

261. Klarquist J, Hennies CM, Lehn MA, Reboulet RA, Feau S, Janssen EM. STING-Mediated DNA Sensing Promotes Antitumor and Autoimmune Responses to Dying Cells. J Immunol. 2014;

262. Corrales L, Glickman LH, McWhirter SM, Kanne DB, Sivick KE, Katibah GE, et al. Direct Activation of STING in the Tumor Microenvironment Leads to Potent and Systemic Tumor Regression and Immunity. Cell Rep. 2015;

263. Erdal E, Haider S, Rehwinkel J, Harris AL, McHugh PJ. A prosurvival DNA damage-induced cytoplasmic interferon response is mediated by end resection factors and is limited by Trex1. Genes Dev. 2017;

264. Gaston J, Cheradame L, Yvonnet V, Deas O, Poupon M-F, Judde J-G, et al. Intracellular STING inactivation sensitizes breast cancer cells to genotoxic agents. Oncotarget. 2016;

265. MacKenzie KJ, Carroll P, Martin CA, Murina O, Fluteau A, Simpson DJ, et al. CGAS surveillance of micronuclei links genome instability to innate immunity. Nature. 2017;

266. Harding SM, Benci JL, Irianto J, Discher DE, Minn AJ, Greenberg RA. Mitotic progression following DNA damage enables pattern recognition within micronuclei. Nature. 2017;

267. Brzostek-Racine S, Gordon C, Van Scoy S, Reich NC. The DNA Damage Response Induces IFN. J Immunol. 2011;

268. Parkes EE, Walker SM, Taggart LE, McCabe N, Knight LA, Wilkinson R, et al. Activation of STING-Dependent Innate Immune Signaling By S-Phase-Specific DNA Damage in Breast Cancer. J Natl Cancer Inst. 2017;109:djw199.

269. Härtlova A, Erttmann SF, Raffi FAM, Schmalz AM, Resch U, Anugula S, et al. DNA Damage Primes the Type I Interferon System via the Cytosolic DNA Sensor STING to Promote Anti-Microbial Innate Immunity. Immunity. 2015;

270. Bakhoum SF, Ngo B, Laughney AM, Cavallo JA, Murphy CJ, Ly P, et al. Chromosomal instability drives metastasis through a cytosolic DNA response. Nature. 2018;

271. Bakhoum SF, Cantley LC. The multifaceted role of chromosomal instability in cancer and its microenvironment. Cell. Elsevier Inc.; 2018;174:1–27.

272. Kondo T, Kobayashi J, Saitoh T, Maruyama K, Ishii KJ, Barber GN, et al. DNA damage sensor MRE11 recognizes cytosolic double-stranded DNA and induces type I interferon by regulating STING trafficking. Proc Natl Acad Sci. 2013;

273. Mullard A. Can innate immune system targets turn up the heat on “cold” tumours?

Nat. Rev. Drug Discov. 2018.

274. Wang H, Hu S, Chen X, Shi H, Chen C, Sun L, et al. cGAS is essential for the antitumor effect of immune checkpoint blockade. Proc Natl Acad Sci U S A. 2017;

275. McGrail DJ, Federico L, Li Y, Dai H, Lu Y, Mills GB, et al. Multi-omics analysis reveals neoantigen-independent immune cell infiltration in copy-number driven cancers. Nat Commun. 2018;

276. Galluzzi L, Buqué A, Kepp O, Zitvogel L, Kroemer G. Immunogenic cell death in cancer and infectious disease. Nat Rev Immunol. 2016;

277. Casares N, Pequignot MO, Tesniere A, Ghiringhelli F, Roux S, Chaput N, et al. Caspase-dependent immunogenicity of doxorubicin-induced tumor cell death. J Exp Med. 2005;

278. Tesniere A, Schlemmer F, Boige V, Kepp O, Martins I, Ghiringhelli F, et al. Immunogenic death of colon cancer cells treated with oxaliplatin. Oncogene. 2010;

279. Dudek AM, Garg AD, Krysko D V., De Ruysscher D, Agostinis P. Inducers of immunogenic cancer cell death. Cytokine Growth Factor Rev. 2013.

280. Obeid M, Tesniere A, Ghiringhelli F, Fimia GM, Apetoh L, Perfettini JL, et al. Calreticulin exposure dictates the immunogenicity of cancer cell death. Nat Med. 2007;

281. Panaretakis T, Joza N, Modjtahedi N, Tesniere A, Vitale I, Durchschlag M, et al. The co-translocation of ERp57 and calreticulin determines the immunogenicity of cell death. Cell Death Differ. 2008;

282. Fucikova J, Kralikova P, Fialova A, Brtnicky T, Rob L, Bartunkova J, et al. Human tumor cells killed by anthracyclines induce a tumor-specific immune response. Cancer Res. 2011;

283. Poon IKH, Lucas CD, Rossi AG, Ravichandran KS. Apoptotic cell clearance: basic biology and therapeutic potential. Nat Rev Immunol. 2014;

284. Kroemer G, Galluzzi L, Kepp O, Zitvogel L. Immunogenic Cell Death in Cancer Therapy. Annu Rev Immunol. 2013;

285. Michaud M, Martins I, Sukkurwala AQ, Adjemian S, Ma Y, Pellegatti P, et al. Autophagy-dependent anticancer immune responses induced by chemotherapeutic agents in mice. Science (80-). 2011;

286. Martins I, Wang Y, Michaud M, Ma Y, Sukkurwala AQ, Shen S, et al. Molecular mechanisms of ATP secretion during immunogenic cell death. Cell Death Differ. 2014;

287. Elliott MR, Chekeni FB, Trampont PC, Lazarowski ER, Kadl A, Walk SF, et al. Nucleotides released by apoptotic cells act as a find-me signal to promote phagocytic clearance. Nature. 2009;

288. Sistigu A, Yamazaki T, Vacchelli E, Chaba K, Enot DP, Adam J, et al. Cancer cell-autonomous contribution of type I interferon signaling to the efficacy of chemotherapy. Nat Med. 2014;

289. Scaffidi P, Misteli T, Bianchi ME. Release of chromatin protein HMGB1 by necrotic cells triggers inflammation. Nature. 2002;

290. Sims GP, Rowe DC, Rietdijk ST, Herbst R, Coyle AJ. HMGB1 and RAGE in Inflammation and Cancer. Annu Rev Immunol. 2010;

291. Yu M, Wang H, Ding A, Golenbock DT, Latz E, Czura CJ, et al. HMGB1 signals through toll-like receptor (TLR) 4 and TLR2. Shock. 2006;

292. Urbonaviciute V, Fürnrohr BG, Meister S, Munoz L, Heyder P, De Marchis F, et al. Induction of inflammatory and immune responses by HMGB1–nucleosome complexes: implications for the pathogenesis of SLE. J Exp Med. 2008;

293. Schiraldi M, Raucci A, Muñoz LM, Livoti E, Celona B, Venereau E, et al. HMGB1 promotes recruitment of inflammatory cells to damaged tissues by forming a complex with CXCL12 and signaling via CXCR4. J Exp Med. 2012;

294. Apetoh L, Ghiringhelli F, Tesniere A, Obeid M, Ortiz C, Criollo A, et al. Toll-like receptor 4-dependent contribution of the immune system to anticancer chemotherapy and radiotherapy. Nat Med. 2007;

295. Vacchelli E, Ma Y, Baracco EE, Sistigu A, Enot DP, Pietrocola F, et al. Chemotherapy-induced antitumor immunity requires formyl peptide receptor 1. Science (80-). 2015;

296. Ma Y, Aymeric L, Locher C, Mattarollo SR, Delahaye NF, Pereira P, et al. Contribution of IL-17-producing gamma delta T cells to the efficacy of anticancer chemotherapy. J Exp Med. 2011;

297. Ohtsukasa S, Okabe S, Yamashita H, Iwai T, Sugihara K. Increased expression of CEA and MHC class I in colorectal cancer cell lines exposed to chemotherapy drugs. J Cancer Res Clin Oncol. 2003;

298. Gasser S, Orsulic S, Brown EJ, Raulet DH. The DNA damage pathway regulates innate immune system ligands of the NKG2D receptor. Nature. 2005;

299. Ramakrishnan R, Huang C, Cho H Il, Lloyd M, Johnson J, Ren X, et al. Autophagy induced by conventional chemotherapy mediates tumor cell sensitivity to immunotherapy. Cancer Res. 2012;

300. van der Most RG, Currie AJ, Cleaver AL, Salmons J, Nowak AK, Mehendran S, et al. Cyclophosphamide chemotherapy sensitizes tumor cells to TRAIL-dependent CD8 T cell-mediated immune attack resulting in suppression of tumor growth. PLoS One. 2009;

301. Leduc C, Adam J, Louvet E, Sourisseau T, Dorvault N, Bernard M, et al. TPF induction chemotherapy increases PD-L1 expression in tumour cells and immune cells in head and neck squamous cell carcinoma. ESMO Open. 2018;

302. Bracci L, Schiavoni G, Sistigu A, Belardelli F. Immune-based mechanisms of cytotoxic chemotherapy: Implications for the design of novel and rationale-based combined treatments against cancer. Cell Death Differ. 2014.

303. Mouw KW, Goldberg MS, Konstantinopoulos PA, D'Andrea AD. DNA damage and repair biomarkers of immunotherapy response. Cancer Discov. 2017.

304. Pfirschke C, Engblom C, Rickelt S, Cortez-Retamozo V, Garris C, Pucci F, et al. Immunogenic Chemotherapy Sensitizes Tumors to Checkpoint Blockade Therapy. Immunity. 2016;

305. Wang L, Amoozgar Z, Huang J, Saleh MH, Xing D, Orsulic S, et al. Decitabine Enhances Lymphocyte Migration and Function and Synergizes with CTLA-4 Blockade in a Murine Ovarian Cancer Model. Cancer Immunol Res. 2015;

306. Lesterhuis WJ, Salmons J, Nowak AK, Rozali EN, Khong A, Dick IM, et al. Synergistic Effect of CTLA-4 Blockade and Cancer Chemotherapy in the Induction of Anti-Tumor Immunity. PLoS One. 2013;

307. Lynch TJ, Bondarenko I, Luft A, Serwatowski P, Barlesi F, Chacko R, et al. Ipilimumab in combination with paclitaxel and carboplatin as first-line treatment in stage IIIB/IV non-small-cell lung cancer: Results from a randomized, double-blind, multicenter phase II study. J Clin Oncol. 2012;

308. Reck M, Bondarenko I, Luft A, Serwatowski P, Barlesi F, Chacko R, et al. Ipilimumab in combination with paclitaxel and carboplatin as first-line therapy in extensive-disease-small-cell lung cancer: results from a randomized, double-blind, multicenter phase 2 trial. Ann Oncol. 2013;

309. Brown JS, Sundar R, Lopez J. Combining DNA damaging therapeutics with immunotherapy: More haste, less speed. Br. J. Cancer. 2018.

310. Order SE. The effects of therapeutic irradiation on lymphocytes and immunity. Cancer. 1977;

311. Slone HB, Peters LJ, Milas L. Effect of host immune capability on radiocurability and subsequent transplantability of a murine fibrosarcoma. J Natl Cancer Inst. 1979;

312. Lugade AA, Moran JP, Gerber SA, Rose RC, Frelinger JG, Lord EM. Local Radiation Therapy of B16 Melanoma Tumors Increases the Generation of Tumor Antigen-Specific Effector Cells That Traffic to the Tumor. J Immunol. 2005;

313. Lee Y, Auh SL, Wang Y, Burnette B, Wang Y, Meng Y, et al. Therapeutic effects of ablative radiation on local tumor require CD8+T cells: Changing strategies for cancer treatment. Blood. 2009;

314. Gerber SA, Sedlacek AL, Cron KR, Murphy SP, Frelinger JG, Lord EM. IFN-γ Mediates the Antitumor Effects of Radiation Therapy in a Murine Colon Tumor. Am J Pathol. 2013;

315. Weichselbaum RR, Liang H, Deng L, Fu YX. Radiotherapy and immunotherapy: A beneficial liaison? Nat. Rev. Clin. Oncol. 2017.

316. Wan S, Pestka S, Jubin RG, Lyu YL, Tsai YC, Liu LF. Chemotherapeutics and radiation stimulate MHC class i expression through elevated interferon-beta signaling in breast cancer cells. PLoS One. 2012;

317. Sharabi AB, Nirschl CJ, Kochel CM, Nirschl TR, Francica BJ, Velarde E, et al. Stereotactic Radiation Therapy Augments Antigen-Specific PD-1-Mediated Antitumor Immune Responses via Cross-Presentation of Tumor Antigen. Cancer

Immunol Res. 2015;

318. Garnett CT, Palena C, Chakarborty M, Tsang KY, Schlom J, Hodge JW. Sublethal irradiation of human tumor cells modulates phenotype resulting in enhanced killing by cytotoxic T lymphocytes. Cancer Res. 2004;

319. Reits EA, Hodge JW, Herberts CA, Groothuis TA, Chakraborty M, K.Wansley E, et al. Radiation modulates the peptide repertoire, enhances MHC class I expression, and induces successful antitumor immunotherapy. J Exp Med. 2006;

320. Verbrugge I, Gasparini A, Haynes NM, Hagekyriakou J, Galli M, Stewart TJ, et al. The Curative Outcome of Radioimmunotherapy in a Mouse Breast Cancer Model Relies on mTOR Signaling. Radiat Res. 2014;

321. Kim JY, Son YO, Park SW, Bae JH, Joo SC, Hyung HK, et al. Increase of NKG2D ligands and sensitivity to NK cell-mediated cytotoxicity of tumor cells by heat shock and ionizing radiation. Exp Mol Med. 2006;

322. Obeid M, Panaretakis T, Joza N, Tufi R, Tesniere A, van Endert P, et al. Calreticulin exposure is required for the immunogenicity of γ-irradiation and UVC light-induced apoptosis [5]. Cell Death Differ. 2007.

323. Gameiro SR, Jammeh ML, Wattenberg MM, Tsang KY, Ferrone S, Hodge JW. Radiation-induced immunogenic modulation of tumor enhances antigen processing and calreticulin exposure, resulting in enhanced T-cell killing. Oncotarget. 2014;

324. Ko A, Kanehisa A, Martins I, Senovilla L, Chargari C, Dugue D, et al. Autophagy inhibition radiosensitizes in vitro, yet reduces radioresponses in vivo due to deficient immunogenic signalling. Cell Death Differ. 2014;

325. Deng L, Liang H, Xu M, Yang X, Burnette B, Arina A, et al. STING-dependent cytosolic DNA sensing promotes radiation-induced type I interferon-dependent antitumor immunity in immunogenic tumors. Immunity. 2014;

326. Lim JYH, Gerber S a, Murphy SP, Lord EM. Type I interferons induced by radiation therapy mediate recruitment and effector function of CD8(+) T cells. Cancer Immunol Immunother. 2014;

327. Brusa D, Migliore E, Garetto S, Simone M, Matera L. Immunogenicity of 56 degrees C and UVC-treated prostate cancer is associated with release of HSP70 and HMGB1 from necrotic cells. Prostate. 2009;

328. Schaue D, Kachikwu EL, McBride WH. Cytokines in Radiobiological Responses: A Review. Radiat Res. 2012;

329. Sharabi AB, Lim M, DeWeese TL, Drake CG. Radiation and checkpoint blockade immunotherapy: Radiosensitisation and potential mechanisms of synergy. Lancet Oncol. 2015.

330. Kuwabara M, Takahashi K, Inanami O. Induction of Apoptosis through the Activation of SAPK/JNK Followed by the Expression of Death Receptor Fas in X-irradiated Cells. J Radiat Res. 2003;

331. Chakraborty M, Abrams SI, Camphausen K, Liu K, Scott T, Coleman CN, et al.

Irradiation of Tumor Cells Up-Regulates Fas and Enhances CTL Lytic Activity and CTL Adoptive Immunotherapy. J Immunol. 2003;

332. Mole RH. Whole Body Irradiation—Radiobiology or Medicine? Br J Radiol. 1953;

333. Demaria S, Ng B, Devitt ML, Babb JS, Kawashima N, Liebes L, et al. Ionizing radiation inhibition of distant untreated tumors (abscopal effect) is immune mediated. Int J Radiat Oncol Biol Phys. 2004;

334. Kaminski JM, Shinohara E, Summers JB, Niermann KJ, Morimoto A, Brousal J. The controversial abscopal effect. Cancer Treat. Rev. 2005.

335. Deng L, Liang H, Burnette B, Beckett M, Darga T, Weichselbaum RR, et al. Irradiation and anti-PD-L1 treatment synergistically promote antitumor immunity in mice. J Clin Invest. 2014;

336. Demaria S, Kawashima N, Yang AM, Devitt ML, Babb JS, Allison JP, et al. Immune-mediated inhibition of metastases after treatment with local radiation and CTLA-4 blockade in a mouse model of breast cancer. Clin Cancer Res. 2005;

337. Dewan MZ, Galloway AE, Kawashima N, Dewyngaert JK, Babb JS, Formenti SC, et al. Fractionated but not single-dose radiotherapy induces an immune-mediated abscopal effect when combined with anti-CTLA-4 antibody. Clin Cancer Res. 2009;

338. Park SS, Dong H, Liu X, Harrington SM, Krco CJ, Grams MP, et al. PD-1 Restrains Radiotherapy-Induced Abscopal Effect. Cancer Immunol Res. 2015;

339. Dovedi SJ, Adlard AL, Lipowska-Bhalla G, McKenna C, Jones S, Cheadle EJ, et al. Acquired resistance to fractionated radiotherapy can be overcome by concurrent PD-L1 blockade. Cancer Res. 2014;

340. Dovedi SJ, Illidge TM. The antitumor immune response generated by fractionated radiation therapy may be limited by tumor cell adaptive resistance and can be circumvented by PD-L1 blockade. Oncoimmunology. 2015;

341. Postow MA, Callahan MK, Barker CA, Yamada Y, Yuan J, Kitano S, et al. Immunologic Correlates of the Abscopal Effect in a Patient with Melanoma. N Engl J Med. 2012;

342. Stamell EF, Wolchok JD, Gnjatic S, Lee NY, Brownell I. The abscopal effect associated with a systemic anti-melanoma immune response. Int J Radiat Oncol Biol Phys. 2013;

343. Golden EB, Demaria S, Schiff PB, Chachoua A, Formenti SC. An abscopal response to radiation and ipilimumab in a patient with metastatic non-small cell lung cancer. Cancer Immunol Res. 2013;

344. Grimaldi AM, Simeone E, Giannarelli D, Muto P, Falivene S, Borzillo V, et al. Abscopal effects of radiotherapy on advanced melanoma patients who progressed after ipilimumab immunotherapy. Oncoimmunology. 2014;

345. Kwon ED, Drake CG, Scher HI, Fizazi K, Bossi A, Van den Eertwegh AJM, et al. Ipilimumab versus placebo after radiotherapy in patients with metastatic castration-resistant prostate cancer that had progressed after docetaxel chemotherapy (CA184-043): A multicentre, randomised, double-blind, phase 3 trial. Lancet Oncol. 2014;

346. Slovin SF, Higano CS, Hamid O, Tejwani S, Harzstark A, Alumkal JJ, et al. Ipilimumab

alone or in combination with radiotherapy in metastatic castration-resistant prostate cancer: results from an open-label, multicenter phase I/II study. Ann Oncol Off J Eur Soc Med Oncol. 2013;

347. Formenti SC, Rudqvist N-P, Golden E, Cooper B, Wennerberg E, Lhuillier C, et al. Radiotherapy induces responses of lung cancer to CTLA-4 blockade. Nat Med. 2018;

348. Kang J, Demaria S, Formenti S. Current clinical trials testing the combination of immunotherapy with radiotherapy. J Immunother Cancer. 2016;

349. Lord CJ, Ashworth A. PARP inhibitors: Synthetic lethality in the clinic. Science (80-.). 2017.

350. Ray Chaudhuri A, Nussenzweig A. The multifaceted roles of PARP1 in DNA repair and chromatin remodelling. Nat. Rev. Mol. Cell Biol. 2017.

351. Zaremba T, Curtin NJ. PARP inhibitor development for systemic cancer targeting. Anticancer Agents Med Chem. 2007;

352. Purnell MR, Whish WJ. Novel inhibitors of poly(ADP-ribose) synthetase. Biochem J. 1980;

353. Farmer H, McCabe N, Lord CJ, Tutt ANJ, Johnson D a, Richardson TB, et al. Targeting the DNA repair defect in BRCA mutant cells as a therapeutic strategy. Nature. 2005;434:917–21.

354. Bryant HE, Schultz N, Thomas HD, Parker KM, Flower D, Lopez E, et al. Specific killing of BRCA2-deficient tumours with inhibitors of poly(ADP-ribose) polymerase. Nature. 2005;

355. Murai J, Huang SYN, Das BB, Renaud A, Zhang Y, Doroshow JH, et al. Trapping of PARP1 and PARP2 by clinical PARP inhibitors. Cancer Res. 2012;

356. Pommier Y, O'Connor MJ, De Bono J. Laying a trap to kill cancer cells: PARP inhibitors and their mechanisms of action. Sci. Transl. Med. 2016.

357. Fong PC, Boss DS, Yap TA, Tutt A, Wu P, Mergui-Roelvink M, et al. Inhibition of Poly(ADP-Ribose) Polymerase in Tumors from BRCA Mutation Carriers. N Engl J Med. 2009;361:123–34.

358. Tutt A, Robson M, Garber JE, Domchek SM, Audeh MW, Weitzel JN, et al. Oral Poly (ADP-ribose) Polymerase Inhibitor Olaparib in Patients with BRCA1 or BRCA2 Mutations and Advanced Breast Cancer: a Proof-of-concept Trial. Lancet. 2010;

359. Audeh MW, Carmichael J, Penson RT, Friedlander M, Powell B, Bell-McGuinn KM, et al. Oral poly (ADP-ribose) Polymerase Inhibitor Olaparib in Patients with BRCA1 or BRCA2 Mutations and Recurrent Ovarian Cancer: A Proof-of-concept trial. Lancet. 2010;376:245–51.

360. Kaufman B, Shapira-Frommer R, Schmutzler RK, Audeh MW, Friedlander M, Balmaña J, et al. Olaparib monotherapy in patients with advanced cancer and a germline BRCA1/2 mutation. J Clin Oncol. 2015;

361. Robson M, Im S-A, Senkus E, Xu B, Domchek SM, Masuda N, et al. Olaparib for Metastatic Breast Cancer in Patients with a Germline *BRCA* Mutation. N Engl J Med.

2017;

362. McCabe N, Turner NC, Lord CJ, Kluzek K, Białkowska A, Swift S, et al. Deficiency in the repair of DNA damage by homologous recombination and sensitivity to poly(ADP-ribose) polymerase inhibition. Cancer Res. 2006;66:8109–15.

363. Lord CJ, Ashworth A. BRCAness revisited. Nat Rev Cancer. 2016;

364. Postel-Vinay S, Bajrami I, Friboulet L, Elliott R, Fontebasso Y, Dorvault N, et al. A high-throughput screen identifies PARP1/2 inhibitors as a potential therapy for ERCC1-deficient non-small cell lung cancer. Oncogene. 2013;32:5377–87.

365. Shen J, Peng Y, Wei L, Zhang W, Yang L, Lan L, et al. ARID1A Deficiency Impairs the DNA Damage Checkpoint and Sensitizes Cells to PARP Inhibitors. Cancer Discov. 2015;5:752–67.

366. Rosado MM, Bennici E, Novelli F, Pioli C. Beyond DNA repair, the immunological role of PARP-1 and its siblings. Immunology. 2013.

367. Navarro J, Gozalbo-López B, Méndez AC, Dantzer F, Schreiber V, Martínez C, et al. PARP-1/PARP-2 double deficiency in mouse T cells results in faulty immune responses and T lymphomas. Sci Rep. 2017;

368. Huang J, Wang L, Cong Z, Amoozgar Z, Kiner E, Xing D, et al. The PARP1 inhibitor BMN 673 exhibits immunoregulatory effects in a Brca1-/-murine model of ovarian cancer. Biochem Biophys Res Commun. 2015;

369. Higuchi T, Flies DB, Marjon NA, Mantia-Smaldone G, Ronner L, Gimotty PA, et al. CTLA-4 Blockade Synergizes Therapeutically with PARP Inhibition in BRCA1-Deficient Ovarian Cancer. Cancer Immunol Res. 2015;

370. Robillard L, Nguyen M, Loehr A, Orsulic S, Kristeleit RS, Lin K, et al. Preclinical evaluation of the PARP inhibitor rucaparib in combination with PD-1 and PD-L1 inhibition in a syngeneic BRCA1 mutant ovarian cancer model. AACR Annu Meet 2017; April 1-5, 2017; Washington, DC. 2017.

371. Drew Y, De Jonge M, Hong S-H, Park YH, Wolfer A, Brown J, et al. An open-label, phase II basket study of olaparib and durvalumab (MEDIOLA): Results in germline BRCA-mutated (gBRCAm) platinum-sensitive relapsed (PSR) ovarian cancer (OC). 49th Annu Meet Soc Gynecol Oncol. 2018.

372. Domchek S, Postel-Vinay S, Bang Y, Park Y, Alexandre J, Delord J, et al. An open-label, multitumor, Phase II basket study of olaparib and durvalumab (MEDIOLA): Results in germline BRCA-mutated (gBRCAm) HER2-negative metastatic breast cancer (MBC). San Antonio Breast Cancer Symp. 2017.

373. Angell HK, Rocher Ros V, Standifer N, Lai Z, Gresty C, Delord J-P, et al. se I/II basket study of olaparib and durvalumab: Biomarker analysis in germline BRCA-mutated (gBRCAm) HER2-negative metastatic breast cancer (MBC) and relapsed small-cell lung cancer (SCLC) patients. 32nd Annu Meet Soc Immunother Cancer. 2017.

374. Olaussen KA, Dunant A, Fouret P, Brambilla E, André F, Haddad V, et al. DNA Repair by ERCC1 in Non–Small-Cell Lung Cancer and Cisplatin-Based Adjuvant

Chemotherapy. N Engl J Med. 2006;

375. Kepp O, Senovilla L, Kroemer G. Immunogenic cell death inducers as anticancer agents. Oncotarget. 2014;5:5190–1.

376. Dréan A, Williamson CT, Brough R, Brandsma I, Menon M, Konde A, et al. Modelling therapy resistance in BRCA1/2 mutant cancers. Mol Cancer Ther. 2017;

377. Pettitt SJ, Krastev DB, Brandsma I, Dréan A, Song F, Aleksandrov R, et al. Genome-wide and high-density CRISPR-Cas9 screens identify point mutations in PARP1 causing PARP inhibitor resistance. Nat Commun. 2018;

378. Friboulet L, Olaussen KA, Pignon J-P, Shepherd FA, Tsao M-S, Graziano S, et al. ERCC1 isoform expression and DNA repair in non-small-cell lung cancer. N Engl J Med. 2013;

379. Touat M, Sourisseau T, Dorvault N, Chabanon RM, Garrido M, Morel D, et al. DNA repair deficiency sensitizes lung cancer cells to NAD+ biosynthesis blockade. J Clin Invest. 2018;

380. Michels J, Adam J, Goubar A, Obrist F, Damotte D, Robin A, et al. Negative prognostic value of high levels of intracellular poly(ADP-ribose) in non-small cell lung cancer. Ann Oncol. 2015;

381. Vennapusa B, Baker B, Kowanetz M, Boone J, Menzl I, Bruey JM, et al. Development of a PD-L1 Complementary Diagnostic Immunohistochemistry Assay (SP142) for Atezolizumab. Appl Immunohistochem Mol Morphol. 2018;

382. Dolled-Filhart M, Locke D, Murphy T, Lynch F, Yearley JH, Frisman D, et al. Development of a prototype immunohistochemistry assay to measure programmed death ligand-1 expression in tumor tissue. Arch Pathol Lab Med. 2016;

383. Hendry S, Salgado R, Gevaert T, Russell PA, John T, Thapa B, et al. Assessing Tumor-Infiltrating Lymphocytes in Solid Tumors: A Practical Review for Pathologists and Proposal for a Standardized Method from the International Immuno-Oncology Biomarkers Working Group: Part 2: TILs in Melanoma, Gastrointestinal Tract Carcinom. Adv. Anat. Pathol. 2017.

384. Martin M. Cutadapt removes adapter sequences from high-throughput sequencing reads. EMBnet.journal. 2011;

385. Dobin A, Davis CA, Schlesinger F, Drenkow J, Zaleski C, Jha S, et al. STAR: Ultrafast universal RNA-seq aligner. Bioinformatics. 2013;

386. Wang L, Wang S, Li W. RSeQC: quality control of RNA-seq experiments. Bioinforma Oxford Engl. 2012;

387. Robinson MD, McCarthy DJ, Smyth GK. edgeR: A Bioconductor package for differential expression analysis of digital gene expression data. Bioinformatics. 2009;

388. Subramanian A, Tamayo P, Mootha VK, Mukherjee S, Ebert BL, Gillette MA, et al. Gene set enrichment analysis: A knowledge-based approach for interpreting genome-wide expression profiles. Proc Natl Acad Sci. 2005;

389. Sergushichev A. An algorithm for fast preranked gene set enrichment analysis using

cumulative statistic calculation. bioRxiv. 2016;

390. Leek JT, Johnson WE, Parker HS, Jaffe AE, Storey JD. The SVA package for removing batch effects and other unwanted variation in high-throughput experiments. Bioinformatics. 2012;

391. Waggott D, Chu K, Yin S, Wouters BG, Liu FF, Boutros PC. NanoStringNorm: An extensible R package for the pre-processing of nanostring mRNA and miRNA data. Bioinformatics. 2012;

392. Lê S, Josse J, Husson F. FactoMineR : An *R* Package for Multivariate Analysis. J Stat Softw. 2008;

393. Ritchie ME, Phipson B, Wu D, Hu Y, Law CW, Shi W, et al. Limma powers differential expression analyses for RNA-sequencing and microarray studies. Nucleic Acids Res. 2015;

394. Shen J, Ju Z, Zhao W, Wang L, Peng Y, Ge Z, et al. ARID1A deficiency promotes mutability and potentiates therapeutic antitumor immunity unleashed by immune checkpoint blockade. Nat Med. 2018;

395. Kandoth C, McLellan MD, Vandin F, Ye K, Niu B, Lu C, et al. Mutational landscape and significance across 12 major cancer types. Nature. 2013;

396. Siegel RL, Miller KD, Jemal A. Cancer statistics, 2018. CA Cancer J Clin. 2018;

397. Pao W, Girard N. New driver mutations in non-small-cell lung cancer. Lancet Oncol. 2011.

398. Mogi A, Kuwano H. TP53 mutations in nonsmall cell lung cancer. J Biomed Biotechnol. 2011;

399. Makowski L, Hayes DN. Role of LKB1 in lung cancer development. Br. J. Cancer. 2008.

400. Scagliotti G, Novello S, von Pawel J, Reck M, Pereira JR, Thomas M, et al. Phase III study of carboplatin and paclitaxel alone or with sorafenib in advanced non-small-cell lung cancer. J Clin Oncol. 2010;

401. Borghaei H, Langer CJ, Gadgeel S, Papadimitrakopoulou VA, Patnaik A, Powell SF, et al. 24-Month Overall Survival from KEYNOTE-021 Cohort G: Pemetrexed and Carboplatin with or without Pembrolizumab as First-Line Therapy for Advanced Nonsquamous Non–Small Cell Lung Cancer. J Thorac Oncol. 2018;

402. Rehman FL, Lord CJ, Ashworth A. Synthetic lethal approaches to breast cancer therapy. Nat. Rev. Clin. Oncol. 2010.

403. Bremnes RM, Busund LT, Kilvaer TL, Andersen S, Richardsen E, Paulsen EE, et al. The Role of Tumor-Infiltrating Lymphocytes in Development, Progression, and Prognosis of Non-Small Cell Lung Cancer. J Thorac Oncol. 2016;

404. Harlin H, Meng Y, Peterson AC, Zha Y, Tretiakova M, Slingluff C, et al. Chemokine expression in melanoma metastases associated with CD8 + T-CeII recruitment. Cancer Res. 2009;

405. Fuertes MB, Kacha AK, Kline J, Woo S-R, Kranz DM, Murphy KM, et al. Host type I IFN signals are required for antitumor CD8 $^{+}$ T cell responses through CD8α $^{+}$ dendritic cells. J Exp Med. 2011;

406. Finotello F, Trajanoski Z. Quantifying tumor-infiltrating immune cells from transcriptomics data. Cancer Immunol. Immunother. 2018.

407. Kitajima S, Ivanova E, Guo S, Yoshida R, Campisi M, Sundararaman SK, et al. Suppression of STING associated with LKB1 loss in KRAS-driven lung cancer. Cancer Discov. 2018;

408. Melton DW, Ketchen AM, Nunez F, Bonatti-Abbondandolo S, Abbondandolo A, Squires S, et al. Cells from ERCC1-deficient mice show increased genome instability and a reduced frequency of S-phase-dependent illegitimate chromosome exchange but a normal frequency of homologous recombination. J Cell Sci. 1998;

409. Niedernhofer LJ, Odijk H, Budzowska M, van Drunen E, Maas A, Theil AF, et al. The Structure-Specific Endonuclease Ercc1-Xpf Is Required To Resolve DNA Interstrand Cross-Link-Induced Double-Strand Breaks. Mol Cell Biol. 2004;

410. Schwartz EK, Heyer WD. Processing of joint molecule intermediates by structure-selective endonucleases during homologous recombination in eukaryotes. Chromosoma. 2011.

411. Dou Z, Ghosh K, Vizioli MG, Zhu J, Sen P, Wangensteen KJ, et al. Cytoplasmic chromatin triggers inflammation in senescence and cancer. Nature. 2017;

412. West AP, Khoury-Hanold W, Staron M, Tal MC, Pineda CM, Lang SM, et al. Mitochondrial DNA stress primes the antiviral innate immune response. Nature. 2015;

413. Gisselsson D, Björk J, Höglund M, Mertens F, Dal Cin P, Åkerman M, et al. Abnormal nuclear shape in solid tumors reflects mitotic instability. Am J Pathol. 2001;

414. Shimizu N. Molecular mechanisms of the origin of micronuclei from extrachromosomal elements. Mutagenesis. 2011.

415. Okamoto A, Utani KI, Shimizu N. DNA replication occurs in all lamina positive micronuclei, but never in lamina negative micronuclei. Mutagenesis. 2012;

416. Glück S, Guey B, Gulen MF, Wolter K, Kang TW, Schmacke NA, et al. Innate immune sensing of cytosolic chromatin fragments through cGAS promotes senescence. Nat Cell Biol. 2017;

417. Shekarian T, Valsesia-Wittmann S, Brody J, Michallet MC, Depil S, Caux C, et al. Pattern recognition receptors: Immune targets to enhance cancer immunotherapy. Ann. Oncol. 2017.

418. Kawai T, Akira S. TLR signaling. Cell Death Differ. 2006.

419. Choi MK, Wang Z, Ban T, Yanai H, Lu Y, Koshiba R, et al. A selective contribution of the RIG-I-like receptor pathway to type I interferon responses activated by cytosolic DNA. Proc Natl Acad Sci. 2009;

420. Takaoka A, Wang Z, Choi MK, Yanai H, Negishi H, Ban T, et al. DAI (DLM-1/ZBP1) is a

cytosolic DNA sensor and an activator of innate immune response. Nature. 2007;

421. Jonsson KL, Laustsen A, Krapp C, Skipper KA, Thavachelvam K, Hotter D, et al. IFI16 is required for DNA sensing in human macrophages by promoting production and function of cGAMP. Nat Commun. 2017;

422. Singh SK, Mishra MK, Eltoum IEA, Bae S, Lillard JW, Singh R. CCR5/CCL5 axis interaction promotes migratory and invasiveness of pancreatic cancer cells. Sci Rep. 2018;

423. Halama N, Zoernig I, Berthel A, Kahlert C, Klupp F, Suarez-Carmona M, et al. Tumoral Immune Cell Exploitation in Colorectal Cancer Metastases Can Be Targeted Effectively by Anti-CCR5 Therapy in Cancer Patients. Cancer Cell. 2016;

424. Geiss GK, Bumgarner RE, Birditt B, Dahl T, Dowidar N, Dunaway DL, et al. Direct multiplexed measurement of gene expression with color-coded probe pairs. Nat Biotechnol. 2008;

425. Veldman-Jones MH, Brant R, Rooney C, Geh C, Emery H, Harbron CG, et al. Evaluating robustness and sensitivity of the nanostring technologies ncounter platform to enable multiplexed gene expression analysis of clinical samples. Cancer Res. 2015;

426. Lyons YA, Wu SY, Overwijk WW, Baggerly KA, Sood AK. Immune cell profiling in cancer: molecular approaches to cell-specific identification. npj Precis Oncol. 2017;

427. Knezevic CE, Wright G, Remsing Rix LL, Kim W, Kuenzi BM, Luo Y, et al. Proteome-wide Profiling of Clinical PARP Inhibitors Reveals Compound-Specific Secondary Targets. Cell Chem Biol. 2016;

428. Rosenberg JE, Hoffman-Censits J, Powles T, Van Der Heijden MS, Balar A V., Necchi A, et al. Atezolizumab in patients with locally advanced and metastatic urothelial carcinoma who have progressed following treatment with platinum-based chemotherapy: A single-arm, multicentre, phase 2 trial. Lancet. 2016;

429. Weber JS, D'Angelo SP, Minor D, Hodi FS, Gutzmer R, Neyns B, et al. Nivolumab versus chemotherapy in patients with advanced melanoma who progressed after anti-CTLA-4 treatment (CheckMate 037): A randomised, controlled, open-label, phase 3 trial. Lancet Oncol. 2015;

430. Green MR, Monti S, Rodig SJ, Juszczynski P, Currie T, O'Donnell E, et al. Integrative analysis reveals selective 9p24.1 amplification, increased PD-1 ligand expression, and further induction via JAK2 in nodular sclerosing Hodgkin lymphoma and primary mediastinal large B-cell lymphoma. Blood. 2010/07/16. 2010;116:3268–77.

431. Ikeda S, Okamoto T, Okano S, Umemoto Y, Tagawa T, Morodomi Y, et al. PD-L1 is upregulated by simultaneous amplification of the PD-L1 and JAK2 genes in non-small cell lung cancer. J Thorac Oncol. 2016;

432. Twa DDW, Chan FC, Ben-Neriah S, Woolcock BW, Mottok A, Tan KL, et al. Genomic rearrangements involving programmed death ligands are recurrent in primary mediastinal large B-cell lymphoma. Blood. 2014;

433. Abiko K, Matsumura N, Hamanishi J, Horikawa N, Murakami R, Yamaguchi K, et al. IFN-γ from lymphocytes induces PD-L1 expression and promotes progression of ovarian cancer. Br J Cancer. 2015;

434. Sun C, Mezzadra R, Schumacher TN. Regulation and Function of the PD-L1 Checkpoint. Immunity. 2018.

435. Burr ML, Sparbier CE, Chan YC, Williamson JC, Woods K, Beavis PA, et al. CMTM6 maintains the expression of PD-L1 and regulates anti-Tumour immunity. Nature. 2017;

436. Mezzadra R, Sun C, Jae LT, Gomez-Eerland R, De Vries E, Wu W, et al. Identification of CMTM6 and CMTM4 as PD-L1 protein regulators. Nature. 2017;

437. Paydas S, Bagir E, Ergin M, Seydaoglu G. Changes in PD-1 and PD-L1 Expression in Cases with Hodgkin Lymphoma after Chemotherapy. Blood. 2015;

438. Ock C-Y, Kim S, Keam B, Kim S, Ahn Y-O, Chung E-J, et al. Changes in programmed death-ligand 1 expression during cisplatin treatment in patients with head and neck squamous cell carcinoma. Oncotarget. 2017;

439. Grabosch S, Zeng F, Zhang L, Strange M, Brozick J, Edwards R, et al. PD-L1 biology in response to chemotherapy in vitro and in vivo in ovarian cancer. J Immunother Cancer. 2015;

440. Tran L, Allen CT, Xiao R, Moore E, Davis R, Park S-J, et al. Cisplatin Alters Antitumor Immunity and Synergizes with PD-1/PD-L1 Inhibition in Head and Neck Squamous Cell Carcinoma. Cancer Immunol Res. 2017;

441. Munari E, Zamboni G, Lunardi G, Marchionni L, Marconi M, Sommaggio M, et al. PD-L1 Expression Heterogeneity in Non–Small Cell Lung Cancer: Defining Criteria for Harmonization between Biopsy Specimens and Whole Sections. J Thorac Oncol. 2018;

442. Zhang M, Li G, Wang Y, Wang Y, Zhao S, Haihong P, et al. PD-L1 expression in lung cancer and its correlation with driver mutations: a meta-analysis. Sci Rep. 2017;

443. Azuma K, Ota K, Kawahara A, Hattori S, Iwama E, Harada T, et al. Association of PD-L1 overexpression with activating EGFR mutations in surgically resected nonsmall-cell lung cancer. Ann Oncol. 2014;25:1935–40.

444. Wang K, Wang J, Wei F, Zhao N, Yang F, Ren X. Expression of TLR4 in non-small cell lung cancer is associated with PD-L1 and poor prognosis in patients receiving pulmonectomy. Front Immunol. 2017;

445. Jiao S, Xia W, Yamaguchi H, Wei Y, Chen MK, Hsu JM, et al. PARP inhibitor upregulates PD-L1 expression and enhances cancer-associated immunosuppression. Clin Cancer Res. 2017;

446. Garcia-Diaz A, Shin DS, Moreno BH, Saco J, Escuin-Ordinas H, Rodriguez GA, et al. Interferon Receptor Signaling Pathways Regulating PD-L1 and PD-L2 Expression. Cell Rep. 2017;

447. Sato H, Niimi A, Yasuhara T, Permata TBM, Hagiwara Y, Isono M, et al. DNA double-

strand break repair pathway regulates PD-L1 expression in cancer cells. Nat Commun. 2017;

448. Li CW, Lim SO, Xia W, Lee HH, Chan LC, Kuo CW, et al. Glycosylation and stabilization of programmed death ligand-1 suppresses T-cell activity. Nat Commun. 2016;

449. Lim SO, Li CW, Xia W, Cha JH, Chan LC, Wu Y, et al. Deubiquitination and Stabilization of PD-L1 by CSN5. Cancer Cell. 2016;

450. Kang HC, Lee Y-I, Shin J-H, Andrabi SA, Chi Z, Gagne J-P, et al. Iduna is a poly(ADP-ribose) (PAR)-dependent E3 ubiquitin ligase that regulates DNA damage. Proc Natl Acad Sci. 2011;

451. DaRosa PA, Wang Z, Jiang X, Pruneda JN, Cong F, Klevit RE, et al. Allosteric activation of the RNF146 ubiquitin ligase by a poly(ADP-ribosyl)ation signal. Nature. 2014;

452. Nakada S. Opposing roles of RNF8/RNF168 and deubiquitinating enzymes in ubiquitination-dependent DNA double-strand break response signaling and DNA-repair pathway choice. J Radiat Res. 2016.

453. Galluzzi L, Vitale I, Aaronson SA, Abrams JM, Adam D, Agostinis P, et al. Molecular mechanisms of cell death: Recommendations of the Nomenclature Committee on Cell Death 2018. Cell Death Differ. 2018.

454. Kepp O, Tartour E, Vitale I, Vacchelli E, Adjemian S, Agostinis P, et al. Consensus guidelines for the detection of immunogenic cell death. Oncoimmunology. 2014.

455. Garg AD, Vandenberk L, Fang S, Fasche T, Van Eygen S, Maes J, et al. Pathogen response-like recruitment and activation of neutrophils by sterile immunogenic dying cells drives neutrophil-mediated residual cell killing. Cell Death Differ. 2017;

456. Vanpouille-Box C, Alard A, Aryankalayil MJ, Sarfraz Y, Diamond JM, Schneider RJ, et al. DNA exonuclease Trex1 regulates radiotherapy-induced tumour immunogenicity. Nat Commun. 2017;

457. Murai J, Huang S-YN, Renaud A, Zhang Y, Ji J, Takeda S, et al. Stereospecific PARP Trapping by BMN 673 and Comparison with Olaparib and Rucaparib. Mol Cancer Ther. 2014;

458. Panaretakis T, Kepp O, Brockmeier U, Tesniere A, Bjorklund AC, Chapman DC, et al. Mechanisms of pre-apoptotic calreticulin exposure in immunogenic cell death. EMBO J. 2009;

459. Chekeni FB, Elliott MR, Sandilos JK, Walk SF, Kinchen JM, Lazarowski ER, et al. Pannexin 1 channels mediate "find-me" signal release and membrane permeability during apoptosis. Nature. 2010;

460. Qu Y, Misaghi S, Newton K, Gilmour LL, Louie S, Cupp JE, et al. Pannexin-1 Is Required for ATP Release during Apoptosis but Not for Inflammasome Activation. J Immunol. 2011;

461. Segawa K, Kurata S, Yanagihashi Y, Brummelkamp TR, Matsuda F, Nagata S. Caspase-mediated cleavage of phospholipid flippase for apoptotic phosphatidylserine exposure. Science (80-). 2014;

462. Rufo N, Garg AD, Agostinis P. The Unfolded Protein Response in Immunogenic Cell Death and Cancer Immunotherapy. Trends in Cancer. 2017.

463. Martins I, Kepp O, Schlemmer F, Adjemian S, Tailler M, Shen S, et al. Restoration of the immunogenicity of cisplatin-induced cancer cell death by endoplasmic reticulum stress. Oncogene. 2011;

464. Fucikova J, Becht E, Iribarren K, Goc J, Remark R, Damotte D, et al. Calreticulin expression in human non-small cell lung cancers correlates with increased accumulation of antitumor immune cells and favorable prognosis. Cancer Res. 2016;

465. Wang Y, Martins I, Ma Y, Kepp O, Galluzzi L, Kroemer G. Autophagy-dependent ATP release from dying cells via lysosomal exocytosis. Autophagy. 2013.

466. Sandilos JK, Chiu YH, Chekeni FB, Armstrong AJ, Walk SF, Ravichandran KS, et al. Pannexin 1, an ATP release channel, is activated by caspase cleavage of its pore-associated C-terminal autoinhibitory region. J Biol Chem. 2012;

467. Fader CM, Aguilera MO, Colombo MI. ATP is released from autophagic vesicles to the extracellular space in a VAMP7-dependent manner. Autophagy. 2012;

468. Ayna G, Krysko D V., Kaczmarek A, Petrovski G, Vandenabeele P, Fésüs L. ATP release from dying autophagic cells and their phagocytosis are crucial for inflammasome activation in macrophages. PLoS One. 2012;

469. Franz S, Herrmann K, Führnrohr B, Sheriff A, Frey B, Gaipl US, et al. After shrinkage apoptotic cells expose internal membrane-derived epitopes on their plasma membranes. Cell Death Differ. 2007;

470. Martins I, Tesniere A, Kepp O, Michaud M, Schlemmer F, Senovilla L, et al. Chemotherapy induces ATP release from tumor cells. Cell Cycle. 2009;

471. Ladoire S, Chaba K, Martins I, Sukkurwala AQ, Adjemian S, Michaud M, et al. Immunohistochemical detection of cytoplasmic LC3 puncta in human cancer specimens. Autophagy. 2012;

472. Andersson U, Wang H, Palmblad K, Aveberger A-C, Bloom O, Erlandsson-Harris H, et al. High Mobility Group 1 Protein (Hmg-1) Stimulates Proinflammatory Cytokine Synthesis in Human Monocytes. J Exp Med. 2000;

473. Park JS, Gamboni-Robertson F, He Q, Svetkauskaite D, Kim J, Strassheim D, et al. High mobility group box 1 protein interacts with multiple Toll-like receptors. AJP Cell Physiol. 2005;

474. Park JS, Svetkauskaite D, He Q, Kim JY, Strassheim D, Ishizaka A, et al. Involvement of Toll-like Receptors 2 and 4 in Cellular Activation by High Mobility Group Box 1 Protein. J Biol Chem. 2004;

475. Dumitriu IE, Baruah P, Bianchi ME, Manfredi AA, Rovere-Querini P. Requirement of HMGB1 and RAGE for the maturation of human plasmacytoid dendritic cells. Eur J Immunol. 2005;

476. Ladoire S, Penault-Llorca F, Senovilla L, Dalban C, Enot D, Locher C, et al. Combined evaluation of LC3B puncta and HMGB1 expression predicts residual risk of relapse

after adjuvant chemotherapy in breast cancer. Autophagy. 2015;

477. Menger L, Vacchelli E, Adjemian S, Martins I, Ma Y, Shen S, et al. Cardiac glycosides exert anticancer effects by inducing immunogenic cell death. Sci Transl Med. 2012;

478. Ghiringhelli F, Apetoh L, Tesniere A, Aymeric L, Ma Y, Ortiz C, et al. Activation of the NLRP3 inflammasome in dendritic cells induces IL-1B-dependent adaptive immunity against tumors. Nat Med. 2009;

479. Meyer C, Rosinsky C, Alme A, Powell J. Expression of CD39 and CD73 as a means of evading anti-tumor immune reponses in lung cancer. J Immunol. 2010;

480. Allard B, Longhi MS, Robson SC, Stagg J. The ectonucleotidases CD39 and CD73: Novel checkpoint inhibitor targets. Immunol. Rev. 2017.

481. Antolín AA, Mestres J. Linking off-target kinase pharmacology to the differential cellular effects observed among PARP inhibitors. Oncotarget. 2014;

482. Song JH, Kraft AS. Pim kinase inhibitors sensitize prostate cancer cells to apoptosis triggered by Bcl-2 family inhibitor ABT-737. Cancer Res. 2012;

483. Cervantes-Gomez F, Chen LS, Orlowski RZ, Gandhi V. Biological effects of the pim kinase inhibitor, SGI-1776, in multiple myeloma. Clin Lymphoma, Myeloma Leuk. 2013;

484. Swisher EM, Lin KK, Oza AM, Scott CL, Giordano H, Sun J, et al. Rucaparib in relapsed, platinum-sensitive high-grade ovarian carcinoma (ARIEL2 Part 1): an international, multicentre, open-label, phase 2 trial. Lancet Oncol [Internet]. 2016;1–13. Available from: http://www.sciencedirect.com/science/article/pii/S1470204516305599%5Cnhttp://www.ncbi.nlm.nih.gov/pubmed/27908594

485. Ho SSW, Zhang WYL, Tan NYJ, Khatoo M, Suter MA, Tripathi S, et al. The DNA Structure-Specific Endonuclease MUS81 Mediates DNA Sensor STING-Dependent Host Rejection of Prostate Cancer Cells. Immunity. 2016;

486. Matos J, West SC. Holliday junction resolution: Regulation in space and time. DNA Repair (Amst). 2014;

487. Ciccia A, McDonald N, West SC. Structural and Functional Relationships of the XPF/MUS81 Family of Proteins. Annu Rev Biochem. 2008;

488. Nimonkar A V., Genschel J, Kinoshita E, Polaczek P, Campbell JL, Wyman C, et al. BLM-DNA2-RPA-MRN and EXO1-BLM-RPA-MRN constitute two DNA end resection machineries for human DNA break repair. Genes Dev. 2011;

489. McNeil EM, Melton DW. DNA repair endonuclease ERCC1-XPF as a novel therapeutic target to overcome chemoresistance in cancer therapy. Nucleic Acids Res. 2012;

490. Sarbajna S, Davies D, West SC. Roles of SLX1-SLX4, MUS81-EME1, and GEN1 in avoiding genome instability and mitotic catastrophe. Genes Dev. 2014;

491. Hanada K, Budzowska M, Davies SL, Van Drunen E, Onizawa H, Beverloo HB, et al. The structure-specific endonuclease Mus81 contributes to replication restart by

generating double-strand DNA breaks. Nat Struct Mol Biol. 2007;

492. Lai X, Broderick R, Bergoglio V, Zimmer J, Badie S, Niedzwiedz W, et al. MUS81 nuclease activity is essential for replication stress tolerance and chromosome segregation in BRCA2-deficient cells. Nat Commun. 2017;

493. Minocherhomji S, Ying S, Bjerregaard VA, Bursomanno S, Aleliunaite A, Wu W, et al. Replication stress activates DNA repair synthesis in mitosis. Nature. 2015;

494. Barefield C, Karlseder J. The BLM helicase contributes to telomere maintenance through processing of late-replicating intermediate structures. Nucleic Acids Res. 2012;

495. Shen YJ, LeBert N, Chitre AA, Koo CXE, Nga XH, Ho SSW, et al. Genome-derived cytosolic DNA mediates type I interferon-dependent rejection of B cell lymphoma cells. Cell Rep. 2015;

496. Lan YY, Londoño D, Bouley R, Rooney MS, Hacohen N. Dnase2a deficiency uncovers lysosomal clearance of damaged nuclear DNA via autophagy. Cell Rep. 2014;

497. Fenech M, Kirsch-Volders M, Natarajan AT, Surralles J, Crott JW, Parry J, et al. Molecular mechanisms of micronucleus, nucleoplasmic bridge and nuclear bud formation in mammalian and human cells. Mutagenesis. 2011.

498. Bartsch K, Knittler K, Borowski C, Rudnik S, Damme M, Aden K, et al. Absence of RNase H2 triggers generation of immunogenic micronuclei removed by autophagy. Hum Mol Genet. 2017;

499. Yang H, Wang H, Ren J, Chen Q, Chen ZJ. cGAS is essential for cellular senescence. Proc Natl Acad Sci. 2017;

500. Adams PD, Ivanov A, Pawlikowski J, Manoharan I, Tuyn J Van, Nelson DM, et al. Lysosome-mediated processing of chromatin in senescence. J Cell Biol. 2013;

501. Dou Z, Xu C, Donahue G, Shimi T, Pan JA, Zhu J, et al. Autophagy mediates degradation of nuclear lamina. Nature. 2015;

502. Ahn J, Ruiz P, Barber GN. Intrinsic Self-DNA Triggers Inflammatory Disease Dependent on STING. J Immunol. 2014;

503. Yang YG, Lindahl T, Barnes DE. Trex1 Exonuclease Degrades ssDNA to Prevent Chronic Checkpoint Activation and Autoimmune Disease. Cell. 2007;

504. Coquel F, Neumayer C, Lin YL, Pasero P. SAMHD1 and the innate immune response to cytosolic DNA during DNA replication. Curr. Opin. Immunol. 2019.

505. Daddacha W, Koyen AE, Bastien AJ, Head PSE, Dhere VR, Nabeta GN, et al. SAMHD1 Promotes DNA End Resection to Facilitate DNA Repair by Homologous Recombination. Cell Rep. 2017;

506. Coquel F, Silva MJ, Técher H, Zadorozhny K, Sharma S, Nieminuszczy J, et al. SAMHD1 acts at stalled replication forks to prevent interferon induction. Nature. 2018;

507. Williams JS, Gehle DB, Kunkel TA. The role of RNase H2 in processing

ribonucleotides incorporated during DNA replication. DNA Repair (Amst). 2017;

508. Mackenzie KJ, Carroll P, Lettice L, Tarnauskaitė Ž, Reddy K, Dix F, et al. Ribonuclease H2 mutations induce a cGAS/STING-dependent innate immune response. EMBO J. 2016;

509. Clifford R, Louis T, Robbe P, Ackroyd S, Burns A, Timbs AT, et al. SAMHD1 is mutated recurrently in chronic lymphocytic leukemia and is involved in response to DNA damage. Blood. 2014;

510. Zimmermann M, Murina O, Reijns MAM, Agathanggelou A, Challis R, Tarnauskaite Ž, et al. CRISPR screens identify genomic ribonucleotides as a source of PARP-trapping lesions. Nature. 2018;

511. Diamond MS, Kinder M, Matsushita H, Mashayekhi M, Dunn GP, Archambault JM, et al. Type I interferon is selectively required by dendritic cells for immune rejection of tumors. J Exp Med. 2011;

512. Li T, Chen ZJ. The cGAS–cGAMP–STING pathway connects DNA damage to inflammation, senescence, and cancer. J Exp Med. 2018;

513. Chien Y, Scuoppo C, Wang X, Fang X, Balgley B, Bolden JE, et al. Control of the senescence-associated secretory phenotype by NF-κB promotes senescence and enhances chemosensitivity. Genes Dev. 2011;

514. Wang H, Yao L, Gong Y, Zhang B. Trim31 regulates chronic inflammation via nf-κb signal pathway to promote invasion and metastasis in colorectal cancer. Am J Transl Res. 2018;

515. Zitvogel L, Galluzzi L, Kepp O, Smyth MJ, Kroemer G. Type I interferons in anticancer immunity. Nat. Rev. Immunol. 2015.

516. Snell LM, McGaha TL, Brooks DG. Type I Interferon in Chronic Virus Infection and Cancer. Trends Immunol. 2017.

517. Taleb K, Auffray C, Villefroy P, Pereira A, Hosmalin A, Gaudry M, et al. Chronic Type I IFN Is Sufficient To Promote Immunosuppression through Accumulation of Myeloid-Derived Suppressor Cells. J Immunol. 2017;

518. Tomic J, Lichty B, Spaner DE. Aberrant interferon-signaling is associated with aggressive chronic lymphocytic leukemia. Blood. 2011;

519. Konno H, Yamauchi S, Berglund A, Putney RM, Mulé JJ, Barber GN. Suppression of STING signaling through epigenetic silencing and missense mutation impedes DNA damage mediated cytokine production. Oncogene. 2018;

520. Xia T, Konno H, Barber GN. Recurrent loss of STING signaling in melanoma correlates with susceptibility to viral oncolysis. Cancer Res. 2016;

521. Xia T, Konno H, Ahn J, Barber GN. Deregulation of STING Signaling in Colorectal Carcinoma Constrains DNA Damage Responses and Correlates With Tumorigenesis. Cell Rep. 2016;

522. Wu L, Cao J, Cai WL, Lang SM, Horton JR, Jansen DJ, et al. KDM5 histone demethylases repress immune response via suppression of STING. PLoS Biol. 2018;

523. Campbell JD, Alexandrov A, Kim J, Wala J, Berger AH, Pedamallu CS, et al. Distinct patterns of somatic genome alterations in lung adenocarcinomas and squamous cell carcinomas. Nat Genet. 2016;

524. Williamson CT, Muzik H, Turhan AG, Zamo A, O'Connor MJ, Bebb DG, et al. ATM Deficiency Sensitizes Mantle Cell Lymphoma Cells to Poly(ADP-Ribose) Polymerase-1 Inhibitors. Mol Cancer Ther. 2010;

525. Siddoo-Atwal C, Haas AL, Rosin MP. Elevation of interferon beta-inducible proteins in ataxia telangiectasia cells. Cancer Res. 1996;

526. Wolf C, Rapp A, Berndt N, Staroske W, Schuster M, Dobrick-Mattheuer M, et al. RPA and Rad51 constitute a cell intrinsic mechanism to protect the cytosol from self DNA. Nat Commun. 2016;

527. Bhattacharya S, Srinivasan K, Abdisalaam S, Su F, Raj P, Dozmorov I, et al. RAD51 interconnects between DNA replication, DNA repair and immunity. Nucleic Acids Res. 2017;

528. Teo MY, Bambury RM, Zabor EC, Jordan E, Al-Ahmadie H, Boyd ME, et al. DNA damage response and repair gene alterations are associated with improved survival in patients with platinum-treated advanced urothelial carcinoma. Clin Cancer Res. 2017.

529. O'Donnell T, Christie EL, Ahuja A, Buros J, Aksoy BA, Bowtell DDL, et al. Chemotherapy weakly contributes to predicted neoantigen expression in ovarian cancer. BMC Cancer. 2018;

530. Jacquelot N, Roberti MP, Enot DP, Rusakiewicz S, Ternès N, Jegou S, et al. Predictors of responses to immune checkpoint blockade in advanced melanoma. Nat Commun. 2017;

531. Schelker M, Feau S, Du J, Ranu N, Klipp E, MacBeath G, et al. Estimation of immune cell content in tumour tissue using single-cell RNA-seq data. Nat Commun. 2017;

532. Shamir ER, Ewald AJ. Three-dimensional organotypic culture: Experimental models of mammalian biology and disease. Nat. Rev. Mol. Cell Biol. 2014.

533. Telli ML, Stover DG, Loi S, Aparicio S, Carey LA, Domchek SM, et al. Homologous recombination deficiency and host anti-tumor immunity in triple-negative breast cancer. Breast Cancer Res. Treat. 2018.

534. Tutt A, Tovey H, Cheang MCU, Kernaghan S, Kilburn L, Gazinska P, et al. Carboplatin in BRCA1/2-mutated and triple-negative breast cancer BRCAness subgroups: The TNT Trial. Nat Med. 2018;

Synthèse en français

Introduction

Les défauts des voies de réparation de l'ADN (DVRA) sont un élément caractéristique des cellules cancéreuses qui participe au développement tumoral en favorisant l'instabilité génomique. Depuis plus de 50 ans, cette caractéristique est exploitée comme opportunité thérapeutique pour le traitement du cancer, avec l'utilisation de chimiothérapies cytotoxiques conventionnelles comme approche « non-sélectionnée ». Plus récemment, de nouvelles thérapies ciblant les DVRA ont vu le jour : la découverte du concept de létalité synthétique – classiquement illustré par la sensibilité des tumeurs BRCA-déficientes aux inhibiteurs de PARP (PARPi) – a notamment permis le développement de thérapies dites ciblées, destinées à des populations sélectionnées. A l'image du succès de ces approches, les PARPi olaparib et rucaparib ont connu un développement clinique accéléré, qui a conduit à leur autorisation de mise sur le marché pour le traitement des cancers *BRCA*-mutés de l'ovaire (olaparib en 2014 ; rucaparib en 2016) et du sein (olaparib en 2018). D'autres interactions de létalité synthétique avec les PARPi ont par ailleurs été décrites, comme la déficience en ERCC1 dans le cancer bronchique non à petite cellule (CBNPC) et les défauts d'ARID1A dans plusieurs types tumoraux. Ces découvertes récentes soutiennent l'importance des PARPi dans l'arsenal thérapeutique contre le cancer, et démontrent également l'intérêt translationnel des approches de létalité synthétique.

Parallèlement à ces avancées, l'avènement de l'immunothérapie dans la dernière décennie a totalement révolutionné le traitement du cancer. En particulier, le développement des inhibiteurs de PD-1/PD-L1 (anti-PD-(L)1) a permis d'améliorer considérablement la survie des patients dans de nombreux cancers agressifs, notamment le mélanome métastatique, les cancers avancés du poumon, du rein, et de la vessie, ainsi que les cancers comportant une instabilité micro-satellitaire élevée. Malgré ces progrès, les patients bénéficiant de ces thérapies sont encore minoritaires (15-45% de patients répondeurs selon les cancers) ; c'est pourquoi, l'identification de combinaisons thérapeutiques rationnelles permettant

d'augmenter la proportion des patients susceptibles de répondre aux anti-PD-(L)1 constitue actuellement un domaine de recherche clinique très actif.

De récentes découvertes concernant l'impact de l'instabilité génomique et des DVRA sur la réponse aux anti-PD-(L)1 ont encouragé le développement d'approches combinatoires avec la chimiothérapie. Cette stratégie a démontré une efficacité thérapeutique exceptionnelle, comme l'illustrent les résultats récents du grand essai clinique de phase III KeyNote-189, dans lequel une amélioration sans précédent de la survie globale et de la survie sans progression a été observée chez des patients atteints de CBNPC, traités en première ligne par pembrolizumab (anti-PD-1) et chimiothérapie à base de platine. Aussi, de plus en plus d'essais cliniques sont initiés afin d'évaluer l'efficacité des anti-PD-(L)1 en combinaison avec d'autres thérapies ciblant les DVRA, en particulier les PARPi.

Objectifs

Dans un contexte où les propriétés immunomodulatrices des PARPi sont essentiellement inconnues, l'objectif de mon projet de thèse a été d'étudier le potentiel immunologique de ces composés sur la cellule cancéreuse, et de caractériser les mécanismes moléculaires à l'origine de ce potentiel – avec pour objectif final d'établir un rationnel scientifique robuste pour les essais cliniques en cours et à venir évaluant la combinaison PARPi + anti-PD-(L)1. Dans ce but, nous avons développé une approche basée sur la cellule tumorale et évalué les propriétés immunomodulatrices des PARPi dans plusieurs contextes histologiques (CBNPC et cancer du sein triple-négatif – CSTN) et moléculaires (présence vs absence de DVRA). Pour cela, nous avons utilisé une combinaison unique de modèles cellulaires isogéniques de CBNPC ERCC1-déficient et de CSTN *BRCA1*-mutés, sensibles ou résistants aux PARPi, et étudié divers aspects du potentiel immunologique des PARPi, notamment leur capacité (i) à stimuler la production de signaux immunitaires de manière autonome par les cellules cancéreuses, via l'activation de la voie cGAS/STING, (ii) à moduler la signalisation interféron (IFN) et l'expression de PD-L1 dans les cellules cancéreuses, et (iii) à provoquer la mort cellulaire immunogène (MCI) des cellules cancéreuses.

Résultats

Les défauts d'ERCC1 dans le CBNPC activent un phénotype immunitaire spécifique des cellules cancéreuses.

La déficience en ERCC1 est le DVRA le plus fréquent dans le CBNPC. Ce défaut confère aux tumeurs de CBNPC une sensibilité accrue aux chimiothérapies à base de platine et aux PARPi ; il constitue ainsi une cible thérapeutique privilégiée et un candidat intéressant pour la modulation de l'immunité anti-tumorale dans cette maladie, où les anti-PD-(L)1 ont démontré une efficacité sans précédent.

Nous avons voulu caractériser les effets immunologiques des défauts d'ERCC1 dans le CBNPC. Pour cela, nous avons tout d'abord conduit une analyse transcriptomique des lignées cellulaires de CBNPC isogéniques A549-ERCC1$^{WT/WT}$ et A549-ERCC1$^{-/-}$, afin d'identifier les changements d'expression génique associés à une perte de fonction d'ERCC1. Cette analyse a montré une up-régulation majeure de nombreuses voies de signalisation immunitaires dans les cellules ERCC1-déficientes, notamment des voies contrôlant la production de cytokines et la réponse IFN de type I. De manière intéressante, nous avons observé que ce phénotype d'activation immunitaire était associé à une réexpression spontanée de la protéine STING dans les cellules ERCC1-déficientes, suggérant une activation constitutive de la voie cGAS/STING en l'absence d'ERCC1.

Nous avons ensuite étudié l'effet de la déficience en ERCC1 sur les caractéristiques du microenvironnement immunitaire tumoral dans une série d'échantillons de tumeurs humaines de CBNPC. Une augmentation significative des niveaux de lymphocytes T infiltrants a été détectée dans les tumeurs présentant une faible expression protéique d'ERCC1, soulignant un potentiel lien entre défauts d'ERCC1 et infiltrat lymphocytaire dans les tumeurs de CBNPC.

Les PARPi stimulent une immunité spécifique des cellules cancéreuses par activation de la voie cGAS/STING.

Les PARPi ciblent spécifiquement les cellules cancéreuses comportant des DVRA tels que les mutations de *BRCA1* et les défauts d'ERCC1. La voie cGAS/STING est un médiateur essentiel de la réponse immunitaire anti-tumorale, qui a récemment montré son implication dans l'activation de signaux immunostimulateurs et inflammatoires en réponse aux DVRA dans la cellule cancéreuse. Nous avons émis l'hypothèse que les PARPi pourraient sélectivement accentuer l'activation de phénotypes immunitaires préexistants dans les cellules porteuses de DVRA, par l'activation de la voie cGAS/STING.

Afin de tester cette hypothèse, nous avons utilisé deux modèles isogéniques de CBNPC précédemment établis dans l'équipe (les lignées cellulaires A549-ERCC1$^{WT/WT}$ / A549-ERCC1$^{-/-}$ et H1975-ERCC1$^{WT/WT}$ / H1975-ERCC1$^{-/-}$) ainsi qu'un modèle isogénique de CSTN développé dans le laboratoire du Prof. Chris Lord à l'Institute of Cancer Research à Londres (lignées cellulaires SUM149-BRCA1$_{mut}$ / SUM149-BRCA1$_{rev}$ / SUM149-PARP1$^{-/-}$), et avons examiné l'activation de la voie cGAS/STING dans ces modèles sous traitement par PARPi. Nos données montrent que plusieurs PARPi cliniques, notamment l'olaparib et le rucaparib, génèrent des fragments d'ADN cytoplasmique ayant les caractéristiques de micronoyaux et ce, de manière cycle cellulaire-dépendante. Ces fragments d'ADN accumulés dans le cytoplasme sont détectés par le senseur cGAS, et déclenchent une cascade de signalisation impliquant les éléments clés de la voie cGAS/STING (y compris TBK1, IRF3 et NF-κB), qui débouche sur l'activation d'une réponse IFN de type I associée à la sécrétion de chimiokines lympho-attractantes telles que CCL5. De manière importante, nous avons observé que ces effets sont largement diminués dans les cellules de CBNPC ré-exprimant ERCC1 et les cellules de CSTN *BRCA1*-révertantes, ce qui suggère que les DVRA amplifient les phénotypes immunitaires associés au traitement par PARPi. En outre, ces effets sont totalement abrogés dans les cellules de CSTN *PARP1*$^{-/-}$, ce qui confirme que les phénotypes observés proviennent d'un effet « on-target » des PARPi sur leur cible.

Afin d'évaluer les propriétés immunomodulatrices des PARPi *in vivo*, nous avons utilisé deux modèles de xénogreffes dérivées de patients atteints de CSTN *BRCA1*-muté.

L'analyse transcriptomique de tumeurs issues de ces modèles, après exposition à l'olaparib *in vivo* chez la souris, a révélé que ce PARPi induit un phénotype immunitaire spécifique des cellules cancéreuses, caractérisé par une up-régulation de nombreux gènes impliqués dans la réponse IFN de type I et dans les mécanismes de présentation antigénique.

Au total, ces résultats suggèrent que les PARPi activent une immunité spécifique des cellules cancéreuses dans le CBNPC et le CSTN, conditionnée par l'activation de la voie cGAS/STING et par la présence de DVRA endogènes.

Les PARPi modulent l'expression de PD-L1 dans les cellules tumorales.

L'expression de PD-L1 dans les cellules tumorales est un biomarqueur prédictif important de la réponse aux anti-PD-(L)1. De récentes études ont démontré un lien entre activation de la voie cGAS/STING et expression de PD-L1, et nous avons par conséquent cherché à mesurer l'effet des PARPi sur l'expression de PD-L1 dans nos modèles de CBNPC.

Nous avons observé que, sous traitement par PARPi, les cellules de CBNPC présentent une induction de l'expression de PD-L1 au niveau transcriptionnel et protéique (à la membrane cellulaire) ; l'ajout d'IFN-γ permet de potentialiser cette induction. Ces effets sont spécifiques de PD-L1, exacerbés dans les cellules de CBNPC ERCC1-déficientes, et résultent d''un effet « on-target » des PARPi sur PARP1. De manière importante, nous avons reproduit ces observations sur des cellules tumorales « fraîches » de patients atteints de CBNPC (isolées à partir d'échantillons de liquide pleural), suggérant que l'induction de PD-L1 par les PARPi se produit aussi *in vivo*.

De façon intéressante, nous avons également montré que ce phénotype ne dépend pas de l'activation de la voie cGAS/STING par les PARPi, ce qui suggère l'implication de mécanismes moléculaires indépendants. Notre observation que la combinaison PARPi + IFN-γ produit un effet synergistique sur l'activation de la voie JAK/STAT suggère que les PARPi influencent – directement ou indirectement – les voies de signalisation contrôlant l'expression de PD-L1 dans la cellule cancéreuse.

Les PARPi génèrent la MCI des cellules cancéreuses.

De nombreux agents cytotoxiques ont été testés pour leur potentiel à générer la MCI des cellules cancéreuses, et plusieurs chimiothérapies cliniques ont été identifiées comme agents inducteurs de la MCI. En tant que thérapies ciblées de la réparation de l'ADN, les PARPi sont également des candidats d'intérêt pour l'induction de la MCI, et nous avons par conséquent évalué la capacité de plusieurs PARPi cliniques à induire les éléments moléculaires clés contrôlant l'immunogénicité de la mort cellulaire dans nos modèles de CBNPC.

Nous avons montré que le rucaparib, utilisé à des concentrations létales, est capable d'activer trois phénotypes essentiels de la MCI : l'exposition de la calréticuline à la surface des cellules cancéreuses, la sécrétion d'ATP et le relargage d'HMGB1 en grandes quantités dans le milieu extracellulaire. De manière intéressante, parmi les autres PARPi testés, aucun n'a démontré des propriétés similaires au rucaparib, suggérant que les phénotypes observés avec ce PARPi découlent d'effets non spécifiques de cette molécule sur des cibles secondaires.

Conclusion

Dans l'ensemble, les résultats de cette étude préclinique suggèrent que les PARPi ont des propriétés immunomodulatrices intrinsèques qui participent à l'activation de réponses immunitaires anti-tumorale. Ce potentiel pourrait être exploité cliniquement en combinaison avec les anti-PD-(L)1 dans des populations adéquatement sélectionnées au plan moléculaire.

université PARIS-SACLAY

ÉCOLE DOCTORALE
Cancérologie, biologie, médecine, santé (CBMS)

GUSTAVE ROUSSY
CANCER CAMPUS
GRAND PARIS

Title

Exploiting DNA repair vulnerabilities to modulate anti-cancer immunity: a study of the immunological potential of PARP inhibitors.

Keywords

PARP inhibitors, DNA repair deficiencies, cGAS/STING, Cancer cell-autonomous immunity, PD-L1, Immunogenic cell death.

Abstract

Poly(ADP-ribose) polymerase inhibitors (PARPi) selectively target cancer cells with DNA repair deficiencies such as BRCA1/2 mutations or ERCC1 defects. Clinically, several PARPi are currently approved for the treatment of BRCA-mutant or platinum-sensitive advanced ovarian and breast cancers, and ongoing clinical trials are investigating the efficacy of PARPi in platinum-sensitive Non-Small Cell Lung Cancer (NSCLC). While PARPi constitute potent targeted therapies for the treatment of DNA repair-deficient malignancies, an increasing number of clinical trials are also evaluating their efficacy in combination with immune checkpoint inhibitor (ICI) in various populations. In this context, it is of critical importance to better understand how PARPi might modulate immune responses against cancer, and to investigate the inherent immunological potential of these agents.

In this study, we show that ERCC1-defective NSCLC cells exhibit an enhanced type I interferon (IFN) transcriptomic signature and that low ERCC1 expression correlates with increased lymphocytic infiltration in human NSCLC tumours. Using isogenic cell lines and patient-derived xenografts, we further demonstrate that several clinical PARPi, including olaparib and rucaparib, display cell-autonomous immunomodulatory properties in ERCC1-defective NSCLC and BRCA1-mutant triple-negative breast cancer (TNBC) models. Mechanistically, PARPi generate cytoplasmic chromatin fragments with micronuclei characteristics; this activates the cGAS/STING pathway and elicits downstream type I IFN signalling and CCL5 secretion. Importantly, these effects are suppressed in BRCA1-reverted TNBC cells and ERCC1-rescued NSCLC cells, suggesting that DNA repair defects exacerbate the innate immunity-related phenotypes triggered by PARPi. Similarly, these effects are totally abrogated in PARP1-null TNBC cells, supporting the on-target effect of PARPi in mediating such phenotypes.

Besides this potential to activate tumour cell-autonomous immunity through cGAS/STING and type I IFN signalling, we also observed that PARPi synergize with type II IFN to induce PD L1 expression in NSCLC cell lines and fresh patient tumour cells, especially in the ERCC1-deficient setting. Moreover, we show that lethal concentrations of some PARPi independently activate the key damage-associated molecular patterns dictating the immunogenicity of cancer cell death, including calreticulin exposure at the tumour cell surface, ATP secretion and HMGB1 release in the extracellular compartment.

Together, these preclinical data suggest that PARPi have intrinsic immunomodulatory properties that activate anti-cancer immune responses; this could be exploited clinically in combination with ICI in appropriately molecularly-selected populations.

Titre

Exploiter les défauts de réparation de l'ADN pour moduler l'immunité anti-cancéreuse : une étude du potentiel immunologique des inhibiteurs de PARP.

Mots-clés

Inhibiteurs de PARP, Défauts de réparation de l'ADN, cGAS/STING, Immunité spécifique des cellules cancéreuses, PD-L1, Mort cellulaire immunogénique.

Résumé

Les inhibiteurs de poly(ADP-ribose) polymérase (PARPi) ciblent sélectivement les cellules porteuses de défauts des voies de réparation de l'ADN tels que les mutations de BRCA1/2 et les défauts d'ERCC1. Sur le plan clinique, plusieurs PARPi ont été approuvés pour le traitement des cancers BRCA-mutés ou platine-sensibles du sein et de l'ovaire, et des essais cliniques sont en cours pour évaluer l'efficacité des PARPi dans le cancer bronchique non-à-petites cellules (CBNPC) platine-sensible. Alors que les PARPi ont un fort potentiel thérapeutique dans les cancers comportant des défauts de réparation de l'ADN, de plus en plus d'essais cliniques évaluent également l'efficacité de ces médicaments en combinaison avec les « inhibiteurs d'immune checkpoints » (ICI) dans diverses populations de patients. Dans ce contexte, il est essentiel de mieux comprendre comment les PARPi modulent la réponse immunitaire anti-tumorale, et d'étudier le potentiel immunologique inhérent de ces médicaments.

Dans cette étude, nous avons établi que les cellules de CBNPC déficientes en ERCC1 expriment fortement la signature interféron (IFN) de type I, et que les tumeurs de CBNPC ayant une faible expression d'ERCC1 ont un infiltrat lymphocytaire renforcé. En utilisant des lignées cellulaires isogéniques et des xénogreffes dérivées de patients, nous avons montré que plusieurs PARPi, notamment l'olaparib et le rucaparib, ont des propriétés immunomodulatrices dans les modèles de CBNPC ERCC1-déficients et de cancers du sein triple-négatifs (CSTN) BRCA1-mutés. D'un point de vue mécanistique, les PARPi génèrent des fragments d'ADN cytoplasmiques ayant les caractéristiques de micronoyaux ; ceux-ci activent la voie cGAS/STING et déclenchent une réponse IFN de type I, associée à la sécrétion de la cytokine CCL5. De manière importante, ces effets sont largement diminués dans les cellules de CSTN BRCA1-révertantes et les cellules de CBNPC ré-exprimant ERCC1, ce qui suggère que les défauts de réparation de l'ADN amplifient les phénotypes immunitaires associés au traitement par PARPi. En outre, ces effets sont totalement abrogés dans les cellules de CSTN PARP1-neutralisées, ce qui confirme que les phénotypes observés dépendent d'un effet spécifique des PARPi sur leur cible.

Au-delà de leur potentiel d'activation d'une immunité spécifique des cellules cancéreuses via cGAS/STING et la signalisation IFN de type I, nous avons également constaté que les PARPi potentialisent les effets inducteurs de l'IFN de type II sur l'expression de PD-L1 dans des lignées cellulaires et cellules tumorales fraîches de patients CBNPC, surtout en présence de défauts d'ERCC1. De plus, nous avons montré que certains PARPi, utilisés à des concentrations létales, activent de manière indépendante les éléments moléculaires clés de la mort cellulaire immunogénique, dont l'exposition de la calréticuline à la surface des cellules cancéreuses, la sécrétion d'ATP et le relargage d'HMGB1 en grandes quantités dans le milieu extracellulaire.

Dans l'ensemble, ces données précliniques suggèrent que les PARPi ont des propriétés immunomodulatrices intrinsèques qui participent à l'activation de réponses immunitaires anti-tumorales ; ce potentiel pourrait être exploité cliniquement en combinaison avec les ICI dans des populations adéquatement sélectionnées au plan moléculaire.